



Durham E-Theses

Bis-terdentate cyclometalated iridium complexes and europium-coordinated macrocycles for luminescent devices

Wilkinson, Andrew John

How to cite:

Wilkinson, Andrew John (2004) *Bis-terdentate cyclometalated iridium complexes and europium-coordinated macrocycles for luminescent devices*, Durham theses, Durham University. Available at Durham E-Theses Online: <http://etheses.dur.ac.uk/1309/>

Use policy

The full-text may be used and/or reproduced, and given to third parties in any format or medium, without prior permission or charge, for personal research or study, educational, or not-for-profit purposes provided that:

- a full bibliographic reference is made to the original source
- a [link](#) is made to the metadata record in Durham E-Theses
- the full-text is not changed in any way

The full-text must not be sold in any format or medium without the formal permission of the copyright holders.

Please consult the [full Durham E-Theses policy](#) for further details.

Academic Support Office, Durham University, University Office, Old Elvet, Durham DH1 3HP
e-mail: e-theses.admin@dur.ac.uk Tel: +44 0191 334 6107
<http://etheses.dur.ac.uk>

BIS-TERDENTATE CYCLOMETALATED
IRIDIUM COMPLEXES AND EUROPIUM-
COORDINATED MACROCYCLES FOR
LUMINESCENT DEVICES

Andrew John Wilkinson

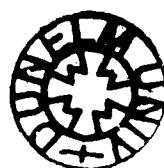
**A copyright of this thesis rests
with the author. No quotation
from it should be published
without his prior written consent
and information derived from it
should be acknowledged.**

Ph.D. Thesis

Department of Chemistry

University of Durham

2004



13 JUN 2005

ABSTRACT

BIS-TERDENTATE CYCLOMETALATED IRIDIUM COMPLEXES AND EUROPIUM-COORDINATED MACROCYCLES FOR LUMINESCENT DEVICES

Andrew John Wilkinson

A great deal of interest currently surrounds the development of electrophosphorescent materials, as they may exhibit efficiencies greater than the theoretical limit of 25% for purely fluorescent materials. The most studied material for such purposes is *fac*-Ir(ppy)₃, which exhibits efficient green phosphorescence in solution and in electroluminescent devices. Europium(III) complexes have also received attention for their narrow bandwidth red emission.

A number of charge-neutral iridium(III) complexes have been prepared as potential electrophosphorescent materials. Bis-terdentate coordination has been investigated, in a quest to provide improved stability with respect to *fac*-Ir(ppy)₃ derivatives, an important objective in commercial development. The complexes described herein are the first examples of iridium bound to N[^]C[^]N coordinating 1,3-di(2-pyridyl)benzene derivatives. Methyl substitution at C⁴ and C⁶ of the phenyl ring (*i.e.* 1,5-di(pyridin-2-yl)-2,4-dimethylbenzene (dpydmbH)) is required to inhibit competitive cyclometalation at these positions. Efficient red emission was observed from Ir(dpydmb-*N,C,N*)(dppy-*C,N,C*) (dppyH₂ = 2,6-diphenylpyridine) ($\lambda_{\text{max}} = 585 \text{ nm}$, $\Phi_{\text{PL}} = 0.21$ in degassed CH₃CN). Fluorination of the dppy ligand at the 2 and 4 positions of the phenyl rings results in a simultaneous blue-shift and increase in efficiency ($\lambda_{\text{max}} = 547 \text{ nm}$, $\Phi_{\text{PL}} = 0.41$ in degassed CH₃CN). These complexes exhibit an unusual meridional geometry, difficult to achieve for tris-bidentate complexes. The complex Ir(dpydmb-*N,C,N*)(ppy-*C,N*)Cl is exceptionally emissive ($\lambda_{\text{max}} = 508 \text{ nm}$, $\Phi_{\text{PL}} = 0.76$ in degassed CH₃CN). Ir(dpydmb-*N,C,N*)(tppic-*C,N,O*) and Ir(dpydmb-*N,C,N*)(hbqc-*C,N,O*) (tppicH₂ = 4-*p*-tolyl-6-phenylpicolinic acid; hbqcH₂ = 4-hydroxybenzo[*h*]quinoline-2-carboxylic acid) were poorly emissive, attributed to a photoactivated labilisation of the Ir–C bond in solution.

The effect of substitution position of a sensitising aminobenzophenone chromophore was investigated in a series of europium(III) macrocyclic complexes. Maximum photoluminescence quantum yield was observed for the *para*-substituted isomer, attributed to the distance dependence of the efficiency of energy transfer. An unexpected rearrangement was observed for the *ortho*-substituted ligand, resulting in a quinoline derivative with a rare *N*-arylated substitution pattern.

ACKNOWLEDGEMENTS

Firstly, I would like to thank my supervisor Dr. J. A. Gareth Williams for his help and support throughout this PhD. Without the numerous discussions and ideas this work would not have progressed as far as it has done. Also I would like to thank Dr. Clive Foster (Avecia Ltd.) for his contribution throughout, and in particular his excellent comments during the writing of this thesis. I must also acknowledge the input of Drs Philipp Stössel and Ingrid Bach (Covion Organic Semiconductors GmbH). I thank the EPSRC and Avecia Ltd. for financial support.

I am grateful to Dr. Andy Beeby for access to the laser for time resolved measurements; Dr. Alan Kenwright, Catherine Heffernan and Ian McKeag for NMR spectroscopy; Dr. Mike Jones and the lovely Lara Turner for mass spectrometry; Jarika Dostal for elemental analysis; Drs Andrés Goeta, Horst Puschmann and Andrei Batsanov for X-ray crystal structures; and to everyone else from the glassblowers to those who provide tea.

My deepest thanks go out to all those whom I have worked alongside in lab CG1 over the past three years. I must thank Dr. Wendy Leslie for her help and friendship from the very start of this work; Kathryn Arm for helping keep me sane, cooking me meals, and being a good friend throughout this PhD; and Dave Rochester for injecting a well needed (!) dose of Morrissey into the lab. I thank Dan, Pete, Chris and Amel for all the great nights out. I also thank, in no particular order, Ximo, Florian, Marc, Anne, Ishmael, Laila, Simon, Les, Jun, Lisa, Jonathan and John.

I am grateful to all the wonderful housemates I've had over the past years; Clare for endless cups of tea and especially for the company and support during the writing of this thesis; Aileen for cooking many meals and being a close friend throughout; and Matt for yet more food and support. I would also like to thank all my other friends during my time in Durham, in particular Ben and Darren for their friendship and nights out walking across all the bridges of Newcastle in a blizzard, to beer festivals that didn't exist, and of course the "interesting" GradSoc parties; Karen for being a good friend, making me dance Salsa, and for providing me a home when I needed it; all members of the Graduate Society Boat Club, in particular the lovely Pascale and Charlie; and my dear friends afar, Heather, Kate and Lyndsey.

My heartfelt thanks go to my fantastic parents and family. Without them I would not have achieved all I have done throughout my life. I love you all.

TABLE OF CONTENTS

1	INTRODUCTION.....	1
1.1	ORGANIC ELECTROLUMINESCENT DEVICES	1
1.1.1	<i>Origins of electroluminescence in organic materials</i>	2
1.1.2	<i>Efficiency of organic electroluminescent devices</i>	5
1.1.3	<i>Fabrication of organic electroluminescent devices</i>	6
1.1.4	<i>Organic materials for OLED applications</i>	7
1.1.4.1	Low molecular weight materials in OLEDs.....	8
1.1.4.2	Polymeric materials in OLEDs	9
1.1.4.3	Hybrid materials in OLEDs	11
1.1.5	<i>Fluorescent dopants in electroluminescent devices</i>	11
1.1.6	<i>Phosphorescent emitters in electroluminescent devices</i>	13
1.2	IRIDIUM COMPLEXES AND THEIR USE IN ELECTROLUMINESCENT DEVICES	14
1.2.1	<i>The inorganic and coordination chemistry of iridium</i>	14
1.2.1.1	<i>N-Heterocyclic complexes of iridium(III)</i>	15
1.2.1.2	<i>Cyclometalated complexes of iridium(III)</i>	16
1.2.2	<i>Photoluminescence and electrochemistry of iridium(III) complexes</i>	22
1.2.3	<i>Electroluminescence of iridium(III) complexes</i>	27
1.3	LANTHANIDE(III) COMPLEXES AND THEIR USE IN ELECTROLUMINESCENT DEVICES	34
1.3.1	<i>The lanthanide series</i>	34
1.3.2	<i>Photophysical properties of the lanthanide(III) ions</i>	35
1.3.3	<i>Coordination and complexation properties of the lanthanide(III) ions</i>	38
1.3.3.1	Europium complexes with macrocyclic ligands	39
1.3.4	<i>Electroluminescence of lanthanide complexes</i>	43
1.3.4.1	Visible electroluminescence of Eu^{3+} and Tb^{3+} complexes	43
1.3.4.2	Electroluminescence from other lanthanide complexes.....	47
1.4	SYNTHESIS OF OLIGOAROMATIC LIGANDS FOR IRIDIUM.....	49
1.4.1	<i>Synthesis of ligands via ring-closing reactions</i>	49
1.4.2	<i>Synthesis of ligands via cross-coupling reactions</i>	51

1.5	SYNTHESIS OF MACROCYCLIC LIGANDS FOR LANTHANIDE COMPLEXES.....	53
2	AIMS AND OBJECTIVES	56
3	SYNTHESIS OF IRIDIUM(III) COMPLEXES	58
3.1	SYNTHESIS OF OLIGOAROMATIC LIGANDS	59
3.1.1	<i>Synthesis of 2,2':6',2''-terpyridine derivatives</i>	<i>59</i>
3.1.2	<i>Synthesis of 1,3-di(pyrid-2-yl)benzene derivatives</i>	<i>61</i>
3.1.3	<i>Synthesis of bis-cyclometalating C^NC ligands and their analogues</i>	<i>66</i>
3.2	COMPLEXATION WITH IRIDIUM(III)	69
3.2.1	<i>Synthesis of Ir(N^CN)(C^NC) complexes</i>	<i>76</i>
3.2.2	<i>Synthesis of complexes of picolinic acid derivatives</i>	<i>83</i>
3.2.3	<i>Cyclometalation via five-membered heterocyclic rings.....</i>	<i>84</i>
3.2.4	<i>Other complexes incorporating mutually trans bis-metalation</i>	<i>86</i>
4	PHOTOPHYSICAL AND COMPUTATIONAL STUDIES OF IRIDIUM(III) COMPLEXES.....	88
4.1	PHOTOPHYSICAL PROPERTIES.....	88
4.1.1	<i>Ir(N^CN)(C^NC) complexes</i>	<i>88</i>
4.1.2	<i>Ir(N^CN)(C^N)Cl complex</i>	<i>93</i>
4.1.3	<i>Ir(N^CN)(C^NO) complexes</i>	<i>96</i>
4.1.4	<i>Ir(N^NN)(C^NC)⁺ complexes</i>	<i>98</i>
4.1.5	<i>Ir(N^CN)(N^NN)²⁺ complexes</i>	<i>101</i>
4.2	COMPUTATIONAL STUDIES	103
4.2.1	<i>Ground-state structures</i>	<i>104</i>
4.2.2	<i>Molecular orbitals.....</i>	<i>107</i>
4.2.3	<i>Ionisation potentials and electron affinities.....</i>	<i>117</i>
4.2.4	<i>Excitation energies.....</i>	<i>118</i>
4.3	CONCLUDING REMARKS: THE EFFECT OF CYCLOMETALATION UPON THE LUMINESCENCE OF IRIDIUM(III) COMPLEXES.....	124
4.4	CONCLUSIONS	127
5	EUROPIUM(III) COMPLEXES.....	130
5.1	SYNTHESIS OF MACROCYCLIC LIGANDS.....	131
5.2	SYNTHESIS OF EUROPIUM(III) COMPLEXES.....	134

5.3	PHOTOPHYSICAL PROPERTIES	139
5.3.1	<i>Absorption spectra</i>	139
5.3.2	<i>Luminescence properties of Eu-127 and Eu-128</i>	140
5.3.3	<i>Luminescence properties of Eu-132 and Eu-133</i>	143
5.4	CONCLUSION.....	146
6	EXPERIMENTAL	147
6.1	SYNTHESIS OF LIGANDS FOR IRIDIUM(III) COMPLEXES	151
6.1.1	<i>[1,1'-Bis(diphenylphosphino)ferrocene]palladium(II) chloride</i>	151
6.1.2	<i>5-Bromo-isophthalic acid diethyl ester</i>	152
6.1.3	<i>4'-Bromo-2,2':6',2''-terpyridine</i>	153
6.1.4	<i>4'-(5,5-Dimethyl-[1,3,2]dioxaborinan-2-yl)-2,2':6',2''-terpyridine</i>	155
6.1.5	<i>5-(2,2':6',2''-Terpyridin-4'-yl)-isophthalic acid diethyl ester 83 [tpyiade]</i> . 156	
6.1.6	<i>4-(2,2':6',2''-Terpyridin-4'-yl)benzoic acid ethyl ester [tpybae]</i>	157
6.1.7	<i>1,3-Di(pyridin-2-yl)benzene 84 [dpybH]</i>	158
6.1.8	<i>1,5-Di(pyrid-2-yl)-2,4-dimethylbenzene 85 [dpydmbH]</i>	159
6.1.9	<i>1,3,5-Tri-pyridin-2-ylpentane-1,5-dione 89</i>	161
6.1.10	<i>1-Pyridin-2-ylpropan-1-one</i>	162
6.1.11	<i>1-(2-Oxo-2-phenylethyl)pyridinium iodide</i>	162
6.1.12	<i>2-(1-(3-Cyanophenyl)-1-oxoethyl)pyridinium iodide</i>	163
6.1.13	<i>1-(2-(2,4-Difluorophenyl)-2-oxoethyl)pyridinium iodide</i>	164
6.1.14	<i>1-(2-Oxo-2-pyridin-2-ylethyl)pyridinium iodide</i>	164
6.1.15	<i>1-(2-Oxo-2-(2-thienyl)ethyl)pyridinium iodide</i>	165
6.1.16	<i>4-p-Tolyl-2,6-diphenylpyridine 91 [tdppyH₂]</i>	166
6.1.17	<i>4-p-Tolyl-2,6-di(3-cyanophenyl)pyridine 92 [tcdppyH₂]</i>	168
6.1.18	<i>2,6-Di(3-cyanophenyl)pyridine 94 [cdppyH₂]</i>	170
6.1.19	<i>2,6-Di(2,4-difluorophenyl)pyridine 96 [F₄dppyH₂]</i>	171
6.1.20	<i>2,6-Di(2-thienyl)pyridine 95 [dthpyH₂]</i>	173
6.1.21	<i>4-p-Tolyl-6-phenylpicolinic acid 93 [tppicH₂]</i>	174
6.1.22	<i>4-Hydroxybenzo[h]quinoline-2-carboxylic acid [hbqcH₂]</i>	176
6.1.23	<i>2,6-Di(2'-indolyl)pyridine 97 [dinpyH₂]</i>	177
6.2	SYNTHESIS OF IRIDIUM(III) COMPLEXES.....	179
6.2.1	<i>Bis(μ-chloro)bis(1,3-di(pyrid-2-yl)-benzene-N,C^{2'},N iridium chloride)</i> <i>[Ir(dpyb)Cl(μ-Cl)]₂</i>	179

6.2.2	<i>Bis(μ-chloro)bis(1,5-di(pyrid-2-yl)-2,4-dimethylbenzene-N,C^{6'},N</i> <i>iridium chloride) 104 [Ir(dpydmb)Cl(μ-Cl)]₂.....</i>	180
6.2.3	<i>Iridium(1,3-di(pyrid-2-yl)-benzene-N,C^{2'},N)(4'-(p-tolyl)-2,2':6',2''-</i> <i>terpyridine)²⁺ 100 [Ir(dpyb)(tppy)]²⁺</i>	181
6.2.4	<i>Iridium(1,5-di(pyrid-2-yl)-2,4-dimethylbenzene-N,C^{6'},N)(2,2':6',2''-</i> <i>terpyridine)²⁺ 105 [Ir(dpydmb)(terpy)]²⁺</i>	182
6.2.5	<i>Iridium(1,5-di(pyrid-2-yl)-2,4-dimethylbenzene-N,C^{6'},N)(4'-(p-tolyl)-</i> <i>2,2':6',2''-terpyridine)²⁺ 106 [Ir(dpydmb)(tppy)]²⁺</i>	183
6.2.6	<i>Iridium(1,5-di(pyrid-2-yl)-2,4-dimethylbenzene-N,C^{6'},N)(5-(2,2':6',2''-</i> <i>terpyridin-4'-yl)-isophthalic acid diethyl ester)²⁺ 107</i> <i>[Ir(dpydmb)(tpyiade)]²⁺</i>	184
6.2.7	<i>Iridium bis(1,5-di(pyrid-2-yl)-2,4-dimethylbenzene-N,C^{6'},N)⁺ 125</i> <i>[Ir(dpydmb)₂]⁺</i>	185
6.2.8	<i>Iridium(1,5-di(pyrid-2-yl)-2,4-dimethylbenzene-N,C^{6'},N)(2-</i> <i>phenylpyridine-N,C^{2'})chloride 115 [Ir(dpydmb)(ppy)Cl].....</i>	186
6.2.9	<i>Iridium(1,5-di(pyrid-2-yl)-2,4-dimethylbenzene-N,C^{6'},N)(2,6-</i> <i>diphenylpyridine-C^{2'},N,C^{2'}) 108 [Ir(dpydmb)(dppy)]</i>	187
6.2.10	<i>Iridium(1,5-di(pyrid-2-yl)-2,4-dimethylbenzene-N,C^{6'},N)(2,6-</i> <i>di(2,4-difluorophenyl)pyridine-C^{6'},N,C^{6'}) 110 [Ir(dpydmb)(F₄dppy)].....</i>	189
6.2.11	<i>Iridium(1,5-di(pyrid-2-yl)-2,4-dimethylbenzene-N,C^{6'},N)(4-p-tolyl-</i> <i>6-phenylpicolinic acid-C^{2'},N,O) 116 [Ir(dpydmb)(tppic)].....</i>	190
6.2.12	<i>Iridium(1,5-di(pyrid-2-yl)-2,4-dimethylbenzene-N,C^{6'},N)(4-</i> <i>hydroxybenzo[h]quinoline-2-carboxylic acid-C¹⁰,N,O) 117</i> <i>[Ir(dpydmb)(hbqc)].....</i>	191
6.2.13	<i>Iridium(1,5-di(pyrid-2-yl)-2,4-dimethylbenzene-N,C^{6'},N)(2,6-di(2'-</i> <i>indolyl)pyridine-C^{3'},N,C^{3'}) 122 [Ir(dpydmb)(dinpy-C^NC)].....</i>	192
6.2.14	<i>Iridium(1,5-di(pyrid-2-yl)-2,4-dimethylbenzene-N,C^{6'},N)(2,6-di(2'-</i> <i>indolyl)pyridine-N,N,N) 123 [Ir(dpydmb)(dinpy-N^NN)].....</i>	193
6.2.15	<i>Iridium(1,5-di(pyrid-2-yl)-2,4-dimethylbenzene-N,C^{6'},N)(2,6-di(2-</i> <i>thienyl)pyridine-C^{3'},N) [Ir(dpydmb)(dthpyH)]⁺</i>	194
6.2.16	<i>Iridium(4-(2,2':6',2''-terpyridin-4'-yl)benzoic acid ethyl</i> <i>ester)(2,6-diphenylpyridine-C^{2'},N,C^{2'})⁺ 124 [Ir(tpybae)(dppy)]⁺</i>	195
6.3	SYNTHESIS OF MACROCYCLIC LIGANDS AND THEIR LANTHANIDE(III) COMPLEXES	197

6.3.1	8-Benzyloxyquinoline-2-carboxaldehyde.....	197
6.3.2	8-Benzyloxy-2-chloromethylquinoline	198
6.3.3	8-Methoxy-4-methylquinoline	200
6.3.4	2-Bromo-1-(4-trifluoromethylphenyl)ethanone	200
6.3.5	1,4,7-Tris-(8-hydroxyquinolin-2-ylmethyl)- 1,4,7,10-tetraazacyclododecane 131	201
6.3.6	1,4,7,10-Tetraazacyclododecane-1,4,7-tris(acetic acid tert-butyl ester) 126 ..	203
6.3.7	Europium(III) 10-((3-Benzoyl-phenylcarbamoyl)methyl)-1,4,7,10- tetraazacyclododecane-1,4,7-trisacetate [Eu- 128].....	204
6.3.8	10-((2-Benzoyl-phenylcarbamoyl)methyl)- 1,4,7,10-tetraazacyclododecane-1,4,7-tris(acetic acid tert-butyl ester)...	207
6.3.9	Europium(III) 10-((2-Benzoyl-phenylcarbamoyl)methyl)-1,4,7,10- tetraazacyclododecane-1,4,7-trisacetate [Eu- 127].....	208
6.3.10	Europium(III) 10-(2-hydroxy-4-phenylquinolin-3-yl)- 1,4,7,10-tetraazacyclododecane-1,4,7-trisacetate [Eu- 132]	210
6.3.11	Yttrium(III) 10-(2-hydroxy-4-phenylquinolin-3-yl)- 1,4,7,10-tetraazacyclododecane-1,4,7-trisacetate [Y- 132].....	211
6.3.12	Europium(III) 10-(2-hydroxy-4-methylquinolin-3-yl)- 1,4,7,10-tetraazacyclododecane-1,4,7-trisacetate [Eu- 133]	212
7	REFERENCES.....	215
A	APPENDIX A – CRYSTAL STRUCTURES	A1
B	APPENDIX B – TD-DFT CALCULATIONS	A32

TABLE OF TABLES

Table 1. Physical properties of elemental iridium.	14
Table 2. Selected bond distances for <i>fac</i> - and <i>mer</i> -Ir(tpy) ₃ (tpyH = 2-(<i>p</i> -tolyl)pyridine).	19
Table 3. Photophysical and electrochemical data for <i>fac</i> -Ir(ppy) ₃ derivatives.	24
Table 4. Photophysical data and decay rates for <i>fac</i> -/ <i>mer</i> -Ir(ppy) ₃ derivatives.	25
Table 5. Characteristics of OLEDs incorporating Ir(C [^] N)(acac) dopants.	31
Table 6. Characteristics of devices fabricated from polymer-bound Ir complexes.	33
Table 7. Attempted conditions for the synthesis of 5-(2,2':6',2''-terpyridin-4'- yl)isophthalic acid diethyl ester by Suzuki cross-coupling.	60
Table 8. Attempted conditions for the synthesis of 1,5-di(pyrid-2-yl)-2,4- dimethylbenzene by Negishi cross-coupling.	62
Table 9. Selected bond lengths and angles for Ir(dpydmb)(DMSO)Cl ₂	74
Table 10. Selected bond lengths and angles for [Ir(dpydmb)(tppy)] ²⁺	75
Table 11. Absorbance data for Ir(N [^] C [^] N)(C [^] N [^] C) complexes in acetonitrile solution at 295 K.	89
Table 12. Luminescence data for Ir(dpydmb)(dppy) 108 , Ir(dpydmb)(F ₄ dppy) 110 and <i>fac</i> -Ir(ppy) ₃ 26 in acetonitrile solution. Data for the <i>fac</i> - and <i>mer</i> -isomers of Ir(ppy) ₃ and Ir(46dfppy) ₃ in dichloromethane solution are included for comparison.	91
Table 13. Radiative, non-radiative and bimolecular oxygen quenching decay rate constants for Ir(dpydmb)(dppy) 108 and Ir(dpydmb)(F ₄ dppy) 110 in acetonitrile solution at 295 K. Data for the <i>fac</i> - and <i>mer</i> -isomers of Ir(ppy) ₃ and Ir(46dfppy) ₃ are included for comparison.	92
Table 14. Absorbance data for Ir(dpydmb)(ppy)Cl 115 in acetonitrile solution at 295 K.	94
Table 15. Luminescence data for Ir(dpydmb)(ppy)Cl 115 in acetonitrile solution.	95
Table 16. Absorbance data for Ir(N [^] C [^] N)(C [^] N [^] O) complexes in acetonitrile solution at 295 K.	96

Table 17. Luminescence data for Ir(dpydmb)(tppic) 116 and Ir(dpydmb)(hbqc) 117 in acetonitrile solution.....	98
Table 18. Radiative, non-radiative and bimolecular oxygen quenching decay rate constants for Ir(dpydmb)(tppic) 116 and Ir(dpydmb)(hbqc) 117 in acetonitrile solution at 295 K.	98
Table 19. Absorbance data for Ir(N [^] N [^] N)(C [^] N [^] C) ⁺ complexes in acetonitrile solution at 295 K.	99
Table 20. Luminescence data for [Ir(tpybae)(dppy)] ⁺ 124 in acetonitrile solution. Complex 34 is included for comparison.	100
Table 21. Radiative, non-radiative and bimolecular oxygen quenching decay rate constants for [Ir(tpybae)(dppy)] ⁺ 124 and 34 in acetonitrile solution at 295 K....	101
Table 22. Absorbance data for Ir(N [^] C [^] N)(N [^] N [^] N) ²⁺ complexes in acetonitrile solution at 295 K.	102
Table 23. Calculated metal–ligand bond lengths for Ir(N [^] C [^] N)(C [^] N [^] C) complexes.....	105
Table 24. Calculated metal–ligand bond lengths for Ir(N [^] C [^] N)(C [^] N [^] O) complexes.....	106
Table 25. Calculated metal–ligand bond lengths for two coordination modes of Ir(dpydmb)(dinpy).	106
Table 26. Calculated metal–ligand bond lengths for [Ir(dpydmb)(terpy)] ²⁺ 105 and [Ir(terpy) ₂] ³⁺ 21 . Also shown for comparison are the respective bond lengths from the X-ray crystal structure of [Ir(dpydmb)(tppy)] ²⁺ 106	107
Table 27. The three highest occupied and three lowest virtual (unoccupied) molecular orbitals of <i>fac</i> -Ir(ppy) ₃ 26 , Ir(dpydmb)(dppy) 108 , Ir(dpydmb)(F ₄ dppy) 110 and Ir(dpydmb)(cdppy) 111	108
Table 28. The three highest occupied and three lowest virtual (unoccupied) molecular orbitals of Ir(dpydmb)(tppic) 116 and Ir(dpydmb)(hbqc) 117	111
Table 29. The three highest occupied and three lowest virtual (unoccupied) molecular orbitals for two binding modes of Ir(dpydmb)(dinpy).....	113
Table 30. The three highest occupied and three lowest virtual (unoccupied) molecular orbitals of [Ir(dpydmb)(terpy)] ²⁺ 105 and [Ir(terpy) ₂] ³⁺ 125	115

Table 31. Calculated ionisation potentials and cationic spin densities for Ir(N [^] C [^] N)(C [^] N [^] C) and Ir(N [^] C [^] N)(C [^] N [^] O) complexes.	117
Table 32. Calculated electron affinities and anionic spin densities for Ir(N [^] C [^] N)(C [^] N [^] C) and Ir(N [^] C [^] N)(C [^] N [^] O) complexes.	117
Table 33. Calculated excitation wavelengths (λ), oscillator strengths (f) and dominant orbital excitations for the ground-state structure of <i>fac</i> -Ir(ppy) ₃ 26 . Orbitals are labelled as in Table 27.....	119
Table 34. Calculated excitation wavelengths (λ), oscillator strengths (f) and dominant orbital excitations for the ground-state structures of Ir(N [^] C [^] N)(C [^] N [^] C) complexes. Orbitals are labelled as in Table 27. Full results are tabulated in Appendix B.	120
Table 35. Luminescence data in acetonitrile solution at 295 K for complexes prepared in this study.	124
Table 36. Absorbance data for europium(III) complexes.	140
Table 37. Photophysical parameters of the europium(III) complexes of 127 and 128 . Included for comparison is Eu· 129	142
Table 38. Calculated values of k^0 , $\sum k_{nr}$ and η_{et} for solutions of the europium(III) complexes of 127 , 128 and 129 in H ₂ O using experimentally determined [$I(0,1)/I_{tot}$], τ_{obs} and Φ_{em} values.	143
Table 39. Photophysical parameters of the europium(III) complexes of 132 and 133	145
Table 40. Calculated values of k^0 , $\sum k_{nr}$ and $\Phi_D\eta_{et}$ for solutions of the europium(III) complexes of 132 and 133 in H ₂ O using experimentally determined [$I(0,1)/I_{tot}$], τ_{obs} and Φ_{em} values.	145

TABLE OF FIGURES

Figure 1. Schematic representation of fluorescence in organic materials.....	2
Figure 2. Schematic representation of electroluminescence in organic materials.	3
Figure 3. Experimentally determined singlet/triplet formation cross-section ratios for some polymeric and oligomeric materials (reproduced from reference 25).	5
Figure 4. Schematic diagram of an organic electroluminescent device.....	7
Figure 5. Effect of doping concentration on a DCM1-doped Alq ₃ device (reproduced from reference 87).	12
Figure 6. Crystal structure of [Ir(Me-ppy) ₂ (μ-Cl)] ₂	17
Figure 7. Room-temperature photoluminescence spectra of air-equilibrated acetonitrile solutions of [Ir(terpy) ₂] ²⁺ (solid line) and [Ir(4'-p-tolyl-terpy) ₂] ²⁺ (dashed line) (adapted from reference 103).	23
Figure 8. Structures of ligands referred to in Table 5.	31
Figure 9. Phosphorescent sensitizers to improve efficiency.	34
Figure 10. Variation in radii of the Ln ²⁺ (▼), Ln ³⁺ (○) and Ln ⁴⁺ (●) ions across the lanthanide series (La ³⁺ is included for completeness).....	35
Figure 11. Typical Eu ³⁺ luminescence spectrum. Also shown are the transitions responsible for the labelled bands.	36
Figure 12. Sensitised emission of lanthanide(III) complexes.	37
Figure 13. Kinetic scheme of sensitised emission from lanthanide complexes (adapted from reference 201).	38
Figure 14. Crystal structure of Na[Eu(DOTA)(H ₂ O)]·4H ₂ O. Cation and water of crystallisation omitted for clarity.	40
Figure 15. Electroluminescence spectrum of a ITO/TPD/Tb(acac) ₃ /Al device (adapted from reference).	43
Figure 16. Two potential binding modes of the 1,3-di(pyridin-2-yl)benzene ligand.....	71
Figure 17. Structure of Ir(dpydmb)(DMSO)Cl ₂ crystallised from DMSO; 120 K, thermal ellipsoids shown at 30% probability.	73

Figure 18. Structure of the $[\text{Ir}(\text{dpydmb})(\text{tppy})]^{2+}$ cation crystallised as the PF_6^- salt from acetone; 120 K, thermal ellipsoids shown at 50% probability.....	75
Figure 19. Ground-state absorbance spectra of $\text{Ir}(\text{dpydmb})(\text{dppy})$ 108 (solid line), $\text{Ir}(\text{dpydmb})(\text{F}_4\text{dppy})$ 110 (dashed line) and <i>fac</i> - $\text{Ir}(\text{ppy})_3$ 26 (dotted line) in acetonitrile solution at 295 K. Also shown is the luminescence excitation spectrum of $\text{Ir}(\text{dpydmb})(\text{dppy})$ 108 (dash-dotted line, displaced for clarity, $\lambda_{\text{em}} = 600$ nm).....	88
Figure 20. Emission spectra of $\text{Ir}(\text{dpydmb})(\text{dppy})$ 108 (solid line, $\lambda_{\text{ex}} = 481$ nm), $\text{Ir}(\text{dpydmb})(\text{F}_4\text{dppy})$ 110 (dashed line, $\lambda_{\text{ex}} = 447$ nm) and <i>fac</i> - $\text{Ir}(\text{ppy})_3$ 26 (dotted line, $\lambda_{\text{ex}} = 400$ nm) in acetonitrile solution at 295 K. Excitation and emission bandpasses were 2.5 nm.....	90
Figure 21. Emission spectra of $\text{Ir}(\text{dpydmb})(\text{dppy})$ 108 in dichloromethane (solid line, $\lambda_{\text{ex}} = 484$ nm), acetonitrile (long dashed line, $\lambda_{\text{ex}} = 481$ nm), THF (dotted line, $\lambda_{\text{ex}} = 484$ nm) and toluene (short dashed line, $\lambda_{\text{ex}} = 485$ nm) following intense irradiation for five minutes. All spectra are normalised to a peak intensity of 1.0 prior to irradiation.	93
Figure 22. Ground-state absorbance spectra of $\text{Ir}(\text{dpydmb})(\text{ppy})\text{Cl}$ 115 (solid line) and $\text{Ir}(\text{dpydmb})(\text{dppy})$ 108 (dashed line) in acetonitrile solution at 295 K. Also shown is the low energy portion of the luminescence excitation spectrum of $\text{Ir}(\text{dpydmb})(\text{ppy})\text{Cl}$ 115 (dash-dotted line, displaced for clarity, $\lambda_{\text{em}} = 507$ nm)....	94
Figure 23. Emission spectrum of $\text{Ir}(\text{dpydmb})(\text{ppy})\text{Cl}$ 115 (solid line, $\lambda_{\text{ex}} = 456$ nm) in acetonitrile solution at 295 K. Excitation and emission bandpasses were 2.5 nm. The emission spectrum of $\text{Ir}(\text{dpydmb})(\text{dppy})$ 108 (dashed line) is included for comparison.....	95
Figure 24. Ground-state absorbance spectra of $\text{Ir}(\text{dpydmb})(\text{tppic})$ 116 and $\text{Ir}(\text{dpydmb})(\text{hbqc})$ 117 in acetonitrile solution at 295 K.	96
Figure 25. Emission spectra of $\text{Ir}(\text{dpydmb})(\text{tppic})$ 116 (solid line, $\lambda_{\text{ex}} = 489$ nm) and $\text{Ir}(\text{dpydmb})(\text{hbqc})$ 117 (dashed line, $\lambda_{\text{ex}} = 459$ nm) in acetonitrile solution at 295 K. Excitation and emission bandpasses were 2.5 nm and 4.0 nm for each complex respectively.....	97

Figure 26. Ground-state absorbance spectrum (solid line) and luminescence excitation spectrum (dash-dotted line, displaced for clarity, $\lambda_{em} = 710$ nm) of $[\text{Ir}(\text{tpybae})(\text{dppy})]^+$ 124 in acetonitrile solution at 295 K.	99
Figure 27. Emission spectrum of $[\text{Ir}(\text{tpybae})(\text{dppy})]^+$ 124 ($\lambda_{ex} = 343$ nm) in acetonitrile solution at 295 K. Excitation and emission bandpasses were 4.0 nm.....	100
Figure 28. Ground-state absorbance spectra of $[\text{Ir}(\text{dpydmb})(\text{terpy})]^{2+}$ 105 (solid line) and $[\text{Ir}(\text{dpydmb})(\text{tppy})]^{2+}$ 106 (dashed line) in acetonitrile solution at 295 K. Also included is the low energy portion of the luminescence excitation spectrum of $[\text{Ir}(\text{dpydmb})(\text{terpy})]^{2+}$ 105 in an ethanol/methanol (4:1 by volume) glass at 77 K (dotted line, offset for clarity, $\lambda_{em} = 501$ nm).	101
Figure 29. Emission spectrum of $[\text{Ir}(\text{dpydmb})(\text{terpy})]^{2+}$ 105 ($\lambda_{ex} = 370$ nm) in an ethanol/methanol (4:1 by volume) glass at 77 K. Excitation and emission bandpasses were 10.0 nm and 5.0 nm respectively.....	102
Figure 30. Optimised ground-state geometry of <i>fac</i> - $\text{Ir}(\text{ppy})_3$ 26	104
Figure 31. Schematic diagram of calculated molecular orbital energies for <i>fac</i> - $\text{Ir}(\text{ppy})_3$ 26 , $\text{Ir}(\text{dpydmb})(\text{dppy})$ 108 , $\text{Ir}(\text{dpydmb})(\text{F}_4\text{dppy})$ 110 and $\text{Ir}(\text{dpydmb})(\text{cdppy})$ 111	107
Figure 32. Contour plots of the HOMO and LUMO of <i>fac</i> - $\text{Ir}(\text{ppy})_3$ 26	109
Figure 33. Contour plots of the HOMO and LUMO of $\text{Ir}(\text{dpydmb})(\text{dppy})$ 108	109
Figure 34. Contour plots of the HOMO and LUMO of $\text{Ir}(\text{dpydmb})(\text{tppic})$ 116	112
Figure 35. Contour plots of the HOMO and LUMO of $\text{Ir}(\text{dpydmb})(\text{hbqc})$ 117	112
Figure 36. Contour plots of the HOMO and LUMO of $\text{Ir}(\text{dpydmb})(\text{dinpy})$ with N [^] N [^] N binding of the dinpy ligand (complex 123).	114
Figure 37. Contour plots of the HOMO and LUMO of $\text{Ir}(\text{dpydmb})(\text{dinpy})$ with C [^] N [^] C binding of the dinpy ligand (complex 122).	114
Figure 38. Contour plots of the HOMO and LUMO of $[\text{Ir}(\text{dpydmb})(\text{terpy})]^{2+}$ 105	116
Figure 39. Contour plots of the HOMO and LUMO of $[\text{Ir}(\text{terpy})_2]^{3+}$ 21	116
Figure 40. Comparison of the experimental absorbance spectrum of <i>fac</i> - $\text{Ir}(\text{ppy})_3$ 26 in acetonitrile solution (solid line, left axis) to singlet (●, right axis) and triplet (▲, arbitrary height) transitions from TD-DFT calculations.....	119

Figure 41. Comparison of the experimental absorbance spectrum of Ir(dpydmb)(dppy) 108 in acetonitrile solution (solid line, left axis) to singlet (●, right axis) and triplet (▲, arbitrary height) transitions from TD-DFT calculations.....	121
Figure 42. Comparison of the experimental absorbance spectrum of Ir(dpydmb)(F ₄ dppy) 110 in acetonitrile solution (solid line, left axis) to singlet (●, right axis) and triplet (▲, arbitrary height) transitions from TD-DFT calculations.....	121
Figure 43. Comparison of the experimental absorbance spectrum of Ir(dpydmb)(tppic) 116 in acetonitrile solution (solid line, left axis) to singlet (●, right axis) and triplet (▲, arbitrary height) transitions from TD-DFT calculations.....	122
Figure 44. Calculated singlet (●, right axis) and triplet (▲, arbitrary height) transitions from TD-DFT calculations for N [^] N [^] N ⁻ (solid shapes) and C [^] N [^] C ⁻ (hollow shapes) binding modes of the dinpy ligand in Ir(dpydmb)(dinpy).....	123
Figure 45. Comparison of the experimental absorbance spectrum of [Ir(dpydmb)(terpy)] ²⁺ 105 in acetonitrile solution (solid line, left axis) to singlet (●, right axis) and triplet (▲, arbitrary height) transitions from TD-DFT calculations.	123
Figure 46. Commission Internationale de L'Eclairage (CIE) colour chart illustrating the observed emission colour of complexes prepared in this study....	125
Figure 47. Pictorial representation of the effect of cyclometalation upon the energy levels and nature of emissive states in a generic series of unsymmetrical bis-terdentate iridium(III) complexes.	127
Figure 48. Pictorial representation of the twisting of acetate groups in the SAP and TSAP geometries of lanthanide(III) DOTA complexes.	136
Figure 49. Effect of ring puckering on the geometries of europium(III)-coordinated cyclen derivatives. Dashed lines represent additional ¹ H- ¹ H COSY cross-peaks.....	137
Figure 50. Ground-state absorbance spectra of Eu· 127 (solid line) and Eu· 128 (dashed line) in aqueous solution at 295 K.	139

Figure 51. Ground-state absorbance spectra of Eu· 132 (solid line) and Eu· 133 (dashed line) in aqueous solution at 295 K. Included for comparison is the published absorbance data for 3-aminoquinolin-2-ol in ethanol (●). ⁴⁴⁰	140
Figure 52. Emission spectra of Eu· 127 (solid line, $\lambda_{\text{ex}} = 259$ nm), Eu· 128 (dashed line, $\lambda_{\text{ex}} = 249$ nm) and Eu· 129 ⁴²⁴ (dotted line, $\lambda_{\text{ex}} = 280$ nm) in aqueous solution at 295 K. Excitation and emission bandpasses were 2.5 nm.....	141
Figure 53. Ground-state absorbance spectrum (solid line) and luminescence excitation spectrum (dashed line, $\lambda_{\text{em}} = 700$ nm) for Eu·128.....	141
Figure 54. Emission spectra of Eu· 132 (solid line, $\lambda_{\text{ex}} = 343$ nm) and Eu· 133 (dashed line, $\lambda_{\text{ex}} = 340$ nm) in aqueous solution at 295 K. Excitation and emission bandpasses were 2.5 nm.....	144
Figure 55. Ground-state absorbance spectrum (solid line) and luminescence excitation spectrum (dashed line, $\lambda_{\text{em}} = 700$ nm) for Eu· 132	144

TABLE OF SCHEMES

Scheme 1. Interconversion pathways for lanthanide DOTA complexes in solution.	40
Scheme 2. The Hantzsch pyridine synthesis.	49
Scheme 3. The Kröhnke pyridine synthesis (X = C or N).	50
Scheme 4. Synthesis of 2,2':6',2''-terpyridine <i>via</i> an enaminone.	51
Scheme 5. Use of a cyclotrimerisation reaction to form pendent pyridyl rings.	51
Scheme 6. The synthesis of 5,5''-dimethyl-2,2':6',2''-terpyridine by a Stille coupling.	52
Scheme 7. Synthesis of 4'-aryl-2,2':6',2''-terpyridines by Suzuki cross-couplings.	53
Scheme 8. Novel synthesis of a 4'-tributylstannyl-2,2':6',2''-terpyridine.	53
Scheme 9. First general synthesis of DO3A.	54
Scheme 10. Mono- <i>N</i> -alkylation of cyclen <i>via</i> phosphoryl-protection.	55
Scheme 11. Generic approaches to charge-neutralisation.	58
Scheme 12. Retrosynthetic analysis of 5-(2,2':6',2''-terpyridin-4'-yl)isophthalic acid diethyl ester (tpyiade).	60
Scheme 13. Synthesis of 5-(2,2':6',2''-terpyridin-4'-yl)isophthalic acid diethyl ester <i>via</i> a Suzuki cross-coupling reaction.	60
Scheme 14. Synthesis of 1,3-di(pyrid-2-yl)benzene and a dimethyl derivative <i>via</i> a Stille cross-coupling reaction.	61
Scheme 15. Attempted synthesis of 1,5-di(pyrid-2-yl)-2,4-dimethylbenzene <i>via</i> a Negishi cross-coupling reaction.	62
Scheme 16. Synthesis of 1,5-di(pyrid-2-yl)-2,4-dimethylbenzene derivatives by Kröhnke type ring-closing of the outer pyridyl rings.	63
Scheme 17. Potential synthesis of 4,6-diacetyl- <i>m</i> -xylene <i>via</i> dilithiation.	64
Scheme 18. Synthesis of dipyridylbenzene derivatives by “C”-insertion.	64
Scheme 19. Formation of a central benzene ring by insertion of nitromethane.	65
Scheme 20. Synthesis of acetic acid 2,5-dinitrophenyl ester by cyclisation of nitromethane and glyoxal.	65

Scheme 21. Synthesis of 2,4,5-triphenylnitrobenzene <i>via</i> the pyranylum salt.	65
Scheme 22. Synthesis of 4- <i>p</i> -tolyl-6-phenylpicolinic acid by ring-closing.	67
Scheme 23. Synthesis of a diphenylpyridine derivative <i>via</i> a Mannich base.	68
Scheme 24. Preparation of 2,6-di(2'-indolyl)pyridine by the Fischer indole synthesis.	69
Scheme 25. Decomposition of Ir(dpydmb)(dppy) to [Ir(dpydmb)(dppyH)L] ⁺	79
Scheme 26. Displacement of a platinum(II) bound chloride by methanol.	79
Scheme 27. Thermally and photochemically activated isomerisation of <i>mer</i> -Ir(ppy) ₃ 27 to <i>fac</i> -Ir(ppy) ₃ 26	80
Scheme 28. Synthesis of [Ir(tpybae)(dppy)] ⁺ 124 by a two-step route.	87
Scheme 29. Synthesis of aminobenzophenone-derivatised DO3A ligands.	132
Scheme 30. Suggested mechanism for the formation of a rearranged <i>ortho</i> - aminobenzophenone derivatised DO3A complex in a basic solution of a Eu ³⁺ salt.	135
Scheme 31. Rearrangement and complexation of a 2-aminoacetophenone derivatised DO3A ligand.	136
Scheme 32. Synthesis of an <i>N</i> -arylated cyclen derivative from an <i>N</i> -aryl precursor. ..	138

Declaration

The work described in this thesis was carried out in the Department of Chemistry at the University of Durham between October 2001 and September 2004. This thesis is the work of the author, except where acknowledged, and has not been submitted for any other degree.

Statement of Copyright

The copyright of this thesis rests with the author. No quotation from it should be published in any form, including electronic, without the author's prior written consent. All information derived from this thesis must be acknowledged appropriately.

ABBREVIATIONS

Terms

Å	Angstrom (10^{-10} m)
CFSE	Crystal field stabilisation energy
CIE	Commission Internationale de L'Eclairage
C [^] N [^] C	Ligands that bind through two peripheral cyclometalating rings and a central pyridine ring
COSY	Correlation spectroscopy
CRT	Cathode-ray tube
CT	Charge transfer
CV	Cyclic voltammetry
DEPT	Distortionless enhancement by polarization transfer
DFT	Density functional theory
EA	Electron affinity
EL	Electroluminescence
<i>fac</i>	Facial
FWHM	Full width at half maximum
GC	Gas chromatography
HF	Hartree-Fock
HOMO	Highest occupied molecular orbital
HRMS	High-resolution mass spectrometry
HSQC	Heteronuclear single quantum correlation
IP	Ionisation potential
IR	Infrared
ISC	Intersystem crossing
LC	Ligand centred
LCD	Liquid crystal display
LED	Light-emitting diode
LLCT	Ligand-to-ligand charge transfer
LUMO	Lowest unoccupied molecular orbital
<i>mer</i>	Meridional
MLCT	Metal-to-ligand charge transfer
MO	Molecular orbital

MS	Mass spectrometry
MS(EI)	Mass spectrometry – Electron impact
MS(ES ⁻)	Mass spectrometry – Negative bias electrospray ionisation
MS(ES ⁺)	Mass spectrometry – Positive bias electrospray ionisation
MS(MALDI)	Mass spectrometry – Matrix assisted laser desorption ionisation
N ^{^C^N}	Ligands that bind through two peripheral pyridine rings and a central cyclometalating phenylene ring
NMR	Nuclear magnetic resonance
N ^{^N^N}	Ligands that bind through three pyridine rings
NOESY	Nuclear Overhauser effect spectroscopy
OELD	Organic electroluminescent device
OLED	Organic light-emitting device/diode
PL	Photoluminescence
PLED	Polymeric light-emitting device/diode
SAP	Square-antiprismatic
SBLCT	Sigma-bond-to-ligand charge transfer
SCF	Self-consistent field
TD-DFT	Time dependent density functional theory
TLC	Thin-layer chromatography
TSAP	Twisted square-antiprismatic
UV	Ultraviolet

Compounds

acacH	Acetylacetone (2,4-Pentanedione)
Alq ₃	Aluminium tris(8-hydroxyquinoline)
bath	Bathophenanthroline (4,7-Diphenyl-1,10-phenanthroline)
bpy	2,2'-Bipyridine
bzqH	Benzo[<i>h</i>]quinoline
CBP	4,4'- <i>N,N'</i> -dicarbazolebiphenyl
cdppyH ₂	2,6-Di(3-cyanophenyl)pyridine
cyclam	1,4,8,11-Tetraazacyclotetradecane
cyclen	1,4,7,10-Tetraazacyclododecane
dinpyH ₂	2,6-Di(2'-indolyl)pyridine
DMF	<i>N,N</i> -Dimethylformamide

DMSO	Dimethyl sulfoxide
DO3A	1,4,7,10-Tetraazacyclododecane-1,4,7-tri(acetic acid)
DOTA	1,4,7,10-Tetraazacyclododecane-1,4,7,10-tetra(acetic acid)
dppyH ₂	2,6-Diphenylpyridine
dpybH	1,3-Di(pyridin-2-yl)benzene
dpydmbH	1,5-Di(pyridin-2-yl)-2,4-dimethylbenzene
dthpyH ₂	2,6-Di(2-thienyl)pyridine
F ₄ dppyH ₂	2,6-Di(2,4-difluorophenyl)pyridine
hbqcH ₂	4-Hydroxybenzo[<i>h</i>]quinoline-2-carboxylic acid
ITO	Indium tin oxide
phen	1,10-Phenanthroline
PPP	Poly(<i>p</i> -phenylene)
PPV	Poly(<i>p</i> -phenylene vinylene)
ppyH	2-Phenylpyridine
PtOEP	2,3,7,8,12,13,17,18-Octaethyl-21 <i>H</i> ,23 <i>H</i> -porphine platinum(II)
PVK	Poly(vinylcarbazole)
py	Pyridine
pydcH ₂	Pyridine-2,6-dicarboxylic acid
tcdppyH ₂	4- <i>p</i> -Tolyl-2,6-di(3-cyanophenyl)pyridine
tdppyH ₂	4- <i>p</i> -Tolyl-2,6-diphenylpyridine
terpy	2,2':6',2''-Terpyridine
THF	Tetrahydrofuran
tppicH ₂	4- <i>p</i> -Tolyl-6-phenylpicolinic acid
tpyba	4-(2,2':6',2''-Terpyridin-4'-yl)benzoic acid
tpybae	4-(2,2':6',2''-Terpyridin-4'-yl)benzoic acid ethyl ester
tpybH ₃	1,3,5-Tri(pyridin-2-yl)benzene
tpyia	5-(2,2':6',2''-Terpyridin-4'-yl)isophthalic acid
tpyiade	5-(2,2':6',2''-Terpyridin-4'-yl)isophthalic acid diethyl ester
TTFA	Thenoyltrifluoroacetate
tppy	4'-(<i>p</i> -Tolyl)-2,2':6',2''-terpyridine
YAG	Yttrium aluminium garnet

CHAPTER 1

INTRODUCTION

1 Introduction

1.1 Organic electroluminescent devices

Until recently, the most common display technology for computers and television screens was the cathode-ray tube (CRT). Yet for mobile devices such as laptop computers and cellular phones, the size, weight and poor durability of CRTs have prevented their usage. It is in these applications that liquid crystal displays (LCDs) have traditionally been employed. Even these are not without their disadvantages; hence a new technology promising energy efficient emissive flat panel displays is highly attractive.

Organic light-emitting devices (OLEDs), also referred to as organic light-emitting diodes or organic electroluminescent devices (OELDs), have received much attention since their conception in the late 1980s, and a number of review articles chart their progress.¹⁻⁵ Electroluminescence (EL) is an electrically activated emission of light, first observed from silicon carbide (SiC) by Henry Round in 1907, and then from zinc sulfide (ZnS) by Georges Destriau in 1936.¹ Inorganic light-emitting diodes (LEDs) based on GaAsP⁶ were commercialised in the early 1960s by General Electric, and further improvements have resulted in luminous efficiencies in excess of 10 lm W^{-1} .¹

Electroluminescence of an organic material was first reported in 1963 with the observation that crystals of anthracene emit light upon the application of over 400 V.⁷ It was another 24 years before Tang and VanSlyke produced a reasonably efficient light-emitting diode incorporating organic fluorophores.⁸ This was the required catalyst to revive research in the area of organic electroluminescent devices. A further breakthrough was published by Friend *et al.* in 1990, reporting the fabrication of an OLED based upon the highly fluorescent conjugated polymer, poly(*p*-phenylene vinylene) (PPV).⁹

The advantages of OLEDs with respect to inorganic LEDs are many and varied. Since only low DC voltages are used, they require less power and may be illuminated uniformly over a large area. Polarised light may be produced,¹⁰ allowing simple integration with existing LCD technologies. Their production and subsequent fabrication into devices by spin-coating, vapour deposition, or other techniques is simpler and less costly than the methods required for inorganic materials. These deposition processes also allow the formation of very thin films and therefore flexible

displays,¹¹ as well as patterned deposition through standard lithographic techniques. Finally, unlike inorganic materials there is much scope for structural modification, facilitating tunability in emission colour and other electroluminescent properties. Inorganic materials however have their advantages, in particular their superior device lifetimes.

For organic LEDs to be fully accepted commercially, lifetimes of 50 000 hours at brightnesses of 250 cd m^{-2} are desirable. Although much research is still required to reach these levels, many companies have already invested in the technology.¹² The first commercially available high-resolution organic electroluminescent display was introduced by Pioneer in a car radio in 1997.¹³ Since then they have been used as efficient backlights for several LCD displays.¹⁴ Looking to the future, Epson have recently demonstrated a prototype 40" full-colour OLED display based on polymeric materials.¹⁵

1.1.1 Origins of electroluminescence in organic materials

To understand electroluminescence it is first advantageous to consider photoluminescence.¹⁶ Photoluminescence is defined as “light emitted by a cold excited body... [that] results from light absorption”,¹⁷ with the main processes summarised in Figure 1. It is initiated by the absorption of a photon of light of suitable wavelength to excite a molecule from the ground (S_0) state to an excited (S_n) state. This is generally followed by rapid relaxation to the lowest excited singlet (S_1) manifold in accordance with Kasha’s rule.¹⁸ Since electronic transitions occur much faster than changes in geometry (the Franck-Condon principle¹⁹), some degree of molecular reorganisation will take place to the lowest vibrational state. A number of processes may follow,

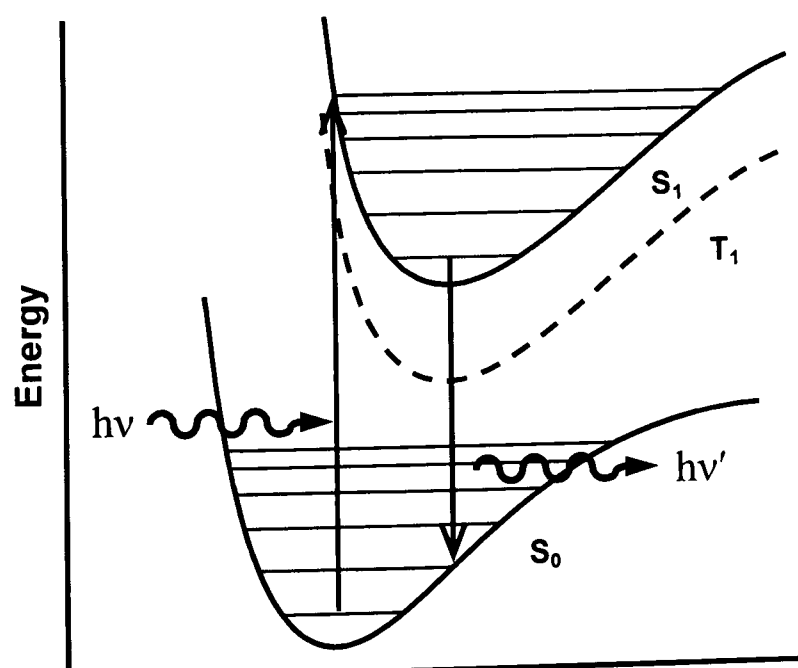


Figure 1. Schematic representation of fluorescence in organic materials.

including chemical reaction or quenching by other species. Most importantly, emission may occur back into a range of vibrationally excited levels of the ground (S_0) manifold, a process termed fluorescence. Alternatively, intersystem crossing (ISC) to a triplet (T_n) state and radiationless relaxation to the lowest excited triplet (T_1) state may occur, followed by phosphorescence. This is most common in the presence of heavy metal atoms, where spin-orbit coupling partially allows the formally forbidden $T_1 \rightarrow S_0$ transition. Due to radiationless losses of energy at each step, the frequency of the emitted photon will be lower than that of the excitation photon. The size of this so called Stokes' shift¹⁹ is dependent on the degree of geometric distortion between the ground and excited states.

Electroluminescence is defined as “a nonthermal generation of light resulting from the application of an electric field to a substrate”²⁰ (*i.e.* the excited state is formed by the application of an electric field rather than the absorption of a photon), summarised in Figure 2. In a simple electroluminescent device, an organic emissive layer is sandwiched between two electrodes. Upon application of an electric potential,

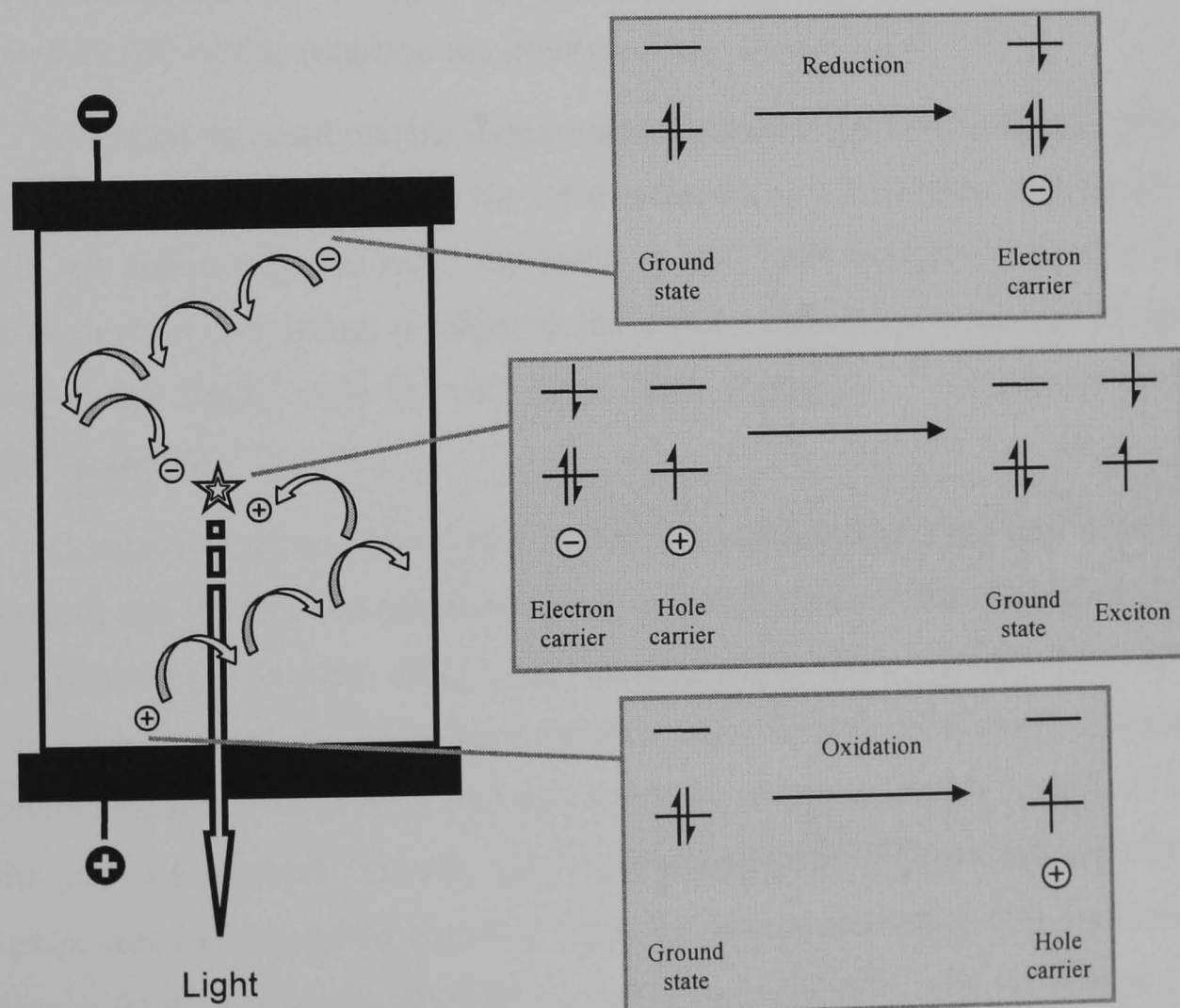


Figure 2. Schematic representation of electroluminescence in organic materials.

the organic layer at the cathode is reduced and at the anode oxidised to give electron and hole carriers respectively. These migrate under the applied field *via* a hopping mechanism until they either reach the opposite electrode, or meet a charge carrier of the opposite sign. When the latter occurs, the two carriers combine to produce one ground state molecule and an exciton. The nature of this exciton is comparable to the excited state produced by transfer of an electron from the HOMO to LUMO (*i.e.* the excited S_1 and T_1 states discussed for photoluminescence). Emission of a photon of light from this level then occurs as for photoluminescence. In fact, it is generally found that the profiles of electroluminescence spectra are identical to those from photoluminescence of the emissive material.

It should be noted that the combination of charge carriers in an electroluminescent device results in the formation of both singlet and triplet excitons. This is in contrast to photoluminescence, where in the absence of significant intersystem crossing only the excited singlet (S_1) state is populated. Since phosphorescence from triplet states is a spin-forbidden process, it is rarely observed in organic molecules at room temperature, and relaxation through non-radiative processes dominates. In an electroluminescent device this results in the generation of unwanted heat.

It is often assumed that the formation of excitons is purely statistical, with a 25% fraction of singlet excitons due to the 1:3 degeneracies of the singlet and triplet states. This is not necessarily the case, especially as the Pauli exclusion principle reduces electron-electron correlation, resulting in the triplet state being lowered in energy with respect to the singlet state by ~ 0.7 eV in both polymeric^{21,22} and small molecular weight²¹ materials.

Comparison of an aluminium tris(8-hydroxyquinoline) (Alq_3) host doped with a fluorescent dye (DCM2) to one doped with a phosphorescent dye (PtOEP) indicates a singlet fraction (χ_s) in Alq_3 of $22 \pm 3\%$, agreeing within error with the 25% statistical ratio.²³ Analysis of the photoluminescence and electroluminescence spectra of a platinum-containing conjugated polymer however, shows a singlet fraction of $57 \pm 4\%$ for the polymeric system, but only $22 \pm 1\%$ for the monomer.²⁴ Photoinduced absorption and photoinduced absorption detected magnetic resonance studies also concluded that the singlet fraction is greater than 25%, varying systematically with the optical gap in a range of conjugated polymers (see Figure 3).²⁵

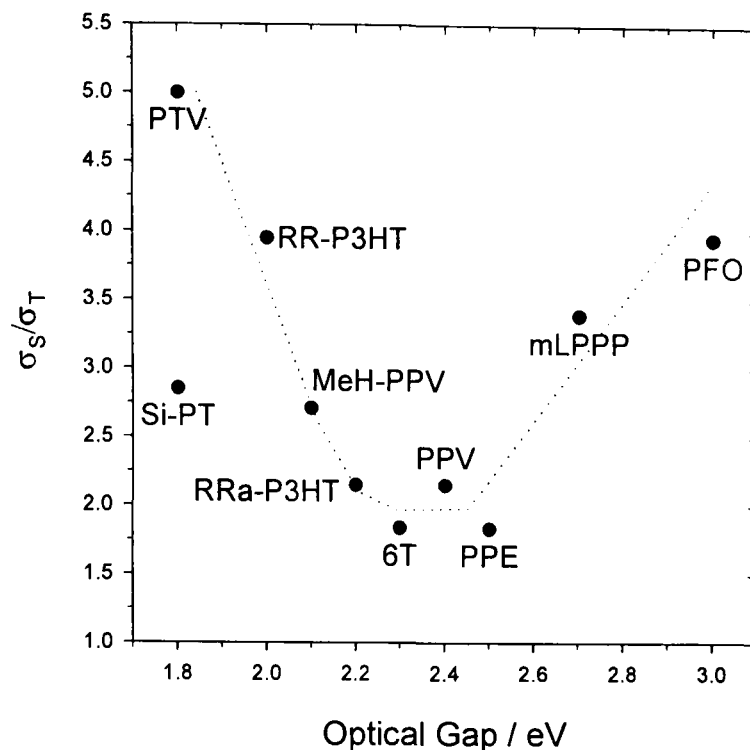


Figure 3. Experimentally determined singlet/triplet formation cross-section ratios for some polymeric and oligomeric materials (reproduced from reference 25).

These conclusions are also evident in theoretical studies of polymeric systems. Molecular orbital perturbation calculations on PPV oligomers²⁶ predict a singlet fraction of 29.7%, although this is raised to 50% by balancing electron and hole injection. By magnetic doping of polymers with transition-metal complexes, it has been predicted that intersystem crossing between the T_2 and S_2 states can be significant, leading to an effective singlet fraction of up to 90%.²⁷ Even if the formation of excitons is statistical, it has been suggested that for energy splittings less than 0.5 eV, thermal repopulation of the singlet state can lead to efficiencies approaching 100%.²⁸

In summary, evidence to date suggests that although singlet formation ratios are limited to 25% for low molecular weight materials, this value in polymers may be larger. Either way, the singlet formation ratio limits the efficiency of traditional electroluminescent devices. Much work has been directed into overcoming this constraint by the use of phosphorescent emitters (see Section 1.1.6).

1.1.2 Efficiency of organic electroluminescent devices

The fundamental quantity of electroluminescence is the internal EL quantum efficiency, η_{int} , which is defined as the ratio of the number of photons emitted to the number of electrons injected. This is the value most comparable to the PL quantum yield, Φ_{PL} , which is the ratio of the number of photons emitted to the number of photons absorbed.

Due to refraction, not all photons produced can escape the bounds of the device. A second quantity, the external EL quantum efficiency η_{ext} , relates the number of photons observed externally to the device to the number of electrons injected. This is related to η_{int} by equation 1,²⁹ where n is the refractive index of the organic material. For a typical polymer, $n = 1.4$, resulting in a four-fold reduction in efficiency.

$$\eta_{\text{int}} = 2n^2\eta_{\text{ext}} \quad (1)$$

Power efficiencies η_{pow} (W W^{-1}) are defined as the ratio of output light power to input electric power. This may be determined from the external EL quantum efficiency by equation 2, where E_p is the average energy of the emitted photons and V is the applied voltage across the device.

$$\eta_{\text{pow}} = \frac{\eta_{\text{ext}} E_p}{V} \quad (2)$$

While this quantity indicates the power of emitted light, the human eye's sensitivity varies as a function of wavelength, being more sensitive to green light than either red or blue. Another term, the luminous efficiency η_{lum} (lm W^{-1}), is determined by applying the eye sensitivity curve S as defined by the Commission Internationale de L'Eclairage (CIE) (equation 3).

$$\eta_{\text{lum}} = \eta_{\text{pow}} S(\lambda) \quad (3)$$

Finally, the brightness of an OLED is often quoted, and specifies the amount of light emitted by a device per unit area (cd m^{-2}). For reference, a typical laptop display reaches a brightness of about 100 cd m^{-2} .¹

1.1.3 Fabrication of organic electroluminescent devices

Organic electroluminescent devices are extremely thin layered configurations of sequentially deposited materials, typically less than 200 nm in total thickness (see Figure 4). These are layered upon a suitable substrate, usually glass, or for flexible displays a polymeric support. One of the electrodes must be semitransparent, with indium tin oxide (ITO) commonly used as the anode. The cathode requires electro-positive metals with low work functions, with Al, Ca, Mg, In, or alloys such as Mg:Ag often used. The organic substrate is sandwiched between the two electrodes, deposited by either vacuum deposition of volatile low molecular weight compounds, or by spin-coating and more recently ink-jet printing³⁰ for polymeric and oligomeric materials. The whole device is protected from the atmosphere to prevent oxidation of the reactive

metal cathode. This requirement is a major hurdle to the development of commercial displays.

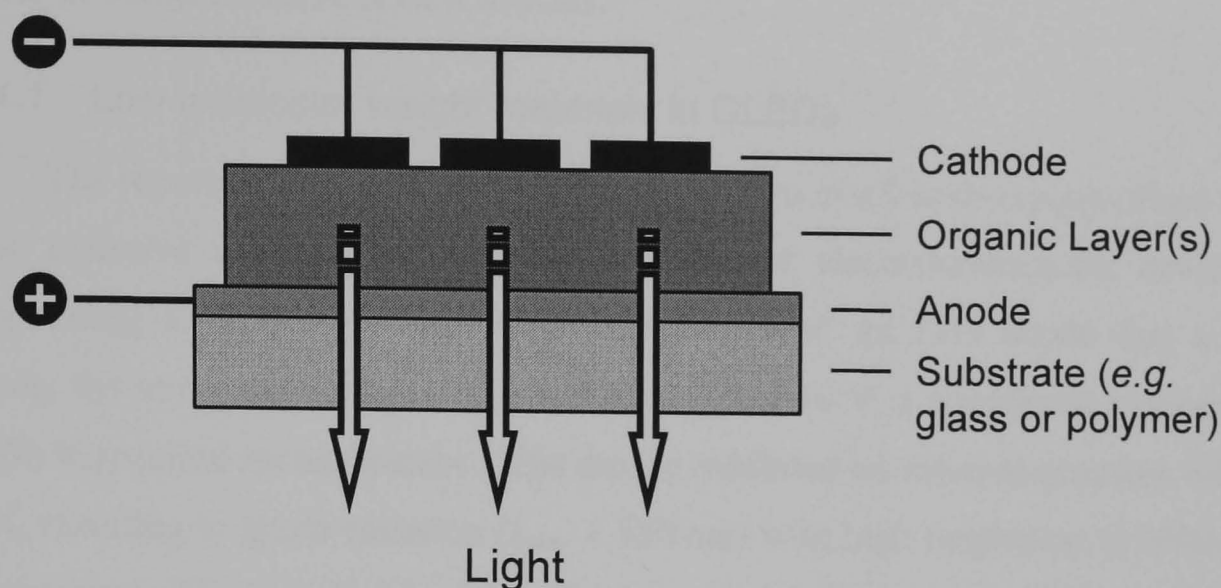


Figure 4. Schematic diagram of an organic electroluminescent device.

Since organic semiconductors are usually intrinsic *p*-type conductors, they are good hole transporters but poor at transporting electrons. Exciton formation therefore occurs a small distance from the cathode, with a detrimental effect on efficiencies and device lifetimes. In order to balance charge injection, multilayer devices have been developed that incorporate additional electron transport layers. The structure of a multilayer device is often written in the form Anode/Organic/Organic:Organic/Cathode, where a solidus (/) separates distinct layers, and a colon (:) denotes a mixture. By the use of suitable device structures, efficient low molecular weight OLEDs have been reported with lifetimes of over 50 000 hours,³¹ and polymeric devices with lifetimes in excess of 10 000 hours.^{32,33}

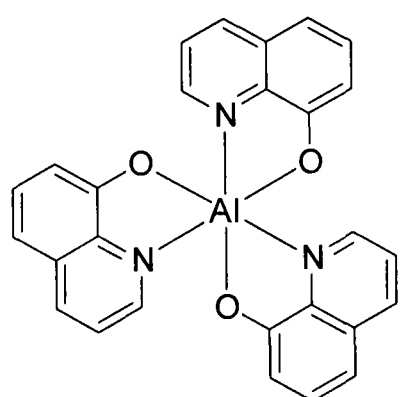
1.1.4 Organic materials for OLED applications

Requirements for organic materials as emitting layers in electroluminescent devices include the ability to undergo charge transfer with neighbouring layers, to transfer that charge through the device, and to efficiently emit light. Two general classes of compounds have been studied, low molecular weight materials and conjugated polymers (sometimes referred to as PLEDs). In an attempt to combine the advantages of each of these, oligomers, and polymers with isolated main-chain or side-chain chromophores have been investigated.

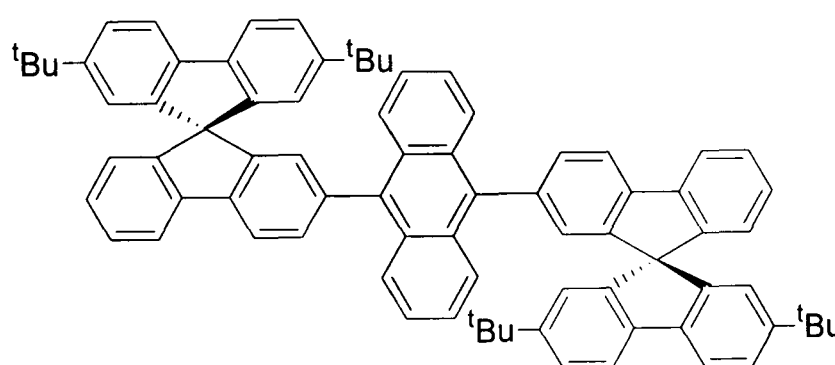
The following sections present an overview of progress in organic materials for electroluminescent devices. For a more thorough account, the reader is directed to a number of comprehensive review articles.¹⁻⁵

1.1.4.1 Low molecular weight materials in OLEDs

The report in 1987 of a device with aluminium tris(8-hydroxyquinoline) (Alq_3) **1** as the emissive material led the way for efficient electroluminescent devices.⁸ By incorporating a bis(triarylamine) hole transport layer, an ITO anode and a Mg:Ag cathode, the operating voltage was lowered to below 10 V, a significant reduction from the 400 V required for anthracene.⁷ The device exhibited an external quantum efficiency of 1%, resulting in green emission ($\lambda_{\text{max}} = 550 \text{ nm}$) with high brightness ($>1000 \text{ cd m}^{-2}$) and luminous efficiency (1.5 lm W^{-1}). To date, Alq_3 **1** is the most widely used electron-transport material due to its high thermal and morphological stability, ease of preparation and inability to form exciplexes. Thin films exhibit a photoluminescence efficiency of $32 \pm 2\%$ ³⁴ and a number of groups have prepared derivatives to further improve its efficiency, thermal stability and film-forming abilities.³⁵⁻³⁷



Alq_3 **1**

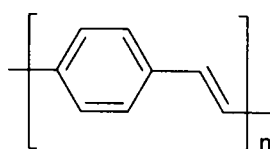


TBSA **2**

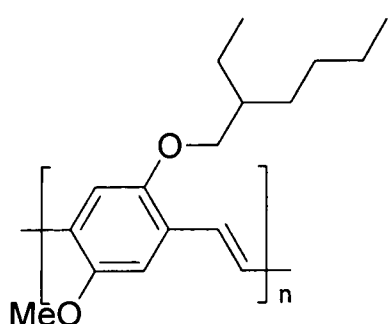
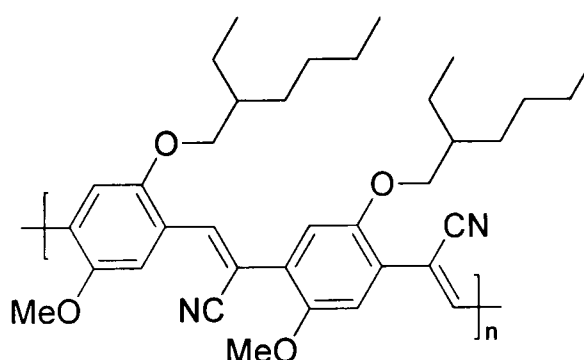
Purely organic emitters generally emit in the blue region,³⁸ a feat that has proven troublesome for inorganic LEDs. The bis(*spiro*bifluorenyl)anthracene **2** (TBSA) is reported to achieve a brightness of 300 cd m^{-2} with CIE coordinates (a measure of the observed colour) of $x = 0.14$; $y = 0.08$,³⁹ claimed to be the closest OLED to the NTSC standard blue. A number of groups have attempted to combine electron transport, hole transport and emitting groups in a single low molecular weight compound.^{40,41} An external quantum efficiency as high as 4% has been achieved, although device lifetimes were poor.⁴⁰

1.1.4.2 Polymeric materials in OLEDs

In 1990, Friend *et al.* demonstrated yellow-green electroluminescence from the conjugated polymer, poly(*p*-phenylene vinylene) (PPV) **3**.⁹ Although PPV itself is insoluble, a precursor may be spin-coated from methanol before thermally activated conversion to PPV. In addition to overcoming the practical difficulties of vapour-deposition techniques, increased stability is expected over sublimed organic films. Although not as high as some low molecular weight devices of the time, a reasonable external EL quantum efficiency of 0.05% was reported.

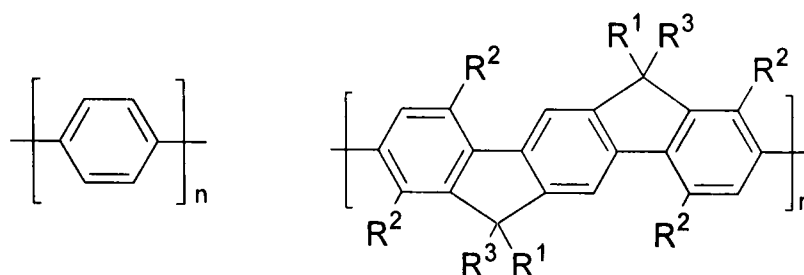
PPV **3**

By incorporating long alkoxy side chains, the polymers become soluble in a range of organic solvents, allowing direct spin-coating without a precursor polymer. The dialkoxy-substituted PPV derivative poly[2-methoxy-5-(2-ethylhexyloxy)-*p*-phenylenevinylene] (MEH-PPV) **4** reaches an external EL quantum efficiency of 1% even in a single-layer device.⁴² The addition of phenyl groups at both vinylene⁴³ and phenylene⁴⁴⁻⁴⁷ positions allow simultaneous improvements in the stability, efficiency and organic solubility, along with a blue-shift in emission. Calculations indicate that the introduction of cyano substituents improve electron injection,⁴⁸ with MEH-CN-PPV **5** shown experimentally to exhibit an external EL quantum efficiency of 2.5%.⁴⁹

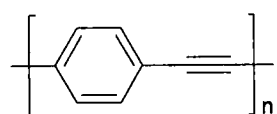
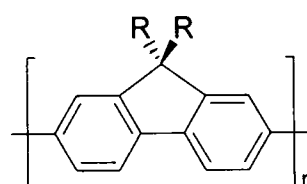
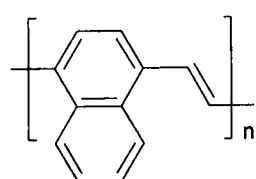
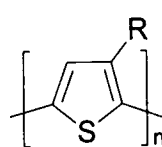
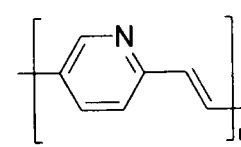
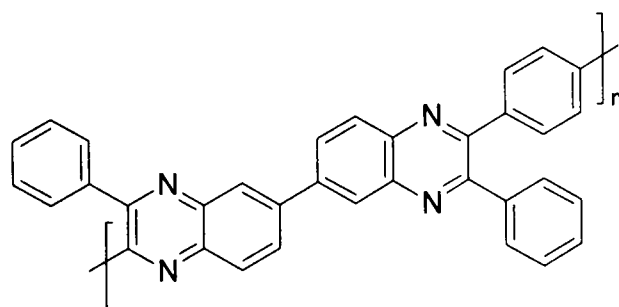
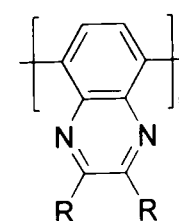
MEH-PPV **4**MEH-CN-PPV **5**

In 1992 Leising *et al.* reported one of the first examples of a blue emitting polymeric OLED by the use of poly(*p*-phenylene) (PPP) **6** ($\lambda_{\text{max}} = 470 \text{ nm}$).^{50,51} The external EL quantum efficiency was 0.05%, comparable to similar PPV based devices. Like PPV, PPP must be spin-coated as a precursor polymer, with alkoxy side-arms

improving solubility.⁵² Ladder-type PPP derivatives **7**⁵³ reduce the twisting between rings induced by side-groups, improving the fluorescence quantum yield.

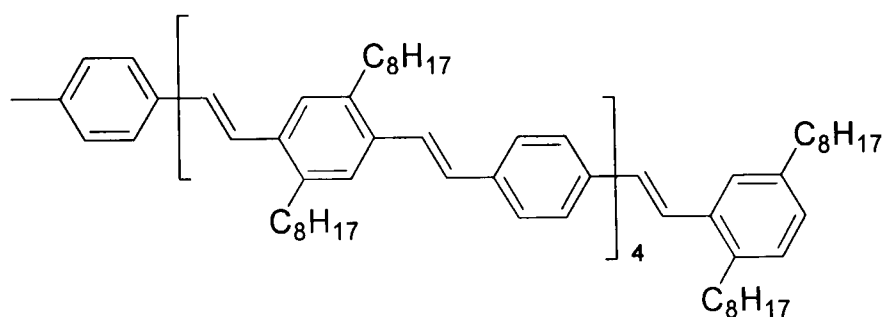
PPP **6**Ladder-type PPP **7**

Other polymeric structures that have been investigated for OLED applications include derivatives of poly(phenylene ethynylene) **8**,⁵⁴ polyfluorene **9**,^{55,56} and poly(naphthalene-vinylene) (PNV) **10**.⁵⁷ Heteroatom containing chains include poly(3-alkylthiophene) (PAT) **11**^{55,58-61} and poly(pyridinevinylene) (PPyV) **12**.^{62,63} Polyquinoxalines (PQxs) are of particular interest, since the low refractive indices of PPQ **13**⁶⁴ and 5,8-derivatives **14**,^{65,66} result in increased external EL efficiencies. Polysilanes exhibit delocalisation of σ -electrons in an analogous manner to the π -electrons of conventional semiconducting polymers, permitting the development of blue- and UV-emitting electroluminescent devices.⁶⁷⁻⁶⁹

Poly(phenylene ethynylene) **8**Polyfluorene **9**PNV **10**PAT **11**PPyV **12**PPQ **13**5,8-PQxs **14**

1.1.4.3 Hybrid materials in OLEDs

Randomly dispersed defects in polymeric materials result in a statistical distribution of conjugation lengths, hence a range of electronic properties. Conjugated oligomers retain the ease of deposition of polymers, but with a well-defined conjugation length. Akin to PPV, oligo(*p*-phenylenevinylene)s (OPVs) have been incorporated into electroluminescent devices, with external EL efficiencies as high as 1.36% for a single-layer of **15**.⁷⁰ The emission wavelength is red-shifted with increasing conjugation length,^{71,72} allowing tuning of the device colour. The first oligothiophene-based device was reported in 1993 exhibiting yellow-orange emission at relatively low voltages, albeit with poor efficiency.⁷³ Much improved performance may be afforded by dearomatisation of a central thienyl ring and replacement with a thienyl-*S,S*-dioxide unit.^{74,75} Oligo(*p*-phenylene)s may be used for blue emission, with efficiencies as high as 3.4%.⁷⁶ Since blue light may be used to excite lower frequency red and green dyes, full colour OLEDs have been produced with sexi(*p*-phenylene) emitters.^{77,78}



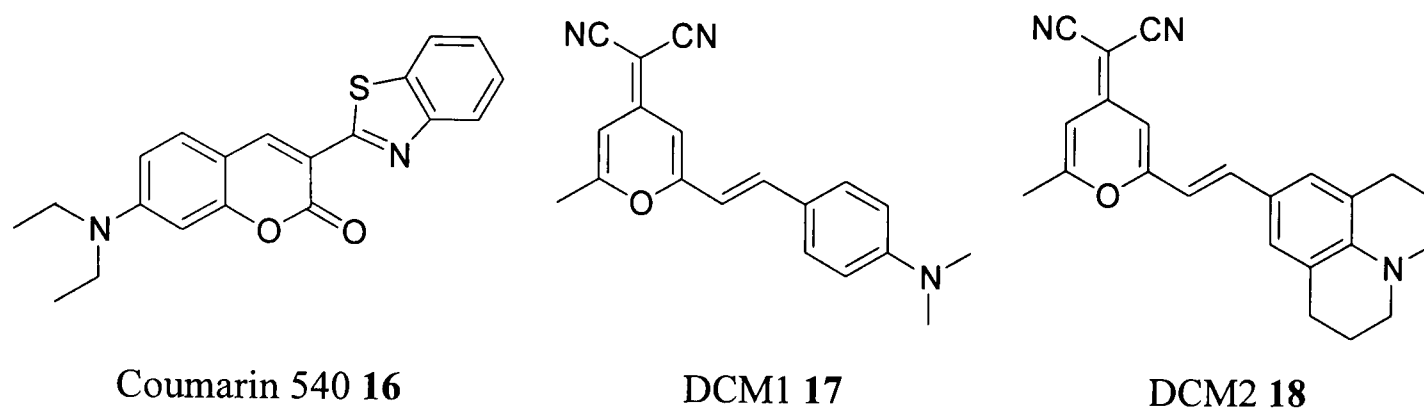
An OPV **15**

Polymers with isolated chromophores provide well-defined, tuneable electronic properties, and suppress π -stacking, recrystallisation and phase separation. By the introduction of regularly spaced ether,⁷⁹ ester,⁸⁰ carbonate,⁸¹ amide,⁸⁰ hexafluoropropylidene⁸² and silane⁸³ groups, the delocalisation of a polymer chain can be broken into sections with distinct conjugation length. Alternatively, side chain appended chromophores allow the direct incorporation of low molecular weight emitters into a polymeric framework. Exciplex formation and crystallisation have hindered the use of multi-nuclear arenes in OLEDs, however pyrene,⁸⁴ fluoranthene,⁸⁴ anthracene⁸⁵ and triphenylene⁸⁶ have all been successfully incorporated when attached to a suitable polymer.

1.1.5 Fluorescent dopants in electroluminescent devices

Two years after the report of Alq₃ as an emitter⁸ it was suggested that the low fluorescence quantum yield limited device performance to about 2%.⁸⁷ By doping with

the highly-emissive dyes coumarin 540 **16**, DCM1 **17** and DCM2 **18**, electroluminescence efficiencies were doubled.⁸⁷ A multilayer device incorporating the 4-methyl derivative of Alq₃ doped with coumarin 540 **16** achieves a maximum luminance in excess of 140 000 cd m⁻² and an external EL quantum efficiency of 7.1%, close to the theoretical limit.⁸⁸ Furthermore, provided that energy transfer is efficient, the emission colour is determined by the dopant.



Doped systems allow the combination of a superior charge transporting host with a highly efficient emitting guest. This also dilutes the guest, reducing self-quenching effects along with their associated broadening and bathochromic shifts. Energy transfer can occur only if the absorption spectrum of the acceptor (guest) overlaps with the emission spectrum of the donor (host). At low dopant concentrations, emission is from both host and guest species. Guest emission is enhanced with increasing concentration, and providing that there is efficient energy transfer, will quench host emission entirely. A further increase in dopant concentration eventually results in a decrease in emission intensity as self-quenching effects dominate (see Figure 5⁸⁷). Optimal dopant concentrations are typically very small, *e.g.* 0.1-0.5% for a DCM1-doped Alq₃ device.⁸⁷

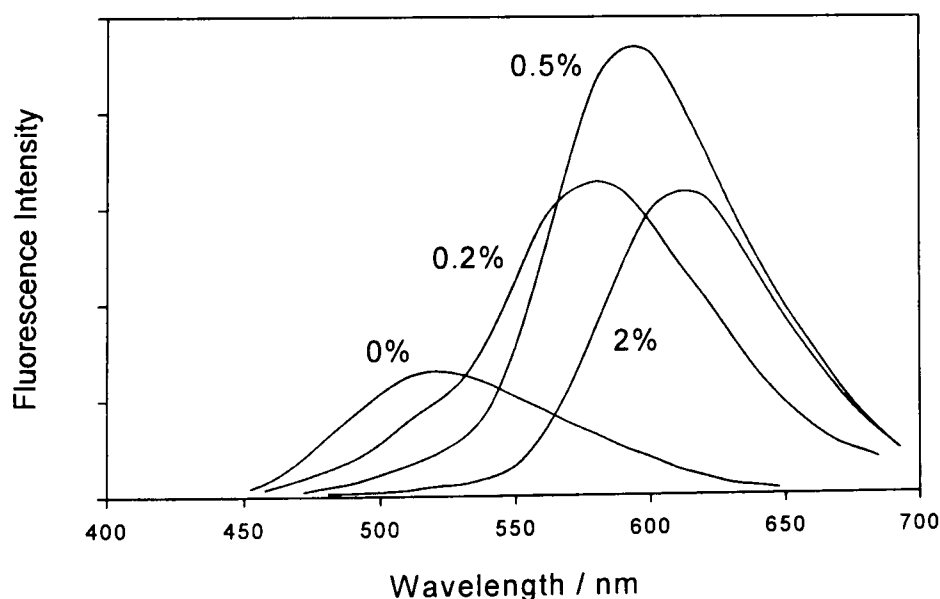
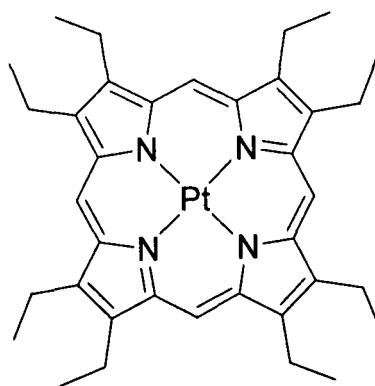
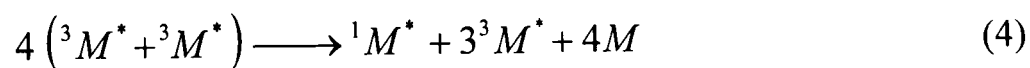


Figure 5. Effect of doping concentration on a DCM1-doped Alq₃ device (reproduced from reference 87).

1.1.6 Phosphorescent emitters in electroluminescent devices

As discussed in Section 1.1.1, the efficiency of purely fluorescent electroluminescent devices is limited by the singlet formation ratio. By incorporating phosphorescent compounds, emission occurs from both singlet and triplet excitons, and 100% internal EL quantum efficiency can potentially be achieved. Dyes containing heavy metal atoms are ideal for this purpose, since the large spin-orbit coupling partially allows previously spin-forbidden emission from triplet states.

Although a device doped with the phosphorescent compound benzophenone was reported in 1996, low efficiency was observed even at 100 K.⁸⁹ The first phosphorescent dye to exhibit efficient electroluminescence was 2,3,7,8,12,13,17,18-octaethyl-21*H*-23*H*-porphine platinum(II) (PtOEP) **19**, with an internal EL quantum efficiency of 23% (corresponding to an external EL quantum efficiency of 4%) when doped into Alq₃.^{90,91} Over 90% of the energy is transferred from Alq₃, confirming that emission occurs from both singlet and triplet excitons. Suitable choice of host raises the internal EL quantum efficiency to 32%.⁹² Doping PtOEP into a polymeric host results in a 40% increase in dopant electroluminescence relative to photoluminescence.⁹³ Unfortunately the long phosphorescence lifetime of PtOEP (>10 μs)⁹⁰ results in triplet-triplet annihilation at high current (equation 4).



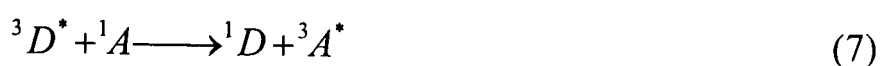
PtOEP **19**

The excited states of dopant molecules may result from either exciton formation in the host followed by charge transfer to the guest, or by direct charge-trapping and exciton formation on the dopant. For the former there are two energy transfer mechanisms, Förster⁹⁴ and Dexter,⁹⁵ both of which require the donor energy levels to be higher in energy than those of the acceptor. Förster transfer⁹⁴ involves coupling of molecular transition dipoles (see equation 5). This is a relatively long range effect (~40–

100 Å) and to be effective requires good overlap of donor emission and acceptor absorption spectra.



Dexter transfer⁹⁵ is the simultaneous exchange of an excited electron from a donor to an acceptor in return for a lower energy electron (see equations 6 and 7). It is dependent upon orbital overlap and hence its efficiency diminishes rapidly with distance.



1.2 Iridium complexes and their use in electroluminescent devices

1.2.1 The inorganic and coordination chemistry of iridium

Iridium^{96,97} is the third row transition metal of group 9 (the cobalt triad). Discovered in 1803 by Tennant, it was named after the Latin *iris* meaning rainbow and the Greek god Iris (ἴρις, whose sign was the rainbow) due to the variety of colours of its compounds. It is an exceedingly rare element, comprising 0.001 ppm of the earth's crust, but may be obtained from osmiridium (~50%) or iridiosmium (~70%). Some physical properties of elemental iridium are summarised in Table 1.

Atomic number	77
Atomic mass	192.217(3)
Natural isotopes	¹⁹¹ Ir (37.3%); ¹⁹³ Ir (62.7%)
Electronic Configuration	[Xe]4f ¹⁴ 5d ⁷ 6s ²
Effective ionic radius	Ir(III) 0.68 Å
(6-coordinate)	Ir(IV) 0.63 Å
	Ir(V) 0.57 Å
Melting Point	2443°C
Boiling Point	4550°C

Table 1. Physical properties of elemental iridium.^{96,97}

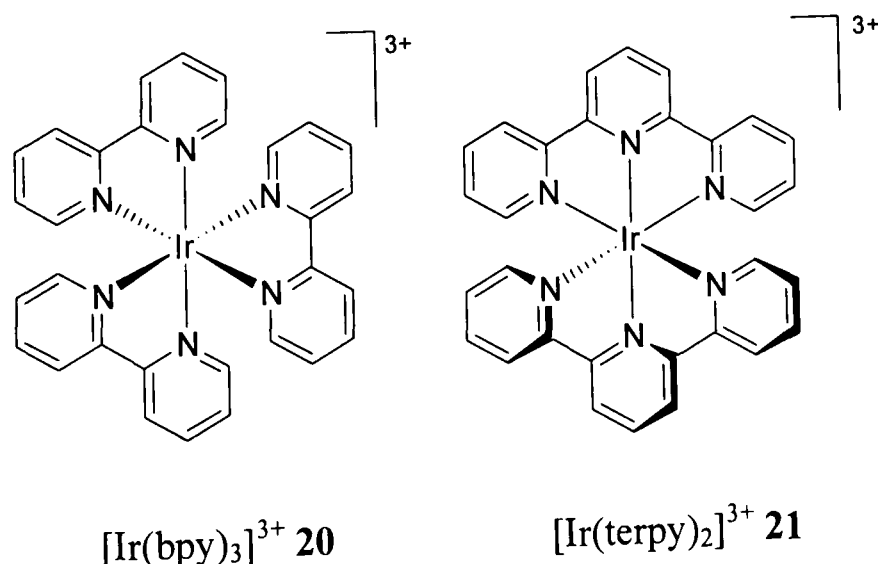
The ground state electronic configuration of iridium is 5d⁷6s², with its accessible oxidation states ranging from -3 ([Ir(CO)₃]³⁻) to +6 (IrF₆). Due to the high crystal field

stabilisation energy (CFSE) resulting from a low-spin octahedral t_{2g}^6 state, Ir^{III} is the most common oxidation state, although Ir^I is well known for π -acceptor ligands. The d^6 low-spin configuration of iridium(III) results in great inertness, with harsh conditions commonly required to substitute ligands.

1.2.1.1 *N*-Heterocyclic complexes of iridium(III)

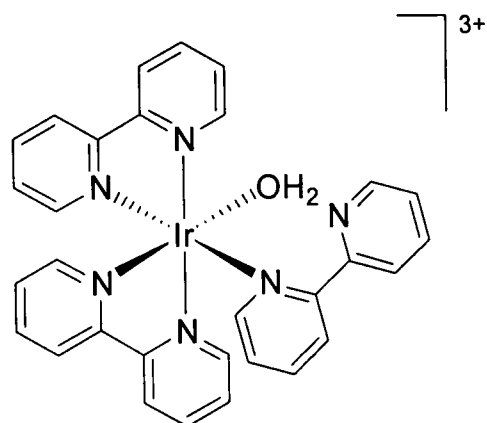
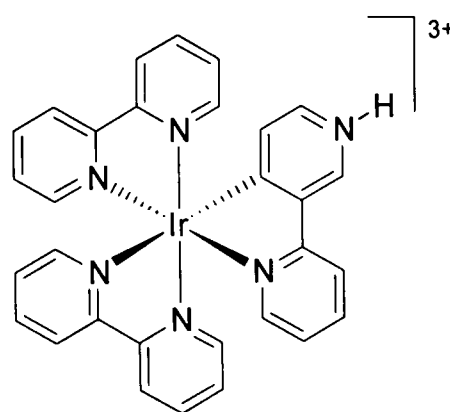
The most straightforward bidentate *N*-heterocyclic ligand is 2,2'-bipyridine (bpy). The preparation of $[\text{Ir}(\text{bpy})_3]^{3+}$ **20** was first reported in 1958 upon heating K_3IrCl_6 in bpy at 272-273°C for 20 minutes,⁹⁸ a route later adapted for $[\text{Ir}(\text{phen})_3]^{3+}$ (phen = 1,10-phenanthroline).⁹⁹ An improved preparation was subsequently published requiring conversion of $\text{K}_3\text{IrCl}_6 \cdot 3\text{H}_2\text{O}$ to its sulfate, reaction with bpy at 230°C under a CO_2 atmosphere and a laborious work-up.¹⁰⁰ A much simplified procedure reported recently involved microwave irradiation of $(\text{NH}_4)_3[\text{IrCl}_6] \cdot \text{H}_2\text{O}$ and 2,2'-bipyridine in ethylene glycol for 15 minutes. Precipitation by addition of a saturated aqueous solution of KPF_6 and recrystallisation gave $[\text{Ir}(\text{bpy})_3]^{3+}$ in 84% yield.¹⁰¹

The tridentate analogue of 2,2'-bipyridine is 2,2':6',2''-terpyridine (terpy). The synthesis of the first iridium(III) bis-terpyridine complex, $[\text{Ir}(\text{terpy})_2]^{3+}$ **21**, was reported in 1990¹⁰² following the harsh conditions used for $[\text{Ir}(\text{bpy})_3]^{3+}$.¹⁰⁰ A milder two-step synthesis was published in 1999.¹⁰³ The first ligand is introduced by reaction with iridium(III) trichloride in refluxing ethanol (or ethylene glycol where solubility is poor) to form an $\text{Ir}(\text{terpy})\text{Cl}_3$ intermediate. Reaction with a second ligand in ethylene glycol at elevated temperatures displaces the chloride ligands. While unsymmetrical complexes may be readily prepared in this way, short reaction times are required to minimise scrambling.

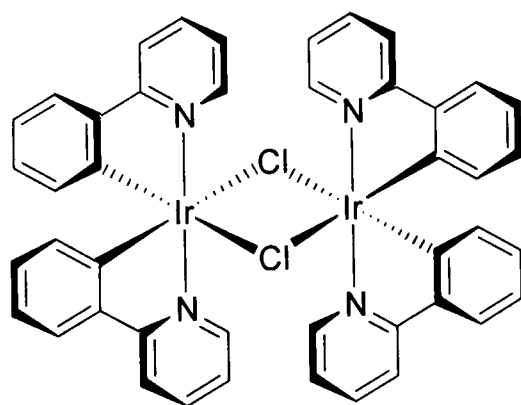
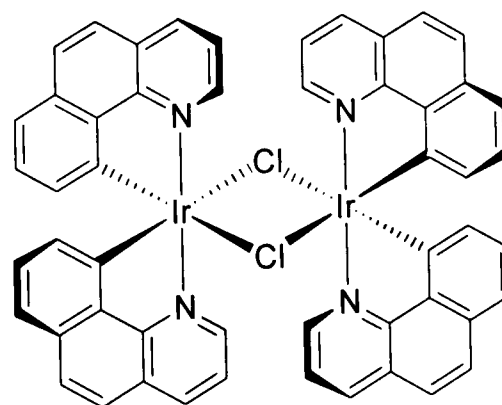


1.2.1.2 Cyclometalated complexes of iridium(III)

The first cyclometalated complex of iridium was prepared in 1977 by reaction of 2,2'-bipyridine (bpy) with iridium(III) trichloride in ethylene glycol at 180°C.¹⁰⁴ Based on the available data it was identified as $[\text{Ir}(\text{bpy-}N,N')_2(\text{bpy-}N)(\text{H}_2\text{O})]^{3+}$ **22**, with one monodentate bipyridine and the sixth coordination site occupied by water. This formulation was controversial,¹⁰⁵⁻¹⁰⁸ and it was not until 1981 that the structure was correctly identified by X-ray crystallography as $[\text{Ir}(\text{bpy-}N,N')_2(\text{Hbpy-C}^3,N')]^{3+}$ **23**.¹⁰⁹


 $[\text{Ir}(\text{bpy-}N,N')_2(\text{bpy-}N)(\text{H}_2\text{O})]^{3+}$ **22**

 $[\text{Ir}(\text{bpy-}N,N')_2(\text{Hbpy-C}^3,N')]^{3+}$ **23**

The prototypical ligand for cyclometalation of iridium(III) is 2-phenylpyridine (ppyH), which must cyclometalate in order to bind in a bidentate manner. In 1985, Watts *et al.* reported the preparation of the dichloro-bridged di-iridium(III) 2-phenylpyridine complex **24** in addition to the benzo[*h*]quinoline (bzqH) analogue **25**.¹¹⁰ The strong *trans*-effect of the cyclometalating ligand directs the bridging chlorides directly opposite the Ir–C bond. A mixture of $\Delta\Delta/\Lambda\Lambda$ isomers is favoured in order to reduce interligand steric interactions, confirmed by subsequent crystallographic studies of $[\text{Ir}(\text{ppy})_2(\mu\text{-Cl})_2]^{111}$ and the 2-(*p*-tolyl)pyridine derivative (see Figure 6).¹¹²


 $[\text{Ir}(\text{ppy})_2(\mu\text{-Cl})_2]$ **24**

 $[\text{Ir}(\text{bzq})_2(\mu\text{-Cl})_2]$ **25**

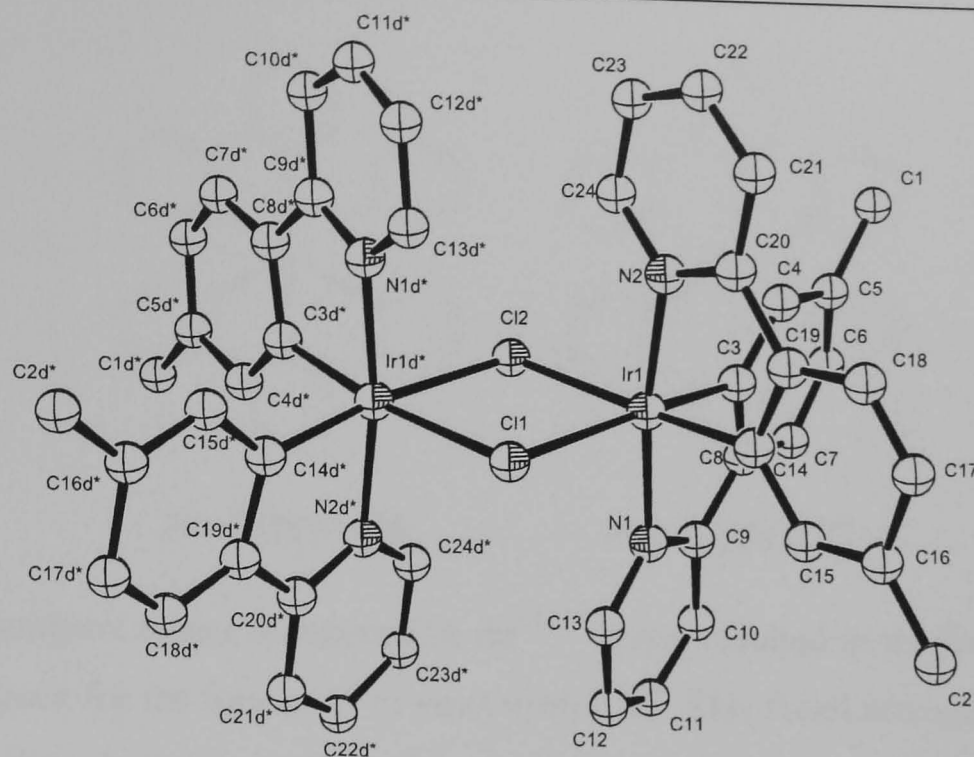
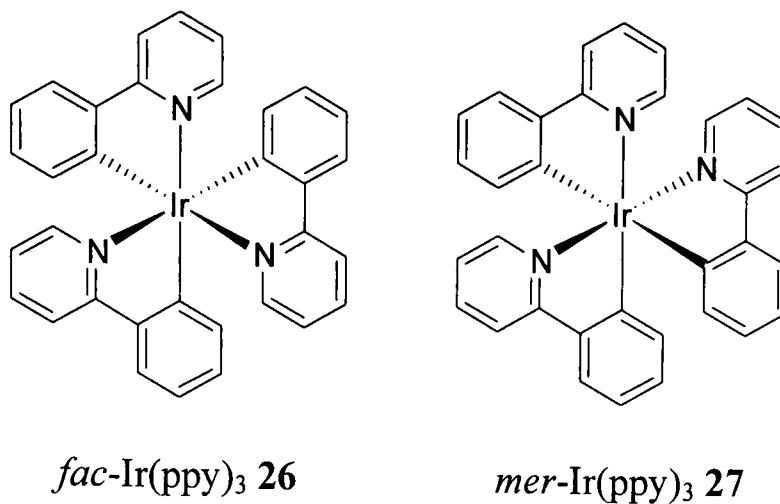


Figure 6. Crystal structure of $[\text{Ir}(\text{Me-ppy})_2(\mu\text{-Cl})]_2$.¹¹²

One side-product in the preparation of $[\text{Ir}(\text{ppy})_2(\mu\text{-Cl})]_2$ was later isolated in low yield (~10%), and identified as the tris-cyclometalated *fac*- $\text{Ir}(\text{ppy})_3$ **26**.¹¹³ The most popular synthesis of this compound to date involves reacting the ligand with $\text{Ir}(\text{acac})_3$ ($\text{acacH} = 2,4\text{-pentanedione}$) in glycerol at reflux for 10 hours (40–75% yield).¹¹⁴ Increased yields have been claimed by firstly converting $[\text{Ir}(\text{ppy})_2(\mu\text{-Cl})]_2$ into the mononuclear $\text{Ir}(\text{ppy})_2(\text{acac})$ by treatment with 2,4-pentanedione and sodium carbonate in 2-ethoxyethanol. Subsequent reaction with 2-phenylpyridine (ppyH) in glycerol at reflux gives *fac*- $\text{Ir}(\text{ppy})_3$ in an overall yield greater than 75%.¹¹⁵

Superior yields (~75%) have also been obtained by reaction of $[\text{Ir}(\text{ppy})_2(\mu\text{-Cl})]_2$ and AgSO_3CF_3 in excess 2-phenylpyridine, with no additional solvent.¹¹⁶ This route has been applied to the preparation of a series of $\text{Ir}(\text{ppy})_3$ derivatives, albeit in lower yield, starting directly from iridium(III) trichloride.¹¹⁷ Similar high yields (75%) are reported upon microwave irradiation of $\text{IrCl}_3 \cdot 3\text{H}_2\text{O}$ and 2-phenylpyridine in ethylene glycol for only one minute.¹¹⁸ By the use of excess ligand and slightly extended reaction times, a quantitative yield is obtained. A smaller quantity of ligand is required if $\text{Ir}(\text{acac})_3$ is used as a precursor, and has been shown to allow access to derivatives inaccessible *via* conventional heating.¹¹⁹



All synthetic routes mentioned so far¹¹³⁻¹¹⁸ have resulted in the facial isomer **26**, with no evidence for the formation of *mer*-Ir(ppy)₃ **27**. This facial arrangement has been attributed to the strong *trans*-effect of cyclometalating ligands directing the nitrogen of a further ppyH into the *trans* site. Subsequent cyclometalation results in a facial arrangement of donor atoms. Evidence for this two-step binding is provided by the isolation of an *N*-coordinated ppyH prior to cyclometalation with Ir.¹²⁰

It has recently been shown that the meridional isomer **27** may be prepared by reaction of [Ir(ppy)₂(μ-Cl)]₂ **24** with ppyH in the presence of potassium carbonate at slightly lower temperatures (140°C).¹²¹ At temperatures greater than 200°C, reaction results predominantly in the facial isomer. These outcomes are also observed for the iridium(III) complexes of 2-(*p*-tolyl)pyridine (tpyH) and 1-phenylpyrazole (ppzH). For the 4,6-difluorinated analogue 2-(4,6-difluorophenyl)pyridine (46dfppyH), a mixture of *fac*- and *mer*-isomers formed even at 140°C, with yet lower temperatures required to isolate the meridional isomer.

The kinetic product, *mer*-Ir(ppy)₃ may be converted into the thermodynamic product, *fac*-Ir(ppy)₃ by either thermal- or photo-isomerisation. Interestingly, although synthesis of *mer*-Ir(46dfppy)₃ requires particularly low temperatures, a similar thermally induced rearrangement does not occur. This suggests that a *mer*→*fac* isomerisation of the intermediate takes place prior to complexation of the third cyclometalating ligand. Photoisomerisation of *mer*-Ir(46dfppy)₃ in acetonitrile solution has an activation energy of 15.2 kJ mol⁻¹, but is quenched by addition of azulene indicating that isomerisation proceeds *via* a triplet state.¹²²

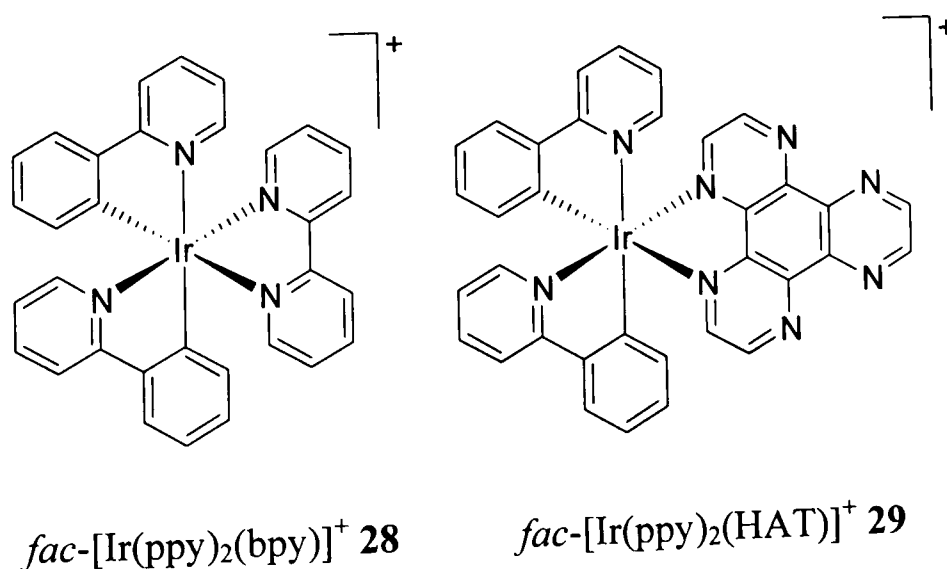
Distinct differences may be observed between the molecular structures of *fac*-Ir(tpy)₃¹¹² and *mer*-Ir(tpy)₃¹²¹ (see Table 2). The mutually *trans* Ir–C and Ir–N bonds of *mer*-Ir(tpy)₃ are comparable in length to those in the facial isomer, as expected from

their similar electronic environments. The Ir–N bonds *trans* to nitrogen however are significantly shortened by the comparatively weak *trans*-influence of the pyridyl group. Similarly, the strong *trans*-influence of a cyclometalated phenyl group lengthens the mutually *trans* Ir–C bonds.

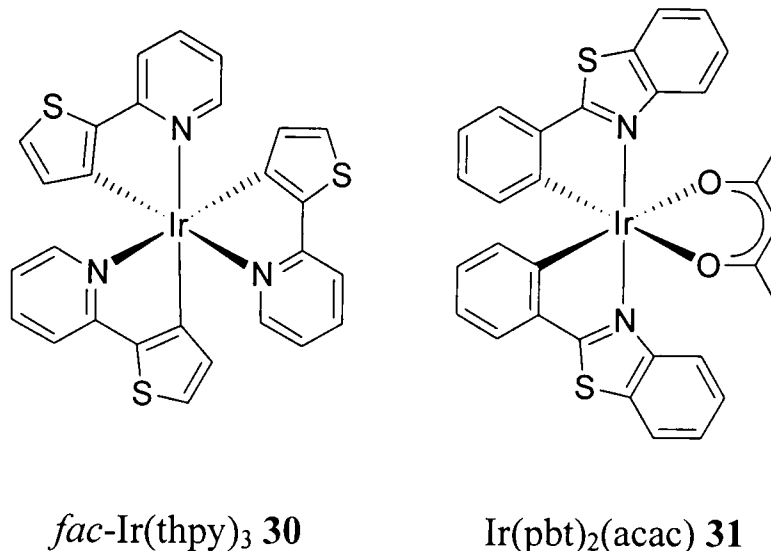
		Bond distances / Å	
		<i>fac</i> -Ir(tpy) ₃ ¹¹²	<i>mer</i> -Ir(tpy) ₃ ¹²¹
Ir-N1	}	2.132(5) (trans to C)	2.151(9) (trans to C3)
Ir-N2			2.044(8) (trans to N3)
Ir-N3			2.065(8) (trans to N2)
Ir-C1	}	2.024(6) (trans to N)	2.076(10) (trans to C2)
Ir-C2			2.086(12) (trans to C1)
Ir-C3			2.020(8) (trans to N1)

Table 2. Selected bond distances for *fac*- and *mer*-Ir(tpy)₃ (tpyH = 2-(*p*-tolyl)pyridine).

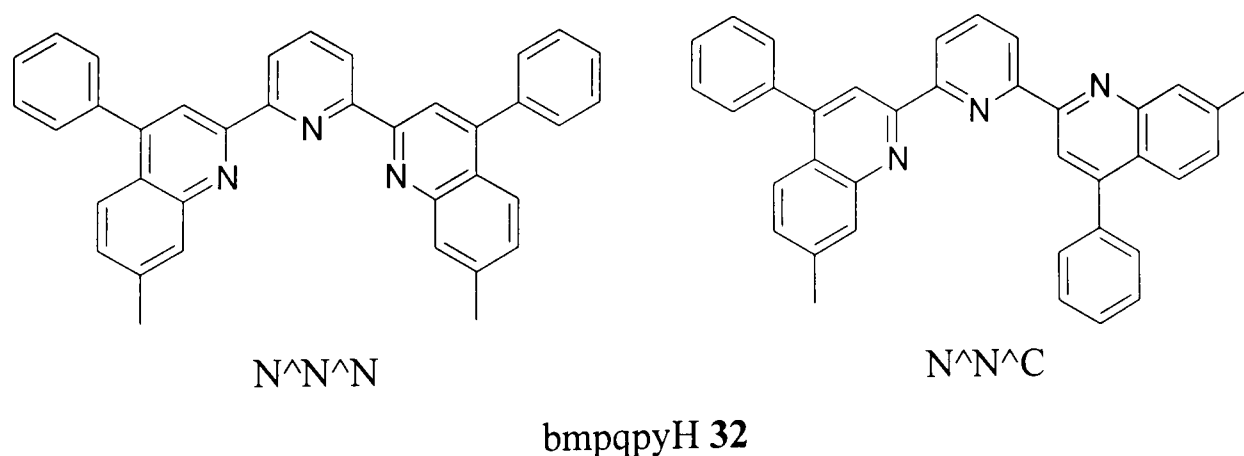
As dichloro-bridged di-iridium(III) intermediates may easily be prepared, this affords ready access to mixed ligand Ir(C[^]N)₂(X[^]X) species. Reaction of [Ir(ppy)₂(μ-Cl)]₂ **24** with 2,2'-bipyridine (bpy) in dichloromethane at room temperature is reported to give [Ir(ppy)₂(bpy)]⁺ **28** in reasonable (~75%) yield.¹²³ Similar reaction with the potentially bridging ligand 1,4,5,8,9,12-hexaazatriphenylene (HAT) also results in the corresponding iridium(III) complex **29**,¹²⁴ allowing the synthesis of mixed-metal dinuclear systems.^{125,126} Where charge-neutral iridium(III) complexes are desired, Ir(C[^]N)(acac) compounds may be prepared as discussed previously.^{115,127,128}



In 1994, the complexation of 2-(2-thienyl)pyridine (thpy) was reported by a solvent-free route.¹¹⁶ The resulting complex (*fac*-Ir(thpy)₃ **30**) exhibits cyclometalation at the 3-position of the thienyl ring. A number of 2-phenylbenzothiazole (pbt) complexes (*e.g.* Ir(pbt)₂(acac) **31**)¹¹⁵ have also been reported.



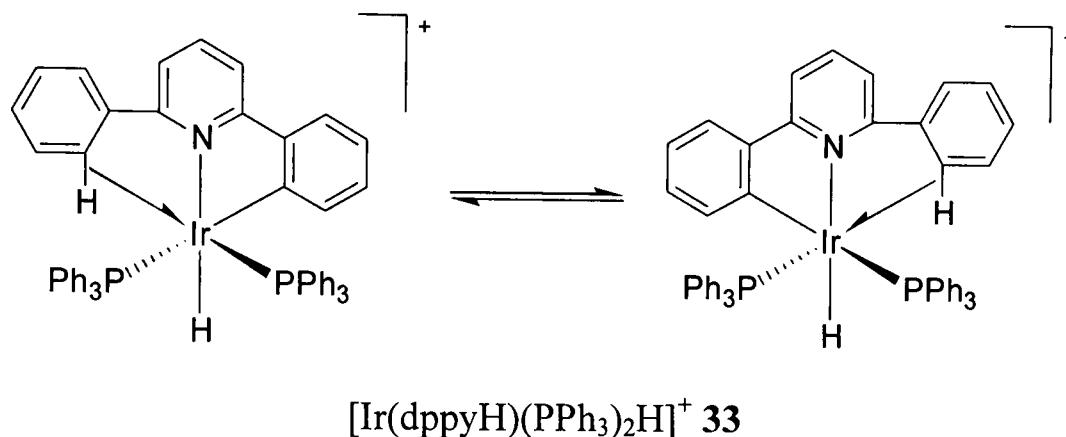
While iridium(III) complexes of C^N binding ligands are common, terdentate coordination of cyclometalating ligands is relatively unexplored. This was first reported in 1997 for the potentially cyclometalating ligand 2,6-bis(7'-methyl-4'-phenyl-2'-quinolyl)pyridine (bmpqpyH) **32**. It is capable of binding through three nitrogens (N^NN) or, by bond rotation, through two nitrogens and a cyclometalating carbon atom (N^NC). Upon reaction with IrCl₃ in glycerol at reflux for 24 hours, both [Ir(bmpqpyH-N^NN)(bmpqpy-N^NC)]²⁺ and [Ir(bmpqpy-N^NC)₂]⁺ were obtained.¹²⁹



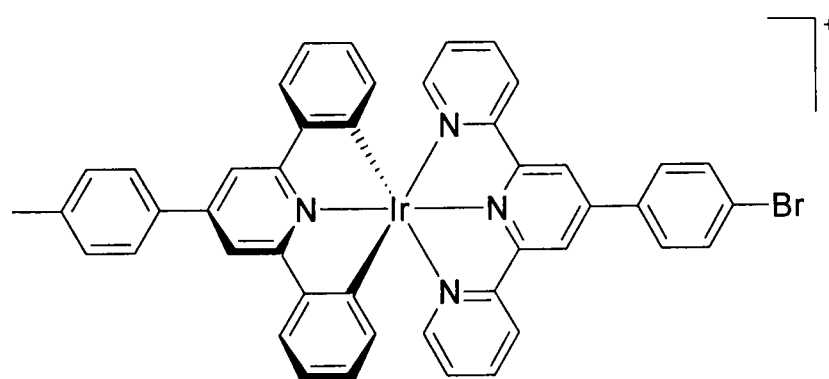
While complexation of 4'-aryl-6'-phenyl-2,2'-bipyridine derivatives has also been investigated,¹³⁰⁻¹³³ the precursor has always been [Ir(ppy)₂(μ-Cl)]₂ **24**, limiting binding to bidentate coordination. The mild reaction conditions employed result in chelation in an N^N manner, with no metalation at the phenyl ring. Crystal structures of

the resulting complexes have shown that the pendent phenyl group is approximately orthogonal to the bipyridine moiety.^{130,131}

The ligand 2,6-diphenylpyridine (dppyH₂) could in principle metalate at both phenyl rings. Early attempts with phosphines as the ancillary ligands were unsuccessful, resulting in the mono-cyclometalated complex [Ir(dppyH)(PPh₃)₂H]⁺ **33**.¹³⁴ The sixth coordination site is stabilised by an agostic C–H···Ir bond, interconverting rapidly with the metalated site in solution.



Very recently, successful dimetalation of 2,6-diphenylpyridine has been reported in complex **34**.¹³⁵ This was synthesised by reaction of a terpyridine iridium trichloride intermediate with 2,6-diphenyl-4-(*p*-tolyl)pyridine) in degassed ethylene glycol at 190°C. The terpyridine fragment binds in a similar manner to that in bis-terpyridine complexes, with the C[^]N[^]C fragment (*i.e.* the ligand binding through two peripheral cyclometalating rings and a central pyridine ring) exhibiting a relatively short Ir–N bond (2.022(6) Å) and relatively long Ir–C bonds (2.122(9) Å and 2.094(9) Å). This again may be explained by the strong *trans*-influence of a cyclometalated phenyl ring.



34

1.2.2 Photoluminescence and electrochemistry of iridium(III) complexes

While iridium(III) polyimine complexes are invariably luminescent, the nature of the emissive state is strongly dependent upon the energy of the highest lying metal-centred orbital. This is determined predominantly by the number of anionic or cyclometalating donor atoms. In addition, $[\text{IrN}_6]^{3+}$ complexes are strong photooxidants, while $[\text{IrN}_3\text{C}_3]$ complexes are strong photoreductants.

When none of the ligands bound to iridium(III) are cyclometalated or anionic, emission generally occurs from ligand centred (LC) states. For example, $[\text{Ir}(\text{bpy})_3]^{3+}$ **20** displays a highly structured emission at 77 K with $\lambda_{\text{em}} \sim 440$ nm and a lifetime of ~ 80 μs .¹⁰⁰ Although predominantly ligand centred, room temperature degassed lifetimes ($\tau = 2.4$ μs)¹³⁶ suggest some metal-to-ligand charge transfer (MLCT) character. Cyclic voltammetry studies show a single irreversible oxidation at +2.05 V, and six one-electron reductions corresponding to the six pyridyl rings.¹³⁷

Iridium bis-terpyridine complexes are also luminescent at room temperature. The emission spectrum of $[\text{Ir}(\text{terpy})_2]^{3+}$ **21** is highly structured, with $\lambda_{\text{em}} = 458$ nm for the highest-energy peak in acetonitrile solution.¹⁰³ This is assigned to an LC emissive state, with a degassed lifetime of 1.2 μs and a quantum yield of 0.025 at 293 K. Emissions from 4'-aryl substituted iridium bis-terpyridine complexes show a systematic red-shift and broadening (see Figure 7).¹⁰³ Although still primarily emission from an LC state, it is likely that this is mixed with energetically accessible ³MLCT states. Two one-electron reduction waves are reported for all complexes, relating to the consecutive reduction of each ligand, while oxidation of Ir(III) to Ir(IV) is not observed.¹⁰³ The interplay between LC and MLCT emissive states is one reason for the investigation of iridium(III) bis-terpyridine complexes as potential luminescent sensors.^{138,139}

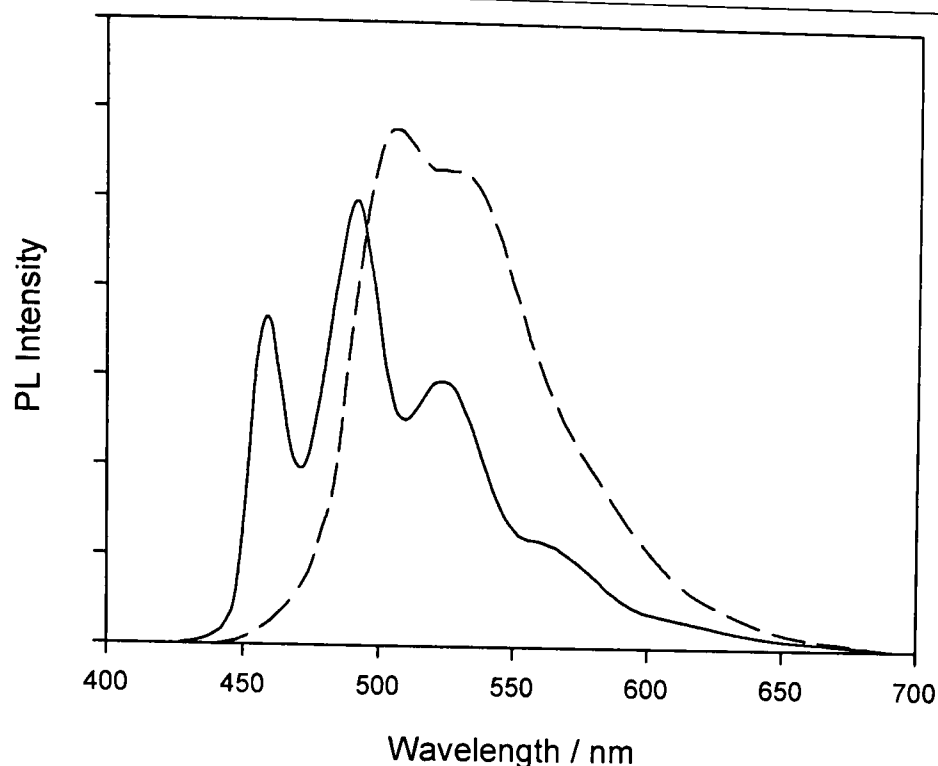


Figure 7. Room-temperature photoluminescence spectra of air-equilibrated acetonitrile solutions of $[\text{Ir}(\text{terpy})_2]^{2+}$ (solid line) and $[\text{Ir}(4'\text{-}p\text{-tolyl-terpy})_2]^{2+}$ (dashed line) (adapted from reference 103).

When anionic or cyclometalating ligands are present, there is sufficient charge compensation to allow oxidation at the metal centre. The energy of metal-to-ligand charge transfer (MLCT) states is reduced to below that of the ligand centred (LC) states and emission is predominantly $^3\text{MLCT}$ in character.

By far the greatest amount of data for such compounds has been acquired for *fac*- $\text{Ir}(\text{ppy})_3$ **26**. Early work by Watts *et al.* reports the photophysical and electrochemical characterisation of a number of tris-cyclometalated iridium(III) complexes (see Table 3).¹¹⁴ At room temperature, a broad structureless emission typical of a $^3\text{MLCT}$ emissive state is observed for all derivatives, an assignment confirmed by excited-state absorption spectroscopy.¹⁴⁰ In degassed toluene solution, *fac*- $\text{Ir}(\text{ppy})_3$ exhibits a high luminescence quantum yield of 0.4 ± 0.1 with a radiative lifetime of about $5 \mu\text{s}$.¹¹³ In contrast with neutral donor ligands, oxidation of the metal atom to Ir^{IV} may be observed, aided by electron-donating substituents.

	$\tau^a / \mu\text{s}$	$\lambda_{\text{em}}^b / \text{nm}$	$E_{\text{oxd}} / \text{V vs. SCE}$
Ir(ppy) ₃	1.90	494	+0.77
Ir(4-F-ppy) ₃	2.04	468	+0.97
Ir(4-MeO-ppy) ₃	2.24	481	+0.75
Ir(4-Me-ppy) ₃	1.94	493	+0.70
Ir(4-CF ₃ -ppy) ₃	2.16	494	+1.08
Ir(4-Pr-ppy) ₃	1.93	496	+0.67
Ir(4- ^t Bu-ppy) ₃	1.97	497	+0.66
Ir(5-MeO-ppy) ₃	2.86	539	+0.55

^a Degassed MeCN, 293 K. ^b Shortest wavelength feature in EtOH/MeOH (1:1) glass at 77 K

Table 3. Photophysical and electrochemical data for *fac*-Ir(ppy)₃ derivatives.¹¹⁴

Electron localisation in the excited state may be considered by two limiting cases, $^*[\text{Ir}^{\text{IV}}(\text{ppy})_2(\text{ppy}^-)]$ and $^*[\text{Ir}^{\text{IV}}(\text{ppy}^{-1/3})_3]$. Electroabsorption spectroscopy has recently been applied to *fac*-Ir(ppy)₃, suggesting that the transition dipole moment is along the molecular three-fold axis, hence electron density is initially distributed evenly amongst the three ppy ligands in the excited state.¹⁴¹ This is consistent with the results of TD-DFT calculations¹⁴² (discussed in Section 4.2). It has been shown, however, that in $[\text{Ru}(\text{bpy})_3]^{2+}$ excitation results in an even distribution of electron density across all three ligands, followed by a localisation on a single bpy prior to emission.¹⁴³

Energy transfer pathways in photoluminescence of *fac*-Ir(ppy)₃ have been studied by transient absorption spectroscopy.¹⁴⁴ Femtosecond measurements upon excitation at 400 nm (¹MLCT) and 266 nm (LC) allow the time constants for the transient species to be determined as,



The average molecular area in Langmuir-Blodgett monolayer films of *fac*-Ir(ppy)₃ is 55 Å².¹⁴⁵ Maximum emission from such films was at 543 nm, resembling the spectrum of solid powder samples. Single molecule detection in poly(methyl methacrylate) (PMMA) films indicate two sites for *fac*-Ir(ppy)₃, distinguished by their bleaching lifetimes and phosphorescence spectra.^{146,147} The emission intensity was found to be highly dependent on the polarisation of the exciting laser. This suggests that

a symmetry distortion due to electrostatic interactions with the environment results in localisation of the emissive state on a single ppy ligand.

Relative to their facial isomers, *mer*-Ir(ppy)₃ **27** and its derivatives are easier to oxidise and show a broader red-shifted emission.¹²¹ The broad spectra are indicative of a large geometric distortion in the excited state. This may include an increase in length of the already long *trans* Ir–C bonds, consistent with the observation of photolytic cleavage and subsequent isomerisation to the facial isomer. Luminescence quantum yields are considerably smaller for the meridional isomers, while radiative decay rates are of a similar magnitude (see Table 4). The poor efficiency is therefore attributed to large non-radiative decay rates associated with the photoisomerisation process ($\Phi_{\text{iso}} = 0.067$ for *mer*-Ir(46dfppy)₃).¹²²

	Φ_{PL}		$\tau / \mu\text{s}$		$k_{\text{r}} / 10^5 \text{ s}^{-1}$		$k_{\text{nr}} / 10^5 \text{ s}^{-1}$	
	<i>fac</i> -	<i>mer</i> -	<i>fac</i> -	<i>mer</i> -	<i>fac</i> -	<i>mer</i> -	<i>fac</i> -	<i>mer</i> -
Ir(ppy) ₃	0.40	0.036	1.9	0.15	2.1	2.4	3.2	64
Ir(tpy) ₃	0.50	0.051	2.0	0.26	2.5	2.0	2.5	36
Ir(46dfppy) ₃	0.43	0.053	1.6	0.21	2.7	2.5	3.6	45

Table 4. Photophysical data and decay rates for *fac*-/*mer*-Ir(ppy)₃ derivatives.¹²¹

For the mono-cyclometalated bmpqpyH **32** complex [Ir(bmpqpyH-N[^]N[^]N)](bmpqpy-N[^]N[^]C)]²⁺, no oxidation of the metal was observed up to +2.00 V vs. SCE.¹²⁹ In contrast, the bis-cyclometalated complex [Ir(bmpqpy-N[^]N[^]C)₂]⁺ shows an oxidation at +1.40 V vs. SCE, continuing the general decrease in oxidation potential with increasing number of cyclometalating atoms. Emission is from ³MLCT states in each case (Ir→(bmpqpyH-N[^]N[^]N) and Ir→(bmpqpy-N[^]N[^]C) respectively). Room temperature luminescence quantum yields in degassed acetonitrile solution are relatively small (mono-cyclometalated complex, $\lambda_{\text{max}} = 620 \text{ nm}$, $\Phi_{\text{PL}} = 0.005$; bis-cyclometalated complex, $\lambda_{\text{max}} = 630 \text{ nm}$, $\Phi_{\text{PL}} = 0.066$), although it was suggested that an upper-lying excited state may contribute to deactivation of the mono-cyclometalated complex.

In contrast to *fac*-Ir(ppy)₃, *fac*-Ir(thpy)₃ **30** shows a structured emission from a ligand-centred (LC) π - π^* transition.¹¹⁶ This is a result of the lowered π - π^* energy (564 nm¹¹⁶) with respect to ppy (460 nm¹⁴⁸), bringing it below that of the ³MLCT state. Metal-ligand vibrations are observed in the narrowed luminescence spectrum of *fac*-Ir(thpy)₃ doped into *fac*-Ir(ppy)₃, suggesting that there is significant mixing with close-

lying MLCT states. A number of *fac*-Ir(thpy)₃ derivatives have been investigated recently for OLED applications.¹⁴⁹ Increasing conjugation, electron donating methyl groups on the thienyl, and electron withdrawing trifluoromethyl groups on the pyridyl, all result in a red-shift of emission. Photoluminescence quantum yields however were low, and incorporation into electroluminescent devices was not attempted.

The electrochemical properties of [Ir(ppy)₂(bpy)]⁺ **28** are between those of Ir(ppy)₃ and [Ir(bpy)₃]³⁺.¹²³ Oxidation of the metal centre (1.26 V vs. SCE) is aided with respect to [Ir(bpy)₃]³⁺, while reduction is more difficult. Emission spectroscopy shows evidence of two components ($\lambda_{\text{max}} = 520 \text{ nm}$ and 550 nm)^{123,150} which, although of a similar lifetime, may be resolved by selective excitation of the lowest energy state with a tunable laser.¹⁵¹ The transitions are assigned to unequilibrated MLCT states, with the lower energy component based on the bpy ligand and the higher energy component on the ppy. These conclusions are consistent with excited state absorption measurements¹⁴⁰ and the solvent dependence of emission.¹⁵² It was suggested that since electronic coupling between the two states is likely to be high, a large viscosity-dependent Franck-Condon barrier is present, consistent with a large red-shift at 77 K.

In contrast, emission from [Ir(ppy)₂(HAT)]⁺ **29** is mono-exponential at room temperature ($\lambda_{\text{max}} > 770 \text{ ns}$, $\tau < 10 \text{ ns}$), while at 77 K dual-emission is again observed.¹²⁴ In this case, the two components are assigned to MLCT and sigma-bond-to-ligand charge transfer (SBLCT) states with lifetimes of $\sim 1.5 \mu\text{s}$ and $3 \mu\text{s}$ respectively.

Solutions of Ir(ppy)₂(acac) exhibit green photoluminescence ($\lambda_{\text{max}} = 516 \text{ nm}$) with a quantum yield of 0.34 in 2-MeTHF.¹¹⁵ Whilst substitution of 2-phenylpyridine with other C[^]N binding ligands allows the tuning of emission from 512 nm to 612 nm,^{115,127} changing the acac ligand results in a relatively minor shift. A study of the Ir(pbt)₂(acac) complex **31** reported the effect of simple modifications to the phenyl-ring of the 2-phenylbenzthiazole (pbtH) ligand.¹²⁸ Fluorination at the 4-position results in a blue-shift of 16 nm but little increase in emission intensity, while fluorination at the 3-position achieves a small red-shift and a tripling of photoluminescence quantum yield relative to the parent compound.

The *trans*-bis-cyclometalated [Ir(terpy)(dppy)]⁺ derivative **34** shows a reversible one-electron oxidation at +1.08 V vs. SCE,¹³⁵ slightly lower than that of other bis-cyclometalated complexes.^{123,129} This is attributed to the enforced *trans* geometry of the cyclometalating carbon atoms (comparable with *mer*-Ir(ppy)₃¹²¹). A one-electron

reduction of the terpyridine ligand is reported at -1.27 V vs. SCE, significantly more negative than that of iridium(III) bis(4'-(*p*-tolyl)-2:2',6':2''-terpyridine) (-0.81 V vs. SCE¹⁰³).

The room-temperature emission spectrum of **34** shows a broad emission ($\lambda_{\max} = 690$ nm) assigned as MLCT with substantial dppy \rightarrow terpy ligand-to-ligand charge transfer (LLCT) character.¹³⁵ Its structureless nature is analogous to that for *mer*-Ir(ppy)₃,¹²¹ and is due to a large geometric distortion in the excited-state. It is significantly red-shifted with respect to bis-terpyridine complexes¹⁰³ since the HOMO is destabilised upon cyclometalation. The emission is relatively weak and the lifetime in degassed acetonitrile solution quite long ($\Phi_{\text{PL}} = 0.032$, $\tau = 1.7$ μs) implying a low radiative rate constant ($k_r = 1.9 \times 10^4$ s⁻¹).

1.2.3 Electroluminescence of iridium(III) complexes

Whilst the first phosphorescent electroluminescent devices utilised platinum complexes as triplet harvesters^{90,91,93} (see Section 1.1.6), the long triplet lifetimes (>10 μs for PtOEP)⁹⁰ limit efficiency due to saturation and triplet-triplet annihilation at high current. More favourable are the relatively short triplet lifetimes (~ 1 μs) of iridium(III) complexes. The first example of a device incorporating such a complex was reported in 1999 for *fac*-Ir(ppy)₃ **26**. Although efficiencies were limited to $\sim 0.8\%$ as a homogeneous film, efficient green emission is observed when doped into a low molecular weight host ($\lambda_{\max} = 510$ nm, $\eta_{\text{pow}(\max)} = 31$ lm W⁻¹, $\eta_{\text{pow}} = 19$ lm W⁻¹ at 100 cd m⁻²).¹⁵³ A peak external EL quantum efficiency of 8% corresponds to an internal EL quantum efficiency of 40%, well above the statistical 25% threshold expected from purely fluorescent emitters.

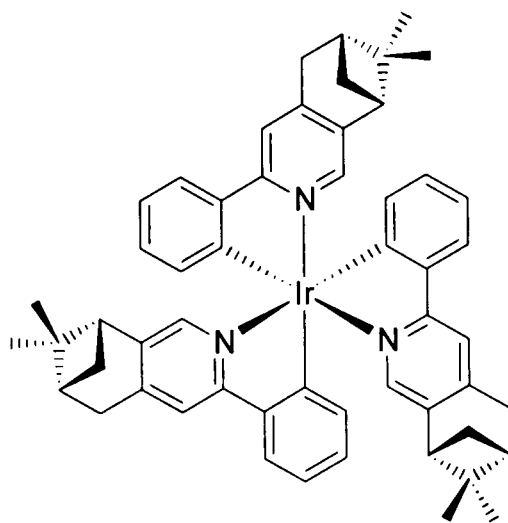
Optimisation of device structure led only a year later to a *fac*-Ir(ppy)₃ doped OLED with an external EL quantum efficiency of $15.4 \pm 0.2\%$ and power efficiency of 40 ± 2 lm W⁻¹.¹⁵⁴ This is a doubling of the internal EL quantum efficiency to 80%, close to the 100% limit. Although greater than the photoluminescence efficiency ($\sim 40\%$ ¹¹³), this was rationalised by the direct generation of triplet states in electroluminescence. By careful choice of materials, a *fac*-Ir(ppy)₃-doped transparent OLED has been developed, emitting light from both sides of the device.¹⁵⁵

The use of a polymeric host was reported in 2000, with a device incorporating a *fac*-Ir(ppy)₃ doped poly(vinylcarbazole) (PVK) emitting layer.¹⁵⁶ The maximum external EL quantum efficiency of 1.9% and peak luminance of 2 500 cd m⁻² is less

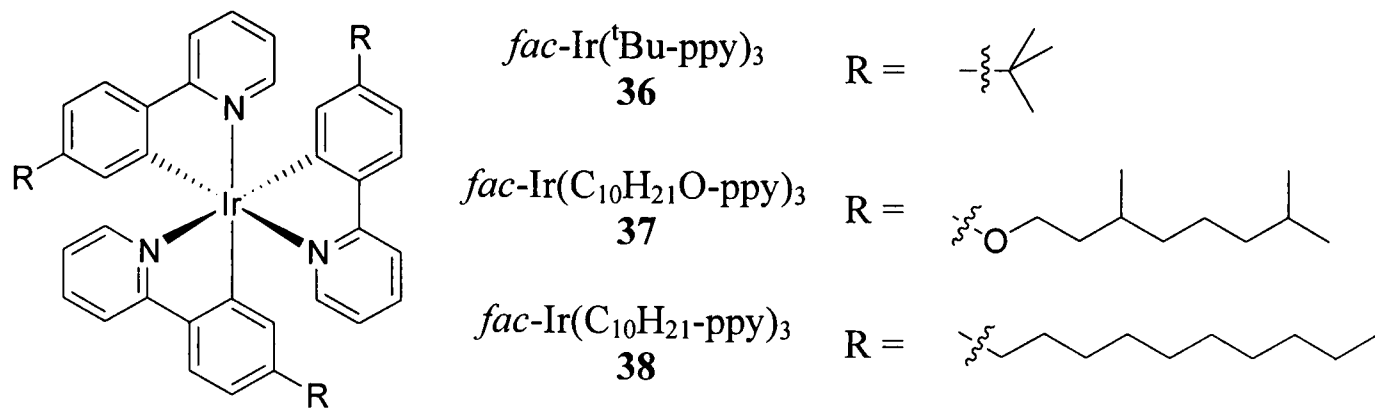
efficient than devices based on low molecular weight emitters, but a significant improvement over the undoped device. By use of a multilayer (ITO/PVK:PBD:*fac*-Ir(ppy)₃/TPBI/Alq₃/Mg:Ag) device, efficiencies were raised to 8.5%.¹⁵⁷ Doping into a hole- and electron-transporting aromatic polyimide host also achieved an improved external EL quantum efficiency of ~7%.¹⁵⁸

Phosphorescent emitters are generally doped in relatively low quantities, since at higher concentrations self-quenching effects become important and efficiency drops. By the incorporation of sterically hindering substituents, the pinene derivative *fac*-Ir(mppy)₃ **35** has an increased photoluminescence quantum yield in solution of 0.71.¹⁵⁹ When incorporated into electroluminescent devices, much higher doping levels can be achieved without a decrease in luminescence (*e.g.* $\eta_{\text{ext}} = 10.2\%$ at 26% by weight).

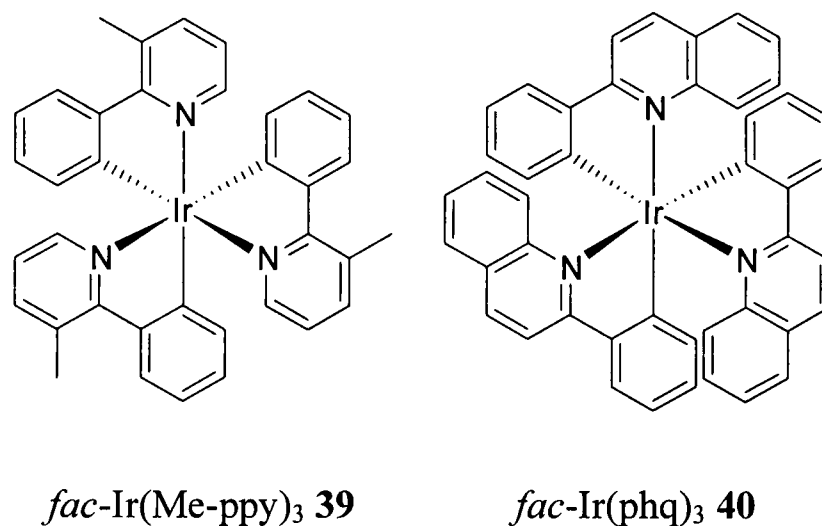
Introduction of *tert*-butyl groups, although not found to significantly decrease self-quenching effects, improve device performance by enhancing the interaction between dopant and polymeric host. An external EL quantum efficiency of 5.1% is reported upon doping *fac*-tris(2-(4-*tert*-butylphenyl)pyridine) iridium(III) (*fac*-Ir(^tBu-ppy)₃) **36** into a PPP-based host.¹⁶⁰ Incorporation of long alkyl and alkoxy chains (complexes **37** and **38**) result in a blue-shift to 495 nm, but a simultaneous decrease in efficiency with respect to *fac*-Ir(ppy)₃.¹⁶¹



fac-Ir(mppy)₃ **35**



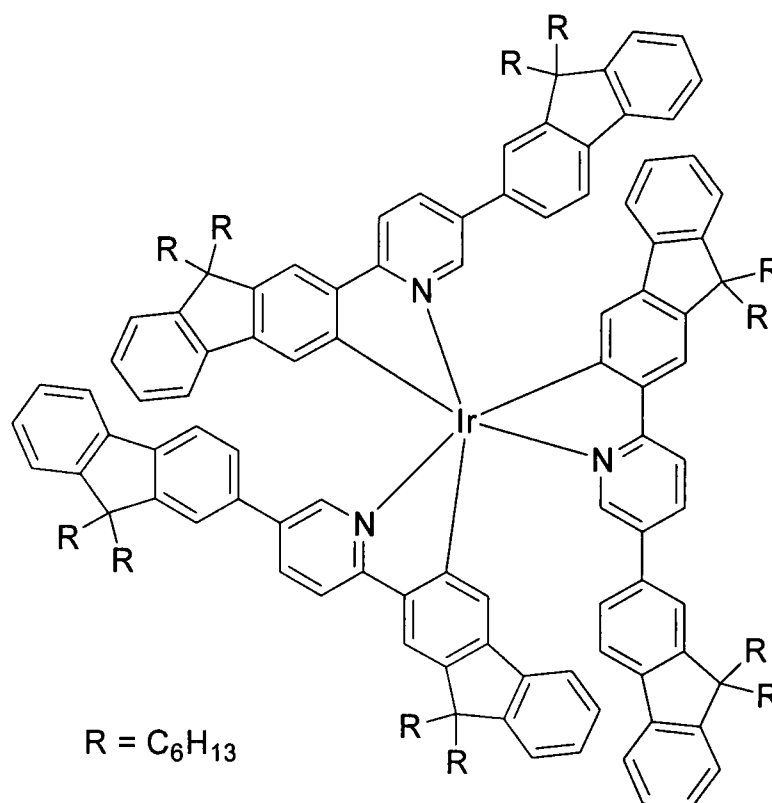
Fine tuning of the HOMO and $^3\text{MLCT}$ states can be achieved by methyl substitution at the 3-position of the pyridyl ring. This induces a slight twisting between the phenyl and pyridyl rings, reducing the extent of delocalisation. An OLED with 2% *fac*-tris(3-methyl-2-phenylpyridine)iridium(III) (*fac*-Ir(Me-ppy) $_3$) **39** doped into a PVK matrix exhibited a reasonable external EL quantum efficiency of 4.5% and peak luminance of 25 000 cd m^{-2} .¹⁶² Increased delocalisation has been achieved by extension of the aromatic rings in Ir(phq) $_3$ **40**, resulting in red-shifted emission ($\lambda_{\text{max}} = 589 \text{ nm}$).¹¹⁹



A number of fluorinated derivatives of *fac*-Ir(ppy) $_3$ show great promise as emitters for electroluminescent devices.^{117,163} Fluorination reduces the rate of radiationless deactivation, improves sublimability, minimises self-quenching and enhances electron mobility. The charge transport and self-quenching properties are improved to the extent that efficient devices may be fabricated without requiring doping into a charge-transporting matrix.

Homogeneous films of iridium complexes have also been reported for fluorene-modified *fac*-Ir(ppy) $_3$ derivatives.¹⁶⁴ Due to the increased bulk, solid state photoluminescence quantum yields of 0.11 ± 0.01 are achieved for the most heavily substituted derivative **41**. The complexes were amorphous, hence able to be spin-coated, and fluorene groups improve charge-transport. Devices without a host material were

successfully fabricated, albeit with poor efficiencies.¹⁶⁴ Fluorene-derivatised iridium complexes doped into polymer matrices have been more successful,¹⁶⁵ with exciton formation reported to result from charge-trapping rather than energy transfer.^{166,167}



41

In addition to *fac*-Ir(ppy)₃, much research has focused on the use of Ir(ppy)₂(acac) as an electrophosphorescent emitter. When incorporated into a wide energy-gap 3-phenyl-4-(1'-naphthyl)-5-phenyl-1,2,4-triazole (TAZ) host, a maximum external EL quantum efficiency of 19±1% was reported.¹⁶⁸ This corresponds to an internal EL quantum efficiency of 87±7%, one of the highest achieved for any electroluminescent device.

A number of Ir(C^N)₂(acac) derivatives have been doped into both low molecular weight (4,4'-*N,N'*-dicarbazolebiphenyl (CBP))¹²⁷ and polymeric (poly(vinyl-carbazole) (PVK))¹⁶⁹ hosts (see Table 5). By substitution of the ligand, the colour may be progressively tuned from green to red. By altering the nature and position of substituents on the 2-phenylbenzothiazole (pbt) fragment of Ir(pbt)₂(acac), finer tuning of the emission properties can be achieved.¹²⁸ An enhancement of red emission to $\eta_{\text{ext}} = 3.5 \pm 0.1\%$ has been accomplished by doubly doping a PVK host with an Ir(btp)₂(acac) emitter and an Ir(ppy)₃ sensitiser.¹⁷⁰

Dopant ^a	Host	Ref.	λ_{\max} / nm	Peak η_{ext} / %
Ir(ppy) ₂ (acac)	CBP ^d	127	525	12.3 ± 0.3
Ir(ppy) ₂ (acac)	PVK ^c	169	516	3.4 ± 0.2
Ir(bzq) ₂ (acac)	PVK ^c	169	548	1.9 ± 0.1
Ir(pbt) ₂ (acac)	CBP ^d	127	565	9.7 ^b
Ir(pbt) ₂ (acac)	PVK ^c	169	557	1.6 ± 0.2
Ir(bsn) ₂ (acac)	PVK ^c	169	606	0.7 ± 0.1
Ir(btp) ₂ (acac)	CBP ^d	127	617	6.6
Ir(btp) ₂ (acac)	PVK ^c	169	612	0.4 ± 0.1

^aStructures of ligands are shown in Figure 8. ^bExternal EL quantum efficiency at 1 mA cm⁻².
^cITO/PVK:PBD:dopant/Mg:Ag/Ag. ^dITO/ α -NPD/CBP:dopant/BCP/Alq₃/Mg:Ag/Ag.

Table 5. Characteristics of OLEDs incorporating Ir(C^N)(acac) dopants.

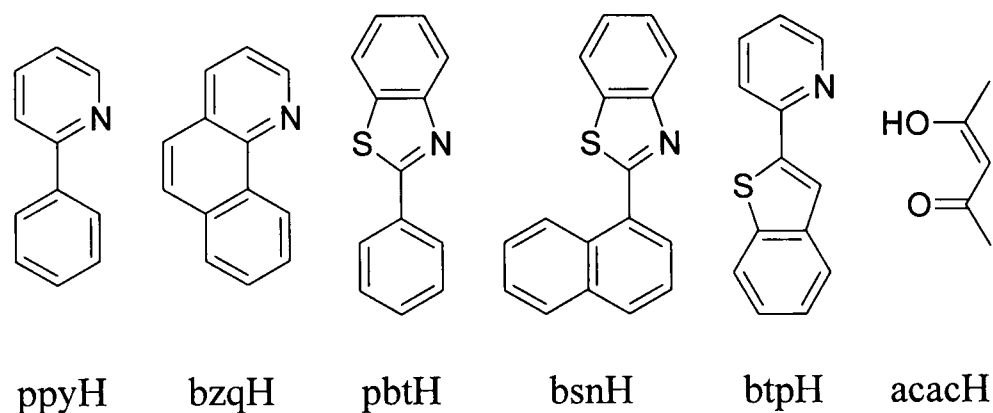
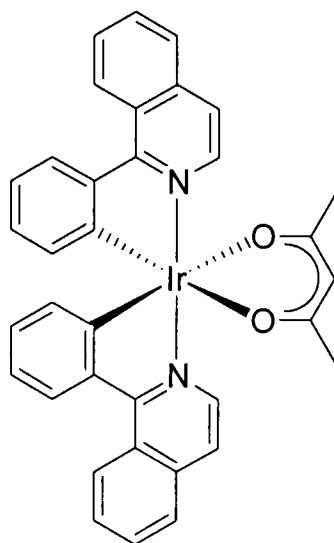


Figure 8. Structures of ligands referred to in Table 5.

Pentafluorophenyl-substituted Ir(C^N)₂(acac) complexes have also been investigated as dopants in electroluminescent devices.¹⁷¹ The bulky pentafluorophenyl groups reduce self-quenching resulting in high external EL efficiencies (11-17%). In addition, a wide gamut of colour is available by altering the position of the substituent (513-578 nm), with a blue-shift observed upon placing the electron withdrawing substituent *para* to the cyclometalating carbon atom.

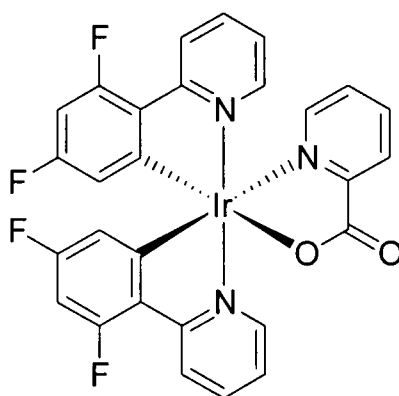
Recently iridium(III) bis(1-phenylisoquinolino-*N,C*^{2'}) acetylacetonate (Ir(piq)₂(acac)) **42** and its derivatives have received some attention as dopants for polymeric^{172,173} and low molecular weight¹⁷⁴ OLEDs. When incorporated into a polymeric PVK host, saturated red emission (CIE coordinates of $x = 0.67$, $y = 0.33$) was achieved

with $\eta_{\text{ext}} = 12\%$, and with high efficiency retained at a luminance of 4322 cd m^{-2} ($\eta_{\text{ext}} = 9.7\%$).¹⁷²



Ir(piq)₂(acac) **42**

The picolinate complex Ir(46dfppy)₂(pic) **43** is of particular note due to its high-efficiency blue emission. Incorporation of fluorine results in a blue-shift of $\sim 40 \text{ nm}$, with the introduction of picolinate contributing a further $\sim 20 \text{ nm}$.¹⁷⁵ When doped into a CBP host, a maximum luminance of 6400 cd m^{-2} was achieved, with a maximum external EL quantum efficiency of $5.7 \pm 0.3\%$.



Ir(46dfppy)₂(pic) **43**

Dendritic architectures promise improved solubility, the ability to spin-coat homogeneous films, and a reduction in self quenching. They also provide the ability to selectively tune physical and electronic properties, determined by the surface groups and core respectively. Photoluminescence studies of thin films of *fac*-Ir(ppy)₃-cored dendrimers show a steady increase in PL quantum yield with increasing generation, along with a reduction in red-shift with respect to solution studies.^{176,177} An approximately ten fold improvement is observed in electroluminescence quantum efficiency between *fac*-Ir(ppy)₃, and iridium(III)-cored dendrimer OLEDs.¹⁷⁸ By mixing with

suitable charge-transport materials, η_{ext} is raised to 10.4%.¹⁷⁹ High efficiency red emission has also been demonstrated from Ir(btp)₃ cored-dendrimers.¹⁸⁰

Alternatively, iridium(III) complexes may be attached as pendent groups to a polymeric backbone (*c.f.* Section 1.1.4.3). A series of Ir(C[^]N)₂(X[^]O) analogues have been attached along with hole-transporting carbazole groups to a non-conjugated polymer. An electroluminescent device with an electron-transporter doped layer of such polymers exhibited red, green and blue emission with reasonable efficiency (see Table 6).¹⁸¹ Ir(btp)₂(acac) has also been attached to a polyfluorene backbone, with a peak external EL quantum efficiency of 1.59%.¹⁸²

Colour	C [^] N	X [^] O	λ_{max} / nm	Peak η_{ext}
Red	2-Benzothiophen-2-yl-pyridine	Acetylacetonate	620	5.5%
Green	2-Phenylpyridine	Acetylacetonate	523	9.0%
Blue	2-(4,6-Difluorophenyl)pyridine	Pyridine-2-carboxylate	475	3.5%

Table 6. Characteristics of devices fabricated from polymer-bound Ir complexes.¹⁸¹

White emission has been achieved by either double-¹⁸³ or triple-doping¹⁷⁰ a polymer with suitable iridium complexes, reaching external EL efficiencies at 100 cd m⁻² of 2.1% and 4.9% respectively. A similar approach utilising polymer-bound iridium complexes has been reported, with CIE coordinates of ($x = 0.34, y = 0.36$) and an external EL quantum efficiency of 4.5%.¹⁸¹

Iridium(III) complexes may also be used as phosphorescent sensitizers for other dyes. Efficient intersystem crossing allows transfer of both singlet and triplet excitons from a host to a fluorescent dye *via* the additional sensitising dopant (see Figure 9). In a 4,4'-*N,N'*-dicarbazole-biphenyl (CBP) host doped in separate layers with *fac*-Ir(ppy)₃ and DCM2 **18**, emission from the fluorescent dye with a peak efficiency of 3.3±0.1% was achieved, significantly higher than the best such devices without a phosphorescent sensitizer.¹⁸⁴ Similar improvements were observed for a polymeric host doped with Ir(ppy)₂(acac) and a Nile Red emitter in a single layer.¹⁸⁵

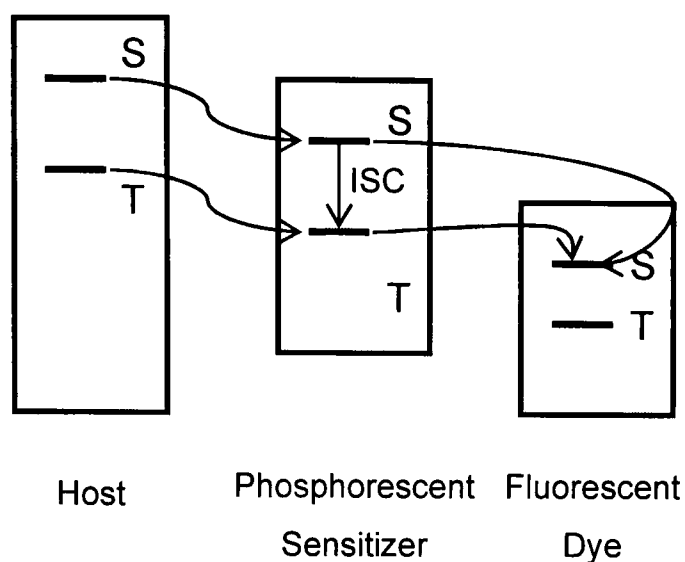


Figure 9. Phosphorescent sensitizers to improve efficiency.

Although charge-neutral dopant molecules have attracted most attention, charged transition metal complexes have also been considered for OLED applications, and formed the subject of a recent review.¹⁸⁶ Although high efficiencies may be attained for single-layer homogeneous films, long turn on times (seconds to several minutes) and poor device stability hinder their application. The first use of a transition metal incorporated a substituted phenanthroline complex of ruthenium(II),¹⁸⁷ but $[\text{Ru}(\text{bpy})_3]^{2+}$ derivatives have led most research.¹⁸⁸ Iridium-based systems to date have been based on $[\text{Ir}(\text{ppy})_2(\text{bpy})]^+$, either as a homogeneous film¹⁸⁹ or doped into a polymeric host.¹⁹⁰

1.3 Lanthanide(III) complexes and their use in electro-luminescent devices

1.3.1 The lanthanide series

The lanthanide series⁹⁶ comprises the fourteen elements from cerium (Ce) to lutetium (Lu), with lanthanum (La) also often included. Although frequently referred to (along with yttrium) as the “rare-earth elements”, most are not particularly rare, with cerium accounting for 66 ppm of the earth’s crust, and the twenty-sixth most abundant of all elements.

The electronic configurations of the lanthanide series are $[\text{Xe}]4f^n5d^06s^2$, with a small number of exceptions (Ce, $[\text{Xe}]4f^15d^16s^2$; Gd, $[\text{Xe}]4f^75d^16s^2$; Lu, $[\text{Xe}]4f^{14}5d^16s^2$). Their chemistry is dominated by the +3 oxidation state, from Ce^{3+} ($[\text{Xe}]4f^1$) to Lu^{3+} ($[\text{Xe}]4f^{14}$). Since 4f orbitals are poor at shielding electrons from the nuclear charge, a regular decrease in ionic radii is observed across the series, termed the “lanthanide contraction” (see Figure 10).

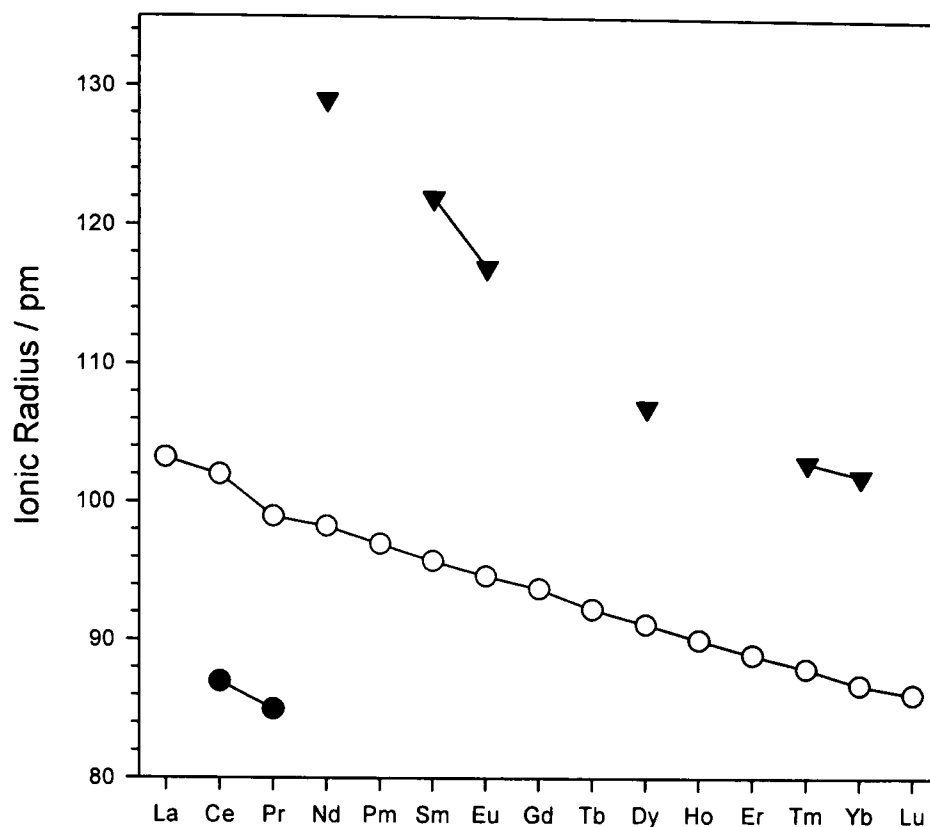


Figure 10. Variation in radii of the Ln^{2+} (▼), Ln^{3+} (○) and Ln^{4+} (●) ions across the lanthanide series (La^{3+} is included for completeness).

Due to unpaired electrons, the ions Ce^{3+} through to Yb^{3+} are paramagnetic. Unlike transition metals, the unpaired 4f electrons are localised deep in the core of lanthanide ions, effectively shielded from their chemical environment. The magnetic properties of lanthanide(III) ions (in particular Eu^{3+} and Yb^{3+}) often result in large shifts of NMR resonances leading to their application as NMR shift reagents.¹⁹¹ For gadolinium(III) there is no shifting of NMR resonances, however enhanced relaxation rates make the complexes effective as magnetic resonance imaging (MRI) contrast agents.¹⁹¹⁻¹⁹³

1.3.2 Photophysical properties of the lanthanide(III) ions

The excited states of lanthanide(III) ions are best represented by the term symbols determined by the Russell-Saunders coupling scheme. Absorption of light may promote a lanthanide ion into any energetically excited state, however this is generally followed by rapid internal conversion to the lowest lying J state of the first excited spectroscopic term. Emission may then occur to any of the J states of the ground spectroscopic term, resulting in a series of bands. For example, emission spectra of europium complexes arise by transitions from the ${}^5\text{D}_0$ excited state to the ${}^7\text{F}_4$, ${}^7\text{F}_3$, ${}^7\text{F}_2$, ${}^7\text{F}_1$ and ${}^7\text{F}_0$ levels of the ground manifold. These transitions give rise to the characteristic red luminescence of europium(III), with the highest energy ${}^5\text{D}_0 \rightarrow {}^7\text{F}_0$ transition at

579 nm, and the most intense being the $\Delta J = 1$ or $\Delta J = 2$ bands around 590 and 615 nm respectively (see Figure 11).

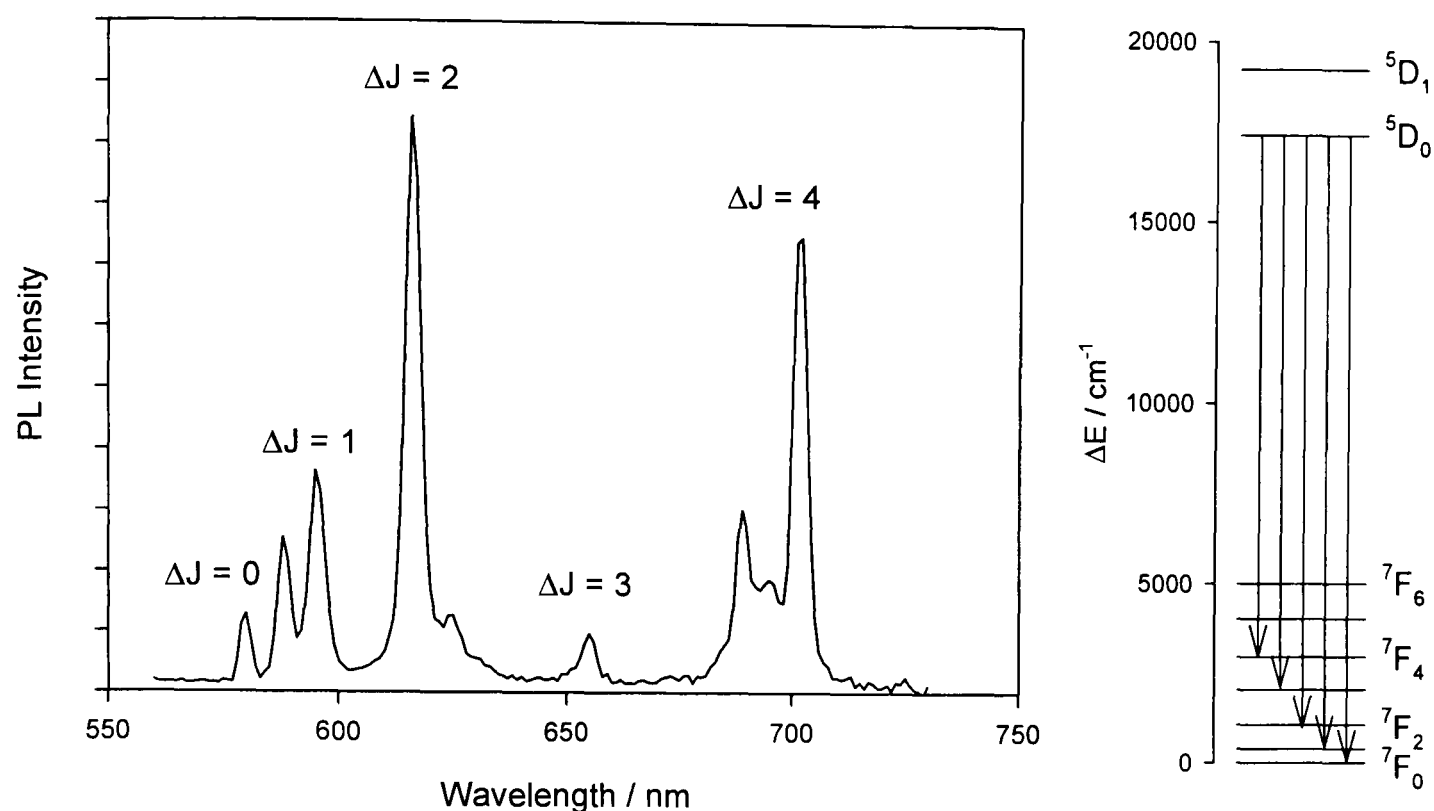


Figure 11. Typical Eu^{3+} luminescence spectrum. Also shown are the transitions responsible for the labelled bands.

Since the highly contracted, “core-like” 4f orbitals are insensitive to their surroundings, ligand-field splittings are small ($\sim 100 \text{ cm}^{-1}$). Emission wavelengths are therefore virtually independent of the coordination environment, and resemble those of the ions in the gas phase. In addition, the bands are sharp since the energies of states are not substantially affected by molecular vibrations. This means that the formally Laporte forbidden $f \rightarrow f$ transitions are very weak ($\epsilon < 1 \text{ mol}^{-1} \text{ dm}^3 \text{ cm}^{-1}$) and low transition probabilities for emission result in long natural lifetimes. This is in contrast to transition metal complexes, where mixing with asymmetric ligand vibrations partially allow $d \rightarrow d$ transitions, and absorptions are significantly more intense.

Although small, ligand-field effects cannot be ignored completely, and fine structure (of the order of 100 cm^{-1}) can be observed in some bands of Ln^{3+} spectra. Changes in fine structure may sometimes be informative, and have been used to determine HCO_3^- concentrations.¹⁹⁴ While the $\Delta J = 1$ band of europium(III) is magnetic dipole allowed, the $\Delta J = 2$ band is an electric dipole transition and significantly more sensitive to the environment. Hence the ratio of the integrated intensities of these two bands provides information on the coordination geometry of the complex.^{195,196}

Although phosphorescence from the excited states of lanthanide ions is efficient, their direct population by absorption of light is hindered by the complex's very weak absorbance spectrum. Intense light sources are required, and direct excitation may be achieved with a laser source. Alternatively, a strongly absorbing chromophore capable of transferring its excitation energy to the lanthanide ion may be used, a process termed as "sensitised emission" (see Figure 12).¹⁹⁷

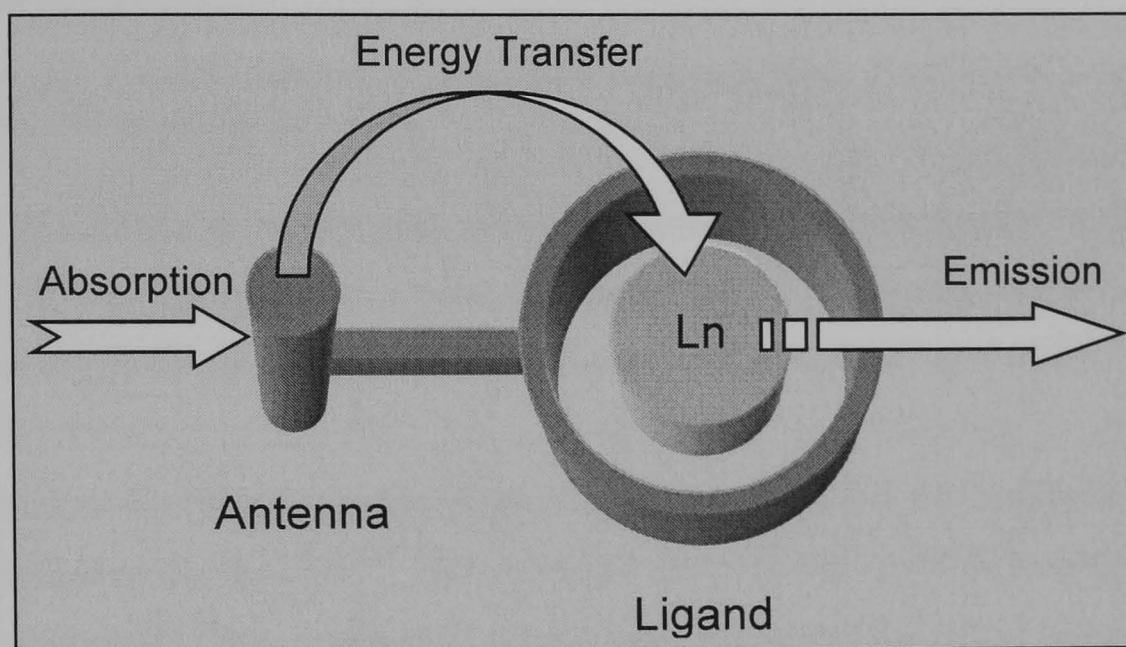


Figure 12. Sensitised emission of lanthanide(III) complexes.

For efficient sensitised emission, it is important to consider the steps involved from excitation of the antenna group to emission from the lanthanide ion (summarised in Figure 13). To maximise emission intensity, a number of criteria must be met. The sensitising chromophore must absorb strongly, followed by efficient intersystem crossing to a triplet state approximately 1700 cm^{-1} higher in energy than the lanthanide emissive state. If this energy gap is much smaller, back energy transfer (k_{BET}) will compete with emission (k_{em} , determined by the lanthanide ion). Minimisation of the distance between chromophore and lanthanide ion will further benefit emission by increasing the efficiency of intramolecular energy transfer (k_{ET} , typically $10^5\text{-}10^7\text{ s}^{-1}$ for distances of $\sim 5\text{ \AA}$ ¹⁹⁸). Any sources of quenching must also be suppressed, especially deactivation by vibrational energy transfer to energy-matched XH oscillators ($k_{\text{q}}[\text{XH}]$).¹⁹⁹ In general, the efficiency of sensitised luminescence (Φ_{em}) can be represented by equation 8, where Φ_{D} is the quantum yield of formation of the antenna state, η_{et} is the efficiency of energy transfer to the lanthanide, and k^0 and τ_{obs} are the radiative rate constant and observed lifetime respectively.²⁰⁰

$$\Phi_{\text{em}} = \Phi_{\text{D}} \eta_{\text{et}} k^0 \tau_{\text{obs}} \quad (8)$$

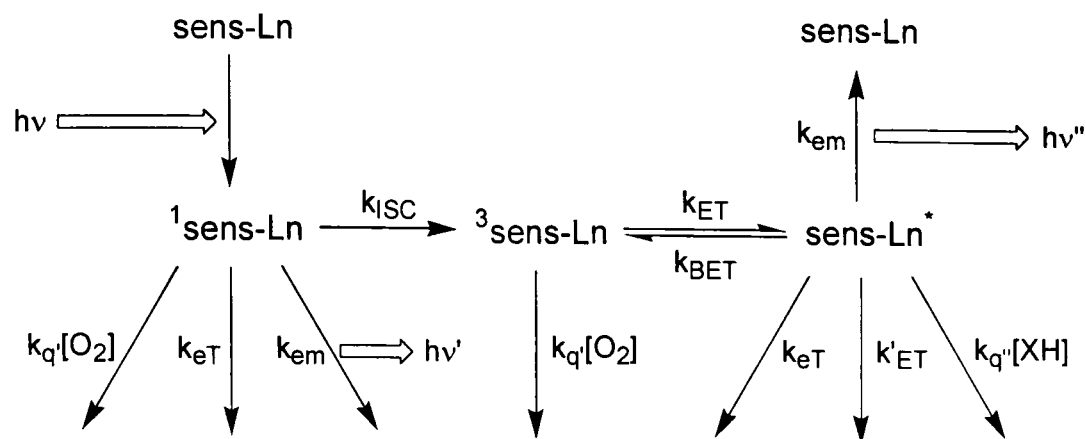


Figure 13. Kinetic scheme of sensitised emission from lanthanide complexes (adapted from reference 201).

Although large energy gaps between emissive and ground states of Eu^{3+} , Gd^{3+} and Tb^{3+} reduce the effect of vibrational quenching,²⁰²⁻²⁰⁴ directly coordinated water molecules are to be avoided. Since the efficiency of vibrational quenching is lessened for D_2O with respect to H_2O (by a factor of ~ 200 times²⁰⁵), comparison of radiative rate constants in each of these solvents allows the estimation of the solution hydration state, q . First demonstrated in 1979,²⁰⁶ Horrocks and Sudnick later proposed equations 9 and 10 for europium(III) and terbium(III) respectively, where τ is measured in ms.²⁰⁷ Parker *et al.* extended this concept by the introduction of correction terms for outer-sphere water molecules.¹⁹⁹ For europium(III) they also introduced terms for any oxygen-bound amide NH groups (equations 11 and 12, where x is the number of oxygen-bound amide NH groups).

$$q^{\text{Eu}} = 1.05(\tau_{\text{H}_2\text{O}}^{-1} - \tau_{\text{D}_2\text{O}}^{-1}) \quad (9)$$

$$q^{\text{Tb}} = 4.2(\tau_{\text{H}_2\text{O}}^{-1} - \tau_{\text{D}_2\text{O}}^{-1}) \quad (10)$$

$$q^{\text{Eu}} = 1.2\left[(\tau_{\text{H}_2\text{O}}^{-1} - \tau_{\text{D}_2\text{O}}^{-1}) - (0.25 + 0.075x)\right] \quad (11)$$

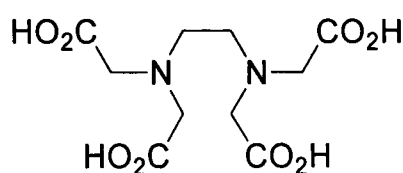
$$q^{\text{Tb}} = 5\left[(\tau_{\text{H}_2\text{O}}^{-1} - \tau_{\text{D}_2\text{O}}^{-1}) - 0.06\right] \quad (12)$$

1.3.3 Coordination and complexation properties of the lanthanide(III) ions

Due to the contracted nature of the lanthanide 4f orbitals, covalent bonding character is very rare, with the charge-dense metal ions favouring electrostatic interactions. Typical hard metal behaviour is observed, with a preference for anionic donors such as carboxylates and phosphates, as well as polarisable neutral donors such as amines and amide oxygens. Since bonding is electrostatic in nature, coordination

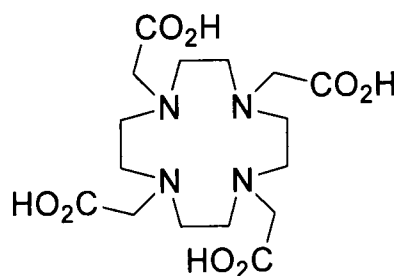
geometries are poorly directional and determined by steric factors. Along with the large ionic radii this results in high coordination numbers, typically eight or nine.

Dissolution of lanthanide(III) salts in water generally leads to the nine-coordinate lanthanide aqua ions $[\text{Ln}(\text{H}_2\text{O})_9]^{3+}$.^{96,200} The high thermodynamic stabilities of such aquated species result in dissociation of many lanthanide complexes in aqueous solution. Design of water stable complexes requires multidentate charged ligands; for example acetylacetonate (acac⁻) forms a tris-complex with lanthanide(III) ions. More thermodynamically stable complexes may be formed with polydentate ligands such as ethylenediaminetetraacetic acid (EDTA) **44** ($K \sim 10^{17}$). Relevant features include five-membered chelate rings, hexadentate binding and a large negative charge. In addition, the loss of water molecules results in a high entropic contribution to stability. Although stable thermodynamically, such complexes are not kinetically stable, with rapid ligand exchange occurring in aqueous solution.

EDTA **44**

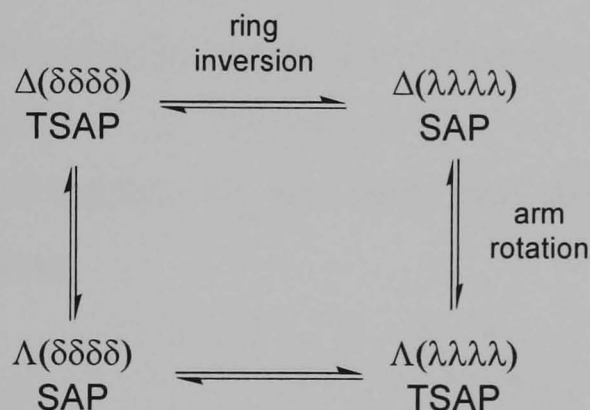
1.3.3.1 Europium complexes with macrocyclic ligands

For high thermodynamic and kinetic stabilities more rigid ligands are preferable, in particular macrocyclic ligands.^{200,201,208} For example 1,4,7,10-tetraazacyclododecane-1,4,7,10-tetra(acetic acid) (DOTA) **45** forms highly stable complexes with lanthanide(III) ions ($K \sim 10^{28}$ for europium(III)²⁰⁹).

DOTA **45**

Lanthanide complexes of DOTA may adopt four geometries; all with a square [3333] ring conformation, and differentiated by their NCCO (Δ/Λ) and NCCN (δ/λ) torsion angles. This results in two enantiomeric pairs; the square-antiprismatic (SAP) geometry ($\Lambda(\delta\delta\delta\delta)$ and $\Delta(\lambda\lambda\lambda\lambda)$) with an N_4/O_4 twist angle of 40° , and the twisted

square-antiprismatic (TSAP) geometry ($\Delta(\delta\delta\delta\delta)$ and $\Lambda(\lambda\lambda\lambda\lambda)$) with an N_4/O_4 twist angle of 29° . For the larger lanthanides (La^{3+} - Nd^{3+}) TSAP is preferred, with SAP favoured for smaller ions (Sm^{3+} - Er^{3+}).^{210,211} In solution these four forms are in dynamic equilibrium *via* ring inversion ($\delta\delta\delta\delta \leftrightarrow \lambda\lambda\lambda\lambda$) and arm rotation ($\Delta \leftrightarrow \Lambda$) (see Scheme 1). Computational studies of these processes suggest that although arm rotation is a concerted process, ring inversion involves a stepwise rotation of the four ethylene groups.²¹² The rate of ring inversion is relatively slow ($\sim 50 \text{ s}^{-1}$ at 298 K), while arm rotation is significantly faster.^{210,213} Both ring inversion²¹⁴ and arm rotation²¹⁵⁻²¹⁷ may be frozen on the NMR timescale by introduction of bulky groups on the ring and arms respectively.



Scheme 1. Interconversion pathways for lanthanide DOTA complexes in solution.

Lanthanide DOTA complexes crystallise in any of the four stereoisomeric conformations dependent on the size of the lanthanide ion.²¹⁸ The most common solid-state structure is the regular square antiprismatic conformation, and is the geometry observed for $Na[Eu(DOTA)(H_2O)] \cdot 4H_2O$ (see Figure 14).²¹⁹ The N_4 and O_4 planes are parallel to each other, with a twist angle dependent on the geometry type. The metal ion does not occupy the centre of the polyhedron, but is shifted towards the O_4 face.

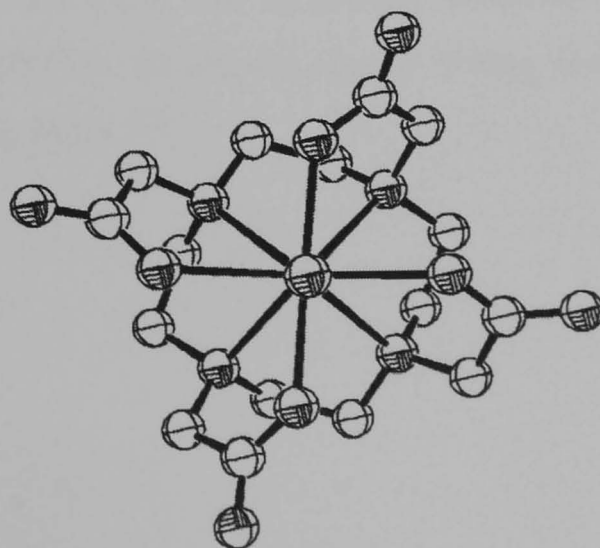
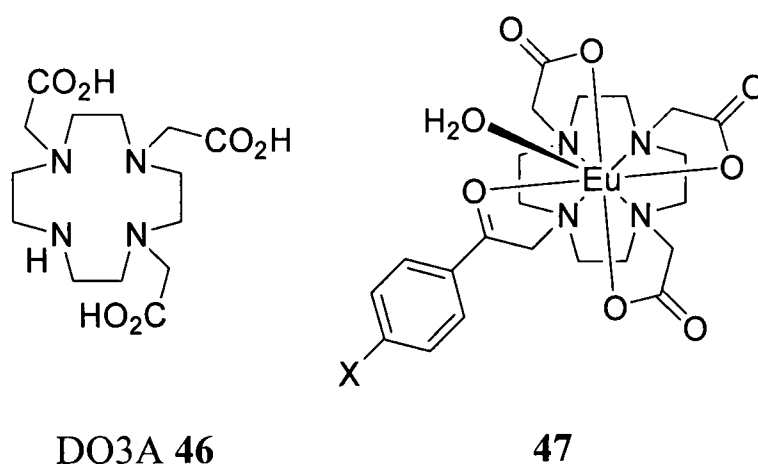


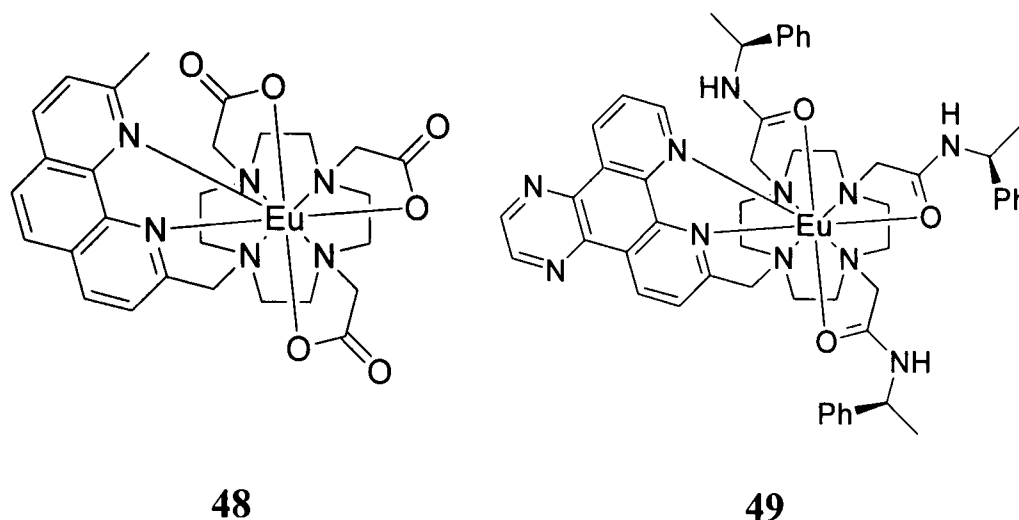
Figure 14. Crystal structure of $Na[Eu(DOTA)(H_2O)] \cdot 4H_2O$.²¹⁹ Cation and water of crystallisation omitted for clarity.

For most luminescent applications,²²⁰ a sensitising group (see Section 1.3.2) must be attached to the macrocyclic ligand. 1,4,7,10-Tetraazacyclododecane-1,4,7-tris(acetic acid) (DO3A) **46** is ideal for this purpose since its complexes show a high stability,²²¹ with a secondary nitrogen capable of being alkylated with a sensitising chromophore.

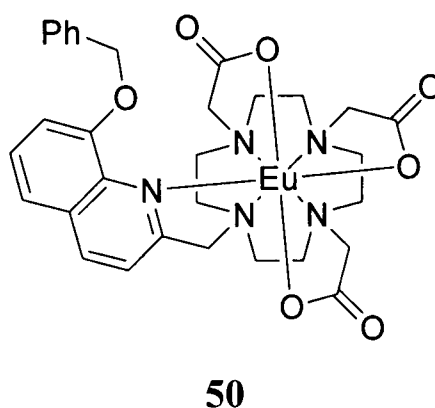
Energy transfer to coordinated lanthanides has been investigated for complex **47** by tuning the triplet energy of the substituent (X = H, 25 300 cm⁻¹ in H₂O; X = OMe, 21 000 cm⁻¹ in H₂O; X = NMe₂, 20 000 cm⁻¹ in H₂O).²²² The improved correlation of donor triplet energy with europium(III) levels (E(⁵D₀) = 17 300 cm⁻¹, E(⁵D₁) = 19 000 cm⁻¹) upon methoxy-substitution results in an increase in energy transfer efficiency. By comparing the shapes of sensitised emission spectra, a systematic increase in relative intensity of the hypersensitive $\Delta J = 2$ band occurs in the series X = H, OMe, NMe₂, rationalised by the increasing Ar=C-O⁻ character of the acetophenone carbonyl group.



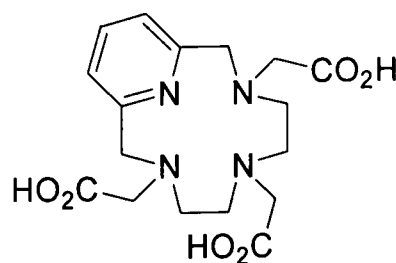
In complex **48**, the phenanthroline moiety is found to bind to europium through both nitrogen atoms, with no inner-sphere water molecules.^{223,224} It exhibits a high photoluminescence quantum yield for sensitised emission of 0.21. The tetraazatriphenylene derivatised complex **49** shows similar strong luminescence, and has been investigated as a probe for DNA.²²⁵



Another attempt to eliminate inner-sphere water molecules, complex **50** exhibits a photoluminescence quantum yield of 0.06 and a q value of 0.21, consistent with the exclusion of all inner-sphere water molecules.²²⁶ The rate constants for non-radiative processes were more than double those of a more remote 8-hydroxyquinoline derivative, despite a significantly greater quantum yield. This apparent anomaly was attributed to an improved efficiency of energy transfer from the sensitising chromophore.



An alternative to pendent sensitising-chromophores is to integrate this group directly into the macrocyclic ring. This has been reported for the europium complex of 3,6,9,15-tetraazabicyclo[9.3.1]pentadeca-1(15),11,13-triene-3,6,9-triacetic acid (111Py12N4) **51**.²²⁷ This exhibits a photoluminescence quantum yield of only 0.029, most likely due to the presence of two bound water molecules.



111Py12N4 **51**

1.3.4 Electroluminescence of lanthanide complexes

Much work has been reported on the application of lanthanide complexes as emitters in electroluminescent devices, the subject of some recent review articles.^{228,229} Early studies utilised terbium(III)²³⁰ and europium(III)²³¹ complexes for their sharp green and red emission respectively. Later work with thulium(III) produced a blue emitting OLED,²³² difficult to achieve with most phosphorescent dyes. Although initially chosen for their sharp emission spectra (FWHM < 5 nm), lanthanide complexes exhibit phosphorescence, and potentially allow 100% internal EL quantum efficiency (see Section 1.1.6). Also, since emission from lanthanide(III) ions is virtually independent of the nature of the ligands, structural modifications may be used to tune physical properties with little or no change in emission colour.

1.3.4.1 Visible electroluminescence of Eu^{3+} and Tb^{3+} complexes

The first OLED incorporating an organolanthanide emitter was demonstrated in 1990 for a homogeneous layer of terbium(III) tris-(acetylacetonate) ($\text{Tb}(\text{acac})_3$) **52**.²³⁰ Bright green emission peaking at 544 nm was observed from the $^5\text{D}_4 \rightarrow ^7\text{F}_5$ transition of the Tb^{3+} ion (see Figure 15). A year later, the same group reported electroluminescence from a europium(III) tris-(thenoyltrifluoroacetate)₃ ($\text{Eu}(\text{TTFa})_3$) **53** doped poly(methylphenylsilane) film.²³¹ Red emission was observed with a turn-on voltage of 12 V, although maximum luminance was only 0.3 cd m^{-2} .

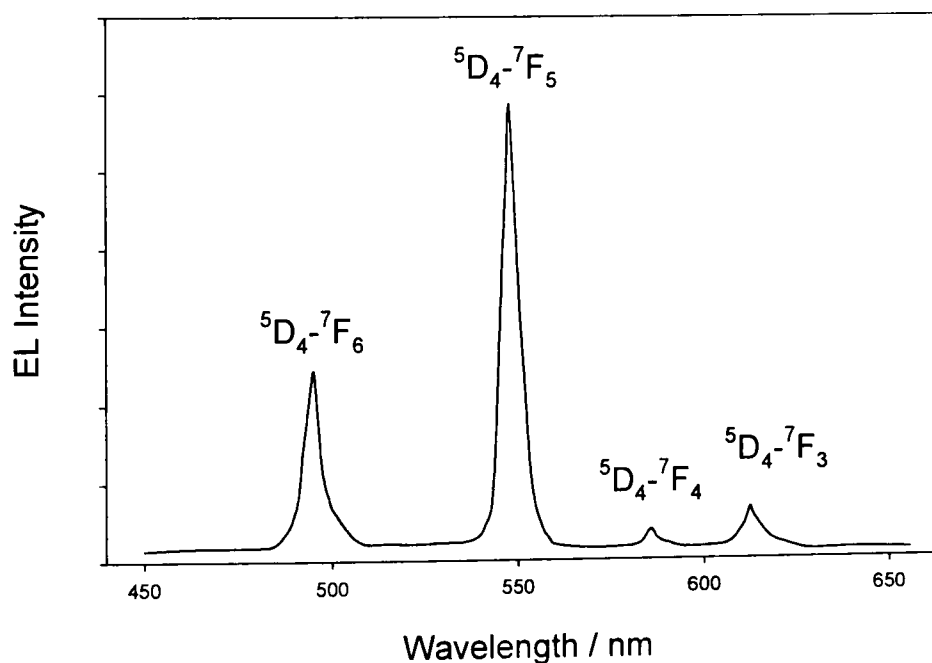
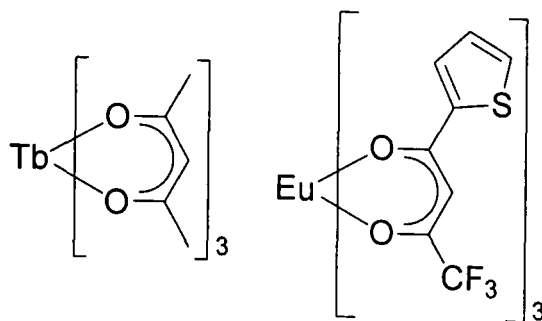
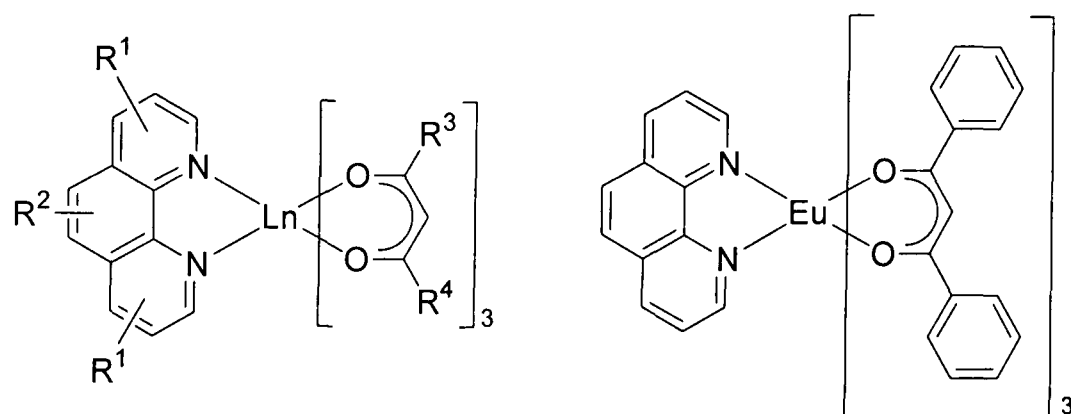


Figure 15. Electroluminescence spectrum of a ITO/TPD/ $\text{Tb}(\text{acac})_3$ /Al device (adapted from reference ²³⁰).



Tb(acac)₃ **52** Eu(TTFA)₃ **53**

Whilst a large volume of work has been published on europium(III) and terbium(III) emitters, there is very little variation in ligand structure. The generic Ln(phen)(acac)₃ structure **54** is by far the most common, with the 1,10-phenanthroline (phen) ligand saturating the coordination number of the lanthanide ion, improving the fluorescence intensity, volatility and stability. One of the first such devices, ITO/TPD/Eu(phen)(DBM)₃ **55**:PBD/Alq₃/Mg:Ag, resulted in a maximum luminance of 460 cd m⁻² ($\lambda_{\text{max}} = 614$ nm), a greater than 10³ fold improvement over **53**.²³³

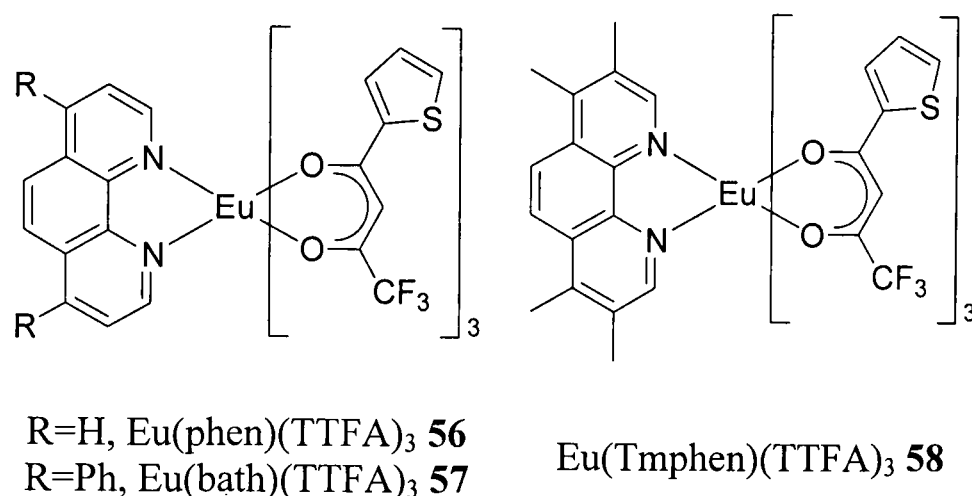


Generic Ln(phen)(acac)₃ structure **54** Eu(phen)(DBM)₃ **55**

Tuning of carrier transport properties,²³⁴ isolation of the emitting region from the cathode,²³⁵ optimisation of device structure²³⁶ and use of a Tb(phen)(acac)₃ sensitiser²³⁷ have all resulted in improved emission efficiencies from europium(III). An external EL quantum efficiency of 4.6% has been achieved, although only at low current densities (0.01 mA cm⁻²).²³⁶ Pure layers of Tb(phen)(acac)₃ have also been investigated,^{238,239} with a maximum luminance of 210 cd m⁻².²³⁹ The improved carrier transport properties of Tb(bath)(acac)₃ result in a luminance of 77 cd m⁻², compared to 30 cd m⁻² for Tb(phen)(acac)₃ under the same conditions.²⁴⁰

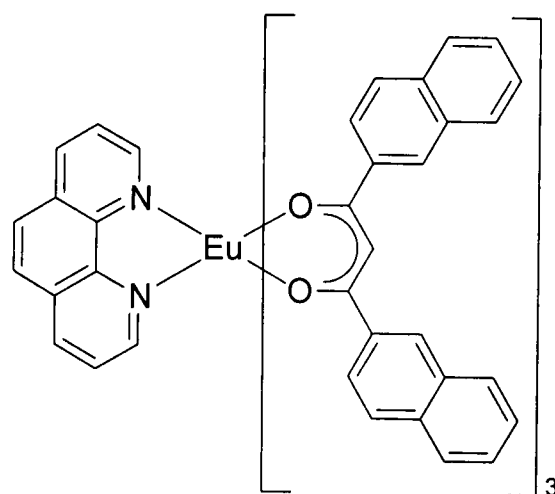
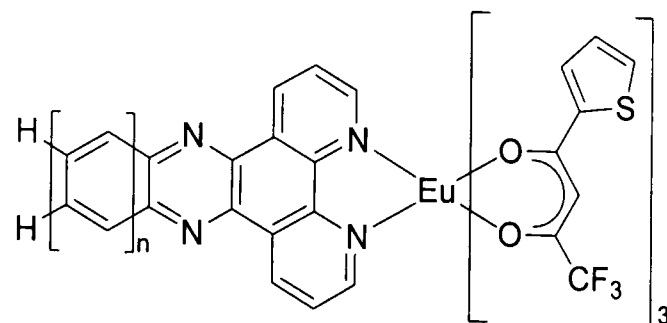
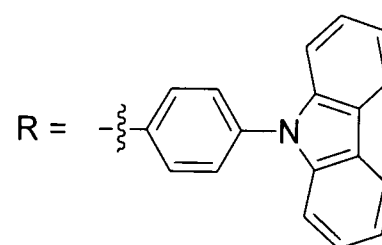
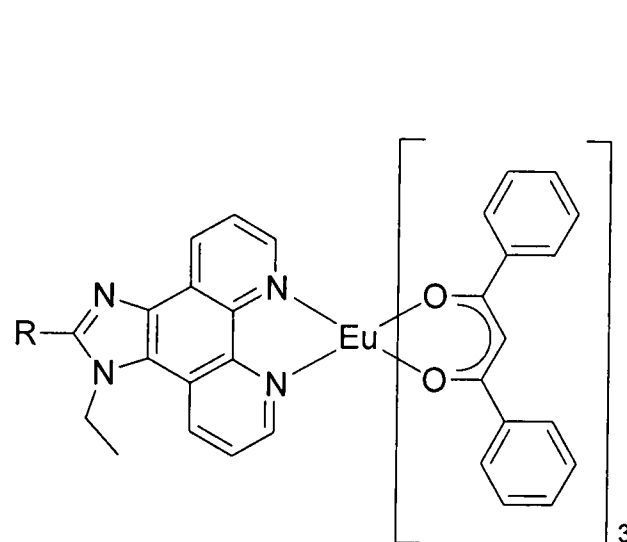
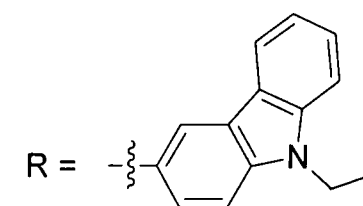
Thenoyltrifluoroacetate (TTFA) is a popular alternative to acac, and homogeneous films of Eu(phen)(TTFA)₃ **56** achieved a luminance of 10 cd m⁻² in

optimised devices.²⁴¹ Microcavity designs with sublimed layers of $\text{Eu}(\text{phen})(\text{TTFA})_3$ **56**²⁴² and $\text{Eu}(\text{bath})(\text{TTFA})_3$ **57**²⁴³ result in highly directional, monochromatic emission at 617 nm, but poor brightness ($\sim 30 \text{ cd m}^{-2}$). Much improved performance has been obtained by doping $\text{Eu}(\text{phen})(\text{TTFA})_3$ into low molecular weight²⁴⁴ and polymeric²⁴⁵ hosts. Further enhancements have been reported upon introduction of methyl groups in $\text{Eu}(\text{Tmphen})(\text{TTFA})_3$ **58** ($\eta_{\text{lum}} = 800 \text{ cd m}^{-2}$, $\eta_{\text{ext}} = 4.3\%$).²⁴⁶ Recently it has been shown that co-doping this with the fluorescent dye DCJTb results in a maximum luminance as high as 2450 cd m^{-2} .²⁴⁷

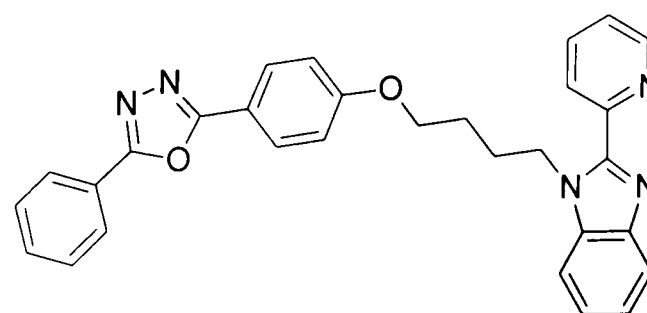
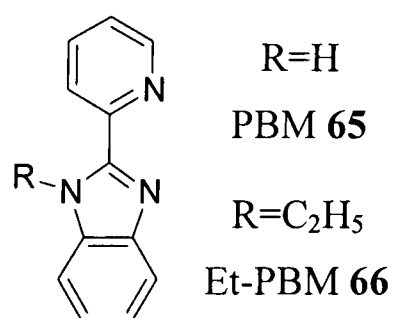


A photoexcited film of $\text{Eu}(\text{phen})(\text{acac})_3$ -doped cyano-substituted PPP results in solely polymer emission, since there is no overlap between polymer emission and europium complex absorption spectra.²⁴⁸ The red-shifted absorption of $(\text{Eu}(\text{phen})(\text{DNM})_3)$ **59** results in sufficient overlap, and emission is solely from the dopant. A similar improvement in electroluminescence efficiencies is however attributed to efficient trapping of charge carriers. A progressive increase in brightness was observed with extended conjugation in the series: $\text{Eu}(\text{phen})(\text{TTFA})_3$ (500 cd m^{-2}) **56**,²⁴⁴ $\text{Eu}(\text{Pyphen})(\text{TTFA})_3$ **60** (1309 cd m^{-2})²⁴⁹ and $\text{Eu}(\text{DPPz})(\text{TTFA})_3$ **61** (1670 cd m^{-2}).²⁵⁰ $\text{Eu}(\text{BDPz})(\text{TTFA})_3$ **62** however exhibited incomplete energy transfer with predominantly ligand-centred emission.²⁴⁹

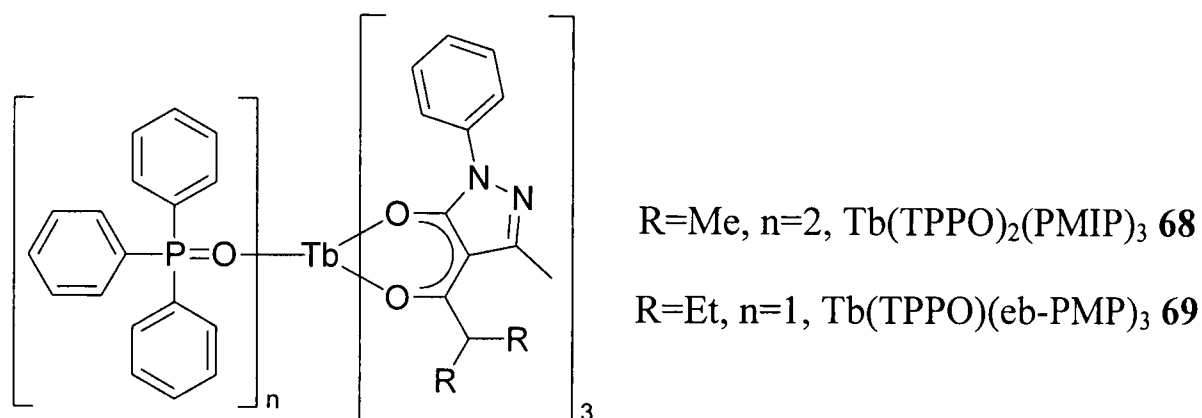
Covalent attachment of a hole-transporting carbazole group, either *N*-bound ($\text{Eu}(\text{CPIP})(\text{DBM})_3$ **63**)²⁵¹ or connected at the 4-position ($\text{Eu}(\text{phencarz})(\text{DBM})_3$ **64**),^{252,253} allows the fabrication of pure films of europium complex with brightnesses of $\sim 1500 \text{ cd m}^{-2}$. The results attainable by this approach are exemplified by the improvement in brightness with increasing hole-transport ability in the phenyl ($\text{R} = \text{Ph}$, 42 cd m^{-2})²⁵⁴, dimethylphenylamine ($\text{R} = \text{C}_6\text{H}_4\text{NMe}_2$, 230 cd m^{-2})²⁵⁵ and triphenylamine ($\text{R} = \text{C}_6\text{H}_4\text{NPh}_2$, 1305 cd m^{-2})²⁵⁶ analogues.

Eu(phen)(DNM)₃ **59**n=0, Eu(Pyphen)(TTFA)₃ **60**n=1, Eu(DPPz)(TTFA)₃ **61**n=2, Eu(BDPz)(TTFA)₃ **62**Eu(CPIP)(DBM)₃ **63**Eu(phencarz)(DBM)₃ **64**

Use of the bidentate 2-(2-pyridyl)benzimidazole (PBM) ligand **65** in pure films of Eu(PBM)(DBM)₃²⁵⁷ and Eu(PBM)(TTFA)₃²⁵⁸ results in poor performance, however ethyl substitution (Et-PBM **66**) increases the brightness to 180 cd m⁻² and 36.6 cd m⁻² respectively. Substantial further improvements were gained by appending a hole-transporting oxadiazole group (OXD-PBM **67**) in a simple double-layer device ($\eta_{\text{lum}} = 322 \text{ cd m}^{-2}$, $\eta_{\text{ext}} = 1.7\%$).²⁵⁹

OXD-PBM **67**

Although pure films of $\text{Eu}(\text{TPPO})(\text{DBM})_3$ ²⁶⁰ and $\text{Eu}(\text{TTPO})_2(\text{TTFA})_3$ ²⁶¹ (TPPO = triphenylphosphine oxide) have been discussed, little quantitative electroluminescence data was reported. When a 1:9 mixture of $\text{Eu}(\text{TPPO})_2(\text{TTFA})_2$ and $\text{Gd}(\text{TPPO})_2(\text{TTFA})_2$ was doped into a polymeric host, red emission (CIE: $x = 0.55$, $y = 0.36$) was observed at 300 K, but a temperature dependence of energy transfer resulted in green-white emission (CIE: $x = 0.35$, $y = 0.49$) at 77 K.²⁶² Pure films of $(\text{Tb}(\text{TPPO})_2(\text{PMIP})_3)$ **68** reach 920 cd m^{-2} at a drive voltage of 18 V, although hole-transport dominates.²⁶³ Balanced charge injection in $(\text{Tb}(\text{TPPO})(\text{eb-PMP})_3)$ **69** results in a remarkable luminance of $12\,000 \text{ cd m}^{-2}$ from optimised devices.²⁶⁴



Of significant note is the incorporation of europium complexes into side chains of conjugated polymers.²⁶⁵ Alternatively, non-conjugated polymers have been functionalised with hole transporting carbazole groups and europium(III) emitters.²⁶⁶ More recently, a non-conjugated polymer has been reported with pendent electron-transporting, hole-transporting and terbium(III) emitter groups.²⁶⁷ Although red and green electroluminescence was observed respectively, the brightnesses were poor.

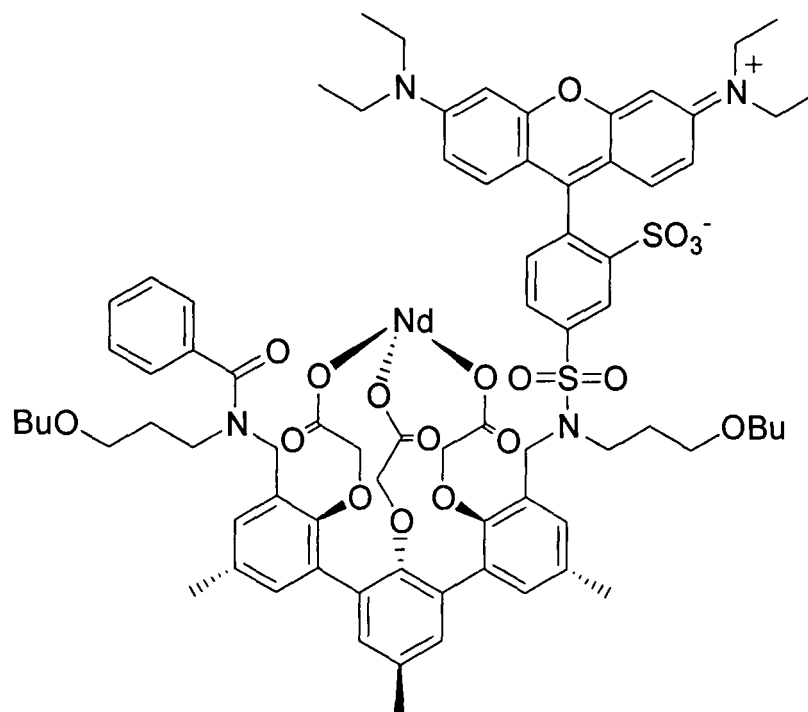
1.3.4.2 Electroluminescence from other lanthanide complexes

Although europium(III) and terbium(III) are the most common organolanthanide electrophosphorescent emitters, orange emission has been observed from complexes of europium(II),²⁶⁸ samarium(III),²⁶⁹ ytterbium(III)²⁷⁰ and erbium(III),²⁷¹ with yellow emission from neodymium(III).²⁷² Much sought after blue emission has been reported from electroluminescent devices of thulium(III) complexes,²³² with lutetium(III) achieving a luminance of 1010 cd m^{-2} from exciplex formation with a diamine hole-transport material.²⁷³

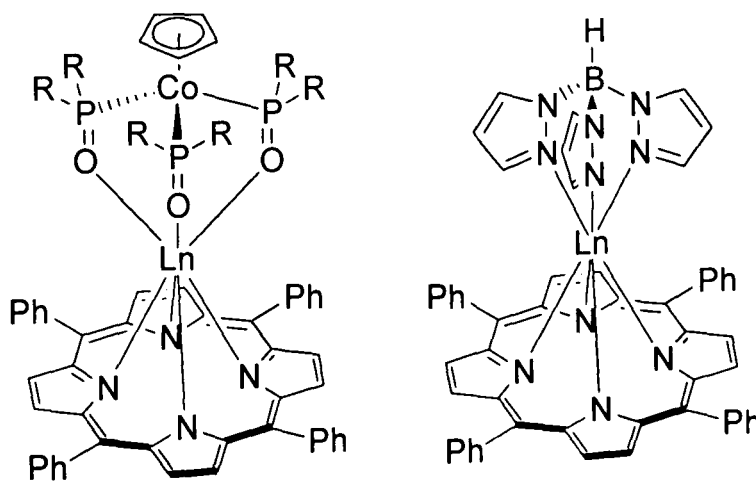
Of interest for optical fibre communication, biomedical, sensor and defence applications are infrared and near-infrared emission, realized for devices containing neodymium(III),²⁷⁴⁻²⁷⁶ holmium(III),^{277,278} erbium(III),^{276,277,279,280} thulium(III)^{277,279} and

ytterbium(III)^{276,277,281,282} complexes. These are of particular note from a structural standpoint, since many have deviated from the simple Ln(phen)(acac)₃ motif, partly since the restrictions upon sensitizer triplet state have been lifted.

Analogous to Alq₃, room-temperature electroluminescence at 1540 nm was reported for an erbium tris(8-hydroxyquinoline) complex.²⁸⁰ The Nd³⁺ complex **70** improves efficiency by appending a lissamine sensitizer group to a tricarboxylate binding fragment.²⁷⁵

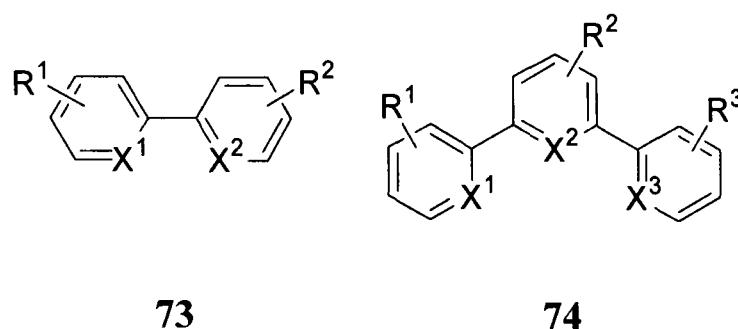
NdLs **70**

The lanthanide tetraphenylporphyrin complexes **71** and **72** have also been investigated as dopants in near-infrared electroluminescent devices.^{276,277,282} The bulky ligands protect the lanthanide from its surrounding environment, and minimise self-quenching. Although the Yb³⁺ complex of **71** is highly photoluminescent, external EL quantum efficiencies were limited to ~0.1%.²⁷⁶

Ln(TPP)(Co complex) **71**Ln(TPP)(TP) **72**

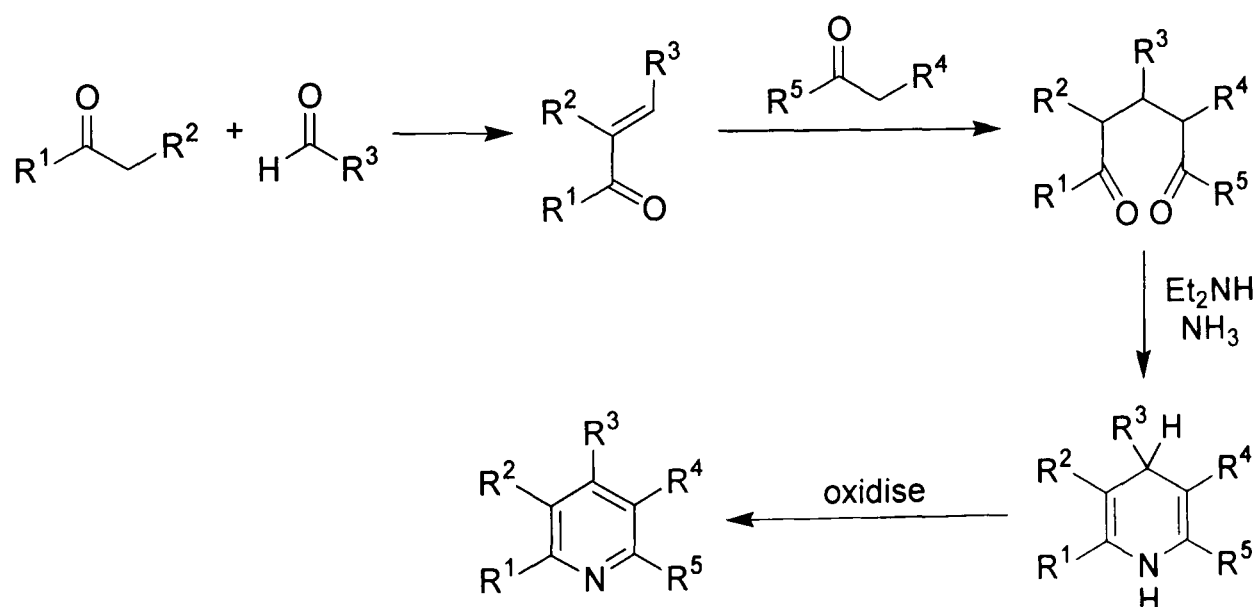
1.4 Synthesis of oligoaromatic ligands for iridium

The synthesis of ligands of the form **73** and **74** may be approached by two general methodologies. The classical route uses ring-closing reactions to form pyridyl rings as required, with any substituents introduced in the starting materials (see Section 1.4.1). The other route uses cross-coupling reactions to form C–C bonds between individual rings, or to append substituents (see Section 1.4.2). A recent report reviews progress in both areas and their application to the synthesis of 4'-substituted 2,2':6',2''-terpyridines (structure **74**, $X^1=X^2=X^3=N$).²⁸³



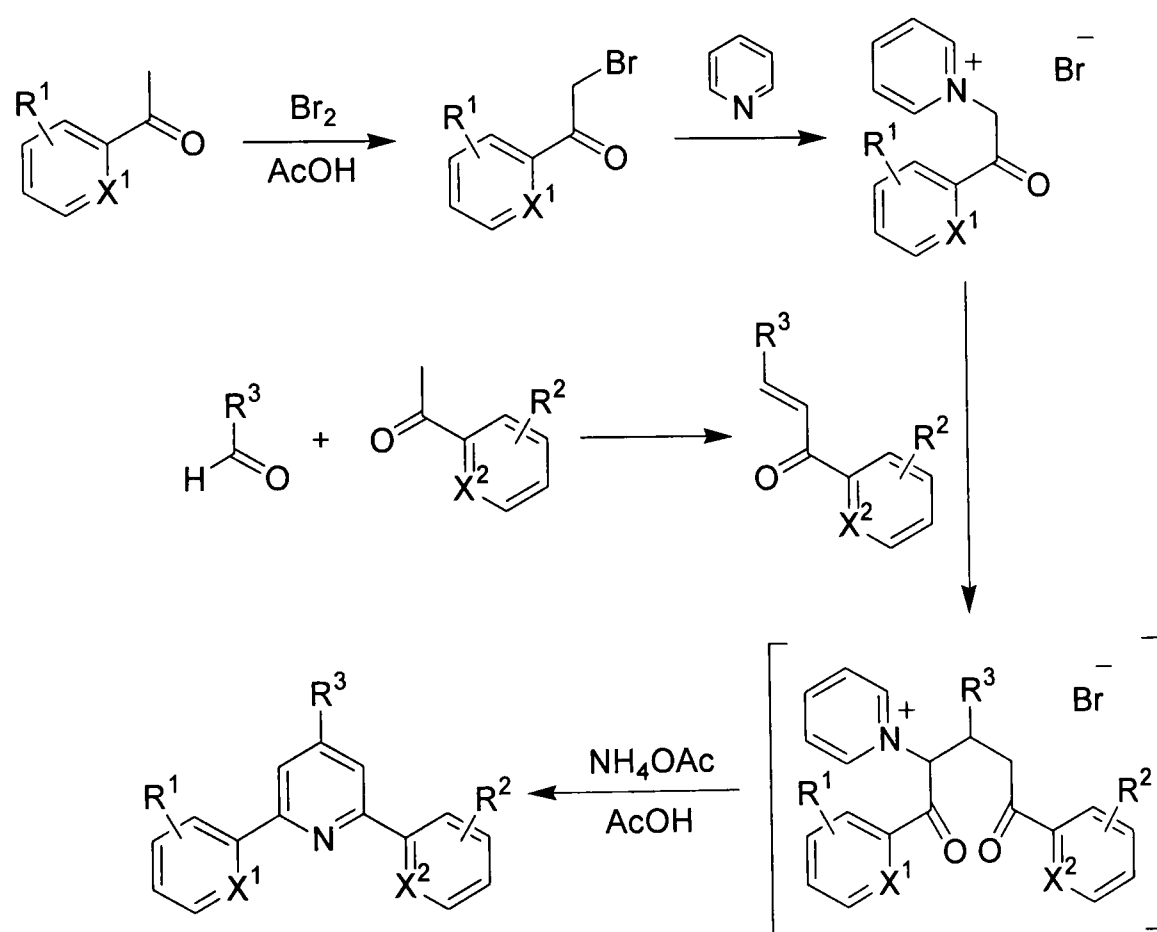
1.4.1 Synthesis of ligands *via* ring-closing reactions

The synthesis of pyridine rings by ring-closing reactions forms the basis of the classical Hantzsch pyridine synthesis (see Scheme 2).²⁸⁴ A diketone is synthesised by a sequence of nucleophilic addition, elimination of water and Michael addition. Insertion of ammonia and ring closing results in the dihydropyridine, which may be readily oxidised (*e.g.* with nitric acid) to the desired pyridine derivative. As can be seen, this provides great flexibility in substitution of the pyridine ring.



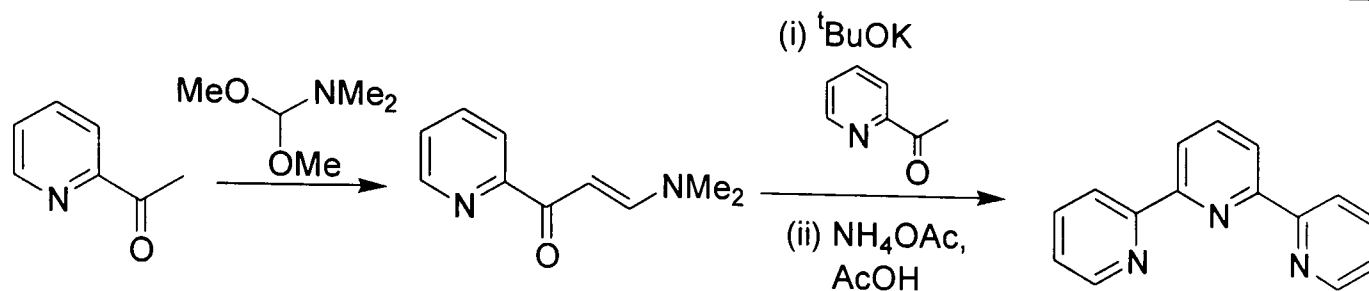
Scheme 2. The Hantzsch pyridine synthesis.

The synthesis of a number of aryl-substituted bipyridine and terpyridine derivatives by the Hantzsch route was reported in 1956.²⁸⁵ An extension of this methodology resulted in the Kröhnke synthesis of pyridines (see Scheme 3), first published in 1962.²⁸⁶ Formation of the pyridinium salt of the ketone activates the α -hydrogens towards Michael addition, and provides a good leaving group circumventing the need for an additional oxidation step. Alternatively, the use of a 2-oxo-4-aryl-but-3-enoic acid in the Michael addition step forms the corresponding bipyridine-carboxylic acid derivative. This may be readily decarboxylated to produce aryl-substituted bipyridines. A review of the application of the Kröhnke synthesis for a large number of pyridine derivatives was published in 1976.²⁸⁷ More recently, similar compounds have been prepared *via* a one-pot solvent-free route.^{288,289}



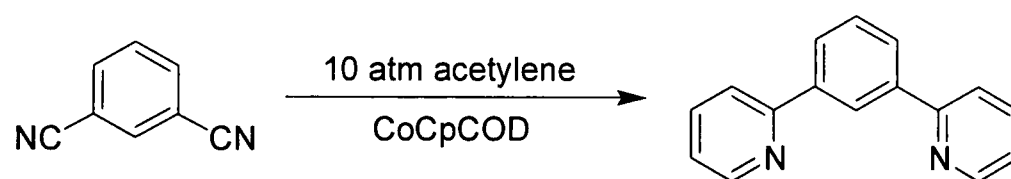
Scheme 3. The Kröhnke pyridine synthesis (X = C or N).

Although applicable to a large number of pyridine derivatives, the Kröhnke synthesis requires an aromatic group in the 4-position. This limitation was overcome by the use of an α -oxoketene dithioacetal in the synthesis of 4'-methylthio-2,2':6'.2''-terpyridine.²⁹⁰ Reduction to terpyridine itself may be afforded by reaction with sodium borohydride in the presence of nickel(II) chloride. This extra step was avoided in a later synthesis by the use of an enaminone (see Scheme 4).²⁹¹ A similar preparation of 2,6-diphenylpyridine has been reported *via* 3-dimethylamino-1-phenyl-propan-1-one.²⁸⁶



Scheme 4. Synthesis of 2,2':6',2''-terpyridine via an enaminone.

An alternative approach is to ring-close the outer pyridyl rings, facilitating the introduction of a central phenylene group. Such a reaction has been reported for the synthesis of 2,2':6',2''-terpyridine via formation of an octahydro-terpyridine.²⁹² Although high-yielding, this route was laborious and very costly. Cyclisation of the pendent pyridyl rings has also succeeded in high yield (90%) by a cyclotrimerisation reaction of 1,3-dicyanobenzene with acetylene in the presence of a cobalt catalyst (see Scheme 5).²⁹³⁻²⁹⁵ This route however is extremely hazardous due to the use of high-pressure acetylene. Although the cyclisation of butadiene with benzonitrile can be envisaged, the only reported reaction of these two reagents to form a pyridyl derivative involves nucleophilic attack at the nitrile, not cyclisation.²⁹⁶



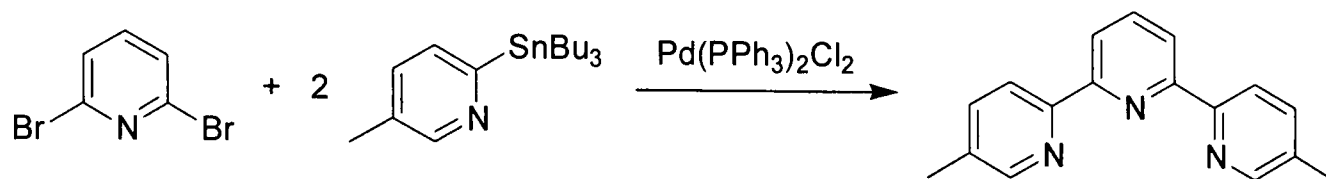
Scheme 5. Use of a cyclotrimerisation reaction to form pendent pyridyl rings.

1.4.2 Synthesis of ligands via cross-coupling reactions

Ever since the report by Murahashi *et al.* of such reactions with Grignard reagents,²⁹⁷ the palladium-catalysed cross-coupling of organometallics has become increasingly used in organic chemistry.²⁹⁸ The field encompasses a range of organometallic coupling reagents for aryl-aryl bond formation including organoboron (Suzuki coupling),²⁹⁹ organosilicon (Hiyama coupling),³⁰⁰ organostannane (Stille coupling)^{301,302} and organozinc (Negishi coupling)³⁰³ compounds.

The use of Suzuki cross-coupling reactions in the synthesis of polypyridyl compounds was reported as early as 1988 for 3,3'- and 3,4'-bipyridine derivatives.³⁰⁴ Although a successful route to 1,3- and 1,4-di(pyrid-2-yl)benzene,³⁰⁵ difficulties are associated with the preparation and use of pyridine-2-boronic acids. Hence Stille and Negishi couplings are favoured for the preparation of 2-pyridyl derivatives. First

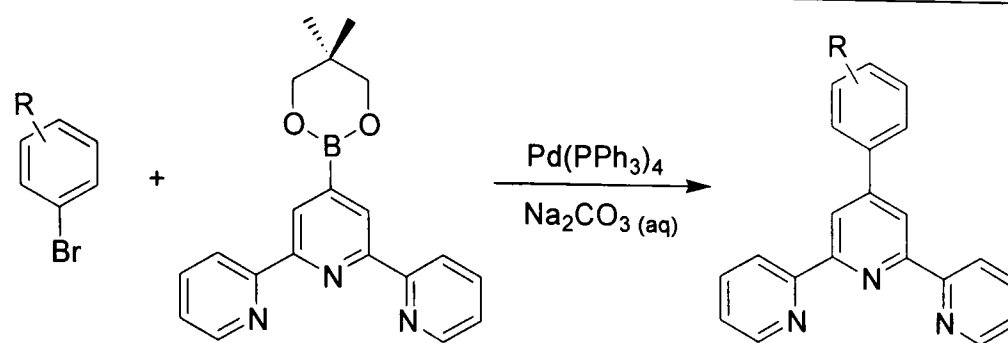
demonstrated in 1996 by Cárdenas and Sauvage,³⁰⁶ Stille couplings have become popular for the synthesis of a number of oligopyridine compounds. They allow the straightforward synthesis of otherwise poorly accessible 5,5''-disubstituted 2,2':6',2''-terpyridine derivatives (see Scheme 6),³⁰⁶ as well as the introduction of strongly electron withdrawing 4'-groups.³⁰⁷



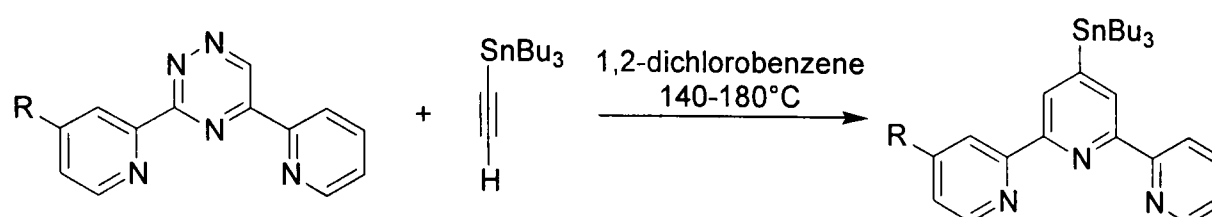
Scheme 6. The synthesis of 5,5''-dimethyl-2,2':6',2''-terpyridine by a Stille coupling.

Since the absence of a central pyridine ring makes conventional ring-closing methodologies unsuitable, Stille couplings have been widely used in the preparation of di(pyrid-2-yl)benzene analogues.³⁰⁸ By control of reaction stoichiometry, selective disubstitution was obtained in the reaction of trimethylstannylpyridine with 1,3,5-tribromobenzene to give 5-bromo-1,3-di(pyrid-2-yl)benzene in 35% yield.³⁰⁹ In an attempt to circumvent the need for highly toxic tin reagents, a series of 5-substituted 1,3-di(pyrid-2-yl)benzene derivatives have been reported in reasonable yield *via* a Negishi cross-coupling procedure.³¹⁰

Alternatively, cross-coupling reactions may be used to attach pendent groups onto a previously prepared ligand. This is particularly useful for the attachment of strongly electron-withdrawing groups at the 4'-position of 2,2':6',2''-terpyridine, hindered in the Kröhnke synthesis owing to inhibition of the Michael reaction step. A large number of such 4'-aryl-substituted compounds have been prepared *via* Suzuki cross-coupling reactions (see Scheme 7).^{311,312} This methodology has even been extended to the coupling of ruthenium complexes to aryl-groups.³¹³ Attachment of pendent groups by Stille couplings has been facilitated by the novel synthesis of a 4'-tributylstannyl-2,2':6',2''-terpyridine (see Scheme 8), which may be converted to the bromide or coupled with arylhalides.³¹⁴



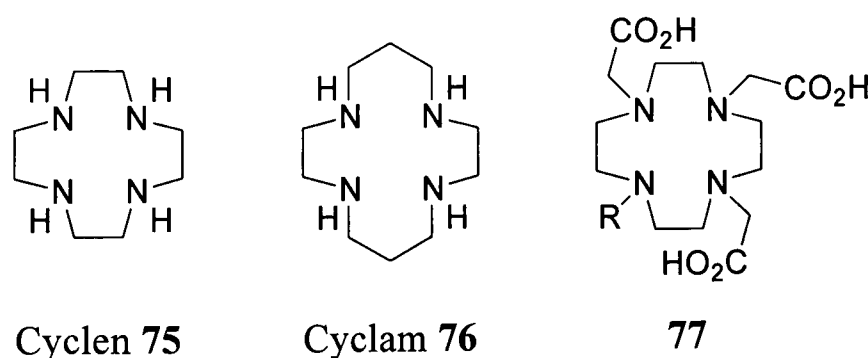
Scheme 7. Synthesis of 4'-aryl-2,2':6',2''-terpyridines by Suzuki cross-couplings.



Scheme 8. Novel synthesis of a 4'-tributylstannyl-2,2':6',2''-terpyridine.

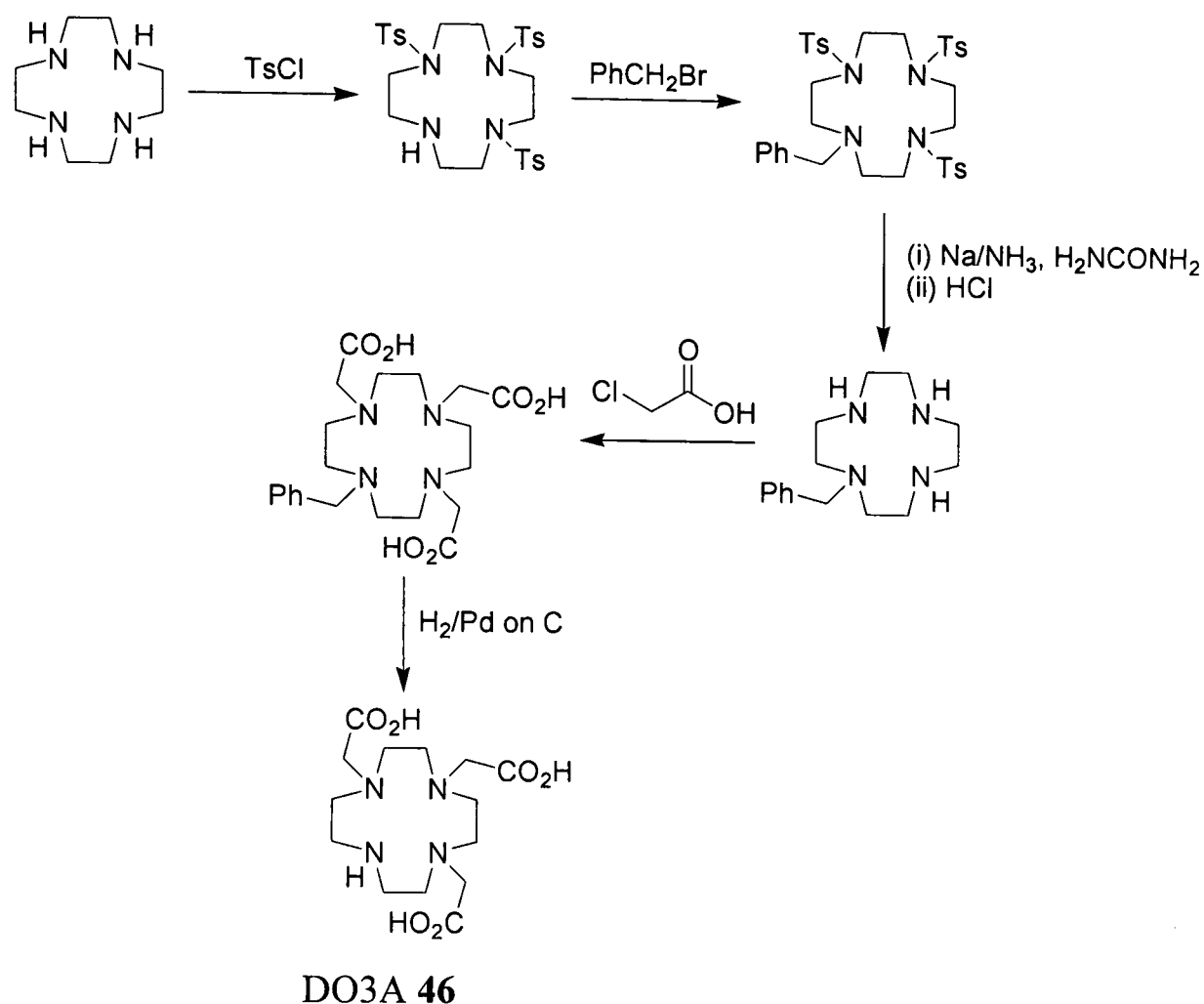
1.5 Synthesis of macrocyclic ligands for lanthanide complexes

While 1,4,7,10-tetraazacyclododecane (cyclen) **75** and the related 1,4,8,11-tetraazacyclotetradecane (cyclam) **76** are commercially available, the primary challenge when synthesising functional derivatives is selectivity in *N*-substitution. While tetra-substituted compounds may usually be prepared by reaction with sufficient alkylating agent,^{315,316} intermediate substitution can be difficult. In order to prepare chromophore appended DO3A derivatives (*i.e.* **77**) two approaches may be considered; selective attachment of the three acetic acid groups followed by the chromophore, or selective mono-alkylation of the chromophore group followed by the acetic acid groups.



The first general synthesis of DO3A **46** was reported in 1991 *via* a six step route.³¹⁷ A benzyl protecting group was used to aid tris-selectivity, which in turn was added after protection with tosyl groups (see Scheme 9). In total four protection and deprotection steps were required. More recently a much simpler one-step synthesis of the *tert*-butyl ester protected derivative has been reported.³¹⁸ Direct reaction of 1,4,7,10-tetraazacyclododecane with *tert*-butyl bromoacetate and three equivalents of sodium hydrogen carbonate leads to tri-alkylation with reasonable selectivity. The choice of a

weak base ensures that a fourth alkylation step is disfavoured, due to protonation of the remaining nitrogen atom.



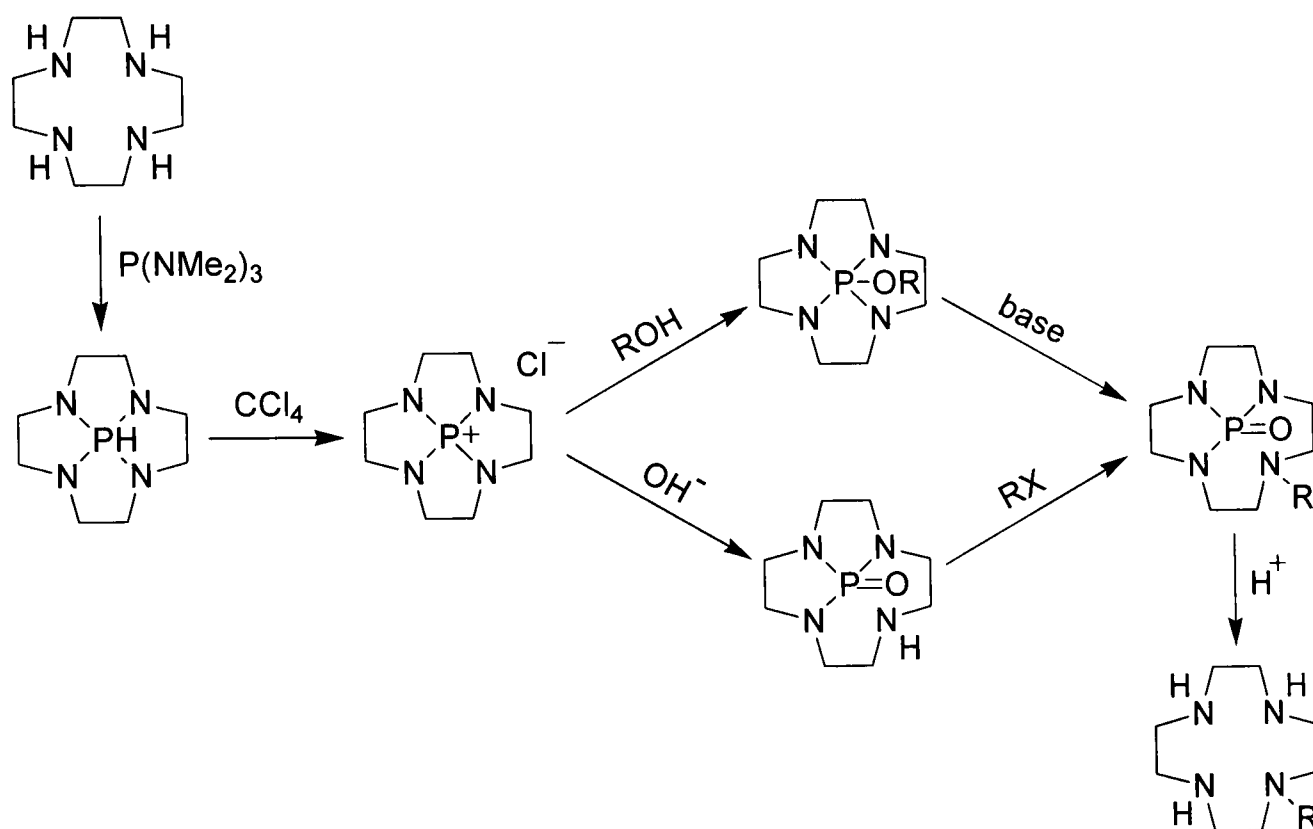
Scheme 9. First general synthesis of DO3A.

Mono-alkylation, on the other hand, may be achieved by a variety of methods. The simplest approach involves direct reaction of an alkylating agent with an excess of macrocycle.^{319,320} Under these conditions mono-alkylation is favoured, with excess starting material able to be isolated and recycled. A much smaller excess is required if acetonitrile is used as the solvent, also allowing the separation of insoluble starting materials by filtration.³²¹ With certain alkylating agents, high selectivity may even be observed with stoichiometric reagent ratios in nonprotic solvents.³²²

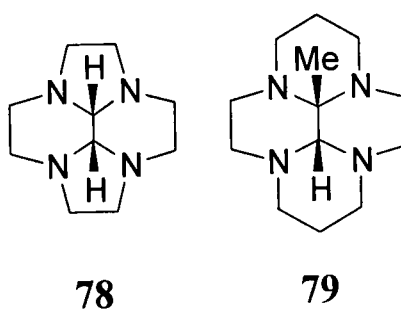
Mono-alkylation has also been accomplished following selective protection of three of the ring amines. Suitable protecting groups include tosyl (Ts),^{317,323} *tert*-butoxycarbonyl (Boc)³²⁴ and formyl (CHO)³²⁵ groups. For greatest selectivity, a single group that binds to three amines simultaneously is ideal. Group 6 metal carbonyls (M(CO)₆, M = Mo, Cr, W) have been shown to bind to 1,4,7,10-tetraazacyclododecane in such a manner, allowing mono-alkylation by alkyl bromides³²⁶ and acid chlorides.³²⁷ Tris(dimethylamino)borane (B(NMe₂)₃) binds similarly, and although highly moisture-sensitive allows deprotection under very mild conditions.³²⁸ High yields (~90% for

mono-benylation of cyclen) have been achieved by phosphoryl-protection.³²⁹ After oxidation with CCl_4 alkylation can be achieved either directly, or *via* an alkoxyphosphorane intermediate (see Scheme 10).

Reaction of cyclen with glyoxal results in the bridged macrocycle **78**. By suitable choice of solvent, high yields of mono- or di-alkylated salts may be prepared, which may then be hydrolysed to the respective cyclen derivatives.^{330,331} Improved mono-selectivity for cyclam can be obtained *via* **79**, with pyruvic acid acting both as a templating group for cyclisation as well as a protecting group.³³²



Scheme 10. Mono-*N*-alkylation of cyclen *via* phosphoryl-protection.



CHAPTER 2

AIMS AND OBJECTIVES

2 Aims and objectives

In the following chapters, the synthesis and characterisation of a number of metal complexes are discussed, with the intention of their investigation as potential electrophosphorescent dopants. In order to meet this aim, a number of design criteria must be realised.

The most important property is that these compounds must be highly luminescent. Although their performance in organic LEDs relates to their solid-state and host-doped electroluminescence properties, these are inherently linked to the photoluminescence properties in solution (see Section 1.1.1). Hence, high photoluminescence quantum yields in solution should maximise the likelihood of efficient emission from electroluminescent devices incorporating the material. In addition, harvesting of both singlet and triplet excitons is desired, and therefore efficient phosphorescence must occur. The large spin-orbit coupling of heavy metal atoms partially allows the otherwise spin-forbidden emission from triplet states, facilitating this requirement. Although efficiency of emission is important, spectral purity of red, green and blue emission is essential for their use as elements in full-colour electroluminescent displays.

Another requirement is overall charge-neutrality. Although high efficiencies have been obtained from electroluminescent devices incorporating charged transition metal complexes,¹⁸⁶ there are a number of disadvantages. Since the application of an electric field will result in the migration of ions to their respective electrodes, it is perhaps unsurprising that device lifetimes are poor. Also, since balanced charge-injection is reliant upon the redistribution of ions under the applied field, turn-on times tend to be long (seconds to several minutes).

A third general requirement in the present work, differentiating it from much of the published literature to date, is a focus upon increased stabilities by the use of multidentate ligands. Whereas previous research on organometallic iridium(III) and europium(III) compounds as electrophosphorescent materials has invariably used bidentate ligands, the design and development of tri- and octa-dentate ligands for these metals respectively, will be described herein.

In chapters 3 and 4, the synthesis, photophysical characterisation and computational study of a number of bis-terdentate iridium(III) complexes are discussed. In order to ensure charge-neutrality, the generic $\text{Ir}(\text{N}^{\wedge}\text{X}^{\wedge}\text{N})(\text{X}^{\wedge}\text{N}^{\wedge}\text{X})$ target structures incorporate a combination of cyclometalating Ir–C bonds, metal bound carboxylates

and amine functionality. The analogous tris-bidentate iridium(III) complex, *fac*-Ir(ppy)₃ **26** has been well studied in electroluminescent device applications, with promising results (see Section 1.2.3). The donor sets described herein enforce a meridional geometry, difficult to achieve otherwise due to the strong *trans*-effect of cyclometalated ligands.

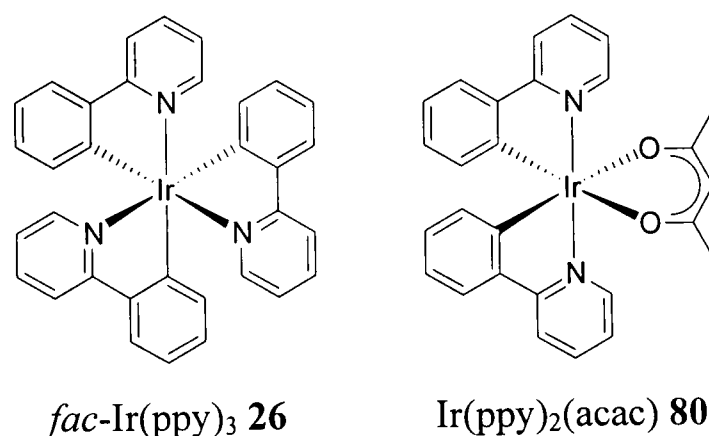
In chapter 5, the synthetic details and photophysical characterisation of a series of europium(III)-coordinated macrocyclic complexes are discussed. They are based around the heptadentate, tricarboxylic acid ligand DO3A **46** (see Section 1.3.3.1), which is derivatised with a sensitising chromophore group by alkylation at the secondary amine.

CHAPTER 3

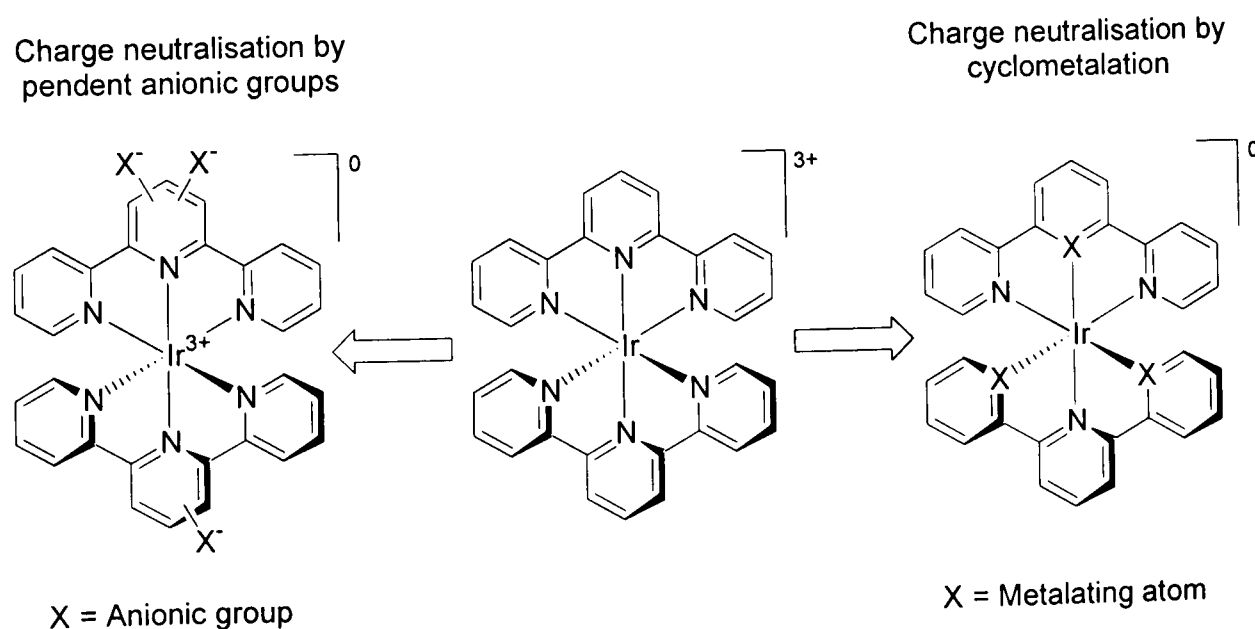
SYNTHESIS OF IRIDIUM(III) COMPLEXES

3 Synthesis of iridium(III) complexes

Although much research has focused upon the use of iridium(III) complexes as electrophosphorescent dopants, they are usually derivatives of the prototypical *fac*-Ir(ppy)₃ **26** and Ir(ppy)₂(acac) **80** structures (see Section 1.2.3). Despite reports of device lifetimes of up to 10 000 hours,³³³ there are concerns with respect to the long-term stability of such materials in electroluminescent devices. In this work, a number of alternative charge-neutral iridium(III) complexes for organic LED applications are explored. By the use of terdentate coordination, it is hoped that high stabilities and therefore improved device lifetimes will be obtained.



As noted in Section 2, charge-neutral complexes are desirable for OLED applications. In the present study, two approaches to overall charge-neutralisation will be considered. Conventional binding of nitrogen donors to the metal centre (see Section 1.2.1.1) may be combined with pendent anionic groups. Alternatively, cyclometalation (see Section 1.2.1.2) provides a route to iridium(III) complexes where neutralisation of molecular charge occurs in the core of the molecule. Generic structures for both these strategies are shown in Scheme 11.



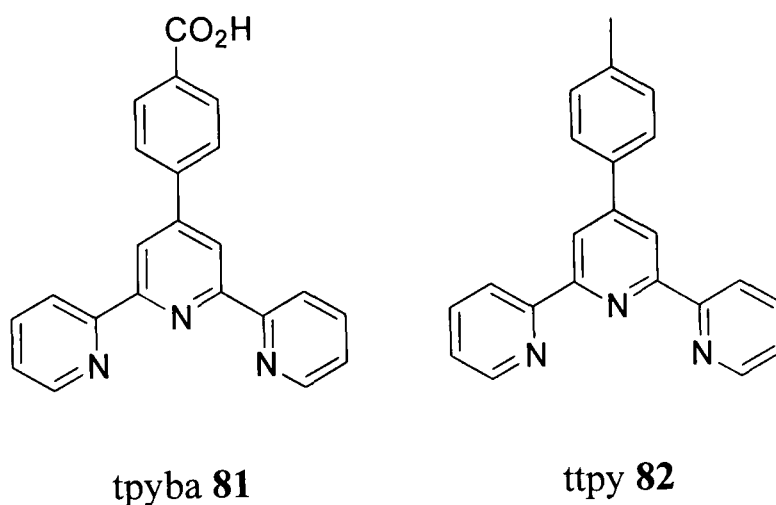
Scheme 11. Generic approaches to charge-neutralisation.

3.1 Synthesis of oligoaromatic ligands

As discussed in Section 1.4, there are two general methodologies for the synthesis of oligoaromatic ligands, ring-closing and cross-coupling reactions. In the course of this work, both routes have been utilised, chosen according to their suitability in each case.

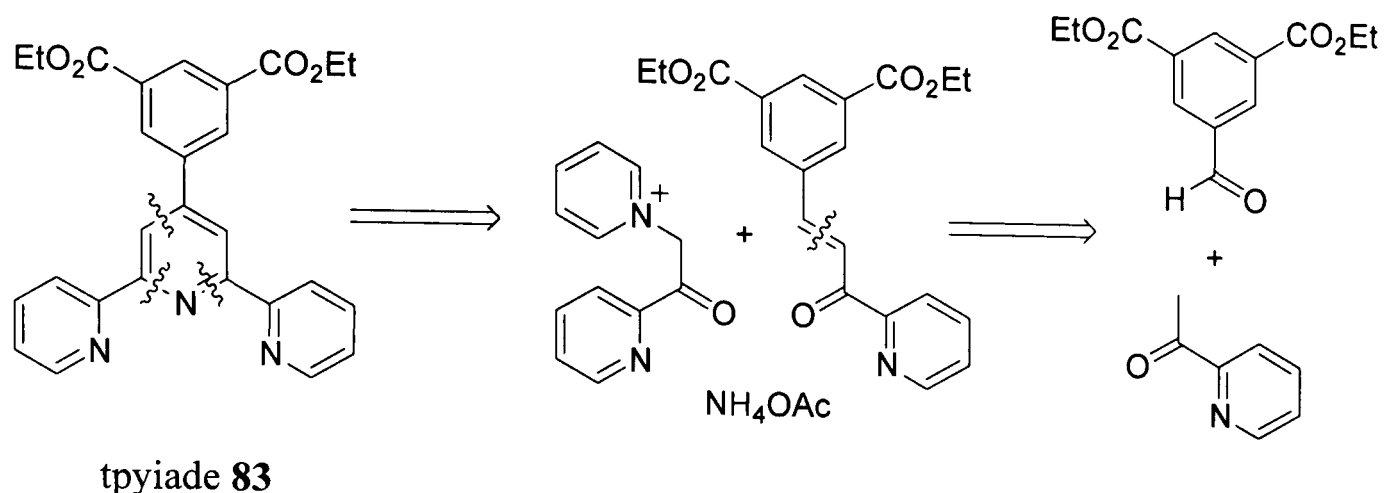
3.1.1 Synthesis of 2,2':6',2''-terpyridine derivatives

The preparation of 2,2':6',2''-terpyridine derivatives is simplified by the presence of the central pyridine ring. This permits the use of the Kröhnke pyridine synthesis (see Scheme 3).²⁸⁶ Another requirement is the presence of a suitable aromatic substituent at the 4'-position. The potentially mono-anionic ligand 4-(2,2':6',2''-terpyridin-4'-yl)-benzoic acid (tpyba) **81** may readily be prepared by such a route, as may 4'-(*p*-tolyl)-2,2':6',2''-terpyridine (tpty) **82**.³³⁴

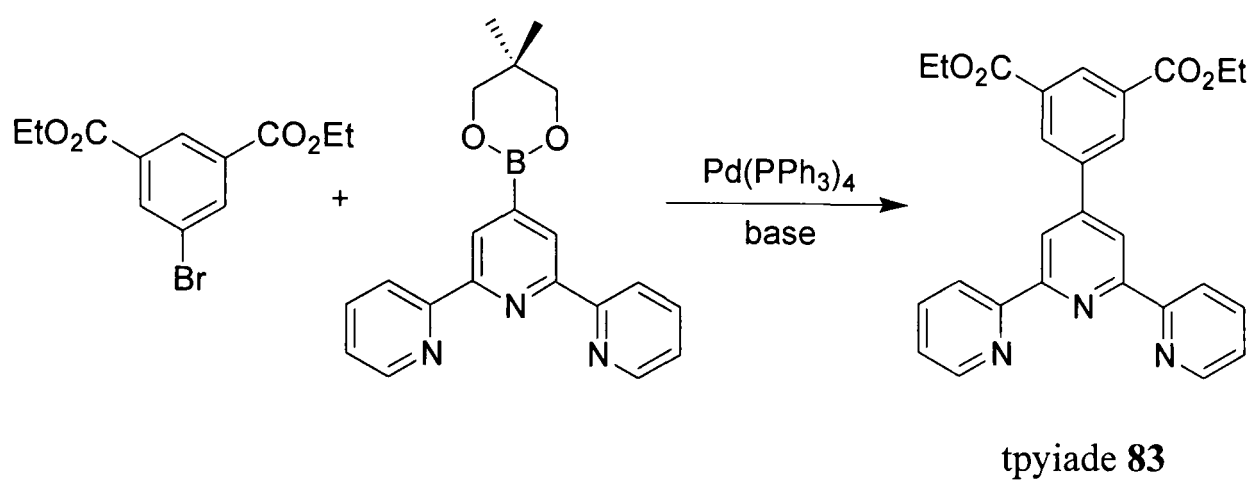


Although the Kröhnke route is seemingly applicable to the synthesis of 5-(2,2':6',2''-terpyridin-4'-yl)isophthalic acid diethyl ester (tpyiade) **83**, retrosynthetic analysis reveals difficulties (see Scheme 12). The preparation of the required aldehyde has been previously reported,^{335,336} however these routes require a synthetically difficult selective reduction of 1,3,5-benzenetricarboxylic acid triethyl ester.

Instead, the Suzuki cross-coupling technique of Williams *et al.*^{311,312} was used to append the 4'-aryl substituent (see Scheme 13). The requisite aryl bromide was readily accessible by oxidation and subsequent esterification of 1-bromo-3,5-dimethyl-benzene, although formation of the boronic ester derivative proved troublesome. Hence 4'-(5,5-dimethyl-[1,3,2]dioxaborinan-2-yl)-2,2':6',2''-terpyridine was prepared from 4'-bromo-2,2':6',2''-terpyridine by Miyaura coupling³³⁷ with bis(neopentyl glycolato)diboron.



Scheme 12. Retrosynthetic analysis of 5-(2,2':6',2''-terpyridin-4'-yl)isophthalic acid diethyl ester (tpyiade).



Scheme 13. Synthesis of 5-(2,2':6',2''-terpyridin-4'-yl)isophthalic acid diethyl ester *via* a Suzuki cross-coupling reaction.

Since solubility of the hydrolysed aryl bromide in organic solvents is poor, the cross-coupling should proceed under conditions that tolerate ester functionality. Standard Suzuki conditions with an aqueous base were found to be highest yielding, with hydrolysis not a significant problem (see Table 7). Anhydrous conditions with either an organic base (NEt_3) or a suspension of inorganic base (K_2CO_3) were shown to give significantly lower yields.

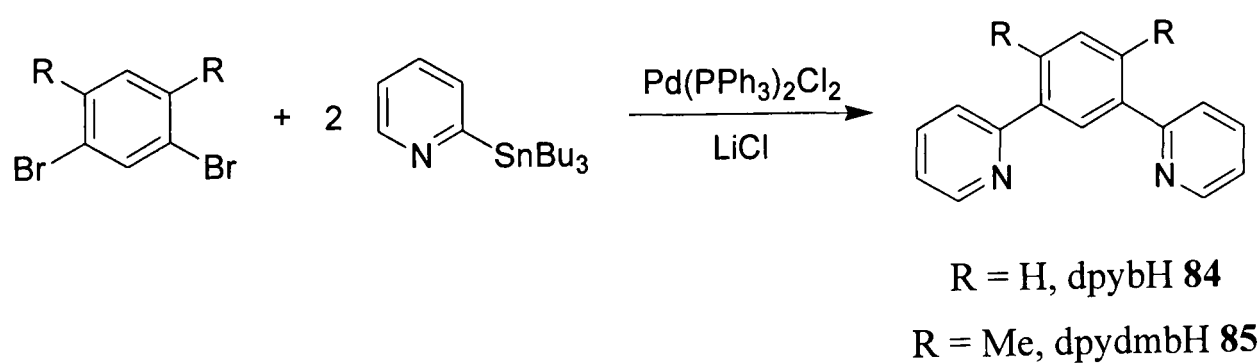
Solvent	Catalyst	Base	Yield
DME	$\text{Pd}(\text{PPh}_3)_4$	Na_2CO_3 (aq)	42%
DMF	$\text{Pd}(\text{PPh}_3)_4$	NEt_3	11%
Toluene	$\text{Pd}(\text{PPh}_3)_4$	K_2CO_3 (s)	6%

Table 7. Attempted conditions for the synthesis of 5-(2,2':6',2''-terpyridin-4'-yl)isophthalic acid diethyl ester *via* a Suzuki cross-coupling reaction.

3.1.2 Synthesis of 1,3-di(pyrid-2-yl)benzene derivatives

Two methodologies have been applied to the preparation of 1,3-di(pyrid-2-yl)benzene in the published literature to date. Reaction of 1,3-dicyanobenzene with acetylene and a cobalt catalyst under high pressure has been shown to result in ring closing of the peripheral pyridyl rings (see Scheme 5).^{293,294} This route was dismissed in the present study due to the extremely hazardous nature of high pressure acetylene. Although pyridyl rings have also been formed by reaction of nitrile compounds with a lithiated derivative of 1,3-butadiene,²⁹⁶ the preparation of this starting material is time-consuming and costly.^{296,338,339}

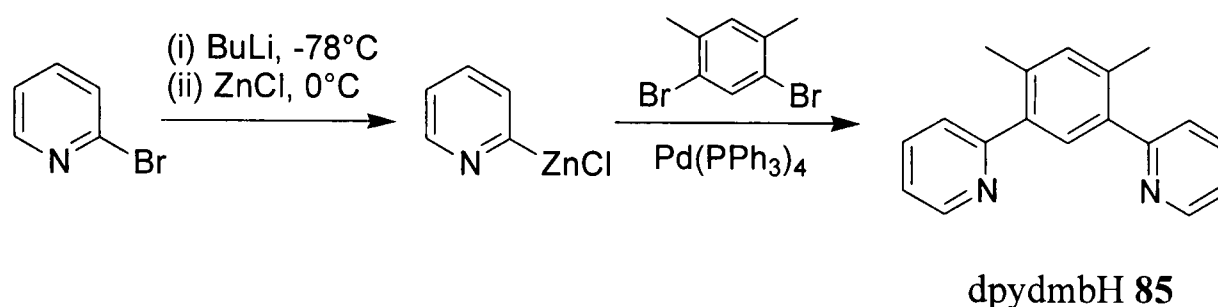
An alternative approach is the coupling of 1,3-dibromobenzene derivatives with organometallic pyridine reagents, previously reported by the cross-coupling procedures of Suzuki,³⁰⁵ Stille³⁰⁸ and Negishi.³¹⁰ Although toxicity of stannane compounds is of some concern, the Stille cross-coupling with 2-tri-*n*-butylstannylpyridine³⁰⁸ was chosen in this work due to the availability and stability of this coupling reagent. Reaction with 1,3-dibromobenzene in the presence of bis(triphenylphosphine)palladium(II) chloride and lithium chloride under an inert atmosphere resulted in 1,3-di(pyridin-2-yl)benzene (dpybH) **84** in reasonable (62%) yield (see Scheme 14). Straightforward dibromination of *meta*-xylene may be achieved by reaction with bromine and a catalytic amount of iodine.* A subsequent Stille cross-coupling allowed the preparation of the new ligand 1,5-di(pyridin-2-yl)-2,4-dimethylbenzene (dpydmbH) **85** in 61% yield.



Scheme 14. Synthesis of 1,3-di(pyrid-2-yl)benzene and a dimethyl derivative via a Stille cross-coupling reaction.

* A less toxic brominating agent, 1,3-dibromo-5,5-dimethylhydantoin (DBH) has been reported for the di- and tri-bromination of mesitylene.³⁴⁰ Numerous attempts at dibromination of *meta*-xylene with DBH were unsuccessful. Poor selectivity resulted in a mixture of dibrominated products, with excess reagent leading to tri- and tetra-bromination (again with poor specificity).

In an attempt to circumvent the use of toxic tin reagents, the zinc-mediated Negishi cross-coupling reaction³⁰³ was evaluated. Its application to the synthesis of 5-methyl-1,3-di(pyrid-2-yl)benzene had already been reported in 86% yield,³¹⁰ hence it was expected to be effective for the preparation of 1,5-di(pyridin-2-yl)-2,4-dimethylbenzene (dpydmbH) **85**. Formation of 2-lithiopyridine by reaction of 2-bromopyridine with *n*-butyl lithium at -78°C was followed by transmetalation with ZnCl_2 at 0°C to give the pyridylzinc chloride. This was coupled without isolation to the required aryl bromide in the presence of a $\text{Pd}(\text{PPh}_3)_4$ catalyst (see Scheme 15). Unfortunately, all attempts were poorly yielding, often with mainly mono-substitution (see Table 8).



Scheme 15. Attempted synthesis of 1,5-di(pyrid-2-yl)-2,4-dimethylbenzene *via* a Negishi cross-coupling reaction.

Solvent	Zinc Reagent	Catalyst	Yield
Aerated THF	ZnCl_2	$\text{Pd}(\text{PPh}_3)_4$	5%
Degassed THF	ZnCl_2	$\text{Pd}(\text{PPh}_3)_4$	15% ^a
Degassed THF	ZnCl_2	$\text{Pd}(\text{PPh}_3)_2\text{Cl}_2$	8% ^a
Degassed THF	Zn powder	$\text{Pd}(\text{PPh}_3)_4$	0%

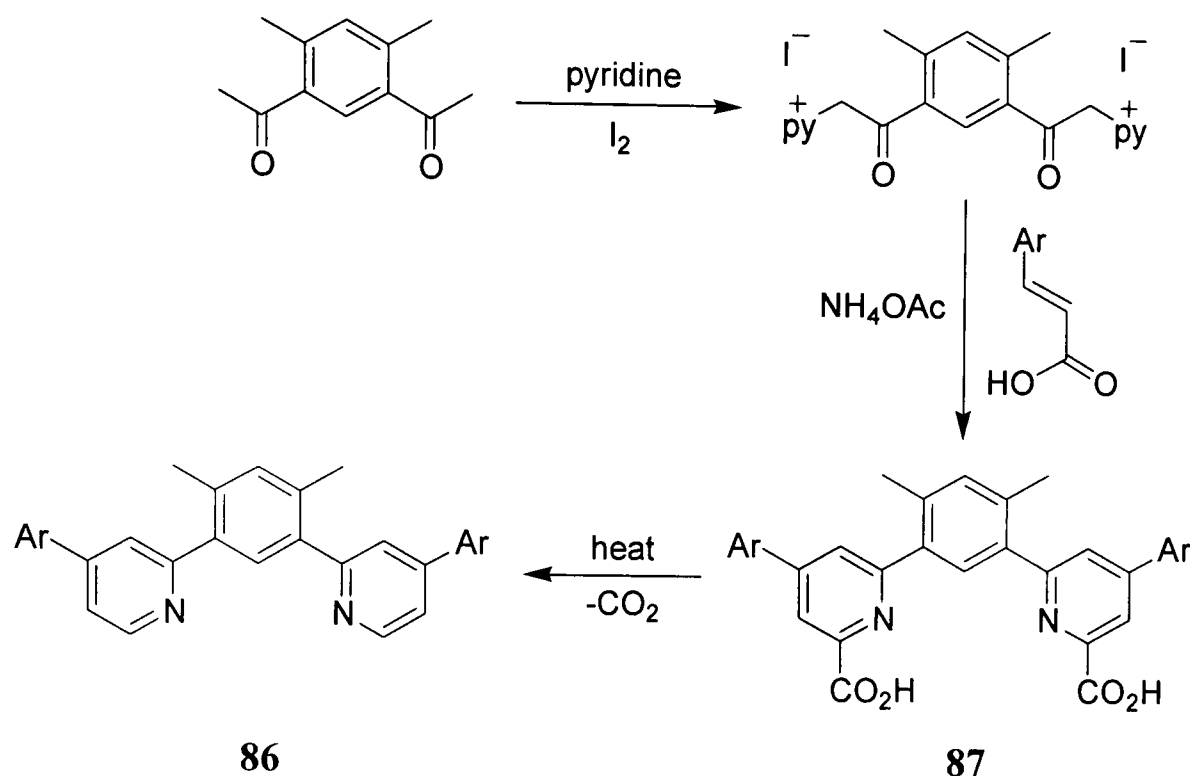
^aUnisolated GC Yield

Table 8. Attempted conditions for the synthesis of 1,5-di(pyrid-2-yl)-2,4-dimethylbenzene *via* a Negishi cross-coupling reaction.

While cross-coupling reactions permit the preparation of a wide range of di-pyridylbenzene derivatives, the need for rigorous degassing and the use of relatively costly, and in some cases toxic reagents hinders their use on larger scales. Ideally, a ring-closing procedure would be available for systems without a central pyridine ring. Two approaches to develop such a route have been investigated in the present work.

Although unable to ring-close a central phenyl ring, the classical Kröhnke synthesis²⁸⁶ could be applied to form the two peripheral pyridine rings. This should allow a straightforward route to structures of the form **86** (see Scheme 16). The inter-

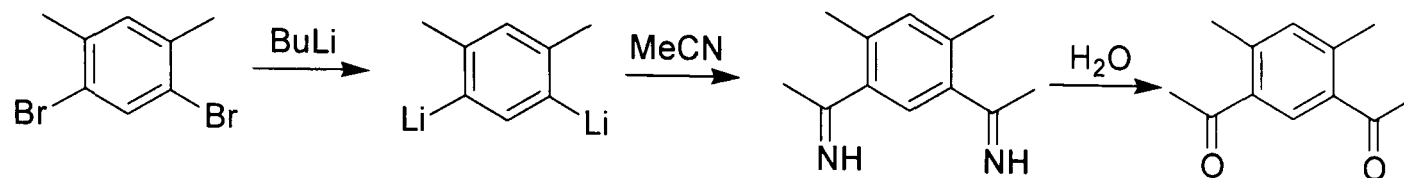
mediate dicarboxylic acid compound **87** is also of interest, since deprotonation of the acid groups results in a ligand capable of balancing the triply positive charge of iridium(III).



Scheme 16. Synthesis of 1,5-di(pyrid-2-yl)-2,4-dimethylbenzene derivatives by Kröhnke type ring-closing of the outer pyridyl rings.

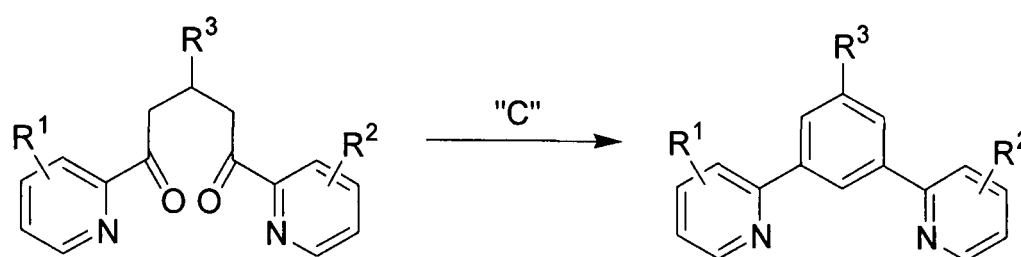
Although Friedel-Crafts acylation normally leads to selective mono-substitution, diacetylation has been reported for mesitylene³⁴¹⁻³⁴⁴ and xylene.³⁴¹ This is attributed to steric inhibition of the resonance interaction between the carbonyl group and the ring, reducing its deactivating effect. However, all attempts at diacetylation in the current work have been unsuccessful. Reaction of *meta*-xylene with two equivalents of either acetyl chloride or acetic anhydride in carbon disulphide with an excess of anhydrous aluminium chloride results in the formation of 4-acetyl-*meta*-xylene in high (82-87%) yield. No evidence of the desired 4,6-diacetyl-*meta*-xylene was observed in either case. This is consistent with the report that sufficient steric inhibition is present in 2-acetyl-*meta*-xylene for a second acylation to take place (55% yield), while 4-acetyl-*meta*-xylene is unreactive.³⁴⁵

Alternatively, if dilithiation could be achieved in the reaction between the readily accessible 1,5-dibromo-2,4-dimethylbenzene and *n*-butyl lithium, subsequent addition of acetonitrile then hydrolysis would yield the desired diacetyl compound (see Scheme 17). Attempts at this reaction showed that only mono-lithiation occurs, with solely monoacetylation resulting. A second independent lithiation of this intermediate is not possible, since butyl lithium is incompatible with the existing ketone.



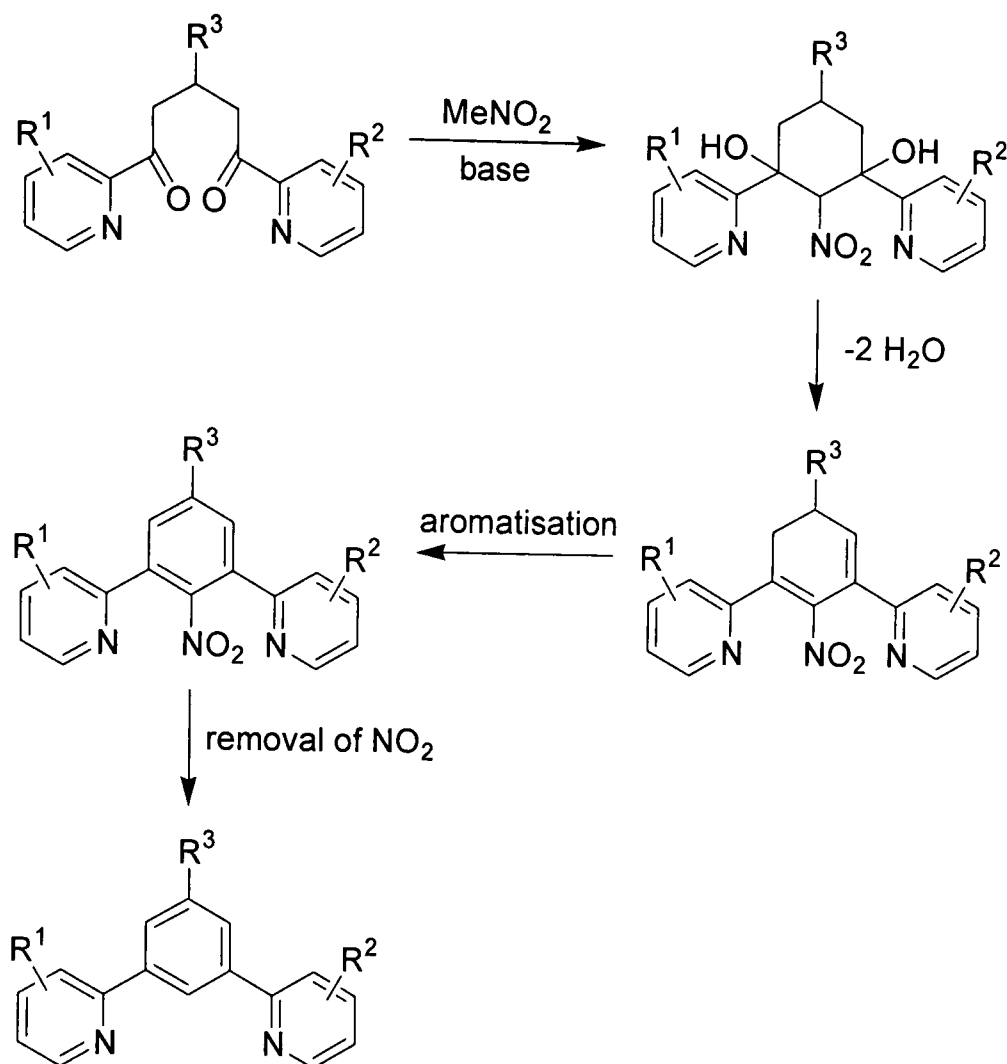
Scheme 17. Potential synthesis of 4,6-diacetyl-*m*-xylene via dilithiation.

A second ring-closing approach to the synthesis of dipyridylbenzene derivatives is to develop a reagent analogous to ammonium acetate, capable of insertion of a carbon atom (see Scheme 18). Such a reagent would require two successive deprotonation and nucleophilic insertion steps, and hence a strongly acidic methyl group. Nitromethane ($\text{pK}_a = 9\text{-}10$)^{346,347} was investigated in the present work with this aim in mind.

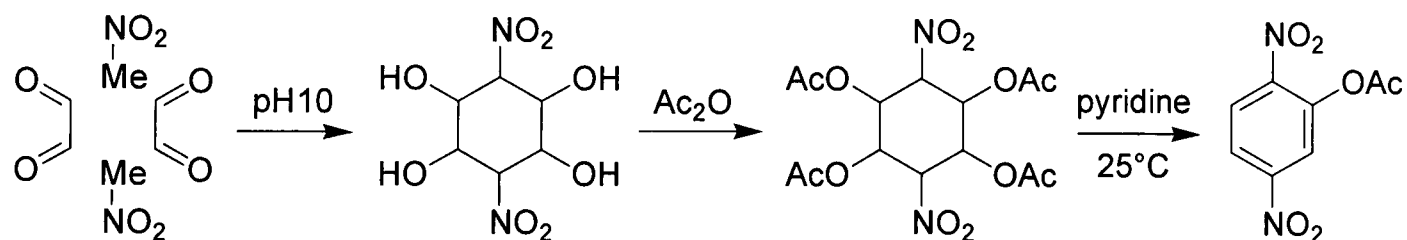


Scheme 18. Synthesis of dipyridylbenzene derivatives by “C”-insertion.

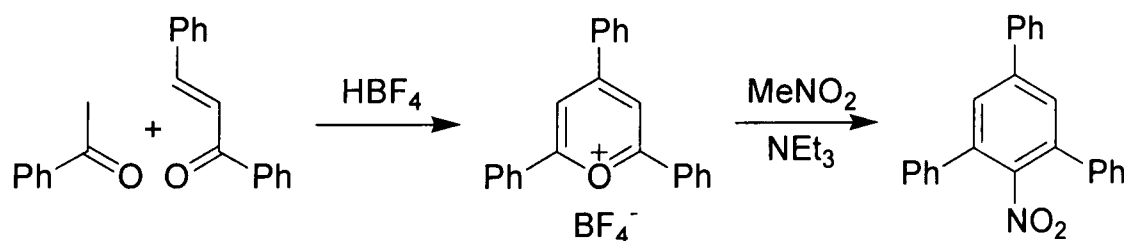
The attack of nitro-stabilised carbanions at carbonyl functionality is referred to as the Henry, or nitroaldol reaction.³⁴⁷ Reaction of nitromethane with dialdehyde compounds to form six-membered rings has received much attention for its use in the preparation of nitro- and amino-substituted sugars.³⁴⁸ The current aim was to develop a procedure whereby reaction of nitromethane with a diketone is followed by dehydration, aromatisation and removal of the nitro-group (see Scheme 19). The cyclisation product of nitromethane with glyoxal has been shown to aromatise following treatment with acetic anhydride (see Scheme 20).³⁴⁹ Alternatively, formation of the 2,4,6-triphenylpyranylium salt³⁵⁰ followed by reaction with nitromethane³⁵¹ leads to direct formation of 2,4,5-triphenylnitrobenzene (see Scheme 21). The latter approach has been demonstrated for a number of 2,4,5-triarylnitrobenzene derivatives.³⁵²⁻³⁵⁵



Scheme 19. Formation of a central benzene ring by insertion of nitromethane.

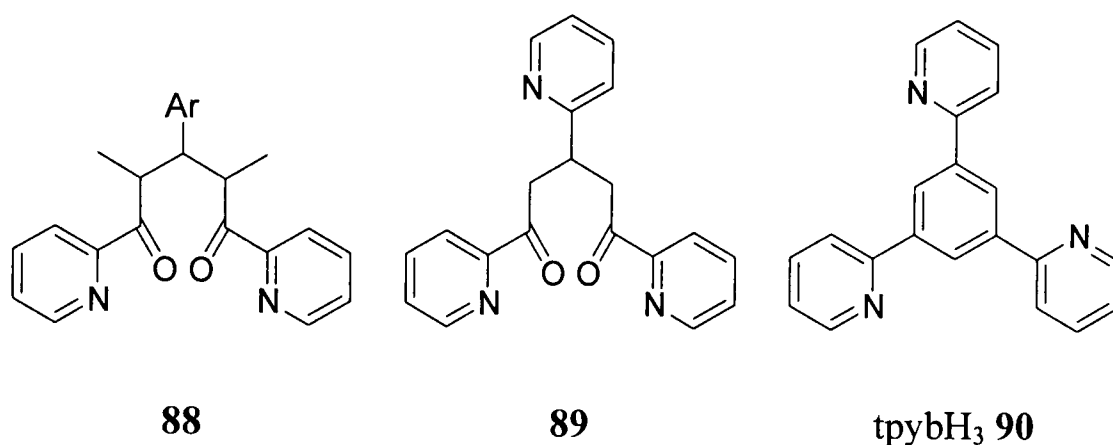


Scheme 20. Synthesis of acetic acid 2,5-dinitrophenyl ester by cyclisation of nitromethane and glyoxal.



Scheme 21. Synthesis of 2,4,5-triphenylnitrobenzene *via* the pyranylum salt.

In order to synthesise N[^]C[^]N binding ligands for iridium(III) (*i.e.* those that bind through two peripheral pyridine rings and a central cyclometalating phenylene ring), a di(pyridin-2-yl)-2,4-dimethylbenzene (dpydmbH) derivative is desired. This requires a diketone intermediate of the form **88**. 1-Pyridin-2-ylpropan-1-one may be prepared by reaction of 2-cyanopyridine with ethylmagnesium bromide at 0°C followed by hydrolysis.³⁵⁶ Preliminary attempts at subsequent reaction with aryl aldehydes to yield **88** suggested such reactions were poorly yielding, leading to a mixture of difficult to separate compounds.



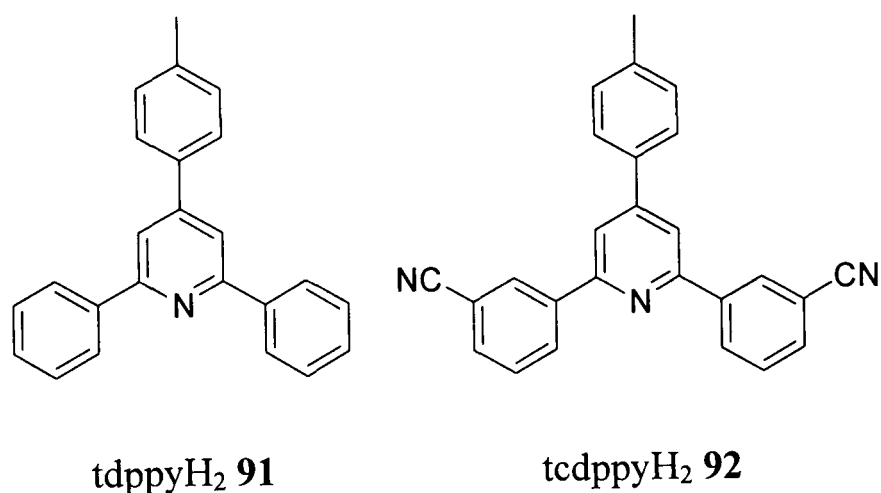
To investigate the effectiveness of ring-closing with nitromethane, the readily accessible dione **89** was synthesised by reaction of two equivalents of 2-acetylpyridine with 2-pyridinecarboxaldehyde in aqueous base. Once cyclised, this should yield the C₃-symmetric, potentially N[^]C[^]N binding ligand 1,3,5-tri(pyridin-2-yl)benzene (tpybH₃) **90**. Dropwise addition of a solution of **89** in nitromethane and dichloromethane to a hot solution of sodium ethoxide in ethanol was followed by heating to reflux at 78°C for three hours. After workup, a mixture of compounds including the desired diol was obtained. This was added without further purification to concentrated sulfuric acid and heated to 150°C overnight. After basification and extraction into dichloromethane, chromatographic purification resulted in the desired compound,[†] although still impure and in very low crude yield (<0.2%).

3.1.3 Synthesis of bis-cyclometalating C[^]N[^]C ligands and their analogues

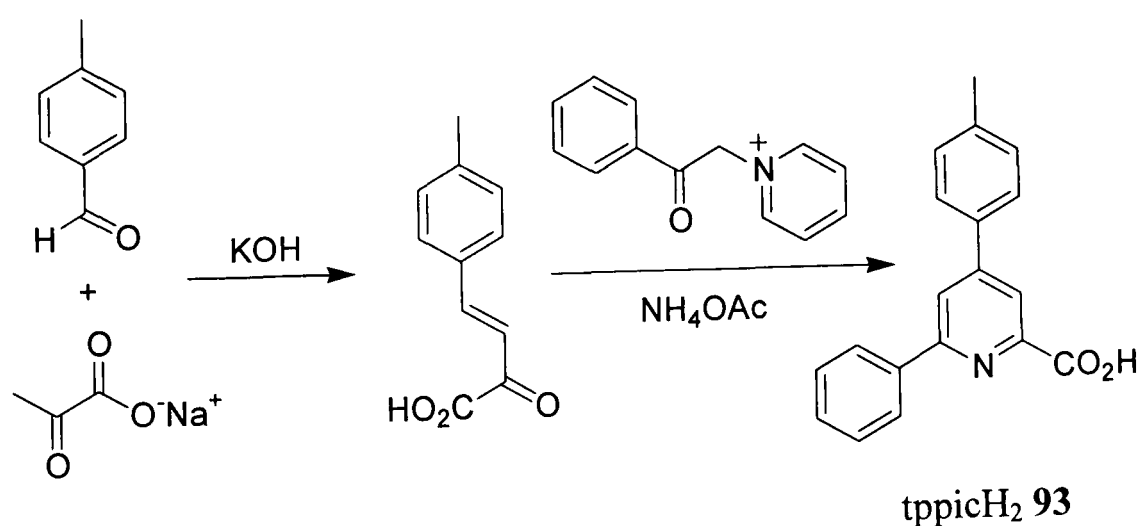
With respect to N[^]C[^]N coordinating ligands, the synthesis of C[^]N[^]C binding compounds is greatly simplified by the presence of a central pyridine ring. In general, Kröhnke methodology²⁸⁶ (see Section 1.4.1) allows access to such compounds from

[†] tpybH₃: ¹H-NMR (CDCl₃, 200 MHz) δ=9.11 (3H, s), 8.75 (3H, d, J=4.9), 8.67 (3H, d, J=7.9), 7.88 (3H, td, J=7.9, 1.8), 7.35 (3H, ddd, J=7.5, 4.8, 1.1). MS(ES+) *m/z*=342 ([2M+Zn]²⁺).

readily available starting materials. When a 4'-aryl substituent was required (*e.g.* 4-*p*-tolyl-2,6-diphenylpyridine (tdppyH₂) **91** and 4-*p*-tolyl-2,6-di(3-cyanophenyl)pyridine (tcdppyH₂) **92**), an acetophenone derivative was reacted with the relevant aryl aldehyde in aqueous base to give the desired chalcone in near quantitative yield. This was then combined with the respective 1-(2-oxo-2-arylethyl)pyridinium iodide and ammonium acetate in glacial acetic acid. Heating to reflux at 116°C for one hour followed by cooling and addition of water precipitated the desired triarylpyridine derivative.



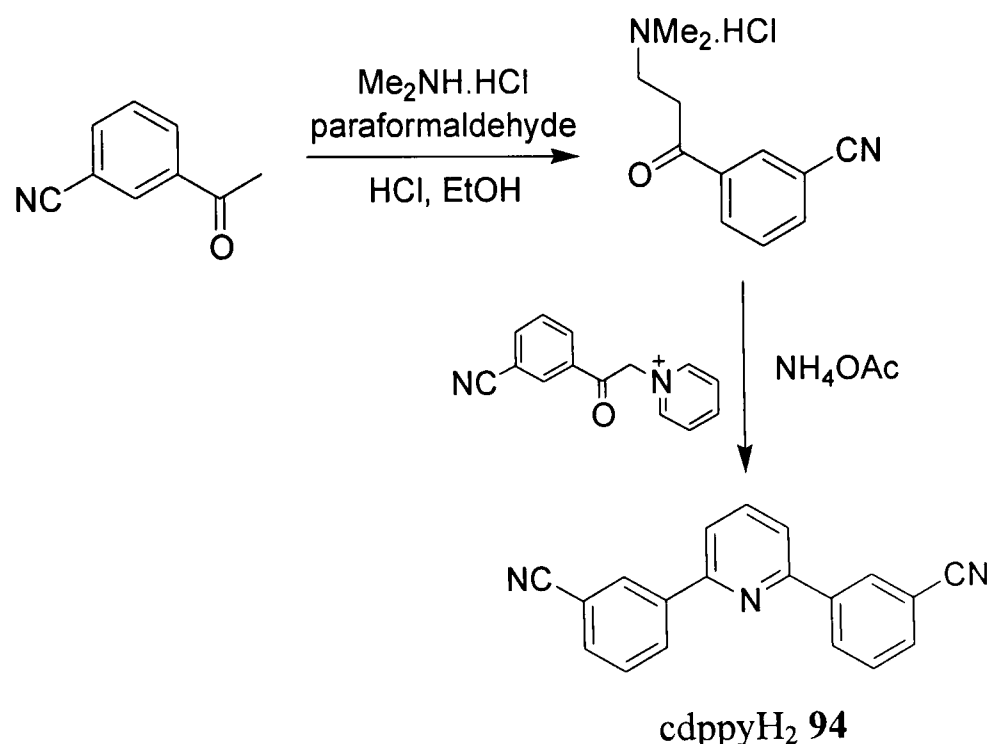
If carboxylic acid functionality was desired (*e.g.* 4-*p*-tolyl-6-phenylpicolinic acid **93** (tppicH₂)), a 2-oxo-4-aryl-but-3-enoic acid derivative was prepared from the aryl aldehyde and sodium pyruvate. Heating this to reflux at 100°C in water with 1-(2-oxo-2-phenylethyl)pyridinium iodide and ammonium acetate resulted in the sought-after ligand, which precipitated from solution upon cooling (see Scheme 22).



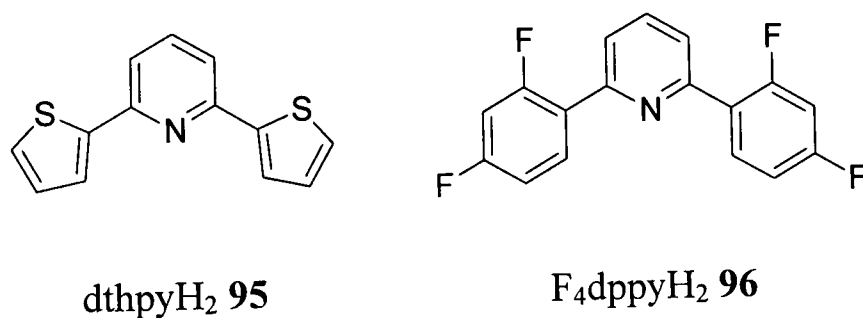
Scheme 22. Synthesis of 4-*p*-tolyl-6-phenylpicolinic acid by ring-closing.

Although necessary for the classical Kröhnke scheme, the requirement of an aryl-group in the 4'-position can be circumvented by the use of a Mannich base, as reported for 2,6-diphenylpyridine.²⁸⁶ The Mannich base derivative of 3-acetylbenzo-

nitrile was prepared in 56% yield by boiling in ethanol with paraformaldehyde, dimethylamine hydrochloride and concentrated hydrochloric acid. Subsequent reaction with 2-(1-(3-cyanophenyl)-1-oxoethyl)pyridinium iodide and ammonium acetate in glacial acetic acid produced 2,6-di(3-cyanophenyl)pyridine (cdppyH₂) **94** in 83% yield. An analogous procedure was used to obtain the thiophene derivative 2,6-di(2-thienyl)pyridine (dthpyH₂) **95**.³⁵⁷

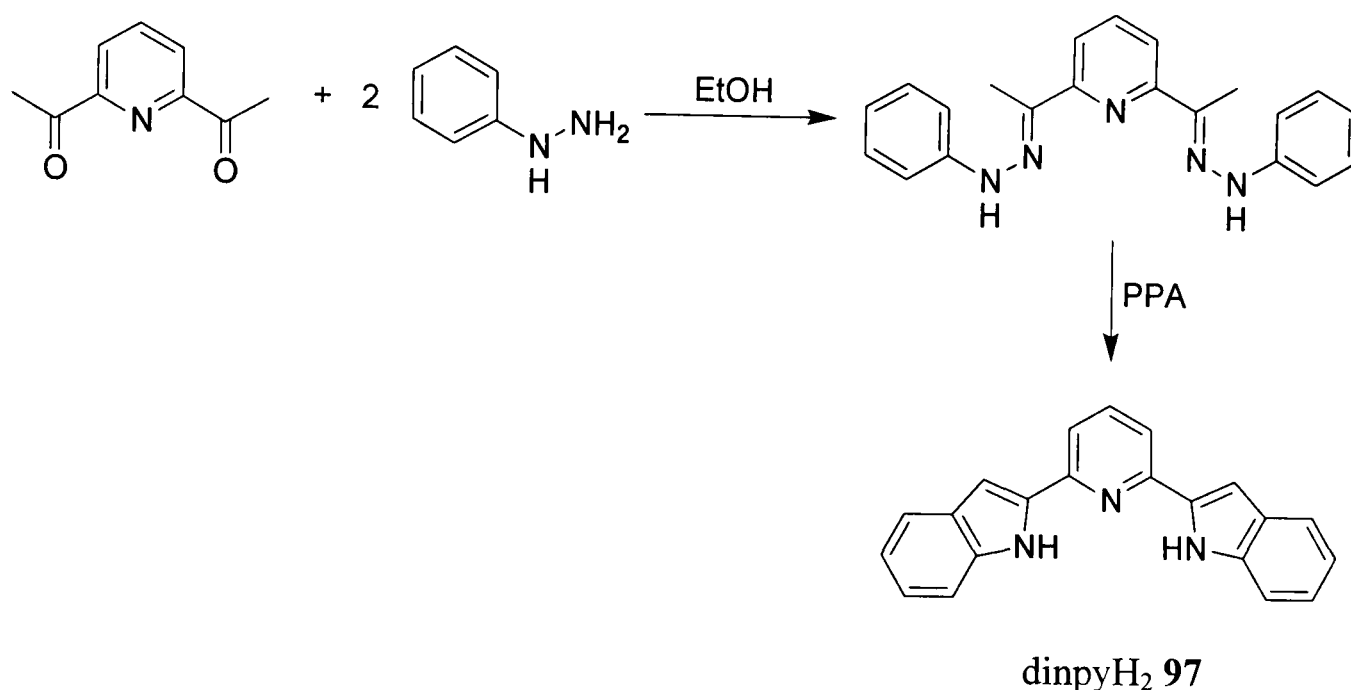


Scheme 23. Synthesis of a diphenylpyridine derivative *via* a Mannich base.



Despite being applicable to many compounds, the above route was unsuccessful in the preparation of 2,6-di(2,4-difluorophenyl)pyridine (F₄dppyH₂) **96**. While the pyridinium salt of 2,4-difluoroacetophenone was synthesised, albeit in lower yield, attempts at formation of the enaminone were unsuccessful. Evidence for nucleophilic aromatic substitution was observed, with dimethylamine replacing fluorine, a problem that was not alleviated by prior mixing of the amine with paraformaldehyde. Instead, a Suzuki cross-coupling²⁹⁹ (see Section 1.4.2) of the commercially available 2,4-difluorophenylboronic acid with 2,6-dibromopyridine in the presence of tetrakis(triphenylphosphine)palladium(0), yielded **96** in 71% yield.

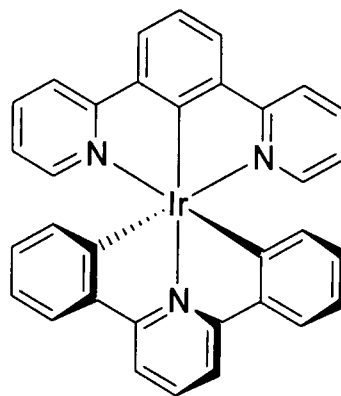
Although X⁻N⁺X ligand systems have concentrated on cyclometalation as a means of charge neutralisation, deprotonation of suitable NH groups may yield an N⁻N⁺N⁻ coordination, satisfying the requirements equally well. 2,6-Di(2'-indolyl)pyridine (dipyH₂) **97** was prepared by the Fischer indole synthesis³⁵⁸⁻³⁶⁰ (see Scheme 24). Condensation of phenyl hydrazine with 2,6-diacetylpyridine was followed by cyclisation of the resulting bis-hydrazone in polyphosphoric acid. Although less viscous and easier to handle, the use of glacial acetic or trifluoroacetic acid failed to promote the cyclisation.



Scheme 24. Preparation of 2,6-di(2'-indolyl)pyridine by the Fischer indole synthesis.

3.2 Complexation with iridium(III)

Since heteroleptic iridium(III) complexes are desired, a two-step complexation strategy was used in their preparation. Initial work focused upon the synthesis of a suitable intermediate for the preparation of Ir(dpyb)(dppy) **98**. The requirement for only a single Ir–C bond suggested that an iridium(III) 1,3-di(pyridin-2-yl)benzene (dpyb) intermediate would be more straightforward than the alternative reaction of IrCl₃ with 2,6-diphenylpyridine (dppyH₂), where two metalating Ir–C bonds must form. Binding of dpyb in the desired manner has previously been reported for Ru(II),³⁶¹⁻³⁶³ Os(II)^{361,362} and Pt(II)^{308,364} systems. The isomeric ligand 6-phenyl-2,2'-bipyridine is also well-known to cyclometalate, exhibiting C⁻N⁺N⁻ coordination to Ru(II),³⁶⁵ Pd(II)^{366,367} and Pt(II).^{366,368,369}

Ir(dpyb)(dppy) **98**

The preparation of chloride-bridged di-iridium(III) intermediates is commonly performed in 2-ethoxyethanol, with addition of water accelerating the reaction (see Section 1.2.1.2). Heating 1,3-di(pyridin-2-yl)benzene (dpybH) **84** with one equivalent of iridium trichloride trihydrate in a 3:1 mixture of 2-ethoxyethanol and water at 130°C for 4½ hours resulted in an orange precipitate. Characterisation by NMR spectroscopy indicated the presence of a complicated mixture of cyclometalated compounds, with purification hindered by poor solubility in all common solvents but DMSO. Shortening or extending reaction times did not result in any improvement, while the absence of water severely impeded the reaction.

To satisfactorily characterise the resulting intermediate compound and confirm that the desired N[^]C[^]N coordination had been achieved, reaction of the product mixture with 2,2'-bipyridine (bpy) and 4'-(*p*-tolyl)-2,2':6',2''-terpyridine (ttpy) in ethylene glycol at 196°C was investigated. In both cases the expected products, [Ir(dpyb)(bpy)Cl]⁺ **99** and [Ir(dpyb)(ttpy)]²⁺ **100** were obtained in small amounts along with a number of other complexes. Although no attempt was made at complete purification, electrospray ionisation mass spectrometry showed that the reaction with 2,2'-bipyridine also resulted in complexes of the form [Ir(dpyb)(bpy)₂]²⁺ and [Ir(dpyb)₂(bpy)]⁺. Similarly, reaction with 4'-(*p*-tolyl)-2,2':6',2''-terpyridine gave compounds of composition [Ir(dpyb)(ttpy)Cl]⁺ and [Ir(dpyb)₂(ttpy)]⁺.

Chromatographic separation of the undesired complexes from reaction with 4'-(*p*-tolyl)-2,2':6',2''-terpyridine allowed their identification as [Ir(dpyb-*N,C*^{4'})(ttpy-*N,N,N*)Cl]⁺ **101** and [Ir(dpyb-*N,C*^{4'})₂(ttpy-*N,N*)]⁺ **102**, where cyclometalation occurs through the C^{4'} position of the phenylene ring (see Figure 16, binding mode **II**). The predominance of this bidentate coordination is not entirely surprising, since the C^{2'} position is more sterically hindered by the pyridyl rings, with metalation likely to be kinetically favoured at the C^{4'} position. A similar coordination has been reported for

complexation of dpybH to palladium(II), with double cyclometalation resulting in a dimeric species.³⁰⁸

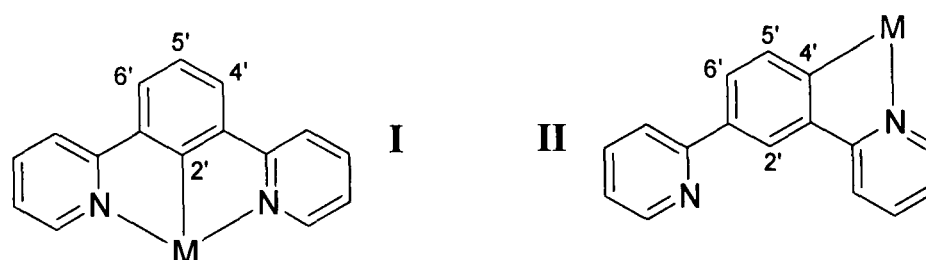
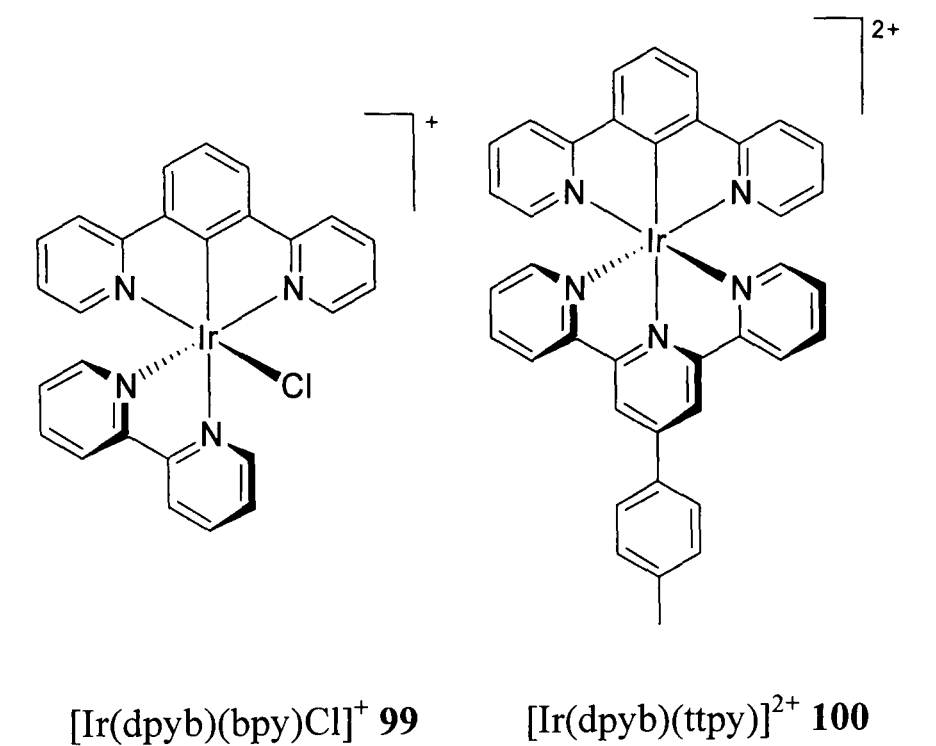
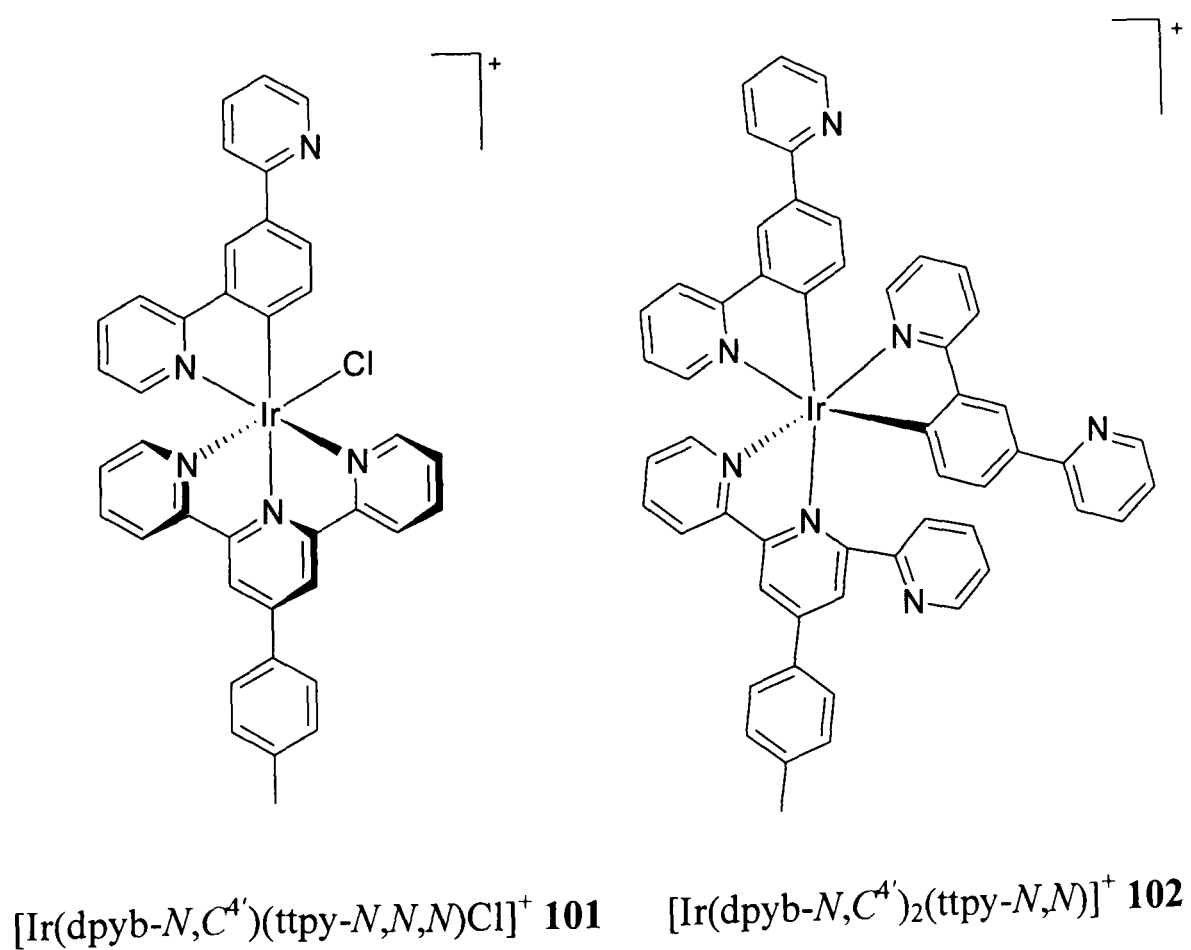


Figure 16. Two potential binding modes of the 1,3-di(pyridin-2-yl)benzene ligand.

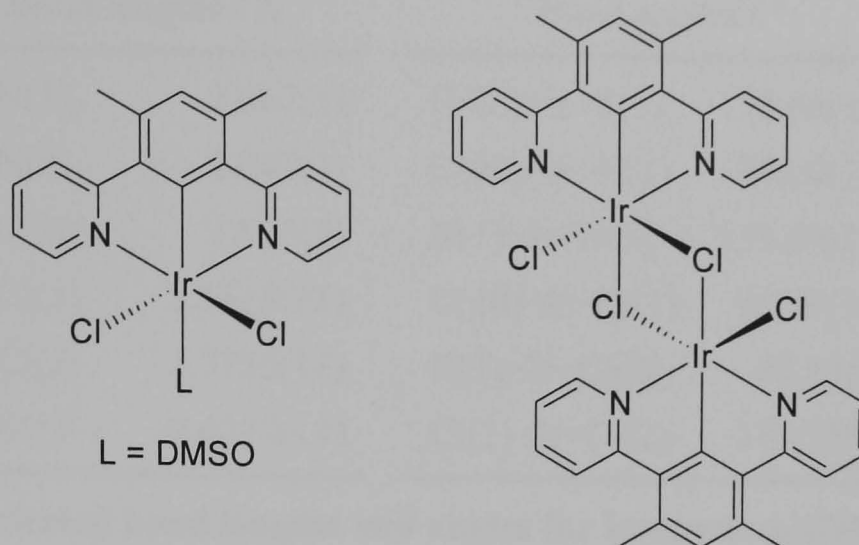


In order to favour terdentate coordination (see Figure 16, binding mode **I**), cyclometalation at the C^{4'} position was blocked by the introduction of methyl substituents. Reaction of 1,5-di(pyridin-2-yl)-2,4-dimethylbenzene (dpydmbH) **85** with iridium trichloride trihydrate in 2-ethoxyethanol at 133°C resulted in the precipitation of a yellow solid. This consisted of a mixture of cyclometalated N[^]C[^]N complex, and an unidentified non-cyclometalated precursor. Cyclometalation is favoured by longer reaction times (*e.g.* ~50% yield after three days, ~71% after five days) or by the addition of water.

However, best results were achieved upon reaction at 80°C with iridium trichloride monohydrate in a 2:1 mixture of 2-ethoxyethanol and water for six hours. Extended reaction times were found to be detrimental to purity, although higher yields may be obtained by removal of the precipitated product, then continued heating of the remaining solution.

Although insoluble in most common solvents, heating the solid in *d*₆-DMSO resulted in a yellow solution. The ¹H NMR spectrum exhibits the same C₂-symmetry as the ligand, but with a loss of the peak due to the phenylene proton between the two pyridine rings. As expected for cyclometalation at this carbon, a significant upfield shift of the resonance attributed to the proton *para* to this position is observed. An X-ray diffraction study of a single crystal obtained from DMSO solution reveals the structure as Ir(dpydmb)(DMSO)Cl₂ **103** (see Figure 17). The desired N[^]C[^]N coordination (see Figure 16, binding mode **I**) is evident, with a sulfur-bound DMSO molecule *trans* to the metalated carbon. MALDI mass spectrometry suggests that the solid isolated initially is the chloride-bridged dimer **104** ([Ir(dpydmb)Cl(μ-Cl)]₂, *m/z* = 1044), which undergoes cleavage of the bridging chloride bond upon solvation in DMSO. Such cleavage of a chloride bridge by a coordinating solvent is not without precedent, being well-established for dimeric iridium(III) ppy derivatives,³⁷⁰ and for platinum(II) dppy complexes.³⁷¹

The structure of Ir(dpydmb)(DMSO)Cl₂ **103** is shown in Figure 17, with selected bond lengths and angles tabulated in Table 9. Further crystallographic data are given in Appendix A. As expected due to the geometric constraints of terdentate binding, the iridium(III) centre exhibits a distorted octahedral geometry, with the cyclometalating ligand bound in the desired manner. The two chloride atoms are approximately perpendicular to the dpydmb ligand, with a sulfur-bound DMSO



$\text{Ir(dpydmb)(DMSO)Cl}_2$ **103** $[\text{Ir(dpydmb)Cl}(\mu\text{-Cl})]_2$ **104**

molecule occupying the remaining site of the iridium(III) centre. The Ir–C bond {1.976(4) Å} is shortened with respect to the analogous bonds in *fac*-Ir(tpy)₃ {2.024(6) Å},¹¹² a result of the constraints imposed by binding of the peripheral pyridine rings. In this sense, the Ir–C bond of Ir(dpydmb)(DMSO)Cl₂ is more comparable to the Ir–N(central pyridine) bond of [Ir(terpy)₂]³⁺ {1.980 Å},¹⁰³ which also exhibits a terdentate binding mode. Similarly, the Ir–N distances of Ir(dpydmb)(DMSO)Cl₂ {2.067(3) Å and 2.087(3) Å} are shortened with respect to *fac*-Ir(tpy)₃ {2.132(5) Å}.¹¹² This is mainly due to the introduction of a strong *trans*-influencing cyclometalated ligand opposite the nitrogen atoms of the latter structure.

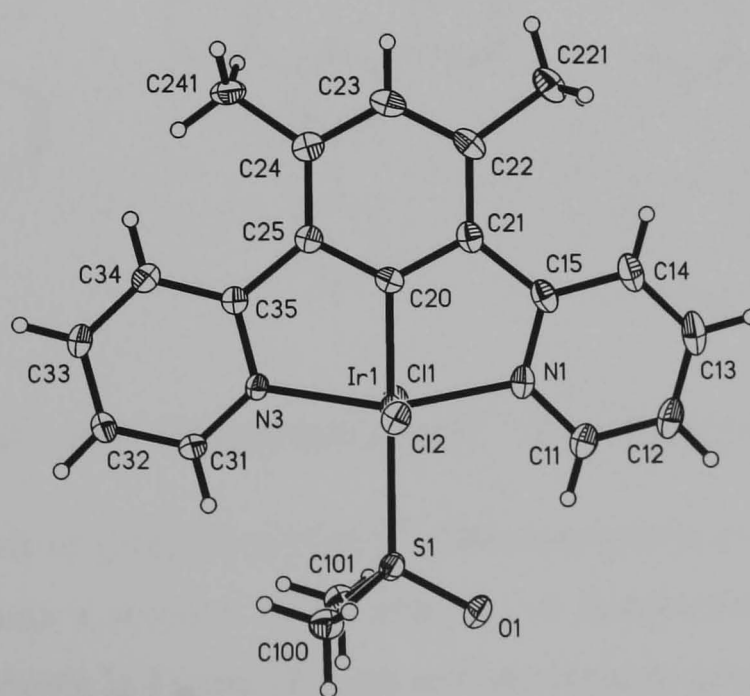
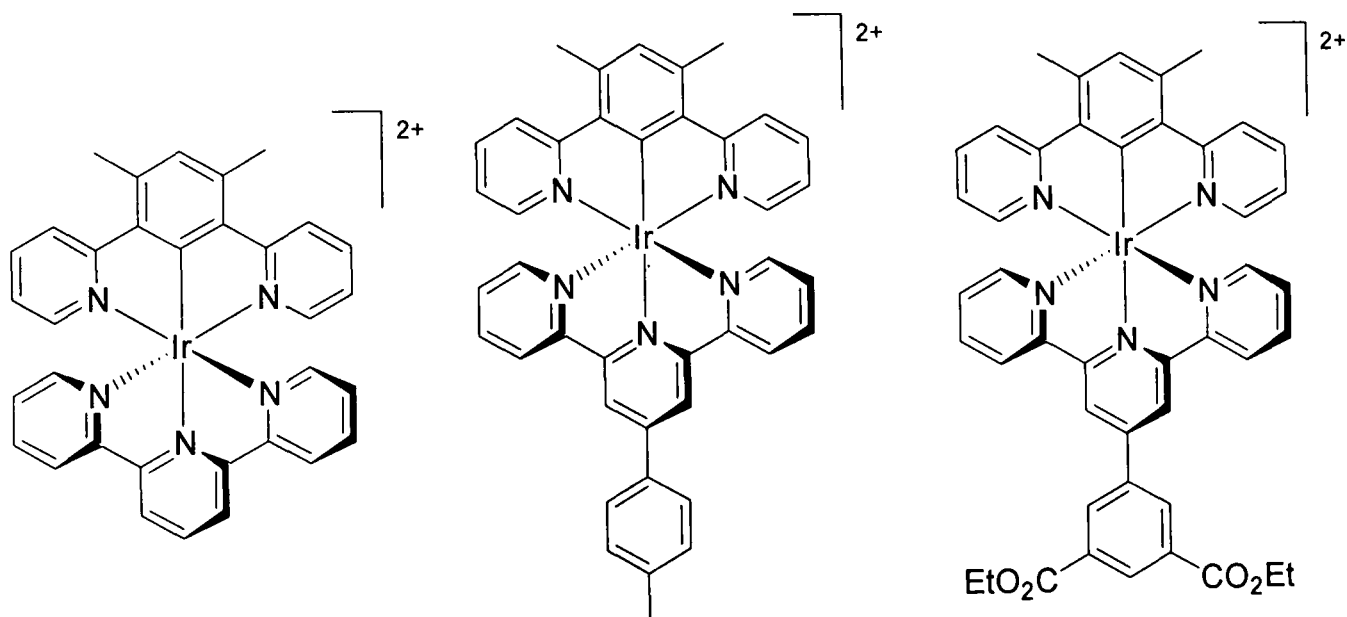


Figure 17. Structure of Ir(dpydmb)(DMSO)Cl₂ crystallised from DMSO; 120 K, thermal ellipsoids shown at 30% probability.

Bond lengths / Å		Bond angles / °	
Ir–N(1)	2.067(3)	C(20)–Ir–S(1)	178.66(10)
Ir–N(3)	2.087(3)	C(20)–Ir–N(1)	80.00(13)
Ir–C(20)	1.976(4)	N(1)–Ir–N(3)	159.89(12)
Ir–Cl(1)	2.3518(15)	C(20)–Ir–Cl(1)	90.94(11)
Ir–Cl(2)	2.3735(14)	N(1)–Ir–Cl(2)	89.29(9)
Ir–S(1)	2.4379(18)	Cl(1)–Ir–Cl(2)	176.20(3)

Table 9. Selected bond lengths and angles for Ir(dpydmb)(DMSO)Cl₂.

Reaction of [Ir(dpydmb)Cl(μ-Cl)]₂ **104** with 4'-(*p*-tolyl)-2,2':6',2''-terpyridine (ttpy) **82** in ethylene glycol at 196°C for 45 minutes gave [Ir(dpydmb)(ttpy)]²⁺ **106** in 87% yield, a marked improvement over that achieved for [Ir(dpyb)(ttpy)]²⁺ **100** (1%). An analogous reaction with 2,2':6',2''-terpyridine (terpy) and 5-(2,2':6',2''-terpyridin-4'-yl)isophthalic acid diethyl ester (tpyiade) **83** yielded [Ir(dpydmb)(terpy)]²⁺ **105** and [Ir(dpydmb)(tpyiade)]²⁺ **107** respectively. The latter complex is of particular interest, since hydrolysis of the ester groups should result in a potentially charge-neutral complex.



[Ir(dpydmb)(terpy)]²⁺ **105** [Ir(dpydmb)(ttpy)]²⁺ **106** [Ir(dpydmb)(tpyiade)]²⁺ **107**

Single crystals of [Ir(dpydmb)(ttpy)]²⁺ **106** were grown as the PF₆⁻ salt by slow diffusion of water into a solution of the complex in *d*₆-acetone. The resulting X-ray crystal structure is shown in Figure 18, with selected bond lengths and angles tabulated in Table 10. Further crystallographic data are given in Appendix A. Due to the geometric constraints of terdentate binding, a distorted octahedral geometry is observed

at the metal centre. The dpydmb ligand binds in a similar manner to that in $\text{Ir}(\text{dpydmb})(\text{DMSO})\text{Cl}_2$ **103**, with a slight shortening of the Ir–C and Ir–N bonds.

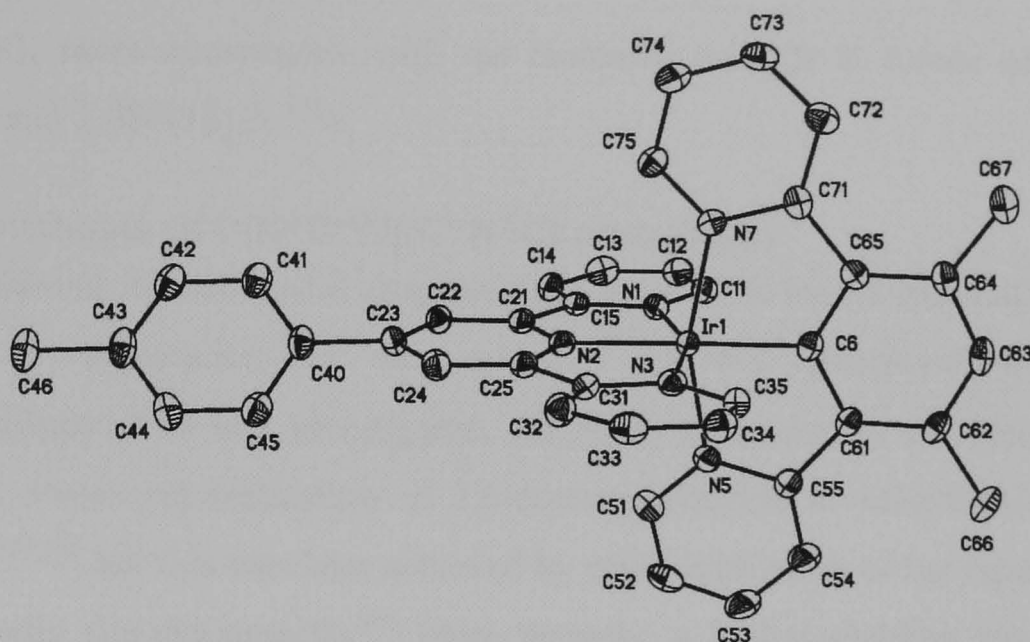


Figure 18. Structure of the $[\text{Ir}(\text{dpydmb})(\text{ttpy})]^{2+}$ cation crystallised as the PF_6^- salt from acetone; 120 K, thermal ellipsoids shown at 50% probability.

Bond lengths / Å		Bond angles / °	
Ir–N(5)	2.046(3)	C(6)–Ir–N(2)	175.76(14)
Ir–N(7)	2.047(3)	C(6)–Ir–N(5)	80.03(15)
Ir–C(6)	1.954(4)	N(5)–Ir–N(7)	160.25(13)
Ir–N(1)	2.046(3)	N(1)–Ir–N(2)	78.82(13)
Ir–N(2)	2.030(3)	N(1)–Ir–N(3)	158.19(13)
Ir–N(3)	2.052(3)	N(1)–Ir–N(5)	90.58(13)

Table 10. Selected bond lengths and angles for $[\text{Ir}(\text{dpydmb})(\text{ttpy})]^{2+}$.

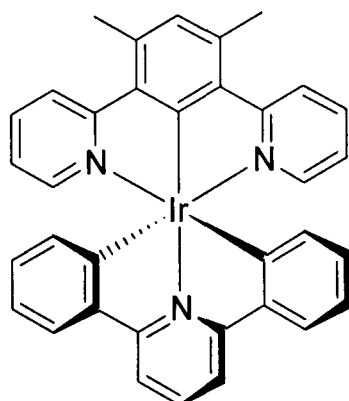
The terpyridine moiety is approximately perpendicular to the cyclometalating ligand, with an N(1)–Ir–N(5) bond angle of $90.58(13)^\circ$. The central pyridine ring is closer to the metal $\{2.030(3) \text{ \AA}\}$ than the two peripheral pyridine rings $\{2.046(3) \text{ and } 2.052(3) \text{ \AA}\}$. This is again attributed to the geometric constraints of a terdentate binding mode (as also observed for $[\text{Ir}(\text{terpy})_2]^{3+}$ ¹⁰³). Comparison to the Ir–N(central terpy) bond length of the $\text{Ir}(\text{N}^{\wedge}\text{N}^{\wedge}\text{N})(\text{C}^{\wedge}\text{N}^{\wedge}\text{C})^+$ complex **34** $\{1.943(6) \text{ \AA}\}$,¹³⁵ and to $[\text{Ir}(\text{terpy})_2]^{3+}$ $\{1.980 \text{ \AA}\}$,¹⁰³ shows a slight lengthening in the present complex. This is a result of the strong *trans*-influence metalated ligand, leading to an increase in length of the Ir–N bond *trans* to metalation. This is analogous to the increased Pt–Cl bond length in $\text{Pt}(\text{dpyb})\text{Cl}$ $\{2.417(2) \text{ \AA}\}$ ³⁷² with respect to $[\text{Pt}(\text{terpy})\text{Cl}]^+$ $\{\sim 2.30 \text{ \AA}\}$.^{373,374} In

complex **34** however it is the second metalating carbon atom that is *trans* to the Ir–C bond.¹³⁵ The consequence is a lengthening of these Ir–C bonds {2.122(9) and 2.094(9) Å} with respect to the present complex and *fac*-Ir(tpy)₃ {1.954(4) and 2.024(6) Å¹¹² respectively}, more comparable with the mutually *trans* Ir–C bonds of *mer*-Ir(tpy)₃ {2.076(10) and 2.086(12) Å¹²¹}.

3.2.1 Synthesis of Ir(N[^]C[^]N)(C[^]N[^]C) complexes

Following the successful preparation of an N[^]C[^]N bound iridium(III) precursor complex, its application to the synthesis of the charge-neutral compound Ir(dpydmb)(dppy) **108** was investigated. As far as other metals are concerned, early attempts at *trans*-cyclometalation of 2,6-diphenylpyridine to palladium(II) were unsuccessful,^{375,376} but this was later achieved by prior dilithiation of the ligand, a strategy also successful for platinum(II).³⁷⁷ More recently, a higher yielding synthesis of the platinum(II) complex has been reported by the use of glacial acetic acid as the reaction solvent.³⁷¹ This has led to numerous studies investigating the effect of substitution upon the ligand³⁷⁸ and the remaining coordination site of the metal.^{379,380} Also of interest is the report of bis-cyclometalation of 6-phenyl-2,2'-bipyridine by “rollover” metalation at the peripheral pyridyl ring.³⁸¹

Unlike the terpyridine complexes **105**, **106** and **107**, reaction of [Ir(dpydmb)Cl(μ-Cl)]₂ **104** with 2,6-diphenylpyridine in ethylene glycol at 196°C for up to two hours yielded none of the desired product. Although ¹H NMR spectroscopy of the isolated compounds showed that the 1,5-di(pyridin-2-yl)-2,4-dimethylbenzene ligand was still bound in an N[^]C[^]N manner, no other protonic resonances could be observed. Electrospray ionisation mass spectrometry suggested that the remaining three coordination sites were occupied by weakly bound solvent molecules. A similar lack of reactivity was observed when the reaction was performed in ethanol at 78°C, or even after five days in a 4:1 mixture of 2-ethoxyethanol and water at 130°C.

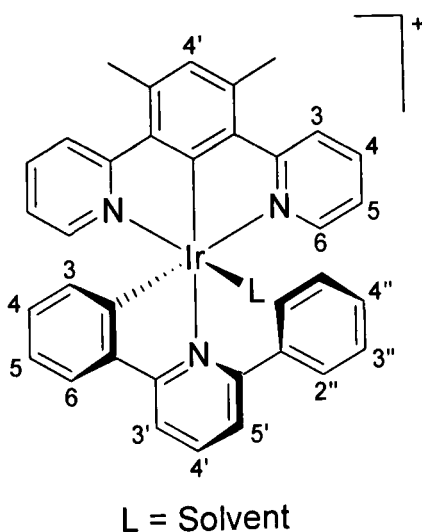


Ir(dpydmb)(dppy) **108**

Heating $[\text{Ir}(\text{dpydmb})\text{Cl}(\mu\text{-Cl})]_2$ **104** and 2,6-diphenylpyridine (dppyH_2) to 196°C in ethylene glycol for 24 hours allowed the chromatographic isolation of a dppy -containing iridium(III) complex. However, ^1H NMR spectroscopy clearly showed that this ligand was only C[^]N-coordinated, with the remaining phenyl group unbound. This complex may also be prepared under much milder conditions (*e.g.* in boiling ethanol for six days) by the addition of Ag^+ salts to promote dechlorination.

This is consistent with early attempts at binding of 2,6-diphenylpyridine (dppyH_2), where a mono-cyclometalated species $[\text{Ir}(\text{dppyH})(\text{PPh}_3)_2\text{H}]^+$ **33** was isolated, with the sixth site of the metal stabilised by an agostic bond.¹³⁴ Five-coordinate iridium complexes have recently been reported where such an agostic interaction is disfavoured, with the site opposite to metalation empty.³⁸² In the present case the pendent phenyl ring is not particularly sterically restricted, and the sixth coordination site is probably occupied by a weakly-bound solvent molecule (*i.e.* $[\text{Ir}(\text{dpydmb})(\text{dppyH})\text{L}]^+$ **109**). ^1H - ^1H NOESY NMR studies show that the unbound phenyl ring is approximately perpendicular to the rest of the dppy ligand, with a through-space interaction between the *ortho*-phenyl protons ($\text{H}^{2''}$) and those adjacent to the nitrogen of the pyridyl rings of dpydmb (H^6).

A similar bidentate binding of 2,2':6',2''-terpyridine has been reported for platinum(II),^{383,384} palladium(II)³⁸³⁻³⁸⁵ and ruthenium(II),³⁸⁶ where a suitable precursor inhibits a third coordination. The Pt(II) and Pd(II) complexes are reported to exhibit fluxional behaviour, with interchange of the bound and unbound pyridyl rings. While a rapid interconversion of metalated and agostic phenyl groups was also observed for $[\text{Ir}(\text{dppyH})(\text{PPh}_3)_2\text{H}]^+$, this was facilitated by a suitably placed hydride.¹³⁴



$[\text{Ir}(\text{dpydmb})(\text{dppyH})\text{L}]^+$ **109**

The use of acetic acid as a solvent has previously been suggested to favour the di-cyclometalation of 2,6-diphenylpyridine to platinum(II).³⁷¹ However, heating of $[\text{Ir}(\text{dpydmb})\text{Cl}(\mu\text{-Cl})]_2$ with dppyH_2 in glacial acetic acid in the presence of silver(I) trifluoromethanesulfonate at 116°C for five days still resulted in **109**.

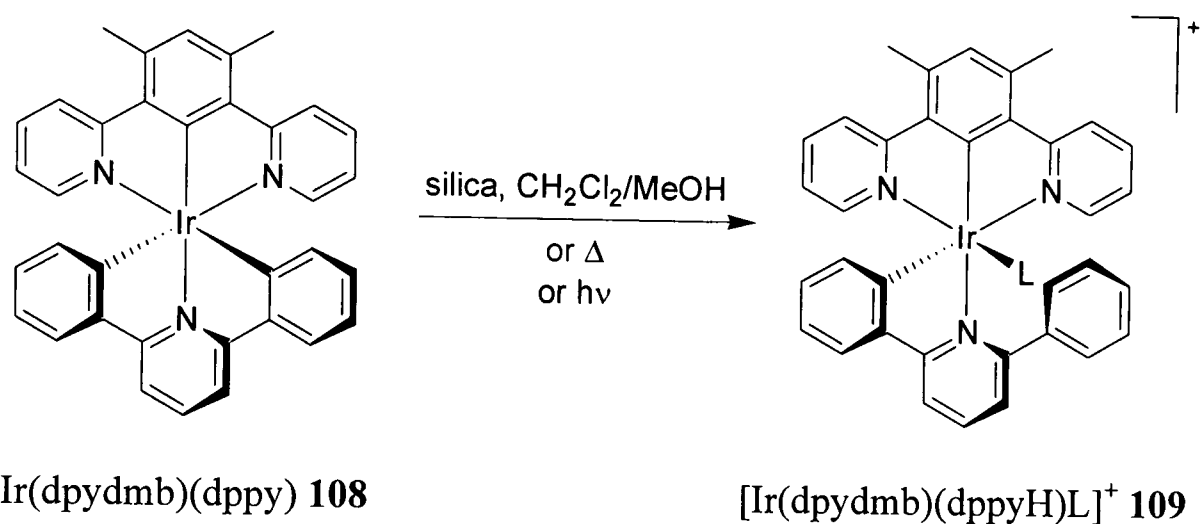
Prior dilithiation of the *ortho*-phenyl carbons of dppyH_2 has been reported to allow bis-transmetalation with platinum(II) and palladium(II),³⁷⁷ whilst the analogous organogold(III) complex has been prepared by transmetalation from the corresponding mercury(II) species.³⁸⁷ The former strategy was considered for the current iridium(III) complexes. Quenching experiments with D_2O , followed by NMR and mass spectrometric characterisation showed that four equivalents of *n*-butyl lithium were sufficient to result in ~40% dilithiation of dppy , with the remainder mainly mono-lithiated. Although larger quantities of *n*-butyl lithium resulted in approximately quantitative dilithiation, butylation *para* to the nitrogen of the pyridyl ring was also observed under these conditions. Nevertheless, addition of $[\text{Ir}(\text{dpydmb})\text{Cl}(\mu\text{-Cl})]_2$ **104** to a diethyl ether solution of dppyLiH and dppyLi_2 , followed by stirring at room temperature resulted in a complex mixture of inseparable compounds.

Since the probable presence of a weakly bound solvent molecule in **109** is likely to stabilise the resulting structure, the absence of potentially coordinating ligands from the reaction may favour the formation of $\text{Ir}(\text{dpydmb})(\text{dppy})$ **108**. Toluene was chosen as a reaction solvent due to its lack of coordinating donor atoms, and its relatively large size, which may obstruct its approach to the sixth coordination site of **109**. Unfortunately, no reaction was observed when $[\text{Ir}(\text{dpydmb})\text{Cl}(\mu\text{-Cl})]_2$ **104** and 2,6-diphenylpyridine were heated to 111°C in toluene for three days.

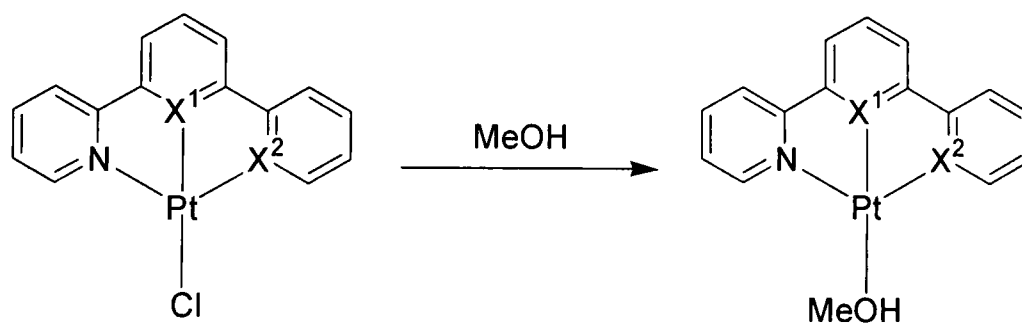
The synthesis of *fac*- $\text{Ir}(\text{ppy})_3$ has been reported with 2-phenylpyridine as both reagent and reaction solvent.^{116,117} Although a solid at room temperature, 2,6-diphenylpyridine melts at 74-76°C. Heating $[\text{Ir}(\text{dpydmb})\text{Cl}(\mu\text{-Cl})]_2$ with silver trifluoromethanesulfonate in molten dppyH at 110°C with no additional solvent, followed by chromatographic purification, did indeed result in the desired complex **108** as an orange solid in 37% yield. The structure was confirmed by ^1H NMR spectroscopy and mass spectrometry.

Although amenable to column chromatography, yields were limited by partial decomposition on the column, an issue reflected in the compound's poor photostability in solution (see Section 4). NMR and mass spectrometric characterisation permitted

identification of the decomposition product as $\text{Ir}(\text{dpydmb})(\text{dppyH})\text{L}$ **109** (see Scheme 25). The instability is probably related to the mutually *trans* cyclometalating carbons, a phenomenon recently referred to as “transphobia”.^{128,388} The strong *trans*-effect of a cyclometalating carbon donor atom labilises the ligand opposite, while its strong *trans*-influence increases the ground state bond length. A dramatic example of the *trans*-effect is provided by a kinetic study of the displacement of chloride from a platinum(II) complex (see Scheme 26). Whereas similar rates of solvation were observed when the central aromatic ring was a pyridine ($X^1 = \text{N}$, $X^2 = \text{N/C}$), substitution with a phenyl ring ($X^1 = \text{C}$, $X^2 = \text{N}$) resulted in an almost 100 000 fold increase.³⁸⁹

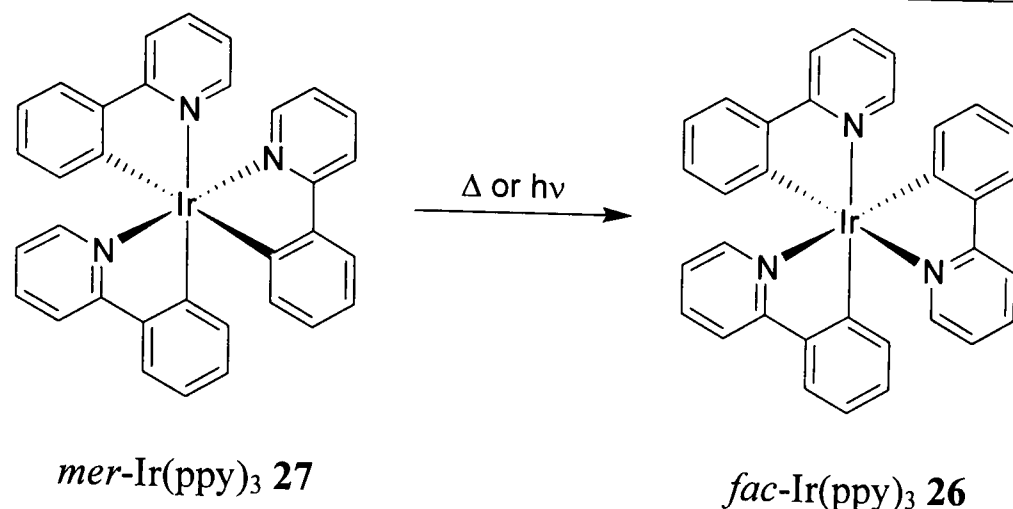


Scheme 25. Decomposition of $\text{Ir}(\text{dpydmb})(\text{dppy})$ to $[\text{Ir}(\text{dpydmb})(\text{dppyH})\text{L}]^+$.



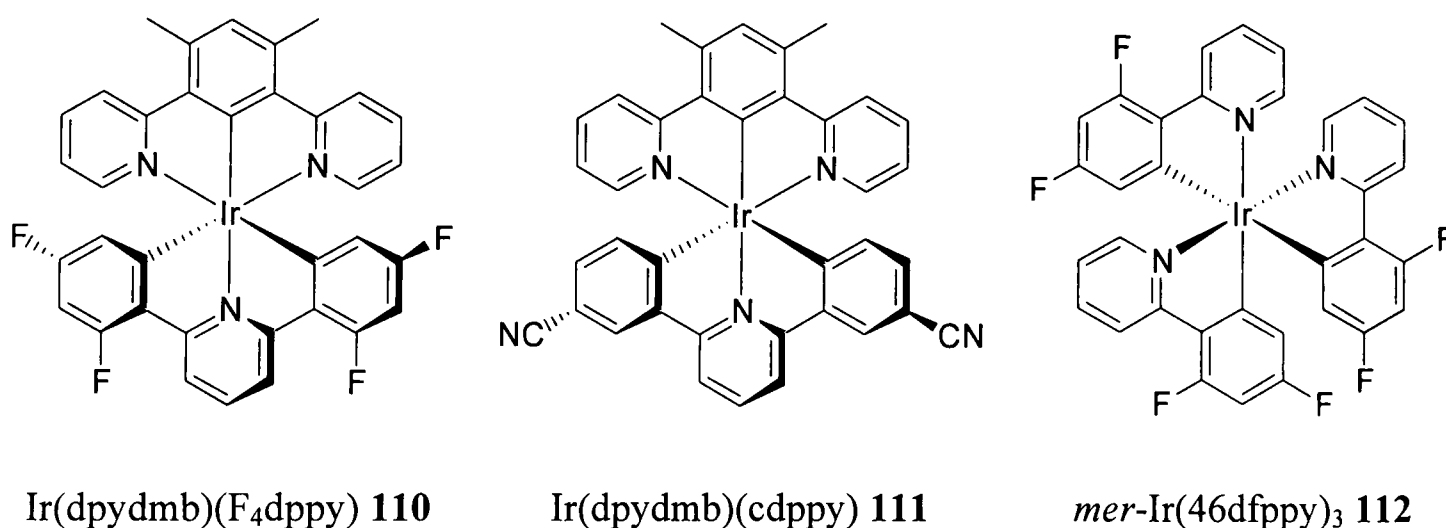
Scheme 26. Displacement of a platinum(II) bound chloride by methanol.

Of particular relevance in the present context is *mer*- $\text{Ir}(\text{ppy})_3$ **27** and derivatives, which undergo a thermally- and photochemically-activated isomerisation to the facial isomers (see Scheme 27).¹²¹ In the present case, the terdentate binding of ligands enforces a meridional geometry, with no opportunity for isomerisation to a facial coordination. Instead, cleavage of one of the mutually *trans* Ir–C bonds is irreversible. It should be noted that, although geometrically constrained, the argument for instability due to steric effects is doubtful due to the high stability in binding of 2,2':6',2''-terpyridine (terpy) derivatives.



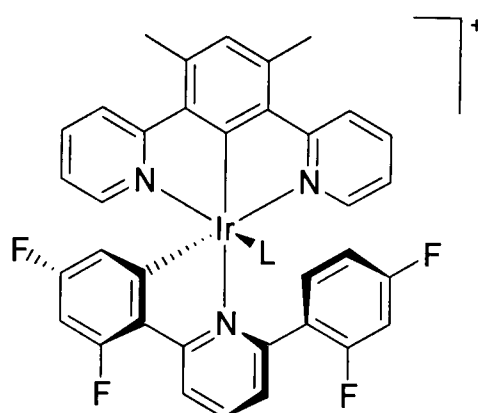
Scheme 27. Thermally and photochemically activated isomerisation of $mer\text{-Ir(ppy)}_3$ **27** to $fac\text{-Ir(ppy)}_3$ **26**.

In order to stabilise Ir(dpydmb)(dppy) **108** with respect to Ir–C bond dissociation, $\text{Ir(dpydmb)(F}_4\text{dppy)}$ **110** and Ir(dpydmb)(cdppy) **111** were considered, incorporating electron-withdrawing substituents in the *meta*- and *para*-positions to the metal respectively. It was hoped that this would stabilise the negative charge at the carbon end of the formal $\text{C}^- \text{--} \text{Ir}^+$ bond, resulting in reduced lability. Difluorination *meta* to cyclometalation has been reported to inhibit the thermal isomerisation of $mer\text{-Ir(46dfppy)}_3$ **112** to the facial isomer,¹²¹ and a recent patent has proposed cyano substitution of Ir(ppy)_3 derivatives.³⁹⁰



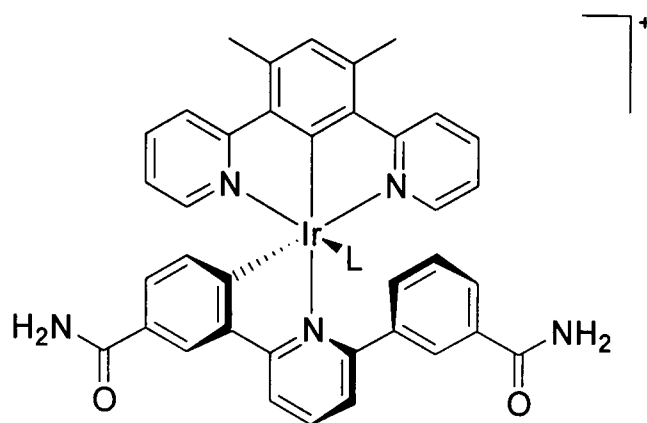
A mixture of $[\text{Ir(dpydmb)Cl}(\mu\text{-Cl})]_2$ **104** and silver trifluoromethanesulfonate in molten 2,6-di(2,4-difluorophenyl)pyridine (F_4dppyH_2) **96** was heated at 110°C with no additional solvent. Following chromatographic purification, $\text{Ir(dpydmb)(F}_4\text{dppy)}$ **110** was obtained as a yellow solid in 21% yield. Although this is in lower yield than for Ir(dpydmb)(dppy) **108**, no evidence of Ir–C bond dissociation was observed upon column chromatography in this case, suggesting that fluorination may be successful in stabilising the system.

Attempts to scale up this reaction were hindered by the increasingly large quantities of the F_4dppyH_2 ligand required. If the ratio of ligand to intermediate is reduced, the mixture no longer melts below 110 °C, and yields are substantially decreased (e.g. 2,6-di(2,4-difluorophenyl)pyridine (116 mg, 0.38 mmol), $[Ir(dpydmb)Cl(\mu-Cl)]_2$ (75 mg, 0.072 mmol) and silver(I) trifluoromethanesulfonate (83 mg, 0.32 mmol) heated to 110 °C for 24 hours resulted in less than 10% yield). Increasing the temperature to 150°C merely resulted in the formation of significant amounts of the decomposed $[Ir(dpydmb)(F_4dppyH)L]^+$ complex **113**. Alternatively, when acetic acid was used as a solvent, no binding of the F_4dppyH_2 ligand was observed whatsoever.



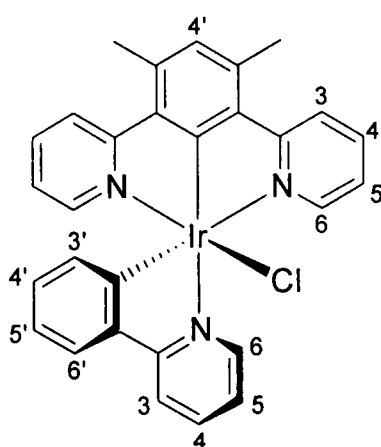
$[Ir(dpydmb)(F_4dppyH)L]^+$ **113**

In the case of $Ir(dpydmb)(cdppy)$ **111**, solvent free reaction conditions are unsuitable due to the high melting point of 2,6-di(3-cyanophenyl)pyridine ($cdppyH_2$) (~188°C). If the reaction temperature is raised to 200°C, a complex mixture of products forms, with no evidence of the desired compound. The use of the conventional solvent diglyme, on the other hand, resulted in no complexation whatsoever upon heating at 110°C. In an attempt to promote cyclometalation, $[Ir(dpydmb)Cl(\mu-Cl)]_2$ was heated with 2,6-di(3-cyanophenyl)pyridine and silver(I) trifluoromethanesulfonate in acetic acid under an inert atmosphere for two days. Although purification of the resulting complex was unsuccessful, it was identified by NMR and mass spectrometry as **114**. In addition to unsymmetrical binding of the $cdppy$ ligand, partial hydrolysis of the cyano-substituents had occurred.



114

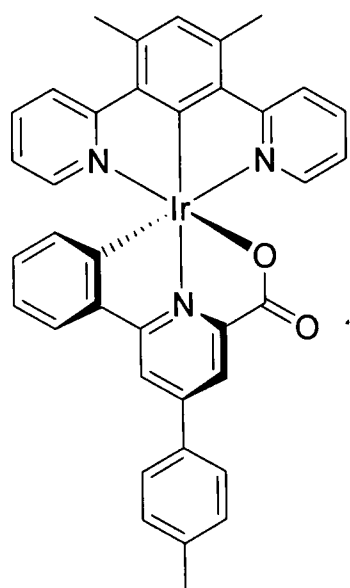
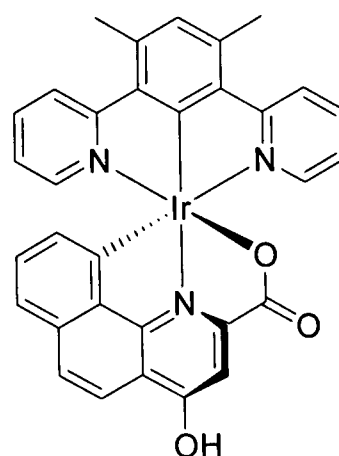
In order to have a model complex with which to investigate the luminescence properties of mixed N⁺C⁻N, C⁻N bound systems (e.g. **109** and **113**), the complex Ir(dpydmb)(ppy)Cl **115** was prepared. Reaction of [Ir(dpydmb)Cl(μ-Cl)]₂ and silver trifluoromethanesulfonate in 2-phenylpyridine (ppyH) gave the desired complex.[‡] Excess ppyH was extracted by washing a dichloromethane solution of the crude product with 1 mol dm⁻³ HCl, followed by chromatographic separation. The use of K₂CO₃ instead of AgSO₃CF₃ (as for the syntheses of *fac*- and *mer*-Ir(ppy)₃¹²¹) in both pure ppyH and ethylene glycol solutions resulted in significantly lower yields. As would be expected for the thermodynamic product, a meridional geometry is observed, confirmed by the presence of a ¹H-¹H NOESY cross-peak between H⁶ of the dpydmb ligand and H⁶ of ppy.

Ir(dpydmb)(ppy)Cl **115**

[‡] Although there is no definitive evidence for the presence of a bound chloride, the low polarity of solvent required upon column chromatography (silica, dichloromethane/methanol, 99.75/0.25) suggests that the obtained product is charge-neutral.

3.2.2 Synthesis of complexes of picolinic acid derivatives

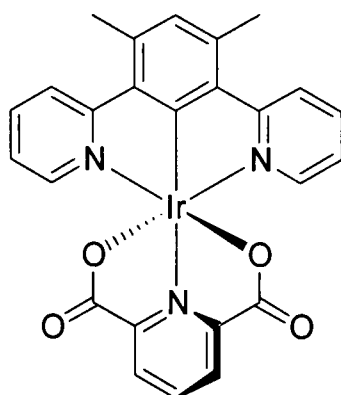
Following successful preparation of Ir(dpydmb)(C^NC) derivatives, the charge-neutral Ir(dpydmb)(C^NO) complexes Ir(dpydmb)(tppic) **116** and Ir(dpydmb)(hbqc) **117**[§] were prepared in molten solutions. Since the ligands themselves are solids at the reaction temperature, the complexations were performed in molten benzoic acid. This was chosen for its suitable melting point (122-123°C) and potential for solubilising pyridine carboxylic acid functionalised ligands. Heating [Ir(dpydmb)Cl(μ-Cl)]₂ with silver trifluoromethanesulfonate and the respective ligand in molten benzoic acid followed by purification by column chromatography resulted in complexes **116** and **117** in reasonable yield (54% and 58% respectively). Interestingly, the attempted preparation of Ir(dpydmb)(dppy) **108** in molten benzoic acid was unsuccessful.

Ir(dpydmb)(tppic) **116**Ir(dpydmb)(hbqc) **117**

The concept of charge-neutralisation by acid functionality may be extended to the target complex Ir(dpydmb)(pydc) **118**, incorporating O^NO coordination of pyridine-2,6-dicarboxylic acid (pydcH₂). The traditional solvents for iridium(III) complexation, 2-ethoxyethanol and ethylene glycol, proved to be inappropriate since rapid esterification of the ligand occurs in competition with complexation. This side reaction is not possible for 1,2-dimethoxyethane (DME), however, heating [Ir(dpydmb)Cl(μ-Cl)]₂ with pyridine-2,6-dicarboxylic acid in DME at 83°C for four days resulted in no evidence for binding of the pydcH₂ ligand. In contrast to the

[§] 4-Hydroxybenzo[*h*]quinoline-2-carboxylic acid (hbqcH₂) was supplied by Avecia Ltd. as the ethyl-ester.

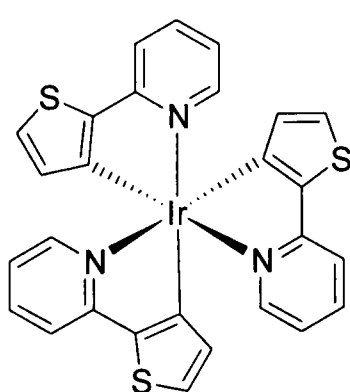
carboxylate bound complexes **116** and **117**, reaction in benzoic acid resulted in a complex mixture of inseparable products. Hence complex **118** has remained elusive.



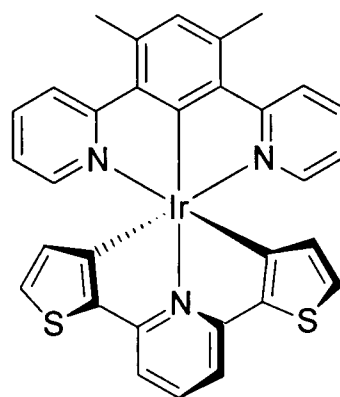
Ir(dpydmb)(pydc) **118**

3.2.3 Cyclometalation *via* five-membered heterocyclic rings

Although most research has focused upon cyclometalation *via* phenyl groups, the formation of Ir–C bonds to five-membered heterocyclic rings has also been reported.^{115,116,127,128,169,170} For example, 2-(2-thienyl)pyridine (thpyH₂) is known to bind in a C^N manner in *fac*-Ir(thpy)₃ **30**.¹¹⁶ The analogous C^N^C coordinated complex is Ir(dpydmb)(dthpy) **119**. The plausibility of coordination in this way is reinforced by the report that reaction of 2,6-di(2-thienyl)pyridine with K₂[PtCl₄] in 2-methoxyethanol/water results in a mixture of C^N^C and C^N binding.³⁵⁷ In the present study, reaction of [Ir(dpydmb)Cl(μ-Cl)]₂ with dthpyH₂ in ethylene glycol at 200°C for 24 hours showed no evidence of complexation. A similar unreactivity was found when heated in an excess of molten ligand. While binding was observed upon replacement of the solvent with glacial acetic acid, this was shown to be only bidentate C^N coordination with the second thienyl ring not bound.



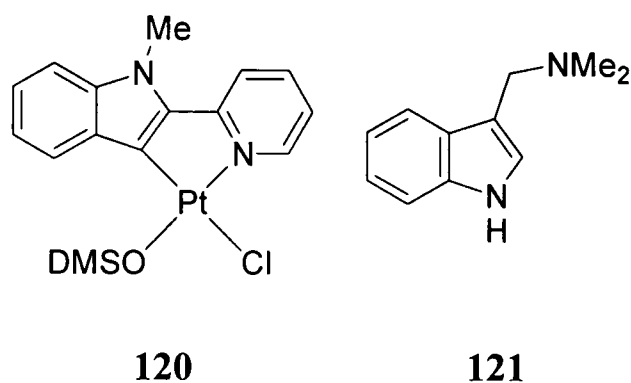
fac-Ir(thpy)₃ **30**



Ir(dpydmb)(dthpy) **119**

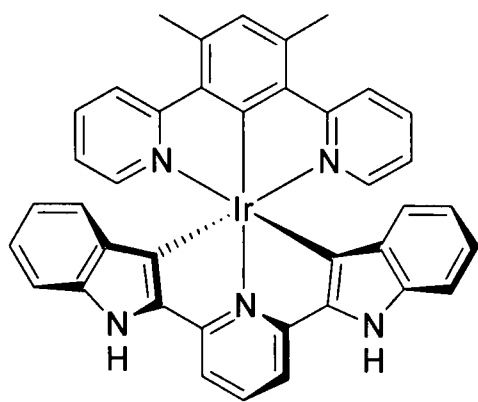
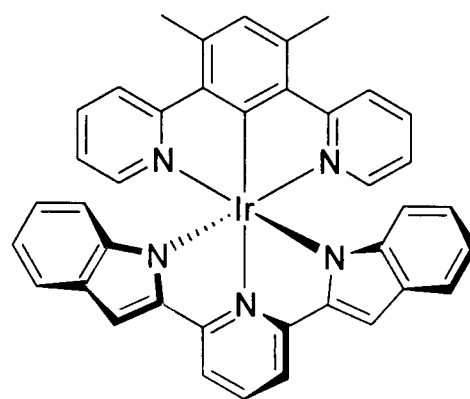
The nitrogen analogue 2,6-di(2'-indolyl)pyridine (dinpyH₂) **97** may either bind to a metal through all three nitrogen atoms, or cyclometalate akin to thpyH₂. Dilithiation

of dinpyH_2 followed by reaction with platinum(II) and palladium(II) precursors has been shown to result exclusively in the former.³⁹¹ Although non-emissive at room temperature, $\text{Pt}(\text{dinpy})(\text{py})$ and $\text{Pt}(\text{dinpy})(\text{SMe}_2)$ exhibited red-orange luminescence ($\lambda_{\text{max}} = 570 \text{ nm}$) at 77 K assigned to a $\pi\text{-}\pi^*$ transition of the dinpy ligand. Reports of the tin(IV) and lead(IV) complexes also reveal an N[^]N[^]N binding mode, with intense luminescence from $\text{Sn}(\text{dinpy})\text{Ph}_2$ even at ambient temperature.³⁹² Similarly, 2-(2'-indolyl)pyridine has been reported to bind in an N[^]N manner to zinc(II),³⁹³ ruthenium(II),³⁹⁴ rhodium(I)³⁹⁵ and palladium(II).³⁹⁶ Cyclometalation at the 3-position has been achieved for the platinum(II) complex **120** by methylation of the indolyl nitrogen atom. ³⁹⁷ Also of note are the palladium(II)³⁹⁸ and platinum(II)³⁹⁹ complexes of **121**, where cyclometalation is observed at the 2-position.



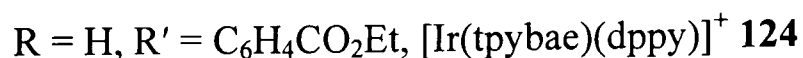
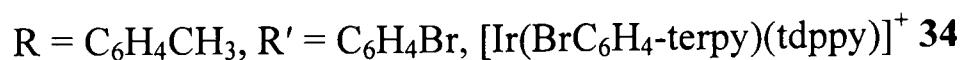
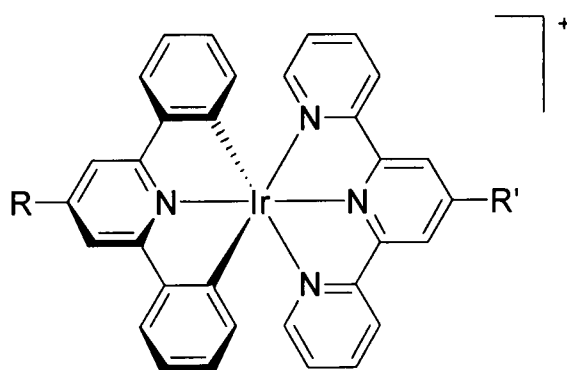
Initial attempts at the preparation of an iridium(III) complex of 2,6-di(2'-indolyl)pyridine (dinpyH_2) involved an adaptation of the molten solid route previously discussed. Since dinpyH_2 has a higher melting point (mp 251.0-253.6°C), it was diluted in molten benzoic acid or, in an attempt to deprotonate the indolyl nitrogen atoms, in diphenylamine or triethylamine. The prior lithiation strategy successful for platinum(II) and palladium(II) complexes was also attempted.³⁹¹ In all cases a complex mixture of inseparable products was obtained.

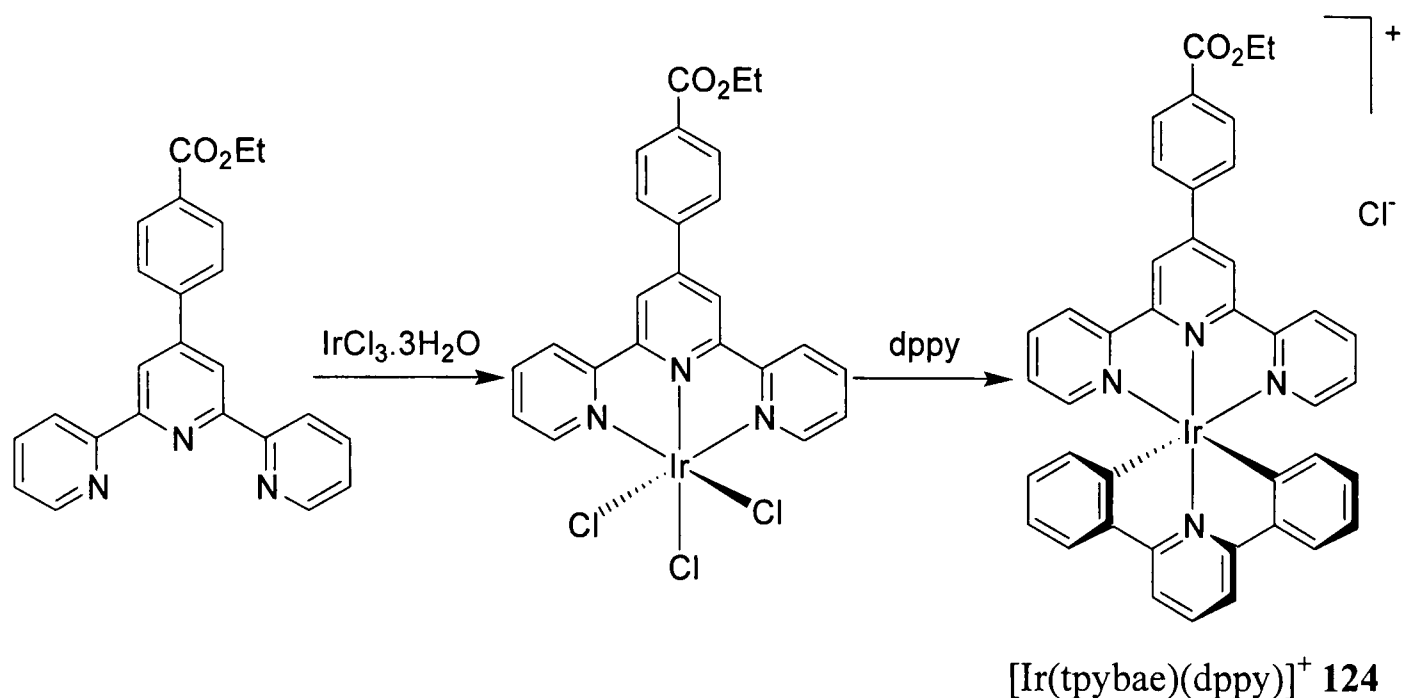
More success was achieved when complexation was promoted by heating in solution, with an intriguing dependence of binding behaviour upon the solvent used. While reaction of $[\text{Ir}(\text{dpydmb})\text{Cl}(\mu\text{-Cl})_2]$ with 2,6-di(2'-indolyl)pyridine in ethylene glycol in the presence of base resulted in the cyclometalated complex $\text{Ir}(\text{dpydmb})(\text{dinpy}\text{-C}^{\wedge}\text{N}^{\wedge}\text{C})$ **122**, the same reaction in acetic acid with a silver salt gave the triply N-bound complex $\text{Ir}(\text{dpydmb})(\text{dinpy}\text{-N}^{\wedge}\text{N}^{\wedge}\text{N})$ **123**. The reactions were unfortunately low yielding (4% and 8% respectively) and product of sufficient purity for photophysical studies has so far not been obtained.

Ir(dpydmb)(dinpy-C^NC) **122**Ir(dpydmb)(dinpy-N^NN) **123**

3.2.4 Other complexes incorporating mutually *trans* bis-metalation

In view of the observation that the instability of C^NC coordinated complexes may be related to the presence of mutually *trans* metalated carbon atoms, other compounds with such a coordination were investigated. The 2,6-diphenylpyridine (dppy) complex [Ir(tpybae)(dppy)]⁺ **124** was prepared by an adaptation of the conventional route to bis-terpyridine complexes (see Section 1.2.1.1). Reaction of 4-(2,2':6',2''-terpyridin-4'-yl)benzoic acid ethyl ester (tpybae) with iridium trichloride trihydrate in ethylene glycol gave the intermediate compound Ir(tpybae)Cl₃. Although some transesterification forming the ethylene glycol derivative contaminates the product, attempts at lower temperatures in 2-ethoxyethanol resulted in incomplete reaction. Subsequent heating with 2,6-diphenylpyridine in ethylene glycol at 196°C followed by chromatographic separation resulted in the desired complex in 4% yield (Scheme 28).

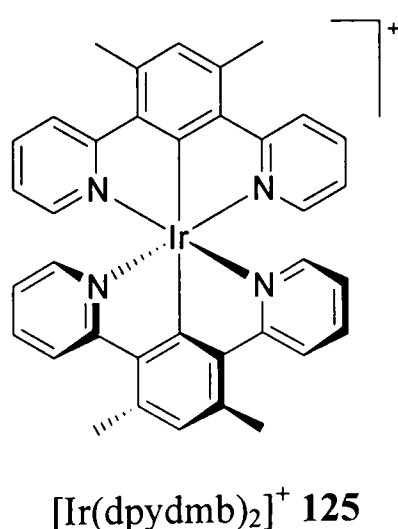




Scheme 28. Synthesis of $[\text{Ir}(\text{tpybae})(\text{dppy})]^+ \text{ 124}$ by a two-step route.

During the course of this work, the preparation of complex **34** was reported in 38% yield *via* an analogous procedure. The improvement in yield is probably due to the absence of ester functionality. It is interesting to note that although both complexes possess a mutually *trans* pair of Ir–C bonds, there is no evidence for any thermal or photochemical instability. This suggests that the labilisation of such bonds in $\text{Ir}(\text{dpydmb})(\text{dppy}) \text{ 108}$ and *mer*- $\text{Ir}(\text{ppy})_3 \text{ 27}$ derivatives is activated by the presence of a third cyclometalating carbon atom in the coordination sphere of the metal.

Another *trans* bis-cyclometalated complex, $[\text{Ir}(\text{dpydmb})_2]^+ \text{ 125}$ was prepared by reaction of the chloride-bridged intermediate compound $[\text{Ir}(\text{dpydmb})\text{Cl}(\mu\text{-Cl})]_2$ with potassium carbonate and a second equivalent of ligand in ethylene glycol at 196°C for 24 hours. Although obtained only in low yield (11%), no instability upon column chromatography was observed.



CHAPTER 4

PHOTOPHYSICAL AND COMPUTATIONAL STUDIES OF IRIDIUM(III) COMPLEXES

4 Photophysical and computational studies of iridium(III) complexes

4.1 Photophysical properties

4.1.1 Ir(N[^]C[^]N)(C[^]N[^]C) complexes

The ground-state absorbance spectra of Ir(dpydmb)(dppy) **108**, Ir(dpydmb)(F₄dppy) **110** and *fac*-Ir(ppy)₃ **26** in acetonitrile solution are shown in Figure 19 (summarised in Table 11). They all show intense bands in the near-UV region between 240 and 300 nm assigned to spin-allowed ¹π-π* transitions of the ligands. These are accompanied by a series of weaker, lower energy features extending well into the visible region, assigned to both allowed and spin-forbidden metal-to-ligand charge transfer (MLCT) bands. The bis-terdentate complexes show significantly lower energy MLCT bands than the tris-bidentate *fac*-Ir(ppy)₃ **26** and *mer*-Ir(ppy)₃ **27** (which exhibit similar absorbance spectra to one another¹²¹). This is attributed to a lowering in energy of the acceptor ligand π*-orbitals upon increased delocalisation across three aromatic rings. The MLCT transitions of the fluorinated Ir(dpydmb)(F₄dppy) **110** complex are blue-shifted with respect to Ir(dpydmb)(dppy) **108**, due to stabilisation of the HOMO as a result of the electron-withdrawing nature of the fluorine substituents.

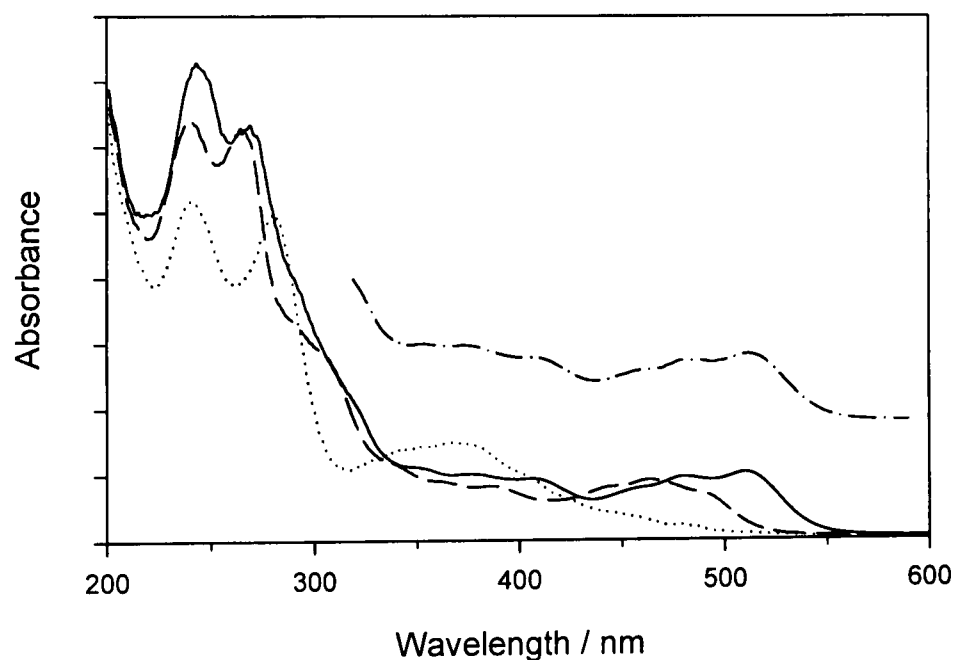


Figure 19. Ground-state absorbance spectra of Ir(dpydmb)(dppy) **108** (solid line), Ir(dpydmb)(F₄dppy) **110** (dashed line) and *fac*-Ir(ppy)₃ **26** (dotted line) in acetonitrile solution at 295 K. Also shown is the luminescence excitation spectrum of Ir(dpydmb)(dppy) **108** (dash-dotted line, displaced for clarity, $\lambda_{em} = 600$ nm).

Complex	λ / nm (ϵ / dm ³ mol ⁻¹ cm ⁻¹)
Ir(dpydmb)(dppy) 108	244 (53 900), 269 (46 900), 349 (7 700), 378 (6 900), 406 (6 500), 458 (5 500), 481 (6 800), 510 (7 300).
Ir(dpydmb)(F ₄ dppy) 110	240 (12 300), 265 (12 000), 290 (6 200), 304 (5 300), 334 (2 100), 360 (1 500), 385 (1 400), 447 (1 400), 464 (1 600), 487 (1 300).

Table 11. Absorbance data for Ir(N[^]C[^]N)(C[^]N[^]C) complexes in acetonitrile solution at 295 K.

The room temperature emission spectra of Ir(dpydmb)(dppy) **108**, Ir(dpydmb)(F₄dppy) **110** and *fac*-Ir(ppy)₃ **26** in acetonitrile solution are shown in Figure 20. All complexes are strongly luminescent in degassed solution, with luminescence excitation spectra comparable to the absorbance spectra in each case (see Figure 19 for Ir(dpydmb)(dppy) **108**). Emission spectra are comprised of a single, broad, structureless band, typical of phosphorescence from an MLCT triplet state. This assignment is supported by TD-DFT calculations, although it is shown to be mixed with significant amounts of ligand centred (LC) and some ligand-to-ligand charge transfer (LLCT) character (see Section 4.2). The Ir(dpydmb)(dppy) **108** luminescence ($\lambda_{\text{max}} = 585$ nm) is noticeably red-shifted with respect to *fac*-Ir(ppy)₃ **26** ($\lambda_{\text{max}} = 528$ nm). This bathochromic shift is attributed to a lowering of the ligand π^* orbital energy upon the increased conjugation which accompanies the introduction of an additional pyridyl ring. Although it may be argued that the effect could arise from a destabilisation of the predominantly metal-based HOMO upon the introduction of two mutually *trans* Ir–C bonds, no significant shift is observed for *mer*-Ir(ppy)₃ **27** (512 nm compared to 510 nm for the *fac*-isomer in the same solvent¹²¹). The blue-shift in emission upon 4,6-difluorination (Ir(dpydmb)(F₄dppy) **110**, $\lambda_{\text{max}} = 547$ nm) is analogous to the hypsochromic shift observed for *fac*-Ir(46dfppy)₃.¹²¹ This is attributed to an increased stabilisation of the HOMO compared to the LUMO upon introduction of the inductively electron-withdrawing fluorine atoms, as was concluded from the absorption spectrum. Molecular orbital plots from DFT calculations substantiate this interpretation, since the LUMO is almost entirely localised on the unsubstituted dpydmb ligand, while the HOMO has a significant portion on the dppy moiety (see Section 4.2.2).

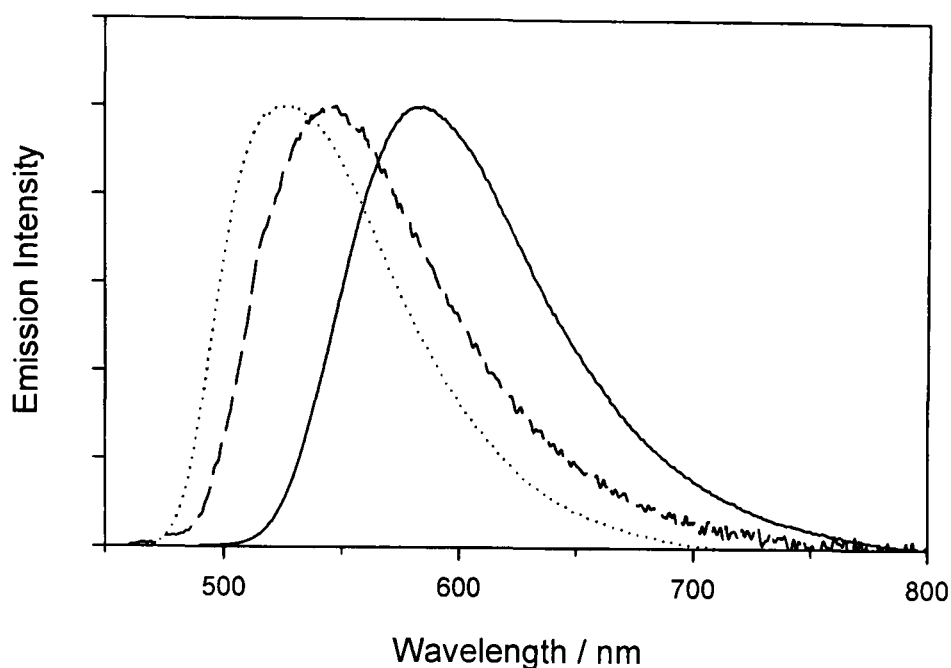


Figure 20. Emission spectra of Ir(dpydmb)(dppy) **108** (solid line, $\lambda_{\text{ex}} = 481$ nm), Ir(dpydmb)(F₄dppy) **110** (dashed line, $\lambda_{\text{ex}} = 447$ nm) and *fac*-Ir(ppy)₃ **26** (dotted line, $\lambda_{\text{ex}} = 400$ nm) in acetonitrile solution at 295 K. Excitation and emission bandpasses were 2.5 nm.

Luminescence data for Ir(dpydmb)(dppy) **108**, Ir(dpydmb)(F₄dppy) **110** and *fac*-Ir(ppy)₃ **26** are summarised in Table 12. The luminescence of Ir(dpydmb)(dppy) **108** and Ir(dpydmb)(F₄dppy) **110** is strongly quenched by oxygen, but in degassed acetonitrile solution the luminescence quantum yields of 0.21 and 0.41 respectively are quite high. While Ir(dpydmb)(dppy) **108** is approximately half as emissive as the related *fac*-Ir(ppy)₃ complexes, a decrease in efficiency is not unexpected. According to the energy gap law,¹⁹ for a homologous series of complexes, a red-shift in emission (as observed in the present case) is likely to be accompanied by a decrease in the luminescence quantum yield. Luminescence quantum yields of both Ir(N[^]C[^]N)(C[^]N[^]C) complexes are however substantially higher than those for *mer*-Ir(ppy)₃ derivatives,¹²¹ which incorporate the same meridional coordination geometry.

Complex	λ_{\max} / nm	CIE coordinates	Aerated		Degassed	
			Φ^a	τ^d / ns	Φ^a	τ^d / ns
Ir(dpydmb)(dppy) 108 ^g	585	$x=0.55, y=0.45$	0.0013 ^b	77 ^e	0.21 ^b	3800 ^e
Ir(dpydmb)(F ₄ dppy) 110 ^g	547	$x=0.43, y=0.55$	0.0036 ^c	<100	0.41 ^c	3700 ^f
<i>fac</i> -Ir(ppy) ₃ ^g	528	$x=0.36, y=0.59$				
<i>fac</i> -Ir(ppy) ₃ ^{h 121}	510				0.40	1900
<i>mer</i> -Ir(ppy) ₃ ^{h 121}	512				0.036	150
<i>fac</i> -Ir(46dfppy) ₃ ^{h 121}	450				0.43	1600
<i>mer</i> -Ir(46dfppy) ₃ ^{h 121}	460				0.053	210

^aQuantum yields of emission, 295 K, measured using an aqueous solution of [Ru(bpy)₃]²⁺ as a standard;⁴⁰⁰ uncertainty $\pm 20\%$. ^b $\lambda_{\text{ex}} = 458$ nm. ^c $\lambda_{\text{ex}} = 447$ nm. ^dLifetimes of emission, $\lambda_{\text{ex}} = 355$ nm, 295 K; uncertainty $\pm 5\%$. ^eMonitored at 580 nm. ^fMonitored at 570 nm. ^gMeasurements in CH₃CN. ^hMeasurements in CH₂Cl₂.

Table 12. Luminescence data for Ir(dpydmb)(dppy) 108, Ir(dpydmb)(F₄dppy) 110 and *fac*-Ir(ppy)₃ 26 in acetonitrile solution. Data for the *fac*- and *mer*-isomers of Ir(ppy)₃ and Ir(46dfppy)₃ in dichloromethane solution are included for comparison.¹²¹

The poor luminescence efficiency of *mer*-Ir(ppy)₃ derivatives was attributed to a competing *mer*-to-*fac* photoisomerisation process, also accounting for the particularly short emission lifetimes.¹²¹ Assuming that formation of the emissive state is efficient, one may calculate the radiative (k_r), non-radiative ($\sum k_{nr}$) and oxygen-quenching (k_q) decay rate constants by application of equations 13 and 14¹⁹ (where Φ and τ are the luminescence quantum yields and lifetimes respectively, and [O₂] is the concentration of oxygen in solution). Whilst *fac*- and *mer*-Ir(ppy)₃ derivatives have similar radiative rate constants, the non-radiative rate constants are more than an order of magnitude greater for the meridional isomers (see Table 13). This is due to the additional *mer*-to-*fac* photoisomerisation process present for these complexes. For Ir(dpydmb)(dppy) **108** and Ir(dpydmb)(F₄dppy) **110**, the non-radiative rate constants are of a comparable magnitude to those for *fac*-Ir(ppy)₃ **26**, suggesting that photodecomposition processes are not of major significance under typical irradiation. Instead, luminescence quantum yields appear to be limited by the relatively low radiative rate constants for these complexes.

$$\tau = \frac{1}{k_r + \sum k_{nr} + k_q [\text{O}_2]} \quad (13)$$

$$\Phi = \frac{k_r}{k_r + \sum k_{nr} + k_q [\text{O}_2]} \quad (14)$$

Complex	$k_r / \text{s}^{-1} \text{ }^a$	$\sum k_{nr} / \text{s}^{-1} \text{ }^a$	$k_q / \text{dm}^3 \text{ mol}^{-1} \text{ s}^{-1} \text{ }^b$
Ir(dpydmb)(dppy) 108	5.5×10^4	2.1×10^5	1.4×10^9
Ir(dpydmb)(F ₄ dppy) 110	1.1×10^5	1.6×10^5	1.1×10^9
<i>fac</i> -Ir(ppy) ₃ ¹²¹	2.1×10^5	3.2×10^5	
<i>mer</i> -Ir(ppy) ₃ ¹²¹	2.4×10^5	6.5×10^6	
<i>fac</i> -Ir(46dfppy) ₃ ¹²¹	2.7×10^5	3.6×10^5	
<i>mer</i> -Ir(46dfppy) ₃ ¹²¹	2.5×10^5	4.5×10^6	

^aEstimated uncertainty $\pm 20\%$. ^bEstimated uncertainty $\pm 10\%$.

Table 13. Radiative, non-radiative and bimolecular oxygen quenching decay rate constants for Ir(dpydmb)(dppy) 108 and Ir(dpydmb)(F₄dppy) 110 in acetonitrile solution at 295 K. Data for the *fac*- and *mer*-isomers of Ir(ppy)₃ and Ir(46dfppy)₃¹²¹ are included for comparison.

Although rates of photodecomposition are likely to be small, such processes were observed for Ir(dpydmb)(dppy) **108** under intense irradiation (Xe discharge lamp). ¹H NMR spectroscopic analysis following irradiation in acetonitrile solution indicates that the major compound present is [Ir(dpydmb)(dppyH)L]⁺ **109**, the result of cleavage of one of the mutually *trans* Ir–C bonds. Whereas *mer*-Ir(ppy)₃ and its derivatives are converted to the *fac*-form following such a dissociation,¹²¹ the terdentate nature of the ligands in Ir(dpydmb)(dppy) **108** prohibit such an isomerisation.

The solvent-dependence of the rate of photodecomposition was investigated, with the results illustrated in Figure 21, which shows the degassed emission spectra following five minutes irradiation, normalised to a peak intensity of 1.0 prior to irradiation. It is suggested that the observed trend is related to the ability of the solvent to solvate the sixth site of the complex. Whilst the smaller dichloromethane and acetonitrile molecules may solvate this site well, the larger THF and toluene molecules are hindered in their approach to this site, impeding the decomposition. Fortunately, there is no sign of decomposition when irradiated in the solid-state, suggesting that stability when incorporated into electroluminescent devices will not be compromised. Although the fluorinated derivative Ir(dpydmb)(F₄dppy) **110** still photodegrades under prolonged irradiation in solution, the rate is significantly decreased, with a significant proportion of the emission intensity retained after irradiation for one hour in acetonitrile solution.

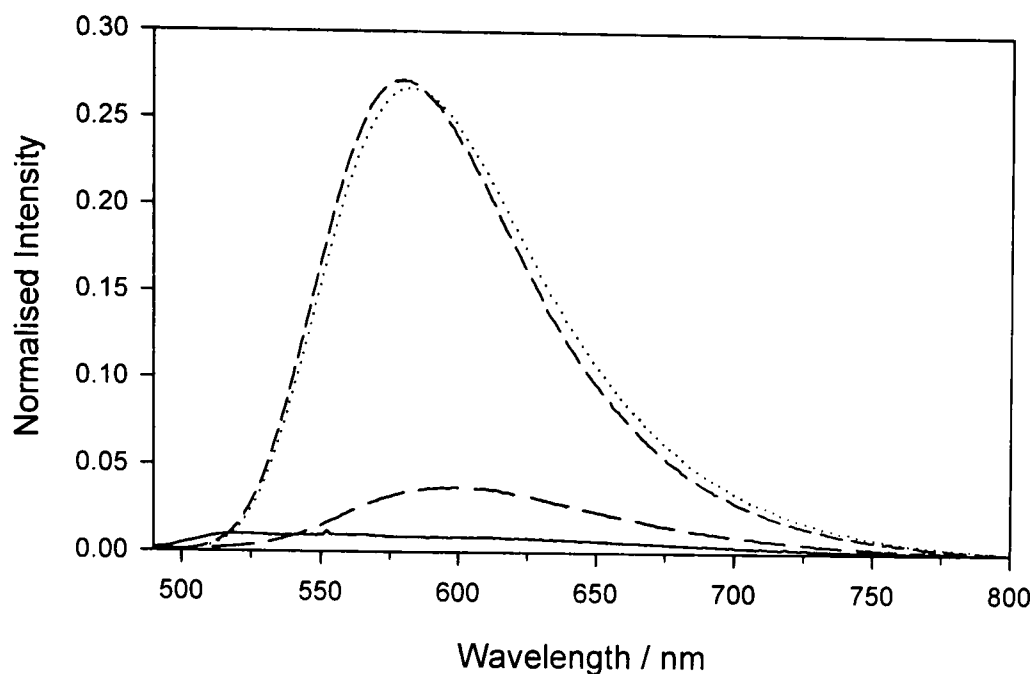


Figure 21. Emission spectra of Ir(dpydmb)(dppy) 108 in dichloromethane (solid line, $\lambda_{\text{ex}} = 484$ nm), acetonitrile (long dashed line, $\lambda_{\text{ex}} = 481$ nm), THF (dotted line, $\lambda_{\text{ex}} = 484$ nm) and toluene (short dashed line, $\lambda_{\text{ex}} = 485$ nm) following intense irradiation for five minutes. All spectra are normalised to a peak intensity of 1.0 prior to irradiation.

4.1.2 Ir(N[^]C[^]N)(C[^]N)Cl complex

The ground-state absorbance spectrum of Ir(dpydmb)(ppy)Cl **115** in acetonitrile solution is compared to that of Ir(dpydmb)(dppy) **108** in Figure 22 (data summarised in Table 14). For Ir(dpydmb)(ppy)Cl **115**, a number of bands are observed below ~ 300 nm due to $^1\pi-\pi^*$ transitions of the ligands, and a series of weaker bands extending into the visible region assigned to metal-to-ligand charge transfer (MLCT) transitions. These are blue-shifted with respect to Ir(dpydmb)(dppy) **108** due to a lowering of the HOMO upon substitution of a cyclometalating carbon atom with a much weaker field chloride ligand.

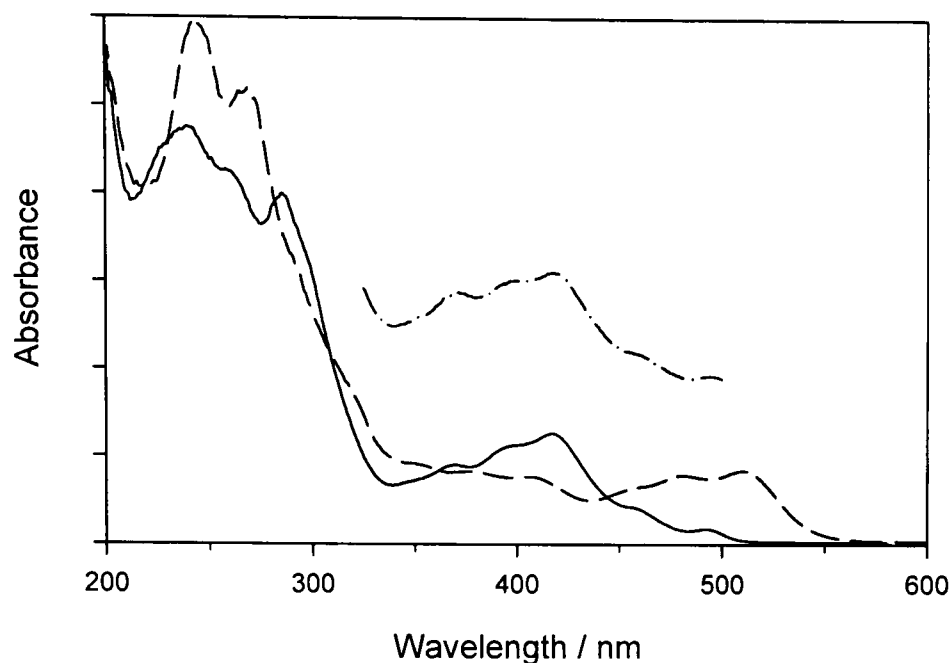


Figure 22. Ground-state absorbance spectra of Ir(dpydmb)(ppy)Cl **115** (solid line) and Ir(dpydmb)(dppy) **108** (dashed line) in acetonitrile solution at 295 K. Also shown is the low energy portion of the luminescence excitation spectrum of Ir(dpydmb)(ppy)Cl **115** (dash-dotted line, displaced for clarity, $\lambda_{em} = 507$ nm).

Complex	λ / nm (ϵ / dm ³ mol ⁻¹ cm ⁻¹)
Ir(dpydmb)(ppy)Cl 115	239 (44 700), 258 (39 700), 285 (37 000), 353 (6 200), 369 (7 800), 399 (10 000), 417 (11 300), 455 (3 600), 492 (1 300).

Table 14. Absorbance data for Ir(dpydmb)(ppy)Cl **115** in acetonitrile solution at 295 K.

The room temperature emission spectrum of Ir(dpydmb)(ppy)Cl **115** in acetonitrile solution is shown in Figure 23, with the luminescence excitation spectrum (matching the absorbance spectrum) shown in Figure 22. In contrast to Ir(dpydmb)(dppy) **108** and *fac*-Ir(ppy)₃ **26**, Ir(dpydmb)(ppy)Cl **115** exhibits structured luminescence at ambient temperature. The emission is significantly blue-shifted with respect to Ir(dpydmb)(dppy) **108**, and is comparable in energy to that of *fac*-Ir(ppy)₃ **26**. A blue-shift is consistent with a lowering of the HOMO upon substitution of a relatively strong field cyclometalating carbon with a chloride, whilst the dpydmb-based LUMO is unchanged. The observation of a more structured emission with a decreased Stokes' shift (16 nm compared to 75 nm* for Ir(dpydmb)(dppy) **108**, in acetonitrile solution at 295 K) is indicative of an increase in ligand-centred (LC) character. Therefore the

* Stokes' shift measured as the difference between the wavelength of maximum emission and that of the lowest energy absorption band.

emission is assigned to a mixed MLCT(Ir→dpydmb)-LC(dpydmb π - π^*) excited state, reflecting the lowering of the predominantly metal-based HOMO in Ir(dpydmb)(dppy) **108** to a similar energy as that of the dpydmb ligand π -orbital.

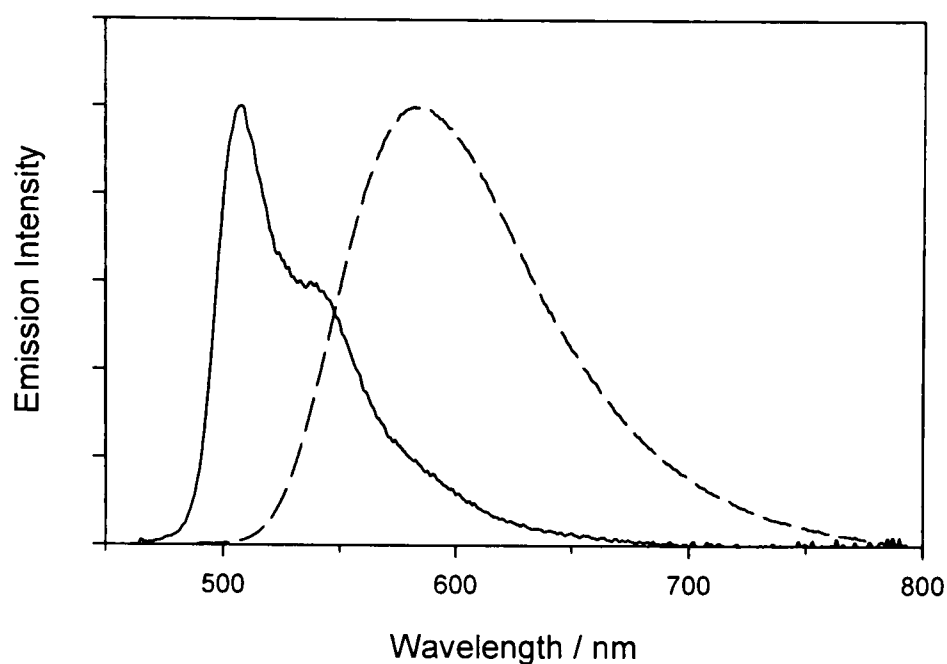


Figure 23. Emission spectrum of Ir(dpydmb)(ppy)Cl **115** (solid line, $\lambda_{\text{ex}} = 456$ nm) in acetonitrile solution at 295 K. Excitation and emission bandpasses were 2.5 nm. The emission spectrum of Ir(dpydmb)(dppy) **108** (dashed line) is included for comparison.

Luminescence data for Ir(dpydmb)(ppy)Cl **115** is summarised in Table 15. The luminescence quantum yield in degassed acetonitrile solution is much greater than that for either Ir(dpydmb)(dppy) **108** ($\Phi_{\text{PL}} = 0.21$) or *fac*-Ir(ppy)₃ **26** ($\Phi_{\text{PL}} = 0.40$ in toluene¹¹³). Application of equations 13 and 14 establish that this improvement is due to a combination of an increased radiative rate constant ($k_r = 4.8 \times 10^5 \text{ s}^{-1}$) and a decreased non-radiative contribution ($\sum k_{\text{nr}} = 1.5 \times 10^5 \text{ s}^{-1}$). The latter is well known for a blue-shift in emission maximum, where the energy-gap law predicts a decrease in the non-radiative rate constant.¹⁹

Complex	λ_{max} / nm	CIE coordinates	Aerated		Degassed	
			Φ	τ / ns	Φ	τ / ns
Ir(dpydmb)(ppy)Cl 115	508	$x=0.29, y=0.64$	0.016 ^a	<100 ^b	0.76 ^a	1600 ^b

^aQuantum yields of emission, $\lambda_{\text{ex}} = 259$ nm, 295 K, measured using an aqueous solution of [Ru(bpy)₃]²⁺ as a standard;⁴⁰⁰ uncertainty $\pm 20\%$. ^bLifetimes of emission monitored at 700 nm, $\lambda_{\text{ex}} = 355$ nm, 295 K; uncertainty $\pm 5\%$.

Table 15. Luminescence data for Ir(dpydmb)(ppy)Cl **115** in acetonitrile solution.

4.1.3 Ir(N[^]C[^]N)(C[^]N[^]O) complexes

The ground-state absorbance spectra of Ir(dpydmb)(tppic) **116** and Ir(dpydmb)(hbqc) **117** in acetonitrile solution are shown in Figure 24 (data summarised in Table 16). There are a series of bands in the near-UV region between 240 and 300 nm, assigned to spin-allowed $^1\pi-\pi^*$ transitions of the ligands. In addition, a set of weaker features stretch out well into the visible region, assigned to both allowed and spin-forbidden metal-to-ligand charge transfer (MLCT) bands. The significant blue-shift with respect to Ir(dpydmb)(dppy) **108** may be explained by the fact that the third Ir–C bond of the latter is more destabilising to the primarily metal-based HOMO than an Ir–O bond.

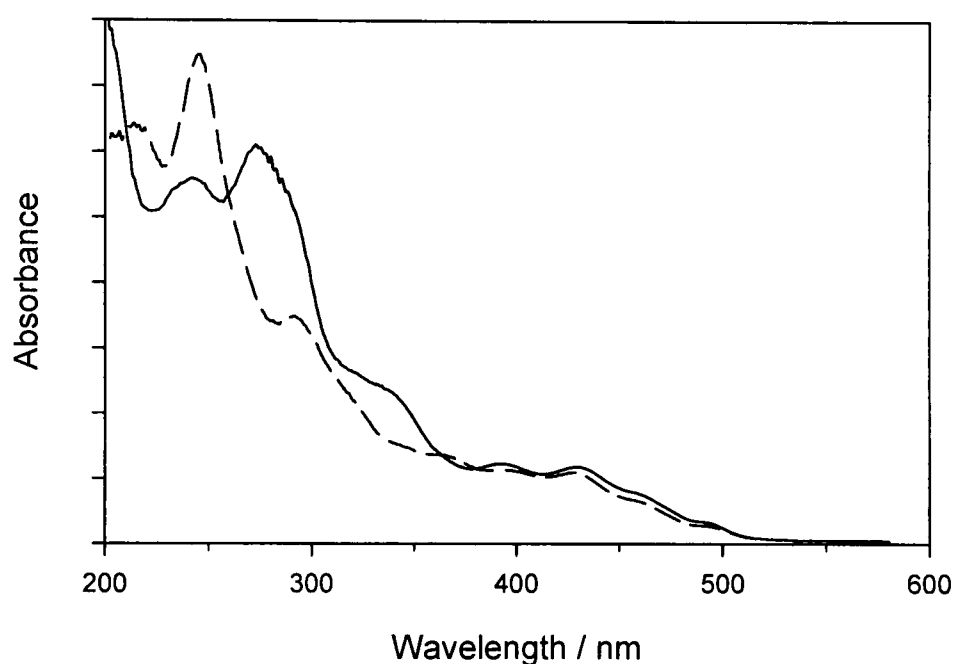


Figure 24. Ground-state absorbance spectra of Ir(dpydmb)(tppic) **116** and Ir(dpydmb)(hbqc) **117** in acetonitrile solution at 295 K.

Complex	λ / nm (ϵ / dm ³ mol ⁻¹ cm ⁻¹)
Ir(dpydmb)(tppic) 116	242 (32 800), 273 (35 700), 290 (30 400), 337 (13 500), 393 (6 900), 429 (6 700), 459 (4 300), 489 (1 700).
Ir(dpydmb)(hbqc) 117	245 (34 500), 290 (16 600), 315 (10 400), 341 (6 500), 363 (5 900), 393 (4 900), 428 (4 600), 459 (2 800), 492 (1 100).

Table 16. Absorbance data for Ir(N[^]C[^]N)(C[^]N[^]O) complexes in acetonitrile solution at 295 K.

The room temperature emission spectra of Ir(dpydmb)(tppic) **116** and Ir(dpydmb)(hbqc) **117** in acetonitrile solution are shown in Figure 25. Both show a broad, structureless emission, typical of phosphorescence from MLCT triplet states,

with luminescence excitation spectra matching those of absorption. The results of DFT calculations (see Section 4.2) however, suggest that there is a significant amount of dpydmb \rightarrow tppic and dpydmb \rightarrow hbqc ligand-to-ligand charge transfer (LLCT) as well as ligand centred (LC) character in each case. The Ir(dpydmb)(hbqc) **117** emission ($\lambda_{\text{max}} = 562$ nm) is blue-shifted with respect to Ir(dpydmb)(dppy) **108** ($\lambda_{\text{max}} = 585$ nm) due to the reduction in number of the strong-field cyclometalating carbon atoms, and hence a lower HOMO energy (as concluded from the absorption spectrum). In contrast, emission from Ir(dpydmb)(tppic) **116** ($\lambda_{\text{max}} = 603$ nm) is significantly red-shifted, even though the absorption spectra of both Ir(N \wedge C \wedge N)(C \wedge N \wedge O) complexes are comparable. This is probably related to the introduction of the *p*-tolyl substituent. Whereas the HOMO-LUMO gap is similar in the ground state, an additional stabilisation is possible in the excited state by rotation of this group with respect to the rest of the molecule.

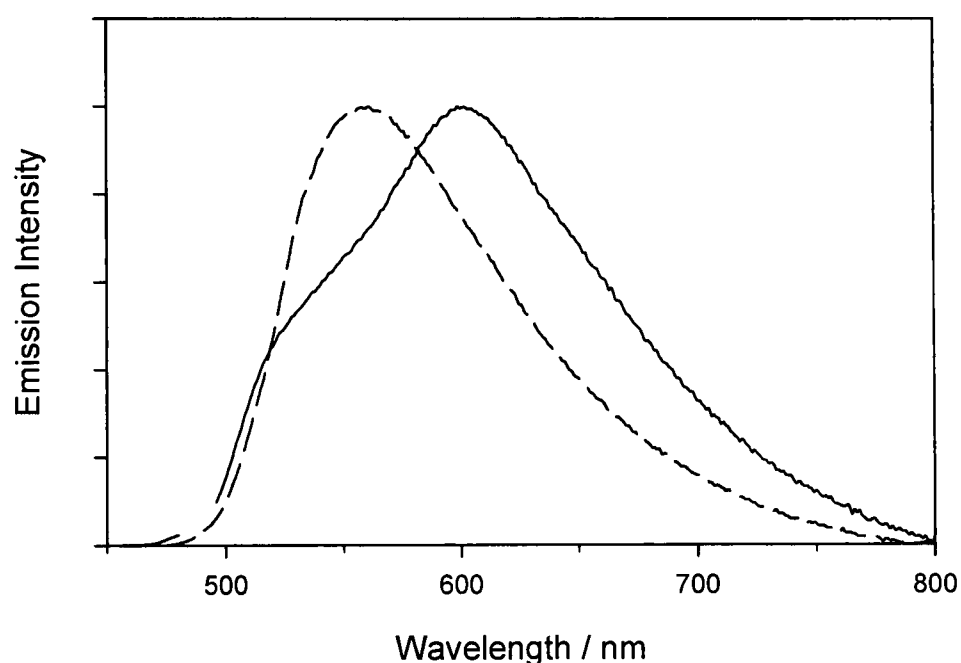


Figure 25. Emission spectra of Ir(dpydmb)(tppic) **116** (solid line, $\lambda_{\text{ex}} = 489$ nm) and Ir(dpydmb)(hbqc) **117** (dashed line, $\lambda_{\text{ex}} = 459$ nm) in acetonitrile solution at 295 K. Excitation and emission bandpasses were 2.5 nm and 4.0 nm for each complex respectively.

Luminescence data for Ir(dpydmb)(tppic) **116** and Ir(dpydmb)(hbqc) **117** are summarised in Table 17. The lifetimes of emission in degassed acetonitrile solution are very short, reflected in the particularly low luminescence quantum yields. Calculation of the radiative and non-radiative decay rate constants (see Table 18) shows that the poor efficiency of emission is due to rapid non-radiative processes, more than an order of magnitude faster than for the Ir(N \wedge C \wedge N)(C \wedge N \wedge C) complexes. While the increase in LLCT character of the emissive state may be argued to be responsible for the poor luminescence efficiency, this is shown for complexes of the form Ir(N \wedge N \wedge N)(C \wedge N \wedge C) $^+$

to be manifested in a low radiative decay rate constant (k_r) (see Section 4.1.4), which is not the case in this instance. Instead, the large non-radiative decay rate constant (k_{nr}) is attributed to a photochemical cleavage of the Ir–O bond in the excited state, analogous to that of the Ir–C bond of Ir(dpydmb)(dppy) **108** resulting in decomposition, and to that of *mer*-Ir(ppy)₃ **27**¹²¹ resulting in isomerisation to the *fac*-isomer. Whereas this process is irreversible for Ir–C bonds, no decomposition is observed for Ir(dpydmb)(tppic) **116** or Ir(dpydmb)(hbqc) **117** upon intense irradiation. Therefore it is concluded that Ir–O bond dissociation is reversible, allowing re-formation of the original complex subsequent to non-radiative relaxation to the ground state.

Complex	λ_{\max} / nm	CIE coordinates	Aerated		Degassed	
			Φ^a	τ^d / ns	Φ^a	τ^d / ns
Ir(dpydmb)(tppic) 116	603	$x=0.52, y=0.47$	0.0092 ^b	39 ^e	0.053 ^b	110 ^e
Ir(dpydmb)(hbqc) 117	562	$x=0.48, y=0.51$	0.0043 ^c	<100 ^f	0.027 ^c	170 ^f

^aQuantum yields of emission, 295 K, measured using an aqueous solution of [Ru(bpy)₃]²⁺ as a standard;⁴⁰⁰ uncertainty $\pm 20\%$. ^b $\lambda_{\text{ex}} = 450$ nm. ^c $\lambda_{\text{ex}} = 459$ nm. ^dLifetimes of emission, $\lambda_{\text{ex}} = 355$ nm, 295 K; uncertainty $\pm 5\%$. ^eMonitored at 600 nm. ^fMonitored at 560 nm.

Table 17. Luminescence data for Ir(dpydmb)(tppic) **116 and Ir(dpydmb)(hbqc) **117** in acetonitrile solution.**

Complex	k_r / s^{-1} ^a	$\sum k_{nr} / \text{s}^{-1}$ ^a	$k_q / \text{dm}^3 \text{mol}^{-1} \text{s}^{-1}$ ^b
Ir(dpydmb)(tppic) 116	4.8×10^5	8.6×10^6	1.8×10^9
Ir(dpydmb)(hbqc) 117	1.6×10^5	5.7×10^6	^c

^aEstimated uncertainty $\pm 20\%$. ^bEstimated uncertainty $\pm 10\%$. ^cNot calculated due to the inaccuracy in determining the aerated lifetime (see Table 17).

Table 18. Radiative, non-radiative and bimolecular oxygen quenching decay rate constants for Ir(dpydmb)(tppic) **116 and Ir(dpydmb)(hbqc) **117** in acetonitrile solution at 295 K.**

4.1.4 Ir(N[^]N[^]N)(C[^]N[^]C)⁺ complexes

The ground-state absorbance spectrum of [Ir(tpybae)(dppy)]⁺ **124** is shown in Figure 26, and summarised in Table 19 along with [Ir(BrC₆H₄-terpy)(tdppy)]⁺ **34**¹³⁵ for comparison. There are three strong absorptions in the UV region at 235 nm, 282 nm and 312 nm assigned to ligand-centred (LC) ¹ π - π^* transitions. In addition, a number of bands (439 nm, 477 nm and 510 nm) extend into the visible region. These are tentatively assigned as MLCT in nature, although it has been shown by DFT calculations that these bands in **34** have a significant amount of dppy→terpy character.¹³⁵ The shapes of the

absorption spectra for $[\text{Ir}(\text{tpybae})(\text{dppy})]^+$ **124** and **34** are very similar, with a small red-shift for the latter.

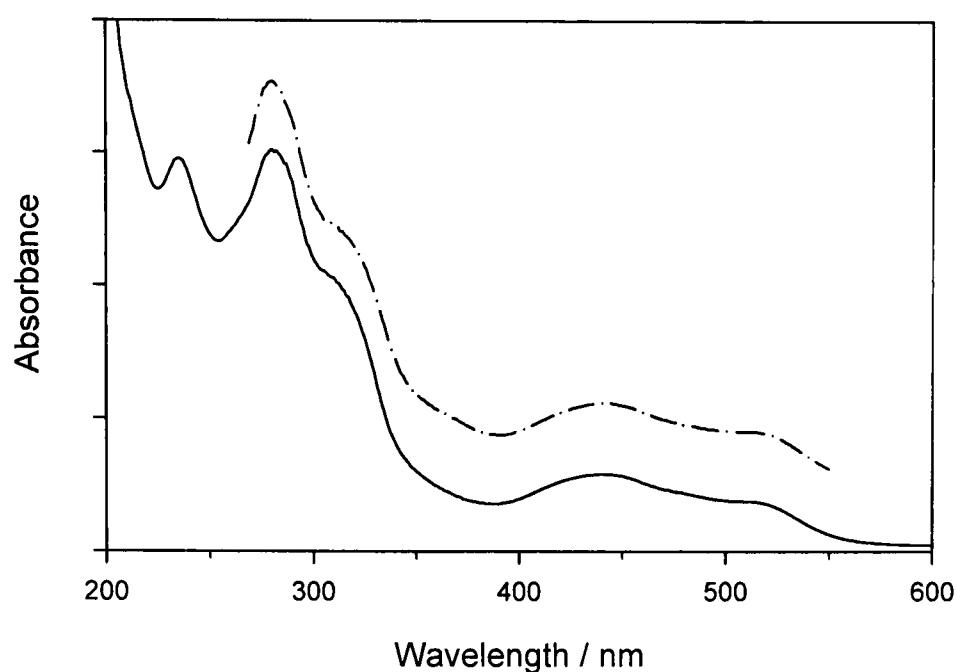


Figure 26. Ground-state absorbance spectrum (solid line) and luminescence excitation spectrum (dash-dotted line, displaced for clarity, $\lambda_{\text{em}} = 710$ nm) of $[\text{Ir}(\text{tpybae})(\text{dppy})]^+$ **124** in acetonitrile solution at 295 K.

Complex	λ / nm (ϵ / $\text{dm}^3 \text{mol}^{-1} \text{cm}^{-1}$)
$[\text{Ir}(\text{tpybae})(\text{dppy})]^+$ 124	235 (16 000), 282 (15 500), 312 (10 600), 439 (2 700), 477 (2 100), 510 (1 700).
34 ¹³⁵	284 (97 500), 320 (66 000), 437 (25 500), 484 (21 200), 520 (19 100).

Table 19. Absorbance data for $\text{Ir}(\text{N}^{\wedge}\text{N}^{\wedge}\text{N})(\text{C}^{\wedge}\text{N}^{\wedge}\text{C})^+$ complexes in acetonitrile solution at 295 K.

The room temperature emission spectrum of $[\text{Ir}(\text{tpybae})(\text{dppy})]^+$ **124** in acetonitrile solution is shown in Figure 27, with the close match between luminescence excitation and absorbance spectra shown in Figure 26. The emission is assigned as MLCT with a substantial LLCT character by analogy with **34**.¹³⁵ Compared with bis-cyclo-metalated complexes of the form $\text{Ir}(\text{C}^{\wedge}\text{N})_2(\text{N}^{\wedge}\text{N})^+$, emission from $\text{Ir}(\text{N}^{\wedge}\text{N}^{\wedge}\text{N})(\text{C}^{\wedge}\text{N}^{\wedge}\text{C})^+$ derivatives is at substantially lower energy (e.g. compared to $\lambda_{\text{max}} = 613$ nm for $[\text{Ir}(\text{ppy})_2(\text{bpy-Ph})]$ in acetonitrile solution⁴⁰¹). This is due to a lowering of the terpyridine π^* based LUMO resulting from increased delocalisation across the terdentate ligand. The emission maximum of $[\text{Ir}(\text{tpybae})(\text{dppy})]^+$ **124** ($\lambda_{\text{max}} = 707$ nm) is slightly red-shifted with respect to **34** ($\lambda_{\text{max}} = 690$ nm). Since an increase in either metal or dppy

π orbital energy is unlikely, this is attributed to a lowering of the terpyridine π^* orbital upon substitution of bromine for a more delocalised ester group.

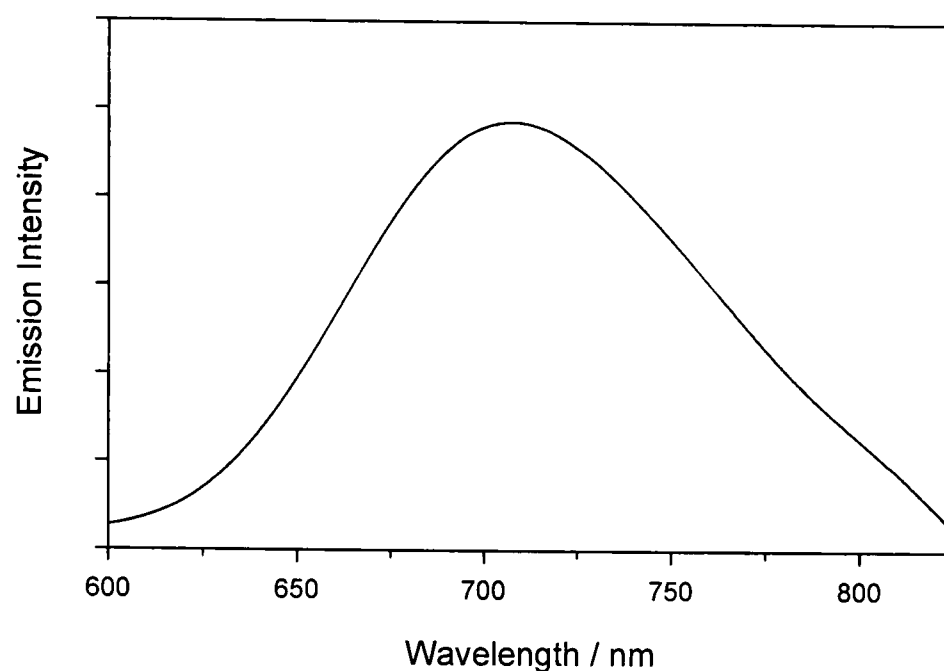


Figure 27. Emission spectrum of $[\text{Ir}(\text{tpybae})(\text{dppy})]^+$ **124** ($\lambda_{\text{ex}} = 343 \text{ nm}$) in acetonitrile solution at 295 K. Excitation and emission bandpasses were 4.0 nm.

Luminescence data for $[\text{Ir}(\text{tpybae})(\text{dppy})]^+$ **124** and **34**¹³⁵ are summarised in Table 20. The quantum yields of emission are significantly lower than for other similar bis-cyclometalated complexes (*e.g.* $\Phi = 0.14$ for $\text{Ir}(\text{ppy})_2(\text{bpy-Ph})$ ⁴⁰¹). This is due to a particularly low radiative rate constant (*e.g.* compared to $2.7 \times 10^5 \text{ s}^{-1}$ for $\text{Ir}(\text{ppy})_2(\text{bpy-NH}_2)$ ⁴⁰²), with results of analysis using equations 13 and 14 shown in Table 21. As proposed for **34**,¹³⁵ this is likely to be attributable to the substantial LLCT character in the emissive state.

Complex	λ_{max} / nm	CIE coordinates	Aerated		Degassed	
			Φ	τ / ns	Φ	τ / ns
$[\text{Ir}(\text{tpybae})(\text{dppy})]^+$ 124	707	$x=0.64, y=0.36$	0.0018 ^a	240 ^b	0.012 ^a	1700 ^b
34 ¹³⁵	690			200	0.032	1700

^aQuantum yields of emission, $\lambda_{\text{ex}} = 259 \text{ nm}$, 295 K, measured using an aqueous solution of $[\text{Ru}(\text{bpy})_3]^{2+}$ as a standard;⁴⁰⁰ uncertainty $\pm 20\%$. ^bLifetimes of emission monitored at 700 nm, $\lambda_{\text{ex}} = 355 \text{ nm}$, 295 K; uncertainty $\pm 5\%$.

Table 20. Luminescence data for $[\text{Ir}(\text{tpybae})(\text{dppy})]^+$ **124** in acetonitrile solution. Complex **34**¹³⁵ is included for comparison.

Complex	$k_r / s^{-1}{}^a$	$\sum k_{nr} / s^{-1}{}^a$	$k_q / dm^3 mol^{-1} s^{-1}{}^b$
$[Ir(tpybae)(dppy)]^+$ 124	7.1×10^3	5.8×10^5	3.9×10^8
34 ¹³⁵	1.9×10^4	5.7×10^5	4.8×10^8

^aEstimated uncertainty $\pm 20\%$. ^bEstimated uncertainty $\pm 10\%$.

Table 21. Radiative, non-radiative and bimolecular oxygen quenching decay rate constants for $[Ir(tpybae)(dppy)]^+$ **124 and **34** in acetonitrile solution at 295 K.**

4.1.5 $Ir(N^A C^A N)(N^A N^A N)^{2+}$ complexes

The ground-state absorbance spectra of $[Ir(dpydmb)(terpy)]^{2+}$ **105** and $[Ir(dpydmb)(tppy)]^{2+}$ **106** in acetonitrile solution are shown in Figure 28 (summarised in Table 22). Both spectra are very similar with a number of intense absorption bands at high energy assigned to ligand-centred (LC) transitions, with lower intensity metal-to-ligand charge transfer (MLCT) bands between 350 and 400 nm. A series of very weak features only resolvable in concentrated solutions stretch out to lower energy. These are assigned as $dpydmb \rightarrow terpy$ ligand-to-ligand charge transfer (LLCT) bands on the basis of DFT calculations (see Section 4.2). Whereas the absorption bands of the previously discussed complexes have often been described as containing LLCT character, this was only as part of predominantly MLCT states. In this case the absorption bands are much weaker, a reflection of the fact that the HOMO has very little metal character, and that the transition is essentially LLCT.

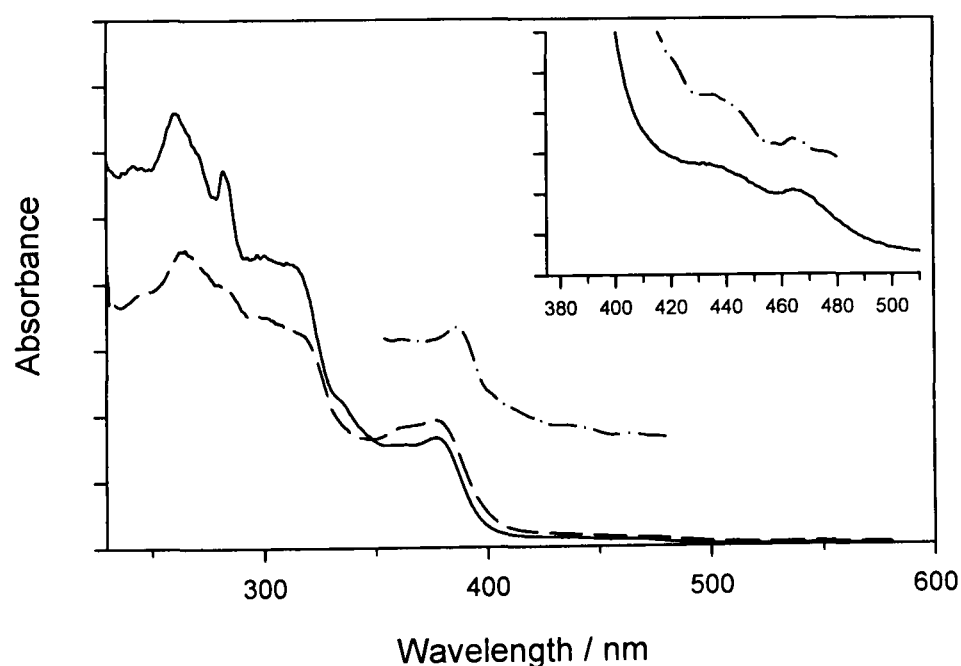


Figure 28. Ground-state absorbance spectra of $[Ir(dpydmb)(terpy)]^{2+}$ **105 (solid line) and $[Ir(dpydmb)(tppy)]^{2+}$ **106** (dashed line) in acetonitrile solution at 295 K. Also included is the low energy portion of the luminescence excitation spectrum of $[Ir(dpydmb)(terpy)]^{2+}$ **105** in an ethanol/methanol (4:1 by volume) glass at 77 K (dotted line, offset for clarity, $\lambda_{em} = 501$ nm).**



Complex	λ / nm ($\epsilon / \text{dm}^3 \text{mol}^{-1} \text{cm}^{-1}$)
$[\text{Ir}(\text{dpydmb})(\text{terpy})]^{2+}$ 105	244 (33 700), 261 (38 500), 270 (35 300), 282 (32 800), 298 (26 000), 311 (25 400), 335 (13 100), 377 (10 100), 435 (700), 465 (500).
$[\text{Ir}(\text{dpydmb})(\text{tppy})]^{2+}$ 106	264 (52 900), 283 (45 100), 301 (39 900), 316 (36 700), 361 (20 300), 377 (21 600), 435 (1 500), 463 (1 000).

Table 22. Absorbance data for $\text{Ir}(\text{N}^{\wedge}\text{C}^{\wedge}\text{N})(\text{N}^{\wedge}\text{N}^{\wedge}\text{N})^{2+}$ complexes in acetonitrile solution at 295 K.

In contrast to all other complexes investigated in the present work, those of the form $\text{Ir}(\text{N}^{\wedge}\text{C}^{\wedge}\text{N})(\text{N}^{\wedge}\text{N}^{\wedge}\text{N})^{2+}$ are virtually non-emissive at room temperature ($\Phi < 0.001$ in degassed acetonitrile solution). Even at 77 K, $[\text{Ir}(\text{dpydmb})(\text{terpy})]^{2+}$ **105** is only weakly emissive, exhibiting a highly structured luminescence at high energy ($\lambda_{\text{max}} = 502 \text{ nm}$) (see Figure 29). The emission is attributed to a $\text{dpydmb} \rightarrow \text{terpy}$ LLCT emissive state. Since there is likely to be a large deviation in molecular structure in states of an LLCT nature, the emission efficiency may be expected to be poor. Hence, the unusually small amount of MLCT character in the emissive states of $\text{Ir}(\text{N}^{\wedge}\text{C}^{\wedge}\text{N})(\text{N}^{\wedge}\text{N}^{\wedge}\text{N})^{2+}$ complexes is probably the main reason for the unexpectedly weak emission.

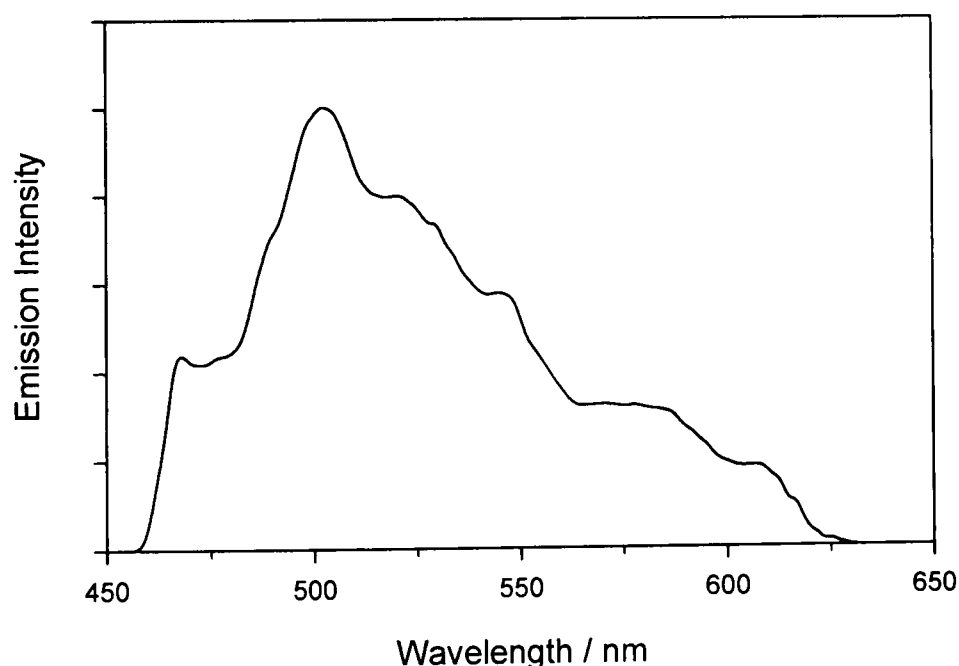


Figure 29. Emission spectrum of $[\text{Ir}(\text{dpydmb})(\text{terpy})]^{2+}$ **105** ($\lambda_{\text{ex}} = 370 \text{ nm}$) in an ethanol/methanol (4:1 by volume) glass at 77 K. Excitation and emission bandpasses were 10.0 nm and 5.0 nm respectively.

Complexes of iridium(III) with an N₅C donor set are very uncommon. The only reported polypyridyl complexes with such a coordination arrangement are [Ir(bpy-*N,N'*)₂(Hbpy-*C³,N'*)]³⁺,¹⁰⁴ [Ir(bpy)₂(ppy)]²⁺^{150,403} and the bis-terdentate [Ir(bmpqpyH-N[^]N[^]N)(bmpqpy-N[^]N[^]C)]²⁺.¹²⁹ Although quantum yield measurements were not reported for [Ir(bpy)₂(ppy)]²⁺, there was no suggestion that emission was particularly weak.¹⁵⁰ The related complex [Ir(bpy-*N,N'*)₂(Hbpy-*C³,N'*)]³⁺ is in fact reported to have a high quantum yield of 0.30.¹⁰⁴ In contrast, the bis-terdentate mono-cyclometalated complex [Ir(bmpqpyH-N[^]N[^]N)(bmpqpy-N[^]N[^]C)]²⁺ exhibits a luminescence quantum yield of only 0.005 in deoxygenated acetonitrile solution,¹²⁹ more consistent with the behaviour observed for [Ir(dpydmb)(terpy)]²⁺ **105**.

4.2 Computational studies

In conjunction with photophysical studies of iridium(III) complexes (see Section 4.1), a number of structures were investigated by computational techniques. The objective of these calculations is to provide an insight into the structural and spectroscopic properties of potentially luminescent iridium(III) compounds.

While empirical molecular mechanics⁴⁰⁴ and semiempirical⁴⁰⁵ methods have found utility in calculations on transition metal complexes, the requirement for suitable parameterisation has limited their use. More common are *ab initio* techniques, in particular Hartree-Fock (HF) methods, which can provide reasonable results for second and third row transition metals.⁴⁰⁶ These however become increasingly impractical with increasing number of atoms, and density functional theory (DFT) calculations are favoured for their similar accuracy at a reduced computational cost as well as their inclusion of electron correlation effects.⁴⁰⁶⁻⁴⁰⁹

Accuracy has reached the stage where DFT calculations may be used almost routinely in combination with experimental studies of transition metal complexes. The common OLED material Alq₃ **1** has been studied by a number of groups with reasonable correlation with experiment.⁴¹⁰⁻⁴¹⁴ Cyclometalated iridium(III) complexes have also been investigated, of particular interest the *fac*- and *mer*-isomers of Ir(ppy)₃.^{121,142}

In the present study, as for previous reports for Ir(ppy)₃,^{121,142} the “hybrid” B3LYP density functional is used throughout. The 6-31G basis set is employed for all ligand atoms, with LANL2DZ⁴¹⁵ used for the iridium(III) atom. Due to the large number of electrons associated with the iridium(III) centre, the chemically inert inner core electrons are replaced with an effective core potential (ECP). Since these electrons

are not involved in bonding, very little loss in accuracy is incurred with a large decrease in calculation time. The more significant outer core $[(5s)^2(5p)^6]$ and valence $(5d)^6$ electrons are still included.

4.2.1 Ground-state structures

The optimised ground-state structure of *fac*-Ir(ppy)₃ **26** is shown in Figure 30. Although no X-ray diffraction studies of this complex have been published, the DFT calculations of Hay¹⁴² and the crystal structure of *fac*-Ir(tpy)₃¹¹² may be used for comparison. The calculated Ir–N bond length of the present study (2.167 Å) is identical to that of Hay, and only slightly longer than the experimentally observed value (2.132(5) Å¹¹²). Similar good agreement is obtained for the Ir–C bond length (2.036 Å) compared to Hay (2.035 Å¹⁴²) and experiment (2.024(6) Å¹¹²). Correlation with the results of Hay is unsurprising since only the starting geometries differ, but comparison with experiment suggests that DFT calculations at this level provide reasonable ground-state geometries.

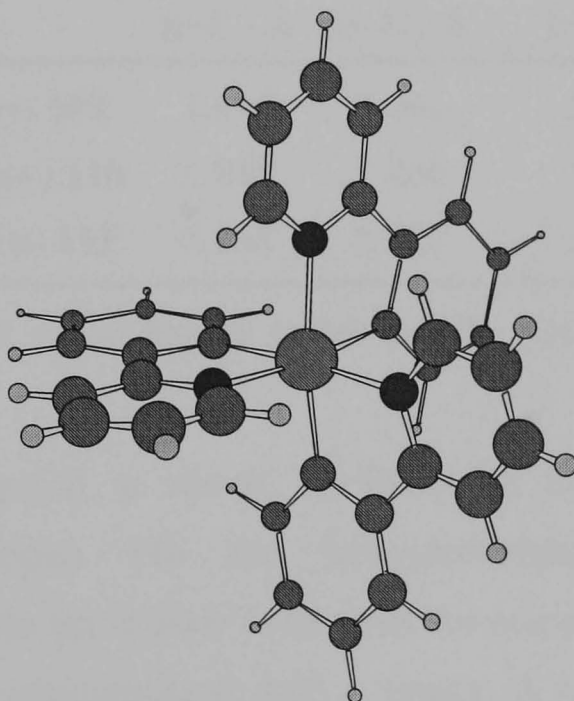


Figure 30. Optimised ground-state geometry of *fac*-Ir(ppy)₃ **26**.

The results of optimised ground-state geometry calculations for the *Ir(N^C^N)(C^N^C)* complexes, Ir(dpydmb)(dppy) **108**, Ir(dpydmb)(F₄dppy) **110** and Ir(dpydmb)(cdppy) **111** are summarised in Table 23. All structures exhibited the expected distorted octahedral geometry with a meridional arrangement of donor atoms. While the Ir–C(dpydmb) bonds are shorter than those of *fac*-Ir(ppy)₃ **26** (2.036 Å) due to the geometric constraints of terdentate binding, the Ir–C(dppy) bonds are significantly longer. Although it may be argued that this is also due to geometric constraints, it

should be noted that these are of a comparable length to those calculated for the mutually *trans* Ir–C bonds of *mer*-Ir(ppy)₃ **27** (2.110 and 2.094 Å¹⁴²) where there are no such restrictions. Instead this is attributed to the strong *trans*-influence of a cyclo-metalating ligand. Similarly, the mutually *trans* nitrogen atoms of the dpydmb ligand are closer to the metal than for *fac*-Ir(ppy)₃ **26** due to the smaller *trans*-influence of an N-donor ligand, mirrored in similar lengths for the analogous atoms of *mer*-Ir(ppy)₃ **27** (2.063 and 2.080 Å¹⁴²).

It is interesting to note that there is very little structural variation upon derivatisation of the dppy ligand in Ir(dpydmb)(dppy) **108**, with the exception of a small (~0.01 Å) decrease in the Ir–C(dppy) bond length upon fluorine substitution. Although within the absolute error, this difference is significant with respect to the other calculations. This suggests an increase in stability of this bond with respect to the parent complex, consistent with experimental observations (see Section 3.2).

Complex	N [^] C [^] N fragment		C [^] N [^] C fragment	
	Ir–C / Å	Ir–N / Å	Ir–C / Å	Ir–N / Å
Ir(dpydmb)(dppy) 108	1.943	2.062	2.113	2.110
Ir(dpydmb)(F ₄ dppy) 110	1.949	2.066	2.100	2.108
Ir(dpydmb)(cdppy) 111	1.948	2.067	2.110	2.103

Table 23. Calculated metal-ligand bond lengths for Ir(N[^]C[^]N)(C[^]N[^]C) complexes.

A similar comparison is shown in Table 24 for the Ir(N[^]C[^]N)(C[^]N[^]O) complexes Ir(dpydmb)(tppic) **116** and Ir(dpydmb)(hbqc) **117**. Although the Ir–N(dpydmb) bond lengths are similar to those of the complexes discussed above, the Ir–C(dpydmb) bonds are approximately 0.05 Å longer. A less pronounced shortening (~0.03 Å) is observed for the opposing Ir–N(C[^]N[^]O) bond. This is accompanied by a simultaneous reduction of the Ir–C(C[^]N[^]O) bond length with respect to those of the dppy ligand. This is due to the loss of a mutually *trans* Ir–C bond, and replacement with a relatively low *trans*-influence Ir–O bond. Comparison of the ground-state structures of Ir(dpydmb)(tppic) **116** and Ir(dpydmb)(hbqc) **117** indicate that the only significant differences are a shortening of the Ir–C(C[^]N[^]O) and lengthening of the Ir–O(C[^]N[^]O) bond in the latter. This shift in the angle of the ligand with respect to the metal centre is due to the increased rigidity of the hbqc ligand upon introduction of the bridging

aromatic ring. Whereas the tpic ligand may distort to accommodate a more symmetrical binding arrangement, this is not possible for the hbqc complex.

Complex	N [^] C [^] N fragment		C [^] N [^] O fragment		
	Ir–C / Å	Ir–N / Å	Ir–C / Å	Ir–N / Å	Ir–O / Å
Ir(dpydmb)(tppic) 116	1.995	2.063	2.039	2.085	2.218
Ir(dpydmb)(hbqc) 117	1.995	2.063	2.053	2.088	2.245

Table 24. Calculated metal-ligand bond lengths for Ir(N[^]C[^]N)(C[^]N[^]O) complexes.

A comparison of bond lengths for two alternative binding modes of the dipy ligand of Ir(dpydmb)(dipy) is shown in Table 25. It is interesting to note that while the structures are remarkably similar, the dipy ligand is slightly further from the metal when it is bound through two cyclometalating carbon atoms. This is again due to the unfavourable arrangement of mutually *trans* Ir–C bonds. The increased distance between the dipy ligand and the metal centre is countered by a nearing of the opposing dpydmb ligand.

Complex	dpydmb fragment		dipy fragment		
	Ir–C / Å	Ir–N / Å	Ir–N(py) / Å	Ir–N(indolyl) / Å	Ir–C / Å
N [^] N [^] N 123	1.959	2.065	2.102	2.086	
C [^] N [^] C 122	1.943	2.061	2.150		2.102

Table 25. Calculated metal-ligand bond lengths for two coordination modes of Ir(dpydmb)(dipy).

The calculated bond lengths for the [Ir(dpydmb)(terpy)]²⁺ complex **105** are shown in Table 26, along with those for [Ir(terpy)₂]³⁺ **21** and the values from the crystal structure of [Ir(dpydmb)(tppy)]²⁺ **106** (see Section 3.2). Reasonable agreement is found between the relative values for calculated and experimental bond lengths, although those from DFT calculations are consistently higher. As expected by the presence of a strong *trans*-influence Ir–C bond, the opposing Ir–N bond length is significantly longer in the cyclometalated complex with respect to [Ir(terpy)₂]³⁺ **21**. In addition, a slight shortening of the Ir–N(peripheral) bonds results from this geometry.

Complex	N^C^N fragment		N^N^N fragment	
	Ir-C / Å	Ir-N / Å	Ir-N(central) / Å	Ir-N(periph.) / Å
[Ir(dpydmb)(terpy)] ²⁺ 105	1.986	2.089	2.056	2.087
[Ir(terpy) ₂] ³⁺ 21			2.009	2.097
[Ir(dpydmb)(tppy)] ²⁺ 106	1.954(4)	2.046(3) 2.047(3)	2.030(3)	2.046(3) 2.052(3)

Table 26. Calculated metal-ligand bond lengths for [Ir(dpydmb)(terpy)]²⁺ **105** and [Ir(terpy)₂]³⁺ **21**. Also shown for comparison are the respective bond lengths from the X-ray crystal structure of [Ir(dpydmb)(tppy)]²⁺ **106**.

4.2.2 Molecular orbitals

In addition to structural information, ground-state DFT calculations provide information on the molecular orbital shapes and, although absolute values should not be relied upon too heavily, orbital energies. This is summarised for *fac*-Ir(ppy)₃ **26**, Ir(dpydmb)(dppy) **108**, Ir(dpydmb)(F₄dppy) **110** and Ir(dpydmb)(cdppy) **111** in Figure 31 and Table 27. Contour plots of the HOMO and LUMO are shown for *fac*-Ir(ppy)₃ **26** and Ir(dpydmb)(dppy) **108** in Figures 32 and 33 respectively.

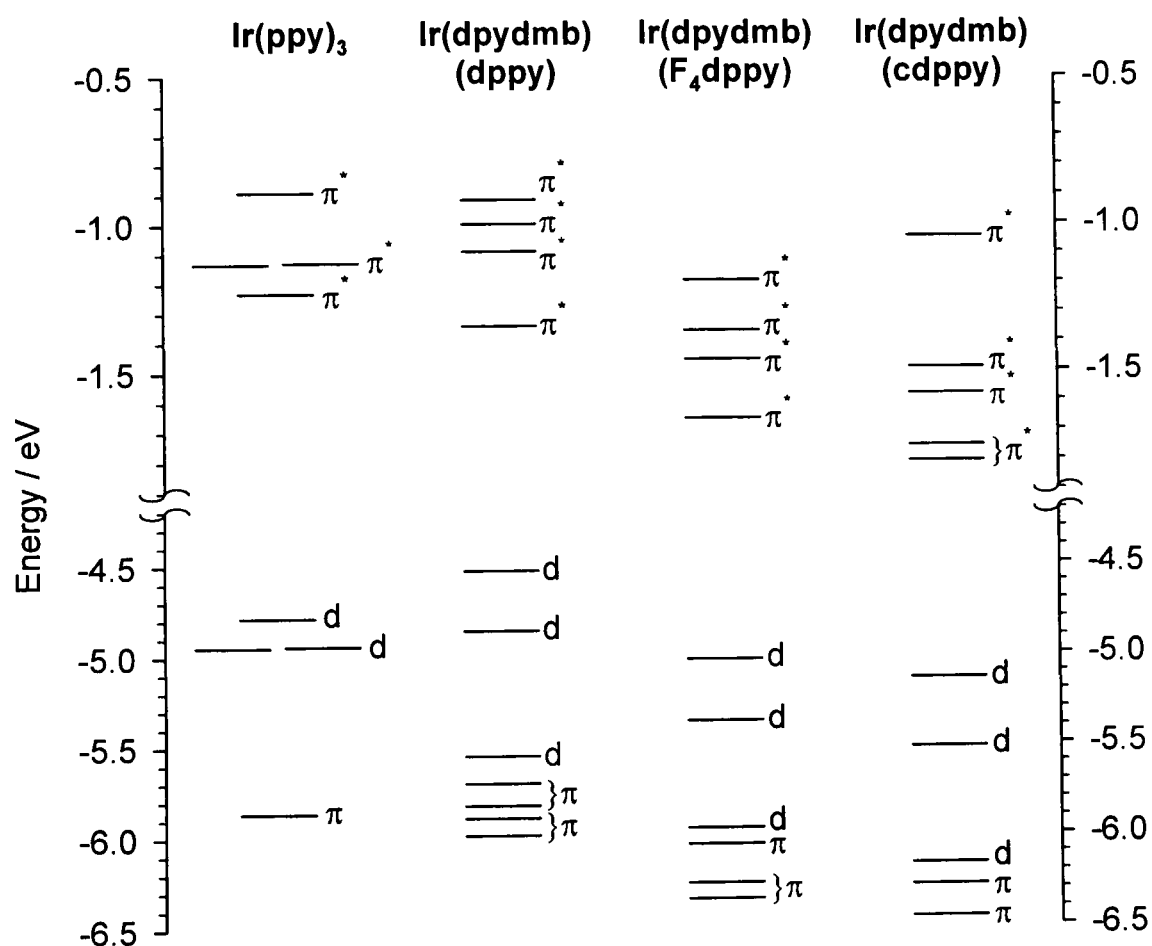


Figure 31. Schematic diagram of calculated molecular orbital energies for *fac*-Ir(ppy)₃ **26**, Ir(dpydmb)(dppy) **108**, Ir(dpydmb)(F₄dppy) **110** and Ir(dpydmb)(cdppy) **111**.

		Orbital	Character	Energy / eV
<i>fac</i> -Ir(ppy) ₃ 26	Virtual	π_{2b}^*	π^* (ppy)	-1.13
		π_{2a}^*	π^* (ppy)	-1.13
		π_1^*	π^* (ppy)	-1.23
	Occupied	d ₁	5d (66%) + π (ppy)	-4.79
		d _{2a}	5d (54%) + π (ppy)	-4.95
		d _{2b}	5d (54%) + π (ppy)	-4.95
Ir(dpydmb)(dppy) 108	Virtual	π_3^*	π^* (dpydmb)	-1.00
		π_2^*	π^* (dppy)	-1.09
		π_1^*	π^* (dpydmb)	-1.34
	Occupied	d ₁	5d (34%) + π (dpydmb/dppy)	-4.53
		d ₂	5d (46%) + π (dppy)	-4.86
		d ₃	5d (63%) + π (dpydmb/dppy)	-5.55
Ir(dpydmb)(F ₄ dppy) 110	Virtual	π_3^*	π^* (dpydmb)	-1.36
		π_2^*	π^* (F ₄ dppy)	-1.46
		π_1^*	π^* (dpydmb)	-1.66
	Occupied	d ₁	5d (37%) + π (dpydmb/F ₄ dppy)	-5.03
		d ₂	5d (46%) + π (F ₄ dppy)	-5.37
		d ₃	5d (63%) + π (dpydmb/F ₄ dppy)	-5.96
Ir(dpydmb)(cdppy) 111	Virtual	π_3^*	π^* (cdppy)	-1.58
		π_2^*	π^* (cdppy)	-1.75
		π_1^*	π^* (dpydmb)	-1.81
	Occupied	d ₁	5d (36%) + π (dpydmb/cdppy)	-5.14
		d ₂	5d (46%) + π (cdppy)	-5.52
		d ₃	5d (64%) + π (dpydmb/cdppy)	-6.16

Table 27. The three highest occupied and three lowest virtual (unoccupied) molecular orbitals of *fac*-Ir(ppy)₃ 26, Ir(dpydmb)(dppy) 108, Ir(dpydmb)(F₄dppy) 110 and Ir(dpydmb)(cdppy) 111.

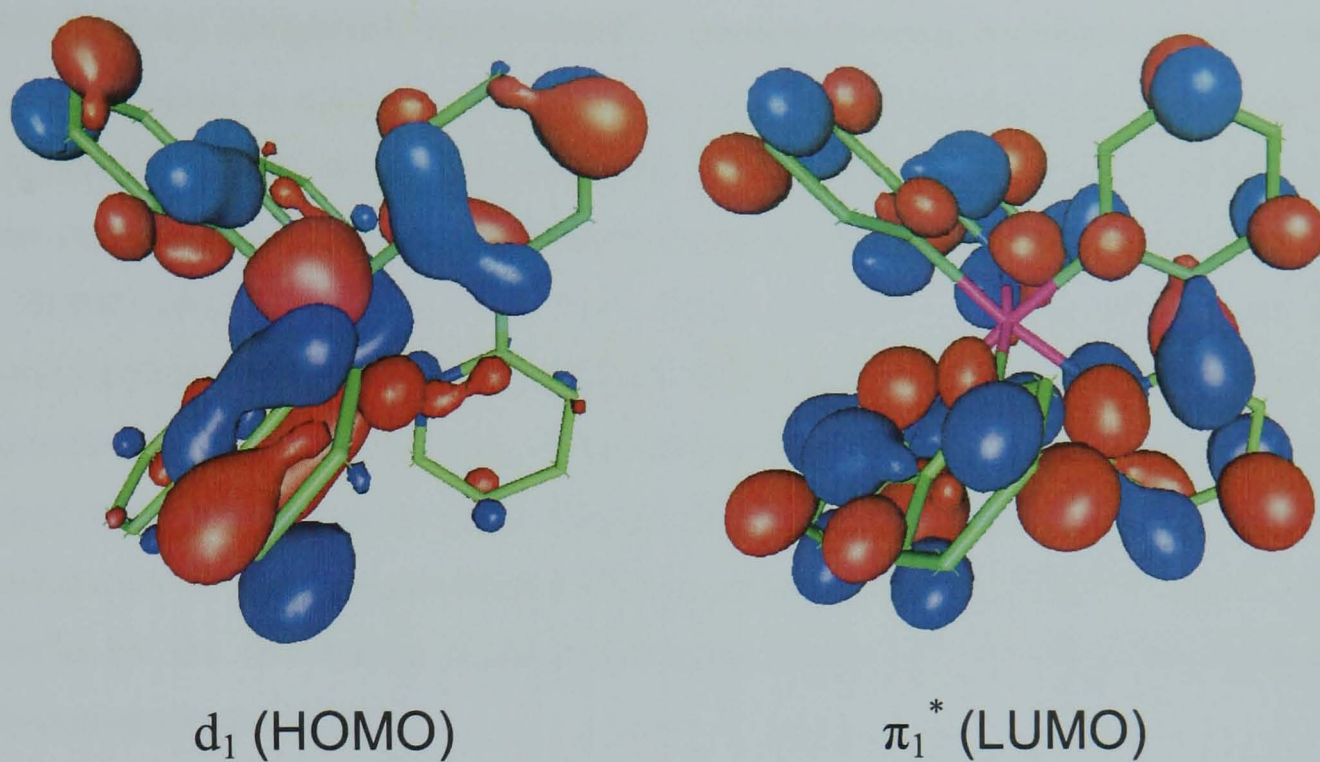


Figure 32. Contour plots of the HOMO and LUMO of *fac*-Ir(ppy)₃ 26.

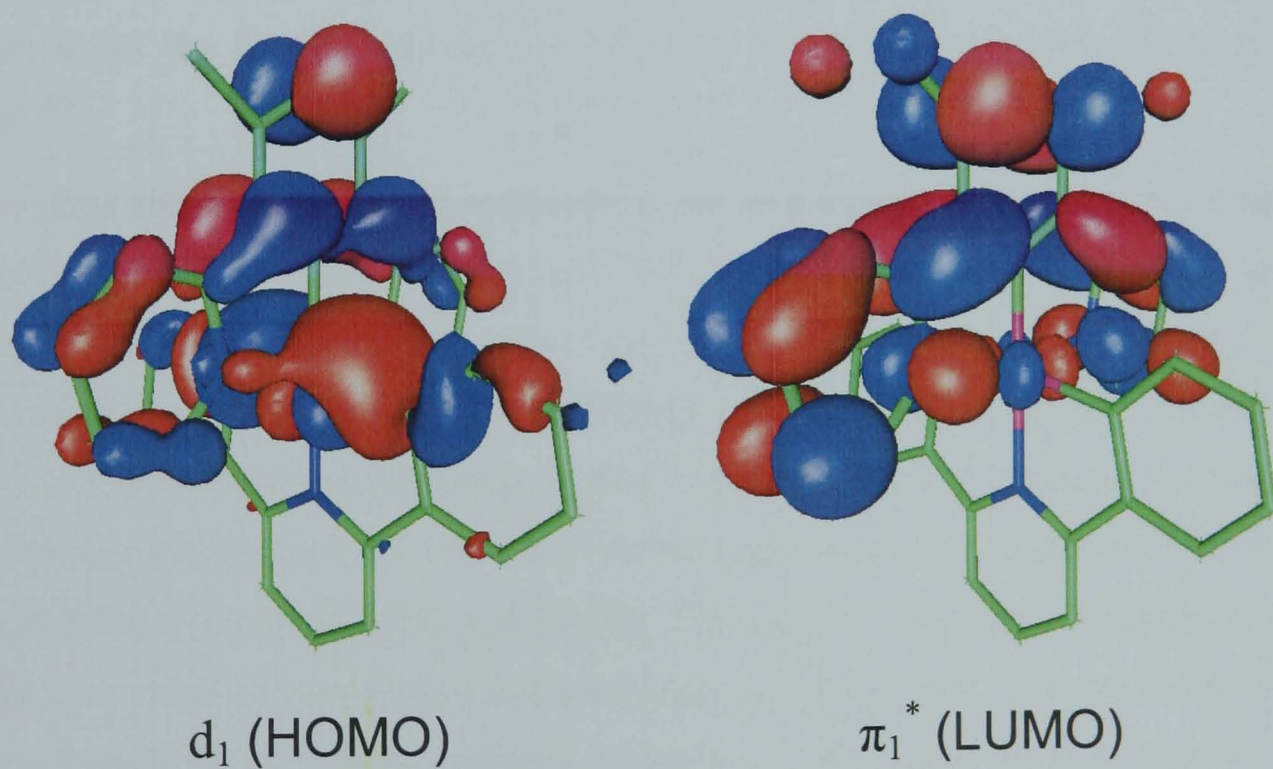


Figure 33. Contour plots of the HOMO and LUMO of Ir(dpydmb)(dppy) 108.

As may be expected for tris-cyclometalated d^6 iridium(III) complexes, the three highest occupied molecular orbitals (HOMOs) are localised on the metal 5d orbitals. While these are designated “metal-based”, it should be noted that there is a significant amount of ligand π character in each case. This is unsurprising considering that the cyclometalating Ir–C bonds are effectively covalent in nature. Even in $[\text{Ru}(\text{bpy})_3]^{2+}$ where coordination is solely through nitrogen atoms, DFT calculations have shown that the HOMO contains approximately 22% ligand character.⁴¹⁶ Thus, although the term metal-to-ligand charge transfer (MLCT) is often used to describe the lowest energy electronic transitions in this class of compound, there is usually considerable ligand-centred (LC) and ligand-to-ligand charge transfer (LLCT) character. An alternative classification is as a sigma-bond-to-ligand charge transfer (SBLCT) state, which accounts for the distribution of electron density across both the metal and metalating carbon atoms in the HOMO.

Although orbital density in the LUMO of *fac*-Ir(ppy)₃ **26** is evenly spread across all three ppy ligands, a change in geometry of the excited state may result in a localisation of electron density on a single ligand prior to emission. This has been shown to be the case for $[\text{Ru}(\text{bpy})_3]^{2+}$ by transient absorption pump-probe spectroscopy.¹⁴³

Due to the lowering of symmetry upon forming unsymmetrical bis-terdentate complexes (the highest order rotation axis is C_2 , compared to C_3 for *fac*-Ir(ppy)₃ **26**), the degeneracy of molecular orbitals observed for *fac*-Ir(ppy)₃ **26** is lost. An increase in delocalisation in the ligands of Ir(dpydmb)(dppy) **108** results in a lowering in energy of the π^* -orbitals with a corresponding raising of the π -orbitals. Introduction of electron-withdrawing substituents has little effect on the shapes of the molecular orbitals, with an overall stabilisation of all MOs as expected. Although it is tempting to suggest that this results in a complex less likely to undergo decomposition processes, such conclusions require knowledge of both ground-state energies and energies of the transition-states for the decomposition process. It should also be noted that although qualitative conclusions may be made by comparison of energy levels, the differences in energy predicted by DFT methods should not be expected to correspond to the observed energies of electronic transitions. For such comparisons to be meaningful, time-dependent DFT (TD-DFT) calculations must be performed (see Section 4.2.4).

Similar conclusions regarding the origin of electronic excited states may be reached for the Ir(N[^]C[^]N)(C[^]N[^]O) complexes, Ir(dpydmb)(tppic) **116** and

Ir(dpydmb)(hbqc) **117** (molecular orbitals summarised in Table 28, with contour plots of the HOMO and LUMO in Figure 34 and Figure 35). The HOMO is a mixed metal-dpydmb orbital, extending a small amount across the carboxylate group of the second ligand. In contrast to complexes of the form Ir(N[^]C[^]N)(C[^]N[^]C) where only a small proportion of the LUMO is on the dppy ligand, the LUMO of Ir(N[^]C[^]N)(C[^]N[^]O) complexes is more evenly spread across both ligands. This results in a much greater contribution of LLCT character to the emissive state.

		Orbital	Character	Energy / eV
Ir(dpydmb)(tppic) 116	Virtual	π_3^*	π^* (dpydmb)	-1.42
		π_2^*	π^* (dpydmb/tppic)	-1.56
		π_1^*	π^* (dpydmb/tppic)	-1.61
	Occupied	d ₁	5d (42%) + π (dpydmb/tppic)	-4.98
		d ₂	5d (50%) + π (tppic)	-5.22
		d ₃	5d (56%) + π (tppic)	-5.75
Ir(dpydmb)(hbqc) 117	Virtual	π_3^*	π^* (dpydmb)	-1.47
		π_2^*	π^* (dpydmb/hbqc)	-1.61
		π_1^*	π^* (dpydmb/hbqc)	-1.63
	Occupied	d ₁	5d (43%) + π (dpydmb/hbqc)	-5.04
		d ₂	5d (45%) + π (hbqc)	-5.25
		d ₃	5d (47%) + π (hbqc)	-5.67

Table 28. The three highest occupied and three lowest virtual (unoccupied) molecular orbitals of Ir(dpydmb)(tppic) **116** and Ir(dpydmb)(hbqc) **117**.

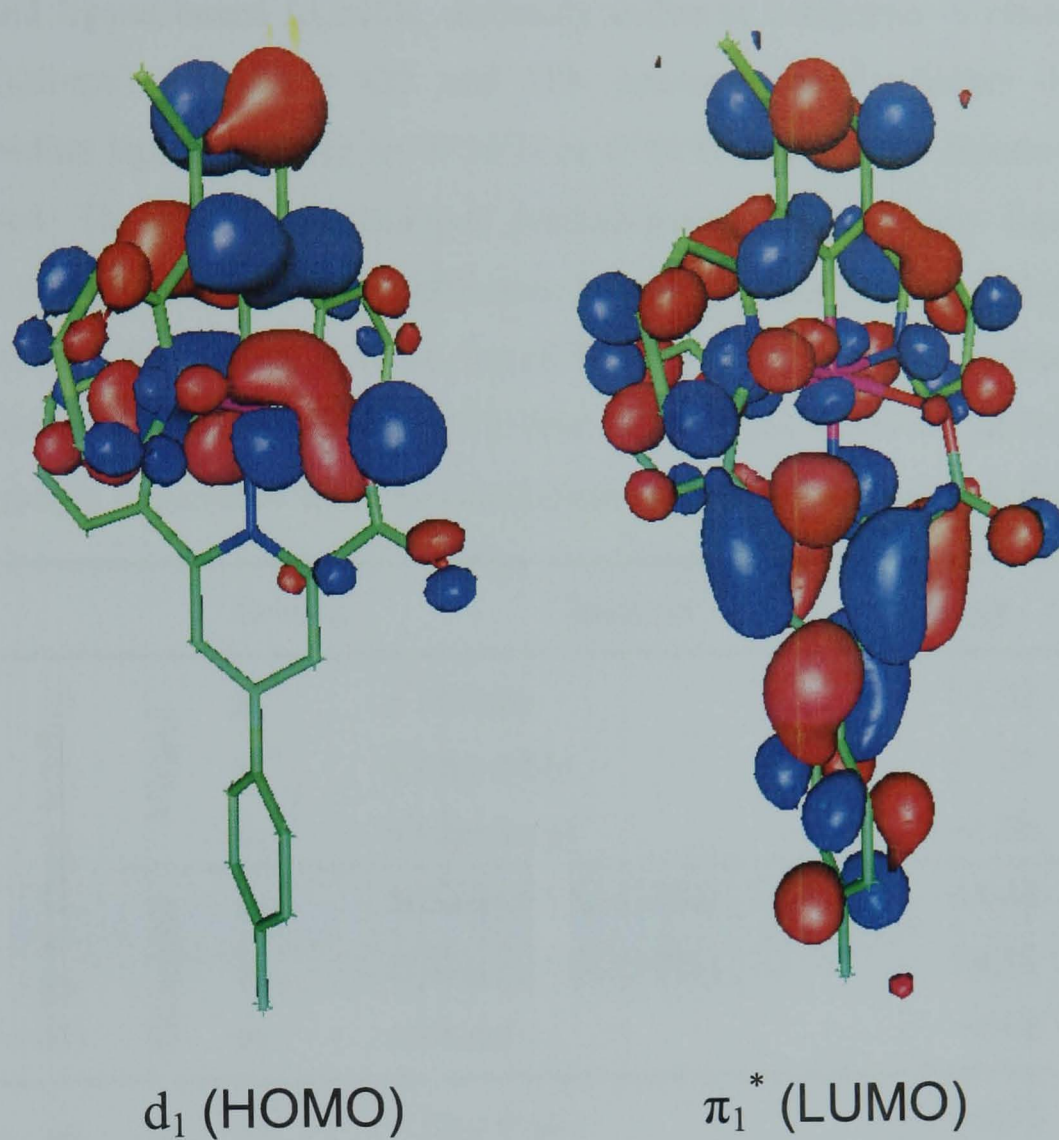


Figure 34. Contour plots of the HOMO and LUMO of Ir(dpydmb)(tppic) 116.

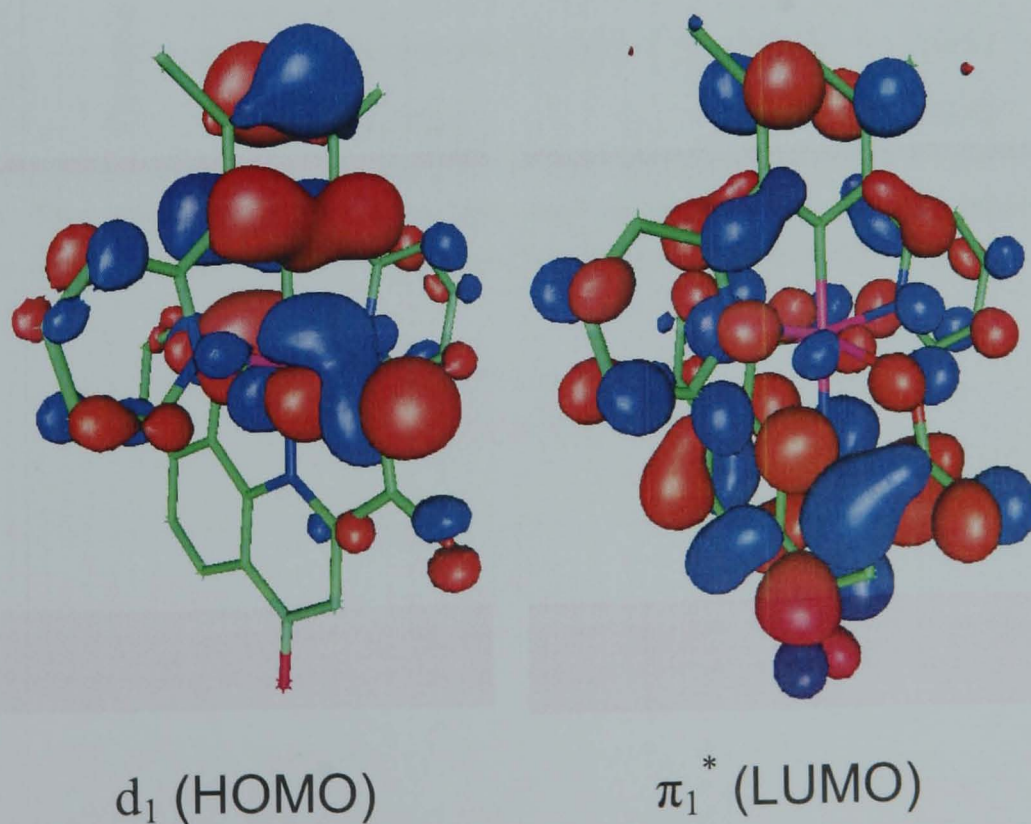


Figure 35. Contour plots of the HOMO and LUMO of Ir(dpydmb)(hbqc) 117.

While the complexes discussed in this section so far have primarily metal-based HOMOs and ligand-based LUMOs, distinctly different behaviour is observed for the Ir(dpydmb)(dinpy) complexes **122** and **123**. Irrespective of whether the 2,6-di(2'-indolyl)pyridine ligand binds in an N[^]N[^]N or C[^]N[^]C manner, the frontier orbitals are ligand based. The HOMO is localised predominantly on the dinpy ligand, and the LUMO on the dpydmb. The main difference between binding modes is that the portion of the HOMO on the central pyridine ring of dinpy is much more pronounced in the bis-cyclometalated complex (see Figure 37). Interestingly, the character of the subsequent states is strongly dependent upon the orientation of the dinpy ligand (see Table 29).

		Orbital	Character	Energy / eV
N [^] N [^] N dinpy binding	Virtual	π_3^*	π^* (dinpy)	-1.22
		π_2^*	π^* (dpydmb)	-1.47
		π_1^*	π^* (dpydmb)	-1.66
	Occupied	π_1	π (dinpy) + 5d (21%)	-4.43
		π_2	π (dinpy) + 5d (10%)	-4.81
		π_3	π (dinpy)	-4.92
C [^] N [^] C dinpy binding	Virtual	π_3^*	π^* (dpydmb)	-0.97
		π_2^*	π^* (dinpy)	-1.08
		π_1^*	π^* (dpydmb)	-1.31
	Occupied	π_1	π (dinpy) + 5d (24%)	-4.28
		π_2	π (dpydmb/dinpy) + 5d (36%)	-4.61
		π_3	π (dinpy)	-4.86

Table 29. The three highest occupied and three lowest virtual (unoccupied) molecular orbitals for two binding modes of Ir(dpydmb)(dinpy).

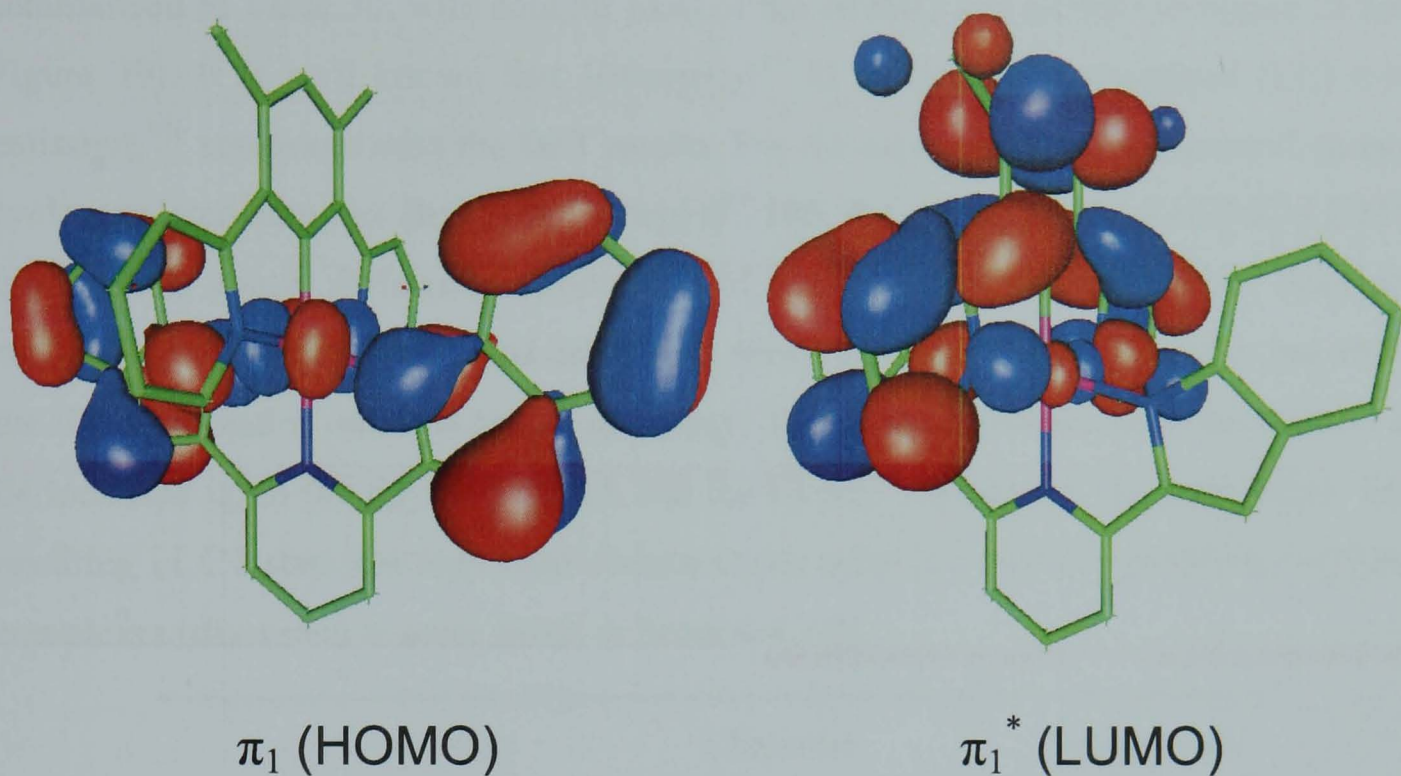


Figure 36. Contour plots of the HOMO and LUMO of Ir(dpydmb)(dinpy) with N^NN binding of the dinpy ligand (complex 123).

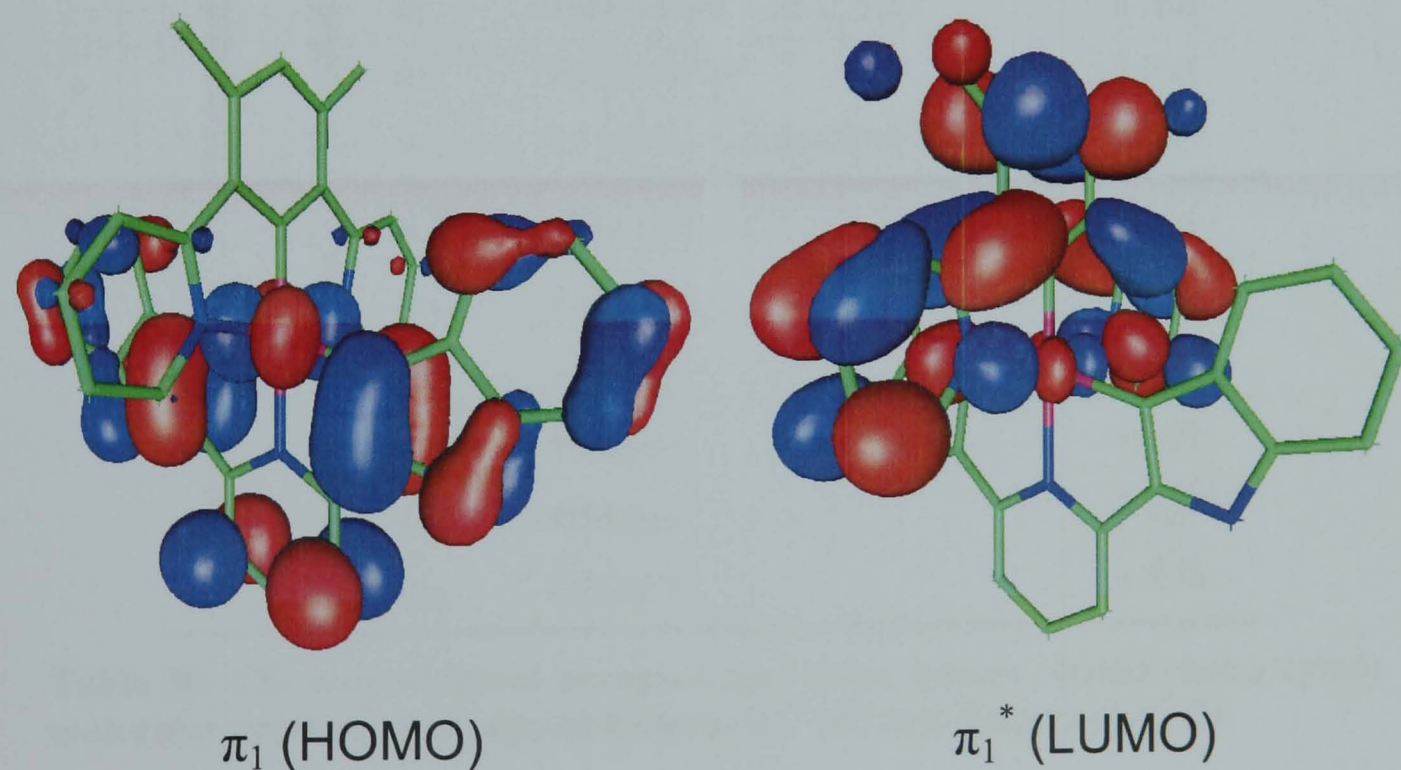


Figure 37. Contour plots of the HOMO and LUMO of Ir(dpydmb)(dinpy) with C^NC binding of the dinpy ligand (complex 122).

The mono-cyclometalated $[\text{Ir}(\text{dpydmb})(\text{terpy})]^{2+}$ **105** and non-cyclometalated $[\text{Ir}(\text{terpy})_2]^{3+}$ **21** have predominantly ligand-based frontier orbitals (molecular orbitals summarised in Table 30, with contour plots of the HOMO and LUMO in Figure 38 and Figure 39). It is well known that $[\text{Ir}(\text{terpy})_2]^{3+}$ **21** exhibits ligand-centred (LC) π - π^* emission,¹⁰³ consistent with the DFT results. For the asymmetrically substituted, mono-cyclometalated complex $[\text{Ir}(\text{dpydmb})(\text{terpy})]^{2+}$ **105**, the character of the HOMO-LUMO transition is subtly different. Introduction of a cyclometalating Ir–C bond does not sufficiently destabilise the metal orbitals to result in a metal-based HOMO, but shifts the ligand π - and π^* -orbitals higher in energy. This is sufficient to allow the HOMO to be localised upon the dpydmb ligand, but the LUMO remains on the terpyridine. The resulting LLCT state has important consequences upon the emission properties of these complexes (discussed in more detail in Section 4.2.4).

		Orbital	Character	Energy / eV
$[\text{Ir}(\text{dpydmb})(\text{terpy})]^{2+}$ 105	Virtual	π_3^*	$\pi^*(\text{dpydmb})$	-6.85
		π_2^*	$\pi^*(\text{terpy})$	-7.84
		π_1^*	$\pi^*(\text{terpy})$	-8.06
	Occupied	π_1	$\pi(\text{dpydmb}) + 5d$ (26%)	-11.04
		π_2	$\pi(\text{dpydmb})$	-11.21
		d_1	$5d$ (60%) + $\pi(\text{dpydmb}/\text{dinpy})$	-12.04
$[\text{Ir}(\text{terpy})_2]^{3+}$ 21	Virtual	π_2^*	$\pi^*(\text{terpy})$	-5.36
		π_{1b}^*	$\pi^*(\text{terpy})$	-5.72
		π_{1a}^*	$\pi^*(\text{terpy})$	-5.72
	Occupied	π_1	$\pi(\text{terpy})$	-9.89
		π_{2a}	$\pi(\text{terpy})$	-15.53
		π_{2b}	$\pi(\text{terpy})$	-15.78

Table 30. The three highest occupied and three lowest virtual (unoccupied) molecular orbitals of $[\text{Ir}(\text{dpydmb})(\text{terpy})]^{2+}$ **105** and $[\text{Ir}(\text{terpy})_2]^{3+}$ **21**.

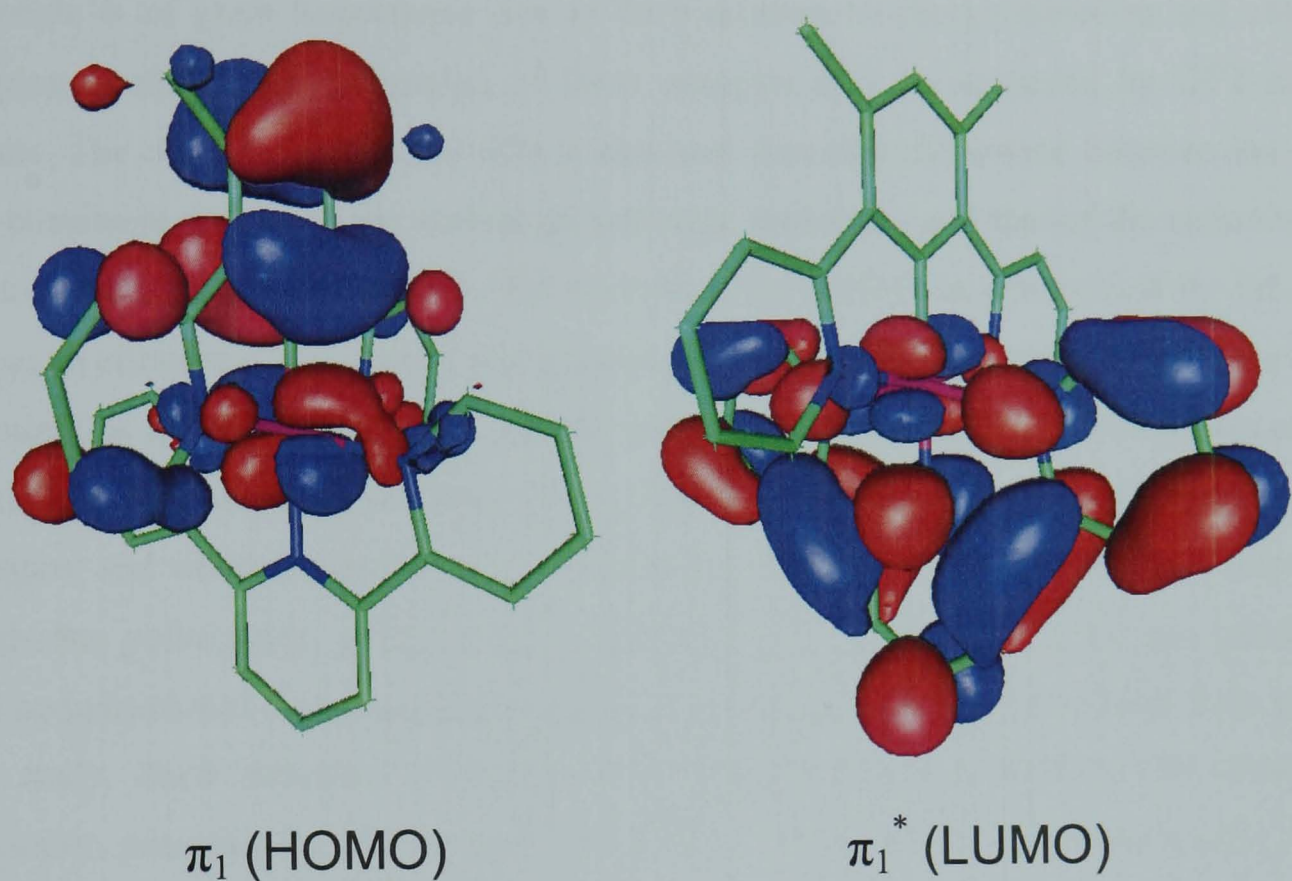


Figure 38. Contour plots of the HOMO and LUMO of $[\text{Ir}(\text{dpymb})(\text{terpy})]^{2+}$ 105.

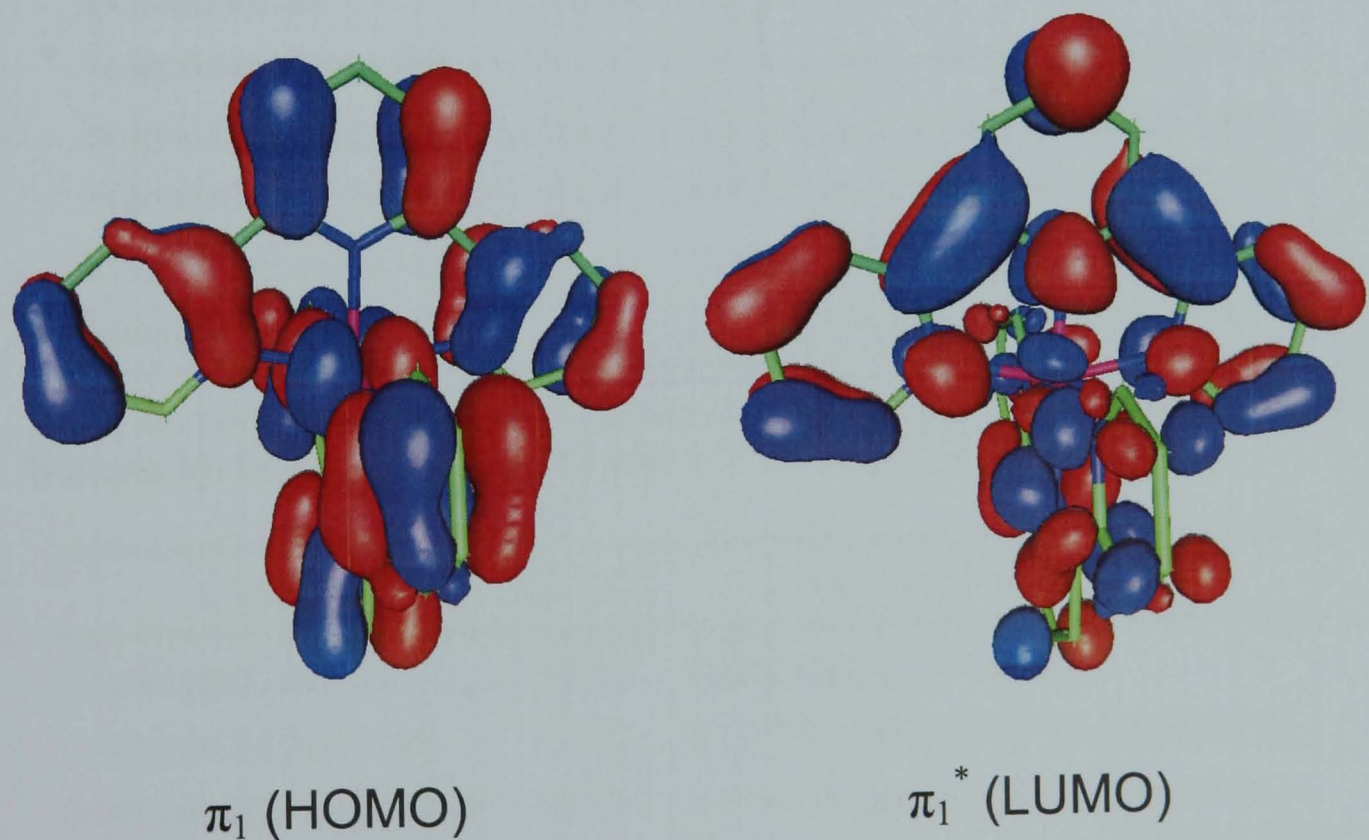


Figure 39. Contour plots of the HOMO and LUMO of $[\text{Ir}(\text{terpy})_2]^{3+}$ 21.

4.2.3 Ionisation potentials and electron affinities

The ionisation potential and electron affinity of potential electroluminescent materials is of great importance due to their relation to charge-injection and charge-trapping qualities. An estimation of these energies may be achieved by DFT calculations. The ionisation potential (IP) is obtained from the difference between the total self-consistent energy of the neutral ground-state molecule, and that of the cation at the ground-state structure. Similarly, the electron affinity (EA) is determined by the difference in energies of the neutral and anionic molecules. Total atomic spin densities from calculations for the cationic and anionic structures also allow the determination of the localisation of charge in each case. The results should ideally be corrected for zero-point energies, and where comparisons to experimental values for the solid-state are required, solid-state polarisation effects (since calculations are performed in the gas phase).⁴¹⁰ The computational cost associated with these corrections however precludes their use in this study. Their influence is evident in the large discrepancy between the calculated ionisation potential for *fac*-Ir(ppy)₃ **26** (+6.00 eV) and that from measurements when doped in a CBP host (+5.2 eV).⁴¹⁷

Complex	IP / eV	Spin density of cation
<i>fac</i> -Ir(ppy) ₃ 26	+6.00	Ir (63%), ppy (12% × 3)
Ir(dpydmb)(dppy) 108	+5.99	Ir (49%), dpydmb (5%), dppy (47%)
Ir(dpydmb)(F ₄ dppy) 110	+6.50	Ir (49%), dpydmb (6%), F ₄ dppy (45%)
Ir(dpydmb)(cdppy) 111	+6.60	Ir (49%), dpydmb (6%), cdppy (46%)
Ir(dpydmb)(tppic) 116	+6.14	Ir (48%), dpydmb (28%), tppic (24%)
Ir(dpydmb)(hbqc) 117	+6.43	Ir (49%), dpydmb (8%), hbqc (43%)

Table 31. Calculated ionisation potentials and cationic spin densities for *fac*-Ir(ppy)₃ **26, Ir(N[^]C[^]N)(C[^]N[^]C) and Ir(N[^]C[^]N)(C[^]N[^]O) complexes.**

Complex	EA / eV	Spin density of anion
<i>fac</i> -Ir(ppy) ₃ 26	+0.27	Ir (2%), ppy (33% × 3)
Ir(dpydmb)(dppy) 108	+0.02	Ir (-2%), dpydmb (59%), dppy (44%)
Ir(dpydmb)(F ₄ dppy) 110	-0.16	Ir (2%), dpydmb (1%), F ₄ dppy (98%)
Ir(dpydmb)(cdppy) 111	-0.53	Ir (-1%), dpydmb (30%), cdppy (71%)
Ir(dpydmb)(tppic) 116	-0.46	Ir (0%), dpydmb (78%), tppic (22%)
Ir(dpydmb)(hbqc) 117	-0.42	Ir (1%), dpydmb (86%), hbqc (14%)

Table 32. Calculated electron affinities and anionic spin densities for *fac*-Ir(ppy)₃ **26, Ir(N[^]C[^]N)(C[^]N[^]C) and Ir(N[^]C[^]N)(C[^]N[^]O) complexes.**

The results of ionisation potential and electron affinity calculations on a number of iridium(III) complexes are summarised in Table 31 (IPs) and Table 32 (EAs). The ionisation potential of *fac*-Ir(ppy)₃ **26** is predicted to be +6.00 eV and the electron affinity +0.27 eV. While the former is in reasonable agreement with the value calculated by Hay (+5.94 eV¹⁴²), the electron affinity is substantially higher (compared to +0.08 eV¹⁴²). In fact some EAs in the present study are negative, suggesting that the anion is more stable than the neutral compound. One difficulty in producing accurate electron affinities is due to the poor ability of the chosen basis set (6-31G) to reproduce the very diffuse molecular orbitals of anionic compounds. While basis sets with diffuse orbitals (*e.g.* 6-31G*) would improve accuracy, this is at the cost of computation time.

The calculated ionisation potential, as expected from the trend in HOMO energies, is progressively increased from Ir(dpydmb)(dppy) **108** upon fluoro and cyano substitution. It is interesting to note that although the spin densities of the cation are similar in each case, they bear poor resemblance to the calculated shape of the HOMO, instead being more comparable to the HOMO+1 orbital. As expected, the electron added on forming the anion is localised on the ligands, with very little spin density at the metal. This is shifted across to the C[^]N[^]C coordinated ligand upon fluorination, and to a lesser extent upon introduction of the cyano substituent.

4.2.4 Excitation energies

Time-dependent DFT (TD-DFT) calculations at the singlet ground-state geometry were performed to determine the excitation energies of electronic transitions. Although a similar calculation at the excited-state geometry should allow the prediction of emission energies, the time required for such computation makes this impractical for molecules as large as those in this study. The results of TD-DFT calculations on *fac*-Ir(ppy)₃ **26** are shown in Table 33. The results are similar to those obtained by Hay's TD-DFT calculation on this structure.¹⁴² Although normally attributed to MLCT(Ir→ppy) excited states, all transitions have a significant proportion of LC(ppy) character as discussed in Section 4.2.2. The calculated excitation wavelengths are compared to the experimentally observed absorbance spectrum in Figure 40. Excellent agreement is found between the two, with T₁ and T₂ states at 482 and 480 nm respectively matching the lowest energy absorption band. This is comparatively weak, consistent with the triplet nature of this MLCT transition.

State	λ / nm	Excitation	State	λ / nm	f	Excitation
T ₁	482	$d_2 \rightarrow \pi_1^*$	S ₁	446	0.0041	$d_2 \rightarrow \pi_1^*$
T ₂	480	$d_2 \rightarrow \pi_{2a}^*$	S ₂	437	0.0019	$d_2 \rightarrow \pi_{2a}^*$
	480	$d_2 \rightarrow \pi_{2b}^*$		437	0.0021	$d_2 \rightarrow \pi_{2b}^*$
T ₃	446	$d_{1a,1b} \rightarrow \pi_{2a,2b}^*$	S ₃	410	0.0213	$d_{1b} \rightarrow \pi_1^*$
T ₄	440	$d_{1a,1b} \rightarrow \pi_{1,2a,2b}^*$		410	0.0222	$d_{1a} \rightarrow \pi_1^*$
	441	$d_{1a,1b} \rightarrow \pi_{1,2a,2b}^*$	S ₄	409	0.0027	$d_{1a,1b} \rightarrow \pi_{2a,2b}^*$
T ₅	423	$d_{1b} \rightarrow \pi_1^*$	S ₅	395	0.0606	$d_{1a,1b} \rightarrow \pi_{2a,2b}^*$
	422	$d_{1a} \rightarrow \pi_1^*$		395	0.0616	$d_{1a,1b} \rightarrow \pi_{2a,2b}^*$
T ₆	417	$d_{1a,1b} \rightarrow \pi_{2a,2b}^*$	S ₆	392	0.0001	$d_2 \rightarrow \pi_3^*$
T ₇	402	$d_2 \rightarrow \pi_3^*$	S ₇	366	0.0060	$d_{1a} \rightarrow \pi_3^*$

Table 33. Calculated excitation wavelengths (λ), oscillator strengths (f) and dominant orbital excitations for the ground-state structure of *fac*-Ir(ppy)₃ 26. Orbitals are labelled as in Table 27.*

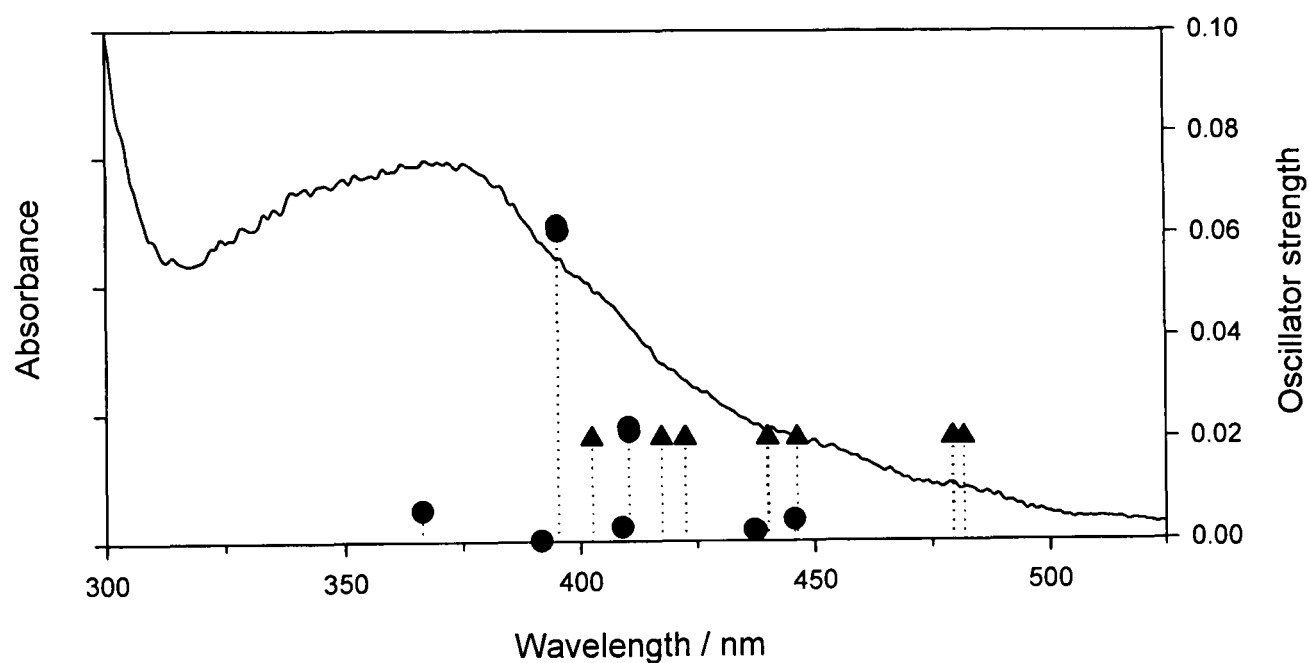


Figure 40. Comparison of the experimental absorbance spectrum of *fac*-Ir(ppy)₃ 26 in acetonitrile solution (solid line, left axis) to singlet (●, right axis) and triplet (▲, arbitrary height) transitions from TD-DFT calculations.

The results of TD-DFT studies of a series of Ir(N[^]C[^]N)(C[^]N[^]C) complexes are shown in Table 34, with full results tabulated in Appendix B. In each case the $d_1 \rightarrow \pi_1^*$ triplet state is at the lowest energy, and hence likely to be the emissive state. Due to the mixing of metal and ligand orbital character in the d_1 state, this may be assigned as

* Orbitals are numbered sequentially by energy. The sub-scripts 'a' and 'b' represent degenerate energy levels.

MLCT(Ir→N[^]C[^]N) with significant LC(N[^]C[^]N) and some LLCT(C[^]N[^]C→N[^]C[^]N) character. The experimentally observed blue-shift in absorption is reflected in the increase in predicted energy of the d₁→π₁^{*} transition upon fluorination. Although the 2,6-di(3-cyanophenyl)pyridine **94** (cdppyH₂) complex was not successfully prepared, TD-DFT calculations suggest that similar absorption properties would be observed.

State	Ir(dpydmb)(dppy) 108		Ir(dpydmb)(F ₄ dppy) 110		Ir(dpydmb)(cdppy) 111	
	λ / nm (<i>f</i>)	Excitation	λ / nm (<i>f</i>)	Excitation	λ / nm (<i>f</i>)	Excitation
T ₁	556	d ₁ → π ₁ [*]	518	d ₁ → π ₁ [*]	524	d ₁ → π ₁ [*]
T ₂	507	d ₁ → π ₂ [*]	477	d ₁ → π ₃ [*]	487	d ₁ → π ₂ [*]
T ₃	484	d ₂ → π ₁ [*]	470	d _{1,2} → π _{1,3} [*]	480	d ₁ → π ₄ [*]
S ₁	482 (0.1019)	d ₁ → π ₁ [*]	451 (0.1125)	d ₁ → π ₁ [*]	472 (0.0000)	d ₁ → π ₂ [*]
S ₂	462 (0.0000)	d ₁ → π ₂ [*]	441 (0.0001)	d ₁ → π ₃ [*]	456 (0.1139)	d ₁ → π ₁ [*]
S ₃	433 (0.0047)	d _{1,2} → π _{1,2} [*]	411 (0.0008)	d ₁ → π ₃ [*]	429 (0.0023)	d ₁ → π ₃ [*]

Table 34. Calculated excitation wavelengths (λ), oscillator strengths (*f*) and dominant orbital excitations for the ground-state structures of Ir(N[^]C[^]N)(C[^]N[^]C) complexes. Orbitals are labelled as in Table 27. Full results are tabulated in Appendix B.

Comparison of the results of TD-DFT calculations with the experimentally observed absorption spectrum for Ir(dpydmb)(dppy) **108** (Figure 41) and for Ir(dpydmb)(F₄dppy) **110** (Figure 42) show good agreement between the two, especially considering the lowering of triplet energies due to spin-orbit coupling effects not included in current TD-DFT calculations.¹⁴² In contrast to the results for *fac*-Ir(ppy)₃ **26**, the lowest energy predicted triplet state does not correspond to a resolvable peak in the absorption spectrum. This suggests that transitions between this state (the emissive state) and the ground state are more strongly forbidden than for *fac*-Ir(ppy)₃ **26**. This is consistent with the relatively long radiative lifetimes (almost 4 μs) observed experimentally for the bis-terdentate analogues.

Although calculations at the ground-state geometry cannot be related directly to emission properties, relative energies of structurally similar compounds may be compared. By calibration with the observed Ir(dpydmb)(dppy) **108** emission (λ_{max} = 585 nm), we may predict that the emission wavelength in acetonitrile solution is ~29 nm higher than the calculated energy of the T₁ state. Application of this correction to the T₁ energy of Ir(dpydmb)(F₄dppy) **110** places the predicted emission at 547 nm,

exactly that experimentally observed. Therefore we may expect with some confidence the emission maximum of the presently inaccessible Ir(dpydmb)(cdppy) complex **111** to be at ~553 nm.

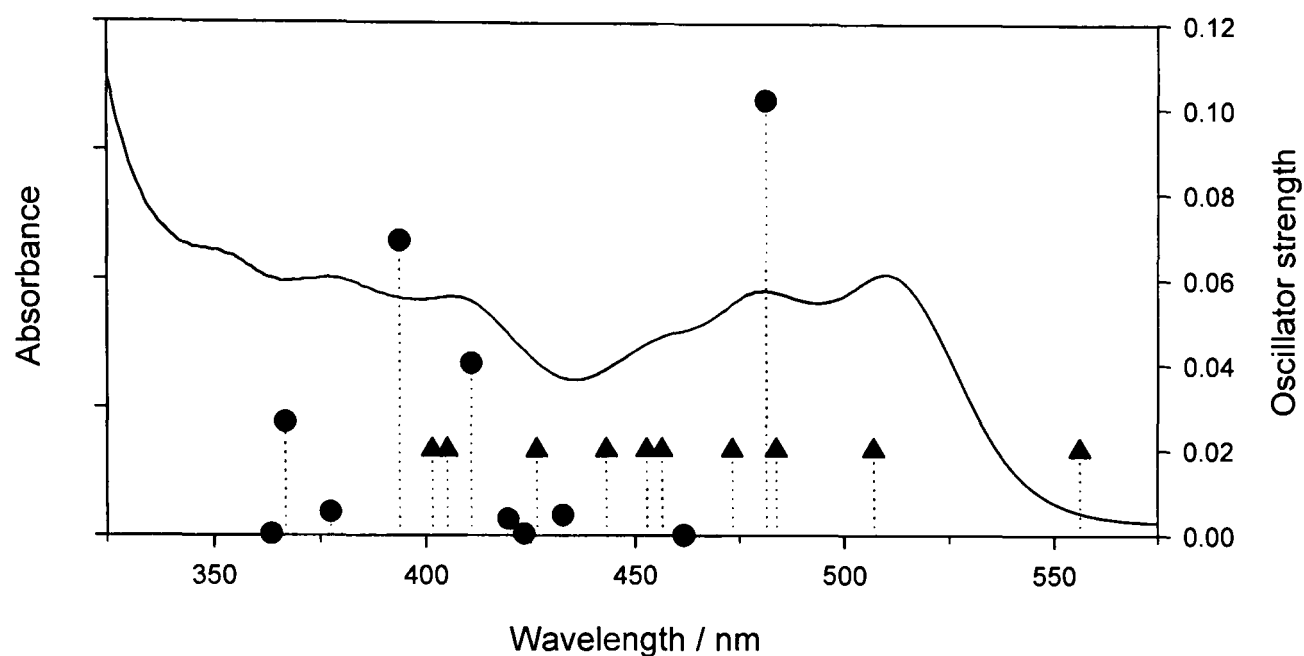


Figure 41. Comparison of the experimental absorbance spectrum of Ir(dpydmb)(dppy) **108** in acetonitrile solution (solid line, left axis) to singlet (●, right axis) and triplet (▲, arbitrary height) transitions from TD-DFT calculations.

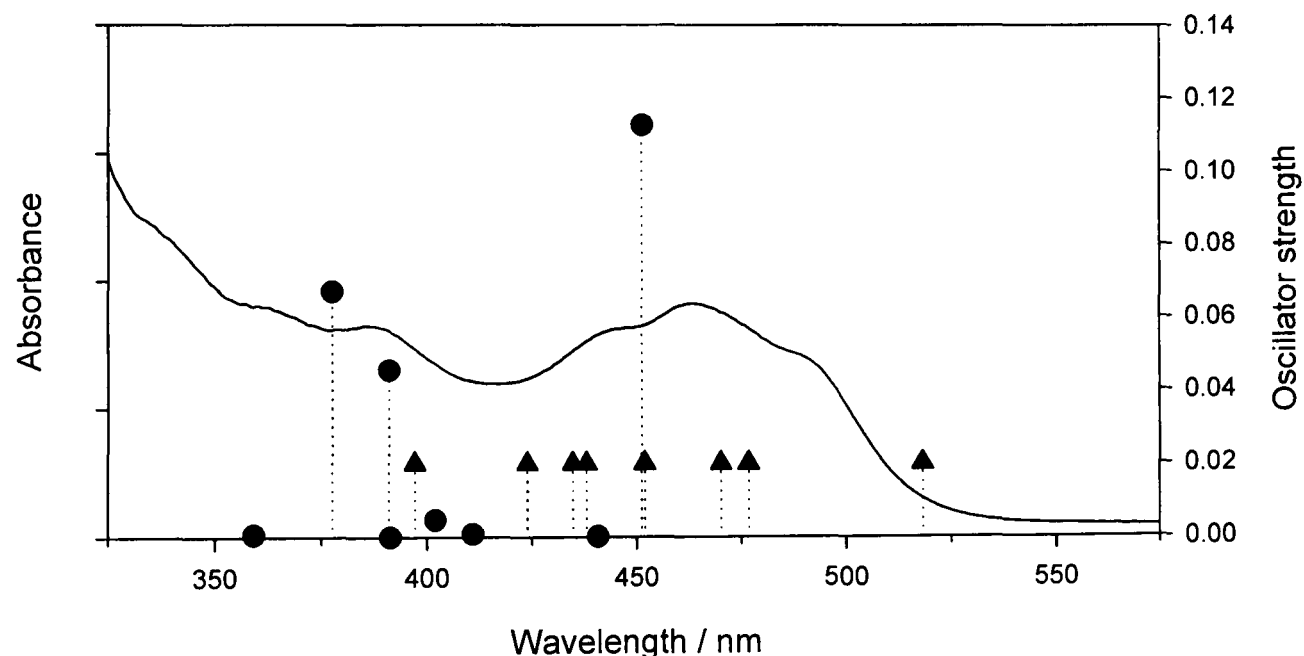


Figure 42. Comparison of the experimental absorbance spectrum of Ir(dpydmb)(F₄dppy) **110** in acetonitrile solution (solid line, left axis) to singlet (●, right axis) and triplet (▲, arbitrary height) transitions from TD-DFT calculations.

A comparison of the absorbance spectrum of Ir(dpydmb)(tppic) **116** with TD-DFT calculations is shown in Figure 43, with similar results obtained for Ir(dpydmb)(hbqc) **117** (full results tabulated in Appendix B). Although the most intense

singlet states from DFT cannot be readily associated with observed bands, the calculations predict the onset of the absorption as 508 nm with reasonable accuracy. The lowest energy excited-state (likely to resemble the emissive state) may be assigned as an MLCT ($d_1 \rightarrow \pi_{1,2}^*$) state. Since the predicted d_1 orbital is delocalised across both ligands as well as the metal, the emissive state is mixed with a large amount of LLCT and LC character, and luminescence efficiency is consequently diminished (see Section 4.1.3).

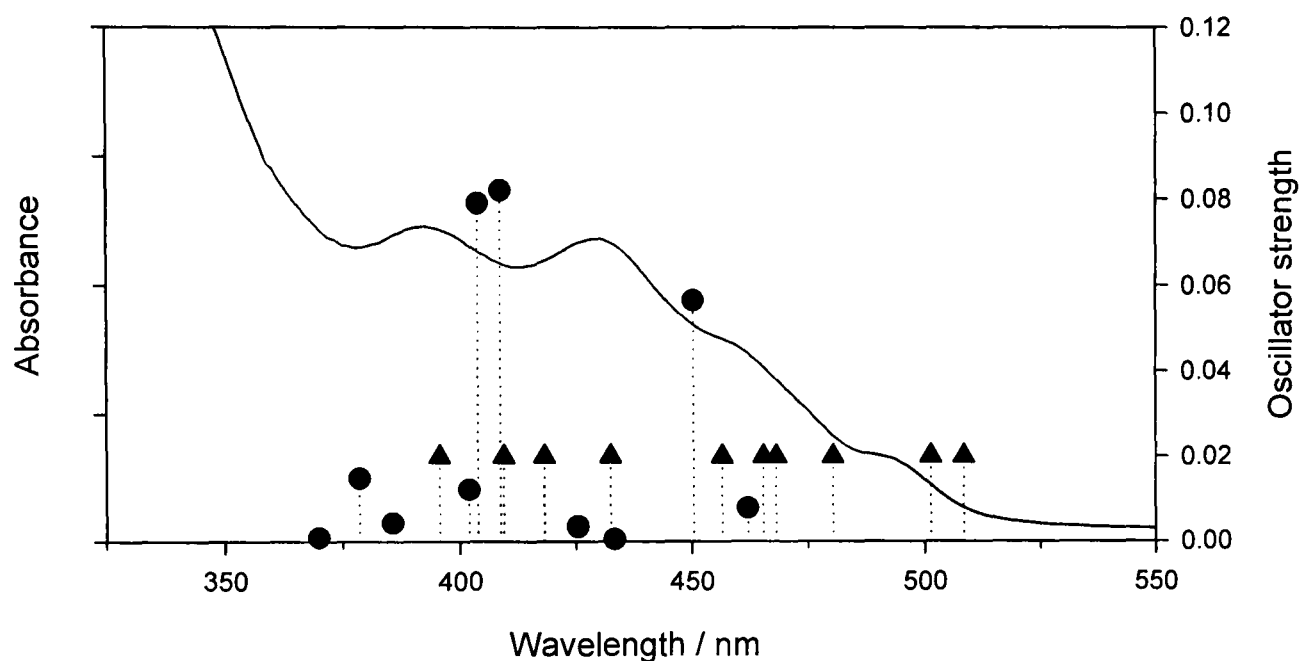


Figure 43. Comparison of the experimental absorbance spectrum of Ir(dpydmb)(tppic) 116 in acetonitrile solution (solid line, left axis) to singlet (●, right axis) and triplet (▲, arbitrary height) transitions from TD-DFT calculations.

The results of TD-DFT calculations on the two Ir(dpydmb)(dinpy) complexes are shown graphically in Figure 44, and tabulated in full in Appendix B. Although the frontier orbitals predicted by DFT calculations are very similar for the two binding modes (see Section 4.2.2), the TD-DFT results show a number of differences. In general the singlet states have very low oscillator strengths, consistent with what is expected for predominantly LLCT transitions. An unexpected exception is the state at 445 nm for the complex incorporating a C^NC-bound dinpy ligand. Consideration of the orbital contribution does not explain the particularly high oscillator strength ($f = 0.1625$) since there is a state predicted at 481 nm with a similar $d_1, \pi_1 \rightarrow \pi_{1,3}^*$ nature, but a substantially lower oscillator strength ($f = 0.0091$). Although samples of either complex with sufficient purity for photophysical studies were not obtained, the TD-DFT results suggest that they would be very poorly emissive due to the LLCT nature of their lowest energy excited states.

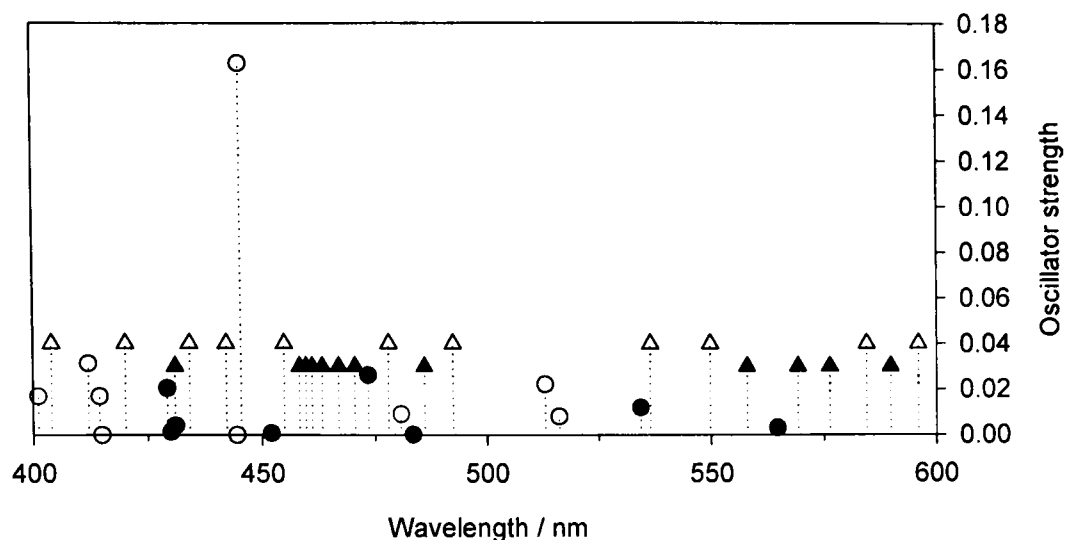


Figure 44. Calculated singlet (●, right axis) and triplet (▲, arbitrary height) transitions from TD-DFT calculations for N^NN⁻ (solid shapes) and C^NC⁻ (hollow shapes) binding modes of the dinpy ligand in Ir(dpydmb)(dinpy).

The experimentally observed absorption spectrum of [Ir(dpydmb)(terpy)]²⁺ **105** is shown alongside TD-DFT results in Figure 45 (full results tabulated in Appendix B). The position of the two most intense singlet states from the present TD-DFT calculation show reasonable correlation with the two very weak absorptions, their low intensity reflected in the small predicted oscillator strengths. These singlet bands are assigned to dpydmb(π_2) \rightarrow terpy(π_1^* and π_2^*) ligand-to-ligand charge transfer (LLCT) transitions. Although a small amount of mixing with metal orbitals is predicted in the HOMO, it is predominantly ligand based with the lowest energy transition assigned therefore as triplet dpydmb(π_1) \rightarrow terpy(π_1^*) LLCT. The unusual nature of this lowest energy state with little contribution of MLCT character may explain the particularly poor luminescence efficiencies of this class of compound even at 77 K (see Section 4.1.5).

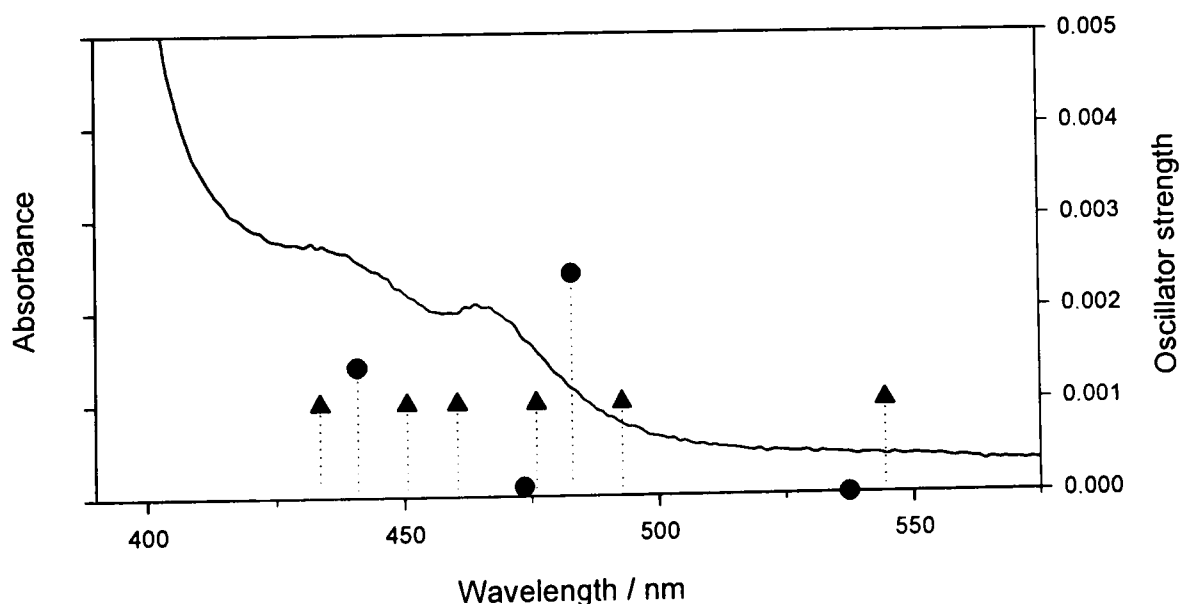


Figure 45. Comparison of the experimental absorbance spectrum of [Ir(dpydmb)(terpy)]²⁺ **105** in acetonitrile solution (solid line, left axis) to singlet (●, right axis) and triplet (▲, arbitrary height) transitions from TD-DFT calculations.

4.3 Concluding remarks: The effect of cyclometalation upon the luminescence of iridium(III) complexes

Luminescence data for the complexes prepared in this study are collated in Table 35 and Figure 46. A number of charge-neutral iridium(III) complexes have been prepared, with emission in acetonitrile solution spanning from green ($\lambda_{em} = 508$ nm) to orange/red ($\lambda_{em} = 603$ nm). There is also a great variation in photoluminescence quantum yields, ranging from virtually non-emissive to highly luminescent ($\Phi = 0.76$ in degassed acetonitrile solution). By a combination of photophysical studies and density functional theory (DFT) calculations, it is possible to explain this breadth of properties resulting from relatively minor modifications in structure.

Complex	λ_{max} / nm	CIE coordinates ^a	Aerated		Degassed	
			Φ^b	τ^c / ns	Φ^b	τ^c / ns
Ir(dpydmb)(dppy) 108	585	$x=0.55, y=0.45$	0.0013	77	0.21	3800
Ir(dpydmb)(F ₄ dppy) 110	547	$x=0.43, y=0.55$	0.0036	<100	0.41	3700
Ir(dpydmb)(ppy)Cl 115	508	$x=0.29, y=0.64$	0.016	<100	0.76	1600
Ir(dpydmb)(tppic) 116	603	$x=0.52, y=0.47$	0.0092	39	0.053	110
Ir(dpydmb)(hbqc) 117	562	$x=0.48, y=0.51$	0.0043	<100	0.027	170
[Ir(tpybae)(dppy)] ⁺ 124	707	$x=0.64, y=0.36$	0.0018	240	0.012	1700
[Ir(dpydmb)(terpy)] ²⁺ 105	502	$x=0.27, y=0.54$	<0.001	^d	<0.001	^d

^aA measure of the observed colour of emission, as defined by the Commission Internationale de L'Eclairage, and plotted in Figure 46. ^bQuantum yields of emission, 295 K, measured using an aqueous solution of [Ru(bpy)₃]²⁺ as a standard;⁴⁰⁰ uncertainty $\pm 20\%$. ^cLifetimes of emission, $\lambda_{ex} = 355$ nm, 295 K; uncertainty $\pm 5\%$. ^dDue to weak emission even at 77 K, luminescence lifetimes were not obtained.

Table 35. Luminescence data in acetonitrile solution at 295 K for complexes prepared in this study.

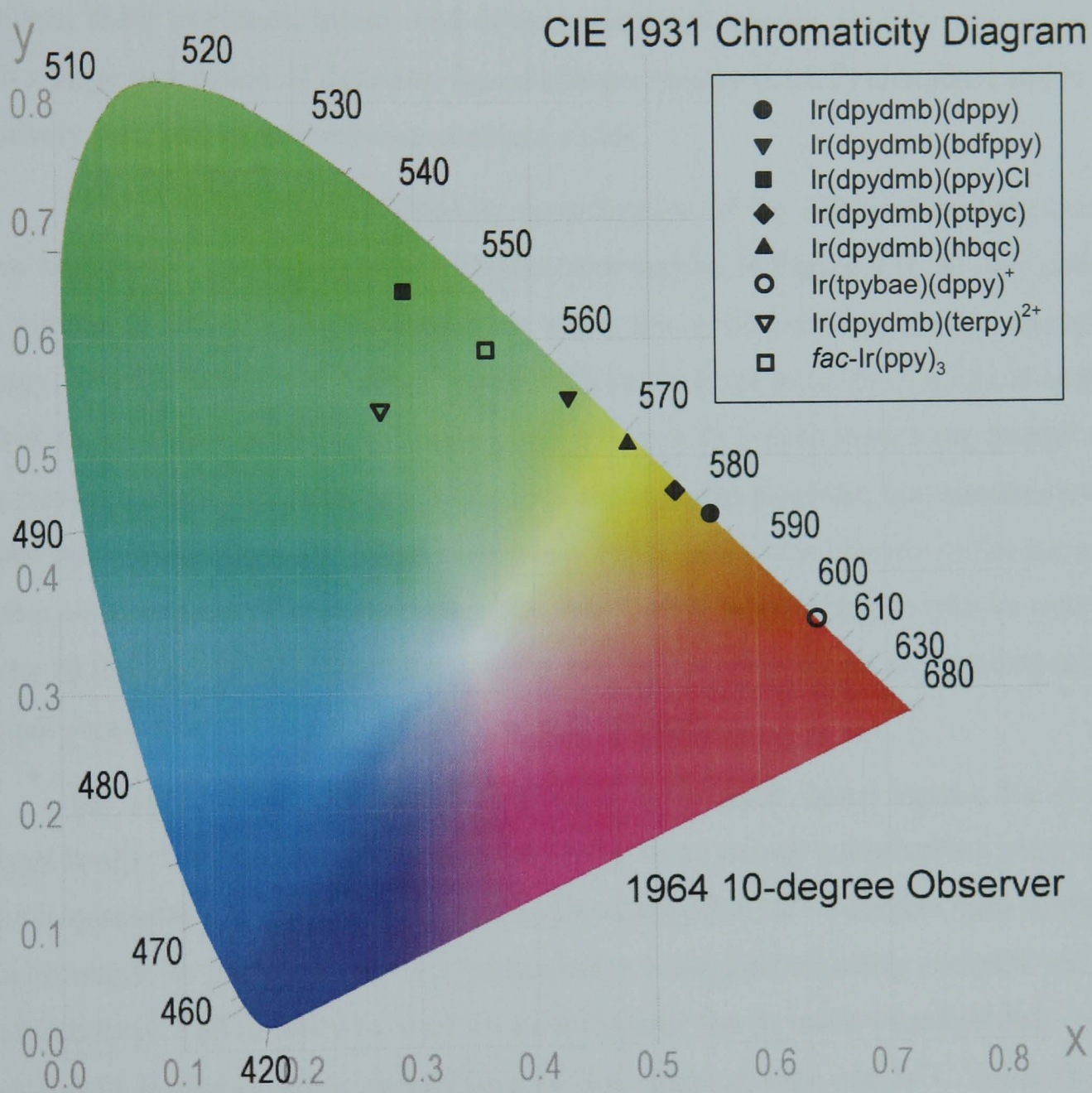


Figure 46. Commission Internationale de L'Eclairage (CIE) colour chart illustrating the observed emission colour of complexes prepared in this study.

The emission properties and luminescence efficiencies of cyclometalated iridium(III) complexes are determined by the nature of their electronic excited states. A steady trend may be observed from the ligand-centred (LC) luminescence of iridium(III) bis-terpyridine complexes to the metal-to-ligand charge transfer (MLCT) states of tris-cyclometalated *fac*-Ir(ppy)₃ **26** and the Ir(C[^]N[^]C)(N[^]C[^]N) complexes of this study. Between these extremes, mono- and di-cyclometalated species exhibit emissive states with a large proportion of ligand-to-ligand charge transfer (LLCT) character, and hence relatively poor photoluminescence quantum yields.

This trend may be explained by consideration of the effect of cyclometalation upon both metal- and ligand-based orbitals (summarised in Figure 47). At one extreme are iridium(III) bis-terpyridine complexes, where the metal d-orbitals are low enough in energy, and the ligand π - π^* energy gap is sufficiently large to result in a ligand-centred emissive state. Replacement of single pyridyl ring with a cyclometalating phenyl ring has two important consequences; it destabilises the metal d-orbital, and simultaneously raises the relevant ligand's π - and π^* -orbitals. Since molecular orbitals of the uncyclometalated ligand are little perturbed by this substitution, a switching in relative ordering of the HOMO or LUMO ligand localisation may occur. This results in a cyclometalated ligand→uncyclometalated ligand LLCT emissive state.

The introduction of a second Ir–C bond in the same ligand repeats the shift in energy levels. This now brings the metal d-orbital to an energy comparable to that of the bis-cyclometalated ligand π -orbital, and a mixed MLCT-LLCT emissive state results. It is worthwhile to comment that a symmetrically bis-cyclometalating complex such as [Ir(dpydmb)₂]⁺ **125** is likely to result in an analogous rise in metal-based orbitals, while each ligand is less severely destabilised by the effect of only one Ir–C bond. On the basis of the scheme presented here this is predicted to result in an MLCT emissive state, and substantially improved emission intensity with respect to Ir(N[^]N[^]N)(C[^]N[^]C)⁺ complexes. This is, in part, the same reasoning as for the efficiently emissive MLCT state of [Ir(ppy)₂(bpy)]⁺ complexes, with an additional destabilisation of ligand-based states due to the reduced delocalisation.

The final introduction of a third cyclometalating carbon atom raises the energy of metal-based orbitals further still, securing a predominantly MLCT emissive state. It is important to note that although electronic transitions have traditionally been labelled with straightforward terms (LC, MLCT, *etc.*), these are simply the extreme situations. In

reality, emission from many complexes is a mixture of these types of transition, with structural modifications influencing their relative proportions.

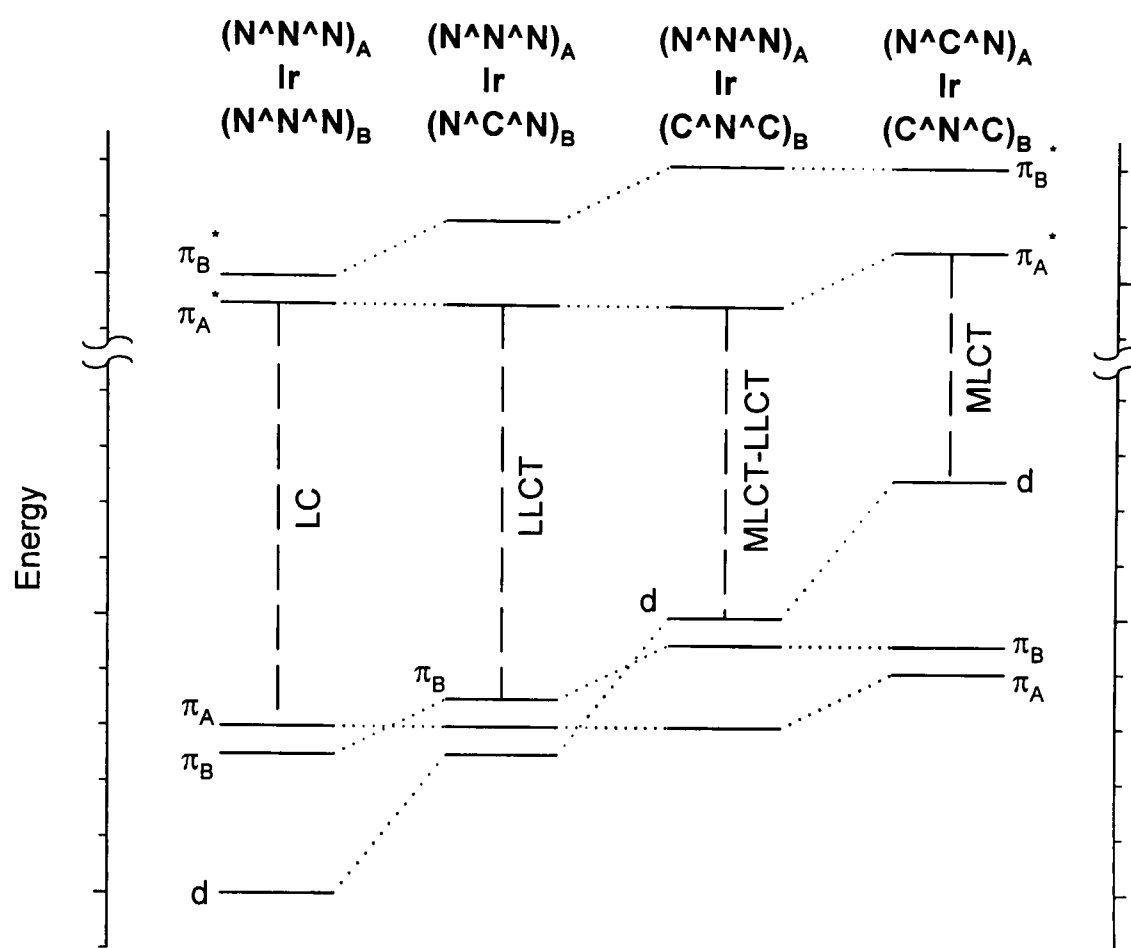


Figure 47. Pictorial representation of the effect of cyclometalation upon the energy levels and nature of emissive states in a generic series of unsymmetrical bis-terdentate iridium(III) complexes.

4.4 Conclusions

In the preceding chapters, the synthesis and photophysical properties of a number of luminescent, bis-terdentate, charge-neutral iridium(III) complexes have been discussed. These are the first examples of iridium(III) complexes incorporating an N^C^N coordinating 1,3-di(pyridin-2-yl)benzene derivative, with the introduction of methyl substituents at C4 and C6 of the phenyl ring blocking competitive metalation at these positions. Charge-neutralisation is obtained by combining this ligand with a C^N^C -, C^N^O - or N^N^N -coordinating analogue. Indeed these are the first examples of bis-terdentate coordination of any metal ion in this way.

Luminescence quantum yields of $Ir(dpydmb)(F_4dppy)$ **110** in degassed acetonitrile solution ($\Phi_{PL} = 0.41$) are comparable to those of the common electrophosphorescent material fac - $Ir(ppy)_3$ **26** ($\Phi_{PL} = 0.4 \pm 0.1$ in degassed dichloromethane solution¹²¹). While luminescence lifetimes are longer ($\tau = 3700$ ns, compared to 1900 ns for fac - $Ir(ppy)_3$), a disadvantage due to an increased probability of triplet-triplet anni-

hilation at high drive currents, they are still substantially shorter than for common platinum(II) based dopants (*e.g.* $>10 \mu\text{s}$ for PtOEP **19**⁹⁰). Investigations into the electroluminescence properties once incorporated into devices are currently underway. The considerable oxygen sensitivity of emission also suggests potential applications as oxygen sensors, promising improved performance with respect to the Ir(ppy)₃ and Ir(ppy)₂(acac) derivatives investigated to date.^{418,419}

Complexes of the form Ir(N[^]C[^]N)(C[^]N[^]C) exhibit an unusual meridional geometry, only recently reported for *mer*-Ir(ppy)₃ **27** and some derivatives.¹²¹ In contrast to these tris-bidentate complexes, the bis-terdentate complexes of the present study are much more emissive and substantially more stable to photodissociation of the Ir–C bond (reflected in the decreased non-radiative decay rate constants, $\sum k_{\text{nr}} = 1.6 \times 10^5 \text{ s}^{-1}$ for Ir(dpydmb)(F₄dppy) **110** compared to $6.4 \times 10^6 \text{ s}^{-1}$ for *mer*-Ir(ppy)₃ **27**¹²¹).

The Ir(N[^]C[^]N)(C[^]N[^]O) complexes Ir(dpydmb)(tppic) **116** and Ir(dpydmb)(hbqc) **117** exhibit comparatively low luminescence quantum yields ($\Phi_{\text{PL}} = 0.053$ and 0.027 respectively), attributed to a competitive photoactivated labilisation of the Ir–O bond. Unlike the Ir(N[^]C[^]N)(C[^]N[^]C) complexes and *mer*-Ir(ppy)₃ **27** derivatives, this is reversible and does not contribute to an overall decomposition process. Although an important limiting factor in solution, dissociation of the Ir–O bond in the excited state may be inhibited in the solid-state, resulting in substantially higher luminescence efficiencies. Current work on fabrication of electroluminescent devices incorporating Ir(dpydmb)(tppic) **116** is hoped to confirm this.

Of particular interest for luminescent applications is Ir(dpydmb)(ppy)Cl **115**, with its particularly high luminescence quantum yield ($\Phi_{\text{PL}} = 0.76$) and reasonably short luminescence lifetime ($\tau = 1600 \text{ ns}$). This is more emissive than some of the best Ir(ppy)₃ derivatives, and yet is not accompanied by any increase in luminescence lifetime. These properties suggest that Ir(dpydmb)(ppy)Cl **115** is an ideal candidate for high efficiency green electroluminescence, with fabrication of test devices currently underway. It should be noted that one of the most efficient OLEDs to date is based upon Ir(ppy)₂(acac) **80** ($\eta_{\text{int}} = 87 \pm 7\%$),¹⁶⁸ whose photoluminescence quantum yield is an unremarkable 0.34 in 2-MeTHF.¹¹⁵

Although designed primarily for organic electroluminescent display applications, bis-terdentate binding geometries make such compounds ideal for the formation

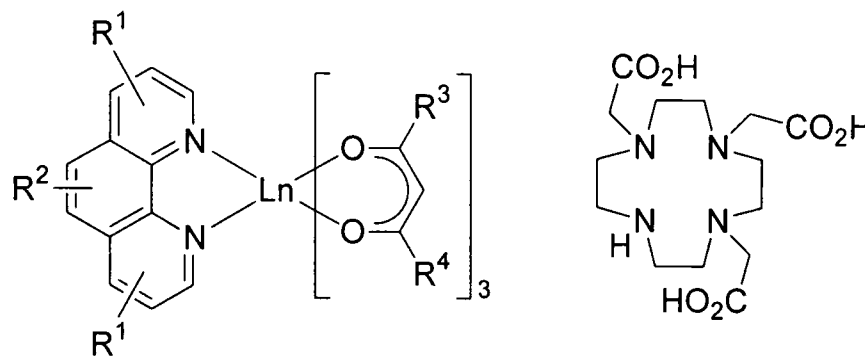
of linear supramolecular architectures,⁴²⁰ an advantage already noted for bis-terpyridine complexes.⁴²¹ The terdentate coordination overcomes problems associated with isomerisation inherent in the structures of the tris-bidentate Ir(ppy)₃ analogues. *fac*-Ir(ppy)₃ **26** is chiral, and hence when two such units are joined together, a mixture of diastereoisomers is formed. In contrast, bis-terdentate complexes are generally achiral. Also, the fixed structural arrangement of two terdentate ligands overcomes issues associated with geometrical isomerism in Ir(ppy)₃ derivatives. In addition, straightforward substitution at the 4'-position allows linear arrays to be readily accessed.

CHAPTER 5

EUROPIUM(III) COMPLEXES

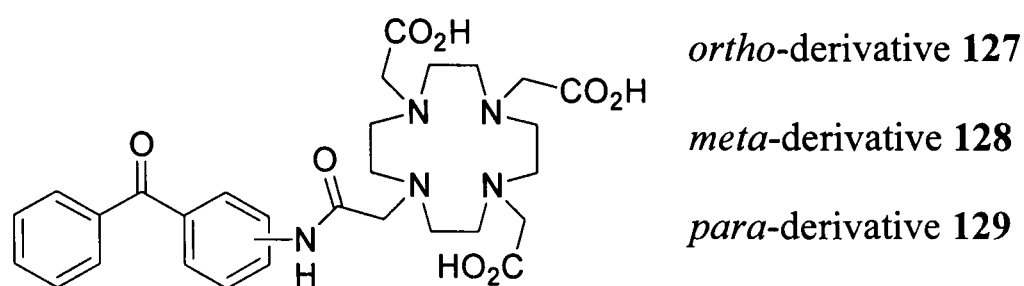
5 Europium(III) complexes

Research on electroluminescent devices incorporating lanthanide dopants has thus far been limited to a very restricted subset of complexes. For visible emitters in particular, work has focused predominantly on complexes of the form $\text{Ln}(\text{phen})(\text{acac})_3$ **54** (see Section 1.3.4). In this chapter, the syntheses of a series of europium-coordinated macrocyclic complexes are described as possible alternative materials for electrophosphorescent dopants.

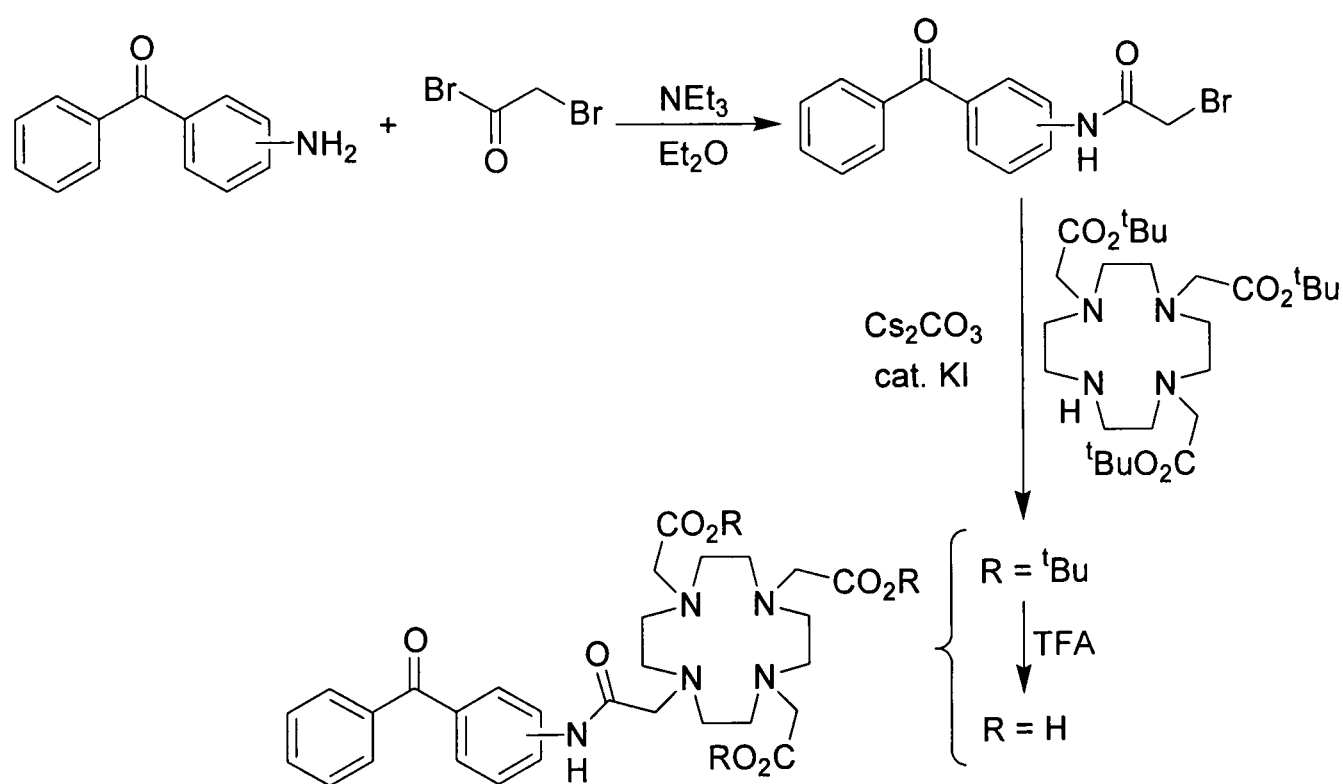
Generic $\text{Ln}(\text{phen})(\text{acac})_3$ structure **54**DO3A **46**

To increase stability and to ensure charge-neutrality, europium(III) complexes based on the heptadentate ligand DO3A **46** were investigated (see Section 1.3.3.1). When a lanthanide(III) ion is introduced, the charge is balanced by binding of the three carboxylic acid groups. Complexes of this ligand are known to exhibit high thermodynamic and kinetic stabilities.²²¹ It is suggested that the improved stability of these complexes with respect to **54** may lead to performance advantages in electroluminescent devices.

Since direct excitation of lanthanide(III) ions is highly inefficient (see Section 1.3.2), a sensitising chromophore group¹⁹⁷ is covalently attached *via* derivatisation of the secondary amine. A substituted benzophenone sensitiser was chosen because of its near-unity quantum yield for formation of the $n-\pi^*$ triplet state.⁴²² Since it is from this state that energy transfer to the lanthanide(III) ion occurs, this should maximise the efficiency of sensitised emission. A highly luminescent ($\Phi_{\text{PL}} = 0.20$) complex has been reported upon mixing 4,4'-bis(*N,N*-dimethylamino)benzophenone (Michler's Ketone) with europium(III) tris(6,6,7,7,8,8,8-heptafluoro-2,2-dimethyloctane-3,5-dione) ($\text{Eu}(\text{fod})_3$) in non-coordinating solvents.⁴²³ Emission is not however observed in coordinating solvents, with the complex readily dissociating in aqueous solution. By attachment of an aminobenzophenone moiety to DO3A, a much increased kinetic and

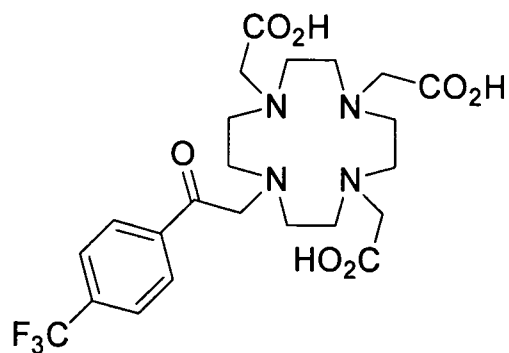


The ligands **127** and **128** were prepared according to Scheme 29. Reaction of the appropriate aminobenzophenone with bromoacetyl bromide and triethylamine gave the respective bromoacetamide derivatives. These were then used to *N*-alkylate the secondary amine of **126**, to give the tri-*tert*-butyl ester-protected derivatives of **127** and **128**. Purification at this stage by column chromatography led to decomposition. Therefore the compounds were used without further purification, with deprotection in trifluoroacetic acid resulting in the desired ligands, and purification postponed until after the complexation step (see Section 5.2).



Scheme 29. Synthesis of aminobenzophenone-derivatised DO3A ligands.

The preparation of the trifluoromethylphenyl-derivatised DO3A ligand **130** was also attempted. Straightforward synthesis of the required alkylating agent was achieved by reaction of 4-(trifluoromethyl)acetophenone with one equivalent of bromine in acetic acid. Although some evidence of dibromination was observed, the desired product was purified by recrystallisation from hexane.

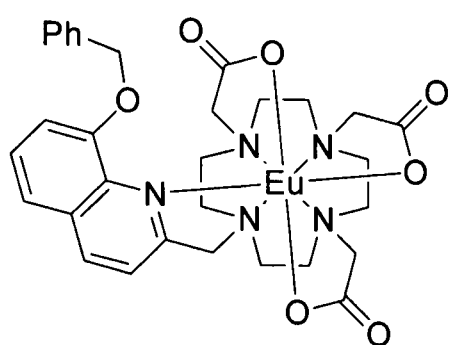


130

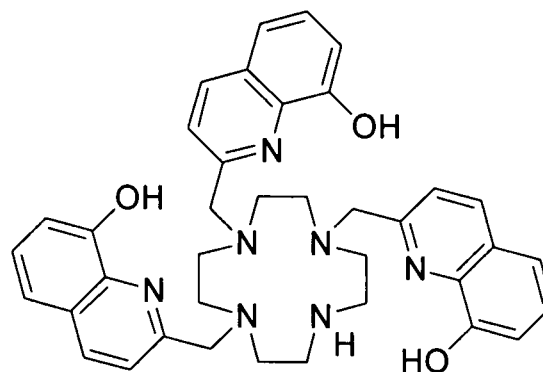
With this alkylating agent, reaction with **126** in the presence of caesium carbonate and a potassium iodide catalyst failed to give the desired product. Further investigation suggested that efficient hydrolysis of the alkylating agent was occurring in competition with alkylation. Triethylamine was considered as an alternative base, since room temperature reaction in the absence of **126** showed evidence of the starting material even after two days. However, reaction of alkylating agent with **126** in the presence of triethylamine failed to yield the desired product. Instead, the bromide was displaced by triethylamine, with no evidence for alkylation of the macrocycle.

By analogy with the europium(III) complex **50**,²²⁶ the tris-8-hydroxyquinoline substituted ligand **131** was synthesised. 8-Benzyloxyquinoline-2-carboxaldehyde was prepared by the route of Williams and Maffeo,²²⁶ *i.e.* oxidation of 2-methylquinolin-8-ol with selenium dioxide following benzyl-protection of the phenol. Reductive amination was then used in the attachment of the quinoline derivative to cyclen. Careful choice of reducing agent (sodium triacetoxyborohydride, NaBH(OAc)₃) allows specific reduction of the imine formed upon reversible condensation of the aldehyde with secondary amines, with little competitive reduction of the aldehyde starting material. Unfortunately, while a single attachment proceeds in high (61%) yield,²²⁶ preliminary attempts at formation of the tri-alkylated product were low yielding (~6%) and purification of the product was problematic. Furthermore, following removal of the benzyl group by reaction with boron tribromide,^{*} **131** was difficult to handle due to a high affinity for unwanted metal ions (for example it would form a precipitate upon addition to standard grade NMR solvents). These complications resulted in the failure of all attempts at formation of the europium(III) complex.

* Although attempted, the use of hydrogen and Pd/C to deprotect the benzyl groups was unsuccessful.



50

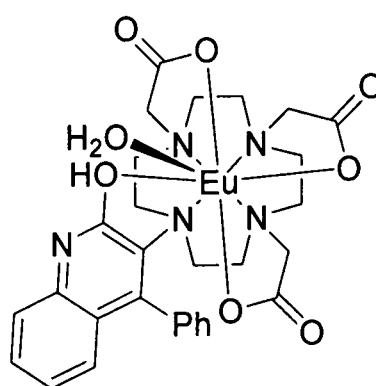


131

5.2 Synthesis of europium(III) complexes

The preparation of europium(III) complexes of DO3A derivatives can generally be performed by boiling an aqueous solution of the ligand with $\text{Eu}(\text{NO}_3)_3 \cdot 5\text{H}_2\text{O}$ at approximately pH 6, although more basic conditions are generally tolerated. One exception is the *ortho*-aminobenzophenone derivative **127**, where basic conditions must be avoided in order to obtain $\text{Eu} \cdot \mathbf{127}$. Initial attempts in basic solution resulted in mass spectrometric and NMR data inconsistent with the desired complex.

Consideration of the observed electrospray ionisation mass spectrum ($m/z = 716$ ($[\text{M}+\text{H}]^+$), 738 ($[\text{M}+\text{Na}]^+$)) suggested a rearrangement had taken place, leading to complex $\text{Eu} \cdot \mathbf{132}$. This was supported by analysis of the ^1H -NMR spectrum, which showed only six protons assignable to NCH_2CO groups. To investigate the resulting compound more fully, identical synthetic conditions were used for a complex of the diamagnetic yttrium(III) ion (for yttrium $I = \frac{1}{2}$). Yttrium(III) is a comparable size to europium(III), and is known to bind to DOTA **45** in a similar manner.⁴²⁵ The much simplified NMR spectrum was consistent with the proposed structure.

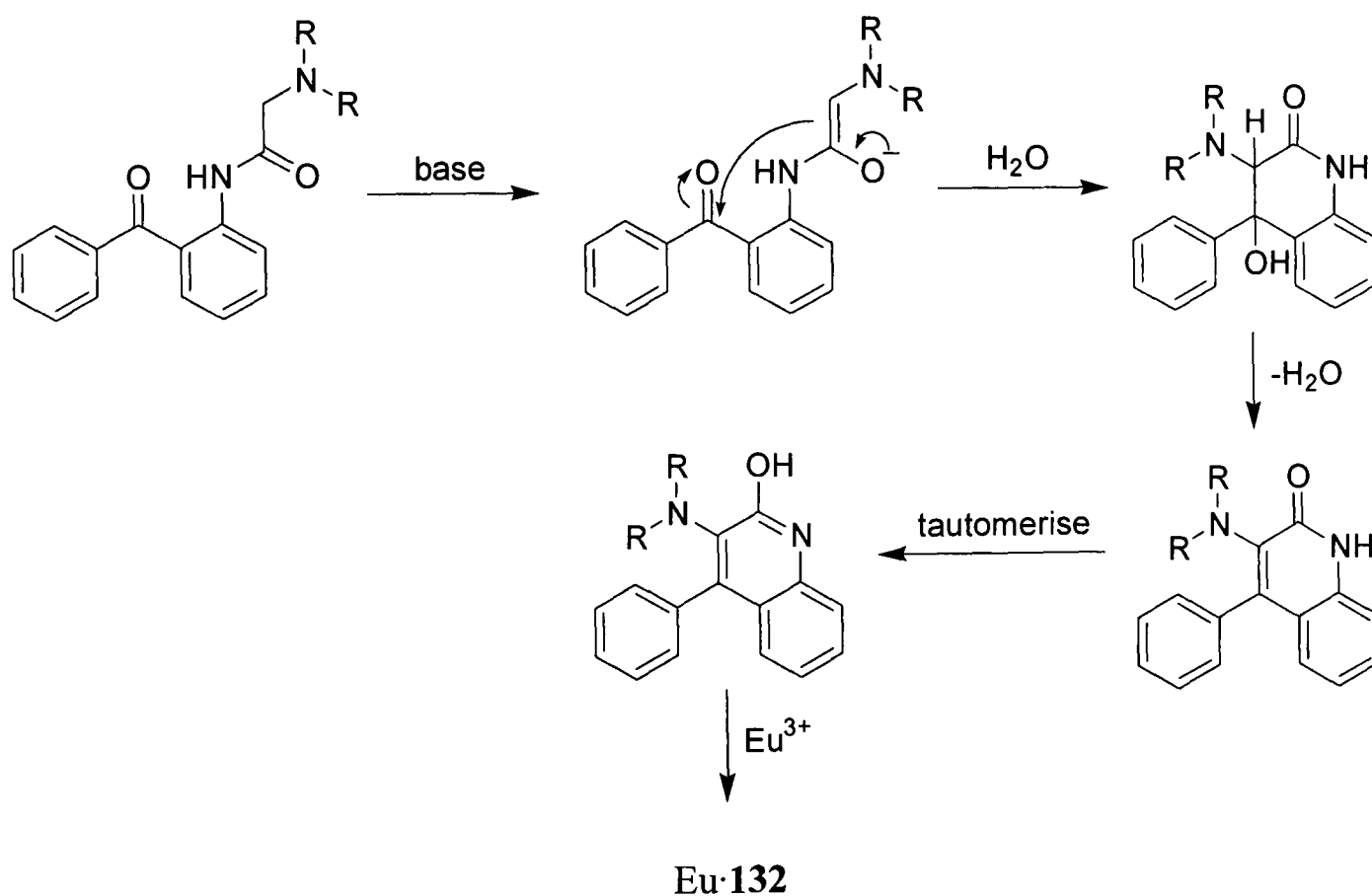


Eu·132

A suggested mechanism for rearrangement is shown in Scheme 30. This only occurs for the *ortho*-aminobenzophenone derivative, since only in this case does attack

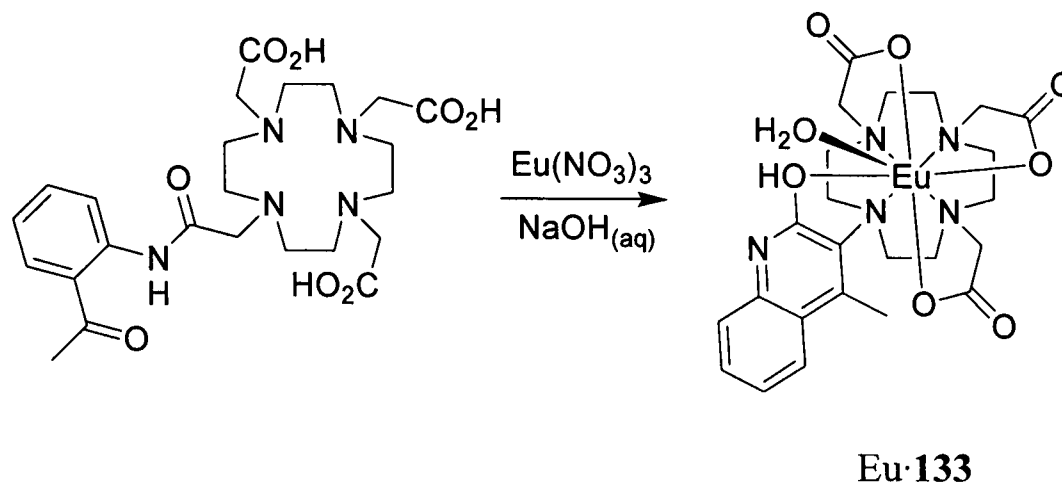
of the enolate ion result in formation of a stable six-membered ring. A search of the literature reveals that such a rearrangement to form 4-hydroxyquinoline derivatives was reported as early as 1899.⁴²⁶

The rearrangement was also found to proceed in the absence of any lanthanide(III) ions. Thus, heating ligand **127** at 100°C in aqueous base for 24 hours results in a yellow solid whose electrospray ionisation mass spectrum ($m/z = 566$ ($[M+H]^+$), 588 ($[M+Na]^+$)) is consistent with the rearranged ligand. No such reaction was observed when an ethanol solution of the tri-*tert*-butyl ester protected **127** derivative was heated to reflux at 78°C for 24 hours in the presence of triethylamine.



Scheme 30. Suggested mechanism for the formation of a rearranged *ortho*-aminobenzophenone derivatised DO3A complex in a basic solution of a Eu^{3+} salt.

Following removal of the OH group, this rearrangement may be useful as a straightforward route to quinolin-3-yl *N*-arylated macrocycles. To investigate its generality, the methyl derivative Eu·**133** was prepared by an analogous procedure (see Scheme 31).



Scheme 31. Rearrangement and complexation of a 2-aminoacetophenone derivatised DO3A ligand.

Although suitable crystals for X-ray diffraction measurements were not obtained and a full dipolar analysis of the NMR data is beyond the scope of this work, a consideration of likely molecular geometries is of interest. In general, complexes of DO3A derivatives are alkylated at the remaining nitrogen *via* a CH₂ spacer group. This allows a twisting of the pendent groups with respect to the N₄ plane, resulting in the typical square-antiprismatic (SAP) and twisted square-antiprismatic (TSAP) geometries (see Figure 48).

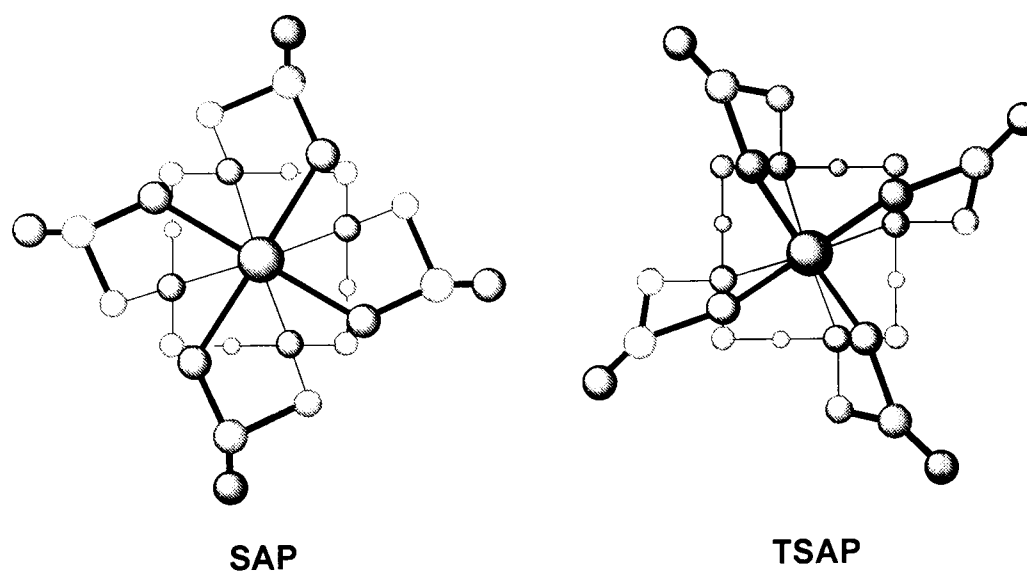


Figure 48. Pictorial representation of the twisting of acetate groups in the SAP and TSAP geometries of lanthanide(III) DOTA complexes.

In Eu·132 however, the direct connection of an aromatic ring to the macrocycle enforces a planar geometry for the organic part of the five-membered Eu–N–C–C–O ring. This will restrict the twisting of the N₄ and O₄ planes, and will potentially induce a change in puckering of the cyclen ring. Evidence for such a distortion in geometry is provided by the ¹H-¹H COSY NMR spectrum (where cross-peaks between protons separated by a many bonds may be observed when they are brought in close spatial

proximity). A number of additional cross-peaks are observed, of particular note being those between the axial protons at 41.81 ppm and 30.78 ppm, and between the equatorial protons at 0.62 ppm and -9.14 ppm. This is consistent with a change in puckering of the ring from a C_4 symmetric form (Figure 49, geometry I), towards a C_2 symmetric form (Figure 49, geometry II). In addition, NMR spectroscopy of the crude product from rearrangement of ligand **127** exhibits remarkably resolved resonances associated with CH_2 protons, suggesting that the conformation is restricted even in the absence of a metal ion.

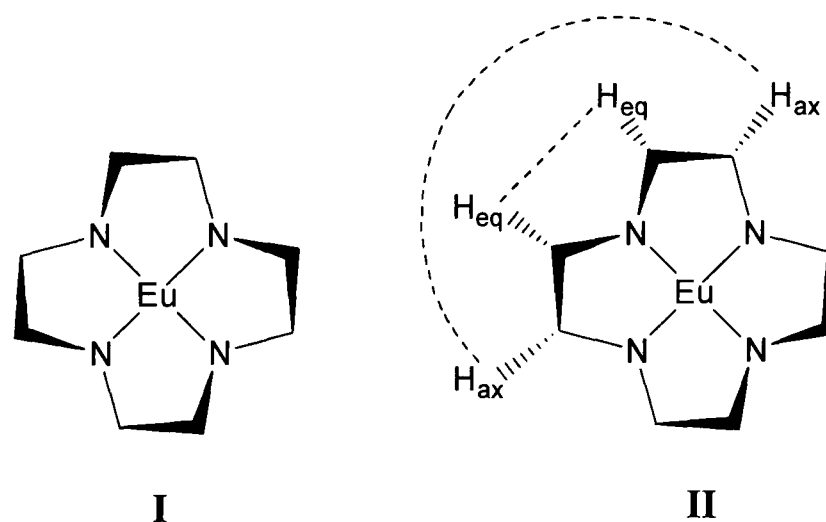
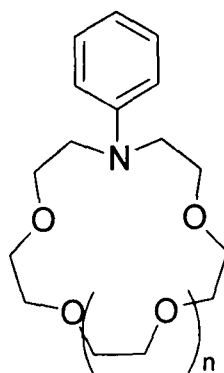


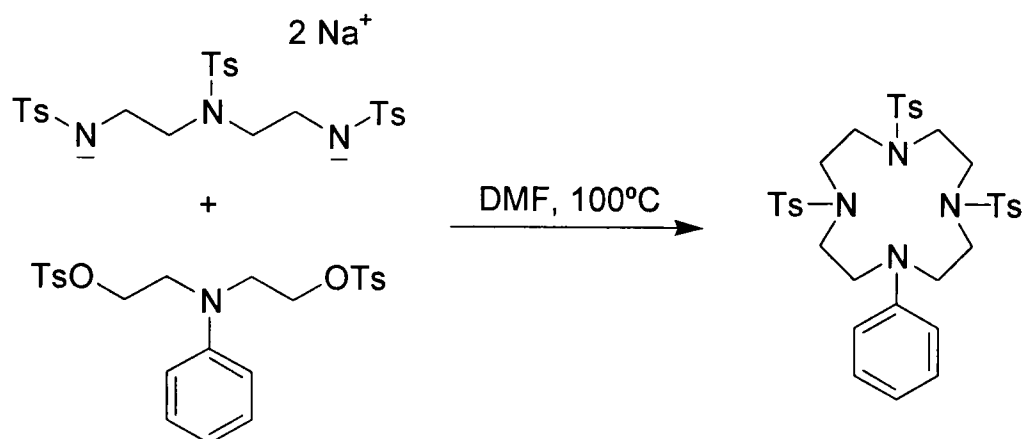
Figure 49. Effect of ring puckering on the geometries of europium(III)-coordinated cyclen derivatives. Dashed lines represent additional 1H - 1H COSY cross-peaks.

Complexes of aromatic chromophores directly attached to cyclen rings have been little studied, with most research focusing on significantly easier to attach compounds with alkyl spacer units. It should be noted that *N*-arylated azacrown ethers are more common. For example, the synthesis of compounds of the form **134** have been reported with $n = 1$,^{427,428} $n = 2$ ^{427,428} and $n = 3$,⁴²⁸ as well as studies of metal complexes of the $n = 1$ derivative.^{429,430}



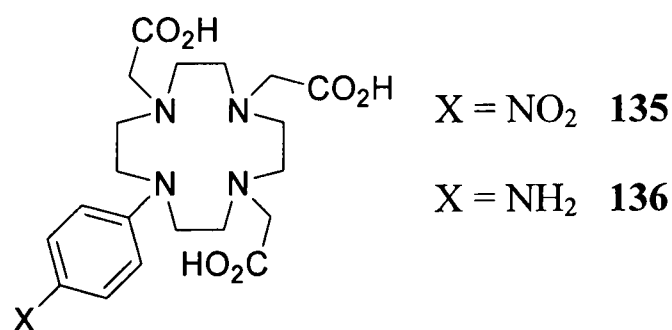
134

Classical *N*-arylation reactions of cyclen are only achievable with electron poor arenes such as fluorinated nitrobenzenes, requiring high temperatures and extended reaction times.^{431,432} Highly activated arylating agents such as 2,4,6-trichloro-1,3,5-triazine have been shown to react under much milder conditions.⁴³³ Attachment of haloarenes that are not particularly electron poor has recently been reported by palladium-catalysed *N*-arylation reactions.⁴³⁴⁻⁴³⁶ Although successful at forming a number of *N*-arylated cyclen derivatives, yields are generally poor, with only a small improvement for pyridine derivatives.⁴³⁴ An alternative strategy involves the formation of the macrocyclic ring from an acyclic aryl-substituted precursor (see Scheme 32).⁴³⁷



Scheme 32. Synthesis of an *N*-arylated cyclen derivative from an *N*-aryl precursor.

The only reported lanthanide complexes of *N*-arylated cyclen derivatives are the europium(III), gadolinium(III) and ytterbium(III) complexes of **135** and **136**.⁴³² Although the magnetic properties of the gadolinium(III) complex were discussed, no luminescence data was reported. Hence, Eu·**132** and Eu·**133** are believed to be the first reported lanthanide(III) complexes based on cyclen incorporating metal-bound *N*-aryl substituents.



5.3 Photophysical Properties

5.3.1 Absorption spectra

Ground-state absorption spectra of the europium(III) complexes Eu·127 and Eu·128 are shown in Figure 50 (data summarised in Table 36). Absorption bands are assigned to $\pi\text{-}\pi^*$ transitions of the benzophenone moiety, as is the single broad feature observed for Eu·129 ($\lambda_{\text{max}} = 295 \text{ nm}$).⁴²⁴ Although only one band may be resolved for Eu·128 and Eu·129, ZINDO⁴³⁸ calculations* suggest that two bands should exist for all three isomers, relating to excitation of an electron from a π -orbital localised on the unsubstituted phenyl ring, and from a π -orbital localised on both phenyl rings. Where a single feature is observed, this is a combination of two unresolved bands. The notable red-shift for the *para*-substituted isomer (Eu·129) is due to an increased delocalisation across the amide group.

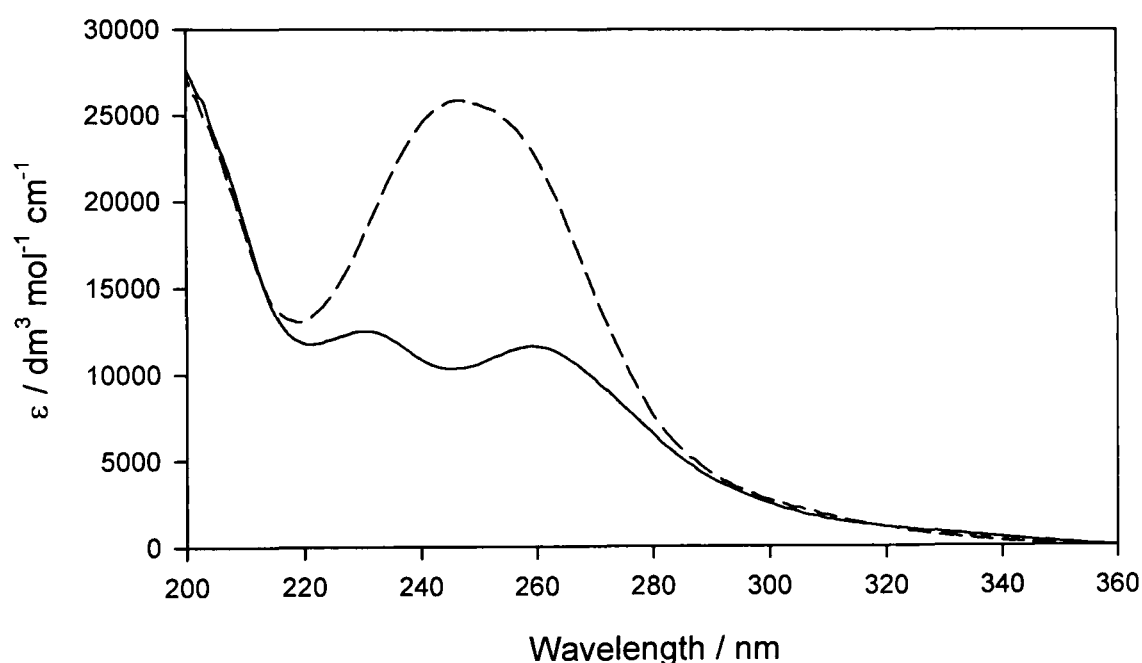


Figure 50. Ground-state absorbance spectra of Eu·127 (solid line) and Eu·128 (dashed line) in aqueous solution at 295 K.

In contrast, the rearranged complexes Eu·132 and Eu·133 absorb out to much longer wavelength (see Figure 51, data summarised in Table 36). This is consistent with the proposed quinoline rearrangement product, and matches absorbance data for the model chromophore, 3-aminoquinolin-2-ol.⁴⁴⁰ The phenyl-substituted derivative Eu·132 is slightly red-shifted with respect to the methyl-derivative Eu·133 due to the increased extent of delocalisation possible in the former.

* ZINDO electronic spectra calculations performed on 2-amino-*N*-(benzoylphenyl)acetamide structures at the MM3 optimised geometries using the CaChe 6.1.1⁴³⁹ software package.

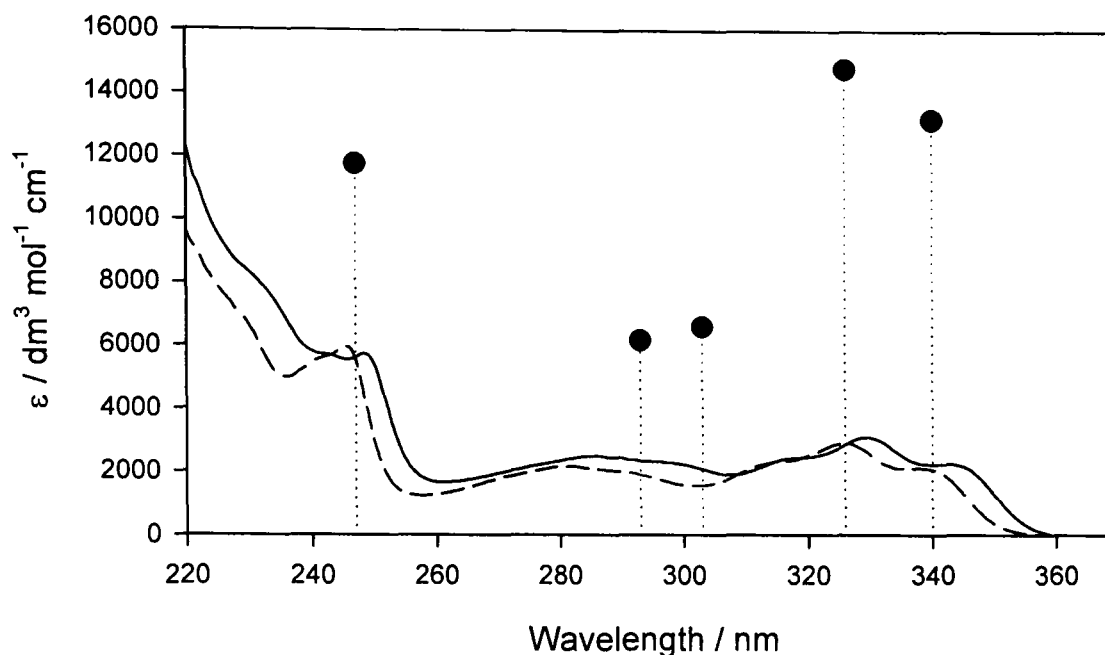


Figure 51. Ground-state absorbance spectra of Eu·132 (solid line) and Eu·133 (dashed line) in aqueous solution at 295 K. Included for comparison is the published absorbance data for 3-aminoquinolin-2-ol in ethanol (●).⁴⁴⁰

Complex	λ / nm ($\epsilon / \text{dm}^3 \text{mol}^{-1} \text{cm}^{-1}$)
Eu·127	231 (12 500), 259 (11 500).
Eu·128	245 (25 800).
Eu·132	205 (22 600), 230 (8 600), 242 (5 900), 248 (5 900), 286 (2 500), 319 (2 500), 329 (3 100), 342 (2 300).
Eu·133	206 (24 500), 246 (6 000), 290 (2 000), 281 (2 200), 315 (2 300), 326 (2 900), 338 (2 100).

Table 36. Absorbance data for europium(III) complexes.

5.3.2 Luminescence properties of Eu·127 and Eu·128

Upon excitation into the $\pi\text{-}\pi^*$ bands of Eu·127, Eu·128 and Eu·129,⁴²⁴ emission characteristic of transitions from the $^5\text{D}_0$ excited state of europium(III) is observed (see Figure 52). The profiles of the spectra (*i.e.* the relative intensity of bands and the fine structure of each) are almost identical, suggesting that the environment at the metal is little affected by substitution position of the chromophore. Luminescence excitation spectra (monitored at 700 nm) match the absorption spectra (shown in Figure 53 for Eu·128), confirming sensitisation of europium(III) emission by the organic chromophore. Notable features include the presence of an obvious $\Delta J = 0$ band, consistent with the low symmetry of the complex. Since both excited ($^5\text{D}_0$) and ground ($^7\text{F}_0$) states are non-degenerate, a single $\Delta J = 0$ band is expected for a single emitting species. Although

multiple $\Delta J = 0$ bands are indicative of a mixture of emitting species, shifts in energy tend to be small and require high-resolution spectra to be distinguished.⁴⁴¹

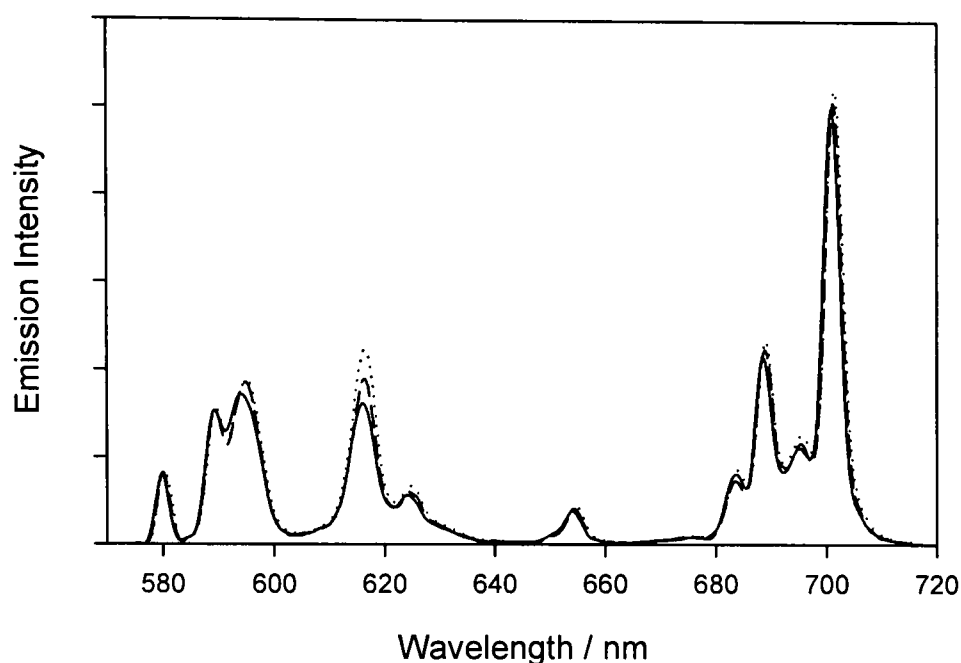


Figure 52. Emission spectra of Eu·127 (solid line, $\lambda_{\text{ex}} = 259$ nm), Eu·128 (dashed line, $\lambda_{\text{ex}} = 249$ nm) and Eu·129⁴²⁴ (dotted line, $\lambda_{\text{ex}} = 280$ nm) in aqueous solution at 295 K. Excitation and emission bandpasses were 2.5 nm.

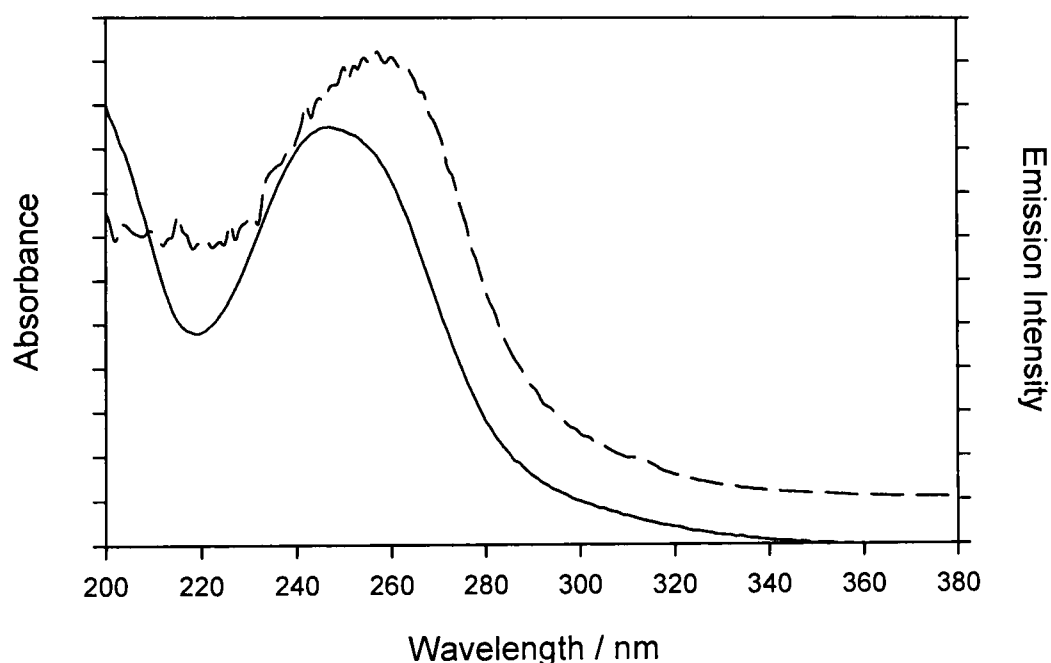


Figure 53. Ground-state absorbance spectrum (solid line) and luminescence excitation spectrum (dashed line, $\lambda_{\text{em}} = 700$ nm) for Eu·128.

Lifetimes of emission and photoluminescence quantum yields in H_2O and D_2O are summarised in Table 37. The quantum yields are unchanged upon degassing, but are increased significantly in D_2O with respect to H_2O . The solution hydration numbers q , were determined by the empirical relationship of Parker *et al.*¹⁹⁹ (equation 11, $x = 1$) as 1.08 and 1.09 for Eu·127 and Eu·128 respectively. This compares well to the value of 1.05 determined for Eu·129,⁴²⁴ suggesting that only a single inner-sphere water

molecule is present in each case. This also provides evidence for binding of the amide carbonyl group to the metal, preventing the entry of a second water molecule.

$$q^{Eu} = 1.2 \left[\left(\tau_{H_2O}^{-1} - \tau_{D_2O}^{-1} \right) - (0.25 + 0.075x) \right] \quad (11)$$

Complex	H ₂ O		D ₂ O		q^e
	τ / ms^a	Φ_{lum}^b	τ / ms^a	Φ_{lum}^b	
Eu·127 ^c	0.59	0.004	2.14	0.027	1.08
Eu·128 ^d	0.60	0.015	2.22	0.16	1.09
Eu·129 ⁴²⁴	0.61	0.095	2.26	0.38	1.05

^aLifetimes of metal-centred emission monitored at 616 nm, 295 K; uncertainty $\pm 5\%$.

^bQuantum yields of europium emission, 295 K, measured using an aqueous solution of [Ru(bpy)₃]²⁺ as a standard,⁴⁰⁰ uncertainty $\pm 20\%$. ^c $\lambda_{\text{ex}} = 259 \text{ nm}$. ^d $\lambda_{\text{ex}} = 249 \text{ nm}$. ^e q is the hydration state as determined by the equation of Parker *et al.*¹⁹⁹

Table 37. Photophysical parameters of the europium(III) complexes of 127 and 128. Included for comparison is Eu·129.⁴²⁴

Comparison of the relative luminescence quantum yields for the three complexes shows a systematic increase from *ortho*-, through *meta*-, to *para*-substitution. Since emission lifetimes are similar, this suggests an increase in the efficiency of energy transfer from the chromophore to the metal (η_{et}). A more detailed analysis may be performed by consideration of the parameters in equation 8. The benzophenone chromophore is known to have a triplet quantum yield of near unity,⁴²² hence $\Phi_{\text{D}} \sim 1$. The pure radiative rate constant (k^0) may not be directly measured. It has been proposed, however, that this value is related to the ratio of the integrated emission intensity of the $^5\text{D}_0 \rightarrow ^7\text{F}_1$ transition (purely magnetic dipole in character) to the total integrated emission intensity (equation 15, where $A(0,1) \sim 32.4 \text{ s}^{-1}$).²²² The results of the analysis are shown in Table 38. It is clear that while the values of k^0 and $\sum k_{\text{nr}}$ are of a similar order of magnitude for all three complexes, the emission intensity is limited by the efficiency of energy transfer from the sensitising chromophore to the europium(III) ion (η_{et}). Whereas the *para*-substituted isomer Eu·129 has an energy transfer efficiency of approximately unity, this decreases significantly for *meta* (Eu·128) and *ortho* (Eu·127) derivatives. This drop is attributed to an increase in the distance between donor and acceptor. While Eu·129 is held rigidly in a position close to the metal, the other isomers may rotate the benzophenone moiety about the N–Ar bond into a sterically favoured position more distant from the metal centre.

$$\Phi_{\text{em}} = \Phi_{\text{D}} \eta_{\text{et}} k^0 \tau_{\text{obs}} \quad (8)$$

$$k^0 = \frac{A(0,1)}{[I(0,1)/I_{\text{tot}}]} \quad (15)$$

	Eu·127	Eu·128	Eu·129
$[I(0,1)/I_{\text{tot}}]^a$	0.22	0.22	0.21
$\tau_{\text{obs}} / \text{ms}$	0.59	0.60	0.61 ⁴²⁴
$k^0{}^b / \text{s}^{-1}$	144	147	155
$\sum k_{\text{nr}}{}^b / \text{s}^{-1}$	1550	1520	1480
Φ_{em}	0.004	0.015	0.095 ⁴²⁴
$\Phi_{\text{D}} \eta_{\text{et}}{}^c$	0.04	0.17	1.01

^aEstimated uncertainty $\pm 5\%$. ^bEstimated uncertainty $\pm 10\%$. ^cEstimated uncertainty $\pm 20\%$.

Table 38. Calculated values of k^0 , $\sum k_{\text{nr}}$ and η_{et} for solutions of the europium(III) complexes of 127, 128 and 129 in H₂O using experimentally determined $[I(0,1)/I_{\text{tot}}]$, τ_{obs} and Φ_{em} values.

5.3.3 Luminescence properties of Eu·132 and Eu·133

Upon excitation into the ligand absorption bands of Eu·132 and Eu·133, emission characteristic of transitions from the ⁵D₀ excited state of europium(III) is observed (see Figure 54). Luminescence excitation spectra (monitored at 700 nm) match the absorption spectra (shown in Figure 55 for Eu·132), confirming sensitisation of europium(III) emission by the organic chromophore. The profiles of the emission spectra are identical, suggesting that the environment at the metal is little affected by substitution at the 4-position of the quinoline ring. With respect to Eu·127, Eu·128 and Eu·129, there is relatively little variation in the form of the emission spectra (compared for example to Eu(TTFA)₃),⁴⁴² evidence that there is a similar set of donor atoms with a similar symmetry. The most notable differences are an increase in intensity of the hypersensitive $\Delta J = 2$ band, and a larger separation of the two components of the $\Delta J = 1$ emission band. This is indicative of an increase in polarisability of the axial donor,¹⁹⁵ as may perhaps be expected for a change from an amide carbonyl group to a phenol.

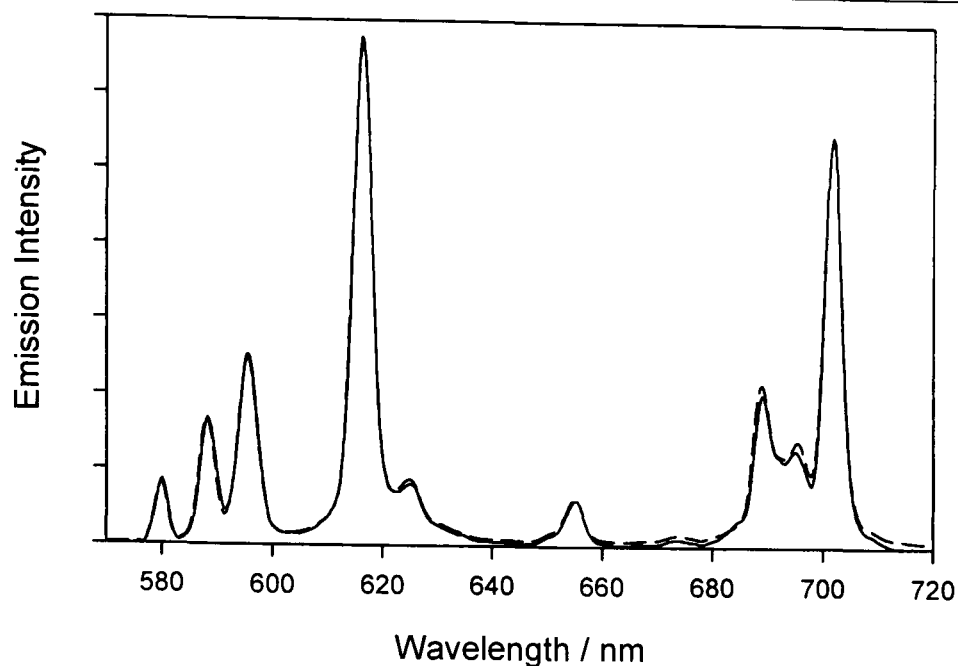


Figure 54. Emission spectra of Eu·132 (solid line, $\lambda_{\text{ex}} = 343$ nm) and Eu·133 (dashed line, $\lambda_{\text{ex}} = 340$ nm) in aqueous solution at 295 K. Excitation and emission bandpasses were 2.5 nm.

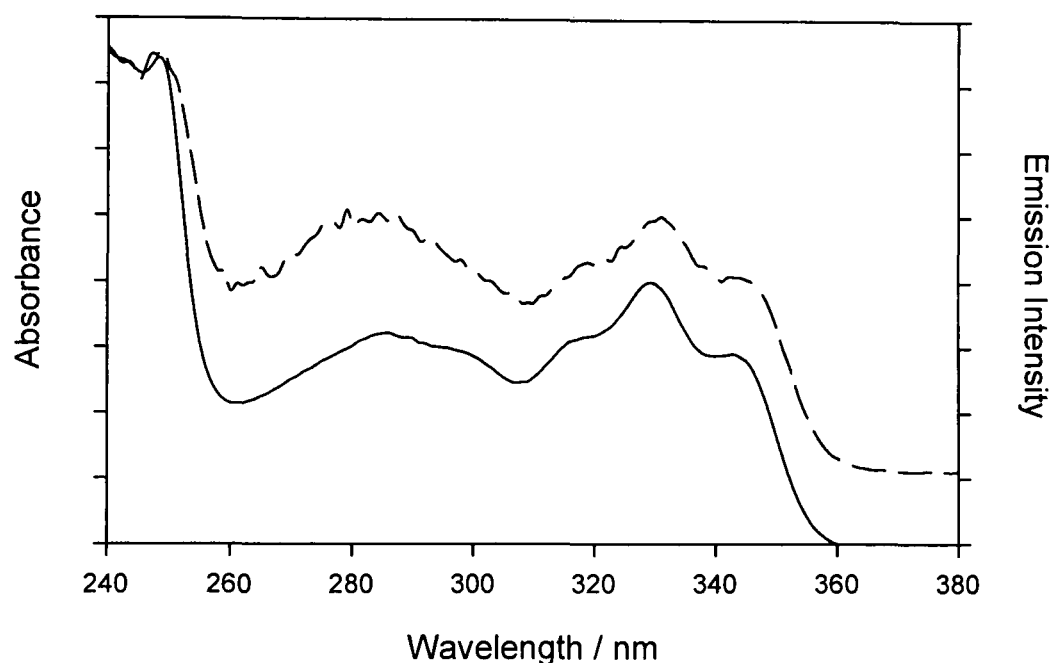


Figure 55. Ground-state absorbance spectrum (solid line) and luminescence excitation spectrum (dashed line, $\lambda_{\text{em}} = 700$ nm) for Eu·132.

Lifetimes for emission in H₂O and D₂O are summarised in Table 39. The solution hydration numbers q , were determined by the empirical relationship of Parker *et al.*¹⁹⁹ (equation 11, $x = 0$) as 1.06 and 1.04 for Eu·132 and Eu·133 respectively. These values suggest that there is only a single inner-sphere water molecule in each case, most likely due to binding of the quinoline hydroxyl-substituent in the eighth coordination site.

Complex	H ₂ O		D ₂ O		q^e
	τ / ms^a	Φ_{lum}^b	τ / ms^a	Φ_{lum}^b	
Eu·132	0.62 ^c	0.003	2.02 ^c	0.011	1.06
Eu·133	0.62 ^d	0.052	2.05 ^d	0.18	1.04

^aLifetimes of metal-centred emission monitored at 616 nm, 295 K; uncertainty $\pm 5\%$.
^bQuantum yields of europium emission, $\lambda_{\text{ex}} = 280$ nm, 295 K, measured using an aqueous solution of $[\text{Ru}(\text{bpy})_3]^{2+}$ as a standard;⁴⁰⁰ uncertainty $\pm 20\%$. ^c $\lambda_{\text{ex}} = 330$ nm.
^d $\lambda_{\text{ex}} = 338$ nm. ^e q is the hydration state as determined by the equation of Parker *et al.*¹⁹⁹

Table 39. Photophysical parameters of the europium(III) complexes of 132 and 133.

The luminescence quantum yield of the phenyl derivative Eu·132 is significantly smaller than that for the methyl derivative Eu·133 despite similar luminescence lifetimes. Although a determination of η_{et} is not possible due to the unknown efficiency of formation of the sensitising chromophore's triplet state, the combined quantity $\Phi_{\text{D}}\eta_{\text{et}}$ may be estimated from equations 8 and 15 (see Table 40). This value is an order of magnitude smaller for Eu·132 than for Eu·133, with a number of possible explanations. Firstly, phenyl substitution on the quinoline chromophore could have a detrimental effect upon the formation of the chromophore triplet state. Secondly, the value of η_{et} may be lowered by an increased distance between the sensitising chromophore and metal centre. Finally, while the quinoline triplet state is high enough in energy ($\sim 22\,000\text{ cm}^{-1}$ ⁴⁴³) to transfer efficiently to the europium(III) ion, there is no guarantee

	Eu·132	Eu·133
$[I(0,1)/I_{\text{tot}}]^a$	0.16	0.17
$\tau_{\text{obs}} / \text{ms}$	0.62	0.62
$k^0{}^b / \text{s}^{-1}$	197	196
$\sum k_{\text{nr}}{}^b / \text{s}^{-1}$	1420	1420
Φ_{em}	0.003	0.052
$\Phi_{\text{D}}\eta_{\text{et}}{}^c$	0.03	0.43

^aEstimated uncertainty $\pm 5\%$. ^bEstimated uncertainty $\pm 10\%$. ^cEstimated uncertainty $\pm 20\%$.

Table 40. Calculated values of k^0 , $\sum k_{\text{nr}}$ and $\Phi_{\text{D}}\eta_{\text{et}}$ for solutions of the europium(III) complexes of 132 and 133 in H₂O using experimentally determined $[I(0,1)/I_{\text{tot}}]$, τ_{obs} and Φ_{em} values.

that phenyl substitution does not lead to an excited state which is too low in energy for this to occur. It is important to note that degassing the samples had no effect upon either luminescence lifetimes or intensities, discounting significant back energy transfer.

5.4 Conclusion

In the preceding sections, a series of luminescent europium(III) containing macrocyclic complexes was discussed. Charge-neutrality as well as high kinetic and thermodynamic stability was ensured by the use of a tricarboxylic acid functionalised cyclen derivative. It is hoped that these complexes will exhibit improved stabilities with respect to compounds of the form **54** when incorporated into electrophosphorescent devices. Investigations of the performance when incorporated into such devices are currently under way. Unfortunately, comparisons with commonly-used electrophosphorescent europium(III) complexes are hindered by the lack of solution photoluminescence data in the literature for acac-based structures.

The preparation and characterisation of europium(III) complexes with DO3A-appended benzophenone groups have been discussed. This chromophore has been shown to result in efficient sensitisation of europium(III) emission in the *para*-substituted isomer Eu-**129**.⁴²⁴ The effect of substitution position was investigated, with a systematic decrease in energy transfer efficiency upon *meta*-, and then *ortho*-substitution. This is attributed to an increased distance between the benzophenone moiety and the metal centre.

During these studies, a rearrangement of the *ortho*-substituted ligand **127** was observed upon heating in basic solution. The resulting ligand incorporates a quinoline substituent directly attached to the secondary amine of DO3A. Although the europium(III) complex is poorly emissive, it may be excited at longer wavelength than with a benzophenone chromophore (up to almost 360 nm). This is of interest in solution-based applications, in particular for biological samples, which tend to absorb strongly at short wavelengths.

CHAPTER 6

EXPERIMENTAL

6 Experimental

All solvents were Analar® quality with the exception of acetonitrile, which was HPLC grade, and were used as supplied unless otherwise stated. Diethyl ether and THF were distilled under a nitrogen atmosphere from sodium wire. Where stated as dry, DMSO and toluene were distilled from calcium hydride under reduced pressure, and stored over 4 Å molecular sieves. Water was purified using the “Purite_{STILL} plus” system and had a conductivity of 0.04 $\mu\text{S cm}^{-1}$ or lower. Reagents were used as supplied.

Thin layer chromatography was carried out using neutral aluminium oxide plates (Merck Art 5550) or silica plates (Merck Art 5554), both types being fluorescent on irradiation at 254 nm. Preparative column chromatography was carried out using neutral alumina (Merck Aluminium Oxide 90, Brockman activity 2-3), or silica (Merck Silica Gel 60, 230-400 mesh).

NMR spectra were recorded on a Varian Mercury-200 (200 MHz for ^1H , 188 MHz for ^{19}F), Bruker AM-250 (250 MHz for ^1H , 63 MHz for ^{13}C), Varian Unity-300 (300 MHz for ^1H , 75 MHz for ^{13}C , 282 MHz for ^{19}F), Varian Mercury-400 (400 MHz for ^1H , 101 MHz for ^{13}C), Bruker Avance-400 (400 MHz for ^1H , 101 MHz for ^{13}C , 128 MHz for ^{11}B) or Varian Inova-500 (500 MHz for ^1H , 126 MHz for ^{13}C , 470 MHz for ^{19}F) spectrometer, and were referenced to residual solvent resonances. All chemical shifts (δ) are quoted in ppm and coupling constants (J) in Hz. ^1H -NMR spectra were assigned with assistance from ^1H - ^1H COSY (correlation spectroscopy, through bond interactions) and ^1H - ^1H NOESY (nuclear Overhauser effect spectroscopy, through space interactions) spectra. ^{13}C -NMR spectra were recorded with proton decoupling, and were assigned with assistance from ^1H - ^{13}C HSQC (heteronuclear single quantum correlation) and ^{13}C DEPT (distortionless enhancement by polarization transfer) spectra. ^{11}B -NMR spectra were recorded with proton decoupling.

Electron-ionisation mass spectra were recorded with a Micromass AutoSpec spectrometer, with GC-MS on a Thermo Finnigan TRACE GCMS. Electrospray ionisation mass spectra were recorded with a Micromass LCT spectrometer with methanol as the carrier solvent. MALDI mass spectra were recorded by the EPSRC National Mass Spectrometry Service at the University of Wales, Swansea. Accurate mass spectra were recorded with a Micromass LCT spectrometer at 5000 resolution using sodium

iodide as the reference. Accurate mass spectra were also recorded by the EPSRC National Mass Spectrometry Service.

Infra-red spectra were recorded with a Perkin-Elmer 1600 FTIR spectrometer operated using GRAMS software. Solid samples were examined as KBr discs, and liquid samples as thin films.

Elemental analysis was performed using an Exeter Analytical E-440 elemental analyser.

Melting points were determined on a Sanyo-Gallenkamp MPD350.BM3.5 melting point apparatus and are uncorrected for the apparatus.

Single crystal X-ray diffraction experiments were carried out on a SMART 3-circle diffractometer with a CCD area detector, using graphite-monochromated Mo K α radiation ($\lambda = 0.71073 \text{ \AA}$). The structures were solved by direct methods and refined by full-matrix least squares against F^2 of all data, using SHELXTL software.⁴⁴⁴

Photophysical Measurements

UV-visible absorption spectra were recorded using a Biotech Instruments XS spectrometer operating with LabPower software. All samples were studied in quartz cuvettes of 1 cm pathlength, against a reference of pure solvent contained within a matched cuvette. Extinction coefficients were determined by a dilution technique and graphical application of the Beer-Lambert law¹⁹ (equation 16, where $A(\lambda)$ is the absorbance at a specified wavelength, $\varepsilon(\lambda)$ is the related extinction coefficient ($\text{dm}^3 \text{ mol}^{-1} \text{ cm}^{-1}$), c is the concentration of the absorbing species (mol dm^{-3}) and l is the path length (cm)).

$$A(\lambda) = \varepsilon(\lambda)cl \quad (16)$$

Steady-state luminescence spectra were recorded using an Instruments S.A. Fluoromax-2 spectrometer, equipped with a Hamamatsu R928 photomultiplier tube. All samples were studied in quartz fluorescence cuvettes of 1 cm pathlength. Solutions were prepared so that the absorbance was ~ 0.1 to minimise inner filter effects. Emission was detected at right angles to the excitation source, with appropriate filters used where required to remove second order peaks. All emission spectra were corrected after data acquisition for dark count and for the spectral response of the detector. Excitation spectra were automatically corrected for lamp output, through use of a beam splitter, which directs 8% of the excitation light to a reference photodiode.

Aerated luminescence quantum yields were recorded using a dilution technique with respect to a standard of ruthenium(II) tris(2,2'-bipyridine) chloride in aqueous solution ($\Phi = 0.028 \pm 0.002$).⁴⁰⁰ The quantum yield to be determined may be calculated with respect to the standard by application of equation 17,⁴⁴⁵ where Φ is the luminescence quantum yield, (dI/dA) is the gradient from the plot of integrated emission intensity vs. absorbance, η is the refractive index of the solvent, and Φ_{ST} , $(dI/dA)_{ST}$ and η_{ST} are the respective values for the standard. Only the gradient of the linear portion of the plot was determined. Degassed quantum yields were obtained from the ratio of integrated emission intensities from degassed and aerated solutions of the same sample. Quantum yields in D₂O were estimated from the ratio of integrated emission intensities from isoabsorbant D₂O and H₂O solutions.

$$\Phi = \Phi_{ST} \left(\frac{\left(\frac{dI}{dA} \right)}{\left(\frac{dI}{dA} \right)_{ST}} \right) \left(\frac{\eta^2}{\eta_{ST}^2} \right) \quad (17)$$

Low temperature (77 K) measurements were obtained from samples held in a 1 cm pathlength quartz cuvette in a liquid nitrogen cooled cryostat (Oxford Instruments Optical Cryostat, DN 1704). The temperature was monitored *via* a temperature controller (Oxford Instruments ITC-601). Steady-state luminescence spectra were recorded using a Perkin-Elmer LS 50 B luminescence spectrometer, equipped with a Hamamatsu R928 photomultiplier tube and operating with FL Winlab 3.0 software. Solutions were prepared so that the absorbance was ~ 0.1 to minimise inner filter effects. Emission was detected at right angles to the excitation source. All spectra were corrected after acquisition for dark count and for the spectral response of the spectrometer.

Samples of iridium(III) complexes for time-resolved spectroscopy were excited in 1 cm pathlength quartz fluorescence cuvettes by third harmonic radiation ($\lambda = 355$ nm, ~ 1 -2 mJ per pulse, pulse length ~ 7 ns) from a Q-switched Nd:YAG laser (Spectra Physics GCE-150-10). Stray light at 1064 nm (fundamental) and 532 nm (second harmonic) was removed by the use of optical filters. Emission was detected at right angles to the excitation source with a photomultiplier tube (Hamamatsu R928) and recorded using a digital storage oscilloscope (Tetronix TDS-340), before transfer to a PC for analysis. The raw data was deconvoluted to account for detector response by reference to a separate sample of 1,4-bis(5-phenyloxazol-2-yl)benzene (POPOP), a

fluorescent dye, and fitted to a single exponential by minimisation of the sum of squared residuals.

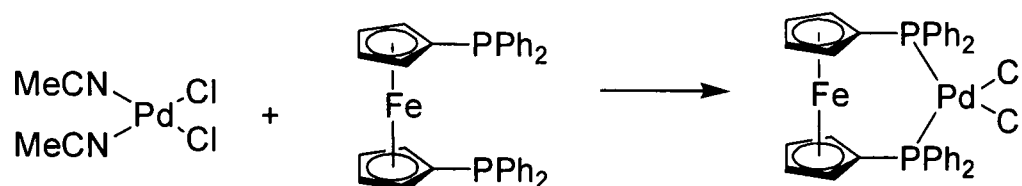
Time-resolved spectroscopy of europium(III) complexes was performed on a Perkin-Elmer LS 55 spectrometer, equipped with a Hamamatsu R928 photomultiplier tube. Luminescence lifetimes were measured by monitoring the integrated intensity of light at 616 nm over a fixed gate time (0.1 ms) following a variable delay time (0.1-10 ms at 0.05 ms intervals for H₂O solutions, 0.1-12.0 ms at 0.10 ms intervals for D₂O solutions). Excitation and emission bandpasses were fixed at 10 nm. Luminescence lifetimes were determined by fitting to a single exponential by minimisation of the sum of squared residuals, and were averaged over three sets of data.

Density Functional Calculations

B3LYP density functional theory calculations were performed using the Gaussian98⁴⁴⁶ software package. “Double- ζ ” quality basis sets were employed for the ligands (6-31G) and the Ir (LANL2DZ⁴¹⁵). The inner core electrons of Ir were replaced with a relativistic effective core potential (ECP), leaving the outer core $[(5s)^2(5p)^6]$ electrons and the $(5d)^6$ valence electrons of Ir(III). The geometries were fully optimised without symmetry constraints. Time-dependent DFT (TD-DFT) calculations were performed at the optimised ground-state geometries using the B3LYP functional.

6.1 Synthesis of ligands for iridium(III) complexes

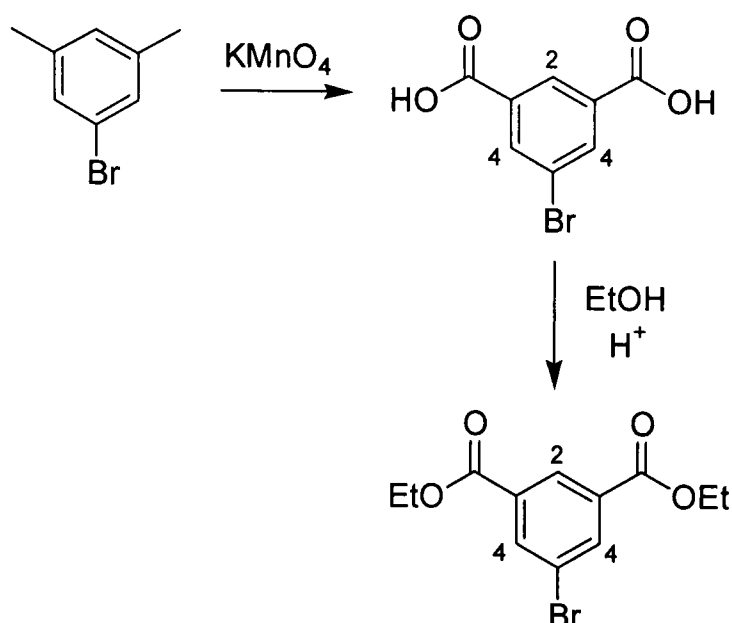
6.1.1 [1,1'-Bis(diphenylphosphino)ferrocene]palladium(II) chloride⁴⁴⁷



1,1'-Bis(diphenylphosphino)ferrocene (292 mg, 0.53 mmol) and *trans*-bis(acetonitrile)palladium(II) chloride (135 mg, 0.52 mmol) were placed in separate Schlenk tubes. Both tubes were evacuated and back filled with nitrogen three times, and dry degassed toluene (10 ml per Schlenk) added to each *via* cannula transfer. Once all the 1,1'-bis(diphenylphosphino)ferrocene had dissolved, it was transferred into the second Schlenk *via* cannula transfer and stirred under a nitrogen atmosphere for 17 h. The solvent was then decanted *via* a filter cannula, and the remaining catalyst residue washed with degassed toluene (3 × 10 ml). Drying under vacuum gave the desired product as a pale orange solid.

¹H-NMR (*d*₆-DMSO, 300 MHz) δ = 7.87 (8H, m, phenyl (*ortho*-)), 7.60 (4H, m, phenyl (*para*-)), 7.51 (8H, m, phenyl (*meta*-)), 4.55 (4H, s, cyclopentadienyl), 4.24 (4H, s, cyclopentadienyl).

6.1.2 5-Bromo-isophthalic acid diethyl ester

*5-Bromo-isophthalic acid*

Potassium permanganate (3.0 g, 18.9 mmol) was added to a stirred solution of 1-bromo-3,5-dimethylbenzene (1.98 g, 10.7 mmol) in water (40 ml) and heated under reflux at 100°C for 3 h. Additional potassium permanganate (9.0 g, 56.6 mmol) was added in 3 g portions over a period of 6 h. After heating under reflux at 100°C for a further 16 h, the resulting solid was removed by filtration of the hot reaction mixture and was washed with hot water. Reduction in volume of the combined filtrates under reduced pressure was followed by addition of concentrated HCl and isolation of the resulting precipitate by filtration to give the desired product as a colourless solid (1.93 g, 73%).

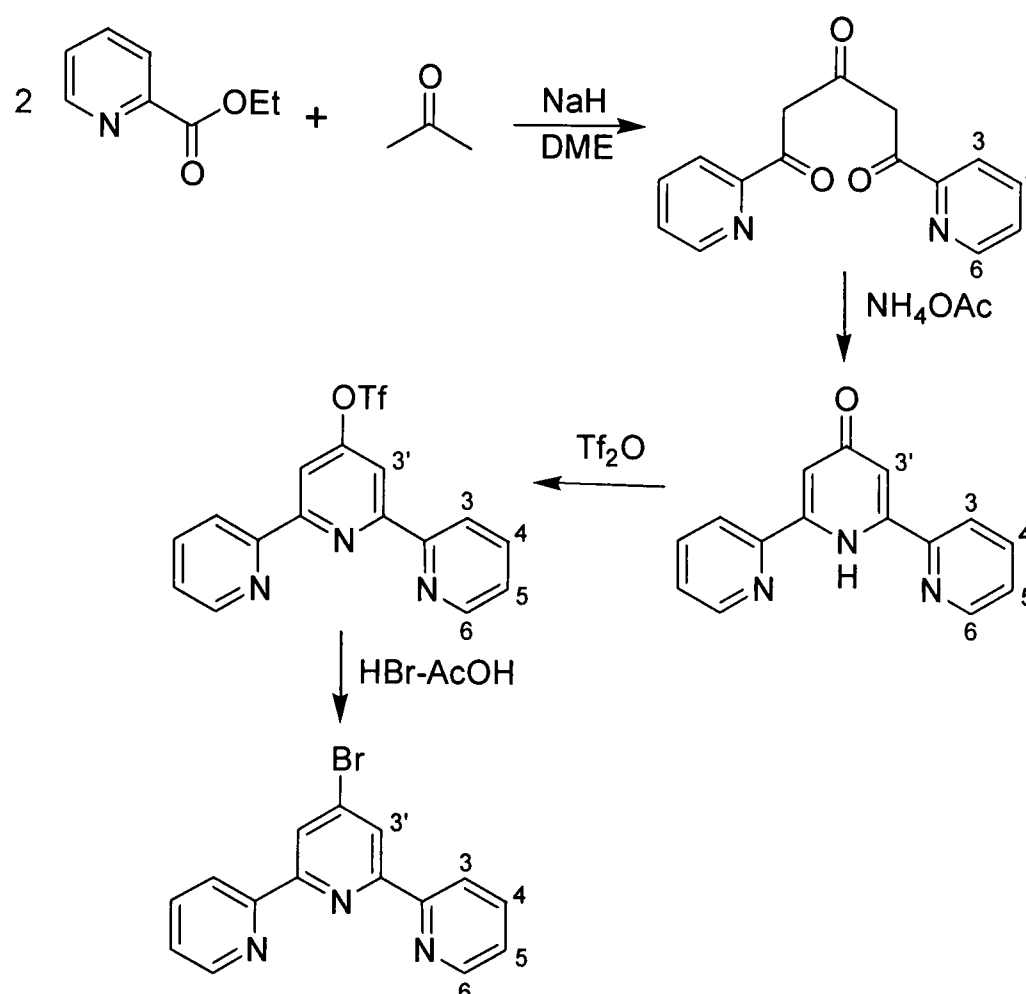
¹H-NMR (*d*₆-Acetone, 200 MHz) δ = 8.66 (1H, t, J = 1.5, H²), 8.40 (2H, d, J = 1.5, H⁴).

5-Bromo-isophthalic acid diethyl ester

Concentrated HCl (1 ml) was added to a solution of 5-bromo-isophthalic acid (1.93 g, 7.87 mmol) in ethanol (80 ml) and heated under reflux at 78°C for 12 h. After cooling to room temperature, the precipitated solid was removed by filtration and the filtrate was neutralised with Na₂CO₃ solution. The precipitated NaCl was removed by filtration, and the solvent removed from the filtrate under reduced pressure. The residue was added to water (50 ml), extracted into dichloromethane (3 × 50 ml) and the combined organic phase dried over MgSO₄. Removal of solvent under reduced pressure and drying under vacuum gave the desired product as a pale yellow solid (890 mg, 38%).

$^1\text{H-NMR}$ (CDCl_3 , 300 MHz) $\delta = 8.60$ (1H, t, $J = 1.5$, H^2), 8.34 (2H, d, $J = 1.5$, H^4), 4.41 (4H, q, $J = 7.2$, OCH_2CH_3), 1.41 (6H, t, $J = 7.2$, OCH_2CH_3). $^{13}\text{C}\{^1\text{H}\}\text{-NMR}$ (CDCl_3 , 63 MHz) $\delta = 164.4$ ($\text{C}=\text{O}$), 136.4 (CH), 132.6 (C^q), 129.1 (CH), 122.4 (C^q), 61.7 (OCH_2CH_3), 14.2 (OCH_2CH_3). MS (EI) $m/z = 300/302$ (M^+), $272/274$ ($\text{M}^+ - \text{C}_2\text{H}_4$), $255/257$ ($\text{M}^+ - \text{OEt}$), $244/246$ ($\text{M}^+ - 2 \times \text{C}_2\text{H}_4$), $227/229$ ($\text{M}^+ - \text{CO}_2\text{Et}$), 221 ($\text{M}^+ - \text{Br}$), $199/201$ ($\text{M}^+ - \text{C}_2\text{H}_4$ & CO_2Et), $254/156$ ($\text{M}^+ - 2 \times \text{CO}_2\text{Et}$), 45 ($\text{EtO}^{+\bullet}$), 29 ($\text{Et}^{+\bullet}$). IR (KBr disc) $\bar{\nu} = 1719$ cm^{-1} (CO_2Et , $\text{C}=\text{O}$ stretch).

6.1.3 4'-Bromo-2,2':6',2''-terpyridine



*1,5-Dipyridin-2-ylpentane-1,3,5-trione*⁴⁴⁸

A solution of pyridine-2-carboxylic acid ethyl ester (14.6 g, 96.5 mmol) and acetone (2.39 ml, 32.5 mmol) in dry degassed 1,2-dimethoxyethane (50 ml) was added to a suspension of sodium hydride (3.92 g, 163 mmol) in dry degassed 1,2-dimethoxyethane (50 ml) under a nitrogen atmosphere. The reaction mixture was stirred at room temperature until a bright orange suspension was obtained (15 minutes), then heated under reflux at 83°C for 6 h. After cooling to room temperature, the solvent was removed under reduced pressure, and the residue dissolved in water (100 ml) and filtered through Celite®. The filtrates were adjusted to pH 7, and the resulting

precipitate isolated by filtration, washed with water and dissolved in diethyl ether. Drying over MgSO_4 and removal of solvent under reduced pressure gave the desired product as a yellow solid (6.12 g, 70%).

$^1\text{H-NMR}$ (CDCl_3 , 300 MHz) δ = 8.61 (2H, d, J = 4.5, H^6), 7.94 (2H, d, J = 8.0, H^3), 7.76 (2H, td, J = 7.7, 1.8, H^4), 7.32 (2H, ddd, J = 7.7, 4.6, 1.2, H^5), 6.74 (2H, s, $\text{CH}=\text{COH}$), 1.49 (2H, s, OH).*

*1'H-2,2':6',2''-Terpyridin-4'-one*⁴⁴⁸

A solution of 1,5-dipyridin-2-ylpentane-1,3,5-trione (7.36 g, 27.4 mmol) and ammonium acetate (15.3 g, 198.0 mmol) in ethanol (100 ml) was heated under reflux at 78°C for 6 h. After cooling to room temperature, the reaction mixture was concentrated under reduced pressure and cooled to give a white precipitate. This was isolated by filtration, washed with cold diethyl ether and dried under vacuum to give the desired product as a white solid (5.37 g, 79%).

$^1\text{H-NMR}$ (CDCl_3 , 200 MHz) δ = 12.09 (1H, br s, NH), 8.80 (2H, dt, J = 4.9, 1.2, H^6), 7.96 (2H, d, J = 8.1, H^3), 7.89 (2H, td, J = 8.1, 1.5, H^4), 7.45 (2H, ddd, J = 7.0, 4.7, 1.7, H^5), 7.23 (2H, s, $\text{H}^{3'}$). Characterisation data are consistent with that in the literature.⁴⁴⁹

*2,2':6',2''-terpyridin-4'-yl trifluoromethanesulfonate*⁴⁵⁰

Trifluoromethanesulfonic anhydride (3.21 g, 11.4 mmol) was added to a stirred solution of 1'H-2,2':6',2''-terpyridin-4'-one (2.64 g, 10.6 mmol) in dry pyridine (25 ml) at 0°C. The mixture was stirred for 30 minutes at 0°C before being allowed to warm to room temperature and stirring for a further 72 h. The reaction mixture was poured into ice/water (200 ml) and stirred for 30 minutes to precipitate a light brown solid. This was isolated by filtration, washed with cold water and recrystallised from hexane to give the desired product as a white flocculent solid (2.01 g, 50%).

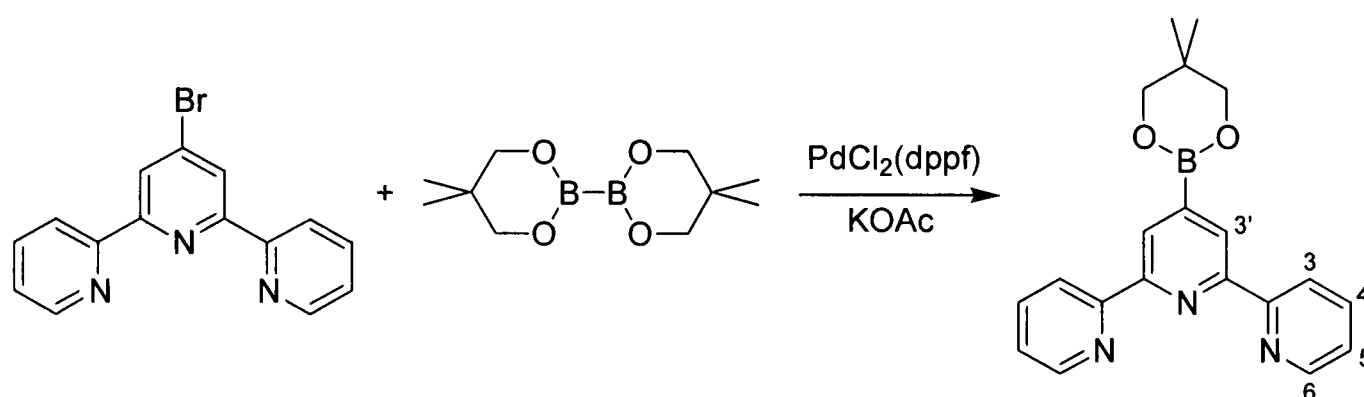
$^1\text{H-NMR}$ (CDCl_3 , 200 MHz) δ = 8.72 (2H, dt, J = 4.8, 0.8, H^6), 8.62 (2H, d, J = 8.0, H^3), 8.42 (2H, s, $\text{H}^{3'}$), 7.89 (2H, td, J = 7.6, 1.6, H^4), 7.39 (2H, ddd, J = 7.53, 4.96, 1.13, H^5). Characterisation data are consistent with that in the literature.⁴⁵⁰

* As discussed by Constable and Ward, 1'H-2,2':6',2''-terpyridin-4'-one may exist as three possible keto-enol tautomers in solution.⁴⁴⁸ The $^1\text{H-NMR}$ data above suggests a large proportion of the di-enol form in this case.

*4'-Bromo-2,2':6',2''-terpyridine*⁴⁵¹

2,2':6',2''-Terpyridin-4'-yl trifluoromethanesulfonate (2.01 g, 5.27 mmol) was added to hydrogen bromide in acetic acid (40 ml) and heated to 110°C for 6 h. After cooling to room temperature, the reaction mixture was poured into ice and stirred until all of the ice had melted. On making basic with KOH solution a pink precipitate formed, which turned white on addition of sufficient base. The solution was extracted into dichloromethane (3 × 100 ml), and the solvent removed under reduced pressure to give the desired product as a pale yellow solid (1.60 g, 98%).

¹H-NMR (CDCl₃, 300 MHz) δ = 8.71 (2H, d, J = 4.7, H⁶), 8.66 (2H, s, H^{3'}), 8.59 (2H, d, J = 8.1, H³), 7.87 (2H, td, J = 7.7, 1.6, H⁴), 7.36 (2H, dd, J = 7.5, 5.2, H⁵). ¹³C{¹H}-NMR (CDCl₃, 101 MHz) δ = 156.6 (C^q), 155.1 (C^q), 149.4 (CH), 137.1 (CH), 135.2 (C^q), 124.4 (CH), 124.3 (CH), 121.5 (CH). MS (EI) *m/z* = 311/313 (M⁺), 232 (M⁺ – Br), 155 (M⁺ – Br, py), 78 (py^{+•}). Characterisation data are consistent with that in the literature.⁴⁵²

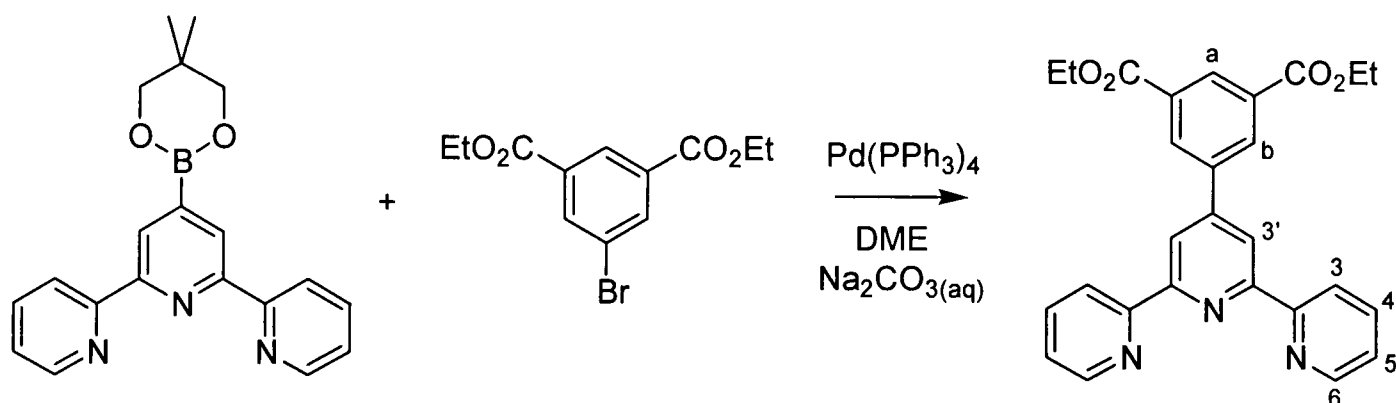
6.1.4 4'-(5,5-Dimethyl-[1,3,2]dioxaborinan-2-yl)-2,2':6',2''-terpyridine³¹³

[1,1'-Bis(diphenylphosphino)ferrocene]palladium(II) chloride (30 mg, 0.04 mmol), potassium acetate (546 mg, 5.57 mmol), bis(neopentyl glycolato)diboron (455 mg, 2.01 mmol) and 4'-bromo-2,2':6',2''-terpyridine (596 mg, 1.91 mmol) were placed in a Schlenk tube, which was then evacuated and back-filled with nitrogen three times. Dry dimethyl sulfoxide (10 ml) was degassed by three freeze-pump-thaw cycles, transferred to the solids by cannula transfer and heated to 80°C for 5½ h. After cooling to room temperature, the reaction mixture was diluted with toluene (100 ml), washed with water (5 × 100 ml) and dried over MgSO₄ before removal of solvent under reduced pressure. The residue was dissolved in a dichloromethane-methanol mixture, followed

by concentration of the solution under reduced pressure.* Isolation of the resulting precipitate and drying under vacuum gave the desired product as a colourless solid (180 mg, 15%).

$^1\text{H-NMR}$ (CDCl_3 , 200 MHz) δ = 8.80 (2H, s, $\text{H}^{3'}$), 8.72 (2H, d, J = 4.8, H^6), 8.61 (2H, d, J = 8.0, H^3), 7.84 (2H, td, J = 7.8, 1.8, H^4), 7.31 (2H, ddd, J = 7.56, 4.79, 1.31, H^5), 3.82 (4H, s, CH_2), 1.04 (6H, s, CH_3). $^{13}\text{C}\{^1\text{H}\}$ -NMR (CDCl_3 , 101 MHz) δ = 156.7 (C^9), 154.7 (C^9), 149.2 (C^6), 136.8 (C^4), 125.7 ($\text{C}^{3'}$), 123.5 (C^5), 121.2 (C^3), 72.4 (OCH_2C), 32.0 ($\text{C}(\text{CH}_3)_2$), 21.9 (CH_3). $^{11}\text{B}\{^1\text{H}\}$ -NMR (CDCl_3 , 128 MHz) δ = 26 ($\text{B}(\text{neo})$). MS (EI) m/z = 345 (M^+), 330 ($\text{M}^+ - \text{Me}$), 260 ($\text{M}^+ - \text{C}_5\text{H}_9\text{O}$), 233 ($\text{M}^+ - \text{B}(\text{neo})$), 78 ($\text{py}^{+\bullet}$). Characterisation data are consistent with that in the literature.³¹³

6.1.5 5-(2,2':6',2''-Terpyridin-4'-yl)-isophthalic acid diethyl ester **83** [tpyiade]



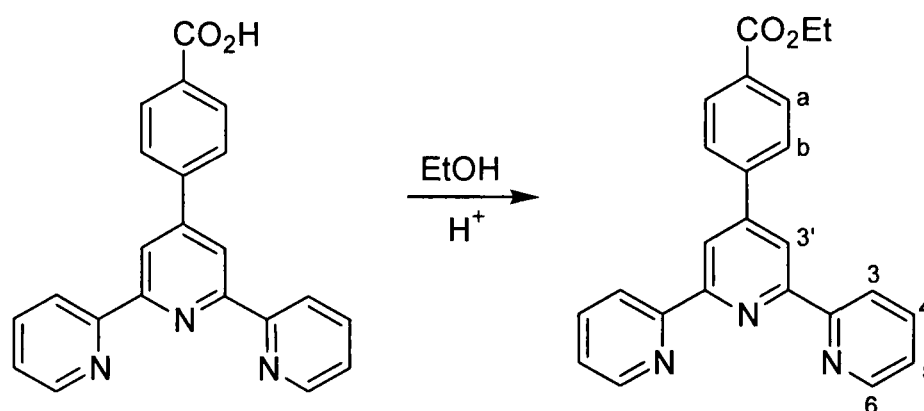
Sodium carbonate (200 mg, 1.89 mmol) in water ($\frac{1}{2}$ ml) was added to a solution of 4'-(5,5-dimethyl-[1,3,2]dioxaborinan-2-yl)-2,2':6',2''-terpyridine (290 mg, 0.84 mmol) and 5-bromo-isophthalic acid diethyl ester (231 mg, 0.77 mmol) in 1,2-dimethoxyethane (10 ml) and degassed by three freeze-pump-thaw cycles. Addition of tetrakis(triphenylphosphine)palladium(0) (49 mg, 0.04 mmol) was followed by stirring at room temperature for 30 minutes then heating to 95°C for 18 h. The progress of the reaction was followed by TLC (alumina, hexane/ether, 50/50). After cooling to room temperature, the precipitated solid was removed by filtration and washed with 1,2-dimethoxyethane, before removal of solvent under reduced pressure. The residue was dissolved in dichloromethane (100 ml), washed with dilute NaHCO_3 solution

* This additional purification, not reported by Aspley and Williams,³¹³ allows removal of unreacted bis(neopentylglycolato)diboron.

(3 × 50 ml) and dried over MgSO₄. Removal of solvent under reduced pressure followed by recrystallisation of the residue from ethanol gave the desired product as a colourless solid (143 mg, 42%), mp = 197.5-198.7°C.

¹H-NMR (CDCl₃, 300 MHz) δ = 8.76 (2H, s, H^{3'}), 8.75-8.77 (1H, obscured by singlet at 8.76 ppm, H^a), 8.73 (2H, br d, J = 4.5, H⁶), 8.70 (2H, d, J = 1.5, H^b), 8.67 (2H, d, J = 8.1, H³), 7.89 (2H, td, J = 7.7, 1.6, H⁴), 7.37 (2H, ddd, J = 7.5, 4.8, 0.9, H⁵), 4.47 (4H, q, J = 7.0, OCH₂CH₃), 1.45 (6H, t, J = 7.1, OCH₂CH₃). ¹³C{¹H}-NMR (CDCl₃, 101 MHz) δ = 165.8 (C=O), 156.4 (C^q), 156.0 (C^q), 149.3 (CH), 148.9 (C^q), 139.8 (C^q), 137.2 (CH), 132.6 (CH), 132.0 (C^q), 131.1 (CH), 124.2 (CH), 121.6 (CH), 119.3 (CH), 61.8 (CO₂CH₂CH₃), 14.5 (CO₂CH₂CH₃). MS (EI) m/z = 453 (M⁺), 408 (M⁺ - OEt), 381 (M⁺ - CO₂Et), 353 (M⁺ - CO₂Et & C₂H₄), 308 (M⁺ - 2 × CO₂Et), 149 (C₆H₄CO₂Et⁺). IR (KBr disc) $\bar{\nu}$ = 1725 cm⁻¹ (CO₂Et, C=O stretch).

6.1.6 4-(2,2':6',2''-Terpyridin-4'-yl)benzoic acid ethyl ester [tpybae]

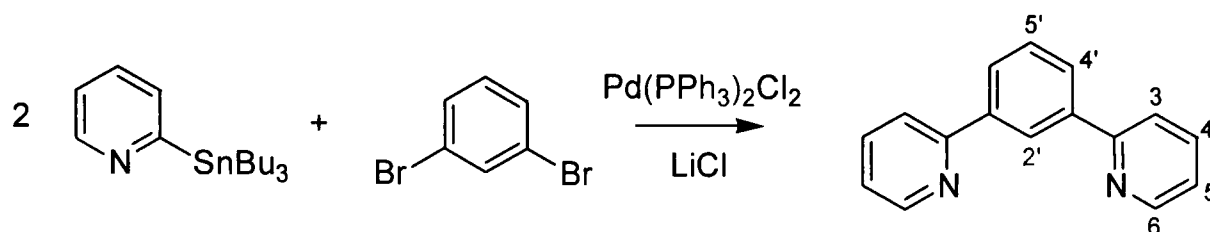


A solution of 4-(2,2':6',2''-terpyridin-4'-yl)benzoic acid (1.40 g, 3.96 mmol) in DMSO (5 ml) was stirred at room temperature for 30 minutes. After this period, ethanol (60 ml) and concentrated H₂SO₄ (1 ml) were added, and the suspension was stirred under reflux at 78°C for three days. After cooling to room temperature, the resulting solid was isolated by filtration and dried under vacuum, to give the desired product as a colourless solid (815 mg, 54%), mp >250°C.

¹H-NMR (d₆-DMSO, 500 MHz) δ = 9.01 (2H, d, J = 7.9, H³), 8.93 (2H, d, J = 5.3, H⁶), 8.89 (2H, s, H^{3'}), 8.44 (2H, td, J = 7.9, 1.3, H⁴), 8.18 (2H, d, J = 8.5, H^b), 8.14 (2H, d, J = 8.5, H^a), 7.88 (2H, ddd, J = 7.7, 5.2, 0.7, H⁵), 4.37 (2H, q, J = 7.2, CO₂CH₂CH₃), 1.37 (3H, t, J = 7.0, CO₂CH₂CH₃). ¹³C{¹H}-NMR (d₆-DMSO, 126 MHz) δ = 165.4 (C=O), 152.3 (C^q), 150.9 (C^q), 149.4 (C^q), 146.6 (C⁶), 142.2 (C⁴), 140.6 (C^q), 131.1 (C^q), 130.1 (C^a), 127.8 (C^b), 126.4 (C⁵), 123.4 (C³), 120.5 (C^{3'}), 61.2

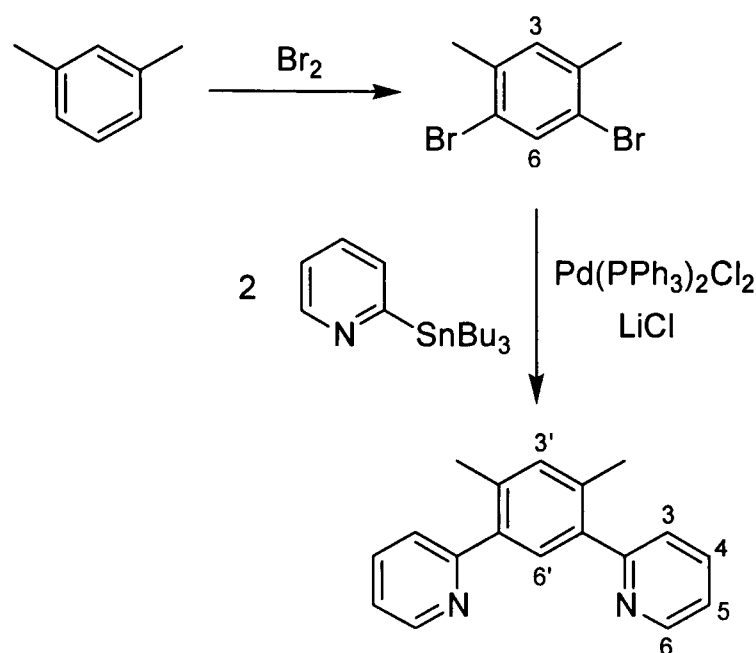
(CO₂CH₂CH₃), 14.3 (CO₂CH₂CH₃). MS(ES+) $m/z = 382$ ([M+H]⁺). IR (KBr disc) $\bar{\nu} = 1699$ cm⁻¹ (CO₂Et, C=O stretch).

6.1.7 1,3-Di(pyridin-2-yl)benzene **84** [dpybH]³⁰⁸



A mixture of 2-tri-*n*-butylstannylpyridine (4.87 g, 77% pure by mass by ¹H NMR assay, 10.2 mmol), 1,3-dibromobenzene (505 μ l, 4.2 mmol), bis-(triphenylphosphine)palladium(II) chloride (187 mg, 0.27 mmol) and lithium chloride (1.45 g, 34.2 mmol) in dry toluene (40 ml) was degassed by three freeze-pump-thaw cycles, then heated under reflux at 111°C under a nitrogen atmosphere for three days. The progress of the reaction was followed by TLC (silica, hexane). After cooling to room temperature, saturated KF solution (15 ml) was added, and the solution stirred for 30 minutes. The precipitated solid was removed by filtration and washed with water (50 ml). NaHCO₃ solution (10%, 100 ml) was then added to the combined filtrates. Extraction into dichloromethane (2 \times 200 ml) and drying over MgSO₄ was followed by removal of solvent under reduced pressure. The residue was purified by column chromatography (silica, hexane/diethyl ether, gradient elution from 100/0 to 30/70) to give the desired product as an orange oil (600 mg, 62%).

¹H-NMR (CDCl₃, 300 MHz) $\delta = 8.72$ (2H, d, $J = 4.7$, H⁶), 8.63 (1H, t, $J = 1.9$, H^{2'}), 8.06 (2H, dd, $J = 7.7, 1.9$, H^{4'}), 7.85 (2H, d, $J = 8.1$, H³), 7.77 (2H, td, $J = 8.0, 1.9$, H⁴), 7.59 (1H, t, $J = 7.8$, H^{5'}), 7.25 (2H, ddd, $J = 7.5, 4.8, 1.2$, H⁵). MS(EI) $m/z = 232$ (M⁺), 231 (M⁺ - H), 154 (M⁺ - C₅NH₅), 78 (C₅NH₄⁺). Characterisation data are consistent with that in the literature.³⁰⁸

6.1.8 1,5-Di(pyrid-2-yl)-2,4-dimethylbenzene **85** [dpydmbH]*1,5-Dibromo-2,4-dimethylbenzene*⁴⁵³

Bromine (43.8 g, 274 mmol) was added over five minutes with stirring to *meta*-xylene (13.0 g, 122 mmol), followed by addition of iodine (0.5 g, 1.97 mmol) over a further 30 minutes, and stirring at room temperature for an additional 3 h. After this period, NaOH solution (4 mol dm⁻³, 100 ml) was added and the reaction mixture was stirred for 15 minutes. The resulting precipitate was isolated by filtration, dried under vacuum, and recrystallised from ethanol to give the desired product as a white solid (15.7 g, 49%).

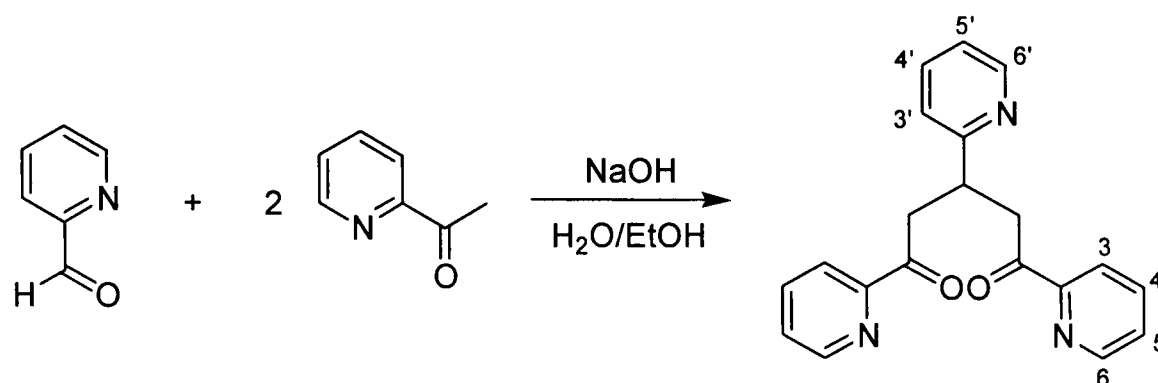
¹H-NMR (CDCl₃, 200 MHz) δ = 7.68 (1H, s, H⁶), 7.10 (1H, s, H³), 2.31 (6H, s, Me). ¹H-NMR (*d*₆-Acetone, 200 MHz) δ = 7.72 (1H, s, H⁶), 7.31 (1H, s, H³), 2.31 (6H, s, Me). ¹³C{¹H}-NMR (CDCl₃, 126 MHz) δ = 137.0 (C^q), 135.0 (CH), 132.7 (CH), 122.1 (C^q), 22.4 (CH₃). MS(EI) *m/z* = 262/264/266 (M⁺), 183/185 (M⁺ – Br), 104 (M⁺ – 2 × Br), 103 (M⁺ – Br, HBr). Characterisation data are consistent with that in the literature.⁴⁵³

1,5-Di(pyrid-2-yl)-2,4-dimethylbenzene 85 [dpydmbH]

A mixture of 2-tri-*n*-butylstannylpyridine (9.32 g, 81% pure by mass by ¹H NMR assay, 20.5 mmol), 1,5-dibromo-2,4-dimethylbenzene (2.28 g, 8.64 mmol), bis-(triphenylphosphine)palladium(II) chloride (225 mg, 0.32 mmol) and lithium chloride (2.68 g, 63.2 mmol) in dry toluene (50 ml) was degassed by five freeze-pump-thaw cycles, then heated under reflux at 111°C under a nitrogen atmosphere for 24 h. The progress of the reaction was followed by TLC (silica, hexane/diethyl ether, 75/25).

After cooling to room temperature, saturated KF solution (20 ml) was added and the solution stirred for 30 minutes. The precipitated solid was removed by filtration and washed with water (50 ml). NaHCO₃ solution (10%, 100 ml) was then added to the combined filtrates, extracted into dichloromethane (2 × 200 ml) and dried over MgSO₄. Removal of solvent under reduced pressure and purification of the residue by column chromatography (silica, hexane/diethyl ether, gradient elution from 100/0 to 10/90) gave the desired product as a pale yellow solid (1.35 g, 61%), mp = 83.8-85.6°C.

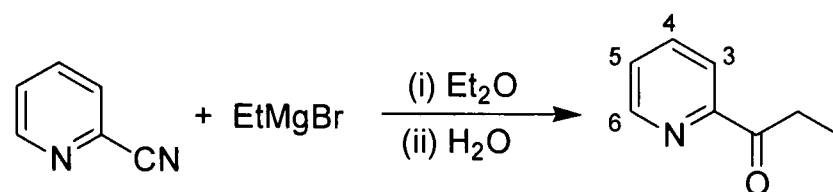
¹H-NMR (CDCl₃, 500 MHz) δ = 8.67 (2H, d, J = 4.9, H⁶), 7.72 (2H, td, J = 7.6, 1.8, H⁴), 7.47 (1H, s, H^{6'}), 7.43 (2H, d, J = 7.7, H³), 7.27 (1H, s, H^{3'}), 7.23 (2H, ddd, J = 7.5, 4.9, 1.2, H⁵), 2.40 (6H, s, Me). ¹H-NMR (d₆-Acetone, 400 MHz) δ = 8.66 (2H, d, J = 4.7, H⁶), 7.85 (2H, td, J = 7.6, 1.9, H⁴), 7.56 (2H, dt, J = 7.9, 1.0, H³), 7.51 (1H, s, H^{6'}), 7.32 (2H, ddd, J = 7.7, 4.9, 1.3, H⁵), 7.23 (1H, s, H^{3'}), 2.41 (6H, s, Me). ¹H-NMR (d₆-DMSO, 400 MHz) δ = 8.66 (2H, d, J = 5.0, H⁶), 7.86 (2H, td, J = 7.7, 1.9, H⁴), 7.57 (2H, dt, J = 7.9, 1.0, H³), 7.43 (1H, s, H^{6'}), 7.35 (2H, ddd, J = 7.6, 4.8, 1.2, H⁵), 7.26 (1H, s, H^{3'}), 2.37 (6H, s, Me). ¹³C{¹H}-NMR (CDCl₃, 126 MHz) δ = 159.8 (C^q), 149.3 (C⁶), 138.2 (C^q), 136.2 (C⁴), 135.9 (C^q), 133.4 (C^{3'}), 131.2 (C^{6'}), 124.3 (C³), 121.6 (C⁵), 20.1 (CH₃). MS(EI) *m/z* = 260 (M⁺), 259 (M⁺ - H), 245 (M⁺ - Me), 78 (C₅NH₄⁺). MS(ES+) *m/z* = 261 ([M+H]⁺), 283 ([M+Na]⁺). HRMS(ES+) *m/z* = 283.1198 ([M+Na]⁺); calc. for C₁₈H₁₆N₂Na, 283.1211. Found: C, 80.85; H, 6.29; N, 10.28%. C₁₈H₁₆N₂·½H₂O requires: C, 80.27; H, 6.36; N, 10.40%. One spot by TLC(silica), R_f = 0.6 in dichloromethane/methanol, 90/10.

6.1.9 1,3,5-Tri-pyridin-2-ylpentane-1,5-dione **89***

A solution of 2-acetylpyridine (8.4 ml, 75.0 mmol), 2-pyridinecarboxaldehyde (3.1 ml, 32.4 mmol) and sodium hydroxide (2.0 g, 50.0 mmol) in a mixture of water (25 ml) and ethanol (35 ml) was stirred at room temperature for 3 h. After this period, water (150 ml) was added and the resulting solid isolated by filtration, washed with water and recrystallised from a 1:1 mixture of ethanol and water, to give the desired product as a colourless solid (6.93 g, 65%).

$^1\text{H-NMR}$ (CDCl_3 , 400 MHz) δ = 8.60 (2H, d, J = 4.6, H^6), 8.40 (1H, d, J = 4.8, $\text{H}^{6'}$), 7.92 (2H, d, J = 8.0, H^3), 7.74 (2H, t, J = 7.6, H^4), 7.53 (1H, t, J = 7.7, $\text{H}^{4'}$), 7.35-7.41 (3H, m, $\text{H}^{3'}$ & H^5), 7.00 (1H, t, J = 6.0, $\text{H}^{5'}$), 4.16 (1H, quintet, 5.0 Hz, CH), 3.87 (2H, dd, J = 18.0, 7.6, CH_2), 3.62 (2H, dd, J = 18.0, 5.6, CH_2). $^1\text{H-NMR}$ (d_6 -DMSO, 500 MHz) δ = 8.70 (2H, d, J = 4.0, H^6), 8.38 (1H, d, J = 4.0, $\text{H}^{6'}$), 7.98 (2H, td, J = 7.7, 1.8, H^4), 7.89 (2H, d, J = 7.7, H^3), 7.67 (1H, td, J = 7.7, 1.8, $\text{H}^{4'}$), 7.64 (2H, ddd, J = 7.7, 4.8, 1.5, H^5), 7.37 (1H, d, J = 8.1, $\text{H}^{3'}$), 7.14 (1H, ddd, J = 7.3, 4.8, 1.1, $\text{H}^{5'}$), 4.09 (1H, quintet, 7.0 Hz, CH), 3.87 (2H, dd, J = 17.8, 7.9, CH_2), 3.53 (2H, dd, J = 17.8, 6.1, CH_2). $^{13}\text{C}\{^1\text{H}\}$ -NMR (d_6 -DMSO, 101 MHz) δ = 199.9 (C=O), 162.9 (C^9), 152.7 (C^9), 149.1 (CH), 148.6 (CH), 137.4 (CH), 136.2 (CH), 127.6 (CH), 123.1 (CH), 121.3 (CH), 121.2 (CH), 42.2 (CH_2), 37.4 (CH). MS(ES+) m/z = 332 ($[\text{M}+\text{H}]^+$). IR (KBr disc) $\bar{\nu}$ = 1696 cm^{-1} (ketone, C=O stretch), 1570 cm^{-1} (ketone, C=O stretch).

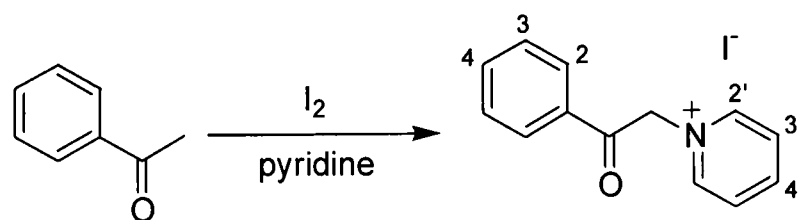
* An adaptation of the procedure used for the synthesis of 1,5-di(pyridin-2-yl)-3-(pyrid-4'-yl)pentane-1,5-dione was followed.⁴⁵⁴

6.1.10 1-Pyridin-2-ylpropan-1-one³⁵⁶

Ethylmagnesium bromide (3.0 mol dm⁻³ solution in diethyl ether, 22.0 ml, 66 mmol) in dry diethyl ether (80 ml) was added dropwise with stirring to a solution of 2-cyanopyridine (8.66 g, 83 mmol) in dry diethyl ether (100 ml) at 0°C under a nitrogen atmosphere. The reaction mixture was then heated under reflux at 35°C for 2½ h. After cooling to 0°C, water (5 ml) was added with care, followed by 2.5 mol dm⁻³ H₂SO₄ (60 ml). The organic layer was separated, and extracted into 1 mol dm⁻³ H₂SO₄ (2 × 30 ml). The combined acid washings were heated in a water bath for 15 min, then neutralised with 1.5 mol dm⁻³ K₂CO₃ solution (150 ml) at 0°C. The resulting white precipitate was extracted into dichloromethane (4 × 100 ml), dried over K₂CO₃, and the solvent removed under reduced pressure to give the desired product as a brown oil (6.91 g, 77%).

¹H-NMR (CDCl₃, 300 MHz) δ = 8.68 (1H, ddd, J = 4.7, 1.6, 0.9, H⁶), 8.05 (1H, dt, J = 7.9, 1.1, H³), 7.83 (1H, td, J = 7.7, 1.7, H⁴), 7.47 (1H, ddd, J = 7.5, 4.7, 1.3, H⁵), 3.25 (2H, q, J = 7.3, CH₂), 1.22 (3H, t, J = 7.2, CH₃). ¹³C{¹H}-NMR (CDCl₃, 101 MHz) δ = 202.7 (C=O), 153.6 (C^q), 149.0 (CH), 136.9 (CH), 127.1 (CH), 121.8 (CH), 31.2 (COCH₂CH₃), 8.1 (COCH₂CH₃). MS(ES⁺) *m/z* = 136 ([M+H]⁺), 271 ([2M+H]⁺). IR (thin film) $\bar{\nu}$ = 1699 cm⁻¹ (ketone, C=O stretch). Characterisation data are consistent with that in the literature.⁴⁵⁵

6.1.11 1-(2-Oxo-2-phenylethyl)pyridinium iodide

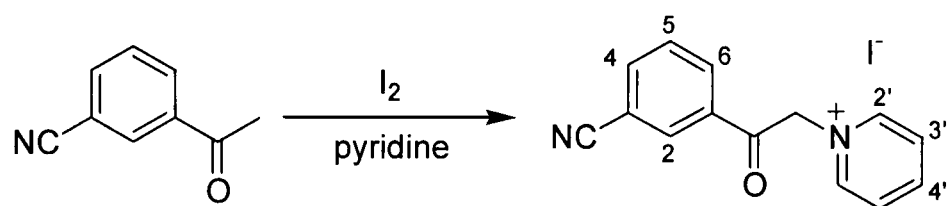


A solution of iodine (5.1 g, 20.1 mmol) in pyridine (15 ml) was added at room temperature to a solution of acetophenone (2.3 ml, 19.7 mmol) in pyridine (5 ml), then heated to 100°C for 3 h. After cooling to room temperature and standing overnight, the resulting precipitate was isolated by filtration and washed with pyridine, dissolved in a

hot mixture of ethanol (120 ml) and water (80 ml), then treated with decolourising charcoal and filtered whilst still hot. Reduction in volume of the filtrate, followed by cooling, resulted in a brown precipitate that was collected by filtration, washed with cold water and dried under vacuum to give the desired product as a pale brown solid (3.85 g, 60%), mp = 190.4-194.8°C.

$^1\text{H-NMR}$ (d_6 -DMSO, 300 MHz) δ = 9.00 (2H, d, J = 5.4, $\text{H}^{2'}$), 8.75 (1H, tt, J = 7.8, 1.2, $\text{H}^{4'}$), 8.29 (2H, dd, J = 7.7, 6.7, $\text{H}^{3'}$), 8.07 (2H, dd, J = 8.6, 1.4, H^2), 7.81 (1H, tt, J = 7.4, 1.2, H^4), 7.67 (2H, t, J = 7.9, H^3), 6.49 (2H, s, CH_2). $^{13}\text{C}\{^1\text{H}\}$ -NMR (d_6 -DMSO, 101 MHz) δ = 190.6 (C=O), 146.4 (C^{py^+}), 146.3 (C^{py^+}), 134.7 (CH), 133.5 (C^{q}), 129.1 (CH), 128.2 (CH), 127.8 (C^{py^+}), 66.2 (CH_2). MS(ES+) m/z = 198 (M^+). MS(ES-) m/z = 127 (I^-). IR (KBr disc) $\bar{\nu}$ = 1697 cm^{-1} (ketone, C=O stretch).

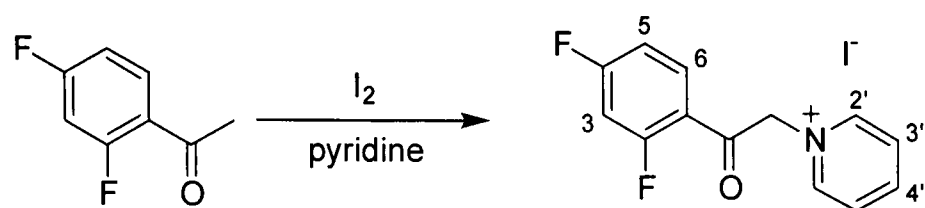
6.1.12 2-(1-(3-Cyanophenyl)-1-oxoethyl)pyridinium iodide



A solution of iodine (5.10 g, 20.1 mmol) in pyridine (15 ml) was added at room temperature to a solution of 3-acetylbenzonitrile (2.75 g, 18.9 mmol) in pyridine (5 ml), then heated to 100°C for 3 h. After cooling to room temperature and standing overnight, the resulting precipitate was isolated by filtration and washed with pyridine, dissolved in a hot mixture of ethanol (120 ml) and water (80 ml), then treated with decolourising charcoal and filtered whilst still hot. Reduction in volume of the filtrate, followed by cooling, resulted in a yellow precipitate that was collected by filtration, washed with cold water and dried under vacuum to give the desired product as a pale yellow solid (4.43 g, 67%), mp = 181.7-183.8°C.

$^1\text{H-NMR}$ (d_6 -DMSO, 300 MHz) δ = 8.98 (2H, d, J = 5.5, $\text{H}^{2'}$), 8.76 (1H, t, J = 7.8, $\text{H}^{4'}$), 8.58 (1H, s, H^2), 8.26-8.37 (4H, m, $\text{H}^{3'}$, H^4 & H^6), 7.89 (1H, t, J = 7.9, H^5), 6.49 (2H, s, CH_2). $^{13}\text{C}\{^1\text{H}\}$ -NMR (d_6 -DMSO, 101 MHz) δ = 189.6 (C=O), 146.6 (C^{py^+}), 146.3 (C^{py^+}), 137.7 (CH), 134.4 (C^{q}), 132.5 (CH), 132.1 (CH), 130.5 (CH), 128.0 (C^{py^+}), 117.8 (C^{q}), 112.3 (C^{q}), 66.3 (CH_2). MS(ES+) m/z = 223 (M^+). MS(ES-) m/z = 127 (I^-). IR (KBr disc) $\bar{\nu}$ = 1701 cm^{-1} (ketone, C=O stretch), 2231 cm^{-1} (nitrile, C \equiv N stretch).

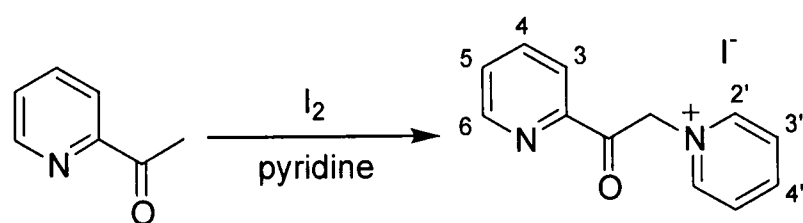
6.1.13 1-(2-(2,4-Difluorophenyl)-2-oxoethyl)pyridinium iodide



2,4-Difluoroacetophenone (2.39 ml, 18.9 mmol) was added at room temperature to a solution of iodine (5.18 g, 20.4 mmol) in pyridine (20 ml), then heated to 100°C for 3 h. After cooling to room temperature and standing for 3 h, the resulting precipitate was isolated by filtration and washed with pyridine, dissolved in a hot mixture of ethanol (50 ml) and water (50 ml), then treated with decolourising charcoal and filtered whilst still hot. Removal of solvent under reduced pressure then recrystallisation from water gave the desired product as a yellow solid (3.17 g, 47%), mp = 176.6-178.5°C.

$^1\text{H-NMR}$ (d_6 -DMSO, 400 MHz) δ = 8.93 (2H, d, J = 5.9, $\text{H}^{2'}$), 8.71 (1H, t, J = 7.7, $\text{H}^{4'}$), 8.24 (2H, dd, J = 7.4, 6.7, $\text{H}^{3'}$), 8.08 (1H, td, J = 8.6, 6.6, H^6), 7.58 (1H, ddd, J = 11.7, 9.2, 2.4, H^3), 7.35 (1H, td, J = 8.5, 2.5, H^5), 6.26 (2H, d, J = 3.2, CH_2). $^{13}\text{C}\{^1\text{H}\}$ -NMR (d_6 -DMSO, 101 MHz) δ = 187.0 (d, J = 5.1, C=O), 166.1 (dd, J = 254.7, 15.6, C^2 or C^4), 162.7 (dd, J = 252.8, 13.4, C^2 or C^4), 146.5 (s, C^{py^+}), 146.2 (s, C^{py^+}), 132.7 (dd, J = 11.3, 3.8, C^6), 127.7 (s, C^{py^+}), 119.0 (dd, J = 13.1, 3.7, C^1), 113.1 (dd, J = 21.9, 3.2, C^5), 105.5 (t, J = 2.5, C^3), 68.6 (d, J = 13.3, CH_2). $^{19}\text{F-NMR}$ (d_6 -DMSO, 282 MHz) δ = -100.1 (1F, m), -103.5 (1F, m). MS(ES+) m/z = 234 (M^+). IR (KBr disc) $\bar{\nu}$ = 1689 cm^{-1} (ketone, C=O stretch).

6.1.14 1-(2-Oxo-2-pyridin-2-ylethyl)pyridinium iodide

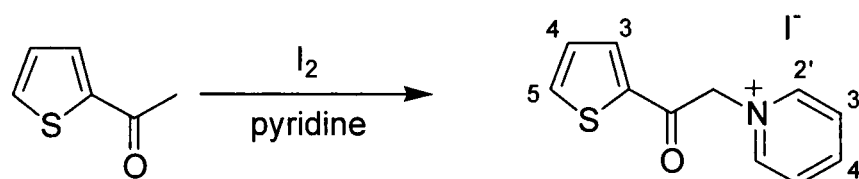


A solution of iodine (6.6 g, 26.0 mmol) in pyridine (15 ml) was added at room temperature to a solution of 2-acetylpyridine (2.8 ml, 25.0 mmol) in pyridine (5 ml), then heated to 100°C for 3 h. After cooling to room temperature and standing overnight, the resulting precipitate was isolated by filtration and washed with pyridine, dissolved in a hot mixture of ethanol (40 ml) and water (80 ml), then treated with decolourising charcoal and filtered whilst still hot. Reduction in volume of the filtrate followed by

cooling resulted in a brown precipitate that was collected by filtration, washed with cold water and dried under vacuum to give the desired product as a pale brown solid (4.71 g, 58%).

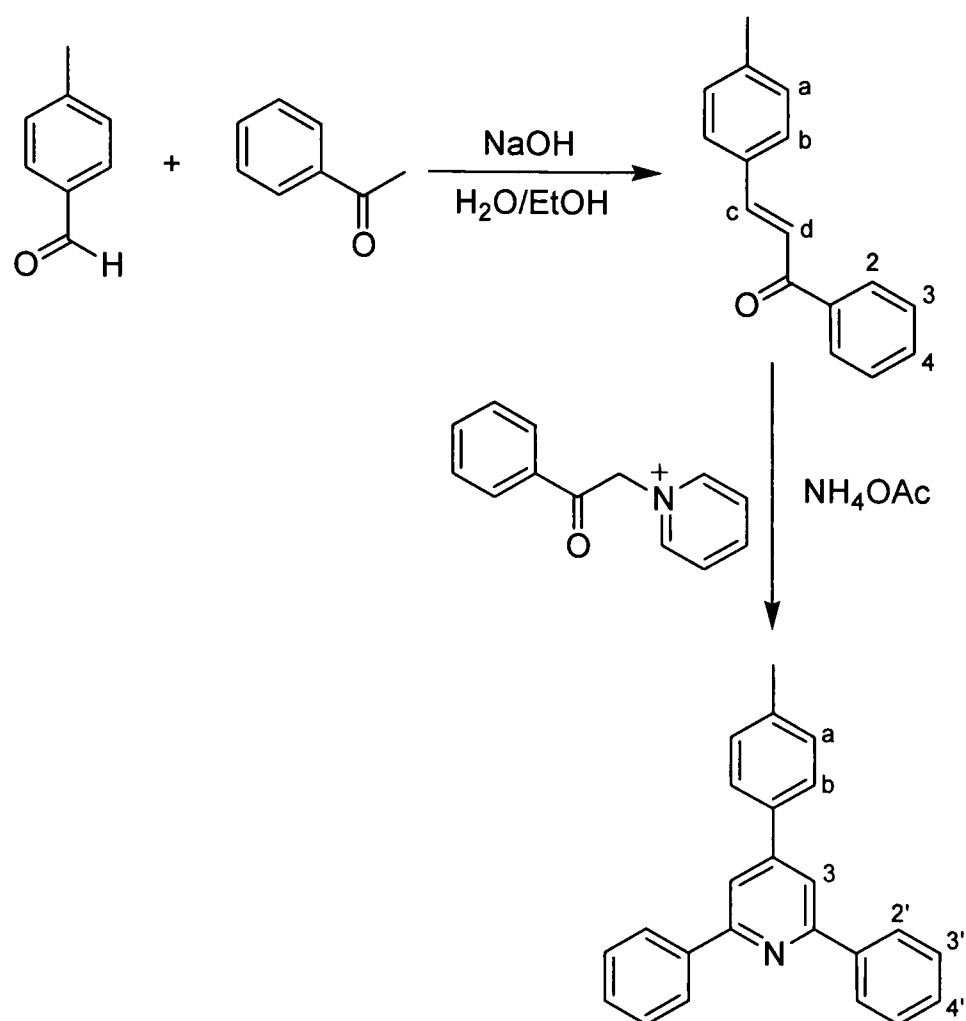
$^1\text{H-NMR}$ (d_6 -DMSO, 300 MHz) δ = 9.02 (2H, d, J = 5.5, $\text{H}^{2'}$), 8.88 (1H, d, J = 4.6, H^6), 8.74 (1H, t, J = 7.8, $\text{H}^{4'}$), 8.29 (2H, dd, J = 7.6, 6.7, $\text{H}^{3'}$), 8.15 (1H, td, J = 7.6, 1.6, H^4), 8.08 (1H, d, J = 7.8, H^3), 7.84 (1H, ddd, J = 7.3, 4.8, 1.4, H^5), 6.52 (2H, s, CH_2). $^{13}\text{C}\{^1\text{H}\}$ -NMR (d_6 -DMSO, 101 MHz) δ = 191.4 (C=O), 150.4 (C^q), 149.5 (CH), 146.3 (C^{py^+}), 146.3 (C^{py^+}), 138.1 (CH), 129.1 (CH), 127.7 (C^{py^+}), 122.0 (CH), 66.6 (CH_2). MS(ES+) m/z = 199 (M^+). MS(ES-) m/z = 127 (I^-). IR (KBr disc) $\bar{\nu}$ = 1710 cm^{-1} (ketone, C=O stretch).

6.1.15 1-(2-Oxo-2-(2-thienyl)ethyl)pyridinium iodide



2-Acetylthiophene (2.05 ml, 19.0 mmol) was added at room temperature to a solution of iodine (5.24 g, 20.6 mmol) in pyridine (20 ml), then heated to 100°C for 4 h. After cooling to room temperature and standing overnight, the resulting precipitate was isolated by filtration and washed with pyridine, dissolved in a hot mixture of ethanol (50 ml) and water (50 ml), then treated with decolourising charcoal and filtered whilst still hot. Reduction in volume of the filtrate followed by cooling resulted in an orange precipitate that was collected by filtration, washed with cold water and dried under vacuum to give the desired product as an orange solid (3.62 g, 58%).

$^1\text{H-NMR}$ (d_6 -DMSO, 400 MHz) δ = 9.03 (2H, d, J = 6.0, $\text{H}^{2'}$), 8.75 (1H, t, J = 7.8, $\text{H}^{4'}$), 8.28 (2H, t, J = 6.9, $\text{H}^{3'}$), 8.24 (1H, dd, J = 4.9, 1.1, H^3 or H^5), 8.22 (1H, dd, J = 3.9, 1.1, H^3 or H^5), 7.42 (1H, dd, J = 4.9, 3.9, H^4), 6.43 (2H, s, CH_2). $^{13}\text{C}\{^1\text{H}\}$ -NMR (d_6 -DMSO, 101 MHz) δ = 183.5 (C=O), 146.5 (C^{py^+}), 146.3 (C^{py^+}), 139.2 (C^q), 136.8 (CH), 134.9 (CH), 129.3 (CH), 127.8 (C^{py^+}), 65.6 (CH_2). MS(ES+) m/z = 204 (M^+). IR (KBr disc) $\bar{\nu}$ = 1662 cm^{-1} (ketone, C=O stretch). Characterisation data are consistent with that in the literature.³⁵⁷

6.1.16 4-*p*-Tolyl-2,6-diphenylpyridine **91** [tdppyH₂]*1-Phenyl-3-p-tolyl-propenone*

A solution of *p*-tolualdehyde (1.9 ml, 16.1 mmol), acetophenone (2.9 ml, 24.5 mmol) and sodium hydroxide (1.00 g, 25.0 mmol) in a mixture of water (30 ml) and ethanol (60 ml) was stirred at room temperature for 2 h. After this period, the resulting precipitate was isolated by filtration, washed with water, and dried under vacuum to give the desired product as a pale yellow solid (3.68 g, 100%).

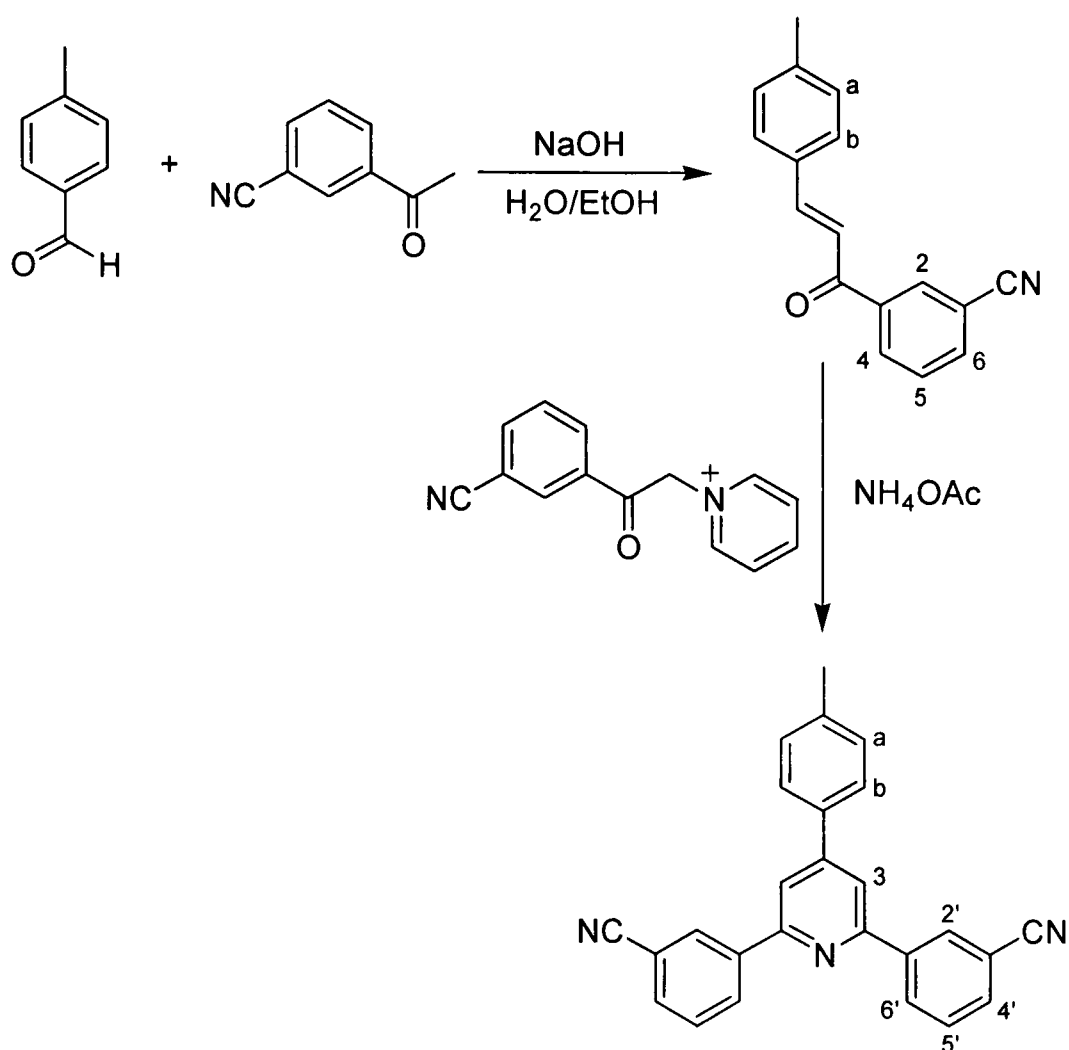
¹H-NMR (CDCl₃, 400 MHz) δ = 8.02 (2H, d, J = 8.1, H²), 7.81 (1H, d, J = 15.7, H^c), 7.47-7.62 (6H, m, H^b, H^d, H³ & H⁴), 7.23 (2H, d, J = 8.1, H^a), 2.40 (3H, s, Me). ¹H-NMR (d₆-DMSO, 500 MHz) δ = 8.14 (2H, dd, J = 8.0, 1.5, H²), 7.89 (1H, d, J = 15.4, H^c), 7.79 (2H, d, J = 8.1, H^b), 7.72 (1H, d, J = 15.8, H^d), 7.67 (1H, tt, J = 7.3, 1.3, H⁴), 7.58 (2H, t, J = 7.5, H³), 7.28 (2H, d, J = 8.1, H^a), 2.36 (3H, s, Me). ¹³C{¹H}-NMR (CDCl₃, 101 MHz) δ = 190.8 (C=O), 145.1 (CH), 141.2 (C^q), 138.5 (C^q), 132.8 (CH), 132.3 (C^q), 129.8 (CH), 128.7 (CH), 128.6 (CH), 128.6 (CH), 121.3 (CH), 21.7 (CH₃). MS(EI) *m/z* = 222 (M⁺), 221 (M⁺ - H), 207 (M⁺ - CH₃), 145 (CH₃C₆H₄CHCH(CO)⁺), 105 (C₆H₅(CO)⁺), 77 (C₆H₅⁺). IR (KBr disc) $\bar{\nu}$ = 1655 cm⁻¹ (ketone, C=O stretch). One spot by TLC(silica), R_f = 0.4 in hexane/diethyl ether, 90/10.

*4-p-Tolyl-2,6-diphenylpyridine 91 [tdppyH₂]**

A solution of 1-phenyl-3-*p*-tolyl-propenone (2.45 g, 11.0 mmol), 1-(2-oxo-2-phenylethyl)pyridinium iodide (3.58 g, 11.0 mmol) and ammonium acetate (11.0 g, 143.0 mmol) in glacial acetic acid (15 ml) was heated under reflux at 116°C for 1 h. After cooling to room temperature and addition of water (50 ml), the resulting precipitate was collected by filtration and washed with water. Recrystallisation from ethanol gave the desired product as a white solid (2.56 g, 73%), mp 114.2-116.4°C.

¹H-NMR (CDCl₃, 300 MHz) δ = 8.20 (4H, dd, J = 6.7, 1.5, H^{2'}), 7.88 (2H, s, H³), 7.66 (2H, d, J = 7.9, H^b), 7.52 (4H, t, J = 7.5, H^{3'}), 7.45 (2H, tt, J = 7.1, 1.4, H^{4'}), 7.34 (2H, d, J = 7.9, H^a), 2.44 (3H, s, Me). ¹³C{¹H}-NMR (CDCl₃, 126 MHz) δ = 157.6 (C^q), 150.2 (C^q), 139.8 (C^q), 139.2 (C^q), 136.2 (C^q), 130.0 (C^a), 129.1 (C^{4'}), 128.8 (C^{3'}), 127.3 (C^{2'}), 127.1 (C^b), 117.0 (C³), 21.4 (CH₃). MS(ES+) *m/z* = 322 ([M+H]⁺). Found: C, 89.59; H, 6.00; N, 4.39%. C₂₄H₁₉N requires: C, 89.68; H, 5.96; N, 4.36%. Characterisation data are consistent with that in the literature.⁴⁵⁶

* An adaptation of the procedure used for the synthesis of 2,4,6-triphenylpyridine was followed.²⁸⁶

6.1.17 4-*p*-Tolyl-2,6-di(3-cyanophenyl)pyridine **92** [tcdppyH₂]*3-(3-p-tolyl-prop-2-enoyl)benzonitrile*

A solution of *p*-tolualdehyde (1.8 ml, 15.4 mmol), 3-acetylbenzonitrile (2.20 g, 15.2 mmol) and sodium hydroxide (0.68 g, 17.0 mmol) in a mixture of water (20 ml) and ethanol (50 ml) was stirred at room temperature for 2½ h. After this period, the resulting yellow precipitate was collected by filtration, washed with water and dried under vacuum, to give the desired product as a pale yellow solid (3.53 g, 94%), mp 152.7-154.2°C.

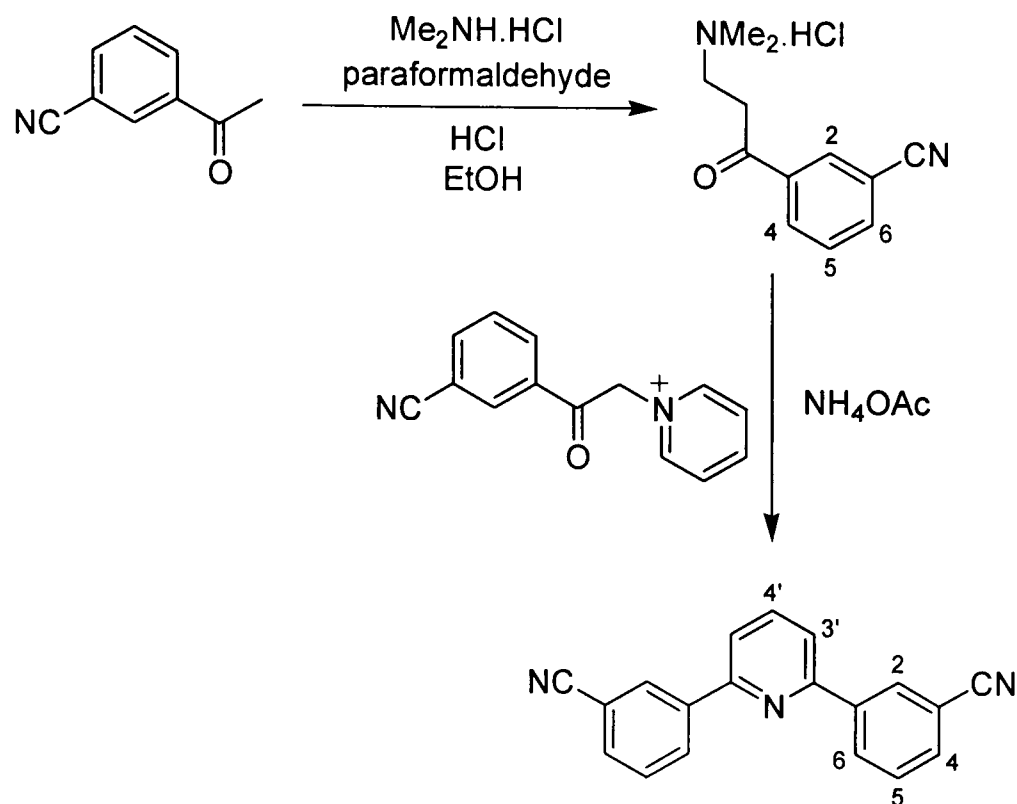
¹H-NMR (CDCl₃, 400 MHz) δ = 8.29 (1H, s, H²), 8.23 (1H, dt, J = 8.3, 1.5, H⁴ or H⁶), 7.86 (1H, dt, J = 7.3, 1.3, H⁴ or H⁶), 7.84 (1H, d, J = 15.9, vinyl), 7.64 (1H, t, J = 7.9, H⁵), 7.57 (2H, d, J = 8.1, H^b), 7.43 (1H, d, J = 15.7, vinyl), 7.25 (2H, d, J = 7.9, H^a), 2.41 (3H, s, Me). ¹H-NMR (*d*₆-DMSO, 300 MHz) δ = 8.70 (1H, t, J = 1.4, H²), 8.40 (1H, dt, J = 8.0, 1.4, H⁴ or H⁶), 8.14 (1H, dt, J = 7.7, 1.3, H⁴ or H⁶), 7.98 (1H, d, J = 15.6, vinyl), 7.75-7.86 (4H, m, vinyl, H^b & H⁵), 7.30 (2H, d, J = 8.0, H^a), 2.38 (3H, s, Me). ¹³C{¹H}-NMR (*d*₆-DMSO, 101 MHz) δ = 187.5 (C=O), 145.3 (CH), 141.1 (C^q), 138.3 (C^q), 136.2 (CH), 132.7 (CH), 132.3 (CH), 131.8 (C^q), 130.1 (CH), 129.5 (CH), 129.2 (CH), 120.4 (CH), 118.2 (C^q), 112.0 (C^q), 21.1 (CH₃). MS(EI) *m/z* = 247 (M⁺),

246 ($M^+ - H$), 232 ($M^+ - CH_3$), 145 ($CH_3C_6H_4CHCH(CO)^+$), 130 ($NCC_6H_4(CO)^+$), 102 ($NCC_6H_4^+$). IR (KBr disc) $\bar{\nu} = 1665\text{ cm}^{-1}$ (ketone, C=O stretch), 2231 cm^{-1} (nitrile, C≡N stretch).

4-p-Tolyl-2,6-di(3-cyanophenyl)pyridine 92 [tcdppyH₂]

A solution of 3-(3-*p*-tolyl-prop-2-enoyl)benzotrile (2.72 g, 11.0 mmol), 2-(1-(3-cyanophenyl)-1-oxoethyl)pyridinium iodide (3.85 g, 11.0 mmol) and ammonium acetate (11.0 g, 143.0 mmol) in glacial acetic acid (15 ml) was heated under reflux at 116°C for 1 h. After cooling to room temperature and addition of water (50 ml), the resulting precipitate was collected by filtration, washed with water, and dried under vacuum to give the desired product as a pale yellow solid (3.51 g, 85%), mp 221.2-223.2°C.

¹H-NMR (CDCl₃, 500 MHz) $\delta = 8.47$ (2H, s, H^{2'}), 8.43 (2H, d, $J = 8.1$, H^{6'}), 7.93 (2H, s, H³), 7.75 (2H, d, $J = 7.5$, H^{4'}), 7.63 - 7.68 (4H, m, H^b & H^{5'}), 7.37 (2H, d, $J = 7.9$, H^a), 2.47 (3H, s, Me). ¹H-NMR (*d*₆-DMSO, 300 MHz) $\delta = 8.72$ (2H, t, $J = 1.8$, H^{2'}), 8.64 (2H, dt, $J = 7.9, 1.8$, H^{5'}), 8.31 (2H, s, H³), 7.98 (2H, d, $J = 7.9$, H^b), 7.89 (2H, dt, $J = 7.5, 1.3$, H^{4'}), 7.74 (2H, t, $J = 7.7$, H^{6'}), 7.37 (2H, d, $J = 7.9$, H^a), 2.41 (3H, s, Me). ¹³C{¹H}-NMR (CDCl₃, 126 MHz) $\delta = 155.5$ (C^q), 151.3 (C^q), 140.4 (C^q), 140.0 (C^q), 135.1 (C^q), 132.7 (C^{4'}), 131.4 (C^{6'}), 130.9 (C^{2'}), 130.2 (C^a), 129.8 (C^b or C^{5'}), 127.1 (C^b or C^{5'}), 118.9 (C^q), 117.9 (C³), 113.2 (C^q), 21.5 (CH₃). MS(ES+) $m/z = 371$ ([M+H]⁺). IR (KBr disc) $\bar{\nu} = 2228\text{ cm}^{-1}$ (nitrile, C≡N stretch). Found: C, 81.69; H, 4.58; N, 11.24%. C₂₆H₁₇N₃·½H₂O requires: C, 82.08; H, 4.77; N, 11.05%. One spot by TLC(silica), R_f = 0.4 in dichloromethane.

6.1.18 2,6-Di(3-cyanophenyl)pyridine **94** [cdppyH₂]*Hydrochloride salt of 3-(3-dimethylaminopropionyl)benzonitrile**

A solution of 3-acetylbenzonitrile (1.44 g, 9.9 mmol), paraformaldehyde (390 mg), dimethylamine hydrochloride (1.06 g, 13.0 mmol) and concentrated hydrochloric acid (20 μ l) in ethanol (10 ml) was heated under reflux at 78°C under a nitrogen atmosphere overnight. After cooling to room temperature, the resulting precipitate was collected by filtration, washed with ethanol, and dried under vacuum to give the desired product as a white solid (1.32 g, 56%), mp 197.8-198.5°C.

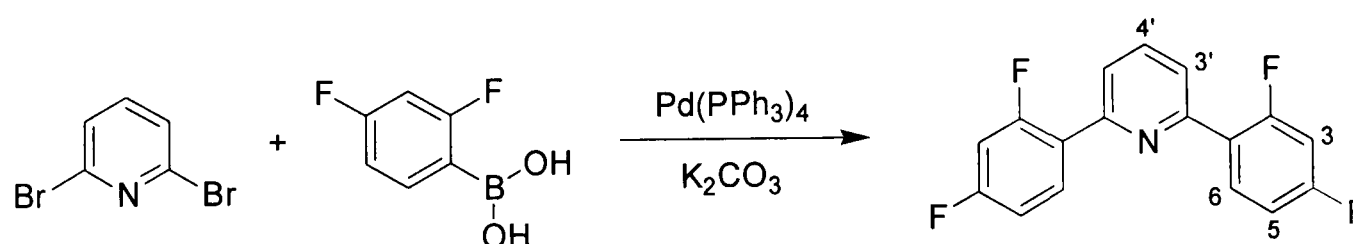
¹H-NMR (*d*₆-DMSO, 400 MHz) δ = 10.70 (1H, br s, NH), 8.51 (1H, t, *J* = 1.6, H²), 8.28 (1H, ddd, *J* = 8.0, 1.7, 1.2, H⁴ or H⁶), 8.16 (1H, dt, *J* = 7.8, 1.4, H⁴ or H⁶), 7.79 (1H, t, *J* = 7.9, H⁵), 3.67 (2H, t, *J* = 7.2, CH₂), 3.40 (2H, t, *J* = 7.1, CH₂), 2.80 (6H, s, Me). ¹³C{¹H}-NMR (*d*₆-DMSO, 101 MHz) δ = 195.4 (C=O), 136.8 (CH), 136.7 (C^q), 132.2 (CH), 132.1 (CH), 130.2 (CH), 118.1 (C^q), 112.0 (C^q), 51.4 (CH₂), 42.1 (CH₃), 33.4 (CH₂). MS(ES+) *m/z* = 203 ([M+H]⁺). IR (KBr disc) $\bar{\nu}$ = 1687 cm⁻¹ (ketone, C=O stretch), 2228 cm⁻¹ (nitrile, C≡N stretch).

* An adaptation of the procedure used for the synthesis of 1-(3-bromophenyl)-3-dimethylaminopropanone was followed.⁴⁵⁷

2,6-Di(3-cyanophenyl)pyridine 94 [cdppyH₂]^{*}

A solution of the hydrochloride salt of 3-(3-dimethylaminopropionyl)benzotrile (1.00 g, 4.19 mmol), 2-(1-(3-cyanophenyl)-1-oxoethyl)pyridinium iodide (1.73 g, 4.94 mmol) and ammonium acetate (4.94 g, 64.1 mmol) in glacial acetic acid (14 ml) was heated under reflux at 116°C for 1 h. After cooling to room temperature, the resulting precipitate was isolated by filtration, washed with water, and dried under vacuum to give the desired product as a pale brown solid (981 mg, 83%), mp 187.5-188.9°C.

¹H-NMR (CDCl₃, 400 MHz) δ = 8.43 (2H, td, J = 1.7, 0.6, H²), 8.38 (2H, ddd, J = 7.9, 1.9, 1.2, H⁴ or H⁶), 7.94 (1H, dd, J = 8.3, 7.3, H⁴), 7.78 (2H, d, J = 7.8, H^{3'}), 7.74 (2H, ddd, J = 7.7, 1.5, 1.3, H⁴ or H⁶), 7.64 (2H, td, J = 7.8, 0.6, H⁵). ¹H-NMR (d₆-DMSO, 300 MHz) δ = 8.68 (2H, s, H²), 8.58 (2H, d, J = 7.8, H⁴ or H⁶), 8.04-8.16 (3H, m, H^{3'} & H⁴), 7.94 (2H, d, J = 7.8, H⁴ or H⁶), 7.75 (2H, t, J = 7.8, H⁵). ¹³C{¹H}-NMR (CDCl₃, 101 MHz) δ = 155.0 (C^q), 140.1 (C^q), 138.5 (C^{4'}), 132.7 (C⁴ or C⁶), 131.3 (C⁴ or C⁶), 130.8 (C²), 129.8 (C⁵), 119.8 (C^{3'}), 118.9 (C^q), 113.2 (C^q). ¹³C{¹H}-NMR (d₆-DMSO, 101 MHz) δ = 153.9 (C^q), 139.5 (C^q), 139.1 (CH), 132.9 (CH), 131.5 (CH), 130.3 (CH), 130.2 (CH), 120.3 (CH), 118.8 (C^q), 112.1 (C^q). MS(ES+) *m/z* = 282 ([M+H]⁺), 304 ([M+Na]⁺). HRMS(ES+) *m/z* = 282.1025 ([M+H]⁺); calc. for C₁₉H₁₂N₃, 282.1026. IR (KBr disc) $\bar{\nu}$ = 2228 cm⁻¹ (nitrile, C≡N stretch). Found: C, 74.60; H, 4.51; N, 13.06%. C₁₉H₁₁N₃·1½H₂O requires: C, 74.01; H, 4.58; N, 13.63%. One spot by TLC(silica), R_f = 0.5 in dichloromethane. Characterisation data are consistent with that in the literature.⁴⁵⁸

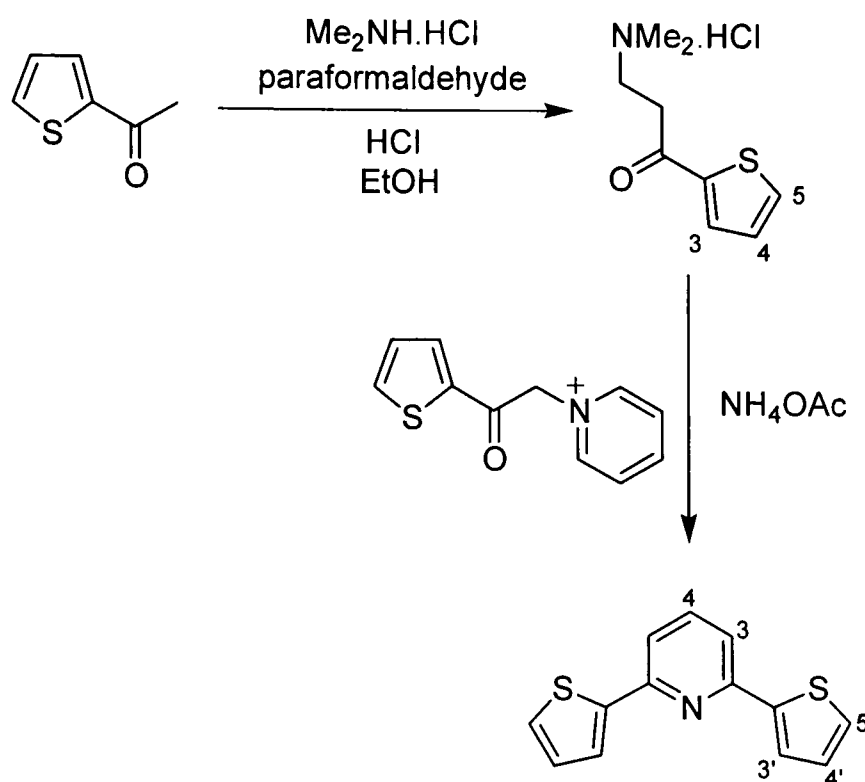
6.1.19 2,6-Di(2,4-difluorophenyl)pyridine 96 [F₄dppyH₂]

A combination of 2,6-dibromopyridine (820 mg, 3.46 mmol), 2,4-difluorophenylboronic acid (1.87 mg, 11.8 mmol) and potassium carbonate (3.23 g, 23.4 mmol) in a mixture of 1,2-dimethoxyethane (16 ml) and water (400 µl) was

^{*} An adaptation of the procedure used for the synthesis of 2,6-diphenylpyridine was followed.²⁸⁶

degassed by three freeze-pump-thaw cycles. Addition of tetrakis(triphenylphosphine)palladium(0) (274 mg, 0.24 mmol) was followed by stirring at room temperature under a nitrogen atmosphere for 30 minutes, before heating to 90°C overnight. The progress of the reaction was followed by TLC (alumina, hexane/ether, 50/50). After cooling to room temperature, the precipitated solid was removed by filtration and washed with 1,2-dimethoxyethane, followed by removal of solvent from the combined filtrates under reduced pressure. The residue was redissolved in dichloromethane (100 ml) and washed with dilute NaHCO₃ solution (3 × 100 ml). The organic layer was dried over MgSO₄ and the solvent removed under reduced pressure, before purification by column chromatography (silica, hexane/diethyl ether, gradient elution from 100/0 to 98/2) to give the desired product as a white solid (929 mg, 88%), mp 83.6-84.4°C.

¹H-NMR (CDCl₃, 500 MHz) δ = 8.14 (2H, td, J = 8.8, 6.8, H⁶), 7.83 (1H, t, J = 7.8, H^{4'}), 7.74 (2H, dd, J = 7.5, 1.9, H^{3'}), 7.03 (2H, td, J = 8.3, 2.1, H⁵), 6.93 (2H, ddd, J = 8.8, 6.3, 2.4, H³). ¹³C{¹H}-NMR (CDCl₃, 126 MHz) δ = 163.2 (dd, J = 309.4, 11.9, C² or C⁴), 161.2 (dd, J = 311.9, 12.1, C² or C⁴), 152.4 (d, J = 2.7, C^{2'}), 137.3 (s, C^{4'}), 132.4 (dd, J = 9.7, 4.5, C⁶), 123.7 (dd, J = 11.7, 3.7, C¹), 122.9 (d, J = 10.2, C^{3'}), 112.0 (dd, J = 21.1, 3.5, C⁵), 104.5 (dd, J = 26.8, 25.5, C³). ¹⁹F-NMR (CDCl₃, 470 MHz) δ = -109.5 (1F, m), -112.8 (1F, m). MS(EI) m/z = 303 (M⁺). Found: C, 66.91; H, 3.01; N, 4.64%. C₁₇H₉F₄N requires: C, 67.33; H, 2.99; N, 4.62%. One spot by TLC(silica), R_f = 0.6 in hexane/diethyl ether, 90/10.

6.1.20 2,6-Di(2-thienyl)pyridine **95** [dthpyH₂]*Hydrochloride salt of 2-(3-dimethylaminopropionyl)thiophene*³⁵⁷

A solution of 3-acetylthiophene (7.1 ml, 65.7 mmol), paraformaldehyde (4.40 g), dimethylamine hydrochloride (5.21 g, 63.9 mmol) and a few drops of concentrated hydrochloric acid in ethanol (30 ml) was heated under reflux at 78°C under a nitrogen atmosphere overnight. After cooling to 0°C, the precipitated solid was collected by filtration, washed with ice-cold ethanol, and dried under vacuum to give the desired product as a white solid (12.1 g, 84%), mp 182.3-184.8°C.

¹H-NMR (*d*₆-DMSO, 400 MHz) δ = 10.67 (1H, br s, NH), 8.07 (2H, t, J = 3.8, H³ & H⁵), 7.30 (1H, t, J = 4.5, H⁴), 3.57 (2H, t, J = 7.3, CH₂), 3.38 (2H, t, J = 7.3, CH₂), 2.78 (6H, s, Me). ¹³C{¹H}-NMR (*d*₆-DMSO, 101 MHz) δ = 189.6 (C=O), 142.7 (C^q), 135.5 (CH), 134.0 (CH), 128.8 (CH), 51.5 (CH₂), 42.2 (CH₃), 33.4 (CH₂). MS(ES+) *m/z* = 184 (M⁺). IR (KBr disc) $\bar{\nu}$ = 1651 cm⁻¹ (ketone, C=O stretch). Characterisation data are consistent with that in the literature.³⁵⁷

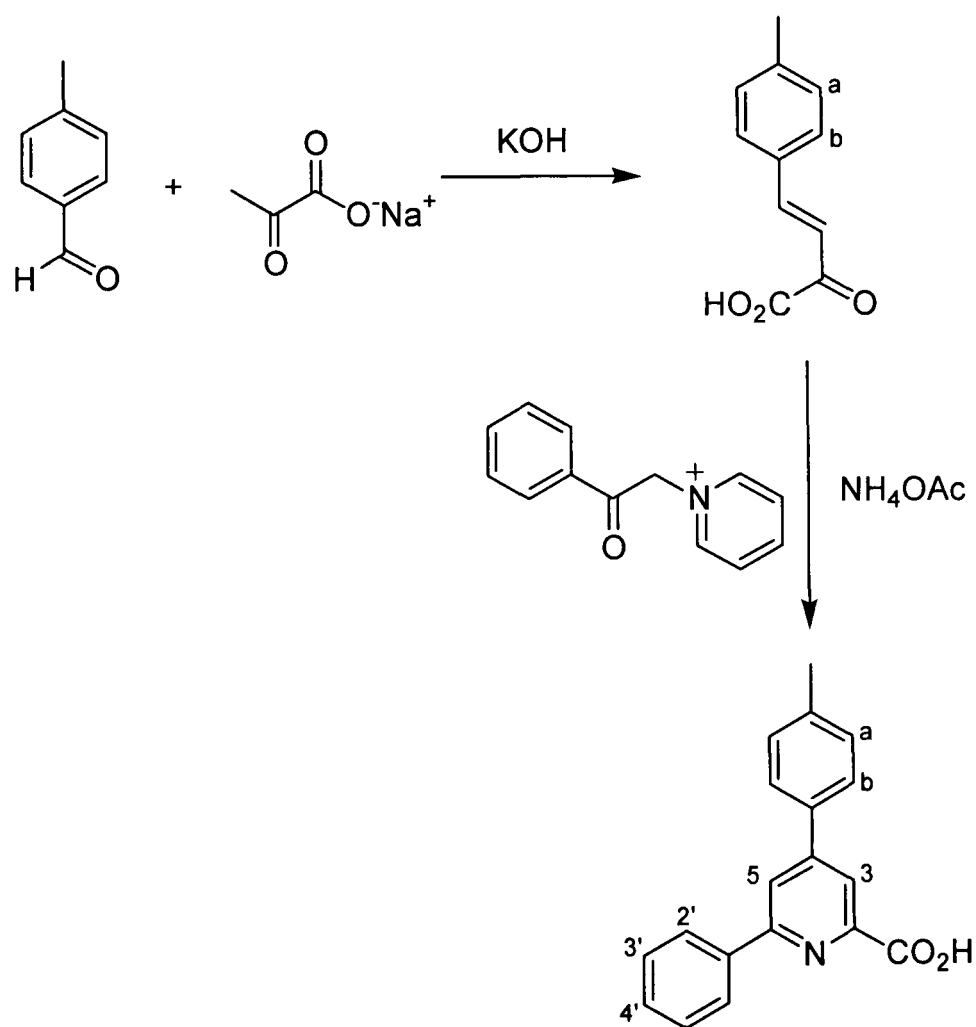
2,6-Di(2-thienyl)pyridine 95 [dthpyH₂]³⁵⁷

A solution of 1-(2-oxo-2-(2-thienyl)ethyl)pyridinium iodide (1.97 g, 5.95 mmol) and dry ammonium acetate (11.17 g, 145 mmol) in glacial acetic acid (12 ml) was heated to 100°C under a nitrogen atmosphere for 10 minutes, followed by addition of the hydrochloride salt of 2-(3-dimethylaminopropionyl)thiophene (1.30 g, 5.92 mmol) and heating to 105°C under a nitrogen atmosphere for 4 h. After cooling to room

temperature, a 1:1 mixture of water and methanol (40 ml) was added, and the solution decanted from the resulting brown oil. Reduction in volume of the aqueous solution precipitated the desired product as a pale yellow solid that was collected by filtration and dried under vacuum. Additional yield was obtained by recrystallisation of the brown oil from methanol, to give the desired product as a pale yellow solid (499 mg, 35%), mp 76.5-78.1°C.

$^1\text{H-NMR}$ (CDCl_3 , 400 MHz) $\delta = 7.67$ (1H, dd, $J = 8.3, 7.4$, H^4), 7.63 (2H, dd, $J = 3.7, 1.1$, $\text{H}^{3'}$), 7.49 (2H, d, $J = 7.8$, H^3), 7.41 (2H, dd, $J = 5.0, 1.1$, $\text{H}^{5'}$), 7.12 (2H, dd, $J = 5.0, 3.7$, $\text{H}^{4'}$). $^{13}\text{C}\{^1\text{H}\}\text{-NMR}$ (CDCl_3 , 101 MHz) $\delta = 152.3$ (C^9), 145.0 (C^9), 137.5 (C^4 or $\text{C}^{5'}$), 128.1 (C^4 or $\text{C}^{5'}$), 127.9 ($\text{C}^{4'}$), 124.8 ($\text{C}^{3'}$), 116.8 (C^3). MS(EI) $m/z = 243$ (M^+), 160 ($\text{M}^+ - \text{C}_4\text{H}_3\text{S}$). Found: C, 62.95; H, 3.85; N, 5.57%. $\text{C}_{13}\text{H}_9\text{NS}_2 \cdot \frac{1}{3}\text{H}_2\text{O}$ requires: C, 62.62; H, 3.91; N, 5.62%. One spot by TLC(silica), $R_f = 0.4$ in hexane/ethyl acetate, 80/20. Characterisation data are consistent with that in the literature.³⁵⁷

6.1.21 4-*p*-Tolyl-6-phenylpicolinic acid **93** [tppicH₂]



2-Oxo-4-*p*-tolyl-but-3-enoic acid⁴⁵⁹

A solution of *p*-tolualdehyde (4.9 ml, 41.6 mmol) in ethanol (200 ml) was combined with a solution of sodium pyruvate (5.02 g, 45.6 mmol) in water (50 ml) and

stirred at room temperature for 15 minutes, resulting in a clear yellow solution. After cooling to 0°C, KOH solution (1.4 mol dm⁻³, 100 ml) was added slowly ensuring that the temperature did not rise above 5°C, followed by stirring at room temperature for an additional 90 minutes. The solution was acidified with concentrated HCl, followed by concentration of the solution under reduced pressure. The resulting precipitate was isolated by filtration, washed with cold water, and purified by recrystallisation from water to give the desired product as a yellow solid (6.79 g, 86%).

¹H-NMR (*d*₆-Acetone, 400 MHz) δ = 7.84 (1H, d, *J* = 16.5, vinyl), 7.70 (2H, d, *J* = 8.0, H^b), 7.34 (1H, d, *J* = 16.5, vinyl), 7.31 (2H, d, *J* = 8.0, H^a), 2.39 (3H, s, Me). ¹³C{¹H}-NMR (*d*₆-Acetone, 101 MHz) δ = 185.2 (C=O), 164.0 (CO₂H), 148.8 (CH), 143.2 (C^q), 132.5 (C^q), 130.7 (CH), 130.0 (CH), 120.6 (CH), 21.5 (CH₃). MS(EI) *m/z* = 190 (M⁺), 145 (M⁺ - CO₂H), 117 (M⁺ - COCO₂H), 115 (M⁺ - COCO₂H, H₂), 91 (C₇H₇⁺), 65 (C₅H₅⁺). IR (KBr disc) $\bar{\nu}$ = 1684 cm⁻¹ (ketone, C=O stretch), 1713 cm⁻¹ (CO₂H, C=O stretch), 2900 cm⁻¹ (br, CO₂H, O-H stretch). Characterisation data are consistent with that in the literature.⁴⁶⁰

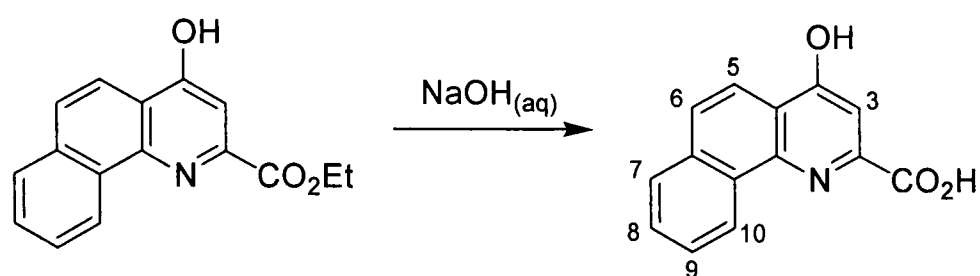
4-p-Tolyl-6-phenylpicolinic acid 93 [tppicH₂]

A solution of 2-oxo-4-*p*-tolyl-but-3-enoic acid (1.52 g, 7.99 mmol), 1-(2-oxo-2-phenylethyl)pyridinium iodide (3.58 g, 11.0 mmol) and ammonium acetate (5.55 g, 72.0 mmol) in water (50 ml) was heated under reflux at 100°C for 5½ h. The progress of the reaction was followed by TLC (silica, dichloromethane/methanol, 80/20). After cooling to room temperature, the resulting precipitate was collected by filtration, washed with acetone (3 × 20 ml), and dried under vacuum to give the desired product as a white solid (1.34 g, 58%), mp 155.6-159.0°C.

¹H-NMR (CDCl₃, 400 MHz) δ = 8.41 (1H, s, H³ or H⁵), 8.16 (1H, s, H³ or H⁵), 8.04 (2H, d, *J* = 7.4, H^{2'}), 7.67 (2H, d, *J* = 8.1, H^a or H^b), 7.48-7.58 (3H, m, H^{3'} & H^{4'}), 7.36 (2H, d, *J* = 7.8, H^a or H^b), 2.45 (3H, s, Me). ¹H-NMR (*d*₆-DMSO, 400 MHz) δ = 8.29 (1H, d, *J* = 1.6, H³ or H⁵), 8.26 (2H, d, *J* = 7.3, H^{2'}), 8.16 (1H, d, *J* = 1.5, H³ or H⁵), 7.84 (2H, d, *J* = 8.1, H^b), 7.51 (2H, t, *J* = 7.6, H^{3'}), 7.46 (1H, t, *J* = 7.1, H^{4'}), 7.35 (2H, d, *J* = 8.0, H^a), 2.37 (3H, s, Me). ¹³C{¹H}-NMR (*d*₆-DMSO, 101 MHz) δ = 167.5 (CO₂H), 156.5 (C^q), 152.7 (C^q), 148.9 (C^q), 139.2 (C^q), 138.5 (C^q), 134.3 (C^q), 129.9 (C^a), 129.3 (C^{4'}), 128.7 (C^{3'}), 127.2 (C³ or C⁵), 127.0 (C^b), 119.9 (C³ or C⁵), 119.1 (C^{2'}), 20.8 (CH₃). MS(ES+) *m/z* = 290 ([M+H]⁺). MS(EI) *m/z* = 289 (M⁺), 245 (M⁺ - CO₂). HRMS(EI) *m/z* = 290.1175 ([M+H]⁺); calc. for C₁₉H₁₆NO₂, 290.1176. IR (KBr disc) $\bar{\nu}$

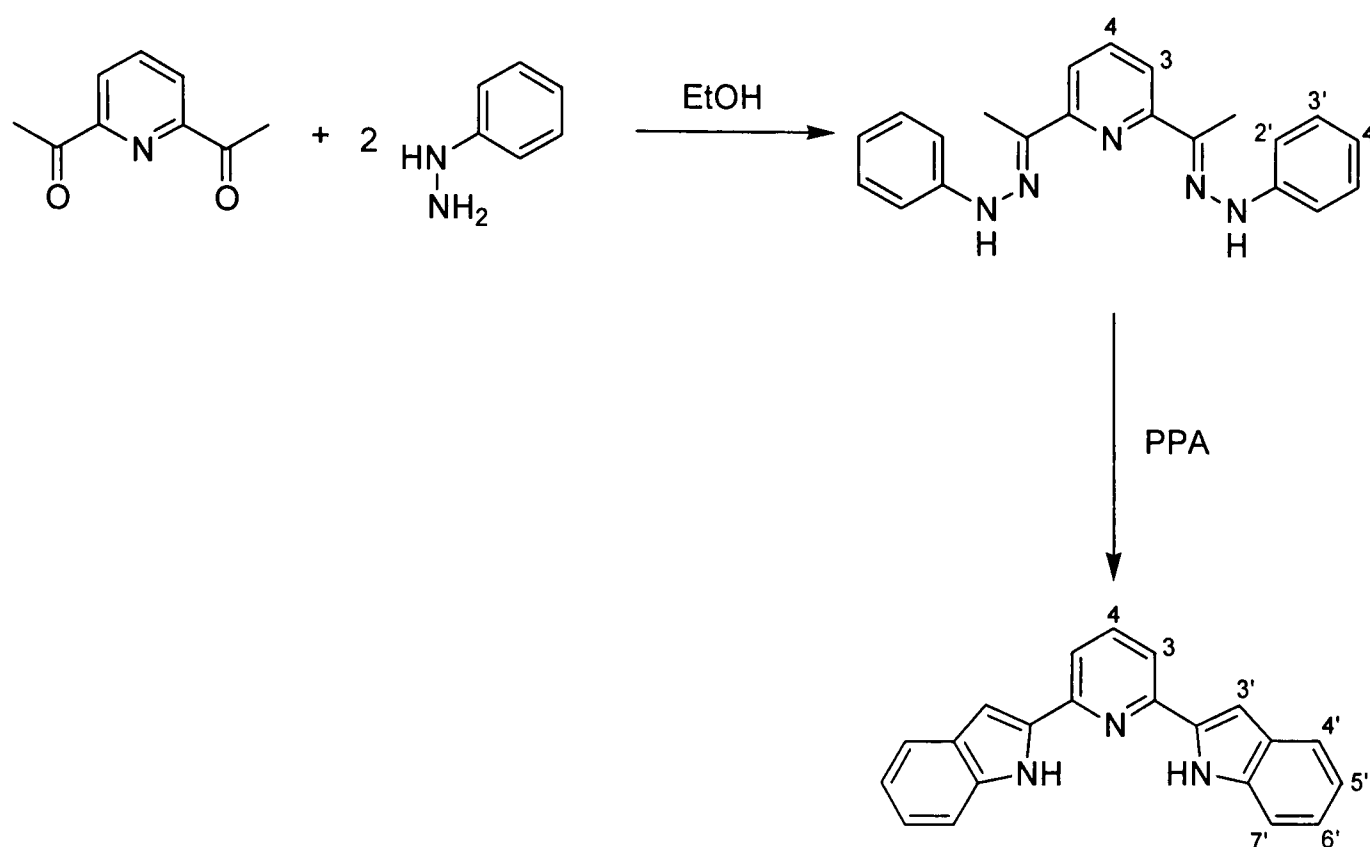
= 1571 cm^{-1} (CO_2H , $\text{C}=\text{O}$ stretch), 3000 cm^{-1} (br, CO_2H , $\text{O}-\text{H}$ stretch). One spot by TLC(silica), $R_f = 0.3$ in dichloromethane/methanol, 90/10.

6.1.22 4-Hydroxybenzo[*h*]quinoline-2-carboxylic acid [hbqcH_2]⁴⁶¹



A solution of 4-hydroxybenzo[*h*]quinoline-2-carboxylic acid ethyl ester (503 mg, 1.88 mmol) in 5% NaOH solution (10 ml) was heated under reflux at 100°C for 5 h. After cooling to room temperature, the reaction mixture was treated with decolourising charcoal and filtered. Addition of HCl (1 mol dm^{-3}) and isolation of the resulting precipitate by filtration, washing with water (2×10 ml), and drying under vacuum gave the desired product as a white solid (380 mg, 85%), mp >250°C.

$^1\text{H-NMR}$ (d_6 -DMSO, 500 MHz) $\delta = 9.31$ (1H, dd, $J = 5.9, 3.4$, H^7), 8.09 (1H, d, $J = 9.0$, H^5), 8.05 (1H, dd, $J = 6.0, 3.4$, H^{10}), 7.96 (1H, d, $J = 9.0$, H^6), 7.75-7.79 (2H, m, H^8 & H^9), 7.65 (1H, br s, H^3). $^{13}\text{C}\{^1\text{H}\}$ -NMR (d_6 -DMSO, 101 MHz) $\delta = 166.3$ (CO_2H), 163.0 (C^9), 147.1 (C^9), 145.8 (C^9), 133.7 (C^9), 130.4 (C^9), 128.7 (C^8 or C^{10}), 128.0 (C^9), 127.5 (C^6), 127.2 (C^8 or C^{10}), 124.8 (C^7), 119.2 (C^5), 119.1 (C^9), 106.8 (C^3). MS(EI) $m/z = 239$ (M^+), 195 ($\text{M}^+ - \text{CO}_2$). IR (KBr disc) $\bar{\nu} = 1627$ cm^{-1} (CO_2H , $\text{C}=\text{O}$ stretch), 3342 cm^{-1} (alcohol, $\text{O}-\text{H}$ stretch), 3400 cm^{-1} (br, CO_2H , $\text{O}-\text{H}$ stretch). Found: C, 67.98; H, 3.80; N, 5.75%. $\text{C}_{17}\text{H}_9\text{F}_4\text{N} \cdot \frac{1}{2}\text{H}_2\text{O}$ requires: C, 67.74; H, 4.06; N, 5.64%.

6.1.23 2,6-Di(2'-indolyl)pyridine **97** [*dinpyH₂*]*2,6-Di(1-N-phenylethanehydrazonoyl)pyridine*³⁹⁶

A solution of 2,6-diacetylpyridine (1.00 g, 6.13 mmol) and phenyl hydrazine (3.42 ml, 97% pure by mass, 34.76 mmol) in ethanol (20 ml), was heated under reflux at 78°C for 30 minutes. After cooling to 0°C, the resulting precipitate was collected by filtration and washed with cold ethanol (~5 ml). Recrystallisation from ethanol gave the desired product as a pale yellow solid (1.56 g, 74%).

¹H-NMR (CDCl₃, 400 MHz) δ = 8.08 (2H, d, J = 7.8, H³), 7.67 (1H, t, J = 7.8, H⁴), 7.54 (2H, br s, NH), 7.31 (4H, t, J = 7.6, H^{3'}), 7.22 (4H, d, J = 7.9, H^{2'}), 6.91 (2H, t, J = 7.3, H^{4'}), 2.45 (6H, s, Me). ¹³C{¹H}-NMR (CDCl₃, 101 MHz) δ = 154.9 (C^q), 144.9 (C^q), 142.6 (C^q), 136.1 (CH), 129.5 (CH), 120.6 (CH), 118.5 (CH), 113.4 (CH), 9.8 (Me). MS(ES+) m/z = 344 ([M+H]⁺), 366 ([M+Na]⁺). Characterisation data are consistent with that in the literature.³⁹⁶

2,6-Di(2'-indolyl)pyridine 97 [*dinpyH₂*]³⁹⁶

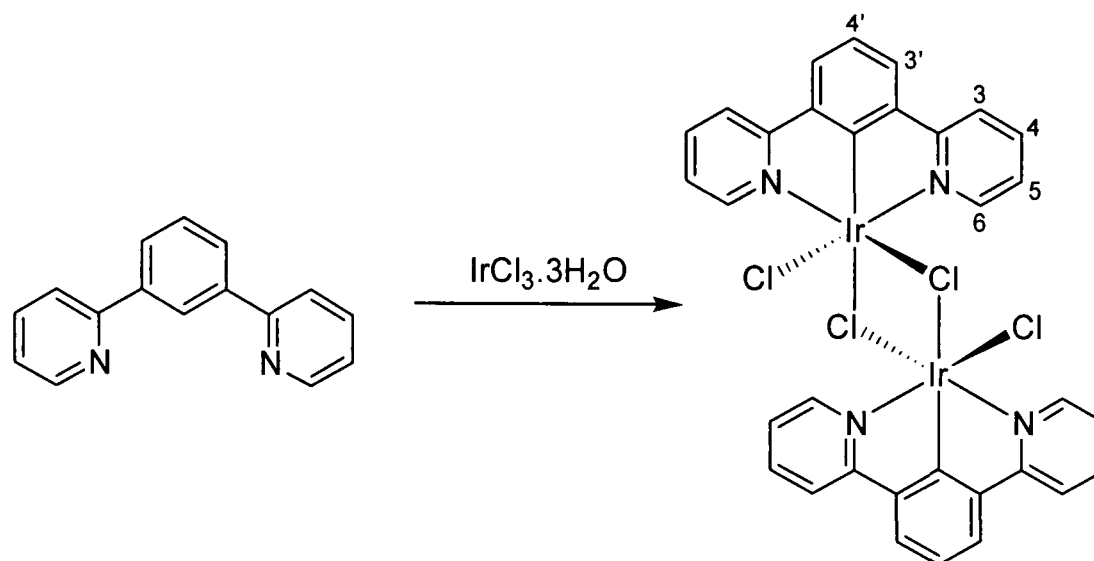
Polyphosphoric acid (~15 g) was added to 2,6-di(1-N-phenylethanehydrazonoyl)pyridine (1.56 g, 4.54 mmol) in a beaker, and heated to 120°C with stirring for 3 h. After cooling to room temperature, the reaction mixture was made basic with 10% NaOH solution. Extraction into dichloromethane (3 × 100 ml), washing with water

(3 × 100 ml), drying over Na₂CO₃ and removal of solvent under reduced pressure gave the desired product as a brown solid (871 mg, 62%), mp 251.0-253.6°C.

¹H-NMR (CDCl₃, 500 MHz) δ = 9.54 (2H, br s, NH), 7.76 (1H, t, J = 7.6, H⁴), 7.67-7.71 (4H, m, H³ & H^{4'}), 7.52 (2H, d, J = 8.2, H^{7'}), 7.27 (2H, ddd, J = 8.0, 7.1, 1.0, H^{6'}), 7.15 (2H, td, J = 7.6, 0.7, H^{5'}), 7.08 (2H, d, J = 1.3, H^{3'}). ¹H-NMR (*d*₆-Acetone, 300 MHz) δ = 11.0 (2H, br s, NH), 7.90 (3H, s, H³ & H⁴), 7.64 (2H, d, J = 8.0, H^{4'}), 7.48 (2H, d, J = 8.2, H^{7'}), 7.23 (2H, d, J = 1.5, H^{3'}), 7.19 (2H, ddd, J = 8.1, 7.1, 1.1, H^{6'}), 7.06 (2H, ddd, J = 8.0, 7.0, 0.7, H^{5'}). ¹³C{¹H}-NMR (CDCl₃, 101 MHz) δ = 149.9 (C^q), 137.4 (C⁴), 136.6 (C^q), 136.5 (C^q), 129.3 (C^q), 123.5 (C^{6'}), 121.4 (C³ or C^{4'}), 120.5 (C^{5'}), 118.4 (C³ or C^{4'}), 111.5 (C^{7'}), 101.4 (C^{3'}). MS(EI) *m/z* = 309 (M⁺). Found: C, 79.83; H, 4.92; N, 13.28%. C₂₁H₁₅N₃·½H₂O requires: C, 79.22; H, 5.07; N, 13.20%. One spot by TLC(silica), R_f = 0.3 in hexane/ethyl acetate, 80/20. Characterisation data are consistent with that in the literature.³⁹⁶

6.2 Synthesis of iridium(III) complexes

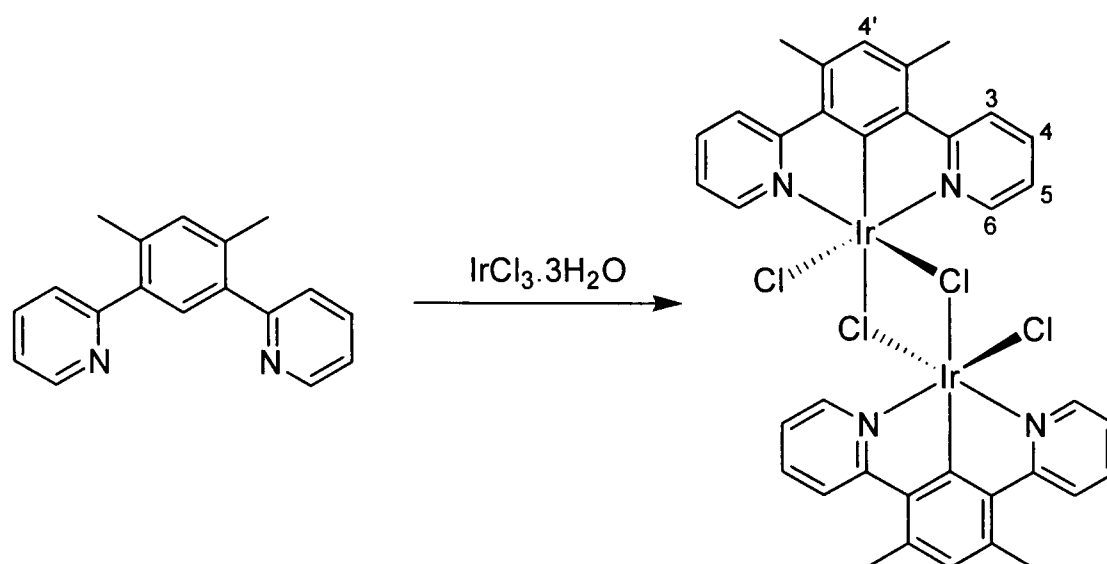
6.2.1 Bis(μ -chloro)bis(1,3-di(pyrid-2-yl)-benzene- $N,C^{2'},N$ iridium chloride) $[\text{Ir}(\text{dpyb})\text{Cl}(\mu\text{-Cl})]_2$



A suspension of 1,3-di(pyridin-2-yl)benzene (dpybH) (201 mg, 0.87 mmol) and iridium trichloride trihydrate (299 mg, 0.85 mmol) in a mixture of 2-ethoxyethanol (15 ml) and water (5 ml) was heated under reflux at 130°C for 2½ h. After cooling to room temperature, the precipitated solid was collected by centrifuge, washed with ethanol (2 × 20 ml), and dried under vacuum to give the desired product as an orange solid (342 mg).

This mixture of intermediate compounds has low solubility in all common solvents, and was used without further purification or characterisation. For further discussion of the nature of this intermediate, see Section 3.2.

6.2.2 Bis(μ -chloro)bis(1,5-di(pyrid-2-yl)-2,4-dimethylbenzene- $N,C^{6'}$, N iridium chloride) **104** $[\text{Ir}(\text{dpydmb})\text{Cl}(\mu\text{-Cl})]_2$



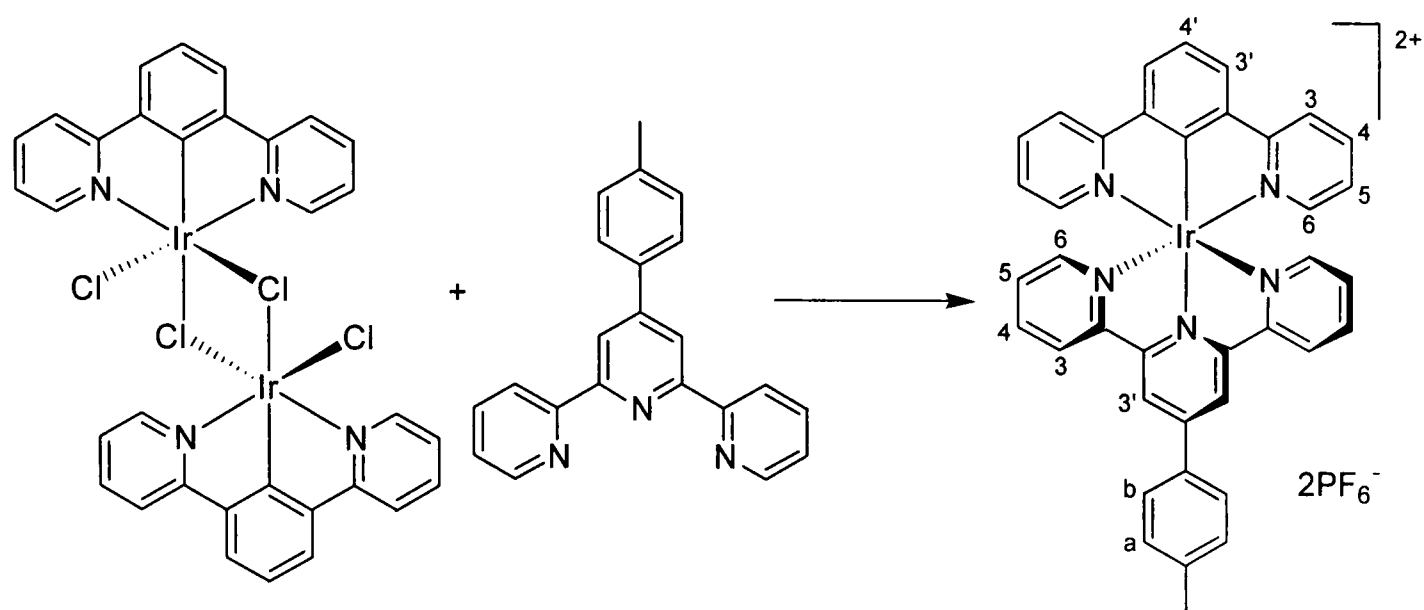
A suspension of 1,5-di(pyrid-2-yl)-2,4-dimethylbenzene (dpydmbH) (435 mg, 1.67 mmol) and iridium trichloride monohydrate (527 mg, 1.66 mmol) in a mixture of 2-ethoxyethanol (28 ml) and water (12 ml) was heated to 80°C for 6 h. After cooling to room temperature, the precipitate was collected by centrifuge, washed with ethanol (3 × 10 ml), and dried under vacuum to give the desired product as a yellow solid (348 mg). Further product was obtained by repeating this procedure with the remaining solution a further two times (total yield 588 mg, 70%), mp > 250°C.

MS(MALDI, DCTB matrix) $m/z = 1259$ ($[\text{M-Cl}+\text{DCTB}]^+$), 1044 (M^+), 737 ($[\text{Ir}(\text{dpydmb})\text{Cl}_2\text{-Cl}+\text{DCTB}]^+$), 522 ($[\text{Ir}(\text{dpydmb})\text{Cl}_2]^+$).

Although the chloride bridged dimer is poorly soluble in all common solvents, heating the solid in d_6 -DMSO results in a solution of the monomeric, d_6 -DMSO solvated, $\text{Ir}(\text{dpydmb})(d_6\text{-DMSO})\text{Cl}_2$.

$^1\text{H-NMR}$ (d_6 -DMSO, 400 MHz) $\delta = 9.21$ (2H, dd, $J = 5.6, 1.2$, H^6), 8.18 (2H, d, $J = 8.4$, H^3), 8.06 (2H, td, $J = 8.0, 2.0$, H^4), 7.54 (2H, ddd, $J = 6.8, 5.6, 1.4$), 6.98 (1H, s, $\text{H}^{4'}$), 2.76 (6H, s, Me). See Section 3.2 and Appendix A for crystal structure.

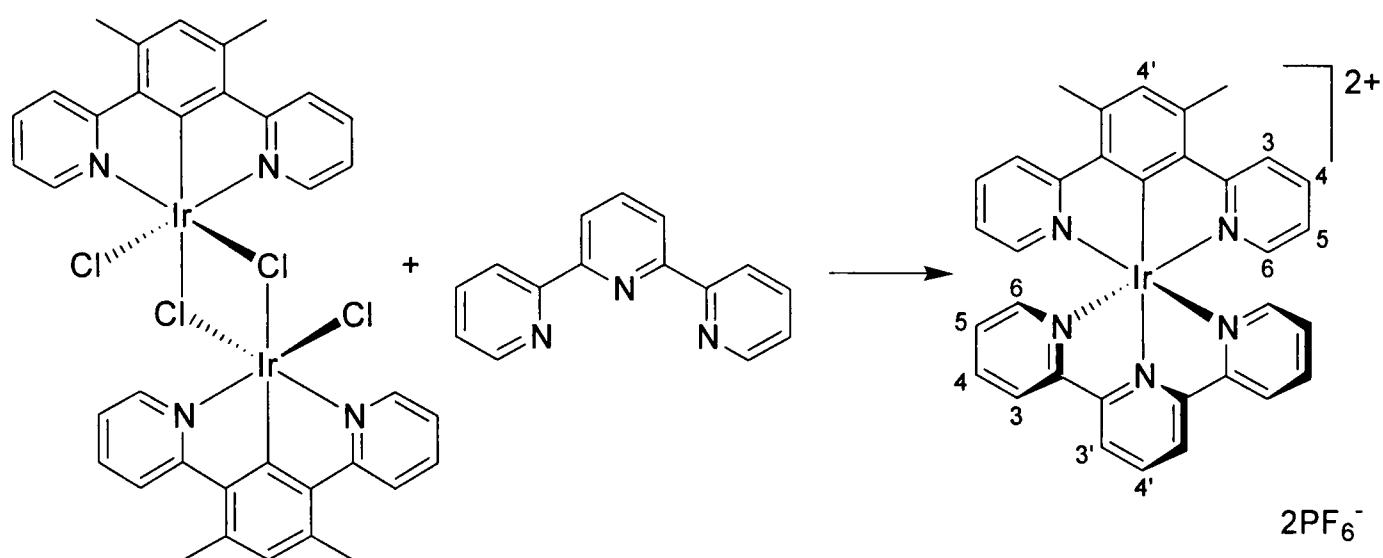
6.2.3 Iridium(1,3-di(pyrid-2-yl)-benzene-N,C^{2'},N)(4'-(*p*-tolyl)-2,2':6',2''-terpyridine)²⁺ **100** [Ir(dpyb)(ttpy)]²⁺



A suspension of bis(μ -chloro)bis(1,3-di(pyrid-2-yl)-benzene-N,C^{2'},N) iridium chloride ([Ir(dpyb)Cl(μ -Cl)]₂) (320 mg) and 4'-(*p*-tolyl)-2,2':6',2''-terpyridine (ttpy) (160 mg, 0.49 mmol) in ethylene glycol (15 ml) was heated to 196°C under a nitrogen atmosphere for 1 h. After cooling to room temperature, the reaction mixture was added to water (20 ml) and filtered. Saturated KPF₆ solution was added, and the resulting red precipitate collected by centrifugation, washed with water (3 × 20 ml) and dried under vacuum. Purification by column chromatography (alumina, acetonitrile) followed by a second column (silica, acetonitrile/water/saturated KNO₃ solution, gradient elution from 100/0/0 to 93.8/6.0/0.2) gave the desired product as a red solid (8 mg, 1%).

¹H-NMR (*d*₆-Acetone, 500 MHz) δ = 9.43 (2H, s, H^{3'} ttpy), 9.03 (2H, d, *J* = 8.2, H³ ttpy), 8.42 (2H, d, *J* = 8.1, H³ dpyb), 8.33 (2H, d, *J* = 7.9, H^{3'} dpyb), 8.23 (2H, d, *J* = 8.2, H^b ttpy), 8.20 (2H, td, *J* = 8.0, 1.3, H⁴ ttpy), 7.98 (2H, td, *J* = 7.9, 1.3, H⁴ dpyb), 7.84 (2H, d, *J* = 5.8, H⁶ dpyb), 7.73 (1H, t, *J* = 7.9, H^{4'} dpyb), 7.57 (2H, dd, *J* = 5.8, 1.2, H⁶ ttpy), 7.54 (2H, d, *J* = 8.0, H^a ttpy), 7.45 (2H, ddd, *J* = 7.8, 5.7, 1.2, H⁵ ttpy), 7.13 (2H, ddd, *J* = 7.3, 5.9, 1.2, H⁵ dpyb), 2.48 (3H, s, Me ttpy). MS(ES⁺) *m/z* = 373.5 (M²⁺), 892 (M(PF₆)⁺).

6.2.4 Iridium(1,5-di(pyrid-2-yl)-2,4-dimethylbenzene-*N,C*^{6'},*N*)(2,2':6',2''-terpyridine)²⁺ **105** [Ir(dpydmb)(terpy)]²⁺

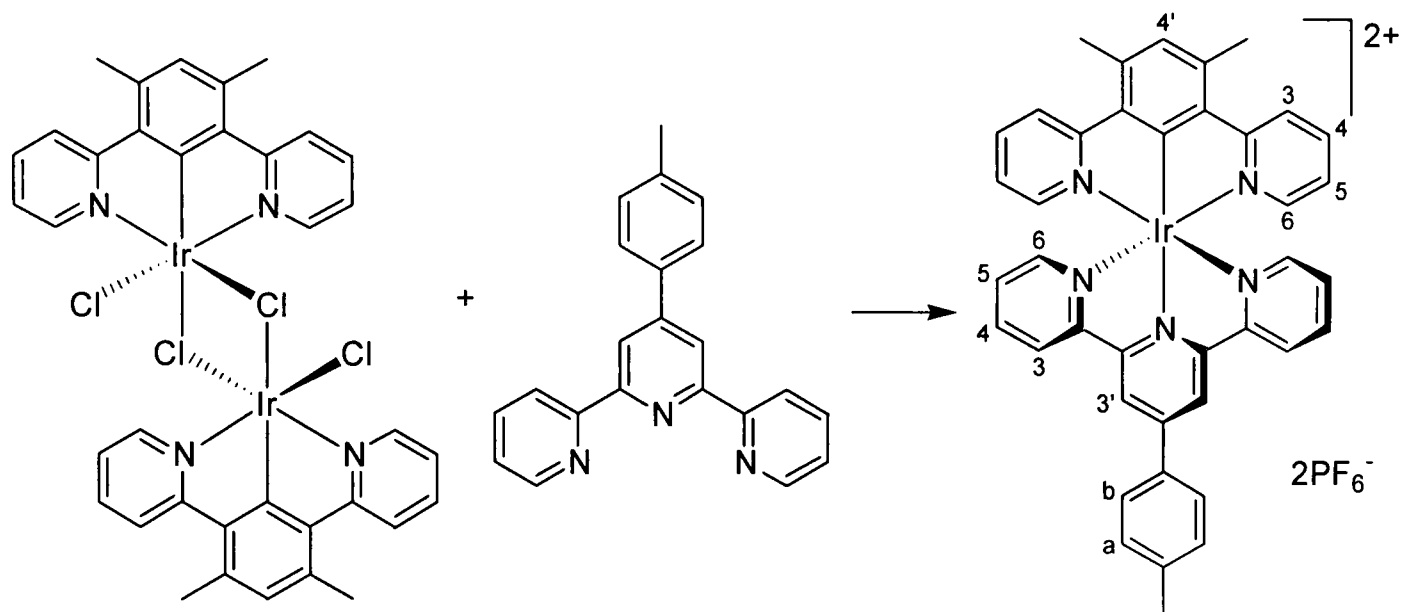


A suspension of bis(μ -chloro)bis(1,5-di(pyrid-2-yl)-2,4-dimethylbenzene-*N,C*^{6'},*N* iridium chloride) ([Ir(dpydmb)Cl(μ -Cl)]₂) (41 mg, 0.039 mmol) and 2,2':6',2''-terpyridine (terpy) (22 mg, 0.094 mmol) in ethylene glycol (5 ml) was heated to 196°C under a nitrogen atmosphere for 1 h. After cooling to room temperature, the reaction mixture was added to water (10 ml) and filtered. Saturated KPF₆ solution (20 ml) was added, and the resulting yellow precipitate collected by centrifugation, washed with water (3 × 10 ml) and dried under vacuum. Purification by column chromatography (silica, acetonitrile/water/saturated KNO₃ solution, gradient elution from 100/0/0 to 93.0/6.8/0.2) gave the desired product as a yellow solid (44 mg, 58%), mp > 250°C.

¹H-NMR (*d*₆-Acetone, 500 MHz) δ = 9.17 (2H, d, *J* = 8.3, H^{3'} terpy), 8.83-8.88 (3H, m, H^{4'} terpy & H³ terpy), 8.46 (2H, d, *J* = 8.5, H³ dpydmb), 8.22 (2H, td, *J* = 8.0, 1.4, H⁴ terpy), 7.98 (2H, ddd, *J* = 8.2, 7.6, 1.6, H⁴ dpydmb), 7.78 (2H, dd, *J* = 5.8, 0.9, H⁶ dpydmb), 7.70 (2H, dd, *J* = 5.8, 0.8, H⁶ terpy), 7.50 (2H, ddd, *J* = 7.6, 5.7, 1.2, H⁵ terpy), 7.43 (1H, s, H^{4'} dpydmb), 7.11 (2H, ddd, *J* = 7.3, 5.8, 1.1, H⁵ dpydmb), 3.02 (6H, s, Me). ¹³C{¹H}-NMR (*d*₆-Acetone, 126 MHz) δ = 178.3 (C^q), 170.7 (C^q), 160.4 (C^q), 156.2 (C⁶ terpy), 154.5 (C^q), 152.8 (C⁶ dpydmb), 142.7 (C^{4'} terpy), 142.1 (C⁴ terpy), 141.4 (C⁴ dpydmb), 140.6 (C^q), 138.0 (C^q), 133.9 (C^{4'} dpydmb), 130.1 (C⁵ terpy), 127.6 (C³ terpy), 126.6 (C^{3'} terpy), 125.5 (C³ dpydmb), 124.6 (C⁵ dpydmb), 22.6 (CH₃). MS(ES⁺) *m/z* = 342.5 (M²⁺), 830 (M(PF₆)⁺). HRMS(ES⁺) *m/z* = 830.1460 (M(PF₆)⁺); calc. for ¹⁹³IrC₃₃H₂₆F₆N₅P, 830.1459. One spot by TLC(silica), R_f = 0.4 in acetonitrile/water/saturated KNO₃ solution, 90/9/1. λ_{max} /nm (Acetonitrile) = 244

($\epsilon/\text{dm}^3 \text{ mol}^{-1} \text{ cm}^{-1}$ 33 700), 261 (38 500), 270 (35 300), 282 (32 800), 298 (26 000), 311 (25 400), 335 (13 100), 377 (10 100), 435 (700), 465 (500).

6.2.5 Iridium(1,5-di(pyrid-2-yl)-2,4-dimethylbenzene- N,C^6',N)(4'-(*p*-tolyl)-2,2':6',2''-terpyridine) $^{2+}$ **106** [Ir(dpydmb)(ttpy)] $^{2+}$



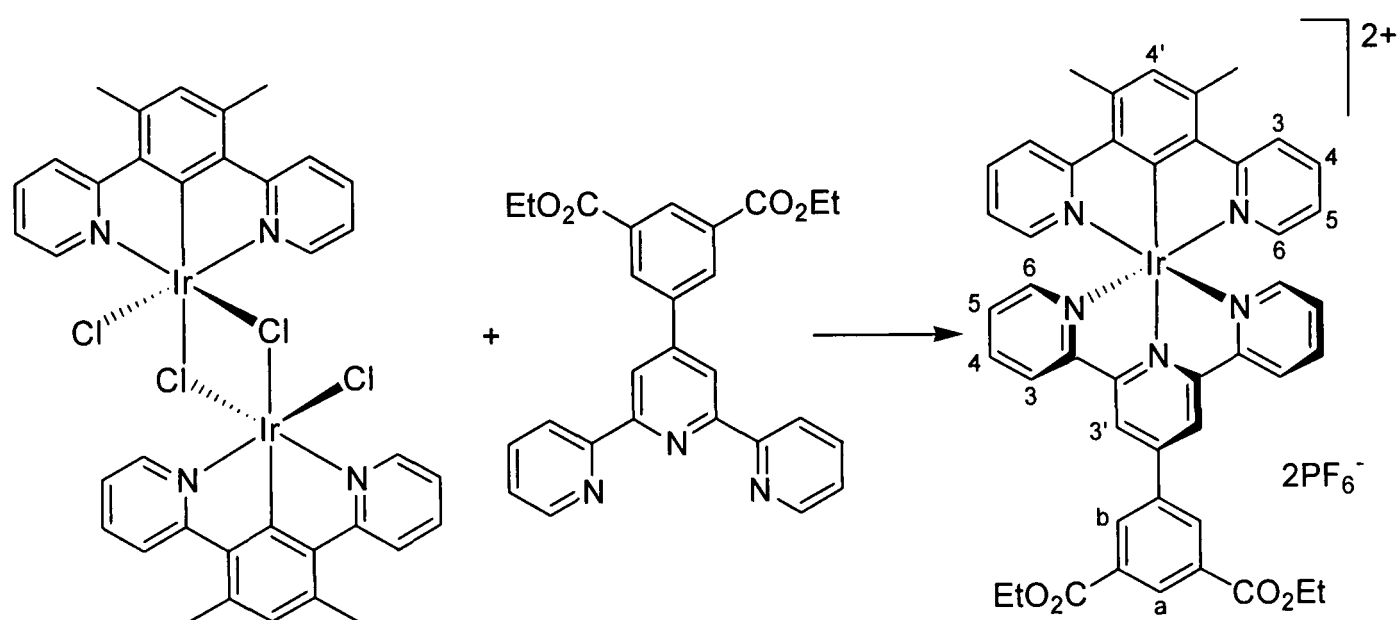
A suspension of bis(μ -chloro)bis(1,5-di(pyrid-2-yl)-2,4-dimethylbenzene- N,C^6',N iridium chloride) ([Ir(dpydmb)Cl(μ -Cl)] $_2$) (24 mg, 0.023 mmol) and 4'-(*p*-tolyl)-2,2':6',2''-terpyridine (ttpy) (15 mg, 0.046 mmol) in ethylene glycol (3 ml) was heated to 196°C under a nitrogen atmosphere for 45 minutes. After cooling to room temperature, the reaction mixture was added to water (5 ml) and filtered. Saturated KPF $_6$ solution was added, and the resulting orange precipitate collected by centrifugation, washed with water (3 \times 5 ml) and dried under vacuum, to give the desired product as an orange solid (43 mg, 87%), mp > 250°C.*

$^1\text{H-NMR}$ (d_6 -Acetone, 400 MHz) δ = 9.49 (2H, s, H $^{3'}$ ttpy), 9.07 (2H, d, J = 8.0, H 3 ttpy), 8.47 (2H, d, J = 8.4, H 3 dpydmb), 8.23 (2H, d, J = 8.1, H b ttpy), 8.23 (2H, td, J = 8.1, 1.4, H 4 ttpy), 7.99 (2H, ddd, J = 8.7, 7.4, 1.6, H 4 dpydmb), 7.89 (2H, dd, J = 5.8, 1.3, H 6 dpydmb), 7.71 (2H, dd, J = 5.5, 1.3, H 6 ttpy), 7.59 (2H, d, J = 7.8, H a ttpy), 7.50 (2H, dd, J = 7.8, 5.9, H 5 ttpy), 7.43 (1H, s, H $^{4'}$ dpydmb), 7.11 (2H, ddd, J = 7.8, 5.9, 1.2, H 5 dpydmb), 3.02 (6H, s, Me dpydmb), 2.53 (3H, s, Me ttpy). $^{13}\text{C}\{^1\text{H}\}$ -NMR (d_6 -Acetone, 101 MHz) δ = 178.7 (C q), 170.8 (C q), 160.7 (C q), 156.2 (CH), 154.7 (C q), 154.6 (C q), 152.7 (CH), 142.7 (C q), 142.0 (CH), 141.4 (CH), 140.6 (C q), 138.1 (C q),

* Purification by column chromatography (alumina, MeCN/H $_2$ O/saturated KNO $_3$ solution, gradient elution from 100/0/0 to 90.0/9.5/0.5) was required to remove small traces of impurity before photophysical studies were performed.

134.1 (CH), 133.9 (q), 131.1 (CH), 130.1 (CH), 129.0 (CH), 127.7 (CH), 125.6 (CH), 124.6 (CH), 123.7 (CH), 22.7 (CH₃ dpydmb), 21.4 (CH₃ tpy). MS(ES⁺) m/z = 388 (M²⁺), 921 (M(PF₆)⁺). HRMS(ES⁺) m/z = 920.1922 (M(PF₆)⁺); calc. for ¹⁹³IrC₄₀H₃₂F₆N₅P, 920.1923. $\lambda_{\text{max}}/\text{nm}$ (Acetonitrile) = 264 ($\epsilon/\text{dm}^3 \text{ mol}^{-1} \text{ cm}^{-1}$ 52 900), 283 (45 100), 301 (39 900), 316 (36 700), 361 (20 300), 377 (21 600), 435 (1 500), 463 (1 000). One spot by TLC(silica), R_f = 0.4 in dichloromethane/methanol, 90/10. See Section 3.2 and Appendix A for crystal structure.

6.2.6 Iridium(1,5-di(pyrid-2-yl)-2,4-dimethylbenzene-*N,C*^{6'},*N*)(5-(2,2':6',2''-terpyridin-4'-yl)-isophthalic acid diethyl ester)²⁺ 107
[Ir(dpydmb)(tpyiade)]²⁺

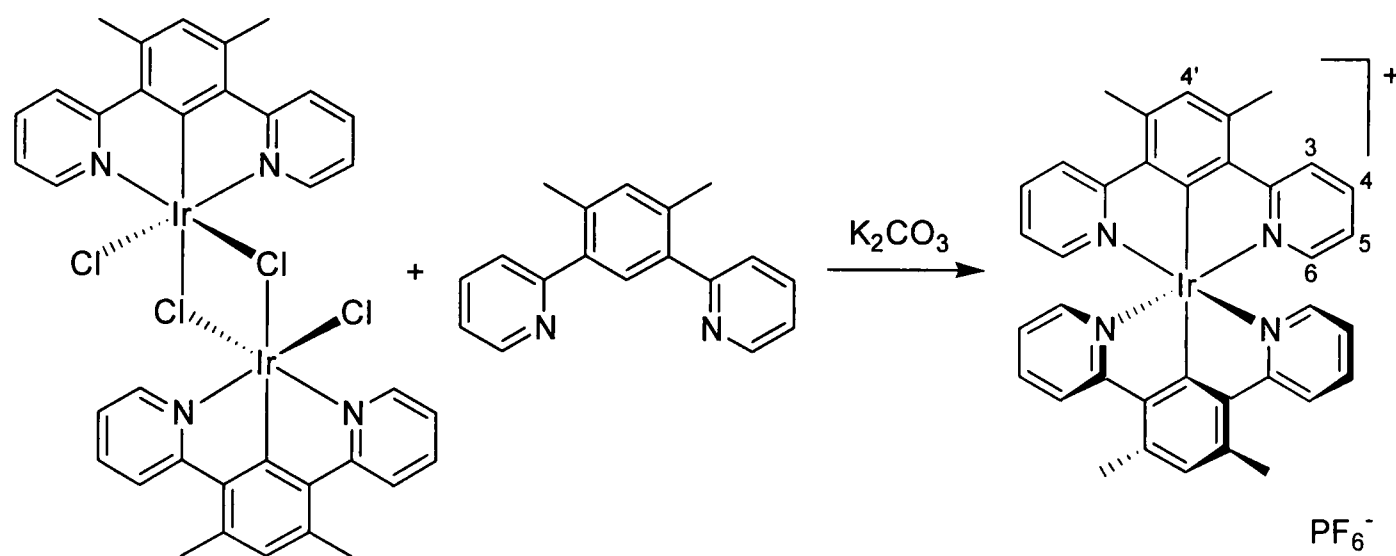


A suspension of bis(μ -chloro)bis(1,5-di(pyrid-2-yl)-2,4-dimethylbenzene-*N,C*^{6'},*N* iridium chloride) ([Ir(dpydmb)Cl(μ -Cl)]₂) (36 mg) and 5-(2,2':6',2''-terpyridin-4'-yl)-isophthalic acid diethyl ester (tpyiade) (31 mg, 0.068 mmol) in ethylene glycol (5 ml) was heated to 196°C under a nitrogen atmosphere for 30 minutes. After cooling to room temperature the reaction mixture was added to water (10 ml). Saturated KPF₆ solution was added, and the resulting brown precipitate collected by centrifugation, washed with water (3 \times 5 ml) and dried under vacuum. Purification by column chromatography (alumina, acetonitrile) followed by a second column (alumina), washed with diethyl ether, then the product collected with acetonitrile gave the desired product as a red solid (14 mg, 35%), mp > 250°C.

¹H-NMR (*d*₆-Acetone, 500 MHz) δ = 9.64 (2H, s, H^{3'} tpyiade), 9.08 (2H, d, J = 8.4, H³ tpyiade), 8.95 (2H, d, J = 1.5, H^b tpyiade), 8.84 (1H, t, J = 1.4, H^a tpyiade), 8.48 (2H, d, J = 8.8, H³ dpydmb), 8.25 (2H, td, J = 7.9, 1.4, H⁴ tpyiade), 8.00 (2H, ddd,

$J = 8.1, 7.8, 1.4, H^4$ dpydmb), 7.92 (2H, d, $J = 5.9, H^6$ dpydmb), 7.75 (2H, d, $J = 5.4, H^5$ tpyiade) 7.53 (2H, ddd, $J = 7.4, 5.8, 1.0, H^6$ tpyiade), 7.45 (1H, s, $H^{4'}$ dpydmb), 7.11 (2H, ddd, $J = 7.3, 5.9, 1.0, H^5$ dpydmb), 4.53 (4H, q, $J = 7.1, CO_2CH_2CH_3$ tpyiade), 3.03 (6H, s, Me dpydmb), 1.47 (6H, t, $J = 7.1, CO_2CH_2CH_3$ tpyiade). $^{13}C\{^1H\}$ -NMR (d_6 -Acetone, 126 MHz) $\delta = 178.5$ (C^q), 170.8 (C^q), 165.6 (C^q), 160.5 (C^q), 156.3 (CH), 154.9 (C^q), 153.3 (C^q), 152.8 (CH), 142.0 (CH), 141.4 (CH), 140.7 (C^q), 139.0 (C^q), 138.1 (C^q), 134.0 (CH), 134.0 (CH), 133.4 (C^q), 132.3 (CH), 130.3 (CH), 127.9 (CH), 125.6 (CH), 125.3 (CH), 124.6 (CH), 62.6 ($CO_2CH_2CH_3$ tpyiade), 22.7 (CH_3 dpydmb), 14.6 ($CO_2CH_2CH_3$ tpyiade). MS(ES+) $m/z = 452.5$ (M^{2+}), 1050 ($M(PF_6)^+$). IR (KBr disc) $\bar{\nu} = 1718\text{ cm}^{-1}$ (CO_2Et , C=O stretch), 1605 cm^{-1} (CO_2Et , C=O stretch).

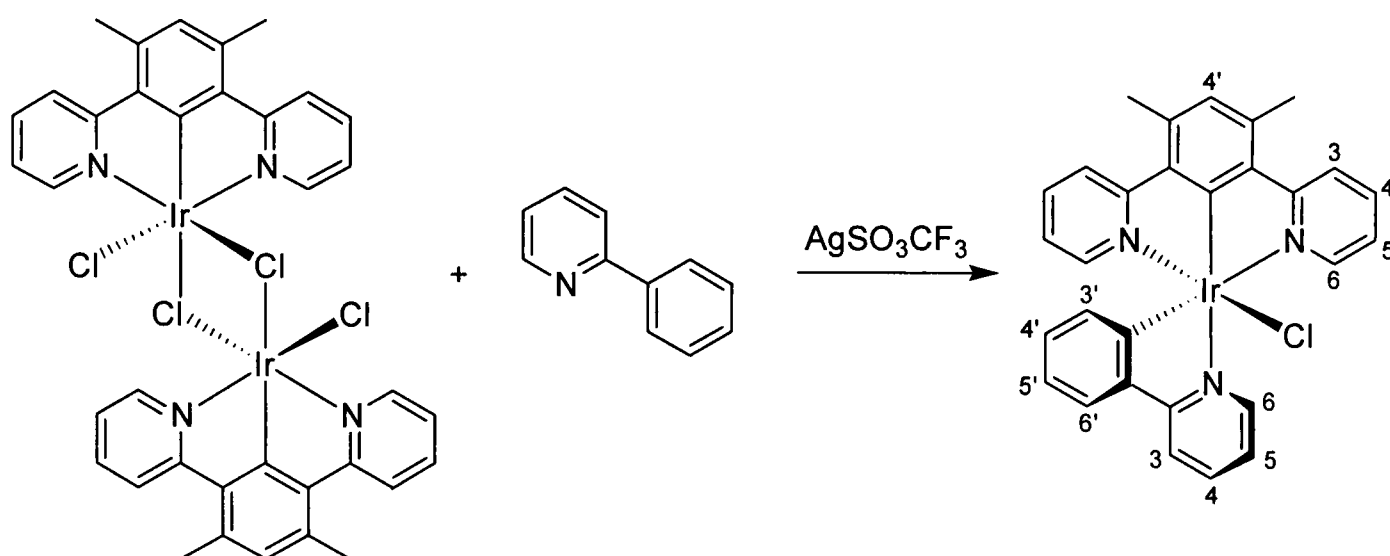
6.2.7 Iridium bis(1,5-di(pyrid-2-yl)-2,4-dimethylbenzene- N,C^6',N)⁺ **125** [Ir(dpydmb)₂]⁺



A suspension of bis(μ -chloro)bis(1,5-di(pyrid-2-yl)-2,4-dimethylbenzene- N,C^6',N iridium chloride) ($[Ir(dpydmb)Cl(\mu-Cl)]_2$) (40 mg, 0.038 mmol), 1,5-di(pyrid-2-yl)-2,4-dimethylbenzene (dpydmbH) (21 mg, 0.081 mmol) and potassium carbonate (55 mg, 0.40 mmol) in ethylene glycol (2 ml) was heated to 196°C under a nitrogen atmosphere for 24 h. After cooling to room temperature the reaction mixture was added to water (8 ml), and any precipitated solid removed by centrifuge and washed with water (3×10 ml). The combined solutions were added to saturated KPF_6 solution, and the resulting yellow precipitate collected by centrifugation, washed with water (3×10 ml) and dried under vacuum. Purification by column chromatography (silica, dichloromethane/methanol, gradient elution from 100/0 to 98/2) gave the desired product as a yellow solid (3 mg, 11%).

$^1\text{H-NMR}$ (CDCl_3 , 400 MHz) $\delta = 8.13$ (4H, d, $J = 8.4$, H^3), 7.66 (4H, ddd, $J = 8.5$, 7.6, 1.8, H^4), 7.31 (4H, dd, $J = 5.7$, 1.6, H^6), 7.17 (2H, s, H^4), 6.74 (4H, ddd, $J = 7.4$, 5.7, 1.4, H^5), 2.96 (12H, s, Me). MS(ES+) $m/z = 711$ (M^+).

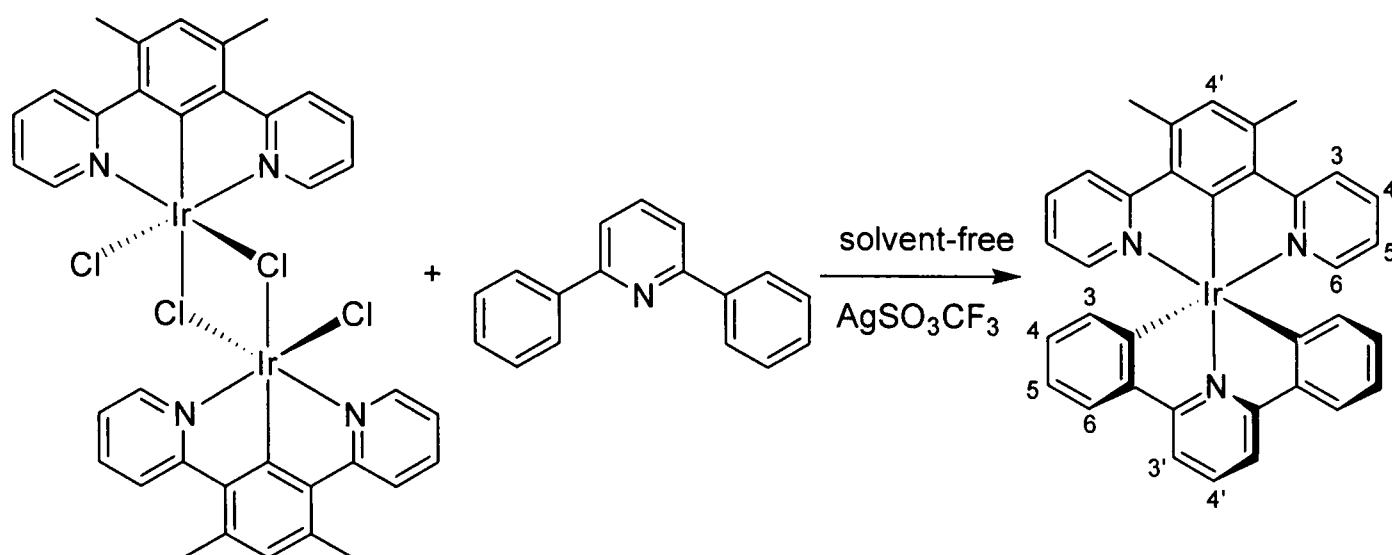
6.2.8 Iridium(1,5-di(pyrid-2-yl)-2,4-dimethylbenzene- $\text{N},\text{C}^{6'}$, N)(2-phenylpyridine- $\text{N},\text{C}^{2'}$)chloride **115** [$\text{Ir}(\text{dpydmb})(\text{ppy})\text{Cl}$]



Bis(μ -chloro)bis(1,5-di(pyrid-2-yl)-2,4-dimethylbenzene- $\text{N},\text{C}^{6'}$, N iridium chloride) ($[\text{Ir}(\text{dpydmb})\text{Cl}(\mu\text{-Cl})]_2$) (35 mg, 0.033 mmol) and silver(I) trifluoromethanesulfonate (44 mg, 0.17 mmol) in 2-phenylpyridine (ppyH) (250 μl , 1.75 mmol) were heated to 110°C under a nitrogen atmosphere for 24 h. After cooling to room temperature, dichloromethane (25 ml) was added and the remaining solid removed by filtration. Washing of the filtrate with HCl (1 mol dm^{-3} , 3×25 ml), drying over MgSO_4 , and removal of solvent under reduced pressure gave a yellow residue. This was purified by column chromatography (silica, dichloromethane/methanol, gradient elution from 100/0 to 99.75/0.25) to give the desired product as a yellow solid (25 mg, 59%), $\text{mp} > 250^\circ\text{C}$.

$^1\text{H-NMR}$ (CDCl_3 , 500 MHz) $\delta = 10.12$ (1H, d, $J = 5.3$, H^6 ppy), 8.07 (1H, d, $J = 8.0$, H^3 ppy), 8.00 (2H, d, $J = 8.4$, H^3 dpydmb), 7.96 (1H, td, $J = 8.0$, 1.4, H^4 ppy), 7.65 (2H, d, $J = 5.6$, H^6 dpydmb), 7.59 (1H, d, $J = 7.7$, $\text{H}^{6'}$ ppy), 7.51-7.55 (3H, m, H^4 dpydmb & H^5 ppy), 6.88 (1H, s, $\text{H}^{4'}$ dpydmb), 6.75 (2H, ddd, $J = 7.2$, 5.9, 1.0, H^5 dpydmb), 6.71 (1H, td, $J = 7.4$, 1.2, $\text{H}^{5'}$ ppy), 6.54 (1H, td, $J = 7.5$, 1.0, $\text{H}^{4'}$ ppy), 6.00 (1H, d, $J = 7.7$, $\text{H}^{3'}$ ppy), 2.83 (6H, s, Me). MS(ES+) $m/z = 606$ ($[\text{M} - \text{Cl}]^+$), 638 ($[\text{M} - \text{Cl} + \text{MeOH}]^+$). $\lambda_{\text{max}}/\text{nm}$ (Acetonitrile) = 239 ($\epsilon/\text{dm}^3 \text{mol}^{-1} \text{cm}^{-1}$ 44 700), 258 (39 700), 285 (37 000), 353 (6 200), 369 (7 800), 399 (10 000), 417 (11 300), 455 (3 600), 492 (1 300).

6.2.9 Iridium(1,5-di(pyrid-2-yl)-2,4-dimethylbenzene-*N,C*^{6'},*N*)(2,6-diphenylpyridine-*C*^{2'},*N,C*^{2'}) **108** [Ir(dpydmb)(dppy)]

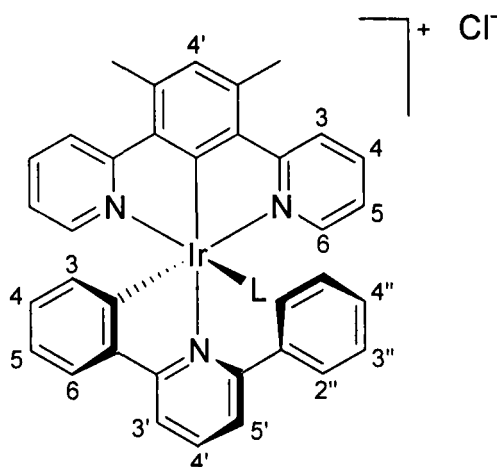


Bis(μ -chloro)bis(1,5-di(pyrid-2-yl)-2,4-dimethylbenzene-*N,C*^{6'},*N* iridium chloride) ([Ir(dpydmb)Cl(μ -Cl)]₂) (31 mg, 0.030 mmol), 2,6-diphenylpyridine (dppyH₂) (416 mg, 1.80 mmol) and silver(I) trifluoromethanesulfonate (34 mg, 0.13 mmol) were ground together in an agar mortar. The resulting fine powder was heated to 110°C and stirred under a nitrogen atmosphere for 24 h. After cooling to room temperature, the product was extracted into ethanol (30 ml) and the remaining solid removed by filtration. Removal of solvent from the filtrate under reduced pressure gave a pale yellow residue. This was purified by column chromatography (silica, dichloromethane/methanol, gradient elution from 100/0 to 98/2) followed by a second column (alumina, dichloromethane) to give the desired product as an orange solid (15 mg, 37%), mp > 250°C.

¹H-NMR (CDCl₃, 400 MHz) δ = 8.04 (2H, d, *J* = 8.4, H³ dpydmb), 7.81 (3H, s, H^{3'} dppy & H^{4'} dppy), 7.67 (2H, d, *J* = 7.7, H⁶ dppy), 7.62 (2H, d, *J* = 5.9, H⁶ dpydmb), 7.38 (2H, td, *J* = 7.9, 1.8, H⁴ dpydmb), 6.97 (1H, s, H^{4'} dpydmb), 6.79 (2H, td, *J* = 7.2, 1.5, H⁵ dppy), 6.55 (2H, td, *J* = 7.2, 1.2, H⁴ dppy), 6.52 (2H, td, *J* = 6.5, 1.2, H⁵ dpydmb), 6.18 (2H, d, *J* = 7.3, H³ dppy), 2.95 (6H, s, Me dpydmb). ¹H-NMR (CD₂Cl₂, 400 MHz) δ = 8.12 (2H, d, *J* = 8.5, H³ dpydmb), 7.85 (3H, s, H^{3'} dppy & H^{4'} dppy), 7.69 (2H, d, *J* = 7.8, H⁶ dppy), 7.66 (2H, d, *J* = 5.8, H⁶ dpydmb), 7.49 (2H, t, *J* = 8.0, H⁴ dpydmb), 7.02 (1H, s, H^{4'} dpydmb), 6.79 (2H, t, *J* = 7.4, H⁵ dppy), 6.61 (2H, t, *J* = 6.6, H⁵ dpydmb), 6.52 (2H, t, *J* = 7.1, H⁴ dppy), 6.08 (2H, d, *J* = 7.3, H³ dppy), 2.97 (6H, s, Me dpydmb). MS(EI) *m/z* = 681 (M⁺), 340.5 (M²⁺). HRMS(EI) *m/z* = 679.1720 (M⁺); calc. for ¹⁹¹IrC₃₅H₂₆N₃, 679.1727. λ_{\max}/nm (Acetonitrile) = 244 ($\epsilon/\text{dm}^3 \text{ mol}^{-1} \text{ cm}^{-1}$

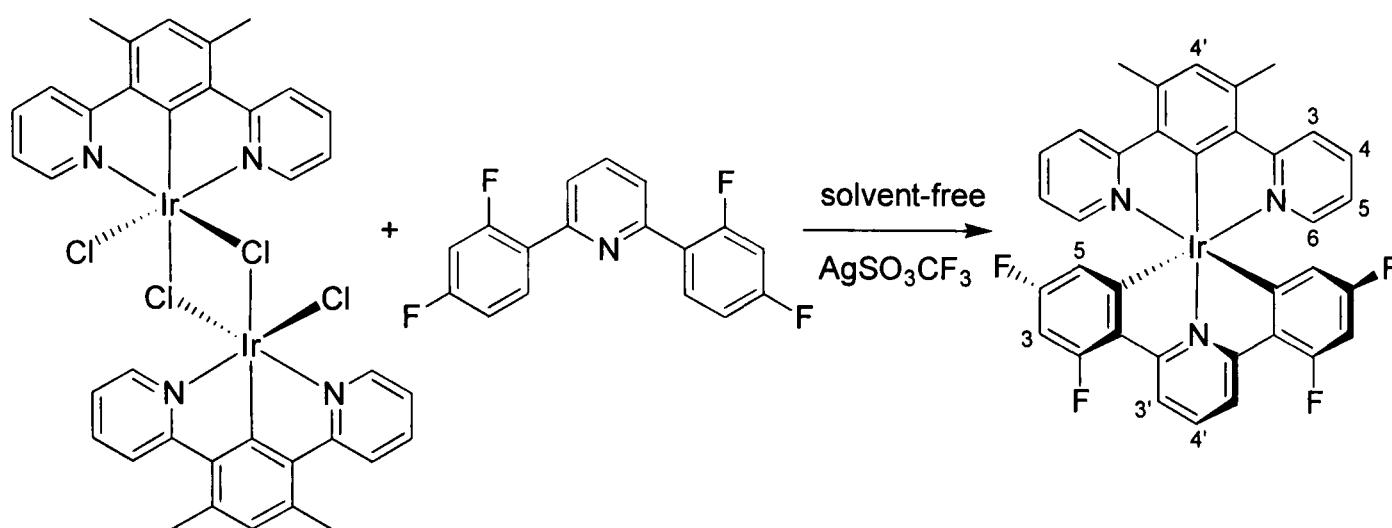
53 900), 269 (46 900), 349 (7 700), 378 (6 900), 406 (6 500), 458 (5 500), 481 (6 800), 510 (7 300).

Iridium(1,5-di(pyrid-2-yl)-2,4-dimethylbenzene-*N,C*^{6'},*N*)(2,6-diphenylpyridine-*C*^{2'},*N*) [Ir(dpydmb)(dppyH)]⁺ was often also obtained from column chromatography of the crude product mixture (silica, dichloromethane/methanol, gradient elution from 100/0 to 97.5/2.5).



¹H-NMR (CDCl₃, 400 MHz) δ=8.21 (1H, d, J=8.2, H^{3'} dppy or H^{5'} dppy), 8.10 (1H, t, J=7.8, H^{4'} dppy), 7.99 (2H, d, J=8.3, H³ dpydmb), 7.81 (2H, d, J=5.7, H⁶ dpydmb), 7.64-7.69 (3H, m, H⁶ dppy & H⁴ dpydmb), 7.59 (2H, d, J=7.6, H^{2''} dppy), 7.47-7.52 (3H, m, H^{3''} dppy & H^{3'} dppy or H^{5'} dppy), 7.41 (1H, t, J=7.3, H^{4''} dppy), 6.98 (2H, t, J=6.6, H⁵ dpydmb), 6.89 (1H, s, H^{4'} dpydmb), 6.78 (1H, t, J=7.6, H⁵ dppy), 6.57 (1H, t, J=7.3, H⁴ dppy), 6.05 (1H, d, J=7.8, H³ dppy), 2.76 (6H, s, Me). MS(ES+) *m/z*=682 (M⁺).

6.2.10 Iridium(1,5-di(pyrid-2-yl)-2,4-dimethylbenzene-*N,C*^{6'},*N*)(2,6-di(2,4-difluorophenyl)pyridine-*C*^{6'},*N,C*^{6'}) **110** [Ir(dpymdb)(F₄dppy)]



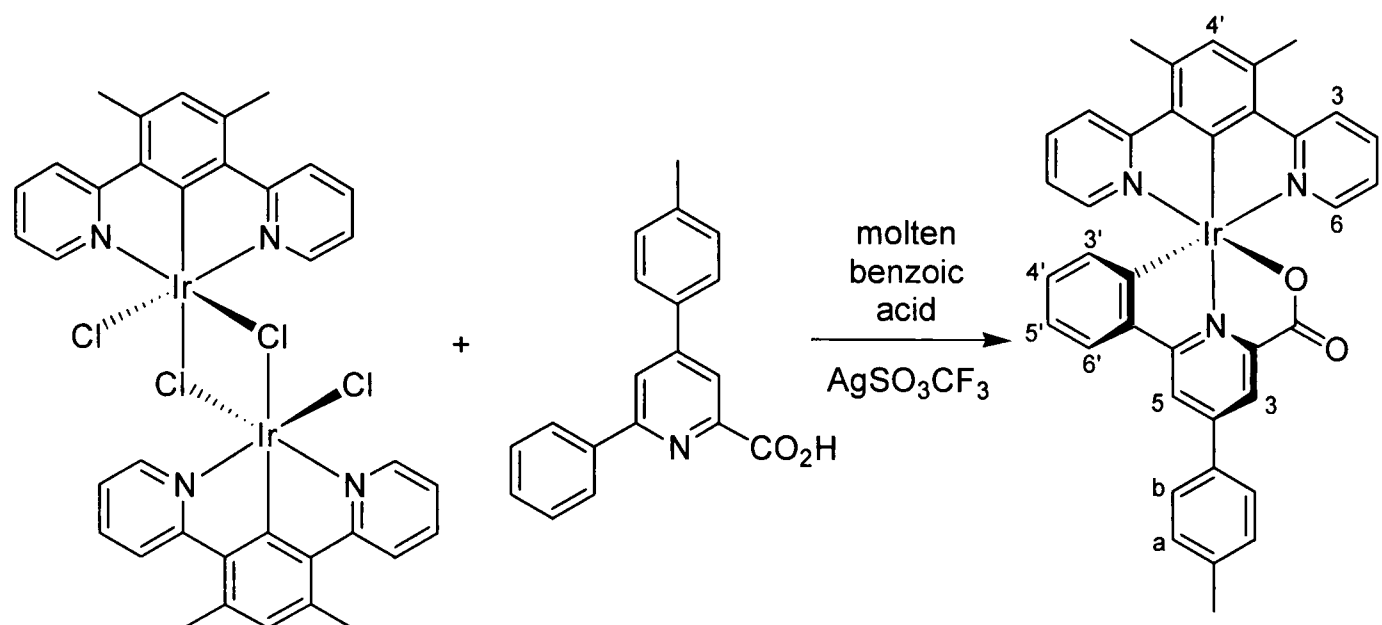
Bis(μ -chloro)bis(1,5-di(pyrid-2-yl)-2,4-dimethylbenzene-*N,C*^{6'},*N*) iridium chloride ([Ir(dpymdb)Cl(μ -Cl)]₂) (41 mg, 0.039 mmol), 2,6-di(2,4-difluorophenyl)pyridine (F₄dppyH₂) (227 mg, 0.75 mmol) and silver(I) trifluoromethanesulfonate (40 mg, 0.16 mmol) were ground together in an agar mortar. The resulting fine powder was heated to 110°C and stirred under a nitrogen atmosphere for 24 h. After cooling to room temperature, the product was extracted into dichloromethane (30 ml), and the remaining solid removed by filtration. Removal of solvent under reduced pressure gave a brown residue. This was purified by column chromatography (silica, hexane/diethyl ether, gradient elution from 100/0 to 95/5)* followed by a second column (silica, hexane/diethyl ether, gradient elution from 100/0 to 98/2) to give the desired product as a yellow solid (12 mg, 21%), mp > 250°C.

¹H-NMR (CDCl₃, 500 MHz) δ = 8.16 (2H, d, *J* = 8.2, H^{3'} F₄dppy), 8.07 (2H, d, *J* = 8.3, H³ dpymdb), 7.85 (1H, t, *J* = 8.1, H^{4'} F₄dppy), 7.57 (2H, dd, *J* = 5.7, 1.1, H⁶ dpymdb), 7.49 (2H, ddd, *J* = 7.5, 6.0, 1.5, H⁴ dpymdb), 6.97 (1H, s, H^{4'} dpymdb), 6.63 (2H, ddd, *J* = 5.8, 4.9, 1.0, H⁵ dpymdb), 6.20 (2H, ddd, *J* = 12.8, 9.1, 2.4, H³ F₄dppy), 5.65 (2H, dd, *J* = 7.2, 2.4, H⁵ F₄dppy), 2.94 (6H, s, Me dpymdb). ¹³C{¹H}-NMR (CDCl₃, 126 MHz) δ = 191.2 (C^q), 176.1 (C^q), 168.6 (C^q), 163.1 (dd, *J* = 259.9, 10.3, CF), 162.2 (dd, *J* = 260.8, 10.3, CF), 161.2 (d, *J* = 7.21, C^q), 149.8 (CH), 138.4 (CH), 137.0 (C^q), 134.8 (C^q), 133.8 (CH⁶ dpymdb), 131.0 (C^q), 127.2 (CH^{4'} dpymdb), 122.6 (CH³ dpymdb), 120.5 (CH), 118.0 (dd, *J* = 13.5, 2.6, CH⁵ F₄dppy), 117.6 (d, *J* = 18.8, CH^{3'} F₄dppy), 97.6 (t, *J* = 26.2, CH³ F₄dppy), 23.0 (CH₃). ¹⁹F-NMR (CDCl₃, 282 MHz)

* Note that unreacted ligand may be recovered, eluting at lower polarity (hexane/diethyl ether, 98/2).

$\delta = -110.77$ (2F, q, $J = 8.8$), -111.02 (2F, dd, $J = 13.4, 9.0$). MS(ES+) $m/z = 754$ ($[M+H]^+$). HRMS(ES+) $m/z = 754.1440$ ($[M+H]^+$); calc. for $^{193}\text{IrC}_{35}\text{H}_{23}\text{F}_4\text{N}_3$, 754.1452. One spot by TLC(silica), $R_f = 0.2$ in hexane/diethyl ether, 90/10. $\lambda_{\text{max}}/\text{nm}$ (Acetonitrile) = 240 ($\epsilon/\text{dm}^3 \text{ mol}^{-1} \text{ cm}^{-1}$ 12 300), 265 (12 000), 290 (6 200), 304 (5 300), 334 (2 100), 360 (1 500), 385 (1 400), 447 (1 400), 464 (1 600), 487 (1 300).

6.2.11 Iridium(1,5-di(pyrid-2-yl)-2,4-dimethylbenzene- $N, C^{6'}$, N)(4-*p*-tolyl-6-phenylpicolinic acid- C^2, N, O) 116 [Ir(dpydmb)(tppic)]

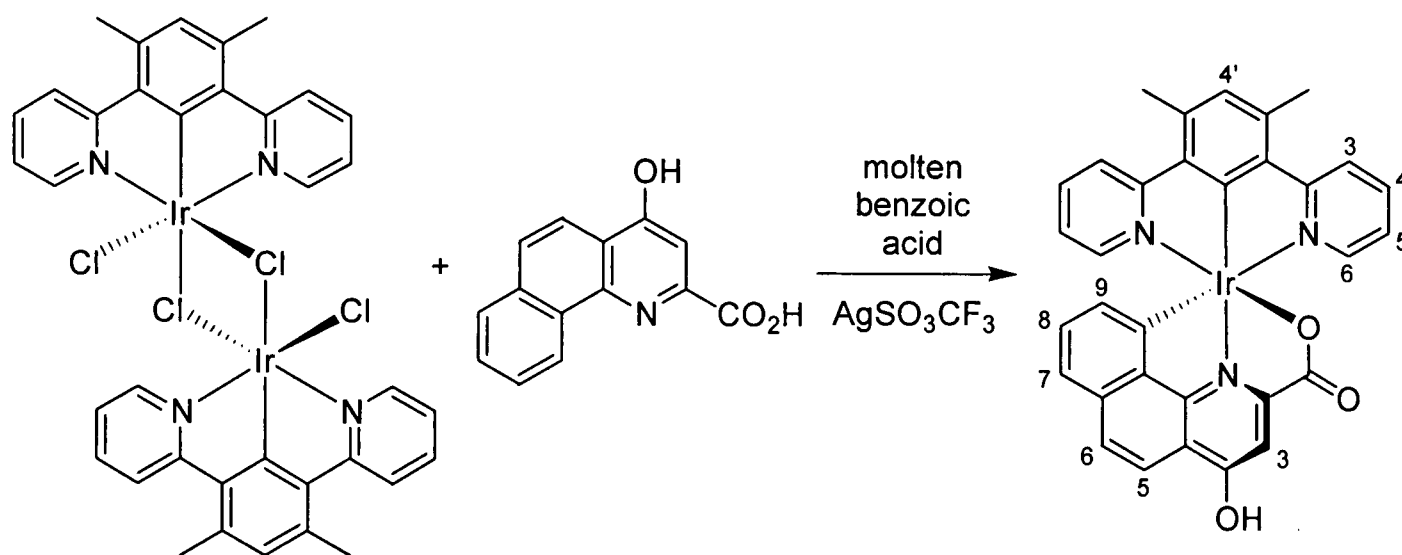


Bis(μ -chloro)bis(1,5-di(pyrid-2-yl)-2,4-dimethylbenzene- $N, C^{6'}$, N iridium chloride) ($[\text{Ir}(\text{dpydmb})\text{Cl}(\mu\text{-Cl})_2]$) (373 mg, 0.36 mmol), 4-*p*-tolyl-6-phenylpicolinic acid (tppicH_2) (1.03 g, 3.55 mmol), silver(I) trifluoromethanesulfonate (552 mg, 2.15 mmol) and benzoic acid (3.49 g, 28.6 mmol) were ground together in an agar mortar. The resulting fine powder was heated to 150°C and stirred under a nitrogen atmosphere for 24 h. After cooling to room temperature, the product was dissolved in dichloromethane (50 ml) and washed with sodium hydrogen carbonate solution (1 mol dm^{-3} , $3 \times 50 \text{ ml}$). Drying over Na_2CO_3 was followed by removal of solvent under reduced pressure. The brown residue was purified by column chromatography (silica, dichloromethane/methanol, gradient elution from 100/0 to 97/3) to give the desired product as an orange solid (286 mg, 54%), $\text{mp} > 250^\circ\text{C}$.

$^1\text{H-NMR}$ (CDCl_3 , 500 MHz) $\delta = 8.48$ (1H, d, $J = 1.3$, H^3 phtpyca), 8.31 (1H, d, $J = 1.4$, H^5 phtpyca), 8.04 (2H, d, $J = 8.1$, H^6 dpydmb), 7.86 (2H, d, $J = 8.1$, H^b phtpyca), 7.70 (1H, dd, $J = 7.9, 1.3$, $\text{H}^{6'}$ phtpyca), 7.59 (2H, ddd, $J = 8.1, 7.7, 1.5$, H^5 dpydmb), 7.41-7.44 (4H, m, H^a phtpyca & H^3 dpydmb), 6.94 (1H, s, $\text{H}^{4'}$ dpydmb), 6.79 (2H, ddd, $J = 7.1, 6.0, 1.0$, H^4 dpydmb), 6.78 (1H, ddd, $J = 8.7, 7.7, 1.3$, $\text{H}^{5'}$ phtpyca),

6.57 (1H, td, $J = 7.5, 1.2$, $H^{4'}$ phtpyca), 5.82 (1H, dd, $J = 7.8, 1.0$, $H^{3'}$ phtpyca), 2.86 (6H, s, Me dpydmb), 2.51 (3H, s, Me phtpyca). MS(ES+) $m/z = 740$ ($[M+H]^+$). MS(EI) $m/z = 739$ (M^+), 695 ($M^+ - CO_2$), 347.5 ($M^{2+} - CO_2$). HRMS(ES+) $m/z = 740.1881$ ($[M+H]^+$); calc. for $^{193}\text{IrC}_{37}\text{H}_{29}\text{O}_2\text{N}_3$, 740.1884. One spot by TLC(silica), $R_f = 0.5$ in dichloromethane/methanol, 90/10. $\lambda_{\text{max}}/\text{nm}$ (Acetonitrile) = 242 ($\epsilon/\text{dm}^3 \text{ mol}^{-1} \text{ cm}^{-1}$ 32 800), 273 (35 700), 290 (30 400), 337 (13 500), 393 (6 900), 429 (6 700), 459 (4 300), 489 (1 700).

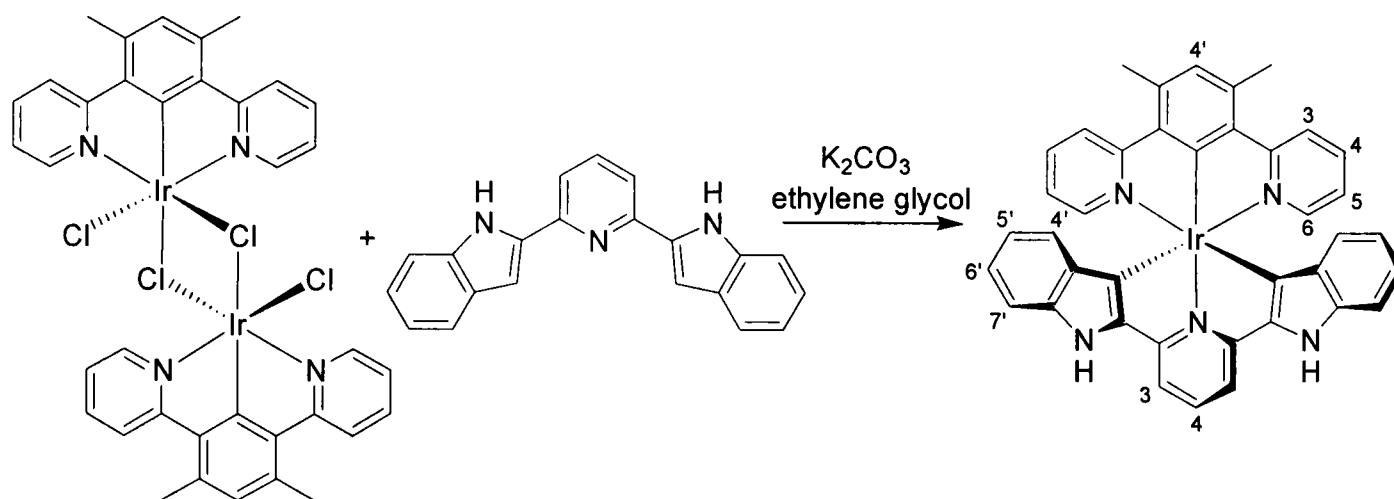
6.2.12 Iridium(1,5-di(pyrid-2-yl)-2,4-dimethylbenzene- $N, C^{6'}$, N)(4-hydroxybenzo[h]quinoline-2-carboxylic acid- C^{10} , N, O 117)
[Ir(dpydmb)(hbqc)]



Bis(μ -chloro)bis(1,5-di(pyrid-2-yl)-2,4-dimethylbenzene- $N, C^{6'}$, N iridium chloride) ($[\text{Ir}(\text{dpydmb})\text{Cl}(\mu\text{-Cl})_2]$) (40 mg, 0.038 mmol), 4-hydroxybenzo[h]quinoline-2-carboxylic acid (hbqcH_2) (87 mg, 0.36 mmol), silver(I) trifluoromethanesulfonate (59 mg, 0.23 mmol) and benzoic acid (314 mg, 2.57 mmol) were ground together in an agar mortar. The resulting fine powder was heated to 110°C and stirred under a nitrogen atmosphere for 24 h. After cooling to room temperature, the solid was extracted into acetonitrile and filtered through Celite®, followed by removal of solvent under reduced pressure. The residue was dissolved in the minimum amount of acetonitrile and added to water (50 ml). The resulting yellow precipitate was collected by centrifugation, washed with water (3×10 ml) and dried under vacuum. The solid may be solubilised in dichloromethane with the addition of a couple of drops of trifluoroacetic acid, and was purified by column chromatography (silica, dichloromethane/methanol, gradient elution from 100/0 to 97.5/2.5) to give the desired product as an yellow solid (30 mg, 58%), mp $> 250^\circ\text{C}$.

$^1\text{H-NMR}$ (CDCl_3 , 500 MHz) δ = 8.12 (1H, d, J = 9.0, H^5 hbqc), 8.12 (1H, s, H^3 hbqc), 8.06 (2H, d, J = 8.4, H^3 dpydmb), 7.83 (1H, d, J = 9.0, H^6 hbqc), 7.63 (2H, td, J = 7.9, 1.7, H^4 dpydmb), 7.28 (2H, d, J = 5.8, H^6 dpydmb), 7.25 (1H, d, J = 7.4, H^7 hbqc), 7.00 (1H, br s, $\text{H}^{4'}$ dpydmb), 6.90 (1H, t, J = 7.6, H^8 hbqc), 6.78 (2H, ddd, J = 7.0, 5.8, 1.0, H^5 dpydmb), 5.86 (1H, d, J = 7.5, H^9 hbqc), 2.87 (6H, s, Me dpydmb). $^{13}\text{C}\{^1\text{H}\}$ -NMR (CDCl_3 , 126 MHz) δ = 183.8, 175.3, 171.0, 163.3, 151.5, 151.0, 144.5, 140.8, 138.1 (C^4 dpydmb), 138.1, 137.8, 134.8, 133.3, 130.7 (C^6 hbqc), 130.4, 129.4 (C^8 hbqc), 123.0 (C^3 dpydmb), 122.2 (C^5 dpydmb), 120.9, 120.2, 119.5, 118.9, 108.1 (C^5 hbqc or C^3 hbqc), 22.6 (CH_3 dpydmb). MS(ES+) m/z = 690 ($[\text{M}+\text{H}]^+$). HRMS(ES+) m/z = 690.1364 ($[\text{M}+\text{H}]^+$); calc. for $^{193}\text{IrC}_{32}\text{H}_{23}\text{O}_3\text{N}_3$, 690.1363. One spot by TLC(silica), R_f = 0.3 in dichloromethane/methanol, 90/10. $\lambda_{\text{max}}/\text{nm}$ (Acetonitrile) = 245 ($\epsilon/\text{dm}^3 \text{mol}^{-1} \text{cm}^{-1}$ 34 500), 290 (16 600), 315 (10 400), 341 (6 500), 363 (5 900), 393 (4 900), 428 (4 600), 459 (2 800), 492 (1 100).

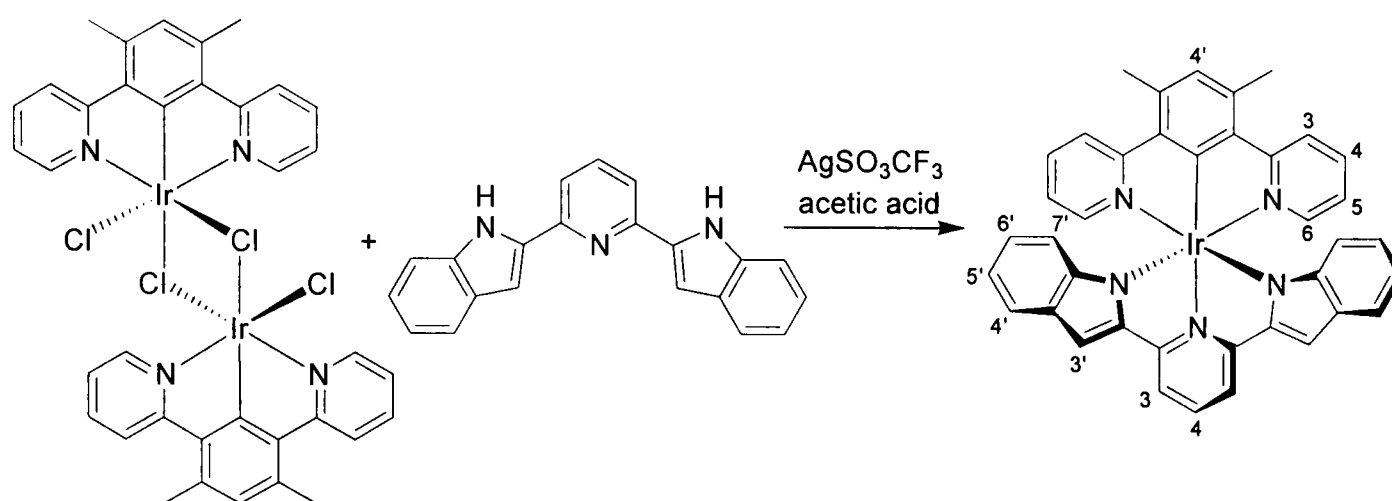
6.2.13 Iridium(1,5-di(pyrid-2-yl)-2,4-dimethylbenzene- $N, \text{C}^{6'}$, N)(2,6-di(2'-indolyl)pyridine- $\text{C}^{3'}$, $N, \text{C}^{3'}$) 122 [$\text{Ir}(\text{dpydmb})(\text{dinpy}-\text{C}^{\wedge}\text{N}^{\wedge}\text{C})$]



A suspension of bis(μ -chloro)bis(1,5-di(pyrid-2-yl)-2,4-dimethylbenzene- $N, \text{C}^{6'}$, N iridium chloride) ($[\text{Ir}(\text{dpydmb})\text{Cl}(\mu\text{-Cl})]_2$) (39 mg, 0.037 mmol), 2,6-di(2'-indolyl)pyridine (dinpyH_2) (23 mg, 0.074 mmol) and potassium carbonate (50 mg, 0.36 mmol) in ethylene glycol (2 ml) was heated to 200°C under a nitrogen atmosphere for 24 h. After cooling to room temperature the reaction mixture was added to water (8 ml), and any precipitated solid removed by centrifugation and washed with water (3×10 ml). The solid was extracted into dichloromethane, dried over MgSO_4 and filtered through Celite®. Removal of solvent under reduced pressure followed by purification by column chromatography (silica, dichloromethane) gave the desired product as a brown solid (2 mg, 4%).

$^1\text{H-NMR}$ (CDCl_3 , 400 MHz) δ = 8.38 (2H, d, J = 7.8, H^3 dinpy), 8.32 (1H, t, J = 8.0, H^4 dinpy), 7.87 (2H, d, J = 8.4, H^3 dpydmb), 7.71 (2H, ddd, J = 8.3, 7.7, 1.7, H^4 dpydmb), 7.50 (2H, d, J = 5.8, H^6 dpydmb), 7.09 (2H, ddd, J = 7.3, 5.8, 1.1, H^5 dpydmb), 6.93 (2H, t, J = 7.3, $\text{H}^{7'}$ dinpy), 6.70 (2H, t, J = 7.6, $\text{H}^{6'}$ dinpy), 6.61 (2H, t, J = 7.8, $\text{H}^{5'}$ dinpy), 6.50 (1H, s, $\text{H}^{4'}$ dpydmb), 5.36 (2H, d, J = 7.9, $\text{H}^{4'}$ dinpy), 2.55 (6H, s, CH_3).

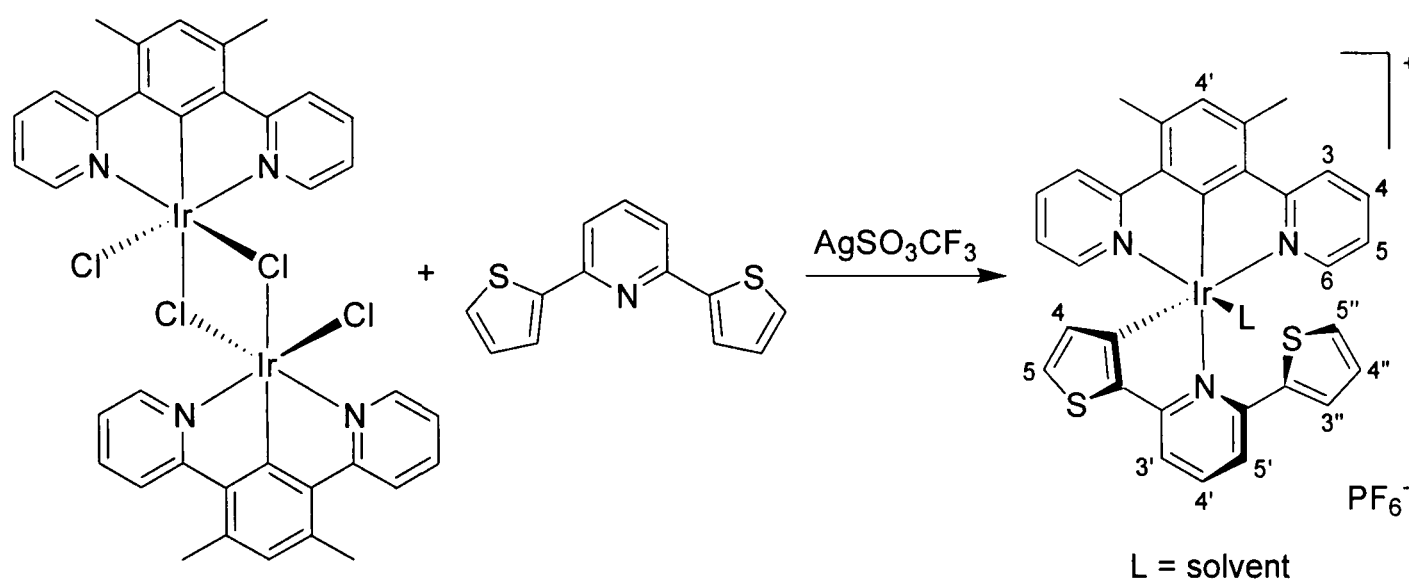
6.2.14 Iridium(1,5-di(pyrid-2-yl)-2,4-dimethylbenzene- $N, C^{6'}$, N)(2,6-di(2'-indolyl)pyridine- N, N, N) **123** [$\text{Ir}(\text{dpydmb})(\text{dinpy-}N^N^N)$]



A suspension of bis(μ -chloro)bis(1,5-di(pyrid-2-yl)-2,4-dimethylbenzene- $N, C^{6'}$, N iridium chloride) ($[\text{Ir}(\text{dpydmb})\text{Cl}(\mu\text{-Cl})]_2$) (41 mg, 0.039 mmol), 2,6-di(2'-indolyl)pyridine (dinpyH_2) (36 mg, 0.12 mmol) and silver(I) trifluoromethanesulfonate (78 mg, 0.30 mmol) in glacial acetic acid (2 ml) was heated to 110°C under a nitrogen atmosphere overnight. After cooling to room temperature, water (20 ml) was added and the mixture extracted into dichloromethane (3×20 ml), dried over MgSO_4 and filtered. Removal of solvent under reduced pressure followed by purification by column chromatography (silica, hexane/ethyl acetate, 75/25) gave the desired product as a brown solid (5 mg, 8%).

$^1\text{H-NMR}$ (CDCl_3 , 400 MHz) δ = 7.94-7.98 (3H, m, H^3 dpydmb & H^4 dinpy), 7.82 (2H, d, J = 7.9, H^3 dinpy), 7.32-7.40 (6H, m, H^4 dpydmb, H^6 dpydmb & $\text{H}^{4'}$ dinpy), 7.23 (1H, s, $\text{H}^{4'}$ dpydmb), 6.97 (2H, s, $\text{H}^{3'}$ dinpy), 6.64 (2H, ddd, J = 7.9, 6.7, 0.7, $\text{H}^{5'}$ dinpy), 6.61 (2H, ddd, J = 7.3, 5.9, 1.0, H^5 dpydmb), 6.48 (2H, ddd, J = 8.3, 6.8, 1.1, $\text{H}^{6'}$ dinpy), 5.73 (2H, dd, J = 8.4, 0.6, $\text{H}^{7'}$ dinpy), 2.96 (6H, s, CH_3). $\text{MS}(\text{ES}^+)$ m/z = 760 ($[\text{M}+\text{H}]^+$).

6.2.15 Iridium(1,5-di(pyrid-2-yl)-2,4-dimethylbenzene-*N,C*^{6'},*N*)(2,6-di(2-thienyl)pyridine-*C*^{3'},*N*) [Ir(dpydmb)(dthpyH)]⁺



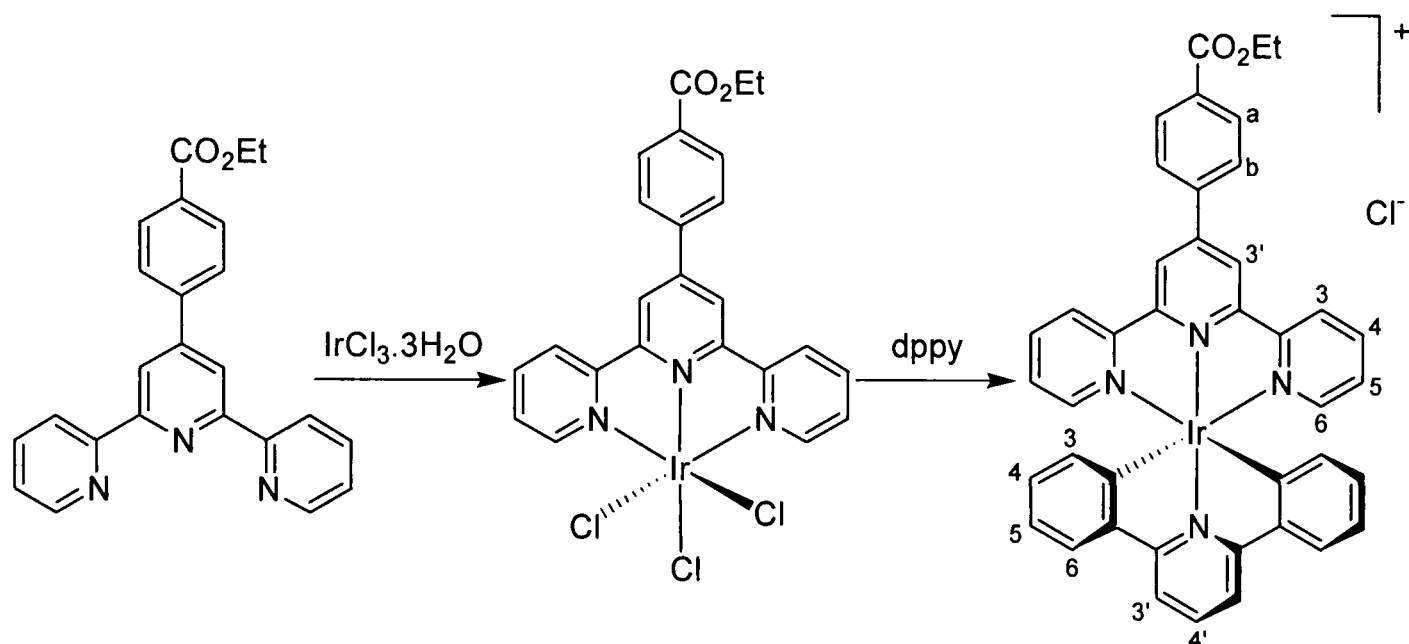
A suspension of bis(μ -chloro)bis(1,5-di(pyrid-2-yl)-2,4-dimethylbenzene-*N,C*^{6'},*N* iridium chloride) ([Ir(dpydmb)Cl(μ -Cl)]₂) (41 mg, 0.039 mmol), 2,6-di(2-thienyl)pyridine (dthpyH₂) (29 mg, 0.12 mmol) and silver(I) trifluoromethanesulfonate (86 mg, 0.33 mmol) in glacial acetic acid (2 ml) was heated to 110°C under a nitrogen atmosphere overnight. After cooling to room temperature, water (20 ml) was added and the mixture extracted into dichloromethane (3 × 20 ml), dried over MgSO₄ and filtered. Removal of solvent under reduced pressure followed by purification by column chromatography (silica, dichloromethane/methanol, gradient elution from 100/0 to 95/5) gave the desired product as a yellow solid (10 mg, 36%*), mp > 250°C.

¹H-NMR (CDCl₃, 400 MHz) δ = 8.22 (1H, dd, *J* = 7.9, 1.4, H^{5'} dthpyH), 8.19 (1H, t, *J* = 7.8, H^{4'} dthpyH), 8.07 (2H, d, *J* = 8.5, H³ dpydmb), 7.95 (1H, dd, *J* = 3.8, 0.8, H^{3''} dthpyH), 7.75 (2H, ddd, *J* = 8.3, 7.6, 1.7, H⁴ dpydmb), 7.70 (1H, dd, *J* = 7.5, 1.4, H^{3'} dthpyH), 7.34 (2H, ddd, *J* = 5.8, 1.6, 0.6, H⁶ dpydmb), 7.17 (1H, dd, *J* = 5.2, 3.8, H^{4''} dthpyH), 7.07 (1H, s, H^{4'} dpydmb), 7.04 (1H, dd, *J* = 5.2, 0.7, H^{5''} dthpyH), 7.03 (1H, d, *J* = 4.9, H⁵ dthpyH), 6.99 (2H, ddd, *J* = 7.5, 5.7, 1.3, H⁵ dpydmb), 5.69 (1H, d, *J* = 4.9, H⁴ dthpyH), 2.86 (6H, s, CH₃). ¹³C{¹H}-NMR (CDCl₃, 101 MHz) δ = 174.2 (C^q), 169.6 (C^q), 159.0 (C^q), 151.7 (CH), 149.2 (C^q), 148.7 (C^q), 140.8 (CH), 139.2 (C^q), 138.8 (C⁴ dpydmb), 138.3 (C^q), 138.0 (C^q), 135.5 (C^q), 134.3 (C^{4''} dthpyH), 132.9 (C^{3''} dthpyH), 131.9 (C^{4'} dpydmb), 130.2 (C⁴ dthpyH), 128.9 (C⁵ dthpyH or C^{5''} dthpyH), 127.8 (CH), 123.4 (C³ dpydmb), 123.2 (C⁵ dpydmb), 117.4 (C^{3'} dthpyH), 117.1 (CH), 22.7 (CH₃).

* Yield based upon the complete removal of the weakly bound solvent molecule, L, upon drying.

MS(ES+) $m/z = 694$ (M^+). HRMS(ES+) $m/z = 694.0966$ (M^+); calc. for $^{193}\text{IrC}_{31}\text{H}_{23}\text{N}_3\text{S}_2$, 694.0963.

6.2.16 Iridium(4-(2,2':6',2''-terpyridin-4'-yl)benzoic acid ethyl ester)(2,6-diphenylpyridine- $C^{2'},N,C^{2'}$) $^+$ 124 [$\text{Ir}(\text{tpybae})(\text{dppy})$] $^+$



Iridium (4-(2,2':6',2''-terpyridin-4'-yl)benzoic acid ethyl ester) trichloride
 $[\text{Ir}(\text{tpybae})\text{Cl}_3]$

A suspension of iridium trichloride trihydrate (177 mg, 0.46 mmol) and 4-(2,2':6',2''-terpyridin-4'-yl)benzoic acid ethyl ester (tpybae) (167 mg, 0.47 mmol) in ethylene glycol (10 ml) was heated to 160°C for 30 minutes. After cooling to room temperature, the precipitated solid was collected by centrifugation, washed with ethanol (2 × 8 ml), water (2 × 8 ml), ethanol (1 × 8 ml) and diethyl ether (2 × 8 ml), then dried under vacuum to give the desired product as pale orange solid (110 mg^{*}).

$^1\text{H-NMR}$ (d_6 -DMSO, 500 MHz) $\delta = 9.23$ (2H, d, $J = 5.5$, H^6), 9.17 (2H, s, H^3), 8.93 (2H, d, $J = 8.0$, H^3), 8.36 (2H, d, $J = 8.5$, H^a or H^b), 8.32 (2H, td, $J = 7.9, 1.4$, H^4), 8.23 (2H, d, $J = 8.5$, H^a or H^b), 8.00 (2H, ddd, $J = 7.0, 5.7, 1.1$, H^5), 4.40 (2H, q, $J = 7.1$, COCH_2CH_3), 1.38 (3H, t, $J = 7.1$, COCH_2CH_3).

^{*} Although contaminated with ~25% of the ethylene glycol ester, this compound is highly insoluble and was used without further purification.

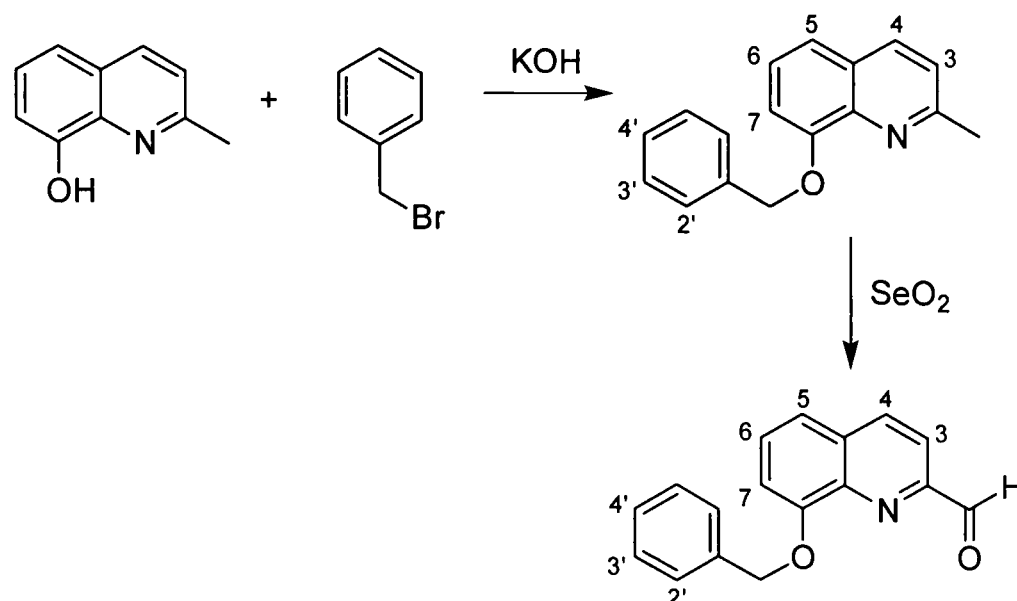
Iridium(4-(2,2':6',2''-terpyridin-4'-yl)benzoic acid ethyl ester)(2,6-diphenylpyridine-C^{2'},N,C^{2'})⁺ 124 [Ir(tpybae)(dppy)]⁺

A suspension of iridium (4-(2,2':6',2''-terpyridin-4'-yl)benzoic acid ethyl ester) trichloride (Ir(tpybae)Cl₃) (110 mg) and 2,6-diphenylpyridine (dppyH₂) (38 mg, 0.16 mmol) in ethylene glycol (5 ml) was heated to 196°C under a nitrogen atmosphere for 45 minutes. After cooling to room temperature, the reaction mixture was added to water (20 ml), extracted into dichloromethane (3 × 30 ml), and dried over MgSO₄. Removal of solvent under reduced pressure followed by purification of the residue by column chromatography (silica, dichloromethane/ethanol, gradient elution from 100/0 to 91/9) gave the desired product as a red solid (6 mg, 4%), mp >250°C.

¹H-NMR (CDCl₃, 400 MHz) δ = 9.25 (2H, s, H^{3'} tpybae), 8.97 (2H, d, J = 7.7, H³ tpybae), 8.37 (4H, s, H^a tpybae & H^b tpybae), 7.96 (1H, t, J = 8.2, H^{4'} dppy), 7.93 (2H, t, J = 7.6, H⁴ tpybae), 7.86 (2H, d, J = 8.0, H^{3'} dppy), 7.73 (2H, d, J = 7.9, H⁶ dppy), 7.61 (2H, d, J = 5.8, H⁶ tpybae), 7.14 (2H, t, J = 6.6, H⁵ tpybae), 6.98 (2H, t, J = 7.8, H⁵ dppy), 6.80 (2H, t, J = 7.2, H⁴ dppy), 6.23 (2H, d, J = 7.3, H³ dppy), 4.45 (2H, q, J = 7.0, CO₂CH₂CH₃ tpybae), 1.47 (3H, t, J = 7.1, CO₂CH₂CH₃ tpybae). ¹H-NMR (d₆-Acetone, 500 MHz) δ = 9.49 (2H, s, H^{3'} tpybae), 9.06 (2H, d, J = 7.5, H³ tpybae), 8.49 (2H, d, J = 7.9, H^a tpybae or H^b tpybae), 8.32 (2H, d, J = 7.6, H^a tpybae or H^b tpybae), 8.16-8.21 (3H, m, H^{3'} dppy & H^{4'} dppy), 8.13 (2H, t, J = 7.1, H⁴ tpybae), 7.99 (2H, d, J = 5.7, H⁶ tpybae), 7.93 (2H, d, J = 7.7, H⁶ dppy), 7.45 (2H, t, J = 6.6, H⁵ tpybae), 6.96 (2H, td, J = 7.6, 1.2, H⁵ dppy), 6.74 (2H, td, J = 7.3, 0.8, H⁴ dppy), 6.32 (2H, d, J = 7.3, H³ dppy), 4.46 (2H, q, J = 7.1, CO₂CH₂CH₃ tpybae), 1.44 (3H, t, J = 7.1, CO₂CH₂CH₃ tpybae). MS(ES⁺) *m/z* = 803 (M⁺). λ_{max}/nm (Acetonitrile) = 235 (ε/dm³ mol⁻¹ cm⁻¹ 16 000), 282 (15 500), 312 (10 600), 439 (2 700), 477 (2 100), 510 (1 700). One spot by TLC(silica), R_f = 0.2 in dichloromethane/methanol, 90/10.

6.3 Synthesis of macrocyclic ligands and their lanthanide(III) complexes

6.3.1 8-Benzyloxyquinoline-2-carboxaldehyde



*8-Benzyloxy-2-methylquinoline*²²⁶

Benzyl bromide (1.8 ml, 15.1 mmol) was added dropwise to a solution of 2-methylquinolin-8-ol (2.0 g, 12.6 mmol) and KOH (760 mg, 13.5 mmol) in ethanol (25 ml) followed by heating under reflux at 78°C for 12 h. The progress of the reaction was followed by TLC (silica, CH₂Cl₂/MeOH, 90/10). Precipitated KBr was removed by filtration and washed with ethanol. The solvent was removed from the filtrate under reduced pressure, and the residue dissolved in water (20 ml). The mixture was acidified with HCl (2 mol dm⁻³) and washed with diethyl ether (2 × 30 ml), followed by addition of NaOH solution (5 mol dm⁻³). The precipitate was isolated by filtration and dried under vacuum to give the desired product as a colourless solid (1.78 g, 57%).

¹H-NMR (CDCl₃, 400 MHz) δ = 7.99 (1H, d, J = 8.5, H³), 7.50 (2H, d, J = 7.4, H^{2'}), 7.35 (2H, tt, J = 7.7, 1.4, H^{3'}), 7.24-7.31 (4H, m, H⁴, H⁶, H^{4'} & H⁵ or H⁷), 6.98 (1H, dd, J = 7.6, 1.4, H⁵ or H⁷), 5.45 (2H, s, CH₂), 2.80 (3H, s, CH₃). MS(EI) m/z = 249 (M⁺), 172 (M⁺ - Ph), 143 (M⁺ - PhCH₂O), 91 (C₇H₇⁺), 65 (C₅H₅⁺). Characterisation data are consistent with that in the literature.²²⁶

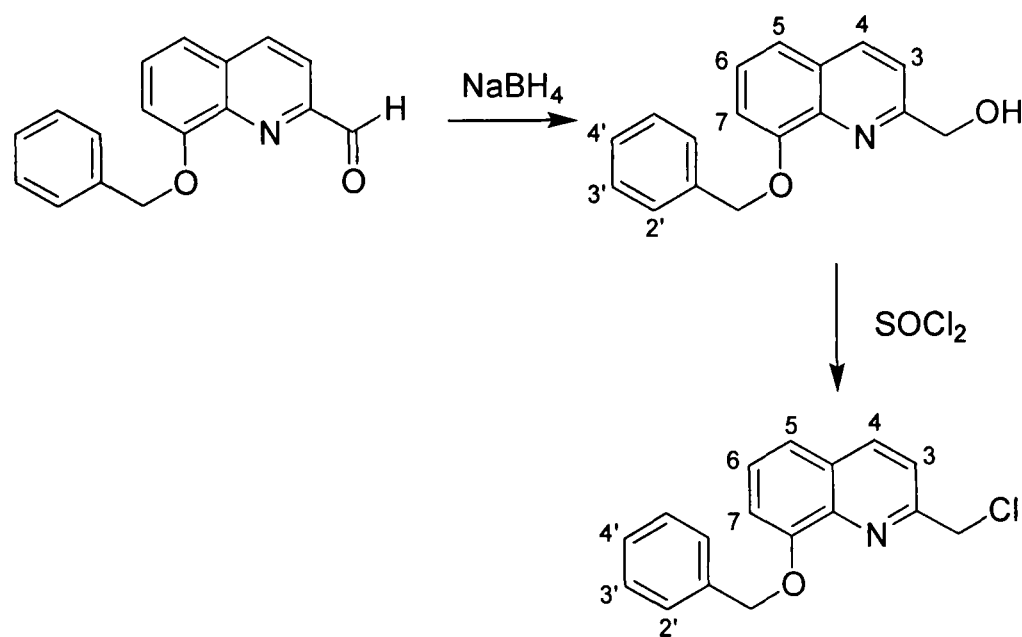
*8-Benzyloxyquinoline-2-carboxaldehyde*²²⁶

8-Benzyloxy-2-methylquinoline (1.35 g, 5.41 mmol) was added to a suspension of selenium oxide (752 mg, 6.78 mmol) in 1,4-dioxane (20 ml) under a nitrogen atmosphere, followed by heating to 80°C for 24 h. The hot mixture was filtered through

Celite® to remove black selenium. The solvent was removed under reduced pressure and the residue redissolved in acetone. The remaining red selenium was removed by filtration and the solvent was removed under reduced pressure. Purification of the residue by column chromatography (silica, CH₂Cl₂/MeOH, gradient elution from 100/0 to 99/1) gave the desired product as a yellow solid (1.15 g, 81%), mp 92.6-93.5°C.

¹H-NMR (CDCl₃, 400 MHz) δ = 10.33 (1H, s, CHO), 8.28 (1H, d, J = 8.5, H³), 8.08 (1H, d, J = 8.5, H⁴), 7.52-7.38 (3H, m, H⁶ & H^{2'}), 7.47 (1H, dd, J = 8.3, 1.2, H⁵ or H⁷), 7.40 (2H, tt, J = 7.8, 1.6, H^{3'}), 7.33 (1H, tt, J = 7.3, 1.4, H^{4'}), 7.16 (1H, dd, J = 7.6, 1.2, H⁵ or H⁷), 5.50 (2H, s, PhCH₂O). ¹³C{¹H}-NMR (CDCl₃, 101 MHz) δ = 194.1 (C=O), 155.4 (C⁹), 151.8 (C⁹), 140.5 (C⁹), 137.4 (CH), 136.7 (C⁹), 131.6 (C⁹), 129.8 (CH), 128.8 (CH), 128.2 (CH), 127.2 (CH), 120.1 (CH), 118.0 (CH), 111.2 (CH), 71.3 (PhCH₂O). MS(EI) *m/z* = 263 (M⁺), 234 (M⁺ - CHO), 186 (M⁺ - Ph), 157 (M⁺ - PhCH₂O), 91 (C₇H₇⁺), 65 (C₅H₅⁺). IR (thin film) $\bar{\nu}$ = 1697 cm⁻¹ (CHO, C=O stretch). Characterisation data are consistent with that in the literature.²²⁶

6.3.2 8-Benzyloxy-2-chloromethylquinoline



*(8-Benzyloxyquinolin-2-yl)methanol**

8-Benzyloxyquinoline-2-carboxaldehyde (1.006 g, 3.92 mmol) in a mixture of methanol (20 ml) and dichloromethane (1 ml) was added dropwise over 10 minutes to a stirred solution of sodium borohydride (87 mg, 2.30 mmol) in methanol (40 ml). The reaction mixture was stirred at room temperature for two days, with additional sodium

* An adaptation of the procedure used for the synthesis of (8-hydroxyquinolin-2-yl)methanol was followed.⁴⁶²

borohydride (160 mg, 4.23 mmol) added after 2½ h and again (159 mg, 4.20 mmol) after 24 h*. The solvent was removed under reduced pressure and the residue dissolved in water (40 ml), neutralised with HCl (1 mol dm⁻³, ~1 ml) and extracted into ethyl acetate (2 × 50 ml). Drying over MgSO₄ followed by removal of solvent under reduced pressure gave the desired product as a yellow solid (771 mg, 75%).

¹H-NMR (CDCl₃, 300 MHz) δ = 8.12 (1H, d, J = 8.5, H³), 7.55 (2H, d, J = 7.7, H^{2'}), 7.32-7.42 (6H, m, H⁷, H⁴, H⁵, H^{3'} & H^{4'}), 7.13 (1H, t, J = 4.5, H⁶), 5.36 (2H, s, PhCH₂O), 4.94 (2H, s, CH₂OH).

8-Benzyloxy-2-chloromethylquinoline[†]

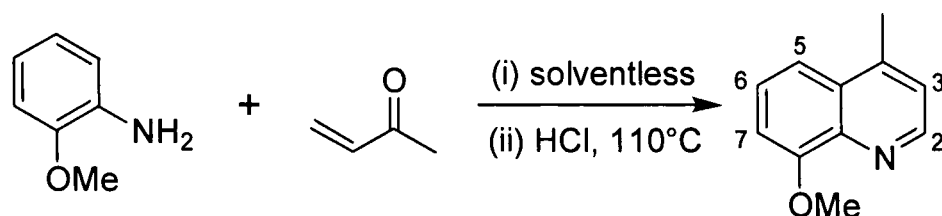
Redistilled thionyl chloride (10 ml) was added over a period of 30 minutes to (8-benzyloxyquinolin-2-yl)methanol (771 mg, 2.91 mmol) at 0°C, followed by stirring at room temperature for 2½ h. The solvent was removed under reduced pressure, and the residue redissolved in dichloromethane then washed with Na₂CO₃ solution. Removal of solvent under reduced pressure followed by recrystallisation of the residue from hexane gave the desired product as a pale yellow solid (160 mg). Further yield (46 mg) was obtained by column chromatography (silica, CH₂Cl₂) of the residue from recrystallisation (giving a total yield of 206 mg, 25%), mp 110.9-111.5°C.

¹H-NMR (CDCl₃, 300 MHz) δ = 8.17 (1H, d, J = 8.6, H³), 7.67 (1H, d, J = 8.5, H⁴), 7.52 (2H, d, J = 7.4, H^{2'}), 7.27-7.43 (5H, m, H⁵, H⁷, H^{3'} & H^{4'}), 7.06 (1H, t, J = 4.6, H⁶), 5.46 (2H, s, PhCH₂O), 4.94 (2H, s, PhCH₂Cl). ¹³C{¹H}-NMR (CDCl₃, 101 MHz) δ = 156.0 (C^q), 154.4 (C^q), 139.6 (C^q), 137.4 (C^q), 137.1 (C^q), 128.9 (C^q), 128.7 (CH), 127.9 (CH), 127.1 (CH), 127.0 (CH), 121.2 (CH), 120.0 (CH), 111.1 (CH), 71.1 (PhCH₂O), 47.8 (CH₂Cl). MS(EI) *m/z* = 283 (M⁺), 248 (M⁺ - Cl), 247 (M⁺ - HCl), 206 (M⁺ - Ph), 177 (M⁺ - PhCH₂O), 91 (C₇H₇⁺), 65 (C₅H₅⁺).

* It is suspected that additional reagent was required due to poor quality of the original sodium borohydride.

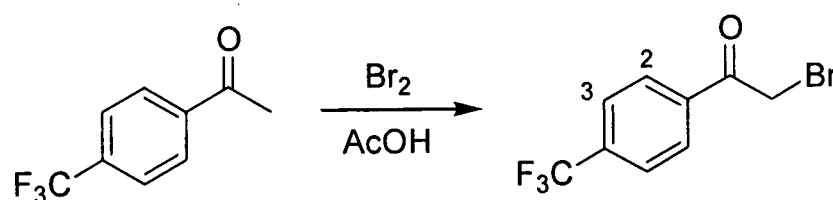
† An adaptation of the procedure used for the synthesis of 8-hydroxy-2-chloromethylquinoline was followed.⁴⁶²

6.3.3 8-Methoxy-4-methylquinoline



2-Methoxyaniline (2.70 ml, 23.9 mmol) and methyl vinyl ketone (3.00 ml, 36.0 mmol) were stirred at 35°C in the absence of solvent for 1 h. Excess starting material was then removed by evaporation at atmospheric pressure. Concentrated HCl (10 ml) was added, and the mixture stirred at 110°C for 20 h. After cooling to room temperature the reaction mixture was diluted with water (50 ml), made basic with KOH solution and extracted into dichloromethane. Drying over MgSO₄, removal of solvent under reduced pressure, column chromatography (silica, CH₂Cl₂/MeOH, gradient elution from 100/0 to 97/3) and recrystallisation from a hexane/diethyl ether mixture gave the desired product as a brown solid (1.59 g, 38%).

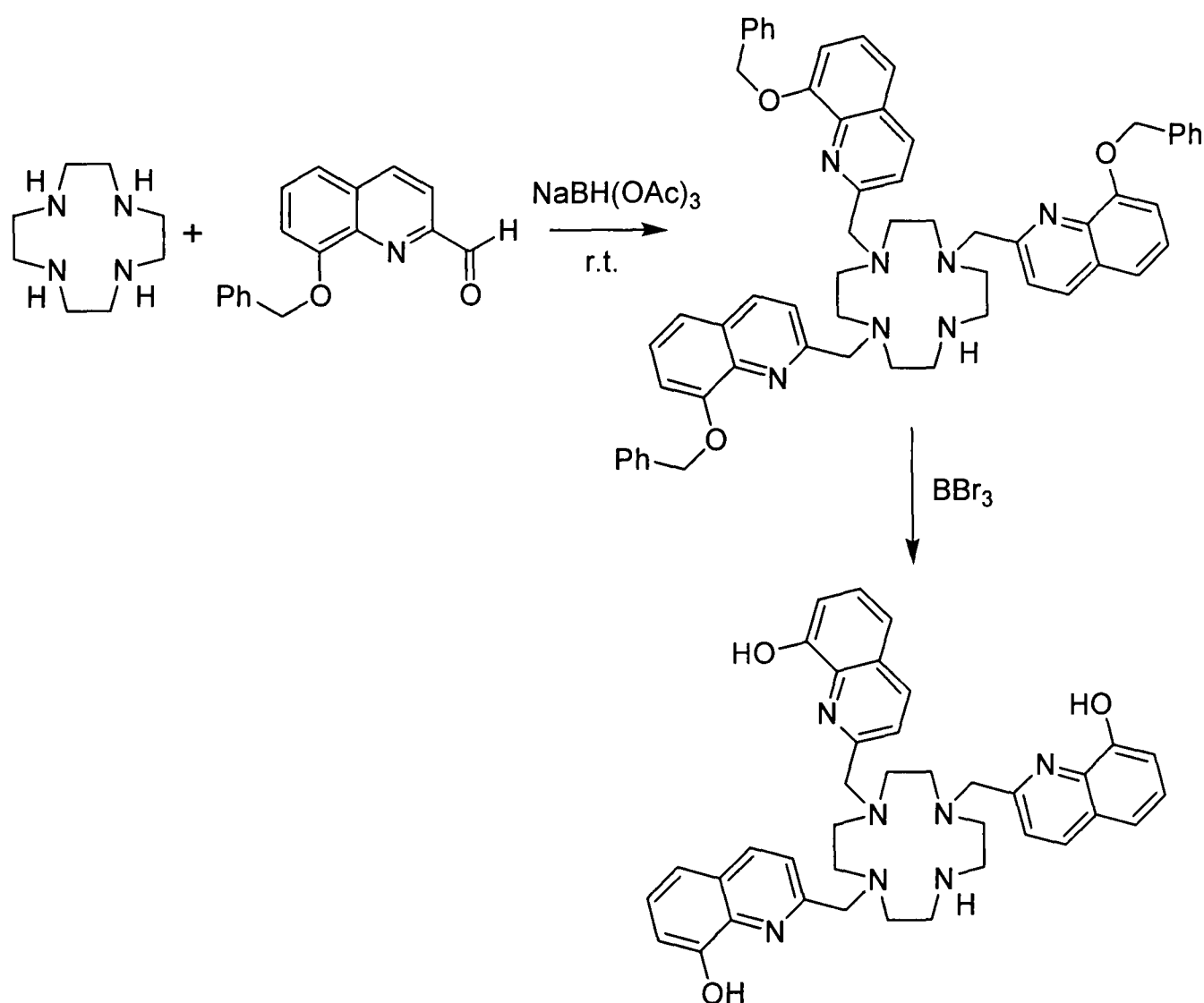
¹H-NMR (CDCl₃, 300 MHz) δ = 8.79 (1H, d, J = 4.3, H²), 7.57 (1H, dd, J = 8.7, 1.3, H⁵), 7.49 (1H, t, J = 8.0, H⁶), 7.27 (1H, d, J = 4.4, H³), 7.06 (1H, dd, J = 7.5, 1.1, H⁷), 4.09 (3H, s, OMe), 2.70 (3H, s, Me). ¹³C{¹H}-NMR (CDCl₃, 63 MHz) δ = 155.9 (C^q), 149.0 (CH), 144.2 (C^q), 140.1 (C^q), 129.4 (C^q), 126.4 (CH), 122.6 (CH), 115.7 (CH), 107.3 (CH), 56.1 (OCH₃), 19.2 (Me). MS(EI) *m/z* = 173 (M⁺), 172 (M⁺ – H), 142 (M⁺ – OMe). Characterisation data are consistent with that in the literature.⁴⁶³

6.3.4 2-Bromo-1-(4-trifluoromethylphenyl)ethanone⁴⁶⁴

4-(Trifluoromethyl)acetophenone (951 mg, 5.05 mmol) and bromine (817 mg, 5.11 mmol) in acetic acid (10 ml) were stirred at room temperature for 1½ h. The progress of the reaction was followed by TLC (silica, hexane/ether, 60/40). After this period, the reaction mixture was poured into ice and extracted into diethyl ether (3 × 30 ml). Drying over MgSO₄, removal of solvent under reduced pressure, and recrystallisation of the residue from hexane gave the desired product as a white crystalline solid (588 mg, 44%), mp 55.2-55.8°C.

$^1\text{H-NMR}$ (CDCl_3 , 300 MHz) $\delta = 8.11$ (2H, d, $J = 8.4$, arom), 7.77 (2H, d, $J = 8.3$, arom), 4.45 (2H, s, COCH_2Br). $^1\text{H-NMR}$ ($d_6\text{-DMSO}$, 400 MHz) $\delta = 8.19$ (2H, d, $J = 8.2$, arom), 7.94 (2H, d, $J = 8.2$, arom), 5.02 (2H, s, COCH_2Br). $^{13}\text{C}\{^1\text{H}\}\text{-NMR}$ (CDCl_3 , 101 MHz) $\delta = 190.5$ (s, $\text{C}=\text{O}$), 136.7 (s, C^1), 135.1 (q, $J = 33$, C^4), 129.3 (s, C^2), 125.9 (q, $J = 4$, C^3), 123.5 (q, $J = 273$, CF_3), 30.6 (s, CH_2). $^{19}\text{F-NMR}$ (CDCl_3 , 188 MHz) $\delta = 63.7$ (CF_3). MS(EI) $m/z = 266/268$ (M^+), 247/249 ($\text{M}^+ - \text{F}$), 173 ($\text{M}^+ - \text{CH}_2\text{Br}$), 145 ($\text{M}^+ - \text{COCH}_2\text{Br}$), 125 ($\text{M}^+ - \text{COCH}_2\text{Br}$, HF). IR (KBr disc) $\bar{\nu} = 1701\text{ cm}^{-1}$ (ketone, $\text{C}=\text{O}$ stretch). Characterisation data are consistent with that in the literature.⁴⁶⁵

6.3.5 1,4,7-Tris-(8-hydroxyquinolin-2-ylmethyl)-1,4,7,10-tetraazacyclododecane **131**



1,4,7-Tris-(8-benzyloxyquinolin-2-ylmethyl)-1,4,7,10-tetraazacyclododecane

8-Benzyloxyquinoline-2-carboxaldehyde (1.16 g, 4.41 mmol) and 1,4,7,10-tetraazacyclododecane (269 mg, 1.56 mmol) in dichloromethane (30 ml) were stirred at room temperature under a nitrogen atmosphere for 1 h. Sodium triacetoxyborohydride (1.16 g, 5.45 mmol) was then added, and the reaction mixture stirred for a further three days. Additional 8-benzyloxyquinoline-2-carboxaldehyde (804 mg, 3.05 mmol) and

sodium triacetoxyborohydride (779 mg, 3.68 mmol) were added in two portions after a further one and two days. The progress of the reaction was followed by TLC (silica, CH₂Cl₂/MeOH, 95/5). The reaction was terminated 18 h after the third addition by treatment with HCl (1 mol dm⁻³, 10 ml) followed by adjustment to pH 10 with KOH solution (1 mol dm⁻³, ~40 ml). The product was extracted into dichloromethane (3 × 30 ml), dried over Na₂CO₃ and the solvent removed under reduced pressure. Purification of the residue by column chromatography (alumina pre-soaked in ethyl acetate, CH₂Cl₂/MeOH, gradient elution from 100/0 to 98/2) followed by recrystallisation from ethyl acetate gave the desired product as a yellow solid (84 mg, 6%).*

MS(ES+) $m/z = 914$ ([M+H]⁺).

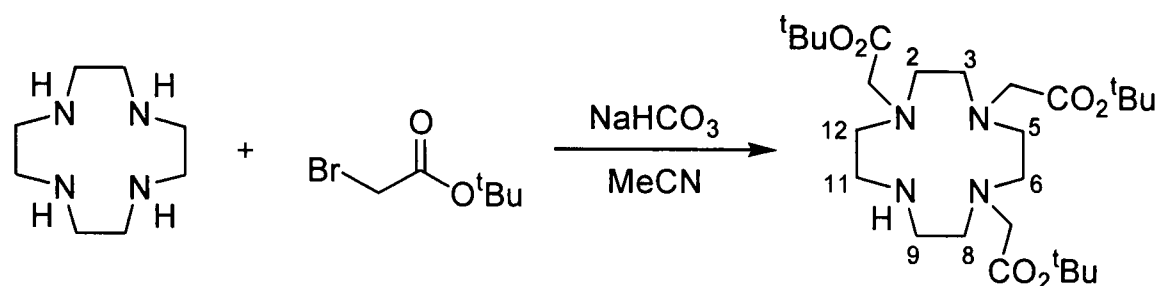
1,4,7-Tris-(8-hydroxyquinolin-2-ylmethyl)-1,4,7,10-tetraazacyclododecane 131[†]

Boron tribromide (1.7 ml, 1.70 mmol) was added to a stirred solution of 1,4,7-tris-(8-benzyloxyquinolin-2-ylmethyl)-1,4,7,10-tetraazacyclododecane (99 mg, 0.11 mmol) in dichloromethane (10 ml) at 0°C under a nitrogen atmosphere. The reaction mixture was allowed to warm to room temperature and stirred under nitrogen overnight, followed by addition of methanol (15 ml) and stirring at room temperature for a further 2 h. Following removal of solvent under reduced pressure, the residue was dissolved in NaOH solution (1 mol dm⁻³, 5 ml) and any solid removed by centrifugation. Neutralisation of the orange solution with HCl (1 mol dm⁻³) precipitated the product, which was collected by centrifugation and dried under vacuum to give the desired product as a white solid (69 mg, 100%).

¹H-NMR (CDCl₃, 200 MHz) $\delta = 6.8-8.4$ (15H, m, arom), 3.91 (4H, br s, NCH₂arom), 3.69 (2H, br s, NCH₂arom), 3.26 (4H, br s, NCH₂CH₂N), 3.03 (4H, br s, NCH₂CH₂N), 2.85 (4H, br s, NCH₂CH₂N), 2.68 (4H, br s, NCH₂CH₂N). MS(ES+) $m/z = 706$ ([M+Cu]⁺).

* Even after column chromatography and recrystallisation, the sample was not entirely pure by ¹H-NMR spectroscopy. Hence, due to the complexity of the spectrum, no assignments have been made.

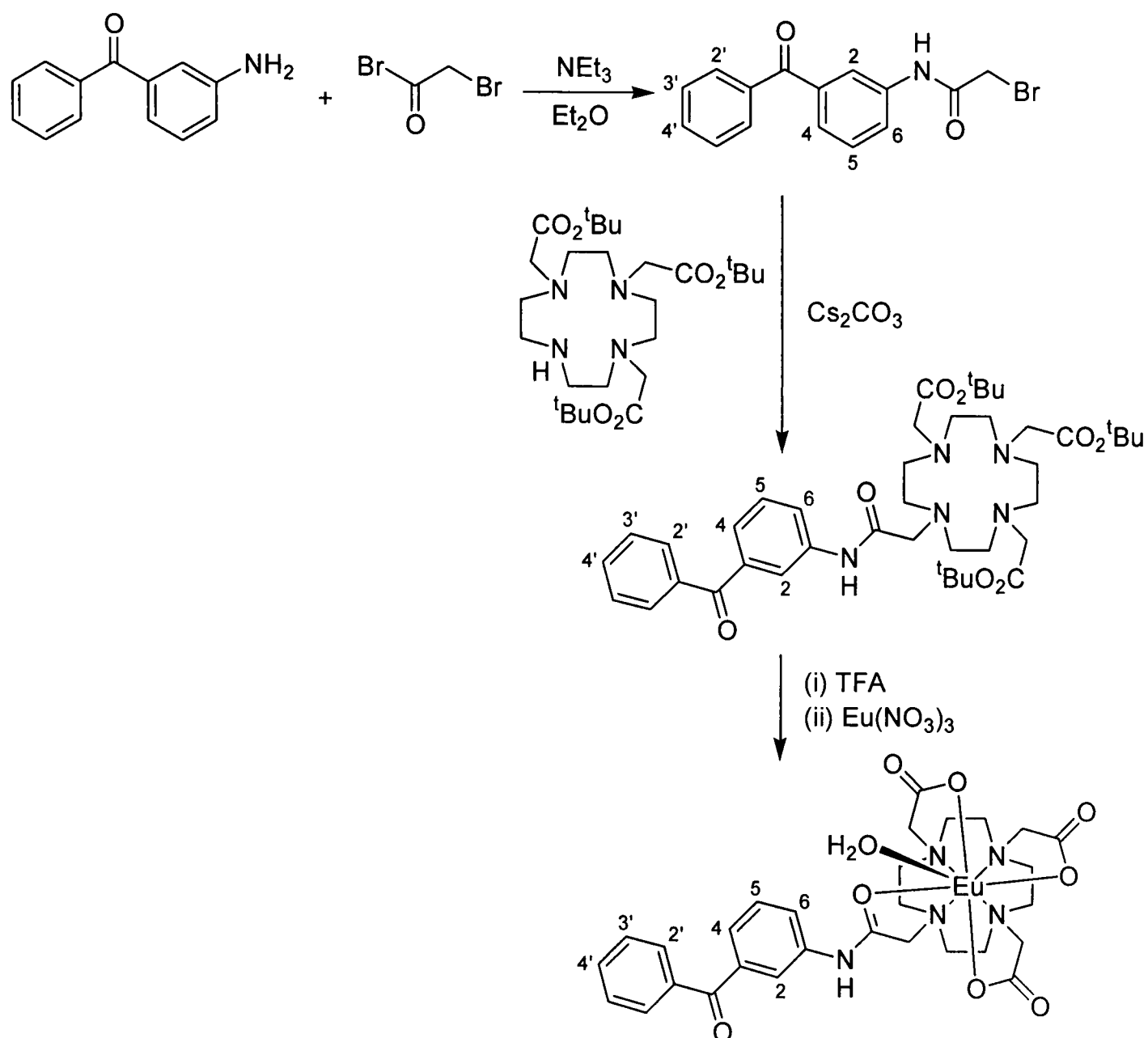
[†] Debonylation to form the 8-hydroxyquinoline derivative was performed as for tris-N-(2-aminoethyl-[8-benzyloxyquinoline-2-carboxamido])amine.⁴⁶⁶

6.3.6 1,4,7,10-Tetraazacyclododecane-1,4,7-tris(acetic acid *tert*-butyl ester) 126³¹⁸


tert-Butyl bromoacetate (7.71 ml, 52.2 mmol) and 1,4,7,10-tetraazacyclododecane (2.97 g, 17.2 mmol) were added to a stirred suspension of sodium hydrogen carbonate (4.47 g, 53.2 mmol) in acetonitrile (120 ml), and the mixture stirred in the presence of a small amount of molecular sieves at room temperature under a nitrogen atmosphere. The progress of the reaction was followed by TLC (silica, CH₂Cl₂/MeOH, 95/5). After 18 h, the solution was decanted from the molecular sieves, which were washed with more acetonitrile. The solvent was removed from the combined solutions under reduced pressure, and the residue added to water (150 ml) followed by extraction into dichloromethane (3 × 150 ml). Removal of solvent under reduced pressure and recrystallisation of the residue from toluene gave the desired product as a colourless solid (5.38 g, 61%), mp = 179.3-180.5°C.

¹H-NMR (CDCl₃, 300 MHz) δ = 10.09 (1H, br s, NH), 3.37 (4H, s, NCH₂CO₂^tBu), 3.28 (2H, s, NCH₂CO₂^tBu), 3.09 (4H, t, J = 8.3, H⁹ & H¹¹), 2.92 (8H, t, J = 8.3, H², H³, H⁵ & H⁶), 2.90 (4H, t, J = 8.3, H⁸ & H¹²), 1.46 (18H, s, ^tBu), 1.45 (9H, s, ^tBu). ¹³C{¹H}-NMR (CDCl₃, 101 MHz) δ = 170.6 (C=O), 169.8 (C=O), 82.0 (C(CH₃)₃), 81.8 (C(CH₃)₃), 58.3 (CH₂), 51.5 (CH₂), 49.4 (CH₂), 47.6 (CH₂), 28.4 (C(CH₃)₃), 28.3 (C(CH₃)₃). MS(ES+) *m/z* = 515 ([M+H]⁺). IR (KBr disc) $\bar{\nu}$ = 1729 cm⁻¹ (CO₂^tBu, C=O stretch), 1718 cm⁻¹ (CO₂^tBu, C=O stretch). Characterisation data are consistent with that in the literature.³¹⁸

6.3.7 Europium(III) 10-((3-Benzoyl-phenylcarbamoyl)methyl)-1,4,7,10-tetraazacyclododecane-1,4,7-trisacetate [Eu-128]



N-(3-Benzoyl-phenyl)-2-bromo-acetamide

Bromoacetyl bromide (2.84 g, 14.1 mmol) was added dropwise to a solution of 3-aminobenzophenone (2.19 g, 11.1 mmol) and triethylamine (1.36 g, 13.4 mmol) in diethyl ether (100 ml) at -10°C , ensuring that the temperature did not rise above 0°C . After warming to room temperature, the precipitated solid was isolated by filtration, re-dissolved in dichloromethane and washed with HCl (1 mol dm^{-3} , $3 \times 50 \text{ ml}$). Drying over MgSO_4 , removal of solvent under reduced pressure and drying under vacuum gave the desired product as a pale brown solid (2.42 g, 68%).

$^1\text{H-NMR}$ (CDCl_3 , 400 MHz) $\delta = 8.32$ (1H, br s, NH), 7.94 (1H, d, $J = 7.8$, H^6), 7.85 (1H, s, H^2), 7.81 (2H, d, $J = 5.6$, $\text{H}^{2'}$), 7.61 (1H, tt, $J = 7.4, 1.4$, $\text{H}^{4'}$), 7.57 (1H, dt, $J = 7.7, 1.3$, H^4), 7.46-7.53 (3H, m, H^5 & $\text{H}^{3'}$), 4.03 (2H, s, CH_2). $^{13}\text{C}\{^1\text{H}\}$ -NMR (CDCl_3 , 101 MHz) $\delta = 196.1$ (C=O), 163.8 (C=O), 138.7 (C^q), 137.3 (C^q), 137.3 (C^q),

132.9 (C^{4'}), 130.2 (C^{2'}), 129.3 (C⁵), 128.6 (C^{3'}), 126.9 (C⁴), 124.1 (C⁶), 121.4 (C²), 29.4 (CH₂). MS(EI) $m/z = 317/319$ (M⁺), 240/242 (M⁺ – Ph), 238 (M⁺ – Br), 197 (PhCOC₆H₄NH₂⁺), 105 (PhCO⁺), 77 (Ph⁺). IR (KBr disc) $\bar{\nu} = 1662$ cm⁻¹ (ketone, C=O stretch), 1655 cm⁻¹ (amide, C=O stretch).

10-((3-Benzoyl-phenylcarbamoyl)methyl)-1,4,7,10-tetraazacyclododecane-1,4,7-tris(acetic acid tert-butyl ester)

1,4,7,10-Tetraazacyclododecane-1,4,7-tris(acetic acid *tert*-butyl ester) (3.76 g, 7.31 mmol), N-(3-benzoyl-phenyl)-2-bromo-acetamide (2.32 g, 7.29 mmol), caesium carbonate (7.36 g, 22.6 mmol) and a few grains of potassium iodide in acetonitrile (150 ml) were stirred at room temperature under a nitrogen atmosphere for two days. The progress of the reaction was followed by TLC (silica, CH₂Cl₂/MeOH, 95/5). The solvent was removed under reduced pressure, and the residue added to water (100 ml) then extracted into dichloromethane (3 × 100 ml). Drying over MgSO₄ and removal of solvent under reduced pressure gave the desired product as a brown solid (4.77 g, 87%).

¹H-NMR (CDCl₃, 300 MHz) $\delta = 11.16$ (1H, br s, NH), 8.65 (1H, d, J = 7.9, H⁶), 8.49 (1H, s, H²), 8.33 (2H, d, J = 7.6, H^{2'}), 7.90-8.12 (5H, m, H⁴, H⁵, H^{3'} & H^{4'}), 3.71 (2H, s, CH₂), 3.68 (2H, s, CH₂), 3.65 (4H, s, CH₂), 3.26-3.40 (12H, m, NCH₂CH₂N), 3.14 (4H, br s, NCH₂CH₂N), 1.93 (9H, s, ^tBu), 1.89 (18H, s, ^tBu). MS(ES⁺) $m/z = 774$ ([M+Na]⁺).

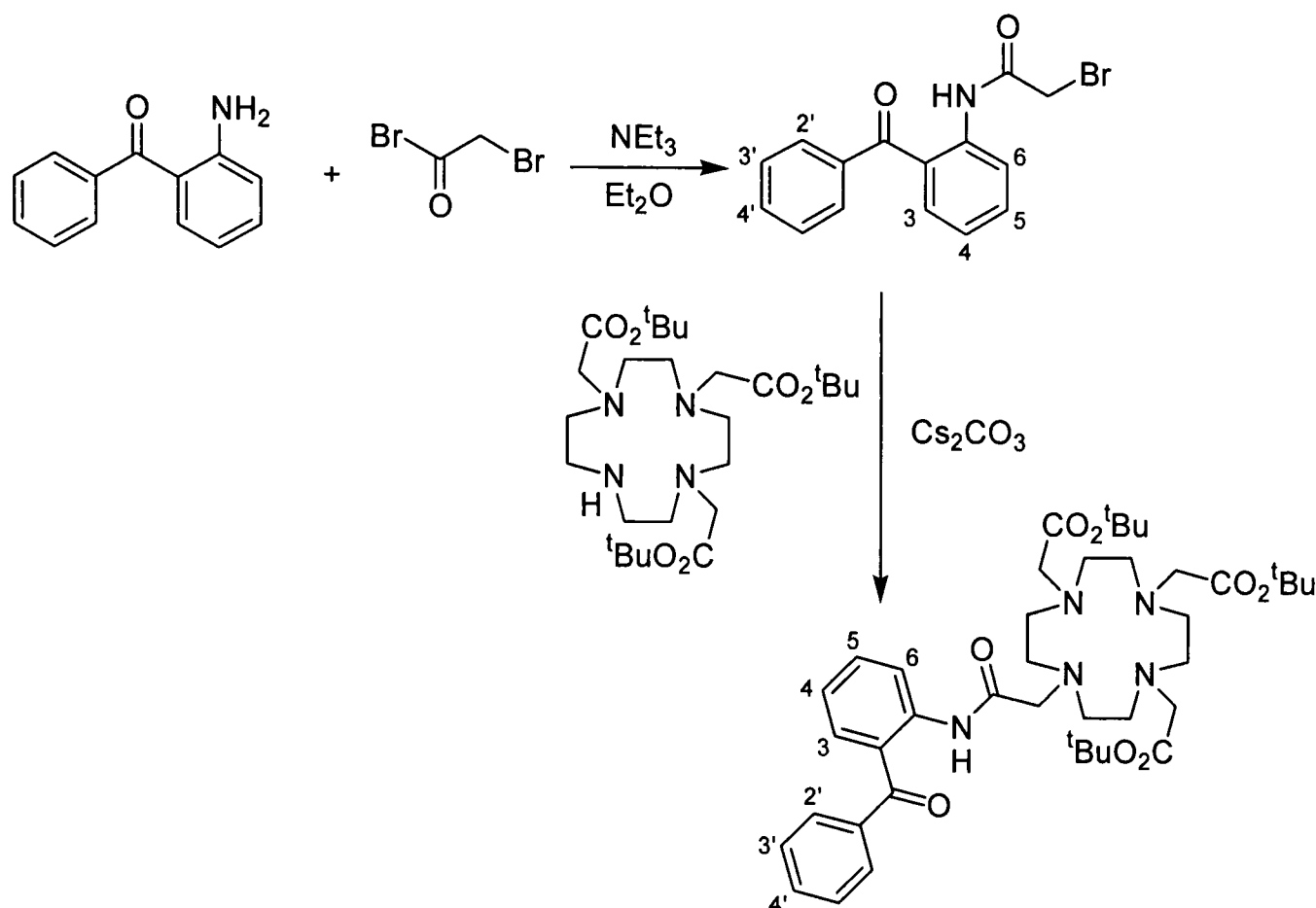
Europium(III) 10-((3-Benzoyl-phenylcarbamoyl)methyl)-1,4,7,10-tetraazacyclododecane-1,4,7-trisacetate [Eu·128]

A solution of 10-((3-benzoyl-phenylcarbamoyl)methyl)-1,4,7,10-tetraazacyclododecane-1,4,7-tris(acetic acid *tert*-butyl ester) (3.55 g, 4.72 mmol) in 80% TFA in dichloromethane (50 ml) was stirred at room temperature for three days. The reaction could be followed by ¹H NMR (D₂O). Removal of solvent under reduced pressure followed by washing with dichloromethane (2 × 100 ml) then diethyl ether (2 × 100 ml) gave 10-((3-benzoyl-phenylcarbamoyl)methyl)-1,4,7,10-tetraazacyclododecane-1,4,7-tris(acetic acid) as a pale brown solid, which was used without further purification.

¹H-NMR (D₂O, 400 MHz) $\delta = 7.84$ (1H, s, arom), 7.76 (3H, d, J = 7.5, arom), 7.71 (1H, t, J = 7.3, arom), 7.49-7.58 (4H, m, arom), 3.86 (8H, br s, CH₂), 3.29 (16H, br s, NCH₂CH₂N). MS(ES⁺) $m/z = 584$ ([M+H]⁺), 606 ([M+Na]⁺).

This was redissolved along with europium(III) nitrate pentahydrate (3.00 g, 7.01 mmol) in water (100 ml), the solution adjusted to pH 6 with NaOH solution (2 mol dm^{-3}) and heated under reflux at 100°C for 24 h. After cooling to room temperature the solvent was removed under reduced pressure. The residue was redissolved in ethanol and all undissolved material removed by filtration. Removal of solvent under reduced pressure and purification of the residue by column chromatography (alumina, $\text{CH}_2\text{Cl}_2/\text{MeOH}$, gradient elution from 100/0 to 95/5) gave the desired product as a colourless solid (1.67 g, 48%), mp $>250^\circ\text{C}$.

$^1\text{H-NMR}$ (D_2O , 500 MHz) $\delta = 34.21$ (1H, s, H_{ax}), 31.35 (1H, s, H_{ax}), 30.24 (1H, s, H_{ax}), 30.03 (1H, s, H_{ax}), 7.82-8.74 (9H, m, arom), 1.14 (1H, s, H_{eq}), -0.50 (2H, s, H_{eq} & $\text{H}_{\text{ax}'}$), -2.99 (1H, s, H_{eq}), -3.86 (2H, s, H_{eq} & $\text{H}_{\text{ax}'}$), -5.09 (1H, s, $\text{H}_{\text{eq}'}$), -7.87 (2H, s, $\text{H}_{\text{eq}'}$ & H_{eq}), -8.10 (1H, s, $\text{H}_{\text{eq}'}$), -10.67 (1H, s, CH_2CO), -11.91 (1H, s, $\text{H}_{\text{ax}'}$), -12.20 (1H, s, CH_2CO), -12.46 (1H, s, $\text{H}_{\text{ax}'}$), -13.82 (1H, s, CH_2CO), -13.96 (1H, s, CH_2CO), -14.90 (1H, s, CH_2CO), -15.10 (1H, s, CH_2CO), -16.21 (1H, s, CH_2CO), -17.54 (1H, s, CH_2CO). MS(ES+) $m/z = 756$ ($[\text{M}+\text{Na}]^+$). HRMS(ES+) $m/z = 734.1702$ ($[\text{M}+\text{H}]^+$); calc. for $\text{EuC}_{29}\text{H}_{35}\text{O}_8\text{N}_5$, 734.1692.

6.3.8 10-((2-Benzoyl-phenylcarbamoyl)methyl)-1,4,7,10-tetraazacyclo-dodecane-1,4,7-tris(acetic acid *tert*-butyl ester)

N-(2-Benzoyl-phenyl)-2-bromo-acetamide

Bromoacetyl bromide (2.89 g, 14.3 mmol) was added dropwise to a solution of 2-aminobenzophenone (2.19 g, 11.1 mmol) and triethylamine (1.50 g, 14.8 mmol) in diethyl ether (100 ml) at -10°C, ensuring that the temperature did not rise above 0°C. After warming to room temperature, the reaction mixture was washed with HCl (1 mol dm⁻³, 3 × 50 ml) and dried over MgSO₄. Removal of solvent under reduced pressure and drying under vacuum gave the desired product as a pale brown solid (3.30 g, 93%).

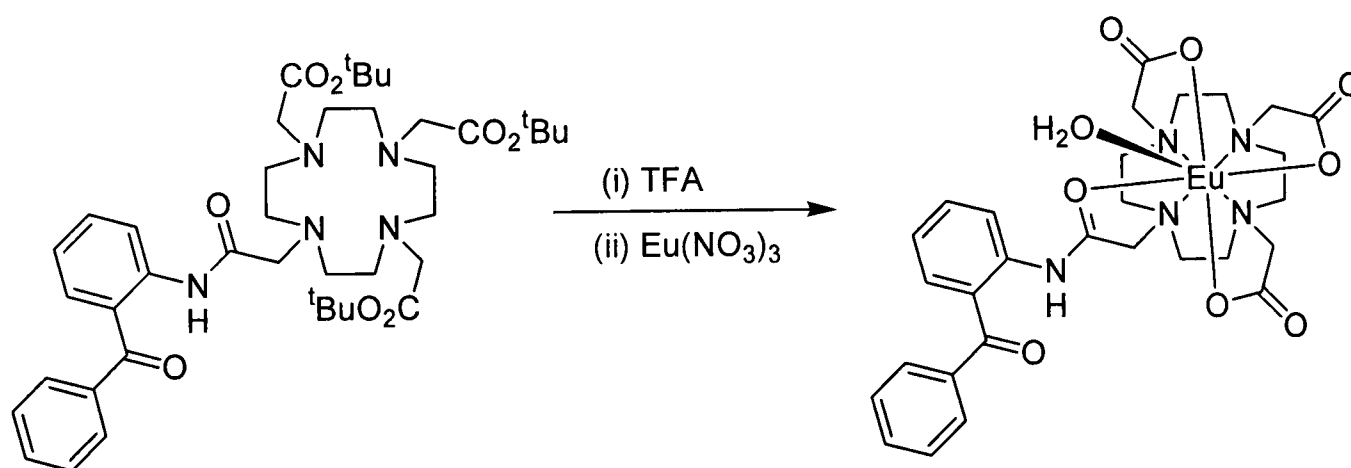
¹H-NMR (CDCl₃, 500 MHz) δ = 11.50 (1H, br s, NH), 8.59 (1H, d, J = 8.2, H⁶), 7.72 (2H, d, J = 7.9, H^{2'}), 7.58-7.63 (3H, m, H³, H⁵ & H^{4'}), 7.49 (2H, t, J = 7.6, H^{3'}), 7.16 (1H, t, J = 7.6, H⁴), 4.03 (2H, s, CH₂). ¹³C{¹H}-NMR (CDCl₃, 126 MHz) δ = 199.4 (C=O), 165.2 (NHC=O), 139.6 (C⁹), 138.4 (C⁹), 134.3 (C³ or C⁵ or C^{4'}), 133.7 (C³ or C⁵ or C^{4'}), 132.8 (C³ or C⁵ or C^{4'}), 130.1 (C^{2'}), 128.5 (C^{3'}), 124.2 (C⁹), 123.2 (C⁴), 121.7 (C⁶), 29.6 (CH₂). MS(EI) *m/z* = 317/319 (M⁺), 240/242 (M⁺ - Ph), 238 (M⁺ - Br), 224 (M⁺ - CH₂Br), 212/214 (M⁺ - PhCO), 196 (M⁺ - COCH₂Br), 105 (PhCO⁺), 77 (Ph⁺). IR (KBr disc) $\bar{\nu}$ = 1684 cm⁻¹ (ketone, C=O stretch), 1630 cm⁻¹ (amide, C=O stretch).

10-((2-Benzoyl-phenylcarbamoyl)methyl)-1,4,7,10-tetraazacyclododecane-1,4,7-tris(acetic acid tert-butyl ester)

1,4,7,10-Tetraazacyclododecane-1,4,7-tris(acetic acid *tert*-butyl ester) (1.88 g, 3.65 mmol), N-(2-benzoyl-phenyl)-2-bromo-acetamide (1.16 g, 3.65 mmol), caesium carbonate (3.68 g, 11.3 mmol) and a few grains of potassium iodide in acetonitrile (75 ml) were stirred at room temperature under a nitrogen atmosphere for two days. The progress of the reaction was followed by TLC (silica, CH₂Cl₂/MeOH, 95/5). The solvent was removed under reduced pressure, and the residue added to water (50 ml) then extracted into dichloromethane (3 × 50 ml). Drying over MgSO₄ and removal of solvent under reduced pressure gave the desired product as a brown solid (2.40 g, 87%).

¹H-NMR (CDCl₃, 300 MHz) δ = 11.27 (1H, br s, NH), 8.23 (1H, d, J = 8.1, H⁶), 7.79 (2H, d, J = 8.0, H^{2'}), 7.56 (1H, tt, J = 7.4, 1.2, H^{4'}), 7.51 (1H, td, J = 8.1, 1.5, H⁵), 7.42-7.47 (3H, m, H³ & H^{3'}), 7.12 (1H, td, J = 7.5, 1.0, H⁴), 3.35 (2H, s, CH₂), 3.25 (4H, s, CH₂), 3.11 (2H, s, CH₂), 2.72-2.91 (16H, m, NCH₂CH₂N), 1.46 (9H, s, ^tBu), 1.39 (18H, s, ^tBu). MS(ES+) *m/z* = 752 ([M+H]⁺), 774 ([M+Na]⁺).

6.3.9 Europium(III) 10-((2-Benzoyl-phenylcarbamoyl)methyl)-1,4,7,10-tetraazacyclododecane-1,4,7-trisacetate [Eu·127]



A solution of 10-((2-benzoyl-phenylcarbamoyl)methyl)-1,4,7,10-tetraazacyclododecane-1,4,7-tris(acetic acid *tert*-butyl ester) (154 mg, 0.20 mmol) in 80% TFA in dichloromethane (2 ml) was stirred at room temperature for three days. The reaction could be followed by ¹H NMR (D₂O). Removal of solvent under reduced pressure followed by washing with dichloromethane (3 × 20 ml) then diethyl ether (3 × 20 ml) gave 10-((2-benzoyl-phenylcarbamoyl)methyl)-1,4,7,10-tetraazacyclododecane-1,4,7-tris(acetic acid) as a pale brown solid, which was used without further purification.

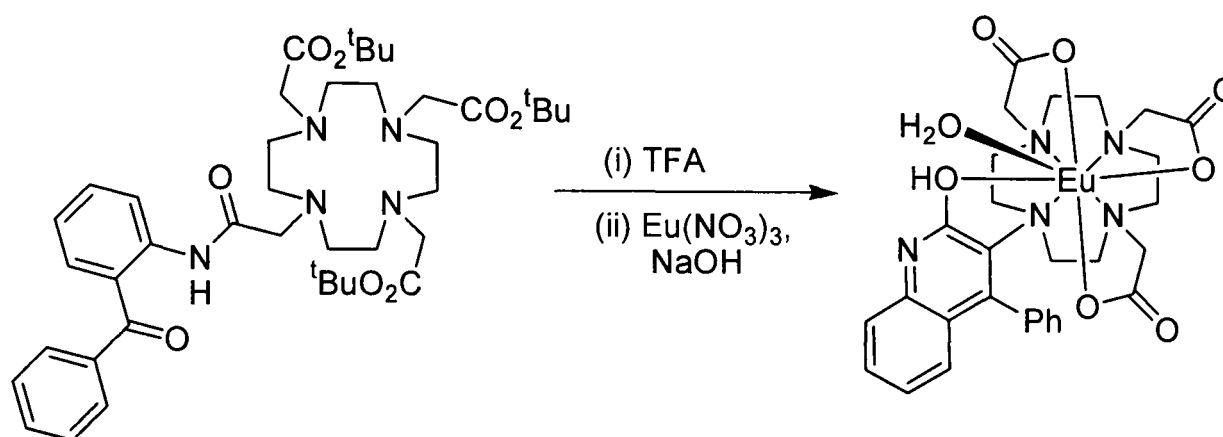
$^1\text{H-NMR}$ (D_2O , 400 MHz) δ = 7.72 (2H, d, J = 7.8, arom), 7.66 (1H, t, J = 7.5, arom), 7.64 (1H, t, J = 8.1, arom), 7.48-7.53 (3H, m, arom), 7.46 (1H, d, J = 8.1, arom), 7.40 (1H, t, J = 7.9, arom), 2.70-3.97 (24H, br m, CH_2). MS(ES+) m/z = 584 ($[\text{M}+\text{H}]^+$), 606 ($[\text{M}+\text{Na}]^+$).

This was redissolved along with europium(III) nitrate pentahydrate (95 mg, 0.22 mmol) in water (3 ml), the solution carefully adjusted to pH 6 with NaOH solution (2 mol dm^{-3}) (NOTE: The reaction must not be carried out under more basic conditions, otherwise the product shown in Section 6.3.10 is obtained) and heated to 40°C for 24 h. After cooling to room temperature the solvent was removed under reduced pressure. The residue was redissolved in ethanol and all undissolved material removed by filtration. Removal of solvent under reduced pressure and purification of the residue by column chromatography (alumina, $\text{CH}_2\text{Cl}_2/\text{MeOH}$, gradient elution from 100/0 to 85/15) gave the desired product as a colourless solid (82 mg, 55%),* mp $>250^\circ\text{C}$.

$^1\text{H-NMR}$ (D_2O , 500 MHz) δ = 33.95 (1H, s, H_{ax}), 31.01 (1H, s, H_{ax}), 29.37 (1H, s, H_{ax}), 28.71 (1H, s, H_{ax}), 7.00-10.00 (9H, m, arom), 1.60 (1H, s), 1.39 (1H, s), -1.01 (1H, s), -3.15 (1H, s), -3.81 (1H, s), -4.78 (1H, s), -4.91 (1H, s), -8.04 (1H, s), -8.48 (2H, s), -9.89 (1H, s), -11.58 (1H, s), -12.44 (1H, s), -13.31 (1H, s), -13.55 (1H, s), -13.68 (1H, s), -14.37 (1H, s), -15.48 (1H, s), -16.50 (1H, s), -18.29 (1H, s). MS(ES+) m/z = 756 ($[\text{M}+\text{Na}]^+$).

* Additional purification by further column chromatography (alumina, $\text{CH}_2\text{Cl}_2/\text{MeOH}$, gradient elution from 100/0 to 85/15) was required to remove small traces of impurity before photophysical studies were performed.

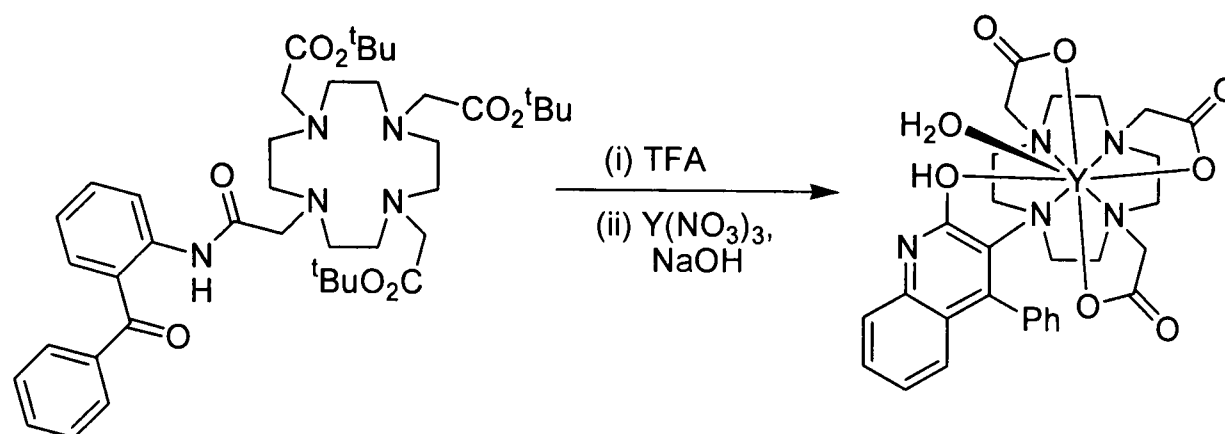
6.3.10 Europium(III) 10-(2-hydroxy-4-phenylquinolin-3-yl)-1,4,7,10-tetraazacyclododecane-1,4,7-trisacetate [Eu·132]



A solution of 10-((2-benzoyl-phenylcarbamoyl)methyl)-1,4,7,10-tetraazacyclododecane-1,4,7-tris(acetic acid *tert*-butyl ester) (1.78 g, 2.37 mmol) in 80% TFA in dichloromethane (25 ml) was stirred at room temperature for three days. The reaction could be followed by ^1H NMR (D_2O). Removal of solvent under reduced pressure followed by washing with dichloromethane (3×50 ml) then diethyl ether (3×50 ml) gave 10-((2-benzoyl-phenylcarbamoyl)methyl)-1,4,7,10-tetraazacyclododecane-1,4,7-tris(acetic acid) as a pale brown solid, which was used without further purification. This was redissolved along with europium(III) nitrate pentahydrate (1.03 g, 2.41 mmol) in water (30 ml), the solution made basic with NaOH solution (2 mol dm^{-3}), and heated under reflux at 100°C for 24 h. After cooling to room temperature the solvent was removed under reduced pressure. The residue was redissolved in ethanol and all undissolved material removed by filtration. Removal of solvent under reduced pressure and purification of the residue by column chromatography (alumina, $\text{CH}_2\text{Cl}_2/\text{MeOH}$, gradient elution from 100/0 to 50/50) gave the desired product as a colourless solid (1.14 g, 68%), mp $>250^\circ\text{C}$.

^1H -NMR (D_2O , 500 MHz) $\delta = 41.81$ (1H, s, H_{ax}), 41.25 (1H, s, H_{ax}), 35.27 (1H, s, H_{ax}), 30.78 (1H, s, H_{ax}), 8.94 (1H, s, arom), 8.29 (2H, s, arom), 7.17 (1H, s, arom), 6.52 (1H, s, H_{eq}), 5.67 (1H, s, arom), 4.00-5.50 (4H, obscured by H_2O , arom), 3.55 (1H, s, H_{eq}), 1.62 (1H, s, H_{eq}), -1.95 (1H, s, H_{eq}), -2.58 (1H, s, H_{ax}), -5.64 (1H, s, H_{eq}), -5.91 (1H, s, H_{eq}), -6.72 (1H, s, H_{ax}), -9.14 (1H, s, H_{eq}), -10.71 (1H, s, H_{eq}), -13.12 (1H, s, H_{ax}), -13.99 (1H, s, H_{ax}), -14.85 (1H, s, CH_2CO), -15.98 (1H, s, CH_2CO), -18.02 (1H, s, CH_2CO), -18.93 (1H, s, CH_2CO), -19.24 (2H, s, CH_2CO). MS(ES+) $m/z = 716$ ($[\text{M}+\text{H}]^+$), 738 ($[\text{M}+\text{Na}]^+$). MS(ES-) $m/z = 714$ ($[\text{M}-\text{H}]^-$). HRMS(ES+) $m/z = 733.1862$ ($[\text{M}+\text{NH}_4]^+$); calc. for $\text{EuC}_{29}\text{H}_{36}\text{O}_7\text{N}_6$, 733.1852.

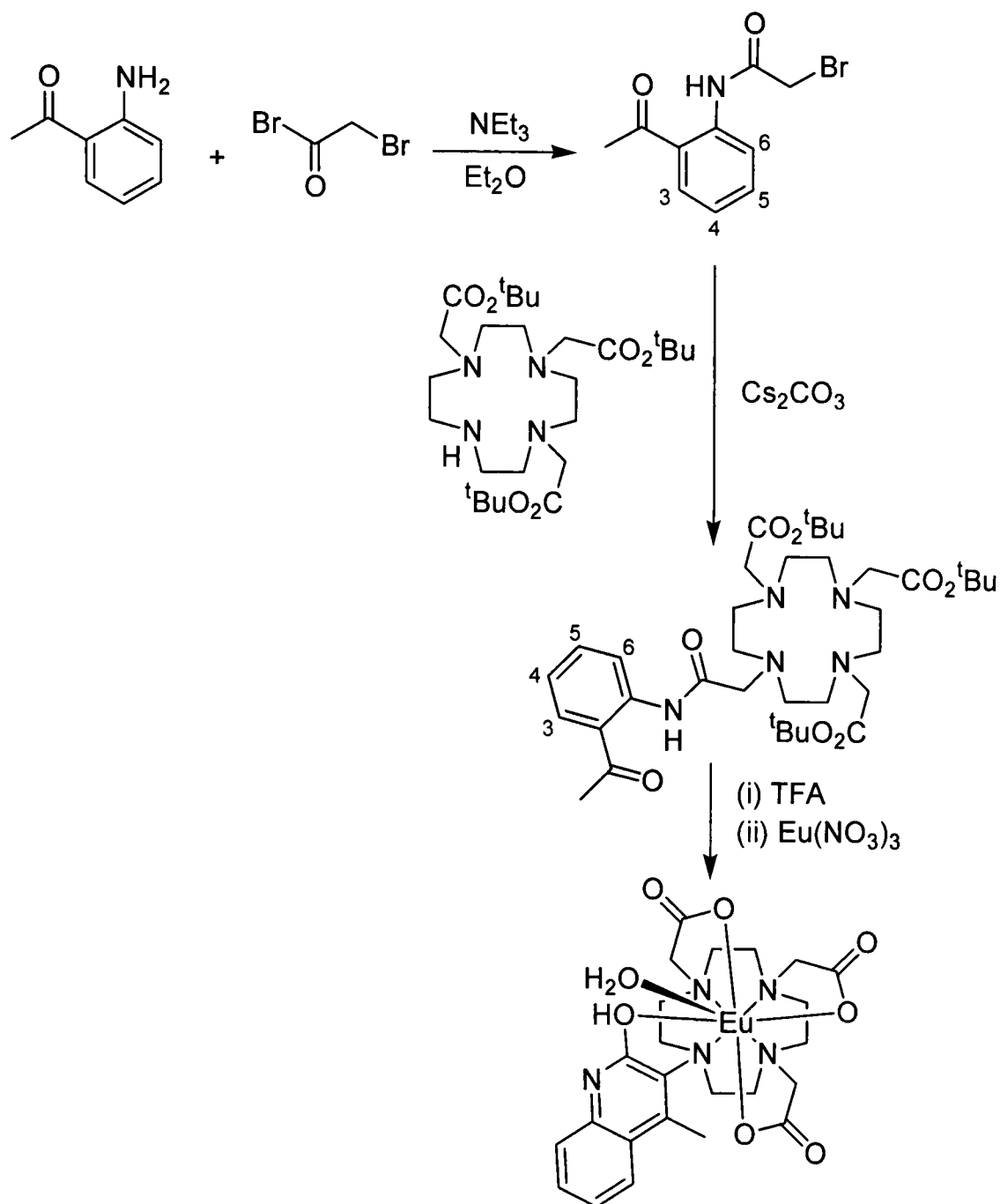
6.3.11 Yttrium(III) 10-(2-hydroxy-4-phenylquinolin-3-yl)-1,4,7,10-tetraazacyclododecane-1,4,7-trisacetate [Y·132]



A solution of 10-((2-benzoyl-phenylcarbamoyl)methyl)-1,4,7,10-tetraazacyclododecane-1,4,7-tris(acetic acid *tert*-butyl ester) (156 mg, 0.21 mmol) in 80% TFA in dichloromethane (2 ml) was stirred at room temperature for three days. The reaction could be followed by ^1H NMR (D_2O). Removal of solvent under reduced pressure followed by washing with dichloromethane (3×20 ml) then diethyl ether (3×20 ml) gave 10-((2-benzoyl-phenylcarbamoyl)methyl)-1,4,7,10-tetraazacyclododecane-1,4,7-tris(acetic acid) as a pale brown solid, which was used without further purification. This was redissolved along with yttrium(III) nitrate (85 mg, 0.31 mmol) in water (3 ml), the solution made basic with NaOH solution (2 mol dm^{-3}) and heated under reflux at 100°C for 24 h. After cooling to room temperature the solvent was removed under reduced pressure. The residue was redissolved in ethanol and all undissolved material removed by filtration. Removal of solvent under reduced pressure and purification of the residue by column chromatography (alumina, $\text{CH}_2\text{Cl}_2/\text{MeOH}$, gradient elution from 100/0 to 20/80) gave the desired product as a colourless solid (87 mg, 62%), mp $>250^\circ\text{C}$.

^1H -NMR (D_2O , 400 MHz) $\delta = 7.67$ (1H, t, $J = 7.5$, arom), 7.58-7.63 (4H, m, arom), 7.39-7.42 (2H, m, arom), 7.23 (1H, t, $J = 7.6$, arom), 7.02 (1H, d, $J = 8.1$, arom), 1.16-4.20 (22H, m, CH_2). MS(ES+) $m/z = 674$ ($[\text{M}+\text{Na}]^+$).

6.3.12 Europium(III) 10-(2-hydroxy-4-methylquinolin-3-yl)-1,4,7,10-tetraazacyclododecane-1,4,7-trisacetate [Eu·133]



N-(2-Acetyl-phenyl)-2-bromo-acetamide

Bromoacetyl bromide (2.89 g, 14.3 mmol) was added dropwise to a solution of 2-aminoacetophenone (1.34 g, 11.1 mmol) and triethylamine (1.50 g, 14.8 mmol) in diethyl ether (100 ml) at -10°C , ensuring that the temperature did not rise above 0°C . After warming to room temperature, the precipitated solid was removed by filtration and washed with diethyl ether (100 ml). The combined filtrates were washed with HCl solution (1 mol dm^{-3} , $3 \times 50\text{ ml}$) and dried over MgSO_4 . Removal of solvent under reduced pressure and drying under vacuum gave the desired product as a pale brown oil that solidified upon standing (2.26 g, 79%).

$^1\text{H-NMR}$ (CDCl_3 , 400 MHz) δ = 12.37 (1H, br s, NH), 8.71 (1H, dd, J = 8.5, 1.0, arom), 7.94 (1H, dd, J = 8.0, 1.6, arom), 7.59 (1H, ddd, J = 8.4, 7.4, 1.6, arom), 7.20 (1H, ddd, J = 7.8, 6.8, 1.1, arom), 4.03 (2H, s, CH_2), 2.70 (3H, s, CH_3). $^{13}\text{C}\{^1\text{H}\}$ -NMR (CDCl_3 , 101 MHz) δ = 202.8 (C=O), 165.7 (CONH), 140.1 (C^q), 135.2 (CH), 131.8 (CH), 123.6 (CH), 122.7 (C^q), 121.0 (CH), 29.7 (CH_2), 28.6 (CH_3). MS(EI) m/z = 255/257 (M^+), 240/242 ($\text{M}^+ - \text{CH}_3$), 212/214 ($\text{M}^+ - \text{COCH}_3$), 176 ($\text{M}^+ - \text{Br}$), 162 ($\text{M}^+ - \text{CH}_2\text{Br}$), 135 ($\text{H}_2\text{NC}_6\text{H}_4\text{COCH}_3^+$), 133 ($\text{M}^+ - \text{COCH}_3, \text{Br}$), 120 ($\text{C}_6\text{H}_3\text{COCH}_3^+$), 77 (C_6H_5^+), 65 (C_5H_5^+), 43 (CH_3CO^+). IR (KBr disc) $\bar{\nu}$ = 1670 cm^{-1} (ketone, C=O stretch), 1655 cm^{-1} (amide, C=O stretch).

10-((2-Acetyl-phenylcarbamoyl)methyl)-1,4,7,10-tetraazacyclododecane-1,4,7-tris(acetic acid tert-butyl ester)

1,4,7,10-Tetraazacyclododecane-1,4,7-tris(acetic acid *tert*-butyl ester) (1.88 g, 3.65 mmol), *N*-(2-acetyl-phenyl)-2-bromo-acetamide (934 mg, 3.65 mmol), caesium carbonate (3.69 g, 11.3 mmol) and a few grains of potassium iodide in acetonitrile (75 ml) were stirred at room temperature under a nitrogen atmosphere for two days. The progress of the reaction was followed by TLC (silica, CH_2Cl_2). The solvent was removed under reduced pressure, and the residue added to water (50 ml) then extracted into dichloromethane (3×50 ml). Drying over MgSO_4 and removal of solvent under reduced pressure gave the desired product as a brown solid (1.93 g, 76%).*

$^1\text{H-NMR}$ (CDCl_3 , 400 MHz) δ = 12.27 (1H, br s, NH), 8.67 (1H, d, J = 8.5, arom), 7.83 (1H, d, J = 7.9, arom), 7.51 (1H, t, J = 7.7, arom), 7.11 (1H, 7.6, arom), 3.39 (2H, s, CH_2), 3.28 (4H, s, CH_2), 3.20 (2H, s, CH_2), 2.75-3.00 (16H, m, $\text{NCH}_2\text{CH}_2\text{N}$), 1.45 (9H, s, ^tBu), 1.41 (18H, s, ^tBu). MS(ES+) m/z = 690 ($[\text{M}+\text{H}]^+$), 712 ($[\text{M}+\text{Na}]^+$).

Europium(III) 10-(2-hydroxy-4-methylquinolin-3-yl)-1,4,7,10-tetraazacyclododecane-1,4,7-trisacetate [Eu-133]

A solution of 10-((2-acetyl-phenylcarbamoyl)methyl)-1,4,7,10-tetraazacyclododecane-1,4,7-tris(acetic acid *tert*-butyl ester) (440 mg, 0.64 mmol) in 80% TFA in dichloromethane (5 ml) was stirred at room temperature for three days. The reaction could be followed by ^1H NMR (D_2O). Removal of solvent under reduced pressure followed by washing with dichloromethane (3×25 ml) then diethyl ether (3×25 ml) gave

* Attempted purification by column chromatography (silica, $\text{CH}_2\text{Cl}_2/\text{MeOH}$) resulted in decomposition, and therefore the product was used without further purification.

10-((2-acetyl-phenylcarbamoyl)methyl)-1,4,7,10-tetraazacyclododecane-1,4,7-tris(acetic acid) as a pale brown solid, which was used without further purification.

$^1\text{H-NMR}$ (D_2O , 400 MHz) δ = 8.06 (1H, d, J = 8.8, arom), 8.03 (1H, d, J = 8.0, arom), 7.64 (1H, t, J = 7.8, arom), 7.34 (1H, t, arom), 3.90 (8H, br s, CH_2), 3.34 (16H, br s, $\text{NCH}_2\text{CH}_2\text{N}$), 2.67 (3H, s, Me).

This was redissolved along with europium(III) nitrate pentahydrate (412 mg, 0.96 mmol) in water (15 ml), the solution made basic with NaOH solution (2 mol dm^{-3}) and heated under reflux at 100°C for 24 h. After cooling to room temperature the solvent was removed under reduced pressure. The residue was dissolved in ethanol and all undissolved material removed by filtration. Removal of solvent under reduced pressure and purification of the residue by column chromatography (alumina, $\text{CH}_2\text{Cl}_2/\text{MeOH}$, gradient elution from 100/0 to 50/50) gave the desired product as a colourless solid (150 mg, 36%), mp $>250^\circ\text{C}$.

$^1\text{H-NMR}$ (D_2O , 500 MHz) δ = 43.10 (1H, s, H_{ax}), 42.40 (1H, s, H_{ax}), 35.42 (1H, s, H_{ax}), 30.30 (1H, s, H_{ax}), 6.76 (1H, s, H_{eq}), 5.83 (1H, s, arom), 5.61 (1H, s, arom), 5.56 (1H, s, arom), 5.20 (1H, s, H_{eq}), 3.95 (1H, s, arom), 3.31 (3H, s, Me), 1.14 (2H, s, $\text{H}_{\text{eq}'}$), -1.25 (1H, s, $\text{H}_{\text{ax}'}$), -1.98 (1H, s, H_{eq}), -4.97 (1H, s, $\text{H}_{\text{eq}'}$), -6.41 (1H, s, $\text{H}_{\text{ax}'}$), -6.76 (1H, s, H_{eq}), -9.60 (1H, s, $\text{H}_{\text{eq}'}$), -11.51 (1H, s, $\text{H}_{\text{eq}'}$), -13.74 (1H, s, $\text{H}_{\text{ax}'}$), -14.30 (1H, s, CH_2CO), -15.07 (1H, s, $\text{H}_{\text{ax}'}$), -15.52 (1H, s, CH_2CO), -17.69 (1H, s, CH_2CO), -18.96 (1H, s, CH_2CO), -20.21 (1H, s, CH_2CO), -20.32 (1H, s, CH_2CO). MS(ES+) m/z = 676 ($[\text{M}+\text{H}]^+$). HRMS(ES+) m/z = 676.1291 ($[\text{M}+\text{Na}]^+$); calc. for $\text{EuC}_{24}\text{H}_{30}\text{N}_5\text{O}_7\text{Na}$, 676.1255.

CHAPTER 7

REFERENCES

7 References

- 1 U. Mitschke and P. Bäuerle, *J. Mater. Chem.*, 2000, **10**, 1471.
- 2 L. S. Hung and C. H. Chen, *Mater. Sci. Eng., R*, 2002, **39**, 143.
- 3 A. Kraft, A. C. Grimsdale and A. B. Holmes, *Angew. Chem., Int. Ed. Engl.*, 1998, **37**, 402.
- 4 L. Akcelrud, *Prog. Polym. Sci.*, 2003, **28**, 875.
- 5 T. Tsutsui, E. Aminaka, C. P. Lin and D. U. Kim, *Philos. Trans. R. Soc. London, Ser. A*, 1997, **355**, 801.
- 6 N. Holonyak, Jr. and S. F. Bevacqua, *Appl. Phys. Lett.*, 1962, **1**, 82.
- 7 M. Pope, H. P. Kallmann and P. Magnante, *J. Chem. Phys.*, 1963, **38**, 2042.
- 8 C. W. Tang and S. A. VanSlyke, *Appl. Phys. Lett.*, 1987, **51**, 913.
- 9 J. H. Burroughes, D. D. C. Bradley, A. R. Brown, R. N. Marks, K. Mackay, R. H. Friend, P. L. Burns and A. B. Holmes, *Nature (London)*, 1990, **347**, 539.
- 10 M. Grell and D. D. C. Bradley, *Adv. Mater.*, 1999, **11**, 895.
- 11 G. Gu, Z. Shen, P. E. Burrows and S. R. Forrest, *Adv. Mater.*, 1997, **9**, 725.
- 12 R. Stevenson, *Chemistry in Britain*, 2003, **39** (1), 33.
- 13 J. Kido, *Physics World*, 1999, **12** (3), 27.
- 14 S. Kelly, *Chemistry in Britain*, 2003, **39** (1), 34.
- 15 http://www.epson.co.jp/e/newsroom/news_2004_05_18.htm, Epson (Accessed 31/8/04)
- 16 D. M. Roundhill and J. P. Fackler, '*Optoelectronic properties of inorganic compounds*', eds. J. P. Fackler, Plenum Press, New York, 1999.
- 17 '*Photoluminescence*', C. Benoit à la Guillaume, in '*Encyclopedia of Applied Physics*', eds. G. L. Trigg, VCH Publishers, New York, 1993, vol. 13, p. 497.
- 18 M. Kasha, *Discuss. Faraday Soc.*, 1950, **9**, 14.
- 19 J. R. Lakowicz, '*Principles of fluorescence spectroscopy*', Kluwer Academic / Plenum Publishers, New York, 2nd edition, 1999.
- 20 '*Electroluminescence*', Y. A. Ono, in '*Encyclopedia of Applied Physics*', eds. G. L. Trigg, VCH Publishers, New York, 1993, vol. 5, p. 295.
- 21 D. Hertel, S. Setayesh, H. G. Nothofer, U. Scherf, K. Müllen and H. Bässler, *Adv. Mater.*, 2001, **13**, 65.

- 22 J. S. Wilson, A. Köhler, R. H. Friend, M. K. Al-Suti, M. R. A. Al-Mandhary, M. S. Khan and P. R. Raithby, *J. Chem. Phys.*, 2000, **113**, 7627.
- 23 M. A. Baldo, D. F. O'Brien, M. E. Thompson and S. R. Forrest, *Phys. Rev. B: Condens. Matter*, 1999, **60**, 14422.
- 24 J. S. Wilson, A. S. Dhoot, A. J. A. B. Seeley, M. S. Khan, A. Köhler and R. H. Friend, *Nature (London)*, 2001, **413**, 828.
- 25 M. Wohlgenannt, K. Tandon, S. Mazumdar, S. Ramasesha and Z. V. Vardeny, *Nature (London)*, 2001, **409**, 494.
- 26 Z. Shuai, D. Beljonne, R. J. Silbey and J. L. Brédas, *Phys. Rev. Lett.*, 2000, **84**, 131.
- 27 C. H. Chen and H. F. Meng, *Phys. Rev. B: Condens. Matter*, 2003, **68**, art. no. 094112.
- 28 A. L. Burin and M. A. Ratner, *J. Chem. Phys.*, 1998, **109**, 6092.
- 29 N. C. Greenham, R. H. Friend and D. D. C. Bradley, *Adv. Mater.*, 1994, **6**, 491.
- 30 T. R. Hebner, C. C. Wu, D. Marcy, M. H. Lu and J. C. Sturm, *Appl. Phys. Lett.*, 1998, **72**, 519.
- 31 M. Arai, K. Nakaya, O. Onitsuka, T. Inoue, M. Codama, M. Tanaka and H. Tanabe, *Synth. Met.*, 1997, **91**, 21.
- 32 G. Yu and A. J. Heeger, *Synth. Met.*, 1997, **85**, 1183.
- 33 K. Pichler, *Philos. Trans. R. Soc. London, Ser. A*, 1997, **355**, 829.
- 34 D. Z. Garbuzov, V. Bulovic, P. E. Burrows and S. R. Forrest, *Chem. Phys. Lett.*, 1996, **249**, 433.
- 35 S. Yin, Y. Hua, X. Chen, X. Yang, Y. Hou and X. Xu, *Synth. Met.*, 2000, **111**, 109.
- 36 H. Jang, L. M. Do, Y. Kim, J. G. Kim, T. Zyung and Y. Do, *Synth. Met.*, 2001, **121**, 1669.
- 37 Y. Shao, Y. Qiu, X. Hu and X. Hong, *Chem. Lett.*, 2000, 1068.
- 38 C. Adachi, T. Tsutsui and S. Saito, *Appl. Phys. Lett.*, 1990, **56**, 799.
- 39 Y. H. Kim, D. C. Shin, S. H. Kim, C. H. Ko, H. S. Yu, Y. S. Chae and S. K. Kwon, *Adv. Mater.*, 2001, **13**, 1690.
- 40 N. Tamoto, C. Adachi and K. Nagai, *Chem. Mater.*, 1997, **9**, 1077.
- 41 H. Tian, W. Zhu and K. Chen, *Synth. Met.*, 1997, **91**, 229.
- 42 D. Braun and A. J. Heeger, *Appl. Phys. Lett.*, 1991, **58**, 1982.

- 43 A. T. H. Koch, D. Beljonne, N. T. Harrison, J. L. Brédas, N. Haylett, R. Daik, W. J. Feast and R. H. Friend, *Opt. Mater. (Amsterdam)*, 1998, **9**, 145.
- 44 B. R. Hsieh, W. C. Wan, Y. Yu, Y. L. Gao, T. E. Goodwin, S. A. Gonzalez and W. A. Feld, *Macromolecules*, 1998, **31**, 631.
- 45 B. R. Hsieh, Y. Yu, E. W. Forsythe, G. M. Schaaf and W. A. Feld, *J. Am. Chem. Soc.*, 1998, **120**, 231.
- 46 F. H. Boardman, A. W. Grice, M. G. Rütger, T. J. Sheldon, D. D. C. Bradley and P. L. Burn, *Macromolecules*, 1999, **32**, 111.
- 47 H. Becker, H. Spreitzer, W. Kreuder, E. Kluge, H. Schenk, I. Parker and Y. Cao, *Adv. Mater.*, 2000, **12**, 42.
- 48 J. L. Brédas and A. J. Heeger, *Chem. Phys. Lett.*, 1994, **217**, 507.
- 49 J. J. M. Halls, D. R. Baigent, F. Cacialli, N. C. Greenham, R. H. Friend, S. C. Moratti and A. B. Holmes, *Thin Solid Films*, 1996, **276**, 13.
- 50 G. Grem, G. Leditzky, B. Ullrich and G. Leising, *Adv. Mater.*, 1992, **4**, 36.
- 51 G. Grem, G. Leditzky, B. Ullrich and G. Leising, *Synth. Met.*, 1992, **51**, 383.
- 52 Y. Yang, Q. Pei and A. J. Heeger, *J. Appl. Phys.*, 1996, **79**, 934.
- 53 G. Grem, C. Paar, J. Stampfl, G. Leising, J. Huber and U. Scherf, *Chem. Mater.*, 1995, **7**, 2.
- 54 C. Weder and M. S. Wrighton, *Macromolecules*, 1996, **29**, 5157.
- 55 M. Uchida, Y. Ohmori, C. Morishima and K. Yoshino, *Synth. Met.*, 1993, **57**, 4168.
- 56 Y. Ohmori, M. Uchida, K. Muro and K. Yoshino, *Jpn. J. Appl. Phys., Part 2*, 1991, **30**, L1941.
- 57 S. Tasch, W. Graupner, G. Leising, L. Pu, M. W. Wagner and R. H. Grubbs, *Adv. Mater.*, 1995, **7**, 903.
- 58 D. Braun, G. Gustafsson, D. McBranch and A. J. Heeger, *J. Appl. Phys.*, 1992, **72**, 564.
- 59 N. C. Greenham, A. R. Brown, D. D. C. Bradley and R. H. Friend, *Synth. Met.*, 1993, **57**, 4134.
- 60 Y. Ohmori, M. Uchida, K. Muro and K. Yoshino, *Jpn. J. Appl. Phys., Part 2*, 1991, **30**, L1938.
- 61 Y. Ohmori, M. Uchida, K. Muro and K. Yoshino, *Solid State Commun.*, 1991, **80**, 605.
- 62 X. C. Li, F. Cacialli, R. Cervini, A. B. Holmes, S. C. Moratti, A. C. Grimsdale and R. H. Friend, *Synth. Met.*, 1997, **84**, 159.

- 63 M. Onoda and A. G. MacDiarmid, *Synth. Met.*, 1997, **91**, 307.
- 64 D. O'Brien, M. S. Weaver, D. G. Lidzey and D. D. C. Bradley, *Appl. Phys. Lett.*, 1996, **69**, 881.
- 65 T. Fukuda, T. Kanbara, T. Yamamoto, K. Ishikawa, H. Takezoe and A. Fukuda, *Appl. Phys. Lett.*, 1996, **68**, 2346.
- 66 T. Yamamoto, K. Sugiyama, T. Kushida, T. Inoue and T. Kanbara, *J. Am. Chem. Soc.*, 1996, **118**, 3930.
- 67 S. Satoh, H. Suzuki, Y. Kimata and A. Kuriyama, *Synth. Met.*, 1996, **79**, 97.
- 68 H. Suzuki, S. Hoshino, C. H. Yuan, M. Fujiki, S. Toyoda and N. Matsumoto, *Thin Solid Films*, 1998, **331**, 64.
- 69 N. Kamata, S. Aihara, M. Umeda, S. Kanezaki, K. Nagumo, D. Terunuma and K. Yamada, *J. Lumin.*, 2000, **87**, 1186.
- 70 T. Goodson III, W. Li, A. Gharavi and L. Yu, *Adv. Mater.*, 1997, **9**, 639.
- 71 V. Gebhardt, A. Bacher, M. Thelakkat, U. Stalmach, H. Meier, H. W. Schmidt and D. Haarer, *Synth. Met.*, 1997, **90**, 123.
- 72 V. Gebhardt, A. Bacher, M. Thelakkat, U. Stalmach, H. Meier, H. W. Schmidt and D. Haarer, *Adv. Mater.*, 1999, **11**, 119.
- 73 F. Geiger, M. Stoldt, H. Schweizer, P. Bäuerle and E. Umbach, *Adv. Mater.*, 1993, **5**, 922.
- 74 G. Gigli, G. Barbarella, L. Favaretto, F. Cacialli and R. Cingolani, *Appl. Phys. Lett.*, 1999, **75**, 439.
- 75 G. Barbarella, L. Favaretto, G. Sotgiu, M. Zambianchi, V. Fattori, M. Cocchi, F. Cacialli, G. Gigli and R. Cingolani, *Adv. Mater.*, 1999, **11**, 1375.
- 76 B. Winkler, F. Meghdadi, S. Tasch, R. Müllner, R. Resel, R. Saf, G. Leising and F. Stelzer, *Opt. Mater. (Amsterdam)*, 1998, **9**, 159.
- 77 A. Niko, S. Tasch, F. Meghdadi, C. Brandstätter and G. Leising, *J. Appl. Phys.*, 1997, **82**, 4177.
- 78 S. Tasch, C. Brandstätter, F. Meghdadi, G. Leising, G. Froyer and L. Athouel, *Adv. Mater.*, 1997, **9**, 33.
- 79 E. Buchwald, M. Meier, S. Karg, P. Pösch, H. W. Schmidt, P. Strohmriegl, W. Rieß and M. Schwoerer, *Adv. Mater.*, 1995, **7**, 839.
- 80 T. S. Novikova, N. N. Barashkov, A. Yassar, M. Hmyene and J. P. Ferraris, *Synth. Met.*, 1996, **83**, 47.
- 81 C. Hosokawa, N. Kawasaki, S. Sakamoto and T. Kusumoto, *Appl. Phys. Lett.*, 1992, **61**, 2503.

- 82 I. D. Parker, Q. Pei and M. Marrocco, *Appl. Phys. Lett.*, 1994, **65**, 1272.
- 83 G. G. Malliaras, J. K. Herrema, J. Wildeman, R. H. Wieringa, R. E. Gill, S. S. Lampoura and G. Hadziioannou, *Adv. Mater.*, 1993, **5**, 721.
- 84 J. Bisberg, W. J. Cumming, R. A. Gaudiana, K. D. Hutchinson, R. T. Ingwall, E. S. Kolb, P. G. Mehta, R. A. Minns and C. P. Petersen, *Macromolecules*, 1995, **28**, 386.
- 85 J. Peng, B. Y. Yu, C. H. Pyun, C. H. Kim and J. I. Jin, *Jpn. J. Appl. Phys., Part 1*, 1996, **35**, 4379.
- 86 A. Bacher, C. H. Erdelen, W. Paulus, H. Ringsdorf, H. W. Schmidt and P. Schuhmacher, *Macromolecules*, 1999, **32**, 4551.
- 87 C. W. Tang, S. A. VanSlyke and C. H. Chen, *J. Appl. Phys.*, 1989, **65**, 3610.
- 88 J. Kido and Y. Iizumi, *Appl. Phys. Lett.*, 1998, **73**, 2721.
- 89 S. Hoshino and H. Suzuki, *Appl. Phys. Lett.*, 1996, **69**, 224.
- 90 M. A. Baldo, D. F. O'Brien, Y. You, A. Shoustikov, S. Sibley, M. E. Thompson and S. R. Forrest, *Nature (London)*, 1998, **395**, 151.
- 91 M. E. Thompson, P. E. Burrows and S. R. Forrest, *Curr. Opin. Solid State Mater. Sci.*, 1999, **4**, 369.
- 92 D. F. O'Brien, M. A. Baldo, M. E. Thompson and S. R. Forrest, *Appl. Phys. Lett.*, 1999, **74**, 442.
- 93 V. Cleave, G. Yahiolu, P. Le Barny, R. H. Friend and N. Tessler, *Adv. Mater.*, 1999, **11**, 285.
- 94 T. Förster, *Discuss. Faraday Soc.*, 1959, **27**, 7.
- 95 D. L. Dexter, *J. Chem. Phys.*, 1953, **21**, 836.
- 96 N. N. Greenwood and A. Earnshaw, '*Chemistry of the Elements*', Butterworth-Heinemann, Oxford, 2nd edition, 1997.
- 97 '*Iridium : Inorganic & coordination chemistry*', C. E. Housecroft, in '*Encyclopedia of Inorganic Chemistry*', eds. R. B. King, John Wiley & Sons Ltd., Chichester, 1994, p. 1606.
- 98 B. Martin and G. M. Waing, *J. Chem. Soc.*, 1958, 4284.
- 99 B. Chiswell and S. E. Livingstone, *J. Inorg. Nucl. Chem.*, 1964, **26**, 47.
- 100 C. M. Flynn and J. N. Demas, *J. Am. Chem. Soc.*, 1974, **96**, 1959.
- 101 N. Yoshikawa, Y. Masuda and T. Matsumura-Inoue, *Chem. Lett.*, 2000, **29**, 1206.

- 102 N. P. Ayala, C. M. Flynn, L. Sacksteder, J. N. Demas and B. A. DeGraff, *J. Am. Chem. Soc.*, 1990, **112**, 3837.
- 103 J.-P. Collin, I. M. Dixon, J.-P. Sauvage, J. A. G. Williams, F. Barigelletti and L. Flamigni, *J. Am. Chem. Soc.*, 1999, **121**, 5009.
- 104 R. J. Watts, J. S. Harrington and J. van Houton, *J. Am. Chem. Soc.*, 1977, **99**, 2179.
- 105 R. J. Watts and S. F. Bergeron, *J. Phys. Chem.*, 1979, **83**, 424.
- 106 R. D. Gillard, R. J. Lancashire and P. A. Williams, *J. Chem. Soc., Dalton Trans.*, 1979, 190.
- 107 J. L. Kahl, K. Hanck and K. DeArmand, *J. Inorg. Nucl. Chem.*, 1979, **41**, 495.
- 108 P. J. Spellane and R. J. Watts, *Inorg. Chem.*, 1981, **20**, 3561.
- 109 W. A. Wickramasinghe, P. H. Bird and N. Serpone, *J. Chem. Soc., Chem. Commun.*, 1981, 1284.
- 110 S. Sprouse, K. A. King, P. J. Spellane and R. J. Watts, *J. Am. Chem. Soc.*, 1984, **106**, 6647.
- 111 F. O. Garces, K. A. King and R. J. Watts, *Inorg. Chem.*, 1988, **27**, 3464.
- 112 F. O. Garces, K. Dedeian, N. L. Keder and R. J. Watts, *Acta Crystallogr., Sect. C: Cryst. Struct. Commun.*, 1993, **49**, 1117.
- 113 K. A. King, P. J. Spellane and R. J. Watts, *J. Am. Chem. Soc.*, 1985, **107**, 1431.
- 114 K. Dedeian, P. I. Djurovich, F. O. Garces, G. Carlson and R. J. Watts, *Inorg. Chem.*, 1991, **30**, 1685.
- 115 S. Lamansky, P. Djurovich, D. Murphy, F. Abdel-Razzaq, R. Kwong, I. Tsyba, M. Bortz, B. Mui, R. Bau and M. E. Thompson, *Inorg. Chem.*, 2001, **40**, 1704.
- 116 M. G. Colombo, T. C. Brunold, T. Riedener, H. U. Grüdel, M. Förtsch and H. B. Bürgi, *Inorg. Chem.*, 1994, **33**, 545.
- 117 V. V. Grushin, N. Herron, D. D. LeCloux, W. J. Marshall, V. A. Petrov and Y. Wang, *Chem. Commun.*, 2001, 1494.
- 118 H. Konno and Y. Sasaki, *Chem. Lett.*, 2003, **32**, 252.
- 119 K. Saito, N. Matsusue, H. Kanno, Y. Hamada, H. Takahashi and T. Matsumura, *Jpn. J. Appl. Phys., Part 1*, 2004, **43**, 2733.
- 120 F. Neve, M. Ghedini, G. D. Munno and A. Crispini, *Organometallics*, 1991, **10**, 1143.
- 121 A. B. Tamayo, B. D. Alleyne, P. I. Djurovich, S. Lamansky, I. Tsyba, N. N. Ho, R. Bau and M. E. Thompson, *J. Am. Chem. Soc.*, 2003, **125**, 7377.

- 122 T. Karatsu, T. Nakamura, S. Yagai, A. Kitamura, K. Yamaguchi, Y. Matsushima, T. Iwata, Y. Hori and T. Hagiwara, *Chem. Lett.*, 2003, **32**, 886.
- 123 Y. Ohsawa, S. Sprouse, K. A. King, M. K. DeArmond, K. W. Hanck and R. J. Watts, *J. Phys. Chem.*, 1987, **91**, 1047.
- 124 P. Didier, I. Ortmans, A. Kirsch-De Mesmaeker and R. J. Watts, *Inorg. Chem.*, 1993, **32**, 5239.
- 125 P. Didier, L. Jacquet, A. Kirsch-De Mesmaeker, R. Hueber and A. von Dorselaer, *Inorg. Chem.*, 1992, **31**, 4803.
- 126 I. Ortmans, P. Didier and A. Kirsch-De Mesmaeker, *Inorg. Chem.*, 1995, **34**, 3695.
- 127 S. Lamansky, P. Djurovich, D. Murphy, F. Abdel-Razzaq, H.-E. Lee, C. Adachi, P. E. Burrows, S. R. Forrest and M. E. Thompson, *J. Am. Chem. Soc.*, 2001, **123**, 4304.
- 128 I. R. Laskar and T. M. Chen, *Chem. Mater.*, 2004, **16**, 111.
- 129 A. Mamo, I. Stefio, M. F. Parisi, A. Credi, M. Venturi, C. D. Pietro and S. Campagna, *Inorg. Chem.*, 1997, **36**, 5947.
- 130 F. Neve, A. Crispini, S. Campagna and S. Serroni, *Inorg. Chem.*, 1999, **38**, 2250.
- 131 F. Neve and A. Crispini, *Eur. J. Inorg. Chem.*, 2000, 1039.
- 132 F. Neve, A. Crispini, F. Loiseau and S. Campagna, *J. Chem. Soc., Dalton Trans.*, 2000, 1399.
- 133 F. Neve, A. Crispini, S. Serroni, F. Loiseau and S. Campagna, *Inorg. Chem.*, 2001, **40**, 1093.
- 134 A. C. Albéniz, G. Schulte and R. H. Crabtree, *Organometallics*, 1992, **11**, 242.
- 135 M. Polson, S. Fracasso, V. Bertolasi, M. Ravaglia and F. Scandola, *Inorg. Chem.*, 2004, **43**, 1950.
- 136 J. N. Demas, E. W. Harris, C. M. Flynn, Jr. and D. Diemente, *J. Am. Chem. Soc.*, 1975, **97**, 3838.
- 137 J. L. Kahl, K. W. Hanck and K. DeArmond, *J. Phys. Chem.*, 1978, **82**, 540.
- 138 M. Licini and J. A. G. Williams, *Chem. Commun.*, 1999, 1943.
- 139 W. Goodall and J. A. G. Williams, *J. Chem. Soc., Dalton Trans.*, 2000, 2893.
- 140 K. Ichimura, T. Kobayashi, K. A. King and R. J. Watts, *J. Phys. Chem.*, 1987, **91**, 6104.
- 141 W. Stampor, J. Mezyk and J. Kalinowski, *Chem. Phys.*, 2004, **300**, 189.

- 142 P. J. Hay, *J. Phys. Chem. A*, 2002, **106**, 1634.
- 143 A. T. Yeh, C. V. Shank and J. K. McCusker, *Science (Washington, D. C.)*, 2000, **289**, 935.
- 144 K. C. Tang, K. L. Liu and I. C. Chen, *Chem. Phys. Lett.*, 2004, **386**, 437.
- 145 H. A. Samha, T. J. Martinez, M. K. De Armond, F. O. Garces and R. J. Watts, *Inorg. Chem.*, 1993, **32**, 2583.
- 146 M. Vacha, Y. Koide, M. Kotani and H. Sato, *J. Lumin.*, 2004, **107**, 51.
- 147 M. Vacha, Y. Koide, M. Kotani and H. Sato, *Chem. Phys. Lett.*, 2004, **388**, 263.
- 148 A. Sarkar and S. Chakravorti, *J. Lumin.*, 1995, **65**, 163.
- 149 A. Tsuboyama, H. Iwawaki, M. Furugori, T. Mukaide, J. Kamatani, S. Igawa, T. Moriyama, S. Miura, T. Takiguchi, S. Okada, M. Hoshino and K. Ueno, *J. Am. Chem. Soc.*, 2003, **125**, 12971.
- 150 K. A. King and R. J. Watts, *J. Am. Chem. Soc.*, 1987, **109**, 1589.
- 151 A. P. Wilde, K. A. King and R. J. Watts, *J. Phys. Chem.*, 1991, **95**, 629.
- 152 A. P. Wilde and R. J. Watts, *J. Phys. Chem.*, 1991, **95**, 622.
- 153 M. A. Baldo, S. Lamansky, P. E. Burrows, M. E. Thompson and S. R. Forrest, *Appl. Phys. Lett.*, 1999, **75**, 4.
- 154 C. Adachi, M. A. Baldo, S. R. Forrest and M. E. Thompson, *Appl. Phys. Lett.*, 2000, **77**, 904.
- 155 X. Zhou, J. Blochwitz-Nimoth, M. Pfeiffer, B. Maenning, J. Drechsel, A. Werner and K. Leo, *Synth. Met.*, 2003, **137**, 1063.
- 156 C. L. Lee, K. B. Lee and J. J. Kim, *Appl. Phys. Lett.*, 2000, **77**, 2280.
- 157 K. M. Vaeth and C. W. Tang, *J. Appl. Phys.*, 2002, **92**, 3447.
- 158 H. Li, F. Zhang and D. Zheng, *Semicond. Sci. Technol.*, 2003, **18**, 278.
- 159 H. Z. Xie, M. W. Liu, O. Y. Wang, X. H. Zhang, C. S. Lee, L. S. Hung, S. T. Lee, P. F. Teng, H. L. Kwong, H. Zheng and C. M. Che, *Adv. Mater.*, 2001, **13**, 1245.
- 160 W. Zhu, Y. Mo, M. Yuan, W. Yang and Y. Cao, *Appl. Phys. Lett.*, 2002, **80**, 2045.
- 161 W. Zhu, C. Liu, L. Su, W. Yang, M. Yuan and Y. Cao, *J. Mater. Chem.*, 2003, **13**, 50.
- 162 R. R. Das, C. L. Lee, Y. Y. Noh and J. J. Kim, *Opt. Mater. (Amsterdam)*, 2002, **21**, 143.

- 163 Y. Wang, N. Herron, V. V. Grushin, D. LeCloux and V. Petrov, *Appl. Phys. Lett.*, 2001, **79**, 449.
- 164 J. C. Ostrowski, M. R. Robinson, A. J. Heeger and G. C. Bazan, *Chem. Commun.*, 2002, 784.
- 165 X. Gong, J. C. Ostrowski, G. C. Bazan, D. Moses and A. J. Heeger, *Appl. Phys. Lett.*, 2002, **81**, 3711.
- 166 X. Gong, J. C. Ostrowski, D. Moses, G. C. Bazan and A. J. Heeger, *Adv. Funct. Mater.*, 2003, **13**, 439.
- 167 X. Gong, S. H. Lim, J. C. Ostrowski, D. Moses, C. J. Bardeen and G. C. Bazan, *J. Appl. Phys.*, 2004, **95**, 948.
- 168 C. Adachi, M. A. Baldo, M. E. Thompson and S. R. Forrest, *J. Appl. Phys.*, 2001, **90**, 5048.
- 169 S. Lamansky, P. I. Djurovich, F. Abdel-Razzaq, S. Garon, D. L. Murphy and M. E. Thompson, *J. Appl. Phys.*, 2002, **92**, 1570.
- 170 Y. Kawamura, S. Tanagida and S. R. Forrest, *J. Appl. Phys.*, 2002, **92**, 87.
- 171 T. Tsuzuki, N. Shirasawa, T. Suzuki and S. Tokito, *Adv. Mater.*, 2003, **15**, 1455.
- 172 C. Jiang, W. Yang, J. Peng, S. Xiao and Y. Cao, *Adv. Mater.*, 2004, **16**, 537.
- 173 W. Zhu, M. Zhu, Y. Ke, L. Su, M. Yuan and Y. Cao, *Thin Solid Films*, 2004, **446**, 128.
- 174 C. H. Yang, C. C. Tai and I. W. Sun, *J. Mater. Chem.*, 2004, **14**, 947.
- 175 C. Adachi, R. C. Kwong, P. Djurovich, V. Adamovich, M. A. Baldo, M. E. Thompson and S. R. Forrest, *Appl. Phys. Lett.*, 2001, **79**, 2082.
- 176 E. B. Namdas, A. Ruseckas, I. D. W. Samuel, S. C. Lo and P. L. Burn, *J. Phys. Chem. B*, 2004, **108**, 1570.
- 177 S. C. Lo, E. B. Namdas, P. L. Burn and I. D. W. Samuel, *Macromolecules*, 2003, **36**, 9721.
- 178 J. P. J. Markham, S. C. Lo, S. W. Magennis, P. L. Burn and I. D. W. Samuel, *Appl. Phys. Lett.*, 2002, **80**, 2645.
- 179 T. D. Anthopoulos, J. P. J. Markham, E. B. Namdas, I. D. W. Samuel, S. C. Lo and P. L. Burn, *Appl. Phys. Lett.*, 2003, **82**, 4824.
- 180 T. D. Anthopoulos, M. J. Frampton, E. B. Namdas, P. L. Burn and I. D. W. Samuel, *Adv. Mater.*, 2004, **16**, 557.
- 181 S. Tokito, M. Suzuki, F. Sato, M. Kamachi and K. Shirane, *Org. Electron.*, 2003, **4**, 105.

- 182 X. Chen, J. L. Liao, Y. Liang, M. O. Ahmed, H. E. Tseng and S. A. Chen, *J. Am. Chem. Soc.*, 2003, **125**, 636.
- 183 I. Tanaka, M. Suzuki and S. Tokito, *Jpn. J. Appl. Phys., Part 1*, 2003, **42**, 2737.
- 184 M. A. Baldo, M. E. Thompson and S. R. Forrest, *Nature (London)*, 2000, **403**, 750.
- 185 G. He, S. C. Chang, F. C. Chen, Y. Li and Y. Yang, *Appl. Phys. Lett.*, 2002, **81**, 1509.
- 186 J. Slinker, D. Bernardis, P. L. Houston, H. D. Abruña, S. Bernhard and G. G. Malliaras, *Chem. Commun.*, 2003, 2392.
- 187 J. K. Lee, D. S. Yoo, E. S. Handy and M. F. Rubner, *Appl. Phys. Lett.*, 1996, **69**, 1686.
- 188 K. M. Maness, H. Masui, R. M. Wightman and R. W. Murray, *J. Am. Chem. Soc.*, 1997, **119**, 3987.
- 189 J. D. Slinker, A. A. Gorodetsky, M. S. Lowry, J. Wang, S. Parker, R. Rohl, S. Bernhard and G. G. Malliaras, *J. Am. Chem. Soc.*, 2004, **126**, 2763.
- 190 G. B. Cunningham, Y. Li, S. Liu and K. S. Schanze, *J. Phys. Chem. B*, 2003, **107**, 12569.
- 191 J. A. Peters, J. Huskens and D. J. Raber, *Prog. Nucl. Magn. Reson. Spectrosc.*, 1996, **28**, 283.
- 192 P. Caravan, J. J. Ellison, T. J. McMurry and R. B. Lauffer, *Chem. Rev.*, 1999, **99**, 2293.
- 193 S. Aime, M. Botta, M. Fasano and E. Terreno, *Chem. Soc. Rev.*, 1998, **27**, 19.
- 194 J. I. Bruce, R. S. Dickins, L. J. Govenlock, T. Gunnlaugsson, S. Lopinski, M. P. Lowe, D. Parker, R. D. Peacock, J. J. B. Perry, S. Aime and M. Botta, *J. Am. Chem. Soc.*, 2000, **122**, 9674.
- 195 R. S. Dickins, D. Parker, J. I. Bruce and D. J. Tozer, *Dalton Trans.*, 2003, 1264.
- 196 S. Aime, M. Botta, D. Parker and J. A. G. Williams, *J. Chem. Soc., Dalton Trans.*, 1996, 17.
- 197 S. I. Weissman, *J. Chem. Phys.*, 1942, **10**, 214.
- 198 A. Beeby, S. Faulkner, D. Parker and J. A. G. Williams, *J. Chem. Soc., Perkin Trans. 2*, 2001, 1268.
- 199 A. Beeby, I. M. Clarkson, R. S. Dickins, S. Faulkner, D. Parker, L. Royle, A. S. de Sousa, J. A. G. Williams and M. Woods, *J. Chem. Soc., Perkin Trans. 2*, 1999, 493.
- 200 D. Parker and J. A. G. Williams, *J. Chem. Soc., Dalton Trans.*, 1996, 3613.

- 201 D. Parker, *Chem. Soc. Rev.*, 2004, **33**, 156.
- 202 J. L. Kropp and M. W. Windsor, *J. Chem. Phys.*, 1963, **39**, 2769.
- 203 J. L. Kropp and M. W. Windsor, *J. Chem. Phys.*, 1965, **42**, 1599.
- 204 J. L. Kropp and M. W. Windsor, *J. Chem. Phys.*, 1966, **45**, 761.
- 205 Y. Haas and G. Stein, *J. Phys. Chem.*, 1972, **76**, 1093.
- 206 W. D. Horrocks, Jr. and D. R. Sudnick, *J. Am. Chem. Soc.*, 1979, **101**, 334.
- 207 W. D. Horrocks, Jr. and D. R. Sudnick, *Acc. Chem. Res.*, 1981, **14**, 384.
- 208 D. Parker, R. S. Dickins, H. Puschmann, C. Crossland and J. A. K. Howard, *Chem. Rev.*, 2002, **102**, 1977.
- 209 V. Alexander, *Chem. Rev.*, 1995, **95**, 273.
- 210 S. Aime, M. Botta and G. Ermondi, *Inorg. Chem.*, 1992, **31**, 4291.
- 211 S. Aime, M. Botta, M. Fasano, M. P. M. Marques, C. F. G. C. Geraldés, D. Pubanz and A. E. Merbach, *Inorg. Chem.*, 1997, **36**, 2059.
- 212 U. Cosentino, A. Villa, D. Pitea, G. Moro, V. Barone and A. Maiocchi, *J. Am. Chem. Soc.*, 2002, **124**, 4901.
- 213 J. F. Desreux, *Inorg. Chem.*, 1980, **19**, 1319.
- 214 J. F. Desreux, V. Humblet, M. Hermann, V. Jacques, J. Paris, R. S. Ranganathan, C. Sauvage, D. Thonon and M. F. Tweedle, *J. Inorg. Biochem.*, 2004, **86**, 41.
- 215 M. Woods, S. Aime, M. Botta, J. A. K. Howard, J. M. Moloney, M. Navet, D. Parker, M. Pott and O. Rousseaux, *J. Am. Chem. Soc.*, 2000, **122**, 9781.
- 216 F. A. Dunand, R. S. Dickins, D. Parker and A. E. Merbach, *Chem.--Eur. J.*, 2001, **7**, 5160.
- 217 S. Aime, M. Botta, G. Ermondi, E. Terreno, P. L. Anelli, F. Fedeli and F. Uggeri, *Inorg. Chem.*, 1996, **35**, 2726.
- 218 F. Benetollo, G. Bombieri, L. Calabi, S. Aime and M. Botta, *Inorg. Chem.*, 2003, **42**, 148.
- 219 F. Benetollo, G. Bombieri, S. Aime and M. Botta, *Acta Crystallogr., Sect. C: Cryst. Struct. Commun.*, 1999, **55**, 353.
- 220 'Responsive luminescent lanthanide complexes', D. Parker and J. A. G. Williams. in 'Metal ions in biological systems, volume 40: The lanthanides and their interrelations with biosystems', eds. A. Sigel and H. Sigel, Marcel Dekker, New York, 2003, p. 233.
- 221 C. A. Chang, *J. Chem. Soc., Dalton Trans.*, 1996, 2347.

- 222 A. Beeby, L. M. Bushby, D. Maffeo and J. A. G. Williams, *J. Chem. Soc., Dalton Trans.*, 2002, 48.
- 223 S. Quici, G. Marzanni, M. Cavazzini, P. L. Anelli, M. Botta, E. Gianolio, G. Accorsi, N. Armaroli and F. Barigelletti, *Inorg. Chem.*, 2002, **41**, 2777.
- 224 S. Quici, G. Marzanni, A. Forni, G. Accorsi and F. Barigelletti, *Inorg. Chem.*, 2004, **43**, 1294.
- 225 G. Bobba, J. C. Frias and D. Parker, *Chem. Commun.*, 2002, 890.
- 226 D. Maffeo and J. A. G. Williams, *Inorg. Chim. Acta*, 2003, **355**, 127.
- 227 J. M. Siaugue, F. Segat-Dioury, A. Favre-Réguillon, V. Wintgens, C. Madic, J. Foos and A. Guy, *J. Photochem. Photobiol. A*, 2003, **156**, 23.
- 228 R. J. Curry and W. P. Gillin, *Curr. Opin. Solid State Mater. Sci.*, 2001, **5**, 481.
- 229 J. Kido and Y. Okamoto, *Chem. Rev.*, 2002, **102**, 2357.
- 230 J. Kido, K. Nagai and Y. Ohashi, *Chem. Lett.*, 1990, **19**, 657.
- 231 J. Kido, K. Nagai, Y. Okamoto and T. Skotheim, *Chem. Lett.*, 1991, **20**, 1267.
- 232 Z. Hong, W. Li, D. Zhao, C. Liang, X. Liu, J. Peng and D. Zhao, *Synth. Met.*, 1999, **104**, 165.
- 233 J. Kido, H. Hayase, K. Hongawa, K. Nagai and K. Okuyama, *Appl. Phys. Lett.*, 1994, **65**, 2124.
- 234 L. Liu, W. Li, Z. Hong, J. Peng, X. Liu, C. Liang, Z. Liu, J. Yu and D. Zhao, *Synth. Met.*, 1997, **91**, 267.
- 235 C. J. Liang, D. Zhao, Z. R. Hong, D. X. Zhao, X. Y. Liu, W. L. Li, J. B. Peng, J. Q. Yu, C. S. Lee and S. T. Lee, *Appl. Phys. Lett.*, 2000, **76**, 67.
- 236 Z. R. Hong, C. J. Liang, R. G. Li, W. L. Li, D. Zhao, D. Fan, D. Y. Wang, B. Chu, F. X. Zang, L.-S. Hong and S.-T. Lee, *Adv. Mater.*, 2001, **13**, 1241.
- 237 D. Zhao, Z. Hong, C. Liang, D. Zhao, X. Liu, W. Li, C. S. Lee and S. T. Lee, *Thin Solid Films*, 2000, **363**, 208.
- 238 J. Kido, W. Ikeda, M. Kimura and K. Nagai, *Jpn. J. Appl. Phys., Part 2*, 1996, **35**, L394.
- 239 W. Li, J. Yu, G. Sun, Z. Hong, Y. Yu, Y. Zhao, J. Peng and T. Tsutsui, *Synth. Met.*, 1997, **91**, 263.
- 240 Y. Zheng, J. Lin, Q. Lin, Y. Yu, S. Wang, C. Guo and H. Zhang, *Opt. Mater. (Amsterdam)*, 2002, **20**, 273.
- 241 R. A. Campos, I. P. Kovalev, Y. Guo, N. Wakili and T. Skotheim, *J. Appl. Phys.*, 1996, **80**, 7144.

- 242 N. Takada, T. Tsutsui and S. Saito, *Jpn. J. Appl. Phys., Part 2*, 1994, **33**, L863.
- 243 T. Tsutsui, N. Takada, S. Saito and E. Ogino, *Appl. Phys. Lett.*, 1994, **65**, 1868.
- 244 C. Adachi, M. A. Baldo and S. R. Forrest, *J. Appl. Phys.*, 2000, **87**, 8049.
- 245 G. Zhong, K. Kim and J. I. Jin, *Synth. Met.*, 2002, **129**, 193.
- 246 J. Fang and D. Ma, *Appl. Phys. Lett.*, 2003, **83**, 4041.
- 247 J. Fang, H. You, J. Gao and D. Ma, *Chem. Phys. Lett.*, 2004, **392**, 11.
- 248 M. D. McGehee, T. Bergstedt, C. Zhang, A. P. Saab, M. B. O'Regan, G. C. Bazan, V. I. Srdanov and A. J. Heeger, *Adv. Mater.*, 1999, **11**, 1349.
- 249 P. P. Sun, J. P. Duan, J. J. Lih and C. H. Cheng, *Adv. Funct. Mater.*, 2003, **13**, 683.
- 250 P. P. Sun, J. P. Duan, H. T. Shih and C. H. Cheng, *Appl. Phys. Lett.*, 2002, **81**, 792.
- 251 M. Guan, Z. Q. Bian, F. Y. Li, H. Xin and C. H. Huang, *New J. Chem.*, 2003, **27**, 1731.
- 252 H. Xin, F. Y. Li, M. Guan, C. H. Huang, M. Sun, K. Z. Wang, Y. A. Zhang and L. P. Jin, *J. Appl. Phys.*, 2003, **94**, 4729.
- 253 H. Xin, M. Sun, K. Z. Wang, Y. A. Zhang, L. P. Jin and C. H. Huang, *Chem. Phys. Lett.*, 2004, **388**, 55.
- 254 D. Gao, Z. Bian, K. Wang, L. Jin and C. H. Huang, *J. Alloys Compd.*, 2003, **358**, 188.
- 255 Z. Bian, D. Gao, K. Wang, L. Jin and C. Huang, *Thin Solid Films*, 2004, **460**, 237.
- 256 M. Sun, H. Xin, K. Z. Wang, Y. A. Zhang, L. P. Jin and C. H. Huang, *Chem. Commun.*, 2003, 702.
- 257 L. Huang, K. Z. Wang, C. H. Huang, F. Y. Li and Y. Y. Huang, *J. Mater. Chem.*, 2001, **11**, 790.
- 258 L. Huang, K. Z. Wang, C. H. Huang, D. Q. Gao and L. P. Jin, *Synth. Met.*, 2002, **128**, 241.
- 259 F. Liang, Q. Zhou, Y. Cheng, L. Wang, D. Ma, X. Jing and F. Wang, *Chem. Mater.*, 2003, **15**, 1935.
- 260 W. Hu, M. Matsumura, M. Wang and L. Jin, *Appl. Phys. Lett.*, 2000, **77**, 4271.
- 261 Y. J. Fu, T. K. S. Wong, Y. K. Yan and X. Hu, *J. Alloys Compd.*, 2003, **358**, 235.

- 262 X. Zhang, R. Sun, Q. Zheng, T. Kobayashi and W. Li, *Appl. Phys. Lett.*, 1997, **71**, 2596.
- 263 X. C. Gao, H. Cao, C. Huang, B. Li and S. Umitani, *Appl. Phys. Lett.*, 1998, **72**, 2217.
- 264 H. Xin, M. Shi, X. M. Zhang, F. Y. Li, Z. Q. Bian, K. Ibrahim, F. Q. Liu and C. H. Huang, *Chem. Mater.*, 2003, **15**, 3728.
- 265 K. S. Wong, T. Sun, X. L. Liu, J. Pei and W. Huang, *Thin Solid Films*, 2002, **417**, 85.
- 266 M. J. Yang, Q. D. Ling, W. Q. Li, Y. Wang, R. G. Sun, Q. B. Zheng and A. J. Epstein, *Mater. Sci. Eng., B*, 2001, **85**, 100.
- 267 L. Zeng, M. Yang, P. Wu, H. Ye and X. Liu, *Synth. Met.*, 2004, **144**, 259.
- 268 S. P. Shipley, S. Capecchi, O. V. Salata, M. Etchells, P. J. Dobson and V. Christou, *Adv. Mater.*, 1999, **11**, 533.
- 269 R. Reyes, E. N. Hering, M. Cremona, C. F. B. da Silva, H. F. Brito and C. A. Achete, *Thin Solid Films*, 2002, **420**, 23.
- 270 Z. R. Hong, C. J. Liang, R. G. Li, D. Zhao, D. Fan and W. L. Li, *Thin Solid Films*, 2001, **391**, 122.
- 271 R. J. Curry and W. P. Gillin, *Synth. Met.*, 2000, **111-112**, 35.
- 272 G. Wang, Y. Ding and Y. Wei, *Appl. Surf. Sci.*, 1996, **93**, 281.
- 273 H. Xin, M. Shi, F. Y. Li, M. Guan, D. Q. Gao, C. H. Huang, K. Ibrahim and F. Q. Liu, *New J. Chem.*, 2003, **27**, 1485.
- 274 Y. Kawamura, Y. Wada, Y. Hasegawa, M. Iwamuro, T. Kitamura and S. Yanagida, *Appl. Phys. Lett.*, 1999, **74**, 3245.
- 275 L. H. Slooff, A. Polman, F. Cacialli, R. H. Friend, G. A. Hebbink, F. C. J. M. van Veggel and D. N. Reinhoudt, *Appl. Phys. Lett.*, 2001, **78**, 2122.
- 276 T. S. Kang, B. S. Harrison, T. J. Foley, A. S. Knefely, J. M. Boncella, J. R. Reynolds and K. S. Schanze, *Adv. Mater.*, 2003, **15**, 1093.
- 277 K. S. Schanze, J. R. Reynolds, J. M. Boncella, B. S. Harrison, T. J. Foley, M. Bouguettaya and T. S. Kang, *Synth. Met.*, 2003, **137**, 1013.
- 278 F. X. Zang, W. L. Li, Z. R. Hong, H. Z. Wei, M. T. Li, X. Y. Sun and C. S. Lee, *Appl. Phys. Lett.*, 2004, **84**, 5115.
- 279 F. X. Zang, Z. R. Hong, W. L. Li, M. T. Li and X. Y. Sun, *Appl. Phys. Lett.*, 2004, **84**, 2679.
- 280 R. J. Curry and W. P. Gillin, *Appl. Phys. Lett.*, 1999, **75**, 1380.

- 281 Y. Kawamura, Y. Wada, M. Iwamuro, T. Kitamura and S. Yanagida, *Chem. Lett.*, 2000, **29**, 280.
- 282 T. S. Kang, B. S. Harrison, M. Bouguettaya, T. J. Foley, J. M. Boncella, K. S. Schanze and J. R. Reynolds, *Adv. Funct. Mater.*, 2003, **13**, 205.
- 283 R. A. Fallahpour, *Synthesis*, 2003, 155.
- 284 'Pyridines', D. T. Davies, in '*Aromatic Heterocyclic Chemistry*', Oxford University Press, Oxford, 1999, p. 35.
- 285 F. H. Case and T. J. Kasper, *J. Am. Chem. Soc.*, 1956, **78**, 5842.
- 286 F. Kröhnke, W. Zecher, J. Curtze, D. Drechsler, K. Pfléghar, K. E. Schnalke and W. Weis, *Angew. Chem., Int. Ed. Engl.*, 1962, **1**, 626.
- 287 F. Kröhnke, *Synthesis*, 1976, 1.
- 288 G. W. V. Cave and C. L. Raston, *Chem. Commun.*, 2000, 2199.
- 289 G. W. V. Cave and C. L. Raston, *J. Chem. Soc., Perkin Trans. 1*, 2001, 3258.
- 290 K. T. Potts, P. Ralli and G. Theodoridis, *Org. Synth.*, 1985, **64**, 189.
- 291 D. L. Jameson and L. E. Guise, *Tetrahedron Lett.*, 1991, **32**, 1999.
- 292 J. C. Adrian, Jr., L. Hassib, N. D. Kimpe and M. Keppers, *Tetrahedron*, 1998, **54**, 2365.
- 293 M. Beley, J. P. Collin, R. Louis, B. Metz and J. P. Sauvage, *J. Am. Chem. Soc.*, 1991, **113**, 8521.
- 294 M. Beley, J. P. Collin and J. P. Sauvage, *Inorg. Chem.*, 1993, **32**, 4539.
- 295 H. Bönnemann, *Angew. Chem., Int. Ed. Engl.*, 1978, **17**, 505.
- 296 J. Chen, Q. Song, C. Wang and Z. Xi, *J. Am. Chem. Soc.*, 2002, **124**, 6238.
- 297 M. Yamamura, I. Moritani and S. I. Murahashi, *J. Organomet. Chem.*, 1975, **91**, C39.
- 298 E. Negishi, *J. Organomet. Chem.*, 2002, **653**, 34.
- 299 N. Miyaura and A. Suzuki, *Chem. Rev.*, 1995, **95**, 2457.
- 300 T. Hiyama and Y. Hatanaka, *Pure Appl. Chem.*, 1994, **66**, 1471.
- 301 D. Milstein and J. K. Stille, *J. Am. Chem. Soc.*, 1979, **101**, 4992.
- 302 J. K. Stille, *Angew. Chem., Int. Ed. Engl.*, 1986, **25**, 508.
- 303 E. J. Negishi, *J. Org. Chem.*, 1977, **42**, 1821.

- 304 W. J. Thompson, J. H. Jones, P. A. Lyle and J. E. Thies, *J. Org. Chem.*, 1988, **53**, 2052.
- 305 M. D. Sindkhedkar, H. R. Mulla, M. A. Wurth and A. Cammers-Goodwin, *Tetrahedron*, 2001, **57**, 2991.
- 306 D. J. Cárdenas and J. P. Sauvage, *Synlett*, 1996, 916.
- 307 R. A. Fallahpour, *Eur. J. Inorg. Chem.*, 1998, 1205.
- 308 D. J. Cárdenas, A. M. Echavarren and M. C. R. de Arellano, *Organometallics*, 1999, **18**, 3337.
- 309 M. Beley, S. Chodorowski, J. P. Collin and J. P. Sauvage, *Tetrahedron Lett.*, 1993, **34**, 2933.
- 310 M. Chavarot and Z. Pikramenou, *Tetrahedron Lett.*, 1999, **40**, 6865.
- 311 W. Goodall and J. A. G. Williams, *Chem. Commun.*, 2001, 2514.
- 312 W. Goodall, K. Wild, K. J. Arm and J. A. G. Williams, *J. Chem. Soc., Perkin Trans. 2*, 2002, 1669.
- 313 C. J. Aspley and J. A. G. Williams, *New J. Chem.*, 2001, **25**, 1136.
- 314 G. R. Pabst and J. Sauer, *Tetrahedron*, 1999, **55**, 5067.
- 315 H. Stetter, W. Frank and R. Mertens, *Tetrahedron*, 1981, **37**, 767.
- 316 S. Buøen, J. Dale, P. Groth and J. Krane, *J. Chem. Soc., Chem. Commun.*, 1982, 1172.
- 317 D. D. Dischino, E. J. Delaney, J. E. Emswiler, G. T. Gaughan, J. S. Prasad, S. K. Srivastava and M. F. Tweedle, *Inorg. Chem.*, 1991, **30**, 1265.
- 318 A. Dadabhoy, S. Faulkner and P. G. Sammes, *J. Chem. Soc., Perkin Trans. 2*, 2002, 348.
- 319 M. Studer and T. A. Kaden, *Helv. Chim. Acta*, 1986, **69**, 2081.
- 320 I. M. Helps, D. Parker, J. R. Morphy and J. Chapman, *Tetrahedron*, 1989, **45**, 219.
- 321 C. Li and W. T. Wong, *Tetrahedron Lett.*, 2002, **43**, 3217.
- 322 W. J. Kruper, P. R. Rudolf and C. A. Langhoff, *J. Org. Chem.*, 1993, **58**, 3869.
- 323 P. S. Pallavicini, A. Perotti, A. Poggi, B. Seghi and L. Fabbrizzi, *J. Am. Chem. Soc.*, 1987, **109**, 5139.
- 324 E. Kimura, S. Aoki, T. Koike and M. Shiro, *J. Am. Chem. Soc.*, 1997, **119**, 3068.
- 325 V. Boldrini, G. B. Giovenzana, R. Pagliarin, G. Palmisano and M. Sisti, *Tetrahedron Lett.*, 2000, **41**, 6527.

- 326 J. J. Yaouanc, N. Le Bris, G. Le Gall, J. C. Clément, H. Handel and H. des Abbayes, *J. Chem. Soc., Chem. Commun.*, 1991, 206.
- 327 V. Patinec, J. J. Yaouanc, J. C. Clément, H. Handel and H. des Abbayes, *Tetrahedron Lett.*, 1995, **36**, 79.
- 328 H. Bernard, J. J. Yaouanc, J. C. Clément, H. des Abbayes and H. Handel, *Tetrahedron Lett.*, 1991, **32**, 639.
- 329 A. Filali, J. J. Yaouanc and H. Handel, *Angew. Chem., Int. Ed. Engl.*, 1991, **30**, 560.
- 330 J. Rohovec, R. Gyepes, I. Cisarová, J. Rudovský and I. Lukeš, *Tetrahedron Lett.*, 2000, **41**, 1249.
- 331 W. C. Baker, M. J. Choi, D. C. Hill, J. L. Thompson and P. A. Petillo, *J. Org. Chem.*, 1999, **64**, 2683.
- 332 F. Boschetti, F. Denat, E. Espinosa and R. Guillard, *Chem. Commun.*, 2002, 312.
- 333 R. C. Kwong, M. S. Weaver, M. H. M. Lu, Y. J. Tung, A. B. Chwang, T. X. Zhou, M. Hack and J. J. Brown, *Org. Electron.*, 2003, **4**, 155.
- 334 J. Coates, P. G. Sammes and R. M. West, *J. Chem. Soc., Perkin Trans. 2*, 1996, 1275.
- 335 O. Félix, M. W. Hosseini, A. De Cian, J. Fischer, L. Catala and P. Turek, *Tetrahedron Lett.*, 1999, **40**, 2943.
- 336 W. Fudickar, J. Zimmermann, L. Ruhlmann, J. Schneider, B. Röder, U. Siggel and J. H. Fuhrhop, *J. Am. Chem. Soc.*, 1999, **121**, 9539.
- 337 T. Ishiyama, M. Murata and N. Miyaura, *J. Org. Chem.*, 1995, **60**, 7508.
- 338 C. Xi, S. Huo, T. H. Afifi, R. Hara and T. Takahashi, *Tetrahedron Lett.*, 1997, **38**, 4099.
- 339 T. Takahashi, W. H. Sun, C. Xi, H. Ubayama and Z. Xi, *Tetrahedron*, 1998, **54**, 715.
- 340 X. Herault, P. Bovonsombat and E. Mc Nelis, *Org. Prep. Proced. Int.*, 1995, **27**, 652.
- 341 L. I. Smith and C. Guss, *J. Am. Chem. Soc.*, 1937, **59**, 804.
- 342 V. Meyer and G. Pavia, *Ber. Dtsch. Chem. Ges.*, 1896, **29**, 2564.
- 343 A. R. Gray, J. T. Walker and R. C. Fuson, *J. Am. Chem. Soc.*, 1931, **53**, 3494.
- 344 P. H. Gore and J. A. Hoskins, *J. Chem. Soc. C*, 1970, 517.
- 345 R. C. Fuson and H. O. House, *J. Org. Chem.*, 1953, **18**, 496.

- 346 'Nitromethane', K. B. G. Torrsell and K. V. Gothelf, in *'Encyclopedia of Reagents for Organic Synthesis'*, eds. L. A. Paquette, John Wiley & Sons Ltd, Chichester, 1995, vol. 6, p. 3742.
- 347 'The Henry (Nitroaldol) Reaction', G. Rosini, in *'Comprehensive Organic Synthesis'*, eds. C. H. Heathcock, B. M. Trost, and I. Fleming, Pergamon Press, Oxford, 1991, vol. 2, p. 321.
- 348 F. W. Lichtenthaler, *Angew. Chem., Int. Ed. Engl.*, 1964, **3**, 211.
- 349 F. W. Lichtenthaler and O. L. Fischer, *J. Am. Chem. Soc.*, 1961, **83**, 2005.
- 350 K. Dimroth, C. Reichardt and K. Vogel, *Org. Synth., Coll. Vol. 5*, 1973, 1135.
- 351 K. Dimroth, A. Berndt and C. Reichardt, *Org. Synth., Coll. Vol. 5*, 1973, 1128.
- 352 K. Dimroth, G. Neubauer, H. Möllenkamp and G. Oosterloo, *Chem. Ber.*, 1957, **90**, 1668.
- 353 K. Dimroth and H. Wache, *Chem. Ber.*, 1966, **99**, 399.
- 354 K. Dimroth, W. Tüncher and H. Kaletsch, *Chem. Ber.*, 1978, **111**, 264.
- 355 E. S. Karaulov and M. N. Tilichenko, *J. Org. Chem. USSR*, 1970, **6**, 182.
- 356 K. B. Prasad and S. C. Shaw, *Chem. Ber.*, 1965, **98**, 2822.
- 357 E. C. Constable, R. P. G. Henney and D. A. Tocher, *J. Chem. Soc., Dalton Trans.*, 1992, 2467.
- 358 E. Fischer and O. Hess, *Ber. Dtsch. Chem. Ges.*, 1884, **17**, 559.
- 359 'Indoles', D. T. Davies, in *'Aromatic Heterocyclic Chemistry'*, Oxford University Press, Oxford, 1999, p. 53.
- 360 'The Fischer indole synthesis', J. Clayden, N. Greeves, S. Warren and P. Wothers, in *'Organic Chemistry'*, Oxford University Press, Oxford, 2001, p. 1204.
- 361 F. Barigelletti, L. Flamigni, M. Guardigli, A. Juris, M. Beley, S. Chodorowski-Kimmes, J. P. Collin and J. P. Sauvage, *Inorg. Chem.*, 1996, **35**, 136.
- 362 F. Barigelletti, L. Flamigni, J. P. Collin and J. P. Sauvage, *Chem. Commun.*, 1997, 333.
- 363 C. Patoux, J. P. Launay, M. Beley, S. Chodorowski-Kimmes, J. P. Collin, S. James and J. P. Sauvage, *J. Am. Chem. Soc.*, 1998, **120**, 3717.
- 364 J. A. G. Williams, A. Beeby, E. S. Davies, J. A. Weinstein and C. Wilson, *Inorg. Chem.*, 2003, **42**, 8609.
- 365 E. C. Constable, R. P. G. Henney, T. A. Leese and D. A. Tocher, *J. Chem. Soc., Dalton Trans.*, 1990, 443.

- 366 F. Neve, A. Crispini and S. Campagna, *Inorg. Chem.*, 1997, **36**, 6150.
- 367 F. Neve, A. Crispini, C. D. Pietro and S. Campagna, *Organometallics*, 2002, **21**, 3511.
- 368 C. M. Che, W. F. Fu, S. W. Lai, Y. J. Hou and Y. L. Liu, *Chem. Commun.*, 2003, 118.
- 369 W. Lu, B. X. Mi, M. C. W. Chan, Z. Hui, C. M. Che, N. Zhu and S. T. Lee, *J. Am. Chem. Soc.*, 2004, **126**, 4958.
- 370 G. A. Carlson, P. I. Djurovich and R. J. Watts, *Inorg. Chem.*, 1993, **32**, 4483.
- 371 G. W. V. Cave, N. W. Alcock and J. P. Rourke, *Organometallics*, 1999, **18**, 1801.
- 372 D. J. Cárdenas, A. M. Echavarren and M. C. R. Arellano, *Organometallics*, 1999, **18**, 3337.
- 373 J. A. Bailey, M. G. Hill, R. E. Marsh, V. M. Miskowski, W. P. Schaefer and H. B. Gray, *Inorg. Chem.*, 1995, **34**, 4591.
- 374 H. K. Yip, L. K. Cheng, K. K. Cheung and C. M. Che, *J. Chem. Soc., Dalton Trans.*, 1993, 2933.
- 375 J. Selbin, K. Abboud, S. F. Watkins, M. A. Gutierrez and F. R. Fronczek, *J. Organomet. Chem.*, 1983, **241**, 259.
- 376 J. Selbin and M. A. Gutierrez, *J. Organomet. Chem.*, 1983, **246**, 95.
- 377 C. Cornioley-Deuschel, T. Ward and A. von Zelewsky, *Helv. Chim. Acta*, 1988, **71**, 130.
- 378 C. P. Newman, G. W. V. Cave, M. Wong, W. Errington, N. W. Alcock and J. P. Rourke, *J. Chem. Soc., Dalton Trans.*, 2001, 2678.
- 379 W. Lu, M. C. W. Chan, K. K. Cheung and C. M. Che, *Organometallics*, 2001, **20**, 2477.
- 380 V. W. W. Yam, R. P. L. Tang, K. M. C. Wong, X. X. Lu, K. K. Cheung and N. Zhu, *Chem.-Eur. J.*, 2002, **8**, 4066.
- 381 A. Zucca, A. Doppiu, M. A. Cinellu, S. Stoccoro, G. Minghetti and M. Manassero, *Organometallics*, 2002, **21**, 783.
- 382 E. Clot, O. Eisenstein, T. Dubé, J. W. Faller and R. H. Crabtree, *Organometallics*, 2002, **21**, 575.
- 383 E. W. Abel, K. G. Orrell, A. G. Osborne, H. M. Pain, V. Šik, M. B. Hursthouse and K. M. A. Malik, *J. Chem. Soc., Dalton Trans.*, 1994, 3441.
- 384 A. Gelling, M. D. Olsen, K. G. Orrell, A. G. Osborne and V. Šik, *J. Chem. Soc., Dalton Trans.*, 1998, 3479.

- 385 L. Barloy, R. M. Gauvin, J. A. Osborn, C. Sizun, R. Graff and N. Kyritsakas, *Eur. J. Inorg. Chem.*, 2001, 1699.
- 386 R. Chotalia, E. C. Constable, M. J. Hannon and D. A. Tocher, *J. Chem. Soc., Dalton Trans.*, 1995, 3571.
- 387 K. H. Wong, K. K. Cheung, M. C. W. Chan and C. M. Che, *Organometallics*, 1998, **17**, 3505.
- 388 J. Vicente, A. Arcas, D. Bautista and M. C. Ramírez de Arellano, *J. Organomet. Chem.*, 2002, **663**, 164.
- 389 A. Hofmann, L. Dahlenburg and R. van Elldik, *Inorg. Chem.*, 2003, **42**, 6528.
- 390 P. Stössel, I. Bach, H. Spreitzer and H. Becker, in '*Rhodium complexes and iridium complexes*' (WO 03/084972), International, 2003.
- 391 Q. Liu, L. Thorne, I. Kozin, D. Song, C. Seward, M. D'Iorio, Y. Tao and S. Wang, *J. Chem. Soc., Dalton Trans.*, 2002, 3234.
- 392 W. L. Jia, Q. D. Liu, R. Wang and S. Wang, *Organometallics*, 2003, **22**, 4070.
- 393 S. F. Liu, Q. Wu, H. L. Schmider, H. Aziz, N. X. Hu, Z. Popovic and S. Wang, *J. Am. Chem. Soc.*, 2000, **122**, 3671.
- 394 F. Wu, C. M. Chamchoumis and R. P. Thummel, *Inorg. Chem.*, 2000, **39**, 584.
- 395 C. Crotti, S. Cenini, B. Rindone, S. Tollari and F. Demartin, *J. Chem. Soc., Chem. Commun.*, 1986, 784.
- 396 R. P. Thummel and V. Hegde, *J. Org. Chem.*, 1989, **54**, 1720.
- 397 S. Tollari, S. Cenini, A. Penoni, G. Granata, G. Palmisano and F. Demartin, *J. Organomet. Chem.*, 2000, **608**, 34.
- 398 S. Tollari, F. Demartin, S. Cenini, G. Palmisano and P. Raimondi, *J. Organomet. Chem.*, 1997, **527**, 93.
- 399 R. Annunziata, S. Cenini, F. Demartin, G. Palmisano and S. Tollari, *J. Organomet. Chem.*, 1995, **496**, C1.
- 400 K. Nakamaru, *Bull. Chem. Soc. Jpn.*, 1982, **55**, 2697.
- 401 K. J. Arm and J. A. G. Williams, *personal communication*, 2004
- 402 K. K. W. Lo, C. K. Chung, T. K. M. Lee, L. H. Lui, K. H. K. Tsang and N. Zhu, *Inorg. Chem.*, 2003, **42**, 6886.
- 403 E. C. Constable and T. A. Leese, *J. Organomet. Chem.*, 1987, **335**, 293.
- 404 '*Metal complexes*', B. P. Hay and O. Clement, in '*Encyclopedia of Computational Chemistry*', eds. P. R. Schleyer, John Wiley & Sons Ltd., Chichester, 1998, p. 1580.

- 405 'Semiempirical methods: Transition metals', A. J. Holder, in 'Encyclopedia of Computational Chemistry', eds. P. R. Schleyer, John Wiley & Sons Ltd., Chichester, 1998, p. 2578.
- 406 'Transition metal chemistry', G. Frenking and T. Wagener, in 'Encyclopedia of Computational Chemistry', eds. P. R. Schleyer, John Wiley & Sons Ltd., Chichester, 1998, p. 3073.
- 407 'Transition metals: Applications', C. W. Bauschlicher Jr., in 'Encyclopedia of Computational Chemistry', eds. P. R. Schleyer, John Wiley & Sons Ltd., Chichester, 1998, p. 3084.
- 408 'Density functional applications', C. H. Hu and D. P. Chong, in 'Encyclopedia of Computational Chemistry', eds. P. R. Schleyer, John Wiley & Sons Ltd., Chichester, 1998, p. 664.
- 409 'Density functional theory applications to transition metal problems', W. Koch and R. H. Hertwig, in 'Encyclopedia of Computational Chemistry', eds. P. R. Schleyer, John Wiley & Sons Ltd., Chichester, 1998, p. 689.
- 410 R. L. Martin, J. D. Kress, I. H. Campbell and D. L. Smith, *Phys. Rev. B: Condens. Matter*, 2000, **61**, 15804.
- 411 M. D. Halls and H. B. Schlegel, *Chem. Mater.*, 2001, **13**, 2632.
- 412 A. Curioni and W. Andreoni, *J. Am. Chem. Soc.*, 1999, **121**, 8216.
- 413 A. Curioni, M. Boero and W. Andreoni, *Chem. Phys. Lett.*, 1998, **294**, 263.
- 414 A. Curioni, W. Andreoni, R. Treusch, F. J. Himpsel, E. Haskal, P. Seidler, C. Heske, S. Kakar, T. van Buuren and L. J. Terminello, *Appl. Phys. Lett.*, 1998, **72**, 1575.
- 415 P. J. Hay and W. R. Wadt, *J. Chem. Phys.*, 1985, **82**, 270.
- 416 K. C. Zheng, J. P. Wang, W. L. Peng, X. W. Liu and F. C. Yun, *J. Mol. Struct. (THEOCHEM)*, 2002, **582**, 1.
- 417 A. J. Mäkinen, I. G. Hill and Z. H. Kafafi, *J. Appl. Phys.*, 2002, **92**, 1598.
- 418 M. C. DeRosa, P. J. Mosher, G. P. A. Yap, K. S. Focsaneanu, R. J. Crutchley and C. E. B. Evans, *Inorg. Chem.*, 2003, **42**, 4864.
- 419 M. C. DeRosa, D. J. Hodgson, G. D. Enright, B. Dawson, C. E. B. Evans and R. J. Crutchley, *J. Am. Chem. Soc.*, 2004, **126**, 7619.
- 420 V. Balzani, A. Juris, M. Venturi, S. Campagna and S. Serroni, *Chem. Rev.*, 1996, **96**, 759.
- 421 C. Sauvage, J. P. Collin, J. C. Chambron, S. Guillerez, C. Coudret, V. Balzani, F. Barigelletti, L. de Cola and L. Flamigni, *Chem. Rev.*, 1994, **94**, 993.
- 422 N. J. Turro, 'Modern Molecular Photochemistry', University Science Books, Sausalito, California, 1991.

- 423 M. H. V. Werts, M. A. Duin, J. W. Hofstraat and J. W. Verhoeven, *Chem. Commun.*, 1999, 799.
- 424 A. Beeby, L. M. Bushby, D. Maffeo and J. A. G. Williams, *J. Chem. Soc., Perkin Trans. 2*, 2000, 1281.
- 425 D. Parker, K. Pulukkody, F. C. Smith, A. Batsanov and J. A. K. Howard, *J. Chem. Soc., Dalton Trans.*, 1994, 689.
- 426 Camps, *Arch. Pharm. (Weinheim, Ger.)*, 1899, **237**, 687 (Beilstein Citation 1010058).
- 427 J. P. Dix and F. Vögtle, *Chem. Ber.*, 1980, **113**, 457.
- 428 J. P. Dix and F. Vögtle, *Angew. Chem., Int. Ed. Engl.*, 1978, **17**, 857.
- 429 M. Geringer and H. Sterk, *Magn. Reson. Chem.*, 1989, **27**, 1148.
- 430 M. V. Alfimov, A. V. Churakov, Y. V. Fedorov, O. A. Fedorova, S. P. Gromov, R. E. Hester, J. A. K. Howard, L. G. Kuz'mina, I. K. Lednev and J. N. Moore, *J. Chem. Soc., Perkin Trans. 2*, 1997, 2249.
- 431 T. Koike, T. Gotoh, S. Aoki, E. Kimura and M. Shiro, *Inorg. Chim. Acta*, 1998, **270**, 424.
- 432 E. Terreno, P. Boniforte, M. Botta, F. Fedeli, L. Milone, A. Mortillaro and S. Aime, *Eur. J. Inorg. Chem.*, 2003, 3530.
- 433 M. Subat, A. S. Borovik and B. König, *J. Am. Chem. Soc.*, 2004, **126**, 3185.
- 434 M. Subat and B. König, *Synthesis*, 2001, 1818.
- 435 S. C. Burdette and S. J. Lippard, *Inorg. Chem.*, 2002, **41**, 6816.
- 436 I. P. Beletskaya, A. D. Averin, A. G. Bessmertnykh, F. Denat and R. Guilard, *Tetrahedron Lett.*, 2002, **43**, 1193.
- 437 T. Hirano, K. Kikuchi, Y. Urano, T. Higuchi and T. Nagano, *Angew. Chem., Int. Ed. Engl.*, 2000, **39**, 1052.
- 438 ZINDO, M. C. Zerner, University of Florida, Gainesville, 1990
- 439 CaChe, Version 6.1.1, Fujitsu Limited, 2003
- 440 I. Baxter and G. A. Swan, *J. Chem. Soc. C*, 1967, 2446.
- 441 M. Albin and W. D. Horrocks, Jr., *Inorg. Chem.*, 1985, **24**, 895.
- 442 O. L. Malta, H. F. Brito, J. F. S. Menezes, F. R. Gonçalves e Silva, C. de Mello Donegá and S. Alves, *Chem. Phys. Lett.*, 1998, **282**, 233.
- 443 'CRC Handbook of Organic Photochemistry', eds. J. C. Scaiano, CRC Press Inc., Boca Raton, Florida, 1989.

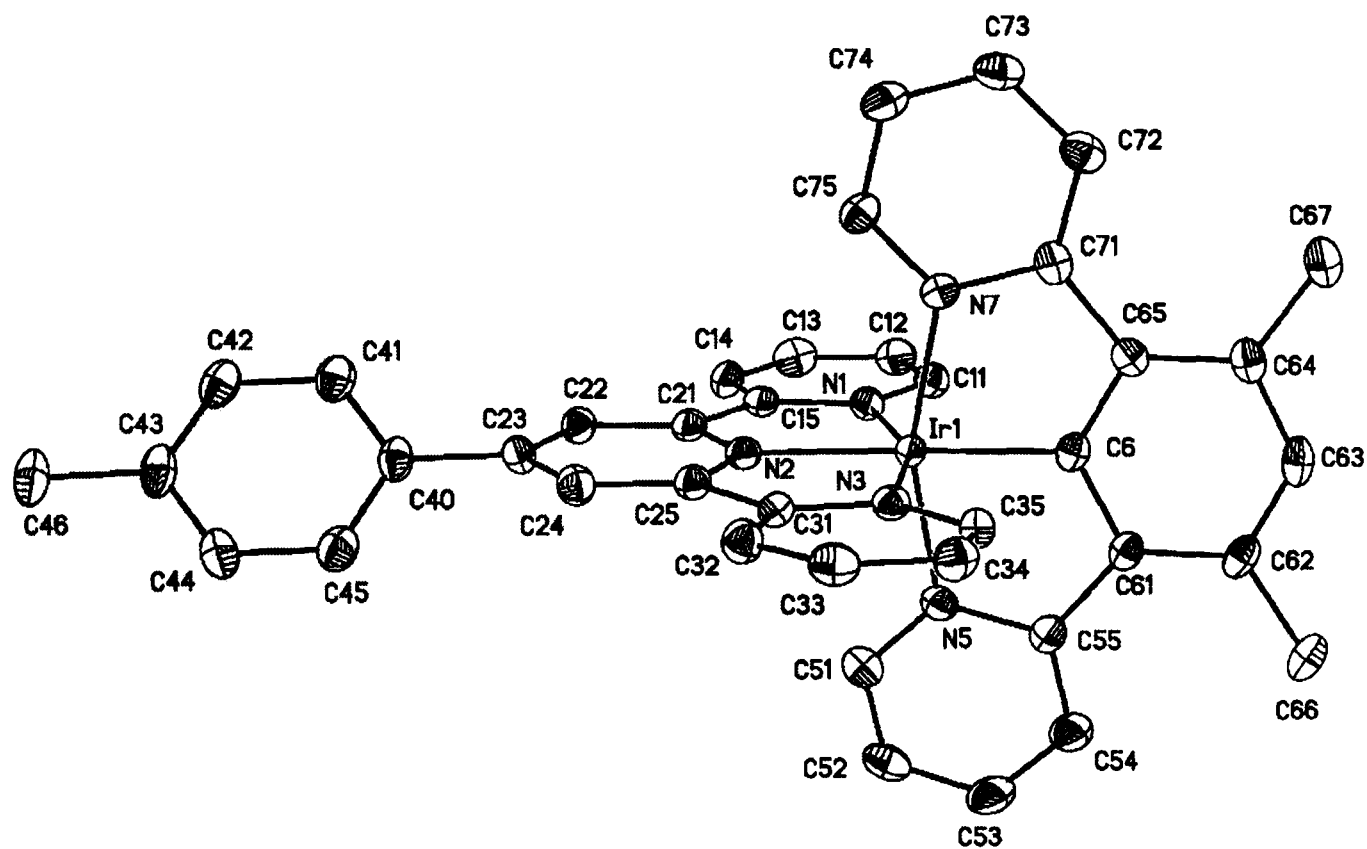
- 444 SHELXTL, Version 5.1, Bruker Analytical X-Ray Systems, Madison, Wisconsin, USA, 1997
- 445 J. N. Demas and G. A. Crosby, *J. Phys. Chem.*, 1971, **75**, 911.
- 446 Gaussian 98, Revision A.9, M. J. Frisch, G. W. Trucks, H. B. Schlegel, G. E. Scuseria, M. A. Robb, J. R. Cheeseman, V. G. Zakrzewski, J. A. Montgomery Jr., R. E. Stratmann, J. C. Burant, S. Dapprich, J. M. Millam, A. D. Daniels, K. N. Kudin, M. C. Strain, O. Farkas, J. Tomasi, V. Barone, M. Cossi, R. Cammi, B. Mennucci, C. Pomelli, C. Adamo, S. Clifford, J. Ochterski, G. A. Petersson, P. Y. Ayala, Q. Cui, K. Morokuma, D. K. Malick, A. D. Rabuck, K. Raghavachari, J. B. Foresman, J. Cioslowski, J. V. Ortiz, A. G. Baboul, B. B. Stefanov, G. Liu, A. Liashenko, P. Piskorz, I. Komaromi, R. Gomperts, R. L. Martin, D. J. Fox, T. Keith, M. A. Al-Laham, C. Y. Peng, A. Nanayakkara, M. Challacombe, P. M. W. Gill, B. Johnson, W. Chen, M. N. Wong, J. L. Andres, C. Gonzalez, M. Head-Gordon, E. S. Replogle and J. A. Pople, Gaussian, Inc., Pittsburgh PA, 1998
- 447 T. Hayashi, M. Konishi and M. Kumada, *Tetrahedron Lett.*, 1979, 1871.
- 448 E. C. Constable and M. D. Ward, *J. Chem. Soc., Dalton Trans.*, 1990, 1405.
- 449 J. D. Holbrey, G. J. T. Tiddy and D. W. Bruce, *J. Chem. Soc., Dalton Trans.*, 1995, 1769.
- 450 K. T. Potts and D. Konwar, *J. Org. Chem.*, 1991, **56**, 4815.
- 451 W. Leslie, 'Cross-coupling reactions in the development of new luminescent bis-terpyridyl complexes', Thesis, University of Durham, Durham, 2003.
- 452 P. Péchy, F. P. Rotzinger, M. K. Nazeeruddin, O. Kohle, S. M. Zakeeruddin, R. Humphry-Baker and M. Grätzel, *J. Chem. Soc., Chem. Commun.*, 1995, 65.
- 453 G. Allinson, R. J. Bushby, M. V. Jesudason, J. L. Paillaud and N. Taylor, *J. Chem. Soc., Perkin Trans. 2*, 1997, 147.
- 454 E. C. Constable and A. M. W. Cargill Thompson, *J. Chem. Soc., Dalton Trans.*, 1992, 2947.
- 455 N. Sato and N. Narita, *Synthesis*, 2001, 1551.
- 456 T. Kobayashi, H. Kawate, H. Kakiuchi and H. Kato, *Bull. Chem. Soc. Jpn.*, 1990, **63**, 1937.
- 457 X. Du, C. Guo, E. Hansell, P. S. Doyle, C. R. Caffrey, T. P. Holler, J. H. McKerrow and F. E. Cohen, *J. Med. Chem.*, 2002, **45**, 2695.
- 458 A. Kumar, R. A. Rhodes, J. Sychala, W. D. Wilson, D. W. Boykin, R. R. Tidwell, C. C. Dykstra, J. E. Hall, S. K. Jones and R. F. Schinazi, *Eur. J. Med. Chem.*, 1995, **30**, 99.

- 459 K. E. Berg, A. Tran, M. K. Raymond, M. Abrahamsson, J. Wolny, S. Redon, M. Andersson, L. Sun, S. Styring, L. Hammarström, H. Toftlund and B. Åkermark, *Eur. J. Inorg. Chem.*, 2001, 1019.
- 460 R. A. Kipp, Y. Li, J. A. Simon and R. H. Schmehl, *J. Photochem. Photobiol. A*, 1999, **121**, 27.
- 461 R. E. Foster, R. D. Lipscomb, T. J. Thompson and C. S. Hamilton, *J. Am. Chem. Soc.*, 1946, **68**, 1327.
- 462 A. Yoneda, G. R. Newkome and K. J. Theriot, *J. Organomet. Chem.*, 1991, **401**, 217.
- 463 B. C. Ranu, A. Hajra, S. S. Dey and U. Jana, *Tetrahedron*, 2003, **59**, 813.
- 464 A. J. Saggiomo, S. Kano, T. Kikuchi, K. Okubo and M. Shinbo, *J. Med. Chem.*, 1972, **15**, 989.
- 465 N. Ikemoto, J. Liu, K. M. J. Brands, J. M. McNamara and P. J. Reider, *Tetrahedron*, 2003, **59**, 1317.
- 466 C. Caris, P. Baret, J. L. Pierre and G. Serratrice, *Tetrahedron*, 1996, **52**, 4659.

APPENDICES

Appendix A – Crystal structures

Crystallographic data for $[\text{Ir}(\text{dpydmb})(\text{ttpy})]^{2+} \cdot 2(\text{PF}_6^-)$



Structure of the $[\text{Ir}(\text{dpydmb})(\text{ttpy})]^{2+}$ cation crystallised as the PF_6^- salt from acetone; 120 K, thermal ellipsoids shown at 50% probability.

Table A1. Crystal data and structure refinement for [Ir(dpydmb)(tppy)]²⁺.2(PF₆⁻).

Empirical formula	C ₄₃ H ₃₈ F ₁₂ IrN ₅ OP ₂	
Formula weight	1122.92	
Temperature	120(2) K	
Wavelength	0.71073 Å	
Crystal system	Orthorhombic	
Space group	Pbca	
Unit cell dimensions	$a = 12.7455(2)$ Å	$\alpha = 90^\circ$
	$b = 19.0106(3)$ Å	$\beta = 90^\circ$
	$c = 33.9410(5)$ Å	$\gamma = 90^\circ$
Volume	8223.9(2) Å ³	
Z	8	
Density (calculated)	1.814 Mg/m ³	
Absorption coefficient	3.423 mm ⁻¹	
F(000)	4432	
Crystal size	0.12 × 0.10 × 0.05 mm ³	
Theta range for data collection	1.20 to 29.22°	
Index ranges	-17 ≤ h ≤ 17, -21 ≤ k ≤ 26, -43 ≤ l ≤ 46	
Reflections collected	52 795	
Independent reflections	10 414 [R(int) = 0.0534]	
Completeness to theta = 29.22°	93.3%	
Absorption correction	Integration	
Max. and min. transmission	0.843 and 0.373	
Refinement method	Full-matrix least-squares on F ²	
Data / restraints / parameters	10 414 / 0 / 577	
Goodness-of-fit on F ²	1.018	
Final R indices [I > 2σ(I)]	R1 = 0.0372, wR2 = 0.0805	
R indices (all data)	R1 = 0.0619, wR2 = 0.0905	
Largest diff. peak and hole	2.616 and -0.819 e.Å ⁻³	

Table A2. Atomic coordinates ($\times 10^4$) and equivalent isotropic displacement parameters ($\text{\AA}^2 \times 10^3$) for $[\text{Ir}(\text{dpydmb})(\text{tppy})]^{2+} \cdot 2(\text{PF}_6^-)$. $U(\text{eq})$ is defined as one third of the trace of the orthogonalized U^{ij} tensor.

	x	y	z	$U(\text{eq})$
Ir(1)	9438(1)	2867(1)	-1349(1)	16(1)
P(1)	7484(1)	6154(1)	16(1)	32(1)
F(1)	6567(3)	6184(2)	-295(1)	92(2)
F(2)	6737(4)	6482(2)	338(2)	104(2)
F(3)	8431(3)	6106(2)	324(1)	58(1)
F(4)	8251(3)	5817(2)	-301(1)	58(1)
F(5)	7125(3)	5380(2)	136(1)	58(1)
F(6)	7846(3)	6912(2)	-118(1)	57(1)
P(2)	5212(1)	4756(1)	2247(1)	26(1)
F(7)	4489(3)	4174(2)	2038(1)	59(1)
F(8)	6212(2)	4468(2)	2012(1)	44(1)
F(9)	5907(3)	5353(2)	2440(1)	58(1)
F(10)	4198(2)	5041(2)	2471(1)	41(1)
F(11)	5452(3)	4242(2)	2602(1)	71(1)
F(12)	4971(2)	5271(2)	1884(1)	38(1)
N(1)	10211(3)	2048(2)	-1086(1)	20(1)
C(11)	10646(3)	1492(2)	-1267(1)	23(1)
C(12)	11190(3)	980(2)	-1065(1)	26(1)
C(13)	11307(3)	1040(2)	-662(1)	28(1)
C(14)	10857(3)	1608(2)	-469(1)	23(1)
C(15)	10297(3)	2101(2)	-683(1)	21(1)
N(2)	9333(2)	3140(2)	-772(1)	19(1)
C(21)	9768(3)	2712(2)	-500(1)	20(1)
C(22)	9690(3)	2887(2)	-105(1)	21(1)
C(23)	9167(3)	3503(2)	1(1)	22(1)
C(24)	8728(3)	3934(2)	-292(1)	23(1)
C(25)	8818(3)	3731(2)	-681(1)	19(1)

N(3)	8611(2)	3790(2)	-1391(1)	19(1)
C(31)	8391(3)	4096(2)	-1033(1)	20(1)
C(32)	7789(3)	4705(2)	-1011(1)	24(1)
C(33)	7389(3)	4996(2)	-1356(1)	24(1)
C(34)	7639(3)	4694(2)	-1714(1)	23(1)
C(35)	8253(3)	4099(2)	-1720(1)	22(1)
C(40)	9092(3)	3727(2)	419(1)	24(1)
C(41)	8868(3)	3246(2)	717(1)	27(1)
C(42)	8785(3)	3471(2)	1105(1)	28(1)
C(43)	8933(3)	4178(3)	1206(1)	28(1)
C(44)	9165(3)	4645(3)	906(1)	29(1)
C(45)	9242(3)	4430(3)	518(1)	28(1)
C(46)	8823(4)	4434(3)	1627(1)	34(1)
N(5)	10838(3)	3329(2)	-1492(1)	20(1)
C(51)	11518(3)	3594(2)	-1229(1)	28(1)
C(52)	12466(4)	3877(3)	-1340(1)	32(1)
C(53)	12724(4)	3895(3)	-1733(1)	35(1)
C(54)	12029(3)	3621(2)	-2005(1)	30(1)
C(55)	11078(3)	3328(2)	-1890(1)	21(1)
C(6)	9481(3)	2668(2)	-1914(1)	18(1)
C(61)	10291(3)	2974(2)	-2138(1)	20(1)
C(62)	10237(3)	2916(2)	-2551(1)	22(1)
C(63)	9395(3)	2543(2)	-2710(1)	24(1)
C(64)	8587(3)	2233(2)	-2494(1)	22(1)
C(65)	8639(3)	2303(2)	-2079(1)	19(1)
C(66)	11028(4)	3240(2)	-2830(1)	29(1)
C(67)	7730(4)	1849(2)	-2713(1)	31(1)
N(7)	8093(3)	2287(2)	-1401(1)	19(1)
C(71)	7883(3)	2051(2)	-1779(1)	21(1)
C(72)	7015(3)	1623(2)	-1840(1)	26(1)
C(73)	6364(3)	1449(2)	-1530(1)	29(1)

C(74)	6576(3)	1690(2)	-1155(1)	28(1)
C(75)	7451(3)	2106(2)	-1103(1)	22(1)
C(1)	4285(4)	6199(3)	681(1)	33(1)
C(2)	4698(5)	6428(3)	1068(2)	54(2)
C(3)	4624(5)	5494(3)	531(2)	55(2)
O(1)	3705(3)	6577(2)	493(1)	50(1)

Table A3. Bond lengths [Å] and angles [°] for [Ir(dpydmb)(tppy)]²⁺.2(PF₆⁻).

Ir(1)-C(6)	1.954(4)	C(23)-C(40)	1.483(5)
Ir(1)-N(2)	2.030(3)	C(24)-C(25)	1.381(5)
Ir(1)-N(5)	2.046(3)	C(25)-C(31)	1.484(5)
Ir(1)-N(1)	2.046(3)	N(3)-C(35)	1.340(5)
Ir(1)-N(7)	2.047(3)	N(3)-C(31)	1.379(5)
Ir(1)-N(3)	2.052(3)	C(31)-C(32)	1.391(6)
P(1)-F(1)	1.575(4)	C(32)-C(33)	1.392(6)
P(1)-F(2)	1.577(4)	C(33)-C(34)	1.381(6)
P(1)-F(6)	1.581(3)	C(34)-C(35)	1.375(6)
P(1)-F(4)	1.588(3)	C(40)-C(41)	1.391(6)
P(1)-F(5)	1.594(3)	C(40)-C(45)	1.393(6)
P(1)-F(3)	1.598(3)	C(41)-C(42)	1.391(6)
P(2)-F(9)	1.581(3)	C(42)-C(43)	1.400(6)
P(2)-F(11)	1.582(3)	C(43)-C(44)	1.384(6)
P(2)-F(10)	1.593(3)	C(43)-C(46)	1.513(6)
P(2)-F(8)	1.600(3)	C(44)-C(45)	1.383(6)
P(2)-F(12)	1.602(3)	N(5)-C(51)	1.342(5)
P(2)-F(7)	1.605(3)	N(5)-C(55)	1.387(5)
N(1)-C(11)	1.342(5)	C(51)-C(52)	1.376(6)
N(1)-C(15)	1.375(5)	C(52)-C(53)	1.373(6)
C(11)-C(12)	1.377(6)	C(53)-C(54)	1.383(6)
C(12)-C(13)	1.381(6)	C(54)-C(55)	1.390(6)
C(13)-C(14)	1.388(6)	C(55)-C(61)	1.473(6)
C(14)-C(15)	1.384(6)	C(6)-C(65)	1.396(5)
C(15)-C(21)	1.479(6)	C(6)-C(61)	1.410(5)
N(2)-C(25)	1.337(5)	C(61)-C(62)	1.406(6)
N(2)-C(21)	1.349(5)	C(62)-C(63)	1.395(6)
C(21)-C(22)	1.385(5)	C(62)-C(66)	1.515(6)
C(22)-C(23)	1.396(6)	C(63)-C(64)	1.394(6)
C(23)-C(24)	1.404(6)	C(64)-C(65)	1.416(5)

C(64)-C(67)	1.509(6)	C(73)-C(74)	1.379(6)
C(65)-C(71)	1.480(6)	C(74)-C(75)	1.379(6)
N(7)-C(75)	1.345(5)	C(1)-O(1)	1.211(6)
N(7)-C(71)	1.386(5)	C(1)-C(2)	1.482(7)
C(71)-C(72)	1.389(6)	C(1)-C(3)	1.496(7)
C(72)-C(73)	1.382(6)		
C(6)-Ir(1)-N(2)	175.76(14)	F(6)-P(1)-F(5)	178.0(2)
C(6)-Ir(1)-N(5)	80.03(15)	F(4)-P(1)-F(5)	88.73(19)
N(2)-Ir(1)-N(5)	100.16(13)	F(1)-P(1)-F(3)	178.3(3)
C(6)-Ir(1)-N(1)	105.42(14)	F(2)-P(1)-F(3)	91.5(3)
N(2)-Ir(1)-N(1)	78.82(13)	F(6)-P(1)-F(3)	91.08(18)
N(5)-Ir(1)-N(1)	90.58(13)	F(4)-P(1)-F(3)	87.4(2)
C(6)-Ir(1)-N(7)	80.45(15)	F(5)-P(1)-F(3)	89.84(18)
N(2)-Ir(1)-N(7)	99.53(13)	F(9)-P(2)-F(11)	91.1(2)
N(5)-Ir(1)-N(7)	160.25(13)	F(9)-P(2)-F(10)	90.75(18)
N(1)-Ir(1)-N(7)	91.74(13)	F(11)-P(2)-F(10)	90.23(16)
C(6)-Ir(1)-N(3)	96.39(14)	F(9)-P(2)-F(8)	90.28(18)
N(2)-Ir(1)-N(3)	79.37(13)	F(11)-P(2)-F(8)	90.79(17)
N(5)-Ir(1)-N(3)	93.68(13)	F(10)-P(2)-F(8)	178.53(18)
N(1)-Ir(1)-N(3)	158.19(13)	F(9)-P(2)-F(12)	89.25(18)
N(7)-Ir(1)-N(3)	91.43(12)	F(11)-P(2)-F(12)	179.5(2)
F(1)-P(1)-F(2)	90.1(3)	F(10)-P(2)-F(12)	90.16(15)
F(1)-P(1)-F(6)	89.5(2)	F(8)-P(2)-F(12)	88.81(15)
F(2)-P(1)-F(6)	90.9(2)	F(9)-P(2)-F(7)	177.6(2)
F(1)-P(1)-F(4)	91.0(2)	F(11)-P(2)-F(7)	91.3(2)
F(2)-P(1)-F(4)	178.8(3)	F(10)-P(2)-F(7)	88.90(17)
F(6)-P(1)-F(4)	89.6(2)	F(8)-P(2)-F(7)	90.02(17)
F(1)-P(1)-F(5)	89.5(2)	F(12)-P(2)-F(7)	88.34(18)
F(2)-P(1)-F(5)	90.8(2)	C(11)-N(1)-C(15)	118.6(4)

C(11)-N(1)-Ir(1)	126.8(3)	C(35)-C(34)-C(33)	119.1(4)
C(15)-N(1)-Ir(1)	114.6(3)	N(3)-C(35)-C(34)	122.8(4)
N(1)-C(11)-C(12)	122.5(4)	C(41)-C(40)-C(45)	119.0(4)
C(11)-C(12)-C(13)	119.2(4)	C(41)-C(40)-C(23)	121.3(4)
C(12)-C(13)-C(14)	119.1(4)	C(45)-C(40)-C(23)	119.7(4)
C(15)-C(14)-C(13)	119.5(4)	C(40)-C(41)-C(42)	120.2(4)
N(1)-C(15)-C(14)	120.9(4)	C(41)-C(42)-C(43)	121.1(4)
N(1)-C(15)-C(21)	116.0(4)	C(44)-C(43)-C(42)	117.6(4)
C(14)-C(15)-C(21)	123.1(4)	C(44)-C(43)-C(46)	120.6(4)
C(25)-N(2)-C(21)	123.4(4)	C(42)-C(43)-C(46)	121.8(4)
C(25)-N(2)-Ir(1)	118.0(3)	C(45)-C(44)-C(43)	122.0(4)
C(21)-N(2)-Ir(1)	118.5(3)	C(44)-C(45)-C(40)	120.1(4)
N(2)-C(21)-C(22)	119.1(4)	C(51)-N(5)-C(55)	120.4(4)
N(2)-C(21)-C(15)	112.0(3)	C(51)-N(5)-Ir(1)	124.5(3)
C(22)-C(21)-C(15)	128.9(4)	C(55)-N(5)-Ir(1)	115.0(3)
C(21)-C(22)-C(23)	119.2(4)	N(5)-C(51)-C(52)	122.1(4)
C(22)-C(23)-C(24)	119.7(4)	C(53)-C(52)-C(51)	119.1(4)
C(22)-C(23)-C(40)	121.3(4)	C(52)-C(53)-C(54)	119.2(4)
C(24)-C(23)-C(40)	119.0(4)	C(53)-C(54)-C(55)	121.4(4)
C(25)-C(24)-C(23)	118.7(4)	N(5)-C(55)-C(54)	117.8(4)
N(2)-C(25)-C(24)	119.8(4)	N(5)-C(55)-C(61)	114.1(3)
N(2)-C(25)-C(31)	112.8(3)	C(54)-C(55)-C(61)	128.0(4)
C(24)-C(25)-C(31)	127.5(4)	C(65)-C(6)-C(61)	123.4(4)
C(35)-N(3)-C(31)	118.7(3)	C(65)-C(6)-Ir(1)	118.0(3)
C(35)-N(3)-Ir(1)	127.5(3)	C(61)-C(6)-Ir(1)	118.1(3)
C(31)-N(3)-Ir(1)	113.7(3)	C(62)-C(61)-C(6)	118.1(4)
N(3)-C(31)-C(32)	120.7(4)	C(62)-C(61)-C(55)	129.8(4)
N(3)-C(31)-C(25)	116.0(3)	C(6)-C(61)-C(55)	112.2(3)
C(32)-C(31)-C(25)	123.3(4)	C(63)-C(62)-C(61)	117.6(4)
C(31)-C(32)-C(33)	119.1(4)	C(63)-C(62)-C(66)	118.4(4)
C(34)-C(33)-C(32)	119.4(4)	C(61)-C(62)-C(66)	124.0(4)

C(64)-C(63)-C(62)	125.4(4)	N(7)-C(71)-C(72)	118.7(4)
C(63)-C(64)-C(65)	116.7(4)	N(7)-C(71)-C(65)	114.0(3)
C(63)-C(64)-C(67)	118.7(4)	C(72)-C(71)-C(65)	127.2(4)
C(65)-C(64)-C(67)	124.6(4)	C(73)-C(72)-C(71)	120.3(4)
C(6)-C(65)-C(64)	118.8(4)	C(74)-C(73)-C(72)	120.5(4)
C(6)-C(65)-C(71)	112.6(3)	C(73)-C(74)-C(75)	117.8(4)
C(64)-C(65)-C(71)	128.5(4)	N(7)-C(75)-C(74)	122.8(4)
C(75)-N(7)-C(71)	119.8(3)	O(1)-C(1)-C(2)	120.5(5)
C(75)-N(7)-Ir(1)	125.6(3)	O(1)-C(1)-C(3)	122.0(5)
C(71)-N(7)-Ir(1)	114.6(3)	C(2)-C(1)-C(3)	117.5(5)

Table A4. Anisotropic displacement parameters ($\text{\AA}^2 \times 10^3$) for $[\text{Ir}(\text{dpydmb})(\text{tppy})]^{2+} \cdot 2(\text{PF}_6^-)$. The anisotropic displacement factor exponent takes the form: $-2\pi^2[h^2 a^{*2} U^{11} + \dots + 2 h k a^* b^* U^{12}]$.

	U^{11}	U^{22}	U^{33}	U^{23}	U^{13}	U^{12}
Ir(1)	16(1)	17(1)	14(1)	0(1)	0(1)	-1(1)
P(1)	30(1)	26(1)	39(1)	3(1)	4(1)	-1(1)
F(1)	55(2)	73(3)	147(4)	48(3)	-60(3)	-17(2)
F(2)	124(4)	62(3)	127(4)	3(2)	88(3)	23(3)
F(3)	79(2)	60(2)	35(2)	5(2)	-23(2)	-17(2)
F(4)	62(2)	67(2)	46(2)	-14(2)	12(2)	2(2)
F(5)	44(2)	36(2)	93(3)	23(2)	3(2)	-3(1)
F(6)	61(2)	42(2)	69(2)	19(2)	-5(2)	-14(2)
P(2)	28(1)	25(1)	25(1)	4(1)	5(1)	5(1)
F(7)	57(2)	41(2)	80(3)	-17(2)	21(2)	-22(2)
F(8)	35(2)	51(2)	46(2)	2(1)	12(1)	16(1)
F(9)	57(2)	72(2)	43(2)	-25(2)	-6(2)	-16(2)
F(10)	40(2)	51(2)	34(2)	11(1)	16(1)	18(1)
F(11)	68(2)	85(3)	61(2)	50(2)	24(2)	45(2)
F(12)	38(2)	45(2)	30(2)	13(1)	1(1)	1(1)
N(1)	17(2)	23(2)	19(2)	-1(1)	-1(1)	-2(1)
C(11)	21(2)	26(2)	22(2)	-3(2)	2(2)	-2(2)
C(12)	24(2)	22(2)	31(2)	-2(2)	5(2)	2(2)
C(13)	22(2)	28(2)	33(2)	6(2)	-2(2)	4(2)
C(14)	26(2)	26(2)	18(2)	3(2)	0(2)	-1(2)
C(15)	17(2)	26(2)	20(2)	0(2)	0(2)	-7(2)
N(2)	17(2)	20(2)	19(2)	2(1)	0(1)	-3(1)
C(21)	16(2)	24(2)	19(2)	1(2)	0(2)	-3(2)
C(22)	20(2)	25(2)	17(2)	1(2)	-2(2)	-1(2)
C(23)	23(2)	24(2)	18(2)	-4(2)	0(2)	-2(2)
C(24)	23(2)	24(2)	22(2)	-2(2)	0(2)	0(2)
C(25)	17(2)	21(2)	19(2)	1(2)	0(2)	-2(2)

N(3)	16(2)	21(2)	19(2)	2(1)	-1(1)	-1(1)
C(31)	20(2)	21(2)	18(2)	-1(2)	3(2)	-4(2)
C(32)	27(2)	23(2)	22(2)	-1(2)	2(2)	2(2)
C(33)	25(2)	17(2)	31(2)	3(2)	-1(2)	3(2)
C(34)	23(2)	25(2)	22(2)	7(2)	-5(2)	1(2)
C(35)	26(2)	24(2)	16(2)	-1(2)	0(2)	-5(2)
C(40)	19(2)	35(2)	17(2)	-3(2)	-1(2)	3(2)
C(41)	25(2)	32(3)	24(2)	0(2)	2(2)	5(2)
C(42)	28(2)	36(3)	20(2)	6(2)	2(2)	5(2)
C(43)	22(2)	42(3)	19(2)	-4(2)	0(2)	9(2)
C(44)	30(2)	33(3)	23(2)	-8(2)	-2(2)	3(2)
C(45)	29(2)	34(3)	22(2)	3(2)	1(2)	0(2)
C(46)	31(2)	50(3)	21(2)	-7(2)	3(2)	7(2)
N(5)	19(2)	20(2)	21(2)	-2(1)	-1(1)	-1(1)
C(51)	29(2)	26(2)	29(2)	-4(2)	-2(2)	-1(2)
C(52)	24(2)	32(2)	40(3)	-4(2)	-7(2)	-9(2)
C(53)	29(2)	38(3)	38(3)	2(2)	12(2)	-9(2)
C(54)	27(2)	31(2)	31(2)	0(2)	7(2)	-4(2)
C(55)	24(2)	19(2)	21(2)	1(2)	3(2)	2(2)
C(6)	21(2)	16(2)	16(2)	5(2)	-1(2)	5(2)
C(61)	23(2)	18(2)	18(2)	1(2)	4(2)	4(2)
C(62)	27(2)	19(2)	20(2)	6(2)	5(2)	8(2)
C(63)	31(2)	25(2)	15(2)	-1(2)	0(2)	11(2)
C(64)	29(2)	19(2)	20(2)	-2(2)	-4(2)	6(2)
C(65)	22(2)	14(2)	21(2)	1(2)	-4(2)	4(2)
C(66)	33(2)	32(2)	22(2)	8(2)	7(2)	5(2)
C(67)	37(3)	34(3)	22(2)	-4(2)	-3(2)	0(2)
N(7)	17(2)	18(2)	21(2)	2(1)	1(1)	1(1)
C(71)	21(2)	19(2)	21(2)	0(2)	-4(2)	7(2)
C(72)	23(2)	24(2)	29(2)	2(2)	-7(2)	0(2)
C(73)	20(2)	30(2)	36(3)	2(2)	-3(2)	-6(2)

C(74)	23(2)	31(2)	30(2)	6(2)	4(2)	-3(2)
C(75)	19(2)	25(2)	22(2)	3(2)	2(2)	3(2)
C(1)	30(2)	44(3)	25(2)	7(2)	9(2)	1(2)
C(2)	58(4)	59(4)	46(3)	0(3)	-11(3)	16(3)
C(3)	51(4)	46(3)	68(4)	-8(3)	21(3)	6(3)
O(1)	51(2)	63(3)	36(2)	10(2)	-1(2)	16(2)

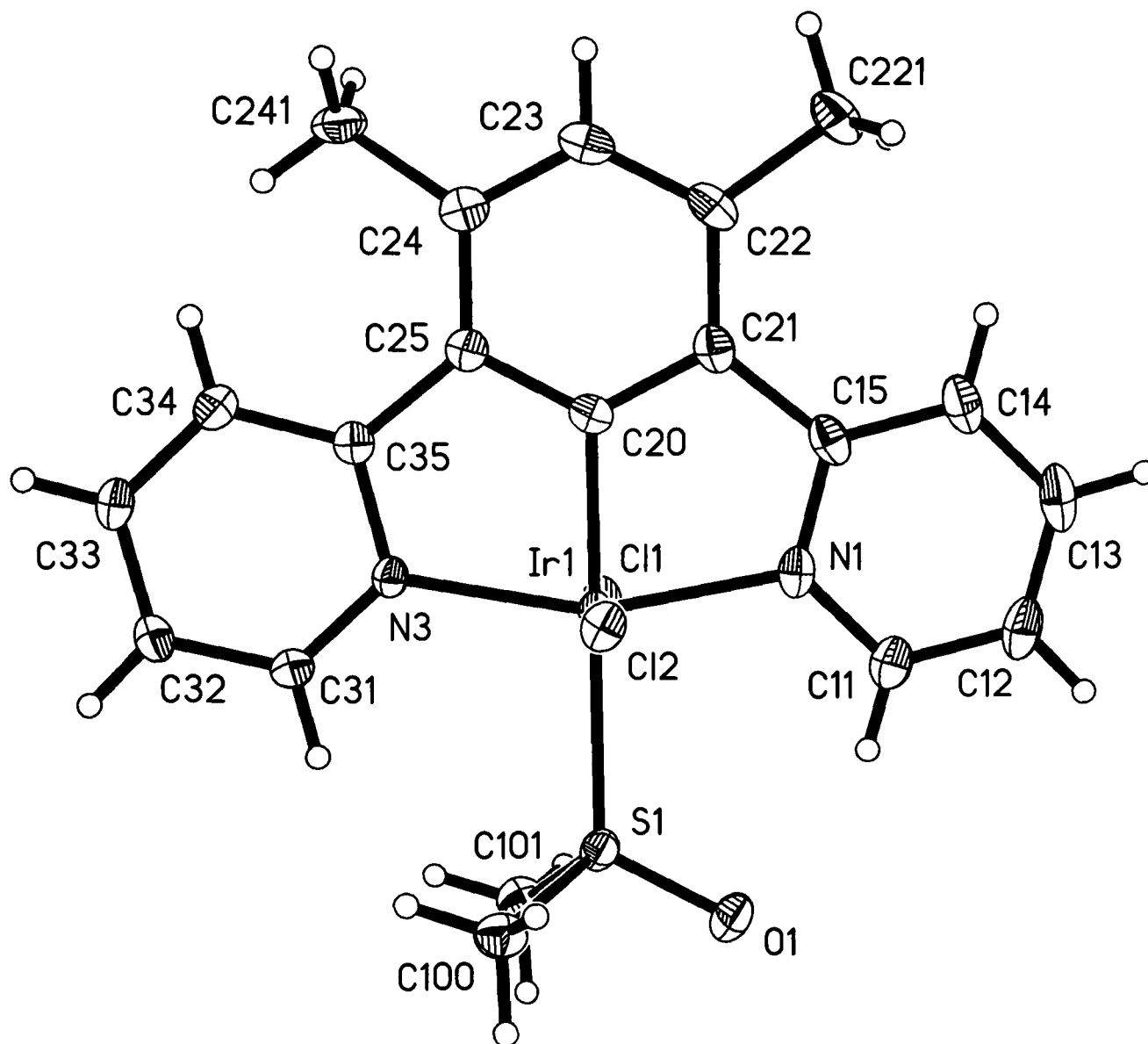
Table A5. Torsion angles [°] for [Ir(dpydmb)(tppy)]²⁺·2(PF₆⁻).

C(6)-Ir(1)-N(1)-C(11)	-0.4(4)	N(3)-Ir(1)-N(2)-C(21)	179.6(3)
N(2)-Ir(1)-N(1)-C(11)	179.6(4)	C(25)-N(2)-C(21)-C(22)	-0.2(6)
N(5)-Ir(1)-N(1)-C(11)	-80.2(3)	Ir(1)-N(2)-C(21)-C(22)	-179.1(3)
N(7)-Ir(1)-N(1)-C(11)	80.2(3)	C(25)-N(2)-C(21)-C(15)	-179.4(3)
N(3)-Ir(1)-N(1)-C(11)	178.4(3)	Ir(1)-N(2)-C(21)-C(15)	1.8(4)
C(6)-Ir(1)-N(1)-C(15)	178.0(3)	N(1)-C(15)-C(21)-N(2)	-3.5(5)
N(2)-Ir(1)-N(1)-C(15)	-2.1(3)	C(14)-C(15)-C(21)-N(2)	176.1(4)
N(5)-Ir(1)-N(1)-C(15)	98.2(3)	N(1)-C(15)-C(21)-C(22)	177.5(4)
N(7)-Ir(1)-N(1)-C(15)	-101.4(3)	C(14)-C(15)-C(21)-C(22)	-2.9(7)
N(3)-Ir(1)-N(1)-C(15)	-3.2(5)	N(2)-C(21)-C(22)-C(23)	-0.4(6)
C(15)-N(1)-C(11)-C(12)	-1.1(6)	C(15)-C(21)-C(22)-C(23)	178.6(4)
Ir(1)-N(1)-C(11)-C(12)	177.2(3)	C(21)-C(22)-C(23)-C(24)	0.2(6)
N(1)-C(11)-C(12)-C(13)	-0.8(6)	C(21)-C(22)-C(23)-C(40)	-177.9(4)
C(11)-C(12)-C(13)-C(14)	1.2(6)	C(22)-C(23)-C(24)-C(25)	0.6(6)
C(12)-C(13)-C(14)-C(15)	0.3(6)	C(40)-C(23)-C(24)-C(25)	178.7(4)
C(11)-N(1)-C(15)-C(14)	2.6(6)	C(21)-N(2)-C(25)-C(24)	1.0(6)
Ir(1)-N(1)-C(15)-C(14)	-176.0(3)	Ir(1)-N(2)-C(25)-C(24)	179.9(3)
C(11)-N(1)-C(15)-C(21)	-177.8(3)	C(21)-N(2)-C(25)-C(31)	-178.5(3)
Ir(1)-N(1)-C(15)-C(21)	3.6(4)	Ir(1)-N(2)-C(25)-C(31)	0.4(4)
C(13)-C(14)-C(15)-N(1)	-2.2(6)	C(23)-C(24)-C(25)-N(2)	-1.2(6)
C(13)-C(14)-C(15)-C(21)	178.3(4)	C(23)-C(24)-C(25)-C(31)	178.3(4)
C(6)-Ir(1)-N(2)-C(25)	0(2)	C(6)-Ir(1)-N(3)-C(35)	0.4(3)
N(5)-Ir(1)-N(2)-C(25)	92.6(3)	N(2)-Ir(1)-N(3)-C(35)	-179.6(3)
N(1)-Ir(1)-N(2)-C(25)	-178.9(3)	N(5)-Ir(1)-N(3)-C(35)	80.8(3)
N(7)-Ir(1)-N(2)-C(25)	-89.0(3)	N(1)-Ir(1)-N(3)-C(35)	-178.4(3)
N(3)-Ir(1)-N(2)-C(25)	0.7(3)	N(7)-Ir(1)-N(3)-C(35)	-80.1(3)
C(6)-Ir(1)-N(2)-C(21)	179(100)	C(6)-Ir(1)-N(3)-C(31)	178.3(3)
N(5)-Ir(1)-N(2)-C(21)	-88.5(3)	N(2)-Ir(1)-N(3)-C(31)	-1.7(3)
N(1)-Ir(1)-N(2)-C(21)	0.1(3)	N(5)-Ir(1)-N(3)-C(31)	-101.4(3)
N(7)-Ir(1)-N(2)-C(21)	90.0(3)	N(1)-Ir(1)-N(3)-C(31)	-0.5(5)

N(7)-Ir(1)-N(3)-C(31)	97.7(3)	N(2)-Ir(1)-N(5)-C(51)	11.6(4)
C(35)-N(3)-C(31)-C(32)	1.4(6)	N(1)-Ir(1)-N(5)-C(51)	-67.1(3)
Ir(1)-N(3)-C(31)-C(32)	-176.7(3)	N(7)-Ir(1)-N(5)-C(51)	-163.9(4)
C(35)-N(3)-C(31)-C(25)	-179.5(3)	N(3)-Ir(1)-N(5)-C(51)	91.5(3)
Ir(1)-N(3)-C(31)-C(25)	2.4(4)	C(6)-Ir(1)-N(5)-C(55)	4.7(3)
N(2)-C(25)-C(31)-N(3)	-1.9(5)	N(2)-Ir(1)-N(5)-C(55)	-171.0(3)
C(24)-C(25)-C(31)-N(3)	178.7(4)	N(1)-Ir(1)-N(5)-C(55)	110.3(3)
N(2)-C(25)-C(31)-C(32)	177.2(4)	N(7)-Ir(1)-N(5)-C(55)	13.5(6)
C(24)-C(25)-C(31)-C(32)	-2.3(6)	N(3)-Ir(1)-N(5)-C(55)	-91.1(3)
N(3)-C(31)-C(32)-C(33)	1.4(6)	C(55)-N(5)-C(51)-C(52)	0.4(7)
C(25)-C(31)-C(32)-C(33)	-177.6(4)	Ir(1)-N(5)-C(51)-C(52)	177.6(3)
C(31)-C(32)-C(33)-C(34)	-3.1(6)	N(5)-C(51)-C(52)-C(53)	0.6(7)
C(32)-C(33)-C(34)-C(35)	1.9(6)	C(51)-C(52)-C(53)-C(54)	-0.8(7)
C(31)-N(3)-C(35)-C(34)	-2.6(6)	C(52)-C(53)-C(54)-C(55)	-0.1(7)
Ir(1)-N(3)-C(35)-C(34)	175.1(3)	C(51)-N(5)-C(55)-C(54)	-1.2(6)
C(33)-C(34)-C(35)-N(3)	1.0(6)	Ir(1)-N(5)-C(55)-C(54)	-178.7(3)
C(22)-C(23)-C(40)-C(41)	-43.0(6)	C(51)-N(5)-C(55)-C(61)	175.8(4)
C(24)-C(23)-C(40)-C(41)	138.9(4)	Ir(1)-N(5)-C(55)-C(61)	-1.7(4)
C(22)-C(23)-C(40)-C(45)	137.3(4)	C(53)-C(54)-C(55)-N(5)	1.0(7)
C(24)-C(23)-C(40)-C(45)	-40.8(6)	C(53)-C(54)-C(55)-C(61)	-175.4(4)
C(45)-C(40)-C(41)-C(42)	0.7(6)	N(2)-Ir(1)-C(6)-C(65)	-86(2)
C(23)-C(40)-C(41)-C(42)	-178.9(4)	N(5)-Ir(1)-C(6)-C(65)	-179.3(3)
C(40)-C(41)-C(42)-C(43)	-0.6(7)	N(1)-Ir(1)-C(6)-C(65)	92.9(3)
C(41)-C(42)-C(43)-C(44)	-0.1(6)	N(7)-Ir(1)-C(6)-C(65)	3.7(3)
C(41)-C(42)-C(43)-C(46)	178.7(4)	N(3)-Ir(1)-C(6)-C(65)	-86.7(3)
C(42)-C(43)-C(44)-C(45)	0.5(7)	N(2)-Ir(1)-C(6)-C(61)	86(2)
C(46)-C(43)-C(44)-C(45)	-178.3(4)	N(5)-Ir(1)-C(6)-C(61)	-7.1(3)
C(43)-C(44)-C(45)-C(40)	-0.4(7)	N(1)-Ir(1)-C(6)-C(61)	-94.9(3)
C(41)-C(40)-C(45)-C(44)	-0.3(6)	N(7)-Ir(1)-C(6)-C(61)	175.9(3)
C(23)-C(40)-C(45)-C(44)	179.4(4)	N(3)-Ir(1)-C(6)-C(61)	85.6(3)
C(6)-Ir(1)-N(5)-C(51)	-172.7(4)	C(65)-C(6)-C(61)-C(62)	0.9(6)

Ir(1)-C(6)-C(61)-C(62)	-170.9(3)
C(65)-C(6)-C(61)-C(55)	179.8(4)
Ir(1)-C(6)-C(61)-C(55)	8.0(4)
N(5)-C(55)-C(61)-C(62)	175.0(4)
C(54)-C(55)-C(61)-C(62)	-8.4(7)
N(5)-C(55)-C(61)-C(6)	-3.8(5)
C(54)-C(55)-C(61)-C(6)	172.8(4)
C(6)-C(61)-C(62)-C(63)	-1.5(6)
C(55)-C(61)-C(62)-C(63)	179.8(4)
C(6)-C(61)-C(62)-C(66)	177.8(4)
C(55)-C(61)-C(62)-C(66)	-0.9(7)
C(61)-C(62)-C(63)-C(64)	1.3(6)
C(66)-C(62)-C(63)-C(64)	-178.0(4)
C(62)-C(63)-C(64)-C(65)	-0.4(6)
C(62)-C(63)-C(64)-C(67)	179.8(4)
C(61)-C(6)-C(65)-C(64)	0.0(6)

Ir(1)-C(6)-C(65)-C(64)	171.8(3)	N(3)-Ir(1)-N(7)-C(71)	96.4(3)
C(61)-C(6)-C(65)-C(71)	-178.4(4)	C(75)-N(7)-C(71)-C(72)	-0.9(5)
Ir(1)-C(6)-C(65)-C(71)	-6.6(4)	Ir(1)-N(7)-C(71)-C(72)	176.8(3)
C(63)-C(64)-C(65)-C(6)	-0.3(5)	C(75)-N(7)-C(71)-C(65)	178.7(3)
C(67)-C(64)-C(65)-C(6)	179.5(4)	Ir(1)-N(7)-C(71)-C(65)	-3.6(4)
C(63)-C(64)-C(65)-C(71)	177.8(4)	C(6)-C(65)-C(71)-N(7)	6.4(5)
C(67)-C(64)-C(65)-C(71)	-2.4(7)	C(64)-C(65)-C(71)-N(7)	-171.8(4)
C(6)-Ir(1)-N(7)-C(75)	177.7(3)	C(6)-C(65)-C(71)-C(72)	-174.0(4)
N(2)-Ir(1)-N(7)-C(75)	-6.6(3)	C(64)-C(65)-C(71)-C(72)	7.8(7)
N(5)-Ir(1)-N(7)-C(75)	168.9(4)	N(7)-C(71)-C(72)-C(73)	1.4(6)
N(1)-Ir(1)-N(7)-C(75)	72.3(3)	C(65)-C(71)-C(72)-C(73)	-178.1(4)
N(3)-Ir(1)-N(7)-C(75)	-86.1(3)	C(71)-C(72)-C(73)-C(74)	-1.0(6)
C(6)-Ir(1)-N(7)-C(71)	0.1(3)	C(72)-C(73)-C(74)-C(75)	0.0(6)
N(2)-Ir(1)-N(7)-C(71)	175.8(3)	C(71)-N(7)-C(75)-C(74)	0.0(6)
N(5)-Ir(1)-N(7)-C(71)	-8.6(5)	Ir(1)-N(7)-C(75)-C(74)	-177.4(3)
N(1)-Ir(1)-N(7)-C(71)	-105.2(3)	C(73)-C(74)-C(75)-N(7)	0.5(6)

Crystallographic data for Ir(dpydmb)(DMSO)Cl₂

Structure of Ir(dpydmb)(DMSO)Cl₂ crystallised from DMSO; 120 K, thermal ellipsoids shown at 30% probability.

Table A6. Crystal data and structure refinement for Ir(dpydmb)(DMSO)Cl₂.

Empirical formula	C ₂₀ H ₂₁ Cl ₂ IrN ₂ OS	
Formula weight	600.55	
Temperature	120(2) K	
Wavelength	0.71073 Å	
Crystal system	Monoclinic	
Space group	P2(1)/n	
Unit cell dimensions	$a = 14.379(11)$ Å	$\alpha = 90^\circ$
	$b = 8.779(7)$ Å	$\beta = 97.811(7)^\circ$
	$c = 15.889(12)$ Å	$\gamma = 90^\circ$
Volume	1987(3) Å ³	
Z	4	
Density (calculated)	2.007 Mg/m ³	
Absorption coefficient	7.107 mm ⁻¹	
F(000)	1160	
Crystal size	0.18 x 0.12 x 0.08 mm ³	
Theta range for data collection	1.79 to 27.50°	
Index ranges	$-18 \leq h \leq 18, -11 \leq k \leq 11, -20 \leq l \leq 20$	
Reflections collected	21 215	
Independent reflections	4559 [R(int) = 0.0377]	
Completeness to theta = 27.50°	99.8%	
Absorption correction	Semi-empirical from equivalents	
Max. and min. transmission	1.000 and 0.729	
Refinement method	Full-matrix least-squares on F ²	
Data / restraints / parameters	4559 / 0 / 244	
Goodness-of-fit on F ²	1.085	
Final R indices [I > 2σ(I)]	R1 = 0.0237, wR2 = 0.0480	
R indices (all data)	R1 = 0.0309, wR2 = 0.0496	
Largest diff. peak and hole	1.031 and -0.719 e.Å ⁻³	

Table A7. Atomic coordinates ($\times 10^4$) and equivalent isotropic displacement parameters ($\text{\AA}^2 \times 10^3$) for Ir(dpydmb)(DMSO)Cl₂. U(eq) is defined as one third of the trace of the orthogonalized U^{ij} tensor.

	x	y	z	U(eq)
Ir(1)	2502(1)	7967(1)	10363(1)	14(1)
S(1)	1806(1)	8436(1)	11655(1)	19(1)
O(1)	1263(2)	7184(3)	11993(2)	31(1)
N(1)	1990(2)	5807(3)	10061(2)	19(1)
Cl(1)	1147(1)	8920(1)	9535(1)	22(1)
Cl(2)	3812(1)	6860(1)	11217(1)	19(1)
N(3)	3196(2)	10034(3)	10264(2)	15(1)
C(11)	1345(2)	5077(4)	10455(2)	22(1)
C(12)	986(3)	3658(4)	10179(3)	28(1)
C(13)	1299(3)	2987(5)	9485(3)	31(1)
C(14)	1953(3)	3752(4)	9079(3)	27(1)
C(15)	2297(2)	5170(4)	9359(2)	20(1)
C(20)	3094(2)	7572(4)	9333(2)	15(1)
C(21)	2952(2)	6134(4)	8955(2)	18(1)
C(22)	3417(2)	5818(4)	8243(2)	21(1)
C(23)	3940(2)	6998(4)	7945(2)	22(1)
C(24)	4048(2)	8455(4)	8300(2)	20(1)
C(25)	3631(2)	8734(4)	9039(2)	17(1)
C(31)	3229(2)	11233(4)	10795(2)	20(1)
C(32)	3738(3)	12542(4)	10703(2)	22(1)
C(33)	4256(3)	12620(4)	10029(2)	21(1)
C(34)	4225(2)	11407(4)	9472(2)	21(1)
C(35)	3694(2)	10108(4)	9580(2)	15(1)
C(100)	2657(3)	8986(5)	12524(2)	26(1)
C(101)	1047(3)	10048(5)	11574(3)	27(1)
C(221)	3398(3)	4314(5)	7780(3)	29(1)
C(241)	4578(3)	9629(5)	7850(2)	26(1)

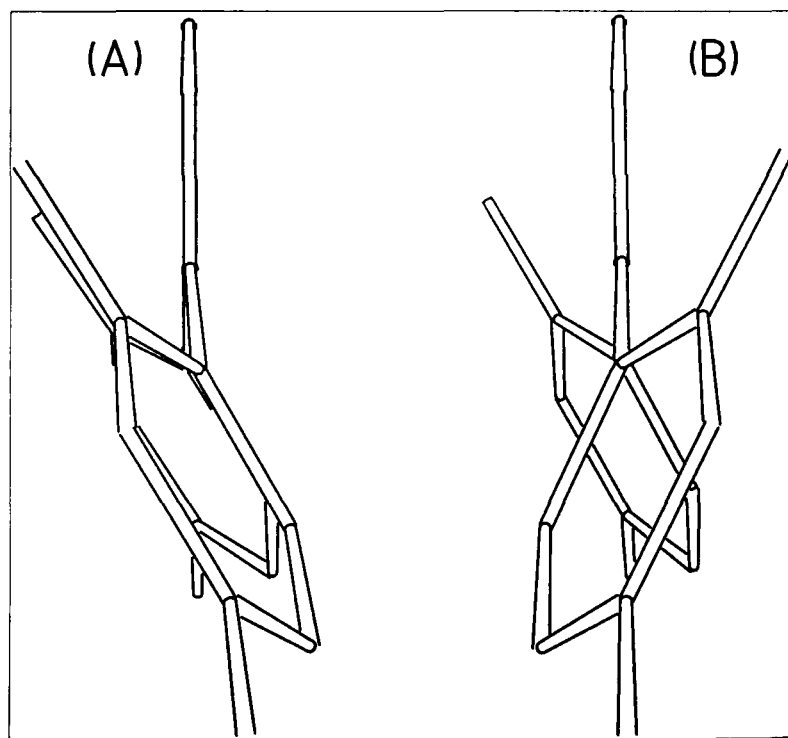
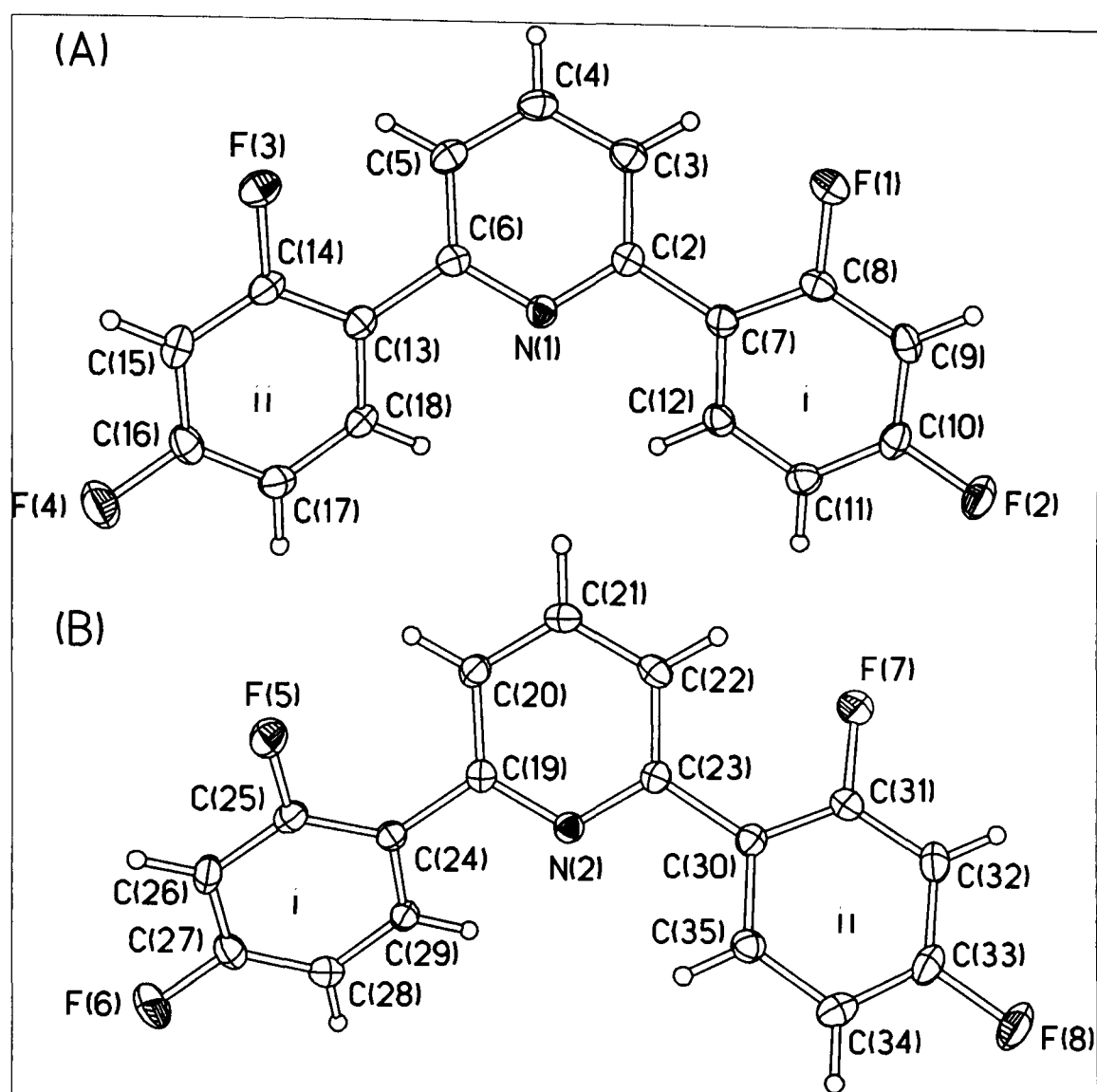
Table A8. Bond lengths [Å] and angles [°] for Ir(dpydmb)(DMSO)Cl₂.

Ir(1)-C(20)	1.976(4)	C(13)-C(14)	1.385(6)
Ir(1)-N(1)	2.067(3)	C(14)-C(15)	1.391(5)
Ir(1)-N(3)	2.087(3)	C(15)-C(21)	1.475(5)
Ir(1)-Cl(1)	2.3518(15)	C(20)-C(25)	1.397(5)
Ir(1)-Cl(2)	2.3735(14)	C(20)-C(21)	1.401(5)
Ir(1)-S(1)	2.4379(18)	C(21)-C(22)	1.419(5)
S(1)-O(1)	1.489(3)	C(22)-C(23)	1.401(5)
S(1)-C(101)	1.782(4)	C(22)-C(221)	1.510(5)
S(1)-C(100)	1.783(4)	C(23)-C(24)	1.397(5)
N(1)-C(11)	1.349(5)	C(24)-C(25)	1.411(5)
N(1)-C(15)	1.373(5)	C(24)-C(241)	1.518(5)
N(3)-C(31)	1.346(5)	C(25)-C(35)	1.476(5)
N(3)-C(35)	1.383(4)	C(31)-C(32)	1.381(5)
C(11)-C(12)	1.396(5)	C(32)-C(33)	1.386(5)
C(12)-C(13)	1.378(6)	C(33)-C(34)	1.381(5)
		C(34)-C(35)	1.396(5)
C(20)-Ir(1)-N(1)	80.00(13)	Cl(1)-Ir(1)-S(1)	90.40(6)
C(20)-Ir(1)-N(3)	79.99(13)	Cl(2)-Ir(1)-S(1)	88.44(6)
N(1)-Ir(1)-N(3)	159.89(12)	O(1)-S(1)-C(101)	105.43(18)
C(20)-Ir(1)-Cl(1)	90.94(11)	O(1)-S(1)-C(100)	105.02(19)
N(1)-Ir(1)-Cl(1)	87.36(9)	C(101)-S(1)-C(100)	100.9(2)
N(3)-Ir(1)-Cl(1)	90.95(9)	O(1)-S(1)-Ir(1)	118.31(12)
C(20)-Ir(1)-Cl(2)	90.24(11)	C(101)-S(1)-Ir(1)	113.03(14)
N(1)-Ir(1)-Cl(2)	89.29(9)	C(100)-S(1)-Ir(1)	112.35(14)
N(3)-Ir(1)-Cl(2)	92.80(9)	C(11)-N(1)-C(15)	120.0(3)
Cl(1)-Ir(1)-Cl(2)	176.20(3)	C(11)-N(1)-Ir(1)	125.0(3)
C(20)-Ir(1)-S(1)	178.66(10)	C(15)-N(1)-Ir(1)	114.7(2)
N(1)-Ir(1)-S(1)	100.15(9)	C(31)-N(3)-C(35)	118.6(3)
N(3)-Ir(1)-S(1)	99.89(8)	C(31)-N(3)-Ir(1)	127.5(2)

C(35)-N(3)-Ir(1)	113.8(2)
N(1)-C(11)-C(12)	121.8(4)
C(13)-C(12)-C(11)	119.0(4)
C(12)-C(13)-C(14)	118.9(4)
C(13)-C(14)-C(15)	121.3(4)
N(1)-C(15)-C(14)	119.0(3)
N(1)-C(15)-C(21)	114.5(3)
C(14)-C(15)-C(21)	126.5(4)
C(25)-C(20)-C(21)	124.8(3)
C(25)-C(20)-Ir(1)	117.9(3)
C(21)-C(20)-Ir(1)	117.3(3)
C(20)-C(21)-C(22)	117.4(3)
C(20)-C(21)-C(15)	113.3(3)
C(22)-C(21)-C(15)	129.3(3)
C(23)-C(22)-C(21)	117.3(3)
C(23)-C(22)-C(221)	117.2(3)
C(21)-C(22)-C(221)	125.4(4)
C(24)-C(23)-C(22)	125.1(3)
C(23)-C(24)-C(25)	117.3(3)
C(23)-C(24)-C(241)	117.8(3)
C(25)-C(24)-C(241)	124.9(3)
C(20)-C(25)-C(24)	117.9(3)
C(20)-C(25)-C(35)	113.3(3)
C(24)-C(25)-C(35)	128.8(3)
N(3)-C(31)-C(32)	123.9(3)
C(31)-C(32)-C(33)	118.1(3)
C(34)-C(33)-C(32)	118.9(3)
C(33)-C(34)-C(35)	121.5(3)
N(3)-C(35)-C(34)	119.0(3)
N(3)-C(35)-C(25)	115.0(3)
C(34)-C(35)-C(25)	126.0(3)

Table A9. Anisotropic displacement parameters ($\text{\AA}^2 \times 10^3$) for Ir(dpydmb)(DMSO)Cl₂. The anisotropic displacement factor exponent takes the form: $-2\pi^2[h^2 a^{*2}U^{11} + \dots + 2hk a^* b^* U^{12}]$.

	U ¹¹	U ²²	U ³³	U ²³	U ¹³	U ¹²
Ir(1)	14(1)	12(1)	16(1)	0(1)	1(1)	-2(1)
S(1)	19(1)	17(1)	22(1)	1(1)	6(1)	-2(1)
O(1)	37(2)	24(2)	36(2)	0(1)	19(1)	-9(1)
N(1)	17(1)	15(2)	23(2)	3(1)	-3(1)	-2(1)
Cl(1)	19(1)	19(1)	26(1)	2(1)	-3(1)	0(1)
Cl(2)	16(1)	20(1)	20(1)	3(1)	0(1)	-1(1)
N(3)	16(1)	13(1)	16(2)	2(1)	1(1)	-1(1)
C(11)	18(2)	22(2)	26(2)	4(2)	-1(2)	-2(2)
C(12)	28(2)	21(2)	31(2)	10(2)	-5(2)	-5(2)
C(13)	36(2)	16(2)	37(2)	0(2)	-9(2)	-6(2)
C(14)	37(2)	15(2)	27(2)	-2(2)	-4(2)	-2(2)
C(15)	23(2)	16(2)	19(2)	-2(1)	-6(1)	2(1)
C(20)	14(2)	19(2)	12(2)	1(1)	-3(1)	4(1)
C(21)	20(2)	18(2)	15(2)	0(1)	-6(1)	-1(1)
C(22)	23(2)	20(2)	18(2)	-4(2)	-4(2)	8(2)
C(23)	19(2)	29(2)	16(2)	-3(2)	-1(1)	7(2)
C(24)	15(2)	25(2)	18(2)	3(2)	-1(1)	3(1)
C(25)	12(2)	20(2)	17(2)	0(1)	-1(1)	1(1)
C(31)	23(2)	20(2)	16(2)	1(2)	5(1)	-2(2)
C(32)	25(2)	17(2)	23(2)	-3(2)	3(2)	-3(1)
C(33)	20(2)	16(2)	25(2)	3(2)	1(2)	-4(1)
C(34)	20(2)	21(2)	23(2)	2(2)	5(2)	-2(2)
C(35)	13(2)	17(2)	15(2)	2(1)	-3(1)	1(1)
C(100)	29(2)	29(2)	19(2)	0(2)	4(2)	-2(2)
C(101)	22(2)	29(2)	32(2)	-3(2)	5(2)	2(2)
C(221)	36(2)	25(2)	25(2)	-10(2)	-1(2)	-1(2)
C(241)	26(2)	33(2)	20(2)	-2(2)	10(2)	0(2)

Crystallographic data for the F₄dppy ligand

Structure of the F₄dppy ligand crystallised from dichloromethane; 120 K, thermal ellipsoids shown at 30% probability.

Table A10. Crystal data and structure refinement for the F₄dppyH₂ ligand.

Empirical formula	C ₁₇ H ₉ F ₄ N	
Formula weight	303.25	
Temperature	120(2) K	
Wavelength	0.71073 Å	
Crystal system	Monoclinic	
Space group	<i>Cc</i> (No)	
Unit cell dimensions	<i>a</i> = 27.555(2) Å	$\alpha = 90^\circ$
	<i>b</i> = 3.7494(3) Å	$\beta = 105.20(1)^\circ$
	<i>c</i> = 26.323(2) Å	$\gamma = 90^\circ$
Volume	2624.4(3) Å ³	
Z	8	
Density (calculated)	1.535 g/cm ³	
Absorption coefficient	0.130 mm ⁻¹	
F(000)	1232	
Crystal size	0.50 × 0.12 × 0.04 mm ³	
Theta range for data collection	2.49 to 30.03°	
Index ranges	-38 ≤ <i>h</i> ≤ 38, -5 ≤ <i>k</i> ≤ 5, -37 ≤ <i>l</i> ≤ 37	
Reflections collected	16 340	
Independent reflections	3848 [R(int) = 0.0443]	
Reflections with I > 2σ(I)	3317	
Completeness to theta = 30.03°	99.9%	
Absorption correction	None	
Refinement method	Full-matrix least-squares on F ²	
Data / restraints / parameters	3848 / 2 / 397	
Goodness-of-fit on F ²	0.966	
Final R indices [I > 2σ(I)]	R1 = 0.0331, wR2 = 0.0725	
R indices (all data)	R1 = 0.0400, wR2 = 0.0744	
Largest diff. peak and hole	0.267 and -0.242 e.Å ⁻³	

Table A11. Atomic coordinates and equivalent isotropic displacement parameters ($\text{\AA}^2 \times 10^3$) for the F_4dppyH_2 ligand. $U(\text{eq})$ is defined as one third of the trace of the orthogonalized U^{ij} tensor.

	$x \times 10^5$	$y \times 10^4$	$z \times 10^5$	$U(\text{eq})$
F(1)	3779(4)	942(3)	48828(4)	283(3)
F(2)	20871(4)	2151(4)	57143(5)	317(3)
F(3)	-3433(4)	2253(4)	20273(5)	303(3)
F(4)	9177(5)	4518(4)	11828(5)	355(3)
N(1)	6045(6)	4237(4)	34674(6)	177(3)
C(2)	4777(7)	4361(5)	39264(7)	179(4)
C(3)	-110(7)	5178(5)	39540(8)	220(4)
C(4)	-3712(7)	5915(5)	34944(8)	233(4)
C(5)	-2454(7)	5818(5)	30193(8)	219(4)
C(6)	2490(7)	4944(5)	30209(7)	181(4)
C(7)	8950(7)	3714(5)	44050(7)	179(4)
C(8)	8378(7)	2125(5)	48623(8)	202(4)
C(9)	12269(8)	1543(5)	53046(8)	209(4)
C(10)	16969(7)	2682(5)	52841(7)	218(4)
C(11)	17872(7)	4307(5)	48499(8)	214(4)
C(12)	13854(7)	4794(5)	44123(8)	188(4)
C(13)	4165(7)	4836(5)	25285(8)	181(4)
C(14)	1219(7)	3552(5)	20518(8)	208(4)
C(15)	2771(8)	3413(5)	15978(8)	237(4)
C(16)	7531(8)	4649(5)	16249(8)	233(4)
C(17)	10691(7)	5983(5)	20802(8)	219(4)
C(18)	8971(7)	6048(5)	25292(8)	192(4)
F(5)	21552(4)	555(3)	19698(5)	282(3)
F(6)	34391(5)	5494(4)	13343(5)	331(3)
F(7)	29015(4)	1377(4)	50178(5)	316(3)
F(8)	45047(5)	-3454(4)	56590(5)	368(3)
N(2)	30400(5)	987(4)	34924(6)	166(3)

C(19)	26851(7)	1870(5)	30557(7)	161(3)
C(20)	21745(7)	1997(5)	30400(7)	191(4)
C(21)	20293(7)	1149(5)	34900(8)	196(4)
C(22)	23921(7)	185(5)	39386(8)	190(4)
C(23)	28978(7)	160(5)	39307(7)	162(4)
C(24)	28747(7)	2834(5)	25928(7)	164(4)
C(25)	26112(7)	2177(5)	20738(8)	194(4)
C(26)	27917(7)	3018(5)	16466(7)	220(4)
C(27)	32560(8)	4592(5)	17496(8)	219(4)
C(28)	35404(7)	5342(5)	22494(8)	208(4)
C(29)	33466(7)	4438(5)	26659(7)	178(4)
C(30)	33115(7)	-836(5)	43940(7)	170(4)
C(31)	33060(7)	-206(5)	49142(8)	207(4)
C(32)	36958(8)	-1038(6)	53444(8)	245(4)
C(33)	41140(8)	-2592(5)	52449(8)	242(4)
C(34)	41508(7)	-3334(5)	47429(8)	230(4)
C(35)	37510(7)	-2429(5)	43244(8)	192(4)

Table A12. Bond lengths [Å] and angles [°] for the F₄dppyH₂ ligand.

F(1)-C(8)	1.357(2)	F(5)-C(25)	1.358(2)
F(2)-C(10)	1.356(2)	F(6)-C(27)	1.361(2)
F(3)-C(14)	1.357(2)	F(7)-C(31)	1.352(2)
F(4)-C(16)	1.356(2)	F(8)-C(33)	1.355(2)
N(1)-C(2)	1.344(2)	N(2)-C(19)	1.341(2)
N(1)-C(6)	1.344(2)	N(2)-C(23)	1.348(2)
C(2)-C(3)	1.401(3)	C(19)-C(20)	1.397(2)
C(2)-C(7)	1.486(3)	C(19)-C(24)	1.491(2)
C(3)-C(4)	1.377(3)	C(20)-C(21)	1.383(3)
C(4)-C(5)	1.383(3)	C(21)-C(22)	1.380(3)
C(5)-C(6)	1.400(2)	C(22)-C(23)	1.399(2)
C(6)-C(13)	1.486(3)	C(23)-C(30)	1.482(3)
C(7)-C(8)	1.389(3)	C(24)-C(25)	1.391(3)
C(7)-C(12)	1.406(3)	C(24)-C(29)	1.400(2)
C(8)-C(9)	1.378(3)	C(25)-C(26)	1.380(3)
C(9)-C(10)	1.378(3)	C(26)-C(27)	1.370(3)
C(10)-C(11)	1.374(3)	C(27)-C(28)	1.372(3)
C(11)-C(12)	1.385(3)	C(28)-C(29)	1.382(3)
C(13)-C(14)	1.390(3)	C(30)-C(31)	1.394(3)
C(13)-C(18)	1.400(3)	C(30)-C(35)	1.405(3)
C(14)-C(15)	1.372(3)	C(31)-C(32)	1.377(3)
C(15)-C(16)	1.375(3)	C(32)-C(33)	1.376(3)
C(16)-C(17)	1.377(3)	C(33)-C(34)	1.380(3)
C(17)-C(18)	1.384(3)	C(34)-C(35)	1.380(3)
C(2)-N(1)-C(6)	118.52(15)	C(4)-C(3)-C(2)	118.66(19)
N(1)-C(2)-C(3)	122.28(17)	C(3)-C(4)-C(5)	119.70(18)
N(1)-C(2)-C(7)	115.52(15)	C(4)-C(5)-C(6)	118.54(18)
C(3)-C(2)-C(7)	122.16(17)	N(1)-C(6)-C(5)	122.30(18)

N(1)-C(6)-C(13)	115.80(16)	C(21)-C(20)-C(19)	118.81(17)
C(5)-C(6)-C(13)	121.88(17)	C(22)-C(21)-C(20)	119.07(17)
C(8)-C(7)-C(12)	116.03(17)	C(21)-C(22)-C(23)	119.31(17)
C(8)-C(7)-C(2)	124.50(16)	N(2)-C(23)-C(22)	121.68(16)
C(12)-C(7)-C(2)	119.46(16)	N(2)-C(23)-C(30)	115.37(15)
F(1)-C(8)-C(9)	116.26(17)	C(22)-C(23)-C(30)	122.93(16)
F(1)-C(8)-C(7)	119.62(17)	C(25)-C(24)-C(29)	115.99(16)
C(9)-C(8)-C(7)	124.08(18)	C(25)-C(24)-C(19)	123.74(16)
C(8)-C(9)-C(10)	116.67(18)	C(29)-C(24)-C(19)	120.26(16)
F(2)-C(10)-C(11)	118.85(18)	F(5)-C(25)-C(26)	116.76(17)
F(2)-C(10)-C(9)	117.98(17)	F(5)-C(25)-C(24)	119.65(16)
C(11)-C(10)-C(9)	123.17(18)	C(26)-C(25)-C(24)	123.58(17)
C(10)-C(11)-C(12)	118.07(18)	C(27)-C(26)-C(25)	117.03(18)
C(11)-C(12)-C(7)	121.97(18)	F(6)-C(27)-C(26)	118.14(18)
C(14)-C(13)-C(18)	116.25(18)	F(6)-C(27)-C(28)	118.70(17)
C(14)-C(13)-C(6)	123.75(17)	C(26)-C(27)-C(28)	123.16(18)
C(18)-C(13)-C(6)	120.00(17)	C(27)-C(28)-C(29)	117.91(17)
F(3)-C(14)-C(15)	116.84(17)	C(28)-C(29)-C(24)	122.33(17)
F(3)-C(14)-C(13)	119.22(17)	C(31)-C(30)-C(35)	115.60(17)
C(15)-C(14)-C(13)	123.91(18)	C(31)-C(30)-C(23)	124.15(17)
C(14)-C(15)-C(16)	116.94(18)	C(35)-C(30)-C(23)	120.22(17)
F(4)-C(16)-C(15)	118.19(18)	F(7)-C(31)-C(32)	116.13(18)
F(4)-C(16)-C(17)	118.83(18)	F(7)-C(31)-C(30)	119.64(17)
C(15)-C(16)-C(17)	122.98(18)	C(32)-C(31)-C(30)	124.22(18)
C(16)-C(17)-C(18)	118.00(18)	C(33)-C(32)-C(31)	116.81(19)
C(17)-C(18)-C(13)	121.92(18)	F(8)-C(33)-C(32)	118.43(19)
C(19)-N(2)-C(23)	118.70(15)	F(8)-C(33)-C(34)	118.67(18)
N(2)-C(19)-C(20)	122.41(17)	C(32)-C(33)-C(34)	122.89(19)
N(2)-C(19)-C(24)	115.31(16)	C(33)-C(34)-C(35)	118.09(18)
C(20)-C(19)-C(24)	122.25(16)	C(34)-C(35)-C(30)	122.37(18)

Table A13. Anisotropic displacement parameters ($\text{\AA}^2 \times 10^4$) for the F_4dppyH_2 ligand. The anisotropic displacement factor exponent takes the form: $-2\pi^2[h^2 a^{*2} U^{11} + \dots + 2 h k a^* b^* U^{12}]$.

	U^{11}	U^{22}	U^{33}	U^{23}	U^{13}	U^{12}
F(1)	237(6)	366(7)	269(7)	49(5)	107(5)	-35(5)
F(2)	294(7)	387(7)	217(6)	40(5)	-29(5)	35(6)
F(3)	203(6)	406(7)	278(6)	-52(6)	24(5)	-112(5)
F(4)	423(8)	443(8)	232(7)	0(6)	147(6)	-43(6)
N(1)	183(8)	173(8)	170(8)	12(6)	39(6)	0(6)
C(2)	193(9)	152(8)	185(9)	-5(7)	37(7)	-3(7)
C(3)	224(9)	206(9)	247(10)	3(8)	95(8)	20(7)
C(4)	172(9)	229(10)	303(11)	20(8)	74(8)	48(7)
C(5)	182(9)	199(10)	254(11)	23(8)	17(8)	19(7)
C(6)	173(9)	154(8)	213(10)	19(7)	44(8)	-6(7)
C(7)	195(9)	170(9)	179(9)	-17(7)	62(7)	25(7)
C(8)	201(9)	206(10)	219(10)	-24(7)	91(8)	-1(7)
C(9)	294(10)	203(9)	151(9)	-3(7)	95(8)	28(8)
C(10)	244(10)	217(10)	164(9)	-27(7)	4(8)	59(8)
C(11)	195(9)	217(10)	235(10)	-20(8)	63(8)	21(7)
C(12)	219(9)	181(9)	179(9)	-2(7)	78(7)	33(7)
C(13)	185(8)	150(8)	197(9)	20(7)	29(7)	16(7)
C(14)	156(9)	211(9)	228(10)	33(8)	-1(7)	-18(7)
C(15)	271(10)	228(10)	174(9)	3(8)	-10(8)	6(8)
C(16)	298(11)	227(10)	195(10)	47(8)	101(9)	25(8)
C(17)	183(9)	218(10)	254(10)	40(8)	54(8)	3(7)
C(18)	165(9)	193(9)	194(9)	16(7)	1(7)	-4(7)
F(5)	214(6)	387(7)	226(6)	-44(5)	22(5)	-83(5)
F(6)	416(7)	395(8)	233(7)	36(6)	179(6)	-38(6)
F(7)	263(6)	474(8)	220(6)	-25(6)	82(5)	96(6)
F(8)	309(7)	448(8)	269(7)	85(6)	-65(5)	68(6)
N(2)	170(7)	165(7)	159(8)	-6(6)	36(6)	3(6)

C(19)	190(9)	129(8)	161(9)	-5(7)	41(7)	1(7)
C(20)	175(9)	201(9)	178(9)	-8(7)	16(7)	27(7)
C(21)	149(9)	203(9)	244(10)	-25(7)	64(8)	-3(7)
C(22)	200(9)	193(9)	196(9)	-6(7)	88(8)	-29(7)
C(23)	171(9)	148(8)	159(9)	-5(7)	29(7)	-9(7)
C(24)	174(8)	148(8)	171(9)	18(7)	44(7)	33(7)
C(25)	165(9)	203(9)	200(9)	-7(7)	24(7)	5(7)
C(26)	256(10)	244(10)	135(9)	2(7)	7(7)	22(8)
C(27)	284(10)	210(10)	190(10)	28(8)	106(8)	33(8)
C(28)	185(9)	205(9)	239(10)	7(8)	68(8)	9(7)
C(29)	177(9)	195(9)	152(9)	-9(7)	24(7)	32(7)
C(30)	171(8)	157(8)	174(9)	27(7)	35(7)	-20(7)
C(31)	193(9)	239(10)	200(10)	17(8)	72(8)	8(7)
C(32)	286(10)	271(10)	169(9)	44(8)	45(8)	-14(8)
C(33)	222(10)	238(10)	224(10)	78(8)	-18(8)	-2(8)
C(34)	181(9)	198(10)	298(11)	28(8)	37(8)	12(7)
C(35)	187(9)	195(9)	201(9)	7(7)	61(7)	-8(7)

Table A14. Torsion angles [°] for the F₄dppyH₂ ligand.

N(1)-C(2)-C(7)-C(12)	32.2(2)
N(1)-C(6)-C(13)-C(18)	-36.5(2)
N(2)-C(23)-C(30)-C(35)	-28.9(2)
N(2)-C(19)-C(24)-C(29)	-30.9(2)

Appendix B – TD-DFT Calculations

Table B1. Calculated excitation wavelengths (λ), oscillator strengths (f) and dominant orbital excitations for the ground-state structures of Ir(N^{^C^N})(C^{^N^C}) complexes. Orbitals are labelled as in Table 27.

State	Ir(dpydmb)(dppy) 108		Ir(dpydmb)(F ₄ dppy) 110		Ir(dpydmb)(cdppy) 111	
	λ / nm (f)	Excitation	λ / nm (f)	Excitation	λ / nm (f)	Excitation
T ₁	556	d ₁ → π_1^*	518	d ₁ → π_1^*	524	d ₁ → π_1^*
T ₂	507	d ₁ → π_2^*	477	d ₁ → π_3^*	487	d ₁ → π_2^*
T ₃	484	d ₂ → π_1^*	470	d _{1,2} → $\pi_{1,3}^*$	480	d ₁ → π_4^*
T ₄	473	d ₁ → π_2^*	452	d ₁ → π_2^*	469	d _{2, \pi_1} → π_1^*
T ₅	457	d ₂ → π_3^*	438	d ₂ → π_4^*	453	d ₂ → π_2^*
T ₆	453	d ₂ → π_2^*	435	d ₂ → π_2^*	451	d ₂ → π_3^*
T ₇	443	d ₂ → π_2^*	424	d ₂ → π_3^*	437	d ₁ → π_3^*
T ₈	427	d ₁ → π_3^*	397	d ₁ → π_4^*	419	d ₂ → π_4^*
T ₉	405	d _{1,2, \pi_{1,3}} → $\pi_{1,5}^*$			392	d _{2,3} → $\pi_{2,3}^*$
T ₁₀	402	d ₁ → π_4^*			388	d ₁ → π_5^*
S ₁	482 (0.1019)	d ₁ → π_1^*	451 (0.1125)	d ₁ → π_1^*	472 (0.0000)	d ₁ → π_2^*
S ₂	462 (0.0000)	d ₁ → π_2^*	441 (0.0001)	d ₁ → π_3^*	456 (0.1139)	d ₁ → π_1^*
S ₃	433 (0.0047)	d _{1,2} → $\pi_{1,2}^*$	411 (0.0008)	d ₁ → π_3^*	429 (0.0023)	d ₁ → π_3^*
S ₄	423 (0.0004)	d ₁ → π_3^*	402 (0.0046)	d ₂ → π_2^*	418 (0.0000)	d ₂ → π_2^*
S ₅	420 (0.0038)	d ₂ → π_2^*	391 (0.0000)	d ₁ → π_4^*	411 (0.0000)	d ₂ → π_1^*
S ₆	411 (0.0403)	d _{1,2} → $\pi_{1,2}^*$	391 (0.0454)	d ₂ → π_1^*	391 (0.0609)	d ₂ → π_1^*
S ₇	394 (0.0689)	d ₂ → π_2^*	378 (0.0669)	d ₂ → π_3^*	385 (0.0577)	d ₂ → π_4^*
S ₈	377 (0.0054)	d ₁ → π_4^*	359 (0.0006)	d ₁ → π_5^*	375 (0.0085)	d ₂ → π_3^*
S ₉	367 (0.0265)	d _{1,2} → $\pi_{3,5}^*$			367 (0.0007)	d ₁ → π_5
S ₁₀	363 (0.0003)	d ₃ → π_1^*			367 (0.0021)	d ₃ → π_1^*

Table B2. Calculated excitation wavelengths (λ), oscillator strengths (f) and dominant orbital excitations for the ground-state structures of Ir(N[^]C[^]N)(C[^]N[^]O) complexes. Orbitals are labelled as in Table 28.

State	Ir(dpydmb)(tppic) 116		Ir(dpydmb)(hbqc) 117	
	λ / nm (f)	Excitation	λ / nm (f)	Excitation
T ₁	508	$d_1 \rightarrow \pi_{1,2}^*$	506	$d_1 \rightarrow \pi_{1,2}^*$
T ₂	501	$d_1 \rightarrow \pi_3^*$	501	$d_1 \rightarrow \pi_3^*$
T ₃	480	$d_2 \rightarrow \pi_{1,2}^*$	497	$d_{2,3} \rightarrow \pi_{1,2}^*$
T ₄	468	$d_1 \rightarrow \pi_{1,2}^*$	478	$d_2, \pi_2 \rightarrow \pi_{1,2}^*$
T ₅	465	$d_2 \rightarrow \pi_{1,2}^*$	466	$d_1 \rightarrow \pi_{1,2}^*$
T ₆	457	$d_2 \rightarrow \pi_3^*$	455	$d_2 \rightarrow \pi_3^*$
T ₇	433	$d_{2,3} \rightarrow \pi_{1,2,4}^*$	451	$d_{2,3} \rightarrow \pi_{1,2}^*$
T ₈	418	$d_{2,3} \rightarrow \pi_{1,4}^*$	409	$d_2 \rightarrow \pi_4^*$
T ₉	409	$d_1 \rightarrow \pi_4^*$	397	$\pi_1 \rightarrow \pi_{1,2}^*$
T ₁₀	396	$d_2, \pi_2 \rightarrow \pi_2^*$	395	$d_2, \pi_2 \rightarrow \pi_{1,2}^*$
S ₁	462 (0.0078)	$d_1 \rightarrow \pi_1^*$	460 (0.0055)	$d_1 \rightarrow \pi_1^*$
S ₂	450 (0.0565)	$d_1 \rightarrow \pi_2^*$	448 (0.0592)	$d_1 \rightarrow \pi_2^*$
S ₃	433 (0.0005)	$d_{1,2} \rightarrow \pi_{1,3}^*$	432 (0.0006)	$d_{1,2} \rightarrow \pi_{1,3}^*$
S ₄	425 (0.0034)	$d_{1,2} \rightarrow \pi_{1,2,3}^*$	418 (0.0068)	$d_2 \rightarrow \pi_{1,2}^*$
S ₅	409 (0.0821)	$d_2 \rightarrow \pi_3^*$	407 (0.0962)	$d_2 \rightarrow \pi_3^*$
S ₆	404 (0.0791)	$d_2 \rightarrow \pi_2^*$	403 (0.0578)	$d_2 \rightarrow \pi_2^*$
S ₇	402 (0.0121)	$d_1 \rightarrow \pi_4^*$	385 (0.0004)	$d_1 \rightarrow \pi_4^*$
S ₈	386 (0.0043)	$d_2 \rightarrow \pi_4^*$	378 (0.0007)	$d_3 \rightarrow \pi_{1,2}^*$
S ₉	378 (0.0148)	$d_3 \rightarrow \pi_{1,2}^*$	372 (0.0004)	$d_2 \rightarrow \pi_3^*$
S ₁₀	370 (0.0008)	$d_1 \rightarrow \pi_5^*$	370 (0.0001)	$\pi_1 \rightarrow \pi_{1,2}^*$

Table B3. Calculated excitation wavelengths (λ), oscillator strengths (f) and dominant orbital excitations for the ground-state structures of two binding modes of Ir(dpydmb)(dinpy). Orbitals are labelled as in Table 29.

State	N [^] N [^] N dinpy binding		C [^] N [^] C dinpy binding	
	λ / nm (f)	Excitation	λ / nm (f)	Excitation
T ₁	590	$\pi_1 \rightarrow \pi_1^*$	596	$\pi_1 \rightarrow \pi_2^*$
T ₂	576	$\pi_{1,2} \rightarrow \pi_{3,4}^*$	585	$\pi_{1,2} \rightarrow \pi_{2,4}^*$
T ₃	569	$\pi_{1,2} \rightarrow \pi_{3,4}^*$	550	$\pi_1 \rightarrow \pi_1^*$
T ₄	558	$\pi_1 \rightarrow \pi_2^*$	537	$d_1 \rightarrow \pi_1^*$
T ₅	486	$\pi_2 \rightarrow \pi_1^*$	492	$\pi_1 \rightarrow \pi_3^*$
T ₆	471	$\pi_3 \rightarrow \pi_4^*$	478	$d_1 \rightarrow \pi_3^*$
T ₇	467	$d_1 \rightarrow \pi_1^*$	455	$d_1 \rightarrow \pi_2^*$
T ₈	463	$\pi_2 \rightarrow \pi_2^*$	442	$\pi_{1,2} \rightarrow \pi_{2,4}^*$
T ₉	461	$d_2, \pi_3 \rightarrow \pi_1^*$	434	$\pi_3 \rightarrow \pi_1^*$
T ₁₀	460	$\pi_3 \rightarrow \pi_3^*$	420	$\pi_2 \rightarrow \pi_{1,4}^*$
S ₁	565 (0.0030)	$\pi_1 \rightarrow \pi_1^*$	516 (0.0081)	$\pi_1 \rightarrow \pi_1^*$
S ₂	534 (0.0120)	$\pi_1 \rightarrow \pi_2^*$	513 (0.0222)	$\pi_1 \rightarrow \pi_2^*$
S ₃	483 (0.0001)	$\pi_2 \rightarrow \pi_1^*$	481 (0.0091)	$d_1, \pi_1 \rightarrow \pi_{1,3}^*$
S ₄	474 (0.0261)	$\pi_1 \rightarrow \pi_3^*$	445 (0.1625)	$d_1, \pi_1 \rightarrow \pi_{1,3}^*$
S ₅	458 (0.0000)	$\pi_2 \rightarrow \pi_2^*$	445 (0.0000)	$d_1 \rightarrow \pi_2^*$
S ₆	452 (0.0007)	$\pi_3 \rightarrow \pi_1^*$	415 (0.0000)	$\pi_2 \rightarrow \pi_1^*$
S ₇	431 (0.0040)	$\pi_1 \rightarrow \pi_4^*$	414 (0.0169)	$d_1 \rightarrow \pi_3^*$
S ₈	431 (0.0000)	$\pi_3 \rightarrow \pi_2^*$	412 (0.0313)	$\pi_1 \rightarrow \pi_4^*$
S ₉	430 (0.0012)	$\pi_1 \rightarrow \pi_5^*$	401 (0.0169)	$\pi_1 \rightarrow \pi_6^*$
S ₁₀	429 (0.0204)	$\pi_{2,4} \rightarrow \pi_{1,3}^*$		

Table B4. Calculated excitation wavelengths (λ), oscillator strengths (f) and dominant orbital excitations for the ground-state structure of $[\text{Ir}(\text{dpydmb})(\text{terpy})]^{2+}$. Orbitals are labelled as in Table 30.

[Ir(dpydmb)(terpy)] ²⁺ 105		
State	λ / nm (f)	Excitation
T ₁	545	$\pi_1 \rightarrow \pi_1^*$
T ₂	493	$\pi_2 \rightarrow \pi_1^*$
T ₃	476	$\pi_1 \rightarrow \pi_2^*$
T ₄	460	$d_2 \rightarrow \pi_1^*$
T ₅	451	$\pi_2 \rightarrow \pi_4^*$
T ₆	434	$d_{1,2}, \pi_{2,3} \rightarrow \pi_{1,2}^*$
S ₁	537 (0.0000)	$\pi_1 \rightarrow \pi_1^*$
S ₂	483 (0.0024)	$\pi_2 \rightarrow \pi_1^*$
S ₃	473 (0.0001)	$\pi_1 \rightarrow \pi_2^*$
S ₄	441 (0.0014)	$\pi_2 \rightarrow \pi_2^*$

